STRUCTURAL SYSTEMS

RESEARCH PROJECT

Report No.
SSRP–06/11

THE ASSESSMENT OF ASPECTS RELATED TO DEFECT CRITICALITY IN CFRP STRENGTHENED CONCRETE FLEXURAL MEMBERS

by

JASON C. DELANEY

VISTASP M. KARBHARI

Final Report Submitted to the California Department of Transportation Under Contract No. 59A0337.

May 2006

Department of Structural Engineering
University of California, San Diego
La Jolla, California 92093-0085

University of California, San Diego
Department of Structural Engineering
Structural Systems Research Project

Report No. SSRP–06/11

The Assessment of Aspects Related to Defect Criticality in CFRP Strengthened Concrete Flexural Members

by

Jason C. Delaney
Graduate Student Researcher

Vistasp M. Karbhari
Professor of Structural Engineering

Final Report Submitted to the California Department of Transportation
Under Contract No. 59A337.

Department of Structural Engineering
University of California, San Diego
La Jolla, California 92093-0085

May 2006

Technical Report Documentation Page

1. Report No.	2. Government Accession No.	3. Recipient's Catalog No.
4. Title and Subtitle The Assessment of Aspects Related to Defect Criticality in CFRP Strengthened Concrete Flexural Members		5. Report Date 5/16/2006 6. Performing Organization Code
7. Author(s) Jason C. Delaney, Vistasp M. Karbhari		8. Performing Organization Report No. UCSD / SSRP- 06/11
9. Performing Organization Name and Address Department of Structural Engineering School of Engineering University of California, San Diego La Jolla, California 92093-0085		10. Work Unit No. (TRAIS) 11. Contract or Grant No. 59A0337
12. Sponsoring Agency Name and Address California Department of Transportation Engineering Service Center 1801 30th St., West Building MS-9 Sacramento, California 95807		13. Type of Report and Period Covered Final Report - 14. Sponsoring Agency Code

15. Supplementary Notes

Prepared in cooperation with the State of California Department of Transportation.

16. Abstract

The effectiveness of externally bonded Carbon Fiber Reinforced Polymer (CFRP) composites in structural rehabilitation is strongly dependent on the bond performance between the CFRP and the reinforced concrete substrate to which it is bonded. Many recent studies have been conducted in an attempt to quantify aspects of bond performance and bond behavior in this situation. Due to the complexity of the problem, most research has been conducted only on idealized specimens. This study investigates how bond performance may be affected in less than ideal conditions involving specific defects that may be encountered in the field. A defect in the FRP, concrete, or at the bond line can result in stress concentrations initiating local bond failure and, therefore, may produce an unfavorable influence on the global strengthening performance. Large-scale flexural tests were utilized to investigate the bond behavior of precracked specimens involving various defects such as crack width, unbonded length, unbonded shape, and unbonded location.

From these tests the critical aspects of defects that have an adverse influence on the global strengthening performance of a rehabilitated section are assessed. The tests demonstrate that current design guidelines pertaining to certain defects may be too conservative and that more attention needs to be paid to the study of the initiation and progression of global failure modes. The resulting data allows for crucial observations to be made pertaining to relating idealized or more "perfect" laboratory behavior to specific "imperfect" field applications. Additionally, the testing program generated important data needed to develop and validate a more precise finite element analysis model for the behavior of CFRP strengthened concrete structures. It is shown that the greatest level of strengthening is not always due to use of maximizing material parameters, but rather optimizing the interaction between them.

17. Key Words	18. Distribution Statement
FRP, Rehabilitation, Defect, Finite Element Analysis	No Restrictions

19. Security Classification (of this report)	20. Security Classification (of this page)	21. No. of Pages	22. Price
Unclassified	Unclassified	410	

Form DOT F 1700.7 (8-72) Reproduction of completed page authorized

DISCLAIMER

The opinions expressed in this report are those of the authors and do not represent positions of the California Department of Transportation.

TABLE OF CONTENTS

TECHNICAL REPORT DOCUMENTATION PAGE i
DISCLAIMER ii
TABLE OF CONTENTS iii
LIST OF FIGURES ix
LIST OF TABLES xv
ACKNOWLEDGEMENTS xvii
ABSTRACT xviii

1. INTRODUCTION 1
1.1 Overview of Strengthening and Rehabilitation of Concrete Structures 1
1.2 History and Literature Review of Defects with FRP Strengthening 5
1.2.1 Cracking with FRP 6
1.2.2 Unbonded Regions 7
1.2.3 Investigating Strengthening in the Presence of Defects 8
1.2.4 Effect of Preloading 11
1.2.5 Design Guideline Recommendations for Defects 13
1.3 Rationale of Study 16
1.4 Structure of Report 18

2 EXPERIMENTAL PROGRAM 22
2.1 Choice of Specimen Type 22
2.2 Specimen Design 24
2.3 Details of Loading Method 26
2.4 Defects Considered 28
2.4.1 Disbonds 31
2.4.2 Cracks 35
2.5 Material Data 35
2.5.1 Composite Characteristics 35
2.5.2 Concrete Properties 38

2.5.3 Steel Properties 40
2.6 Instrumentation 40
2.7 Loading Protocol 42
2.8 Preloading 42
2.9 Wet Layup Procedure 52
2.10 Final Testing 55

3. DEFECT MODELING USING FEA 57
3.1 FE Analysis Program 58

4. RESULTS 73
4.1. Control Specimens 73
4.1.1 Unstrengthened Control Specimens 74
4.1.2 Non-Preloaded, Strengthened Control Specimens 76
4.1.3 Preloaded, Strengthened Control Specimens 77
4.2. Critical Disbond Size 87
4.2.1 Circular Disbond 88
4.2.2 Rectangular Disbonds 100
4.3. Critical Disbond Location 115
4.3.1 Circular Disbond 115
4.4 Effect of Excessive Preload Cracking 136
4.4.1 0mm to 1.5mm Crack Widths 136
4.4.2 1.0mm Crack Widths with Disbonds 144
4.4.3 Submerging FRP in Water 154
4.5 Interlaminar Disbonds 155

5. DISCUSSION OF RESULTS 164
5.1 Significant Observations of Results 164
5.2 Comparison with FEA 172

6. CONCLUSIONS 189

Appendix A: Failure Modes 196

Appendix B: Specimen Test Synopsis 201

A.B.1: Control Specimens 201

Specimen 1: Unstrengthened control specimen tested 12/16/2004 (Control_1_S1) 201

Specimen 2: Unstrengthened control specimen tested 1/7/2005 (Control_2_S2) 204

Specimen 3: Unstrengthened control specimen tested 1/14/2005 (Control_3) 206

Specimen 7: Strengthened, preloaded control specimen tested 5/18/2005 (R_C_Control_1_S7) 208

Specimen 26: Strengthened, non-preloaded control specimen tested 5/26/2005 (R_UC_Control_1_S26) 213

Specimen 9: Strengthened, preloaded control specimen tested 6/13/2005 (R_C_Control_2_S9) 216

Specimen 27: Strengthened, non-preloaded control specimen tested 6/15/2005 (R_UC_Control_2_S27) 219

Specimen 6: Strengthened, non-preloaded control specimen tested 6/16/2005 (R_C_Control_3_S6) 222

Specimen 28: Strengthened, non-preloaded control specimen tested 6/17/2005 (R_UC_Control_3_S28) 226

Specimen 29: Strengthened, non-preloaded control specimen tested 6/20/2005 (R_UC_Control_4_S29) 229

Specimen 10: Strengthened, preloaded control specimen tested 6/22/2005 (R_C_Control_4_S10) 233

A.B.2 Specimens with inserted defects 236

Specimen 14: 150x100mm rectangular disbond inserted in the adhesive interface 185mm from the midspan tested 6/22/2005 (150R_185_S14) 236

Specimen 17: 150mm diameter circular disbond inserted in the adhesive interface 185mm from the midspan tested 6/23/2005 (150C_185_S17) 240

Specimen 15: 100mm diameter circular disbond inserted in the adhesive interface 185mm from the midspan tested 6/23/2005 (100C_185_S15) 244

Specimen 8: 100mm x 150mm rectangular disbond inserted in the adhesive interface 185mm from the midspan tested 6/27/2005 (100R_185_S8) 248

Specimen 19: 50mm x 150mm rectangular disbond inserted in the adhesive interface 185mm from the midspan tested 6/28/2005 (50R_185_S19) 251

Specimen 21: 50mm diameter circular disbond inserted in the adhesive interface 185mm from the midspan tested 6/29/2005 (50C_185_S21) 254

Specimen 13: 25mm x 150mm rectangular disbond inserted in the adhesive interface 185mm from the midspan tested 7/6/2005 (25R_185_S13)..... 258

Specimen 12: 25mm diameter circular disbond inserted in the adhesive interface 185mm from the midspan tested 7/7/2005 (25C_185_S12)..... 261

Specimen 4: 100mm x 150mm rectangular disbond inserted in the adhesive interface 185mm from the midspan tested 7/8/2005 (100R_185_S4)..... 264

Specimen 16: 100mm diameter circular disbond inserted in the adhesive interface 185mm from the midspan tested 7/8/2005 (100C_185_S16_2)..... 268

Specimen 25: 100mm x 150mm rectangular disbond inserted in the adhesive interface located at the midspan tested 7/11/2005 (100R_0_S25) 271

Specimen 18: Strengthened, preloaded control specimen tested 7/11/2005 (R_C_Control_5_S18)..... 275

Specimen 24: 100mm diameter circular disbond inserted in the adhesive interface 428mm from the midspan tested 7/12/2005 (100C_428_S24)..... 278

Specimen 20: 100mm diameter circular disbond inserted in the adhesive interface 185mm from the end of the FRP tested 7/12/2005 (100C_185E_S20)..... 281

Specimen 11: 150mm x 150mm rectangular disbond inserted in the adhesive interface located 185mm from the midspan, tested 7/13/2005 (150R_185_S11_2)..... 285

Specimen 5: 100mm diameter circular disbond inserted in the adhesive interface 185mm from the midspan tested 7/13/2005 (100C_185_S5_3)..... 289

Specimen 23: 100mm diameter circular disbond inserted in the adhesive interface located at the midspan tested 7/14/2005 (100C_0_S23) 292

Specimen 22: 150mm diameter circular disbond inserted in the adhesive interface 185mm from the midspan tested 7/14/2005 (150C_185_S22_2)..... 295

Specimen 30: Unstrengthened control specimen tested 7/28/2005 (Control_4_S30) 299

Specimen 31: 100mm x 150mm rectangular disbond inserted in the adhesive interface 185mm from the midspan tested 9/2/2005 (100R_185_S31)..... 301

Specimen 36: Strengthened, preloaded control specimen tested 9/13/2005 (R_C_Control_6_S36)..... 304

Specimen 35: 250mm x 150mm rectangular disbond inserted in the adhesive interface located 185mm from the midspan, tested 9/20/2005 (250R_185_S35)..... 308

Specimen 32: 50mm x 150mm rectangular disbond inserted in the adhesive interface 185mm from the midspan tested 9/20/2005 (50R_185_S32_2)..... 311

Specimen 33: 150x100mm rectangular disbond inserted in the adhesive interface 185mm from the midspan tested 9/20/2005 (150R_185_S33_3)..... 315

Specimen 34: 200mm by 150mm rectangular disbond inserted in the adhesive interface 185mm from the midspan tested 9/22/2005 (200R_185_S34)..... 319

Specimen 37: 100mm x 150mm rectangular disbond inserted in the interface between FRP layers located 185mm from the midspan tested 9/27/2005 (100RI_185_S37) 323

Specimen 40: 100mm x 150mm rectangular disbond inserted in the interface between FRP layers and in the adhesive located 185mm from the midspan tested 9/28/2005 (100RAI_185_S40) 326

Specimen 38: 100mm x 150mm rectangular disbond inserted in the adhesive interface 185mm from the midspan tested 9/28/2005 (100R_185_S38_4)..... 330

Specimen 43: 100mm diameter circular disbond inserted in the interface between FRP layers and in the adhesive interface, located 185mm from the midspan tested 9/30/2005 (100CAI_185_S43) 334

Specimen 42: Strengthened, preloaded control specimen tested 9/30/2005 (R_C_Control_7_S42)..... 337

Specimen 45: 100mm x 150mm rectangular disbond inserted in the interface between FRP layers and in the adhesive interface located at the midspan tested 10/25/2005 (100RAI_0_S45) 341

Specimen 44: 100mm x 150mm rectangular disbond inserted in the interface between FRP layers and in the adhesive interface located at the midspan tested 10/26/2005 (100RAI_428_S44) 344

Specimen 41: 100mm x 150mm rectangular disbond inserted in the interface between FRP layers and in the adhesive located 185mm from the midspan tested 10/26/2005 (100RAI_185_S41_2) 348

Specimen 39: 100mm x 150mm rectangular disbond inserted in the interface between FRP layers located 185mm from the midspan tested 10/28/2005 (100RI_185_S39_2) 352

Specimen 55: 100mm x 150mm rectangular disbond inserted in the adhesive interface, submerged in water for seven days, located 185mm from the midspan, tested 11/2/2005 (100RS7_185__1.0cw_S55) 355

Specimen 61: 200mm by 150mm rectangular disbond inserted in the adhesive interface 185mm from the midspan tested 11/2/2005 (200R_185_S61_2)..... 358

Specimen 46: 50mm x 150mm rectangular disbond inserted in the adhesive interface 185mm from the midspan tested 11/4/2005 (50R_185_S46_3)..... 362

Specimen 53: 100mm x 150mm rectangular disbond inserted in the adhesive interface 185mm from the midspan tested 11/4/2005 (100R_185_1.0cw_S53) 366

Specimen 52: Specimen preloaded to a 1.0mm residual maximum crack width 11/7/2005 (1.0cw_S52) 369

Specimen 51: Specimen preloaded to a 0.6mm residual maximum crack width 11/8/2005 (0.6cw_S51) 374

Specimen 50: Specimen preloaded to a 0.2mm residual maximum crack width 11/9/2005 (0.2cw_S50) 378

Specimen 47: Strengthened, preloaded control specimen tested 11/9/2005 (R_C_Control_8_S47) 381

Specimen 48: Specimen preloaded to a 1.5mm residual maximum crack width 11/10/2005 (1.5cw_S48) 385

Specimen 54: 100mm x 150mm rectangular disbond inserted in the adhesive interface, submerged in water for twenty-one days, located 185mm from the midspan, tested 11/14/2005 (100RS21_185_1.0cw_S54) 389

Specimen 57: 100mm x 150mm rectangular disbond inserted in the adhesive interface 185mm from the midspan in both directions tested 11/15/2005 (100R2_185_1.0cw_S57) 392

Specimen 58: 100mm x 150mm rectangular disbond inserted in the adhesive interface 185mm from the midspan tested 11/16/2005 (100R_185_1.0cw_S58) 395

Specimen 60: 50mm diameter circular disbond inserted in the adhesive interface 185mm from the midspan tested 11/17/2005 (50C_185_S60_2) 398

Specimen 59: 25mm diameter circular disbond inserted in the adhesive interface 185mm from the midspan tested 11/17/2005 (25C_185_S59_2) 401

Specimen 56: 200mm by 150mm rectangular disbond inserted in the adhesive interface 185mm from the midspan tested 11/18/2005 (200R_185_1.0cw_S56) 404

Specimen 49: 250mm x 150mm rectangular disbond inserted in the adhesive interface located 185mm from the midspan, tested 11/18/2005 (250R_185_S49_2) 407

LIST OF FIGURES

Figure 1-1: Test setup. 3
Figure 2-1: Three types of failure modes 23
Figure 2-2: Test specimen design. 25
Figure 2-3: Test setup 27
Figure 2-4: Defect locations considered (in mm from the midspan location), loading regions, and shear and moment diagrams. 32
Figure 2-5: Sketch of disbond locations 33
Figure: 2-6: 100mm by 150mm rectangular Teflon disbond. 34
Figure 2-7: Concrete Compressive Strength vs. Cure Time 39
Figure 2-8: Casting of the reinforced concrete beam specimens. 39
Figure 2-9: Instrumentation layout for test program 41
Figure 2-10: Residual crack width after unloading vs. maximum midspan deflection. 47
Figure 2-11: 0.2mm residual crack width (max beam deflection = 8.02mm) 48
Figure 2-12: 0.6mm residual crack width (max beam deflection = 10.04mm) 48
Figure 2-13: 1.0mm residual crack width (max beam deflection = 13.07mm) 49
Figure 2-14: 1.4mm residual crack width (max beam deflection = 20.06mm) 49
Figure 2-15: 1.5mm residual crack width (max beam deflection = 21.04mm) 50
Figure 2-16: Picture before preloading and after preloading to 35.6kN. 51
Figure 2-17: Wet lay-up procedure. 54
Figure 3-1: Local bond-slip curves for bond performance between concrete and FRP…. 58
Figure 3-2: Graphical representation of the FE model. 60
Figure 3-3: Coefficients for determination of the fracture energy (CEB-FIP 1993). 61
Figure 3-4: Stress-strain material model for concrete behavior 63
Figure 3-5: Steel material model utilized in the FE model 64
Figure 3-6: Model CEB-FIP MC90 describing steel-concrete bond behavior 65
Figure 3-7: Failure modes: debonding through the adhesive layer and debonding through the concrete cover. 66

Figure 3-8: FRP stress-strain material model. 67
Figure 3-9: Simplified linear softening model for mode II fracture. 68
Figure 3-10: Simplified linear softening model for mode I fracture. 68
Figure 4-1: Load vs. Displacement plots for the unstrengthened control specimens. 75
Figure 4-2: Typical failed unstrengthened control specimen. 75
Figure 4-3: Crack pattern and debonding failure of a typical non-preloaded, strengthened beam. 77
Figure 4-4: Crack pattern and debonding failure of a typical precracked, rehabilitated beam. 78
Figure 4-5: Representative Load vs. Displacement plots for the three types of control specimens. 80
Figure 4-6: Representative Steel Strain vs. Load plots for the three types of control specimens. 80
Figure 4-7: Representative strain profiles for preloaded and non-preloaded control specimens. 84
Figure 4-8: Representative load versus midspan displacement plots for the three different debonding failure modes observed during testing of the control specimens. 86
Figure 4-9: Representative strain profiles the three different debonding failure modes observed during testing of the control specimens. 87
Figure 4-10: Sketch of disbond locations 88
Figure 4-11: Example placement of a 100mm diameter circular disbond for investigating the critical defect size. 89
Figure 4-12: Characteristic load vs. midspan displacement plots for circular disbonds with different failure modes. 92
Figure 4-13: Representative Steel Strain vs. Load plots for representative circular disbond specimens and the control specimens. 93
Figure 4-14: Typical cracking patterns for specimens with circular disbond defects. The circled regions represent the approximate locations of the disbond(s). 94
Figure 4-15: Representative strain profiles for beams with circular disbonds. 95
Figure 4-16: Max load vs. circular disbond diameter. 97
Figure 4-17: Displacement at debonding vs. circular disbond diameter. 97
Figure 4-18: Maximum load vs. circular disbond diameter for “deep concrete, steel” failure mode. 99

Figure 4-1-9: Displacement at debonding vs. circular disbond diameter for “deep concrete, steel” failure mode. 99

Figure 4-20: Peak FRP strain vs. circular disbond diameter for “deep concrete, steel” failure mode. 100

Figure 4-21: FRP strain profile at steel yielding load. 100

Figure 4-22: Placement of a 100mm rectangular disbond for investigating the critical defect size. 101

Figure 4-23: Characteristic load vs. displacement plots for rectangular disbond sets…... 106

Figure 4-24: Representative Steel Strain vs. Load plots for representative rectangular disbond specimens and the control specimens. 107

Figure 4-25: Typical cracking patterns for specimens with disbond defects. The circled regions represent the approximate locations of the disbond(s). 108

Figure 4-26: Representative strain profiles for beams with rectangular disbonds. 109

Figure 4-27: Max load vs. rectangular disbond length. 112

Figure 4-28: Displacement at debonding vs. rectangular disbond length. 112

Figure 4-29: Displacement at debonding vs. rectangular disbond length with failure mode “thick concrete bondline”. 113

Figure 4-30: Displacement at steel yield vs. rectangular disbond length with failure mode “thick concrete bondline”. 114

Figure 4-31: FRP strain at debonding vs. rectangular disbond length with failure mode “thick concrete bondline”. 114

Figure 4-32: Characteristic load vs. displacement plots for various disbond locations. 116

Figure 4-33: Representative Steel Strain vs. Load plots for various disbond locations. 117

Figure 4-34: Representative strain profiles. 120

Figure 4-35: Max load vs. circular disbond location. 121

Figure 4-36: Displacement at debonding vs. circular disbond location. 122

Figure 4-37: Load at steel yield vs. circular disbond location for “thick concrete bondline” debonding mode. 123

Figure 4-38: Displacement at steel yield vs. circular disbond location for “thick concrete bondline” debonding mode. 124

Figure 4-39: FRP strain at steel yield vs. circular disbond location for “thick concrete bondline” debonding mode. 124

Figure 4-40: Maximum FRP strain vs. circular disbond location for “thick concrete bondline” debonding mode. 125

Figure 4-41: Characteristic load vs. displacement plots for various disbond locations. 127

Figure 4-42: Characteristic load vs. displacement plots for various disbond locations. 128

Figure 4-43: Representative Steel Strain vs. Load plots for various disbond locations. 128

Figure 4-44: Representative strain profiles. 131

Figure 4-45: Max load vs. rectangular disbond location. 132

Figure 4-46: Displacement at debonding vs. rectangular disbond location. 133

Figure 4-47: Max load vs. circular disbond location. 134

Figure 4-48: Displacement at debonding vs. circular disbond location. 134

Figure 4-49: Displacement at debonding vs. rectangular disbond location. 135

Figure 4-50: Displacement at debonding vs. rectangular disbond location. 136

Figure 4-51: Characteristic load vs. displacement plots for various preload crack widths.. 139

Figure 4-52: Representative Steel Strain vs. Load plots for various disbond locations 139

Figure 4-53: Representative strain profiles. 141

Figure 4-54: Max load vs. residual preload crack width. 143

Figure 4-55: Displacement at debonding vs. residual preload crack width. 143

Figure 4-56: Characteristic load vs. displacement plots for various preload crack widths.. 145

Figure 4-57: Representative strain profiles. 147

Figure 4-58: representative photos of large primary crack (top) and a multiple distributed cracks (bottom). 148

Figure 4-59: Max load versus defect(s) size and characteristics. 150

Figure 4-60: Displacement at debonding versus defect(s) size and characteristics. 150

Figure 4-61: Max load versus defect(s) size and characteristics for specimens debonding by the “deep concrete, steel” failure mode. 152

Figure 4-62: Displacement at debonding versus defect(s) size and characteristics for specimens debonding by the “deep concrete, steel” failure mode. 152

Figure 4-63: Load at steel yield versus defect(s) size and characteristics for specimens debonding by the “deep concrete, steel” failure mode. 152

Figure 4-64: Midspan displacement at yield versus defect(s) size and characteristics for debonding by the “deep concrete, steel” failure mode. 153

Figure 4-65: FRP strain at yield versus defect(s) size and characteristics for specimens debonding by the “deep concrete, steel” failure mode. 153

Figure 4-66: Maximum FRP strain versus defect(s) size and characteristics for specimens debonding by the “deep concrete, steel” failure mode. 153

Figure 4-67: Ultimate load versus defect(s) size and characteristics for specimens soaked in water. 154

Figure 4-68: Ultimate load versus defect(s) size and characteristics for specimens soaked in water. 154

Figure 4-69: Maximum FRP strain versus defect(s) size and characteristics for specimens debonding by the “deep concrete, steel” failure mode. 155

Figure 4-70: Characteristic load vs. displacement plots for various interface disbond locations. 156

Figure 4-71: Representative steel strain vs. load plots for interlaminar disbonds.. 156

Figure 4-72: Representative strain profiles. 158

Figure 4-73: Max load vs. disbond characteristics 159

Figure 4-74: Displacement at debonding versus disbond characteristics 160

Figure 4-75: Max load vs. disbond characteristics for specimens debonding through the “resin interface” failure mode. 161

Figure 4-76: Displacement at debonding vs. disbond characteristics for specimens debonding through the “resin interface” failure mode. 162

Figure 4-77: Maximum FRP strain vs. disbond characteristics for specimens debonding through the “resin interface” failure mode. 162

Figure 5-1: Debonding load versus failure mode 168

Figure 5-2: Specimen failure mode distribution in each rehabilitation set. 168

Figure 5-3: Four debonding failure modes that occurred. 169

Figure 5-4: Load versus displacement comparison for unstrengthened control beams.. 173

Figure 5-5: Load versus midspan displacement for specimens strengthened with FRP. 173

Figure 5-6: Behavior changes resulting from changes in material properties. 175

Figure 5-7: Changed debonding failure mode due to different material properties (top is debonding through the concrete substrate, while the bottom image is debonding through the adhesive)..... 175

Figure 5-8: Load versus midspan displacement for disbonds located at the midspan..... 180

Figure 5-9: Load vs midspan displacement for disbonds located at 185mm from the midspan..... 180

Figure 5-10: Load vs midspan displacement for disbonds located at 428mm from the midspan..... 181

Figure 5-11: Load vs midspan displacement for disbonds located at 660mm from the midspan..... 181

Figure 5-12: Load versus midspan displacement for disbonds located at 750mm from the midspan..... 182

Figure 5-13: Comparison between FEA predicted cracking pattern for a rehabilitated beam without defects and a failed specimen without defects..... 183

Figure 5-14: Comparison between FEA predicted cracking pattern of a beam and a failed specimen with a 250mm disbond located 185mm from the midspan. 183

Figure 5-15: Displacement at debonding versus disbond location from midspan for FEA and laboratory results..... 185

Figure 5-16: Load versus disbond location from midspan for FEA and laboratory results..... 186

LIST OF TABLES

Table 2-1: Summary of defects investigated. 29
Table 2-2: Key for table 2-1 30
Table 2-3: Tensile coupon data summary 37
Table 2-4: Concrete compressive strengths 38
Table 2-5: Steel bar properties 40
Table 2-6: Test specimen summary. 44
Table 2-7: Key for table 2-6 45
Table 3-1: Material Properties Used in the FEA 69
Table 4-1: Unstrengthened control specimen beam characteristics. 76
Table 4-2: Strengthened control specimen beam characteristics. 81
Table 4-2 (continued): Strengthened control specimen beam characteristics. 82
Table 4-3: Average response characteristics for strengthened control specimens. .. 83
Table 4-4: Load vs. measured crack width (mm) during testing. 84
Table 4-5: Beam behavior characteristics for determination of critical circular disbond size. 90
Table 4-6: Load vs. measured crack width (mm) during testing. 95
Table 4-7: Beam behavior characteristics for determination of critical rectangular disbond size. 104
Table 4-7 (continued): Beam behavior characteristics for determination of critical rectangular disbond size. 105
Table 4-8: Load vs. measured crack width (mm) during testing. 110
Table 4-9: Beam behavior characteristics for determination of critical circular disbond locations. 118
Table 4-10: Load vs. measured crack width (mm) during testing. 120
Table 4-11: Beam behavior characteristics for determination of critical rectangular disbond location. 130
Table 4-12: Load vs. measured crack width (mm) during testing. 131
Table 4-13: Strengthened control specimen beam characteristics. 140

Table 4-14: Load vs. measured crack width (mm) during testing. 142
Table 4-15: Beam behavior characteristics for determination of critical rectangular disbond location. 146
Table 4-16: Load vs. measured crack width (mm) during testing. 149
Table 4-17: Beam behavior characteristics for determination of the effect of interlaminar disbonds. 157
Table 4-18: Load vs. measured crack width (mm) during testing. 158
Table 5-1: Summary of the Effect of Defects 170
Table 5-1(continued): Summary of the Effect of Defects 171
Table 5-2: Summary of FEA Results. 187

ACKNOWLEDGEMENTS

The authors would like to express their gratitude to the California Department of Transportation for their financial support and to Fyfe Co for donating materials used on this project. They would also like to thank Dr. Karbhari's research group for their expertise and support.

ABSTRACT

The Assessment of Aspects Related to Defect Criticality in CFRP Strengthened Concrete Flexural Members

The effectiveness of externally bonded Carbon Fiber Reinforced Polymer (CFRP) composites in structural rehabilitation is strongly dependent on the bond performance between the CFRP and the reinforced concrete substrate to which it is bonded. Many recent studies have been conducted in an attempt to quantify aspects of bond performance and bond behavior in this situation. Due to the complexity of the problem, most research has been conducted only on idealized specimens. This study investigates how bond performance may be affected in less than ideal conditions involving specific defects that may be encountered in the field. A defect in the FRP, concrete, or at the bond line can result in stress concentrations initiating local bond failure and, therefore, may produce an unfavorable influence on the global strengthening performance. Large-scale flexural tests were utilized to investigate the bond behavior of precracked specimens involving various defects such as crack width, unbonded length, unbonded shape, and unbonded location.

From these tests the critical aspects of defects that have an adverse influence on the global strengthening performance of a rehabilitated section are assessed. The tests demonstrate that current design guidelines pertaining to certain defects may be too

conservative and that more attention needs to be paid to the study of the initiation and progression of global failure modes. The resulting data allows for crucial observations to be made pertaining to relating idealized or more “perfect” laboratory behavior to specific “imperfect” field applications. Additionally, the testing program generated important data needed to develop and validate a more precise finite element analysis model for the behavior of CFRP strengthened concrete structures. It is shown that the greatest level of strengthening is not always due to use of maximizing material parameters, but rather optimizing the interaction between them.

1. INTRODUCTION

1.1 Overview of Strengthening and Rehabilitation of Concrete Structures

The twentieth century yielded great advances in the building and transportation construction industry. New innovations, technologies, and improved engineering skills lead to the use of construction materials such as reinforced concrete at previously unprecedented rates. Very large, complex, and relatively economical structures were erected using innovative engineering techniques. This progress lead to the cities and roadways we see before us today. However, as many structures age, their performance capabilities may decline, or their service demands often change and there is an immediate need to improve them structurally. In the case of structures such as bridges, continuously increasing traffic along with the exposure to harsh environments over time has led to significant physical and chemical damage resulting in cracking and spalling of the concrete, and corrosion of the steel reinforcement (Kaiser 2002). Other reasons that rehabilitation may be needed include improper design or construction, poor materials, physical damage due to excessive or improper loading, or deficiencies in previous design codes that may require rehabilitation to improve structural behavior. Complete reconstruction of such structures is often not the preferred action due either to cost or perhaps historical value. One of the most effective and fastest growing ways to rehabilitate a structure is using externally bonded fiber reinforced polymer (FRP) composites.

Considerable research has been conducted on this topic in the past ten years and many applications have already been implemented. Several text books and design guidelines have been written on this topic (ACI 440 2002), (NCHRP Report 514), (Teng et al, 2002). Many of these applications have proven very successful. However, there is still much more work that needs to be done to optimize design and verify long term performance capabilities of FRP rehabilitated structures. The effect of common defects found in the FRP strengthening process involving the behavior and response of the rehabilitated structure is one of these areas that need to be addressed further. As an effort to fulfill the need for information in this area, this investigation consisted of laboratory testing of a total of 62 large scale flexural concrete members that were rehabilitated with carbon fiber reinforced polymer (CFRP). As part of the testing process, these concrete members were first preloaded to create a damaged structure. Figure 1-1 is a picture of the laboratory test setup. They were then rehabilitated with CFRP composite bonded to the tension face before being tested to failure. During the preloading and rehabilitation phases, many of these specimens were purposely manufactured to possess some of the common defects that may be encountered in the field. In addition to the laboratory testing program, a finite element analysis model was developed with the capability to accurately model the behavior of FRP strengthened flexural members either with or without defects.

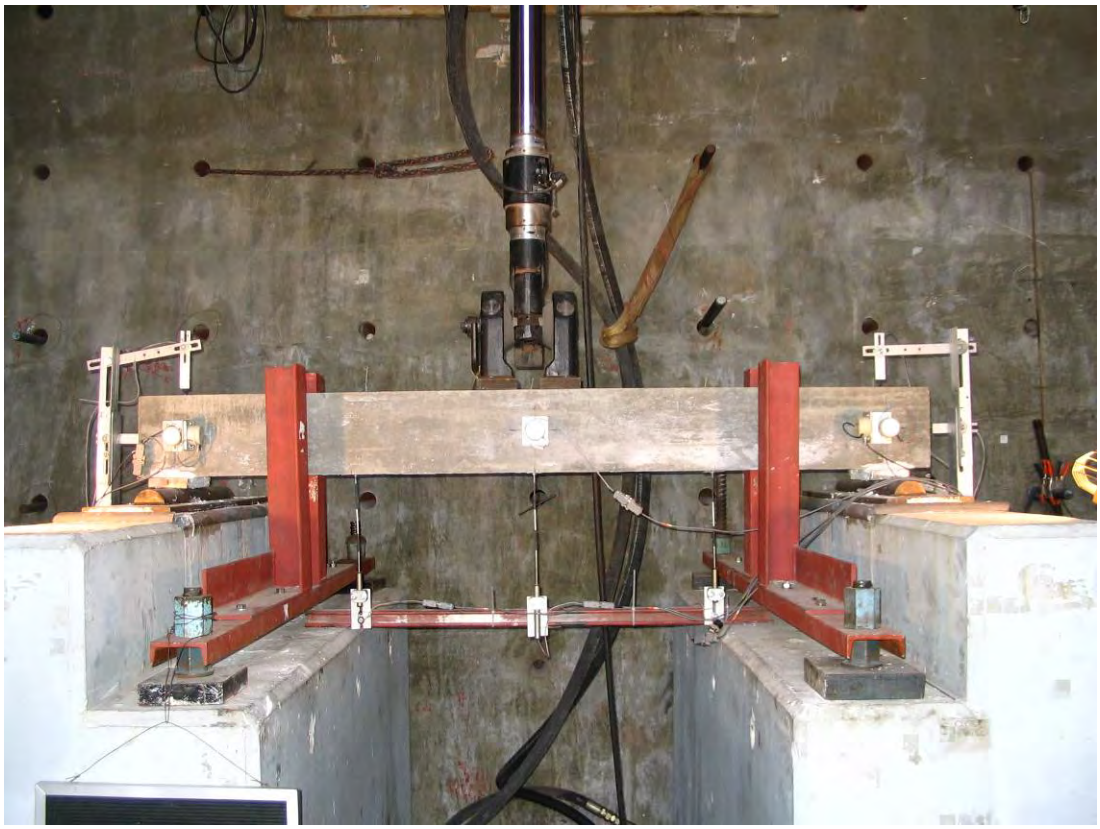

Figure 1-1: Test setup.

The primary purpose of applying externally bonded FRP is to utilize the composites strength and stiffness characteristics to increase structural capacity or serviceability. FRP materials hold useful advantages over other methods of external strengthening such as steel plate bonding or external post-tensioning due to their high stiffness and strength to weight ratios which ease the difficulty of application and decrease the additional mass that would have been added to the structure. Additionally, the relatively high durability of appropriately cured FRP permits much less potential for environmental degradation than steel. There exist a number of different structural

applications for externally bonded FRP, all to improve the flexural or shear capabilities of the structure. The most common applications involve bonding FRP:

1. To the tension face of a flexural member to improve flexural capacity.
2. Transversely to the body of a flexural member to improve shear capacity.
3. To the tension face of a slab to improve flexural and punching shear capacities.
4. Around a column for additional concrete confinement.

The two principle methods of creating and applying the FRP composites for use in civil infrastructure include wet layup of fabric and adhesive bonding of prefabricated elements. Additionally, the resin infusion method may also be used in cases where application is practical (Kaiser 2002).

The wet layup method is the most commonly used fabrication process due to cost efficiency and ease of application. However, it presents the most variability, and the possibility for defects to occur. In the wet layup method, resin is applied to the concrete followed by wetting of the fabric, which is then applied to the substrate and compacted prior to curing. In the wet layup method the resin used as a constituent of the composite also functions as the adhesive to bond the concrete and the FRP together.

Using prefabricated strips generally eliminates much of the potential for flaws in the FRP component of the system (Kaiser 2002). This leaves only the concrete substrate and adhesive to be likely sources of defects, thus prefabricated applications tend to have better quality control. In this process the FRP is manufactured, generally

by the pultrusion method, to a specified geometry off-site in a controlled environment. The composite is then adhesively bonded to the concrete surface. Disadvantages to this method include difficulty creating complex geometries, cost of manufacturing the FRP strips, and difficulty achieving an optimal, defect free, bondline between materials.

Before the composite materials are applied to the concrete surface a degree of surface preparation is necessary. Generally the concrete surface is sandblasted to remove the laitance followed by a thorough cleaning either by blasting the surface with air or cleaning it with a solvent. In the case of old, damaged, or weak concrete a primer layer of the resin/adhesive may be applied and allowed to set in order to achieve more uniform bonding conditions.

1.2 History and Literature Review of Defects with FRP Strengthening

To date, only a limited number of studies have been conducted involving FRP defects in civil infrastructure. Most existing studies are focused on the strengthening of new structures and very few studies exist on structures with defects. In an effort to isolate performance impacts for modeling purposes the investigations including defects were conducted primarily at the component level or with atypical loading scenarios (for example, using a mixed-mode peel test), such that the failure modes were different from those in a practical structure. These tests revealed important information, however, in reality defects may not play the same critical role if tests are

conducted in which specimens are loaded similarly to what is commonly encountered in the field (i.e. flexural or shear strengthening configurations).

1.2.1 Cracking with FRP

Bizindavyi and Neale (1999), through single lap shear tests, suggested that concrete cracking may increase stress transfer length, particularly shear cracking in the form of local debonding at high loads. Bizindavyi and Neale further suggested that the relation between the transfer length and the load level can be approximated as a bilinear relationship. Ueda et al (2002) investigated bond response in FRP strengthened concrete tension members. The results of this investigation suggested that the application of FRP reduced crack spacing and reduced the crack width. This cracking deteriorated bond response by creating diagonal cracks near main cracks, thus reducing shear transfer capabilities. Additionally, it was observed that a greater FRP stiffness or number of layers seems to lead to increased average bond stress and corresponding average shear stress near the concrete surface. More research is needed to clarify the impact of concrete cracking on FRP strengthening behavior. Also, more comprehensive models must be developed for application of future design and analysis. Karbhari et al (2004) stated, “While the FRP can be expected to provide a level of resistance to crack opening the movement of crack faces wider than 0.25 mm could result in the initiation of delamination and fiber crushing in local areas and hence it is suggested that the cracks be repaired through the use of epoxy injection.” Injection could provide resistance to debonding by minimizing these effects as well as

protecting internal steel reinforcement from further corrosion. It is also acknowledged here that there is still a need for further refinement in a number of aspects pertaining to FRP composite construction specifications for the bonded repair and retrofit of concrete structures. Wu and Niu (2000) conducted an analytical investigation on stress concentrations near cracks and determined that interfacial shear transfer and debonding at the end of a localized crack may be similar to the behavior seen in simple shear tests, suggesting that such debonding from a localized crack may be predicted by results of a simple shear test. In an experimental program consisting of FRP strengthened flexural members in three-point bending, it was noted that there were two typical flexural crack patterns that accompanied debonding failure (Niu and Wu, 2005). These two crack patterns were either a single localized crack near the maximum moment region, or multiple distributed cracks across the span of the strengthened RC beams. Physical testing of the flexural members as well as finite element modeling using the discrete crack model determined that with either cracking pattern the resulting failure was debonding of the FRP from flexural cracks near the midspan.

1.2.2 Unbonded Regions

Through the flexural rehabilitation of a slab, Seim et al. (2001) investigated the effect of incomplete bonding of FRP reinforcement. Incomplete bond could be the consequence of misapplication or it could be intentional for the purposes of influencing ductility. Each slab was strengthened by two 1.83-m long strips. The slabs

had the bond configurations of full bond, bond at the ends only (50% of full bond length), and bond at each end and middle (75% of full bond length). The maximum load of the slab with FRP bonded at the ends was only 21% lower than the slab with fully bonded FRP strips. The midspan deflection at which significant load drop occurred, however, increased by 15%. This showed that changing bond and anchorage configurations could influence load capacity and ductility. For the slab strengthened with FRP bonded at the ends and middle, the maximum load decreased by 9%, and the deflection at failure decreased by 4%, demonstrating that partial bond may lower the capacity of the strengthened beam. However, the ultimate load of the slab with only ends bonded was still 59% higher than the as-built slab. Additionally, slight decreases in stiffness behavior were observed prior to global failure.

1.2.3 Investigating Strengthening in the Presence of Defects

Kaiser (2002) studied the effect of different defects in the application of wet lay-up of FRP to concrete using a fracture mechanics approach. A mixed-mode peel-type test was utilized to compare fracture energy release rates (FERR) to control specimens on the basis that the presence of defects in the bond between FRP and concrete could influence the resistance to debonding. The fracture energy release rate was calculated for each specimen by measuring crack propagation with the aid of video cameras. The effects of damage to free edges, incorrect stoichiometry, inadequate primer, concrete cavities, and prolonged primer cure were tested to measure the corresponding detriment to FERR. The most harmful action to fracture

toughness was over application of the primer. This reduced fracture toughness by up to 90%. At a 25% change in resin mixture ratio, the fracture toughness was reduced. Most pertinent to this study, (a) minor concrete cavities did not appear to be detrimental to fracture toughness due to an increase of the fracture path and (b) the critical size of a circular disbond was found to be of a diameter equivalent to half the width of the FRP. Similarly, Navada (2004) also used FERR in mixed-mode peel tests to investigate the impact of defects occurring in critical environments. Defects such as inadequate primer, excessive primer, substrate moisture, delaminations, and disbonds were subjected to various environments such as ambient conditions, heat, freeze, immersion, and ponding to determine changes in FERR.

Fiber waviness is also a very common occurrence in the field due to working in difficult arrangements and improper care taken during the process. Yang et al. (2002) investigated the effects of fiber misalignment in tensile coupons and found that a deviation in fiber orientation as small as 5° can have a significant influence (as much as 14%) on the strength and stiffness. Kaiser (2001) conducted an extensive literature review describing a wide variety of defects that may occur in the application of FRP to concrete structures. These defects were defined at four different levels: the materials level, the preparation level, the installation phase, and the service level. At the materials level, the defects described included: incorrect resin system, over-aged materials, contaminations and inclusions, moisture entrapment, incorrect fiber type, kinked or wavy bundles, broken fibers, fabric wrinkles, sheared fabric, damage to free edges, loose fibers, fiber gaps, voids or process induced defects, and transportation

and handling damage. Defects described involving site preparation and processing included: improper storage, improper stoichiometry, improper mixing, inadequate primer application, disbonding in marked regions, concrete imperfections, inclusions, inadequate grinding of substrate, and galvanic corrosion. Defects that occur during field installation were described as: sagging material, non-uniform concrete/composite interface, porosity, and voids. Intrinsic to the composite material, defects described were: porosity, voids, debonding, delamination, fabric waviness, resin richness/poorness, indentations, damaged edges, missing layers and defects at the material interfaces. Finally, at the service level defects described included: moisture and chemicals, heat damage, interlaminar matrix cracking, surface scratches, and impact damage. Kaiser (2002) also described the relative potential for such defects to occur and offered suggestions on the need for further investigation of critical defects. Karbhari et al (2004) suggested that all voids and depressions should be filled, reasoning that "failure to do this will result in the bridging of FRP material over a void that then acts as a crack/debond initiator, as well as a location for collection of moisture."

Karbhari (2001) conducted a research review pertaining to material considerations in FRP rehabilitated structures, noting that the efficacy of the external composite is largely dependent on the bond between the composite and the concrete. Here, it was suggested that beyond sand blasting and abrasion very little research has been conducted pertaining to bond quality as related to concrete strengthening, noting that various surface preparations may influence both durability and fracture behavior.

1.2.4 Effect of Preloading

The effectiveness of strengthening structurally deteriorated RC beams (specifically considering cracked concrete) was demonstrated using glass fiber reinforced polymers (GFRP) and steel plates respectively (Sharif et al. 1994, Hussain et al. 1995). The specimens used in the experiment were preloaded to 85 percent of the ultimate load level and then unloaded prior to the application of FRP or steel plates. These studies were significant because they verified that epoxy bonded plates are an effective way to strengthen not only undamaged concrete structures, but damaged specimens with pre-existing cracks as well. However, the experimental programs lacked the necessary testing to quantify the behavior difference between strengthened specimens that have been precracked and those left undamaged. Arduini and Nanni (1997b) also investigated precracked flexural members. In their test program, the effect of maintaining the preload level during the application and curing of FRP was examined. Some specimens were preloaded to 30% of the nominal capacity, then unloaded before the application of FRP, while in two other specimens the load was maintained during placement and curing of the FRP before loading to failure. The test series suggests the possibility to simulate and predict experimental load-deflection behavior, strain distribution, and the failure mode of FRP strengthened beams, including the effects of precracking. Additionally, the conclusion was that the performance of a strengthened precracked specimen is not significantly different from that of a strengthened non-precracked specimen. Shahawy et al. (2001) conducted a

detailed investigation on the effectiveness of FRP strengthening of preloaded full-scale flexural members under service loads. The strengthening program included specimens that were fully wrapped to cover the entire flange of the T-girder as well as specimens that were only partially wrapped to cover the soffit and two inches up the sides of each girder. The main objective was to evaluate the performance of precracked, strengthened girders. The girders were loaded to a predefined stress level based on the percent of steel yield, locked into place, and then retrofitted with CFRP. The girders were preloaded to levels of 0, 65, 85, and 117% of the yield moment and locked in place prior to strengthening with two layers of FRP before loading up to failure. These tests found that the level of preload does not conclusively affect the overall behavior of the "fully wrapped" specimens, however, the preloaded "partially wrapped" girders exhibit less ductility and strength than the corresponding preloaded "fully wrapped" members due to an altered failure mode. Chan (2001) investigated the effect of preload in one-way slabs retrofitted with CFRP plates. Relevant specimens consisted of two control specimens without FRP and six specimens to study the effects of preloading at levels of 0, 60, and 80% of ultimate load before the application of composite. Key observations in this study were there are insignificant differences in the load carrying capacity for slabs with and without preload, but the deflections were higher in the specimens that were preloaded. Also noted, was that the application of FRP can significantly improve cracking behavior in both cracked and previously uncracked applications.

1.2.5 Design Guideline Recommendations for Defects

There are currently two primary sources of information providing guidance to designers about the criticality of defects. These are the *Guide for the Design and Construction of Externally Bonded FRP Systems for Strengthening Concrete Structures* (ACI 440, 2002) and the *National Cooperative Highway Research Program Report 514* (NCHRP 514, 2004). Both documents provide guidance pertaining to crack limitations and repair requirements, out of plane variations on concrete surfaces, substrate holes, and fiber misalignment. Delaminations are also addressed in both documents, defining them in categories of small, medium, and large. Finally, guidelines are presented pertaining to substrate cleanliness and dryness.

ACI Committee 440 (2002) states, "some manufacturers have reported that the movement of cracks 0.01 in. (0.3mm) and wider can affect the performance of the externally bonded FRP system through delamination or fiber crushing." Thus, cracks wider than 0.3mm should be pressure injected. The guide also states that the maximum allowable out-of-plane variation of the concrete surface is not to exceed 1/32 inches or the recommended tolerances by the FRP system manufacturer, the system should be kept dry, and bug holes must be filled. In compliance with tensile coupon research, fiber misalignment must remain less than five degrees or otherwise approved by the engineer.

The ACI Committee 440 (2002) gives guidelines pertaining to delaminations as well. The cured FRP system should be evaluated for delaminations or air voids between multiple plies or between the FRP system and the concrete. Inspection

methods should be capable of detecting delaminations of 2 square inches or greater. Methods such as acoustic sounding, ultrasonics, and thermography can be used to detect delaminations. Specifically, small delaminations less than 2 square inches each are permissible as long as the delaminated area is less than 5% of the total laminate area and there are no more than 10 such delaminations per 10 square foot area. Medium delaminations are those between 2 and 25 square inches and may be repaired by resin injection or ply replacement. Large delaminations are classified as those being larger than 25 square inches in area. It is stated these large delaminations can affect the performance of the installed FRP and should be repaired by selectively cutting away the affected sheet and applying an overlapping sheet patch of equivalent plies (ACI 440, 2002).

NCHRP 514 (2004) states, "Although there is a general consensus on the characteristics of a sound FRP system and on the type and size of defects that are absolutely unacceptable, the thresholds for critical defects are not yet sufficiently researched. Significant research is needed to determine critical defects, their identification using rapid methods of NDE techniques, and the effect of such defects on the long-term performance of FRP repair systems."

The guidelines currently provided by NCHRP 514 (2004) are somewhat similar to those in ACI 440 (2002). In the case of a missing portion of the concrete cross section, repair material is required to fill the area of the removed concrete substrate, and any void larger than 12.7mm (1/2") in diameter and depth. All cracks in the surface of the concrete or substrate that are wider than 0.25mm (1/100 in) are

required to be filled using pressure injection of epoxy. Like ACI 440 (2002), any deviation in the alignment more than 5 degrees is not acceptable and installed fibers are required to be free of kinks, folds and waviness. Also similar to the guidelines provided by ACI 440 (2002), defects smaller than 6.4mm (1/4 in) in diameter will require no corrective action. Defects larger than 6.4mm, but smaller than 32mm (1 ¼ in) in diameter will be repaired with epoxy injection. Defects larger than 32mm, but smaller than 152 mm (6 in) in diameter, and with a frequency of less than 5 per any unit surface area of 3-m (10ft) length of width, are required to be repaired by patching methods. Larger defects must be repaired by replacing the FRP section. In the commentary, NCHRP 514 (2004) lists many of the potential defects some of which are mentioned earlier, but provides little or no specific guidance pertaining to their effects:

> "Defects in FRP systems may include (i) voids and air encapsulation between concrete and layers of primer, resin, or adhesive and within the FRP system itself; (ii) delaminations between layers of FRP system; (iii) broken or damaged edges of FRP system; (iv) wrinkling and buckling of fiber and fiber tows; (v) discontinuities due to fracture of fibers, breakage in the fabric, or cracks in procured shells; (vi) cracks, blisters, and peeling of the protective coating; (vii) resin-starved areas or areas with nonuniform impregnation or wet-out; (viii) undercured or incompletely cured resin; and (ix) incorrect fiber orientation."

1.3 Rationale of Study

Many studies have been conducted investigating FRP strengthening and bond to concrete structures (Bizindavyi and Neale 1999, Sharif et al 1994, Arduini and Nanni 1997a, Wu and Niu 2000). The majority of these investigations have focused on investigating bond performance for the purpose of assessing the capabilities of FRP strengthening as well as the development of initial material and structural design considerations. As the use of FRP composites continues to increase, demand for more refined and economical design specifications increases. Despite numerous studies and the creation of design specifications, there is still little known about the long-term performance of FRP rehabilitated structures (Navada 2004). The integrity of FRP rehabilitated structures containing defects may be particularly susceptible over time. Thus, more research is necessary to assess bond performance and strengthening of applications containing defects. To date, only a limited number of studies have been conducted involving FRP defects in civil infrastructure. In an effort to isolate performance impacts for modeling purposes these investigations were conducted primarily at the component level or with atypical loading scenarios, such that the failure modes were different from those in a practical structure (Yang et al 2002, Kaiser 2002, Navada 2004). In reality, defects may not play the same critical role if tests are conducted at the structural level. In an effort to create complete design guidelines, very conservative and somewhat arbitrary critical defect aspects were assigned in documents such as ACI 440 (2002) and NCHRP 514 (2004). The values of defect size and type limitations found in these specifications were derived largely from

previous studies conducted for aerospace or automotive applications. Many such defects may not perform the same in the case of FRP rehabilitated concrete. Additionally, such precision as is demanded by these documents is likely somewhat excessive given the large variability that exists in concrete construction in general. The primary purpose of this research project was to improve our understanding of typical defects encountered in FRP rehabilitated concrete.

Existing analytical and numerical bond models typically assume the presence of a "perfect" bond and, therefore, do not adequately model bond behavior in the presence of defects. Another objective of this project was to investigate the preliminary development of a bond model capable of adequately determining structural and material performance in the presence of a defect. Such a model would allow not only the prediction of defect criticality and performance, but in the process would also provide a more complete and accurate model for determining bond performance of non-defective specimens. The resulting improved model would provide the groundwork and knowledge for the development of an accurate, simplified bond model to be created in the future for engineering design and analysis purposes.

From both the perspective of the designer, and the inspector, it is important that defects are identified in appropriate classes and that the effects of these defects are quantifiable. For example, if a disbond is noted during the inspection of a FRP rehabilitated structure it would be useful to be able to assess whether

a) the size and location of the disbond were such that it could affect overall response (and if so, by how much), and

b) the defect could conceivably be affected by loading or environmental conditions over its service-life, resulting in growth.

Thus, not only is it important to know the effect of defects in terms of overall short-term behavior, but also in terms of both time to criticality and influence of local phenomena at the global response level.

1.4 Structure of Report

Chapter 2 discusses the experimental program. This includes the choice of the specimen type, specimen design, specimen loading method, defects considered, material data, instrumentation, and the wet layup method procedure.

Chapter 3 describes the development of the FEA model used to model the beam specimen behavior observed in the laboratory. This chapter includes a description of the material models utilized, the FEA mesh, as well as the material properties and loading procedures used.

The fourth chapter highlights the results obtained in this investigation. It includes the individual specimen test results and compiled analysis of the laboratory testing.

The fifth chapter involves a discussion of the results from chapter 4. It includes a discussion of the effectiveness of FRP strengthening, describes the effect of each defect type investigated, results from the FEA model, and comparisons of the FEA model and laboratory test results.

Chapter 6 discusses the conclusions of the study and recommendations for implementation.

References

ACI Committee 440, *Guide for the Design and Construction of Externally Bonded FRP Systems for Strengthening Concrete Structures*, ACI 440.2R-02, American Concrete Institute, Farmington Hills, MI, USA, pp. 103, 2002.

Arduini, M. and A. Nanni, *Behavior of Precracked RC Beams Strengthened with Carbon FRP Sheets*, Journal of Composites for Construction, Vol. 1, No. 2, p. 63-70, 1997a.

Arduini, M. and A. Nanni, *Parametric Study of Beams with Externally bonded FRP Reinforcement*. Journal of Composites for Construction, Vol. 94, No. 5, p. 493-501, 1997b.

Bizindavyi L. and K.W. Neale, *Transfer Lengths and Bond Strengths for Composites Bonded to Concrete*, ASCE Journal of Composites for Construction, Vol. 3 No. 4, p. 153, 1999.

Chan, T. K. and M. Niall, *Strengthening of One-way Slabs Using Carbon Fibre Plates: The Effect of Preload*, CSE Research Bulletin, No.14, 2001.

Hussain M., A. Sharif, I.A. Basunbul, M.H. Baluch, and G.J. Al-Sulaimani, *Flexural Behavior of Precracked Reinforced Concrete Beams Strengthened Externally by Steel Plates*, ACI Structural Journal, Vol. 92, No. 1, pp. 14-22, 1995.

Kaiser, H., *Assessment of Defect Criticality and Non-destructive Monitoring of CFRP-rehabilitated Civil Structures*, Masters Thesis *Department of Structural Engineering*, UCSD: La Jolla, CA, 2002.

Kaiser, H. and V.M. Karbhari, *Quality and Monitoring of Structural Rehabilitation Measures – Part 1: Description of Potential Defects*. University of California, San Diego: La Jolla, CA, p. 60, 2001.

Karbhari, V.M., A. Mirmiran, M. Shahawy, and A. Nanni, *Construction Specifications for Bonded Repair and Retrofit of Concrete Structures Using FRP Composites – Results of a NCHRP Study*, Composites 2004 Convention and Trade Show, American Composites Manufacturers Association, p. 10, 2004.

Karbhari, V.M., *Materials Considerations in FRP Rehabilitation of Concrete Structures*, Journal of Materials in Civil Engineering, Vol. 13, No. 2, pp. 90-97, 2001.

Navada R., *An Experimental Assessment of Defect Criticality in FRP Rehabilitated Concrete using a Fracture Mechanics Approach*, Masters Thesis *Department of Structural Engineering*, UCSD: La Jolla, CA, 2004.

NCHRP Report 514, Transportation Research Board, Washington, D.C., Section II, p. 1-33, 2004.

Niu H., J. Delaney, V.M. Karbhari, *Effect of Defects on Performance of CFRP Strengthened RC Beams*, Sampe 2005 Long Beach Conference Proceedings, 2005.

Niu H., and Z. Wu, *Numerical Analysis of Debonding Mechanisms in FRP-Strengthened RC Beams*, Computer-Aided Civil and Infrastructure Engineering, Vol. 20, pp 354-368, 2005.

Seim, W., M. Horman, V. Karbhari, and F. Seible, *External FRP Poststrengthening of Scaled Concrete* Slabs, ACSE Journal of Composites for Construction, Vol. 5, No. 2, pp. 67-75, 2001.

Shahawy, M, O. Chaallal, T: E. Beitelman, and A. El-Saa, *Flexural Strengthening with Carbon Fiber-Reinforced Polymer Composites of Preloaded Full-Scale Girders*, ACI Structural Journal, Vol. 98, No. 5, p. 735, 2001.

Sharif, A., G.J. Al-Sulaimani, I.A. Basunbul, M.H. Baluch and B.N. Ghaleb, "*Strengthening of Initially Loaded Reinforced Concrete Beams Using FRP Plates*", ACI Structural Journal, Vol. 91, No. 2, , pp. 160-168. 1994.

Teng, J. G., J. F. Chen, S. T. Smith, and L. Lam, FRP Strengthened RC Structures. John Wiley and Sons, New York, NY, 2002.

Ueda T., R. Yamaguchi, K. Shoji, Y. Sato, *Study on Behavior in Tension of Reinforced Concrete Members Strengthened by Carbon Fiber Sheet*, ASCE Journal of Composites for Construction, Vol. 6, No. 3, p. 168, 2002.

Wu, Z.S. and H.D. Niu, *Study on Debonding Failure Load of RC Beams Strengthened with FRP Sheets*, JSCE Journal of Structural Engineering, Vol. 46A, pp. 1431-1441, 2000.

Yang X., A. Nanni, S. Haug, and C.L. Sun, *Strength and Modulus Degradation of CFRP Laminates from Fiber Misalignment*, Journal of Materials in Civil Engineering, American Society of Civil Engineers, Vol. 14, No. 4, pp. 320-326, 2002.

2 EXPERIMENTAL PROGRAM

2.1 Choice of Specimen Type

Several factors contributed to the decision of the specimen design and type in order to optimize the tests. These factors included scope and number of tests, loading type, simulation of practical field conditions, and feasibility.

In civil structures, strengthening or repair may be conducted for a variety of purposes. Applications include flexural strengthening on the tension face, shear rehabilitation or strengthening, tension member rehabilitation, or column retrofit by wrapping. Pure tension members are not common and defects such as disbonds in column confining applications are generally thought to be less critical (although long-term environmental effects still need to be investigated). Also, load and response conditions in shear applications are complex and not well understood and, therefore, are difficult to predict and reproduce thus they are not currently practical for the initial investigation of the behavior of defects. This leaves flexural applications as the most practical case for this investigation. Behaviors learned from investigations on flexural members are applicable in many ways to the other strengthening applications as well.

FRP bond failure at an interface can occur due to the presence of one or more of three loading types: peeling in tension, sliding by in-plane shear, and sliding by means of out-of-plane shear (Kaiser 2002). These three loading types constitute the three separate failure modes, referred to as modes I, II, and III. Mode I loading involves tearing or peeling normal to the failure surface such that no shear stress exists.

Mode II loading involves in-plane shearing by sliding in the same direction as the failure propagates. Finally, mode III loading involves shearing by sliding parallel to the cracking line. Figure 2-1 displays the three cracking modes. Bond failure typically consists of one or more of these loading modes causing crack propagation.

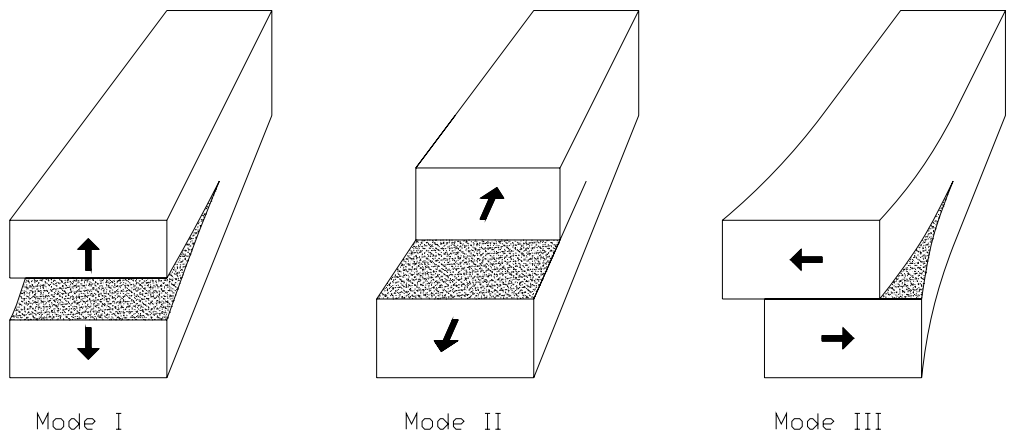

Figure 2-1: Three types of failure modes

Previous investigations involving defects such as those described above conducted by Kaiser (2002) and Navada (2004), utilized a mixed-mode peel test in an effort to measure FERR to quantify performance (Kaiser 2002, Navada 2004). Additionally, tests conducted by Yang (2002) measured the strength and modulus degradation in tensile coupons. Although tests like these have their advantages, particularly as initial investigations of the effect of defects, they do not necessarily yield adequate data in regards to performance of real structures due to the fact that the failure mode

interactions could be significantly different than in a field structure such as a flexural member. Bond behavior in shear strengthening applications involves the application of FRP across shear cracks and the failure experienced is purely Mode II. In flexural strengthening applications, the failure mechanism is somewhat more complicated since both mode I and mode II loading exists in addition to a normal force working to hold the FRP firmly to the concrete surface near a crack.

Large-scale flexural tests were eventually chosen in order to meet the criteria of test specimens that simulated a field component. Many of the FRP strengthening applications are flexural members. Precracking protocols are easiest to design and carry out with flexural members and no studies currently exist involving defects in FRP strengthened concrete flexural members. Additionally this specimen type includes the mixed-modes I and II failure interaction which other tests are not capable of accurately emulating. Also, the flexural test holds a distinct advantage over tension members or peel tests because neither of these is utilized in practical structures in the field. Finally, due to the large size of typical civil structures, relatively large specimens were required in order to test defects relevant to this scale.

2.2 Specimen Design

Figure 2-2 shows a detailed drawing of the test specimen. The concrete specimens were two meters in length with cross sectional dimensions of 150mm width by 200mm depth. Longitudinal reinforcement consisted of two 13mm (#4) bars, top and bottom, providing reinforcement to promote a ductile beam behavior. This

configuration provided for a tension controlled beam with a steel area (A_s) equal to 258mm^2 (0.4in^2) and a corresponding reinforcement ratio (ρ_s) equal to 0.011. The transverse reinforcements were 10mm (#3) diameter stirrups at 80mm spacing. The steel was shaped and tied such that a concrete cover depth of 25mm clear was provided top and bottom. This spacing ensured that shear failure would not occur, but allowing some shear cracks to occur in the FRP strengthened specimens. The concrete mix specified 13mm maximum aggregate size and had a 28 day strength of 35.7 MPa and 32.3 MPa for cast number one and cast number two respectively (see results in section 2.5 for exact data). The beams were designed so a large ductility was provided such that a defect's effect could be observed in a consistent environment (i.e. known virgin beam strength at all given deflections).

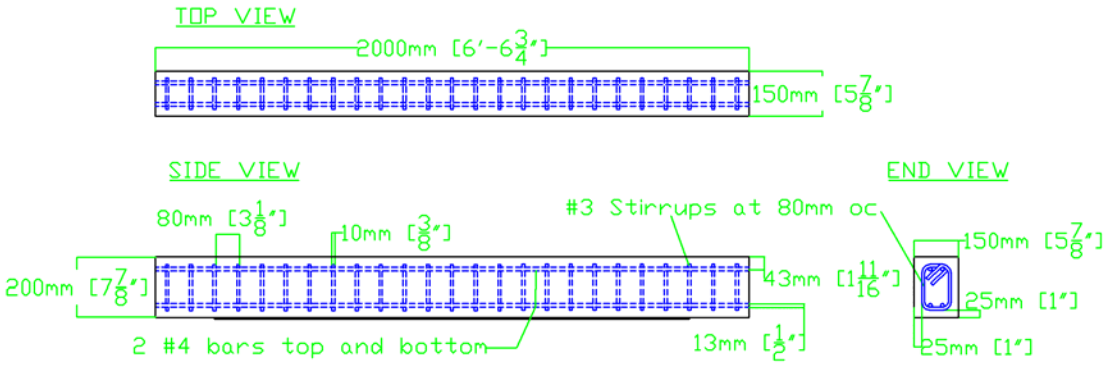

Figure 2-2: Test specimen design.

The specimen size was chosen to be large enough to simulate practical field behavior, but manageable enough that a large number of specimens could be tested over the course of the investigation. The specimens were all instrumented with a total of four strain gages on the longitudinal steel bars, one on each tension bar at the mid-span and one at each quarter point on one of the tension bars. The purpose behind these gages was primarily for control of the extent of precracking and also to compare the steel behavior when testing various defects involving the FRP.

2.3 Details of Loading Method

The test setup was designed to enable testing of flexural components such that the 222kN actuator applied the load directly through two elastomeric pads were symmetrically about the midspan of the beam. The elastomeric pads were 100mm in width and 150mm in length oriented such that they spanned the full width of the beam specimen. The center-to-center spacing of the elastomeric pads was 165mm, leaving a clear gap of 60mm between them. This loading configuration was chosen so additional confining stresses at the mid-span of the beam were avoided, thus ensuring that concrete crushing occurred close to its true compressive strength. Additionally, by loading directly through the head of the actuator, as opposed to using an apparatus to change the load points, a very stable configuration was ensured, minimizing the opportunity for eccentricities to occur. A detailed drawing of the test setup is shown in figure 2-3. It is worth mentioning that, although technically this is a four-point bend test, the center load points are relatively close together, leading to a relatively small constant

moment region of 165 mm. Finally, this setup constitutes a large shear span in which the debonding mechanisms can be studied.

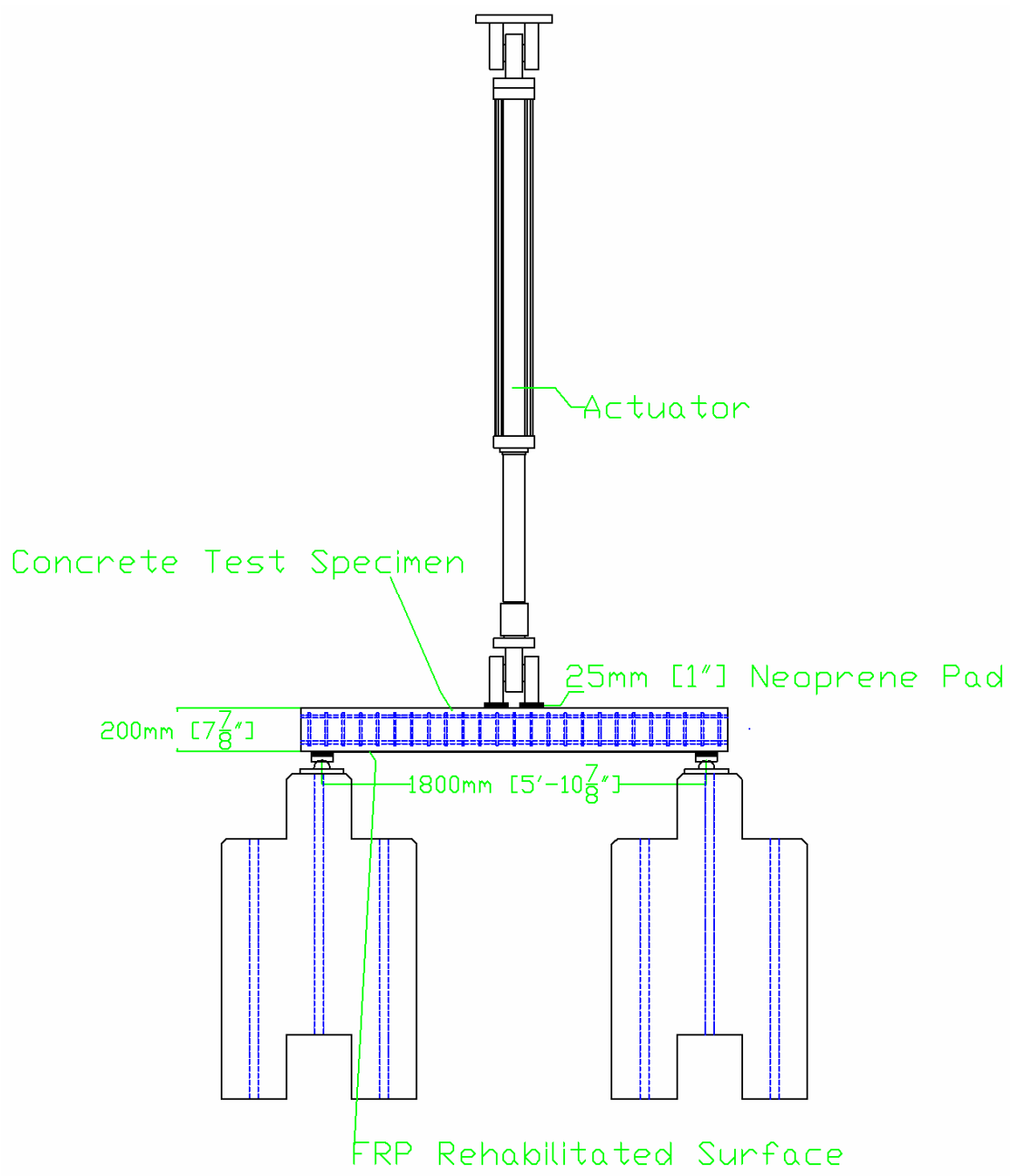

Figure 2-3: Test setup

2.4 Defects Considered

The defects considered in this investigation include disbond shape, disbond size, disbonds located at the concrete resin interface, interlaminar disbonds, disbonds exposed to excessive moisture, typical concrete cracking, and excessive concrete cracking. Table 2-5 details a summary of the defects considered in each specimen while table 2-1 shows a summary of the different categories of defects investigated as well as the various defect configurations utilized to investigate each category. A detailed summary of each specimen can also be found in the individual test descriptions in Chapter 4.

Table 2-1: Summary of defects investigated.

Test Category	Number of Tests	Test Description (Name)	Defect Location (mm)	Defect size (mm)	Defect Shape	Loading Description
Control Specimens	4	Unstrength. Control	-	-	-	-
	4	Uncracked Control	-	-	-	-
	8	Precracked Control	-	-	-	-
Critical Disbond Size	2	25C_185	185	25	Circular	High M, High S
	2	50C_185	185	50	Circular	High M, High S
	3	100C_185	185	100	Circular	High M, High S
	2	150C_185	185	150	Circular	High M, High S
	1	25R_185	185	25	Rectangular	High M, High S
	3	50R_185	185	50	Rectangular	High M, High S
	4	100R_185	185	100	Rectangular	High M, High S
	3	150R_185	185	150	Rectangular	High M, High S
	2	200R_185	185	200	Rectangular	High M, High S
	2	250R_185	185	250	Rectangular	High M, High S
Critical Disbond Location	1	100C_185E	660	100	Circular	Low M, High S
	1	100C_428	428	100	Circular	Low M, High S
	1	100C_0	0	100	Circular	High M, Zero S
	1	100R_0	0	100	Rectangular	High M, Zero S
Excessive Preload Cracking	1	0.2cw	-	-	Crack	-
	1	0.6cw	-	-	Crack	-
	1	1.0cw	-	-	Crack	-
	1	1.5cw	-	-	Crack	-
	2	100R_185_1.0cw	185	100	Rect/ Crack	High M, High S
	1	200R_185_1.0cw	185	200	Rect/ Crack	High M, High S
	1	100R2_185_1.0cw	185	2 x 100	Rect/ Crack	High M, High S
	2	100RS_185_1.0cw	185	100	Rect/ Crack	High M, High S
Interlaminar Disbonds	2	100RI_185	185	100	Rectangular	High M, High S
	2	100RAI_185	185	100	Rectangular	High M, High S
	1	100CAI_185	185	100	Circular	High M, High S
	1	100RAI_0	0	100	Rectangular	High M, Zero S
	1	100RAI_428	428	100	Rectangular	Low M, High S

* See Table 2-2 for table key and explanation

Table 2-2: Key for table 2-1

<table>
<tr><td>Test Category</td><td colspan="2">Describes the various categories of defects that were investigated.</td></tr>
<tr><td rowspan="2">Test Description (Name)</td><td colspan="2">Names and describes each defect configuration tested.</td></tr>
<tr><td>Naming Key</td><td>First # = Defect size in mm (disbond size or crack width)
Second # = Defect location
# cw = crack width in tests investigating excessive preload cracking
R = Rectangular shaped disbond
C = Circular shaped disbond
A = Defect located in the concrete-FRP adhesive layer
I = Defect located between FRP layers (interlaminar)
AI = Defect located both in the adhesive and interlaminar location</td></tr>
<tr><td>Defect Size</td><td colspan="2">Gives the size of the defect (either a disbond or concrete crack width) in mm. In the case of a rectangular disbond this number describes the length of the defect (all rectangular disbonds covered the full width of the FRP strip). For circular disbonds the defect size describes the defect diameter.</td></tr>
<tr><td>Defect Location</td><td colspan="2">Describes the distance (mm) from the midspan of the beam to the centroid of the defect. For example, “185” refers to the center of the defect being located 185mm away from the beams midspan.</td></tr>
<tr><td rowspan="2">Loading Description</td><td colspan="2">Describes beam shear and beam moment characteristics near the location of the defect.</td></tr>
<tr><td colspan="2">High M = High beam moment region

Low M = Low beam moment region

High S = High beam shear region

Zero S = Zero beam shear region</td></tr>
</table>

2.4.1 Disbonds

Disbonds in this test were created using three layers of Teflon each of 0.15mm thickness to ensure a near frictionless disbond with a separation of the FRP from the concrete of one to two millimeters. The Teflon sheets were cut to the specific shape of the disbond specified for each specimen and placed at the appropriate material interface during the application of the FRP material. As can be noted from table 2-1, the size of the disbonds ranged from 25mm to 300mm in length and 25mm to 150mm in width. A large number of tests were conducted using circular shaped disbonds as well as rectangular shaped disbonds in order to measure how stress concentrations, due to varying shapes as well as sizes, affected strengthening performance. Rectangular disbonds spanned the full 150mm width of the specimen and varied in length between 25mm and 300mm. Circular disbonds were seated such that the centroid of the disbond intersected the centerline of the beam. The dimensions of the circular disbonds varied from 25mm diameters to the full width of the specimen of 150mm diameters.

In addition to defect size and shape, another important parameter that was tested was varying the defect location along the length of the specimen. The effect of the disbonds were measured by placing them in regions defined by the beam loading characteristics obtained from the shear and moment diagrams. These regions were defined as high moment/high shear, high moment/zero shear, and low moment/high shear regions. Figure 2-4 shows these various regions along with defect locations

considered and the beam shear and moment diagrams for the loading of the specimens.

A summary of the disbond locations for each specimen may be found in table 2-1.

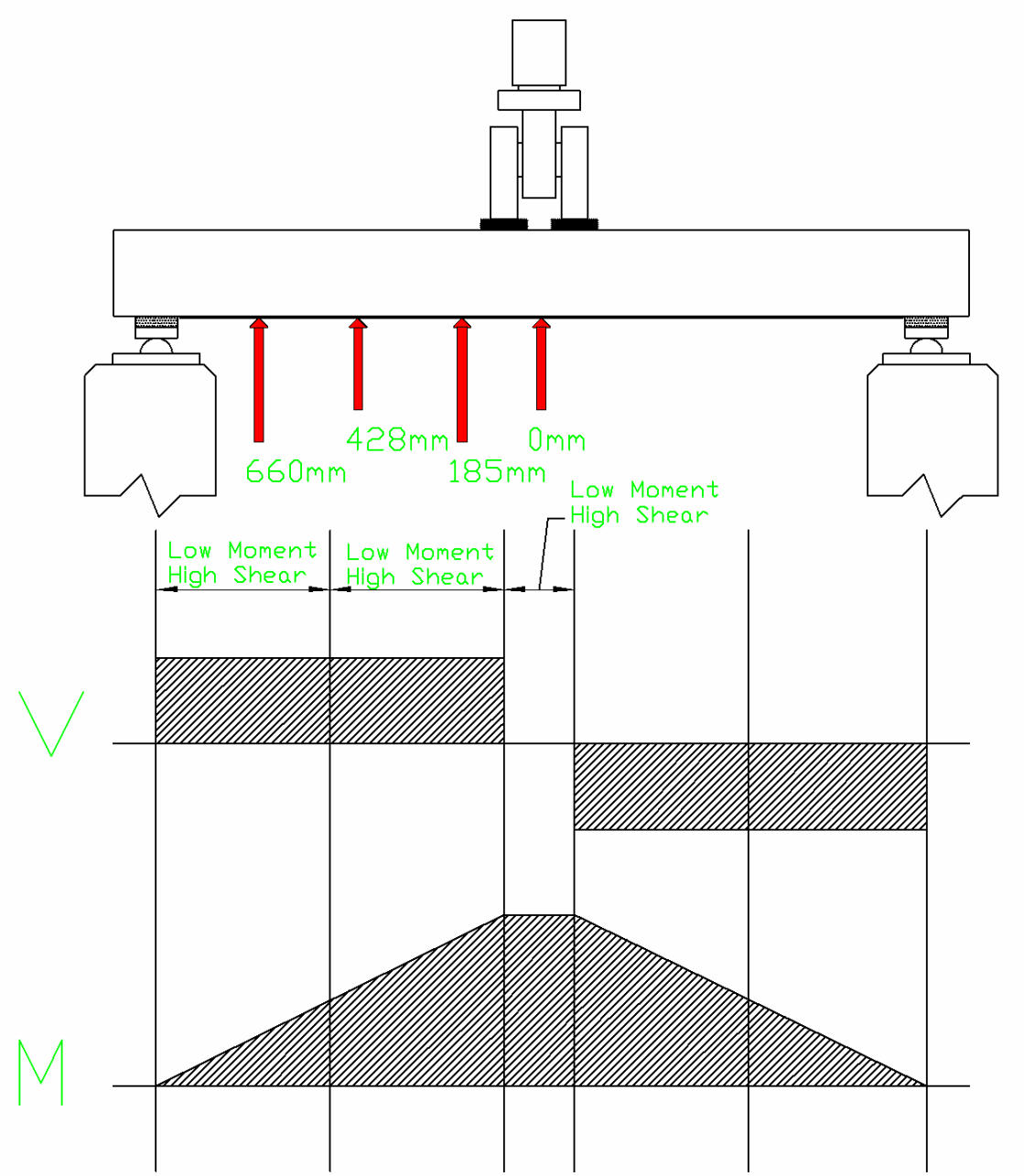

Figure 2-4: Defect locations considered (in mm from the midspan location), loading regions, and shear and moment diagrams.

Another defect variable that was considered in this investigation involved the depth of a disbonds location in terms of whether the defect is located at the concrete/resin interface or between fabric layers. Specimens were tested with disbonds located at the concrete/resin interface, at interlaminar locations, and at both locations. Figure 2-5 shows the location of each of these disbonds. A summary of these locations for each specimen can be seen in table 2-5 in the column labeled “defect depth”. Figure 2-6 shows a typical rectangular Teflon disbond used in the testing program.

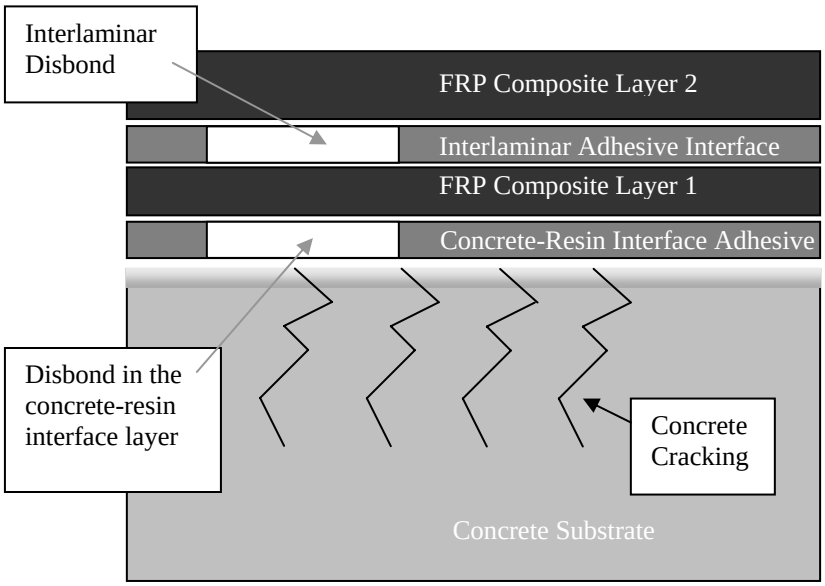

Figure 2-5: Sketch of disbond locations

Two of the specimens included the submersion of disbonds in water for a period of 7 and 21 days before testing. These two specimens (specimens 54 and 55) were submerged three days after the application of FRP, after initial curing had occurred. Only the FRP and the first inch of concrete on the tension face was

submerged in the water with the remainder of the beam left above water. Upon removal from the water, the FRP was strain gauged, and the beam was tested the same day.

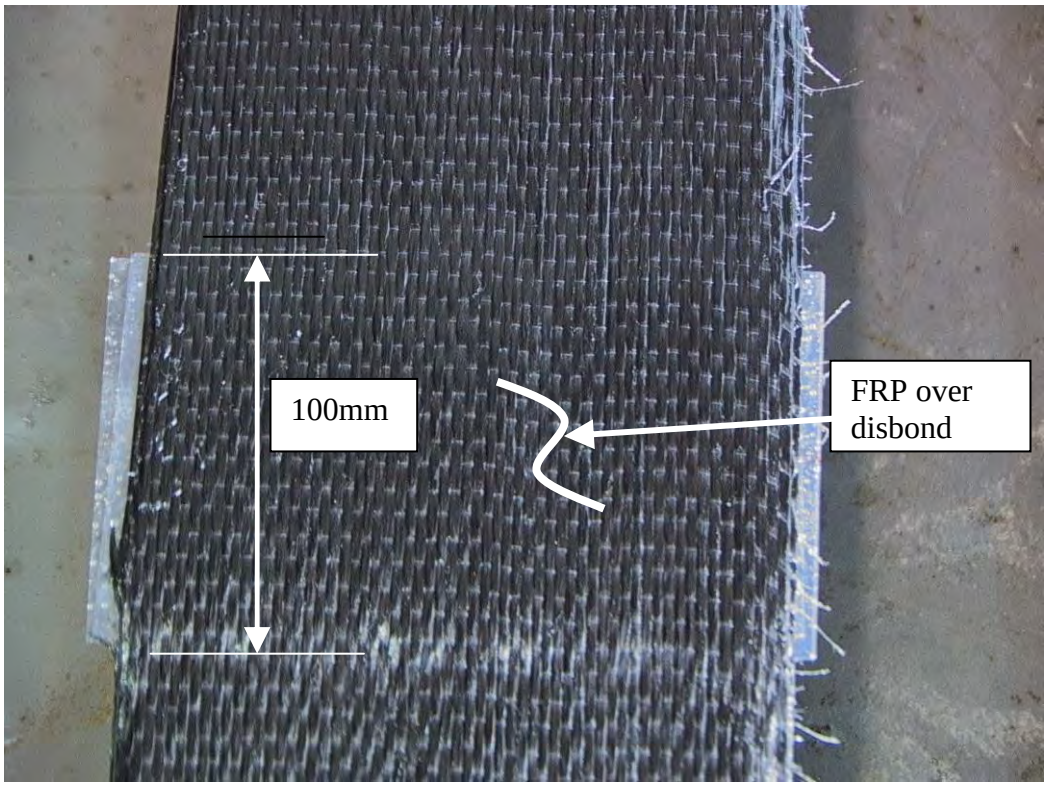

Figure: 2-6: 100mm by 150mm rectangular Teflon disbond.

2.4.2 Cracks

In addition to preloading to simulate actual field conditions, pre-existing cracks in the concrete were treated as a defect and tests were designed using various damage levels to determine the impact of cracking on strengthening performance. Cracks in this study were measured visually in millimeters using a crack width gage that was printed on a transparency sheet to measure the crack width. This is a fast method for measuring crack width and can be used anywhere a crack appears. A summary of the tests conducted to investigate the effect of excessive preload cracking may be found in table 2.1. Details of specific crack widths, ACI (2002) and NCHRP (2004) guidelines, and aggregate interlock issues are explained in section 2.8 (preloading) and a summary of the preload levels applied to each specimen can be found in table 2-5 under the heading "Preload."

2.5 Material Data

2.5.1 Composite Characteristics

Hexcel GA090 unidirectional carbon fiber fabric was utilized for all FRP applications. It is a 12k fabric with a fiber modulus of 227 GPa (33Msi), fabric weight of 302g/m^2 (8.9oz/yd^2) and a thickness of 0.34mm (0.134in), as given by the manufacturer.

The epoxy-resin system utilized to complete the composite system was Tyfo S epoxy-resin manufactured by Fyfe Co. The resin mixture ratio recommended by the manufacturer is 100 parts epoxy to 42 parts hardener. The manufacturer specified

properties for the Tyfo S epoxy-resin included a tensile strength of 72.4 MPa, a tensile modulus of 3.18 GPa, an ultimate elongation of 5%. Upon mixture, this material has a viscosity of 600-700cps, a density of 4.2kg/3.79L at 20°C, and a pot life of 3-6 hours at 20°C.

Several series of tension tests were conducted to determine the composites strength and modulus. For these tension tests, 2-layer panels 305mm by 305mm (12in by 12in) were created on a smooth, flat surface. They were created using the same resin batch that was used for strengthening of the beams, and left to cure near the beams to ensure similar curing conditions. The panels were cut into test coupons using a diamond tipped wet saw. The samples were 25.4mm wide (1in) by 254mm (10in) long. The coupons were tested in tension following the specifications in ASTM D-3039 (2000). Table 2-3 summarizes the tension test results.

All beam specimens were strengthened with two layers of carbon fabric using the wet lay-up method described in section 2.7, with the exception of specimen used as unreinforced controls.

Table 2-3: Tensile coupon data summary

Sample	Thickness	Cross Section Area	Modulus	Strength	Ultimate Strain
	mm	mm^2	MPa	MPa	%
Series 1: Manufactured May 6, 2005					
A-1	1.276	32.4	56700	842.1	1.48
A-2	1.3	32.9	49100	782.2	1.59
A-3	1.274	32.4	47900	839.1	1.75
A-4	1.322	33.3	47900	832.2	1.74
A-5	1.312	33.2	51000	825.7	1.62
A-6	1.298	32.9	60900	829.1	1.36
Mean:	1.30	32.9	52250	825.1	1.59
Std-Dev	0.02	0.383	5366	21.9	0.15
Series 2: Manufactured May 27, 2005					
B-1	1.69	38.4	50130	653.8	1.30
B-2	1.78	37.4	44300	635.8	1.44
B-3	1.756	37.8	44400	713.4	1.61
B-4	1.722	37.6	52900	675.7	1.28
B-5	1.724	38.9	55700	726.7	1.30
B-6	1.632	37.5	44800	747.9	1.67
Mean:	1.72	37.9	48705	692.2	1.43
Std-Dev	0.05	0.592	4934	44.0	0.17
Series 3: Manufactured July 1, 2005					
C-1	1.746	43.9	40100	619.8	1.54
C-2	1.66	42.2	44100	705.4	1.60
C-3	1.54	39.3	49300	592.5	1.20
C-4	1.658	42.4	42500	600.8	1.41
C-5	1.512	38.4	47300	729.1	1.54
C-6	1.596	40.1	41200	607.4	1.47
Mean:	1.62	41.1	44083	642.5	1.46
Std-Dev	0.09	2.120	3585	59.1	0.14
Overall Mean	1.54	37.3	48346	719.9	1.49
Overall Std Dev	0.19	3.7	5590	89.6	0.16

2.5.2 Concrete Properties

The beam specimens were cast in two separate batches. The first casting was on October 19, 2004 and the second casting was on February 8, 2005. Both batches were made with a 13mm maximum aggregate size and relatively low strength concrete mix design was used to more accurately represent field conditions of older structures in need of FRP strengthening. For ease of construction, the steel cages were placed in the forms such that the tension face of the beams was cast facing up. Figure 2-8 shows the steel, forms, and casting of the concrete specimens. After pouring, the beams were covered with plastic and left for at least nine days before the formwork was removed. Each batch had a set of test cylinders, 305mm height by 152mm diameter, prepared for compression testing at 7 days, 21 days, 28 days, day of testing started (DOT started), and day of testing finished (DOT finished). Three cylinders were tested at each of these points. The results of average cylinder strengths for each testing can be seen in Table 2-4. The data is also plotted in Figure 2-7.

Table 2-4: Concrete compressive strengths

Cast 1			**Cast 2**		
Date	Cure Time	Strength	Date	Cure Time	Strength
	days	MPa		days	MPa
10/26/2004	7	29.23	2/15/2005	7	24.89
11/9/2004	21	33.99	3/1/2005	21	30.41
11/16/2004	28	35.65	3/8/2005	28	32.34
12/16/2004	58	40.75	7/29/2005	171	41.58
7/15/2005	269	51.69	12/5/2005	300	46.80

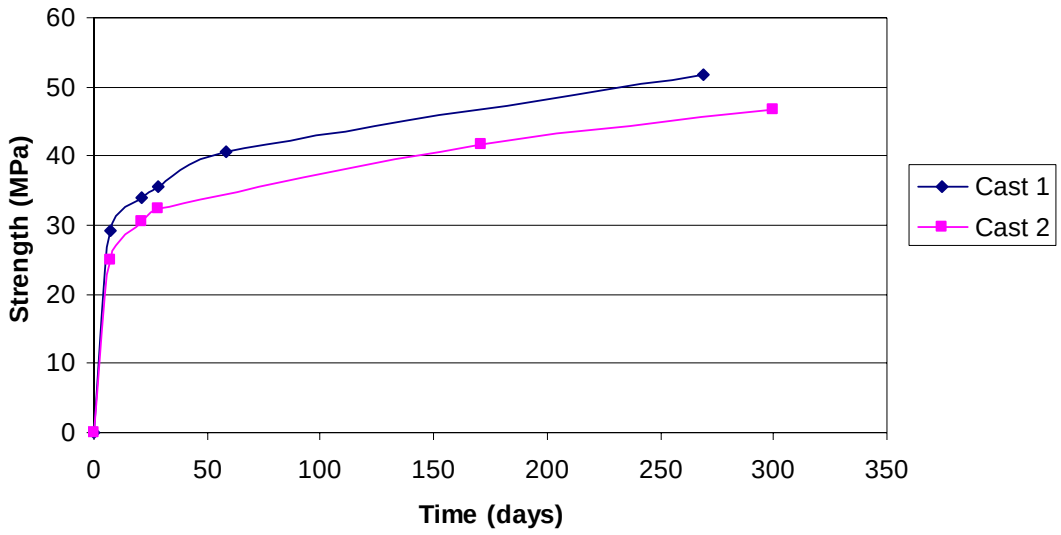

Figure 2-7: Concrete Compressive Strength vs. Cure Time

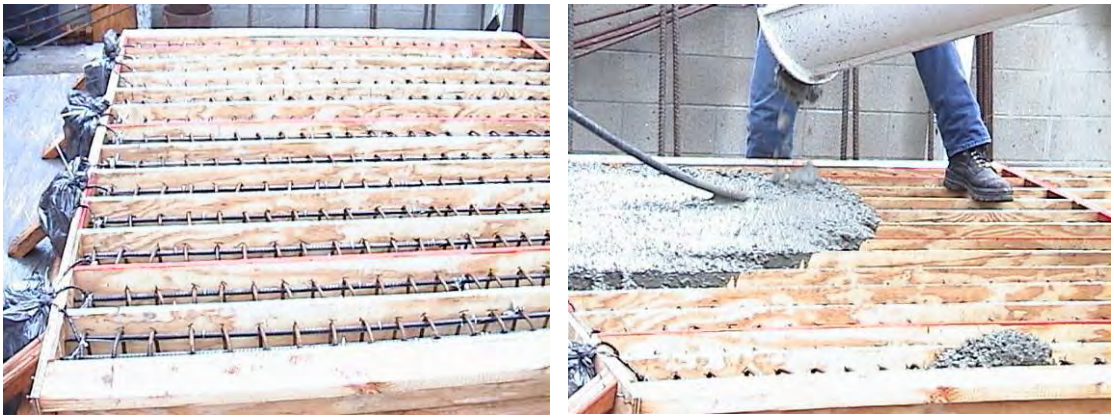

Figure 2-8: Casting of the reinforced concrete beam specimens.

2.5.3 Steel Properties

The beam specimens contained internal reinforcing steel in the form of two 13mm (number four) bars top and bottom as well as 10mm (number three) stirrups at 80mm spacing (see figure 2-2 for details). Both bar types were specified to be 414 MPa steel. Each bar type was tested in tension to determine the yield stress, ultimate stress, ultimate strain, and elastic modulus. Table 2-5 gives the average values for the three specimens that were tested of each size.

Table 2-5: Steel bar properties

Bar	Area	f_y	f_u	ε_y	ε_u	E
	mm^2	MPa	MPa	%	%	GPa
#3	71	451	693	0.23	13.0	197
#4	129	492	679	0.24	11.2	207

2.6 Instrumentation

Figure 2-9 shows a schematic of the displacement and strain related instrumentation used for each specimen. Strain data was collected using attached lead electrical resistance strain gages, while displacement data was collected using linear potentiometers and inclinometers. Instrumentation for all specimens included four 5mm internal steel strain gages (FLA-5-11 manufactured by Tokyo Sokki Kenkyujo Co., Ltd.), seven linear variable displacement transducers (LVDTs), five inclinometers, one to three 60mm concrete strain gages, and several 30mm gages on the FRP surface.

The exact layout of the concrete and FRP strain gages is specimen dependent and is further detailed in the test descriptions in chapter four.

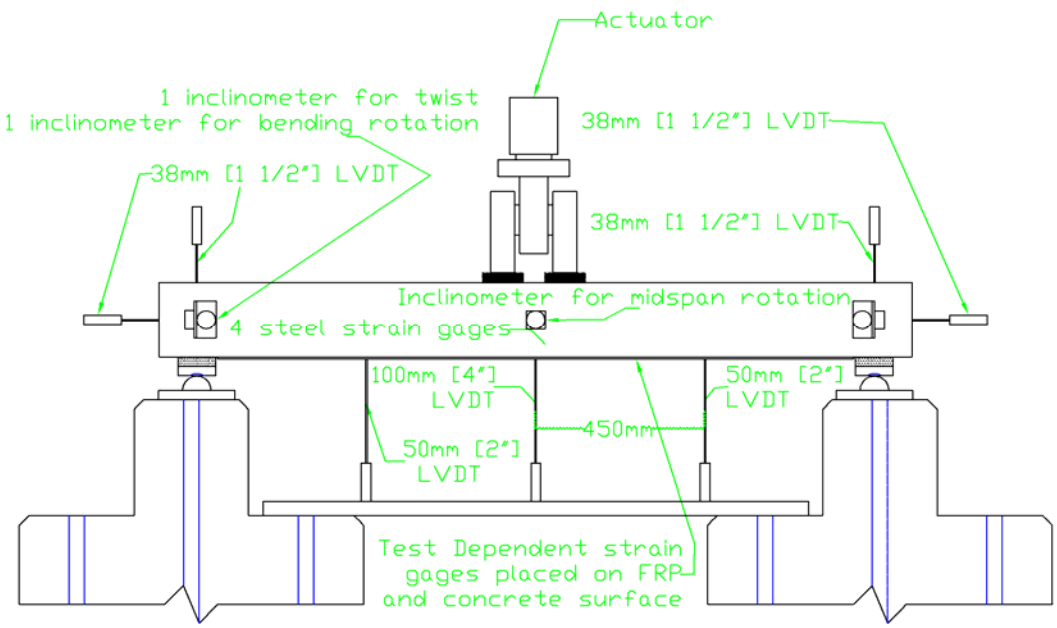

Figure 2-9: Instrumentation layout for test program

The principle displacement readings being taken were at three points along the span length: one at the midspan, and one at each quarterspan. The placement of the target was near the center of the beam's width to collect an average displacement reading taken at that point along the beams length. The remaining LVDTs were placed at the supports to document any inadvertent movement that could occur at this location. The inclinometers were placed two at each end and one at the midspan as shown in figure 2-9 to monitor for asymmetrical bending or twisting in the specimens. All of the

specimens had at least one strain gage measuring the compressive strain at the midspan at a location 20mm below the top edge of the beam, bonded to the face of the beam.

2.7 Loading Protocol

After the initial construction of the concrete specimens testing was divided into two phases. The first phase was the preloading of the virgin specimens to damage or “precrack” the beams as part of the preparation to simulate field conditions. After preloading the FRP was applied and allowed to cure for a minimum of seven days. The second phase of the testing procedure was then conducted in which the strengthened specimens were loaded to failure.

2.8 Preloading

When structures require the application of FRP strengthening in the field, they are generally not new structures and hence have some form of existing damage. These structures can be damaged by long sustained over-loading, by being overloaded by a large single event (such as an earthquake or vehicle impact), or have lost capacity over time due to material degradation and are no longer capable of sustaining the service loads required. At the very least these structures have likely sustained cracking damage to the surface to which the FRP will be applied. It is therefore important to not only conduct tests on specimens with similar cracked conditions, but also to know the specific effects these cracks have on strengthening behavior. The tests conducted in

this project involve specimens with no preloading, preloading to near yielding of internal steel, as well as specimens that were preloaded to various post-yielding displacements so that any differences in behavior due to preloading could be documented. Table 2-6 provides a summary of the important parameters pertaining to the specimen type including a schematic of the preload levels to which each test specimen was subjected.

Table 2-6: Test specimen summary.

Specimen Number	Preload	Defect	Defect Size	Defect Location (from midspan)	Defect Depth	Rehab #	Rehab Date	Test Date	Cast #
1	None	None	-	-	-	-	-	12/16/04	1
2	None	None	-	-	-	-	-	1/7/05	1
3	None	None	-	-	-	-	-	1/14/05	1
7	35.6 kN	None	-	-	-	1	5/6/05	5/18/05	1
26	None	None	-	-	-	1	5/6/05	5/26/05	1
9	35.6 kN	None	-	-	-	2	5/27/05	6/13/05	1
27	None	None	-	-	-	2	5/27/05	6/15/05	1
6	35.6 kN	None	-	-	-	2	5/27/05	6/16/05	1
28	None	None	-	-	-	2	5/27/05	6/17/05	1
29	None	None	-	-	-	2	5/27/05	6/20/05	1
10	35.6 kN	None	-	-	-	2	5/27/05	6/22/05	1
14	35.6 kN	Rectangular	150mm	185	C/R Interface	3	6/16/05	6/22/05	1
17	35.6 kN	Circular	150mm	185	C/R Interface	3	6/16/05	6/23/05	1
15	35.6 kN	Circular	100mm	185	C/R Interface	3	6/16/05	6/24/05	1
8	35.6 kN	Rectangular	100mm	185	C/R Interface	3	6/16/05	6/27/05	1
19	35.6 kN	Rectangular	50mm	185	C/R Interface	3	6/16/05	6/28/05	1
21	35.6 kN	Circular	50mm	185	C/R Interface	3	6/16/05	6/29/05	1
13	35.6 kN	Rectangular	25mm	185	C/R Interface	3	6/16/05	7/6/05	1
12	35.6 kN	Circular	25mm	185	C/R Interface	3	6/16/05	7/7/05	1
16	35.6 kN	Circular	100mm	185	C/R Interface	4	7/1/05	7/8/05	1
4	35.6 kN	Rectangular	100mm	185	C/R Interface	4	7/1/05	7/8/05	1
18	35.6 kN	None	-	-	-	4	7/1/05	7/11/05	1
25	35.6 kN	Rectangular	100mm	0	C/R Interface	4	7/1/05	7/11/05	1
20	35.6 kN	Circular	100mm	660	C/R Interface	4	7/1/05	7/12/05	1
24	35.6 kN	Circular	100mm	428	C/R Interface	4	7/1/05	7/12/05	1
5	35.6 kN	Circular	100mm	185	C/R Interface	4	7/1/05	7/13/05	1
11	35.6 kN	Rectangular	150mm	185	C/R Interface	4	7/1/05	7/13/05	1
22	35.6 kN	Circular	150mm	185	C/R Interface	4	7/1/05	7/14/05	1
23	35.6 kN	Circular	100mm	0	C/R Interface	4	7/1/05	7/14/05	1
30	35.6 kN	None	-	-	-	-	-	7/28/05	2
31	35.6 kN	Rectangular	100mm	185	C/R Interface	5	8/19/05	9/2/05	2
36	35.6 kN	None	-	-	-	5	8/19/05	9/13/05	2
32	35.6 kN	Rectangular	50mm	185	C/R Interface	5	8/19/05	9/20/05	2
33	35.6 kN	Rectangular	150mm	185	C/R Interface	5	8/19/05	9/20/05	2
35	35.6 kN	Rectangular	250mm	185	C/R Interface	5	8/19/05	9/20/05	2
34	35.6 kN	Rectangular	200mm	185	C/R Interface	5	8/19/05	9/22/05	2
37	35.6 kN	Rectangular	100mm	185	Interlaminar	6	9/20/05	9/27/05	2
40	35.6 kN	Rectangular	100mm	185	C/R & Interlaminar	6	9/20/05	9/28/05	2
38	35.6 kN	Rectangular	100mm	185	C/R Interface	6	9/20/05	9/28/05	2
42	35.6 kN	None	-	-	-	6	9/20/05	9/30/05	2
43	35.6 kN	Circular	100mm	185	C/R & Interlaminar	6	9/20/05	9/30/05	2
45	35.6 kN	Rectangular	100mm	0	C/R & Interlaminar	6	9/20/05	10/25/05	2
41	35.6 kN	Rectangular	100mm	185	C/R & Interlaminar	6	9/20/05	10/26/05	2
44	35.6 kN	Rectangular	100mm	428	C/R & Interlaminar	6	9/20/05	10/26/05	2
39	35.6 kN	Rectangular	100mm	185	Interlaminar	6	9/20/05	10/28/05	2
55	16mm	Rect, Crack, Soak	100, 1.0mm	185 (both sides)		7	10/21/05	11/2/05	2
61	35.6 kN	Rectangular	200mm	185	C/R Interface	7	10/21/05	11/2/05	2
46	35.6 kN	Rectangular	50mm	185	C/R Interface	7	10/21/05	11/4/05	2
53	16mm	Rect, Crack	100, 1.0mm	185	C/R Interface	7	10/21/05	11/4/05	2
52	16mm	Crack	1.0mm	N/A	Concrete	7	10/21/05	11/7/05	2
51	11.5mm	Crack	0.6mm	N/A	Concrete	7	10/21/05	11/8/05	2
47	35.6 kN	None	-	-	-	7	10/21/05	11/9/05	2
50	8mm	Crack	0.2mm	N/A	Concrete	7	10/21/05	11/9/05	2
48	14mm	Crack	1.5mm	N/A	Concrete	7	10/21/05	11/10/05	2
54	16mm	Rect, Crack, Soak	100, 1.0mm	185	C/R Interface, Conc	7	10/21/05	11/14/05	2
57	16mm	Rect, Crack	100, 1.0mm	185	C/R Interface, Conc	7	10/21/05	11/15/05	2
58	16mm	Rect, Crack	100, 1.0mm	185	C/R Interface, Conc	7	10/21/05	11/16/05	2
59	35.6 kN	Circular	25mm	185	C/R Interface	7	10/21/05	11/17/05	2
60	35.6 kN	Circular	50mm	185	C/R Interface	7	10/21/05	11/17/05	2
56	16mm	Rect, Crack	100, 1.0mm	185	C/R Interface	7	10/21/05	11/18/05	2
49	35.6 kN	Rectangular	250mm	185	C/R Interface	7	10/21/05	11/18/05	2

* See Table 2-7 for table key and explanation

Table 2-7: Key for table 2-6

Preload	Load level (kN) or crack width (cw) to which the preload level was applied.
Defect	Describes whether the defect inserted was a rectangular disbond (Rectangular or Rect), a circular disbond (Circular) disbond, an excessive crack width (Crack), a soaked disbond (soak), or some combination of these defects.
Defect Size	Gives the size of the defect (either a disbond or concrete crack width) in mm. In the case of a rectangular disbond this number describes the length of the defect (all rectangular disbonds covered the full width of the FRP strip). For circular disbonds the defect size describes the defect diameter.
Defect Location	Describes the distance (mm) from the midspan of the beam to the centroid of the defect. For example, "185" refers to the center of the defect being located 185mm away from the beams midspan.
Defect Depth	Describes where the defect was located in terms of depth within the specimen (for example whether it was located in the FRP, the concrete-resin interface or in the concrete alone).
	C/R Interface – Disbond located in the concrete-resin interface Interlaminar – Disbond located in between fabric layers in the FRP Concrete – Cracking located in the concrete specimen

The preload level used for most of the specimens in this study was the 35.6kN load level, based on the results obtained from testing the control specimens. The reasons for choosing this level were because this corresponded to a load level 0% to 5% below steel yield and the maximum crack opening at this point was approximately 0.20mm to 0.25mm, which is the limit allowed by NCHRP 514 (2004). Similarly, ACI

440 (2002) allows a maximum crack opening of 0.30mm. Additionally, this level was visually sufficient to verify the specimen had suffered damage. After unloading the specimens loaded to this level, the maximum crack openings closed to approximately 0.05 to 0.10mm since the steel had not yielded and were able to reclaim much of their original positions. The cracks remained closed at these widths during the application of FRP. Precracking protocol of specimens loaded to predefined deflections were determined based on cracking data obtained from earlier tests. Displacements of 8mm, 11.5mm, 16mm, and 21mm were used to achieve approximate residual crack widths (after removal of preload) of 0.2mm, 0.5mm, 1.0, and 1.5mm respectively (see figures 2-10, 2-11, 2-12, 2-13, 2-14, and 2-15). Prior to the removal of preload, the crack widths were 0.6mm, 1.0mm, 1.7mm. and 1.8mm, respectively. This was conducted to test what behavioral changes may be observed due to cracks and steel strain hardening. These crack width values were chosen based on the ACI Committee 224 (2004) suggestion that aggregate interlock is lost at 0.9mm (~1.0mm) so that tests are conducted at cracking less than, approximately equal to, and greater than that needed to achieve interlock. Finally, four specimens were strengthened without prior application of preload to serve as control specimens. The loading rate for precracking of the specimens was 0.220 kN per second when the actuator was being operated in load control for the 35.6 kN preload and a rate of 0.04mm/sec for the specimens loaded beyond steel yield. This rate of 0.040mm per second corresponds to the same approximate loading rate as the 0.220 kN per second loading rate based on the

specimen stiffness before steel yield. A typical cracking pattern due to preloading can be seen in Figure 2-16.

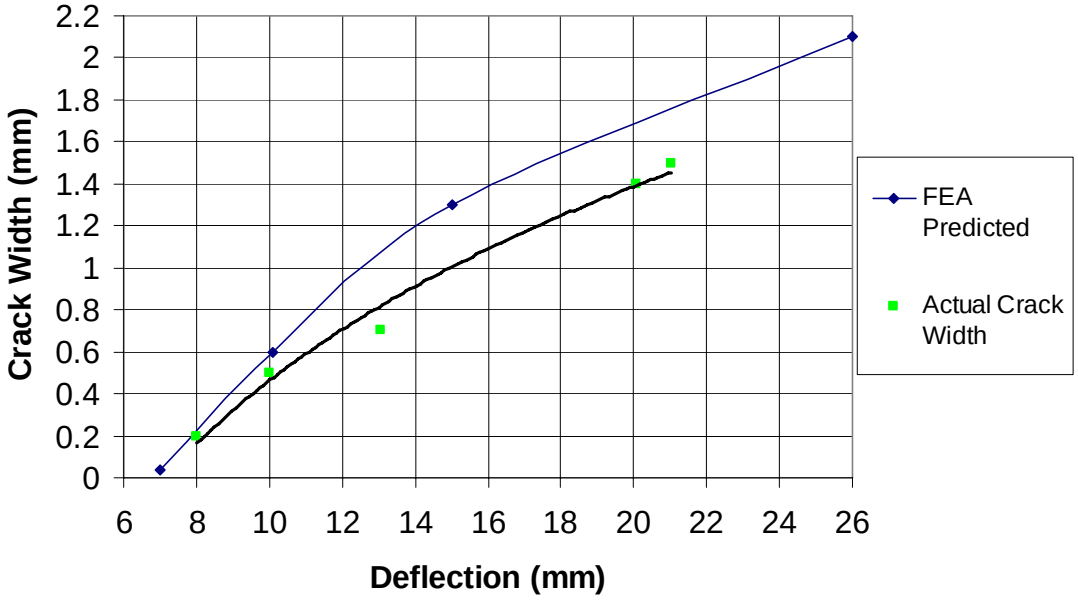

Figure 2-10: Residual crack width after unloading vs. maximum midspan deflection.

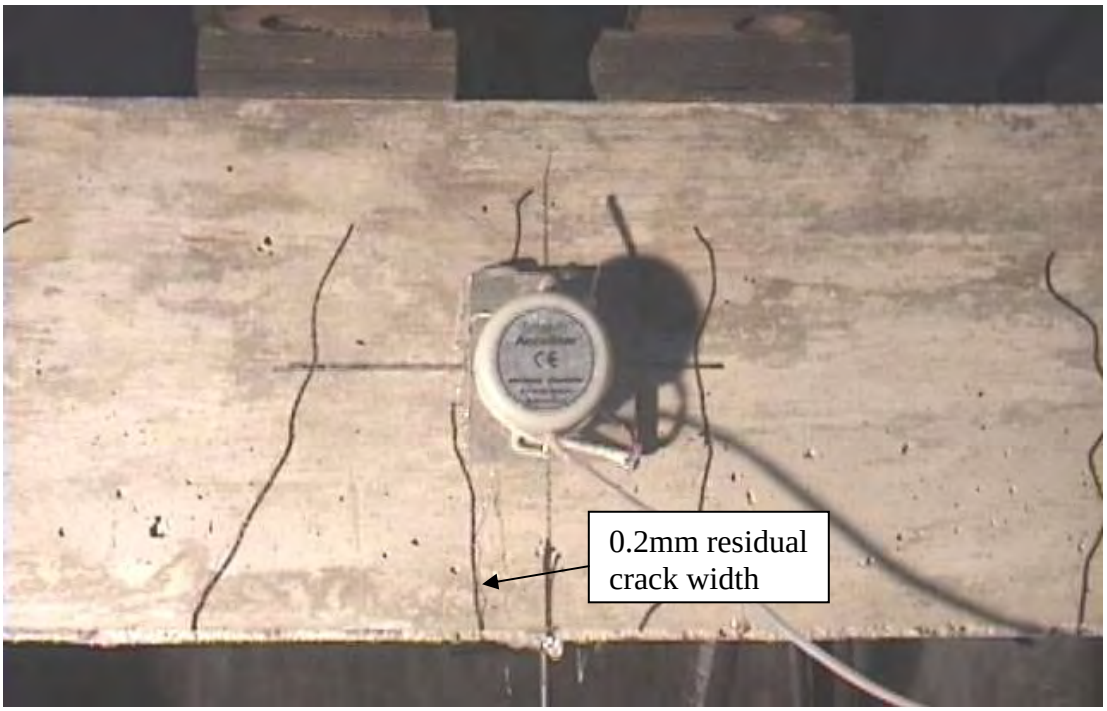

Figure 2-11: 0.2mm residual crack width (max beam deflection = 8.02mm)

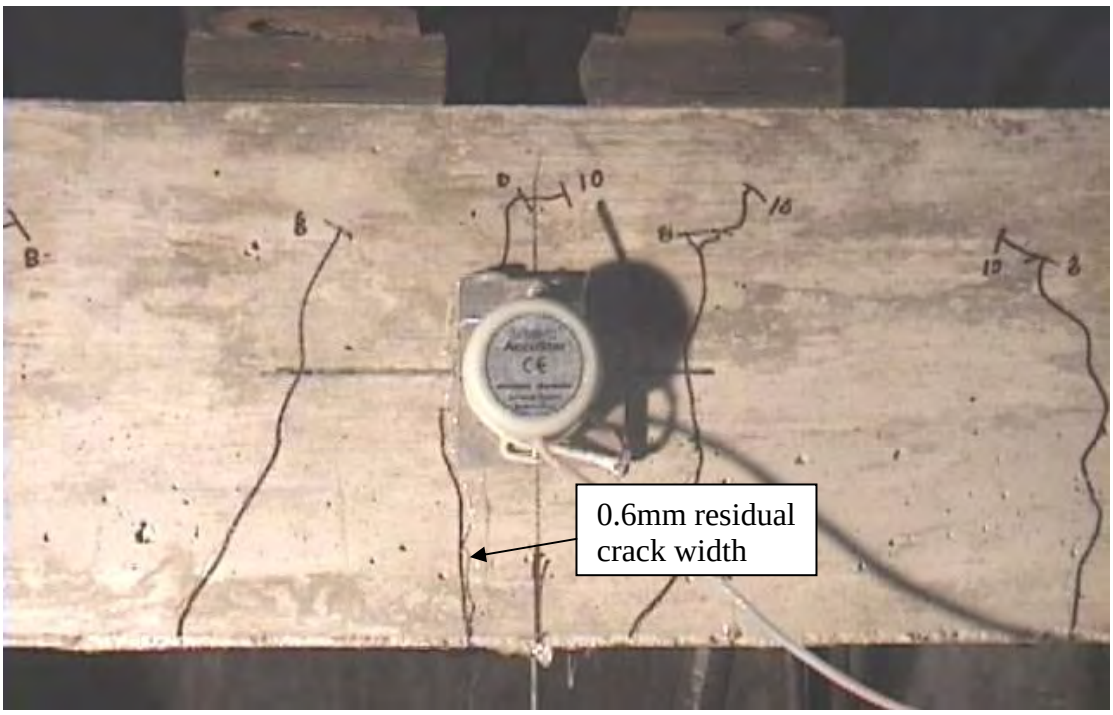

Figure 2-12: 0.6mm residual crack width (max beam deflection = 10.04mm)

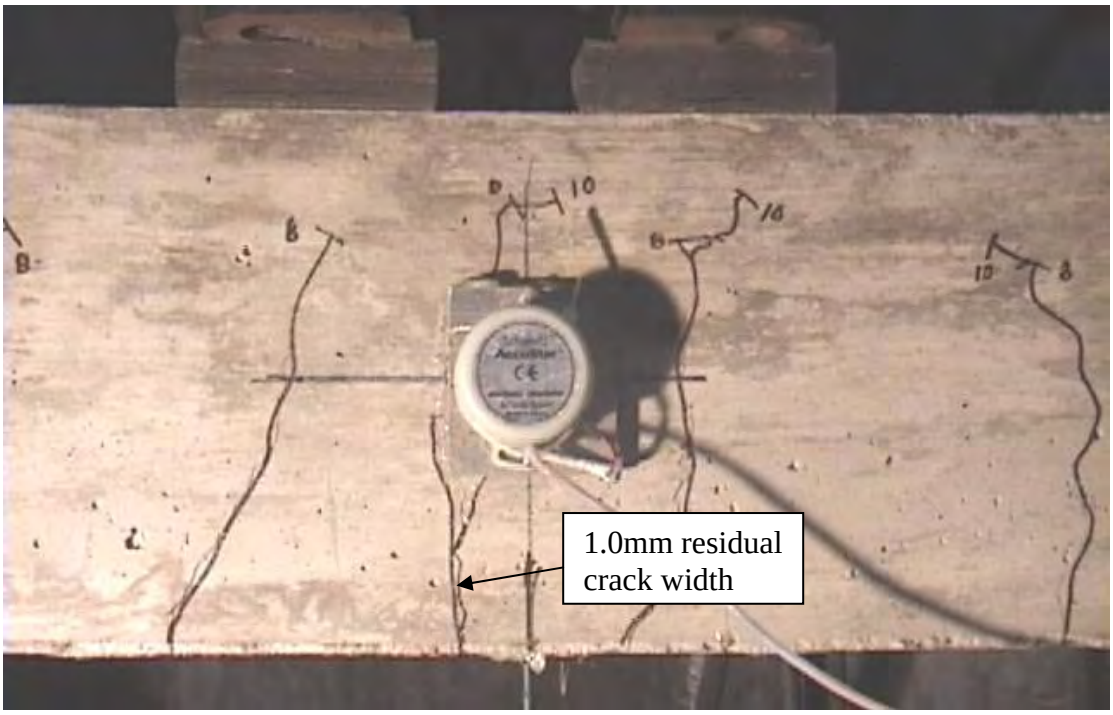

Figure 2-13: 1.0mm residual crack width (max beam deflection = 13.07mm)

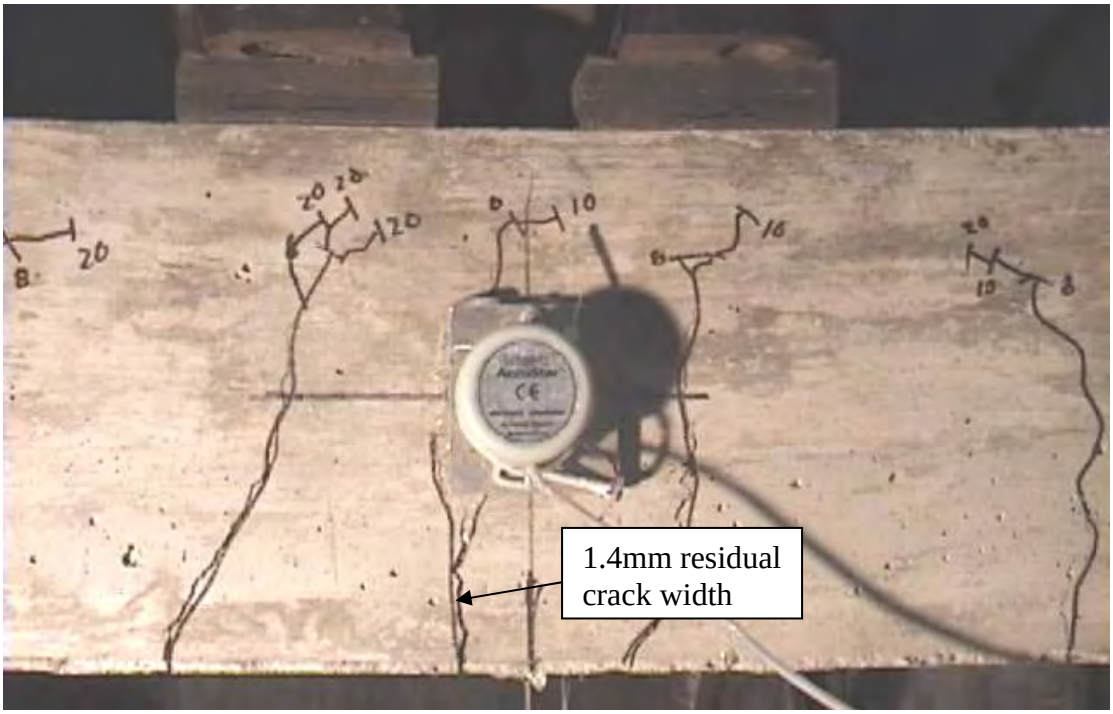

Figure 2-14: 1.4mm residual crack width (max beam deflection = 20.06mm)

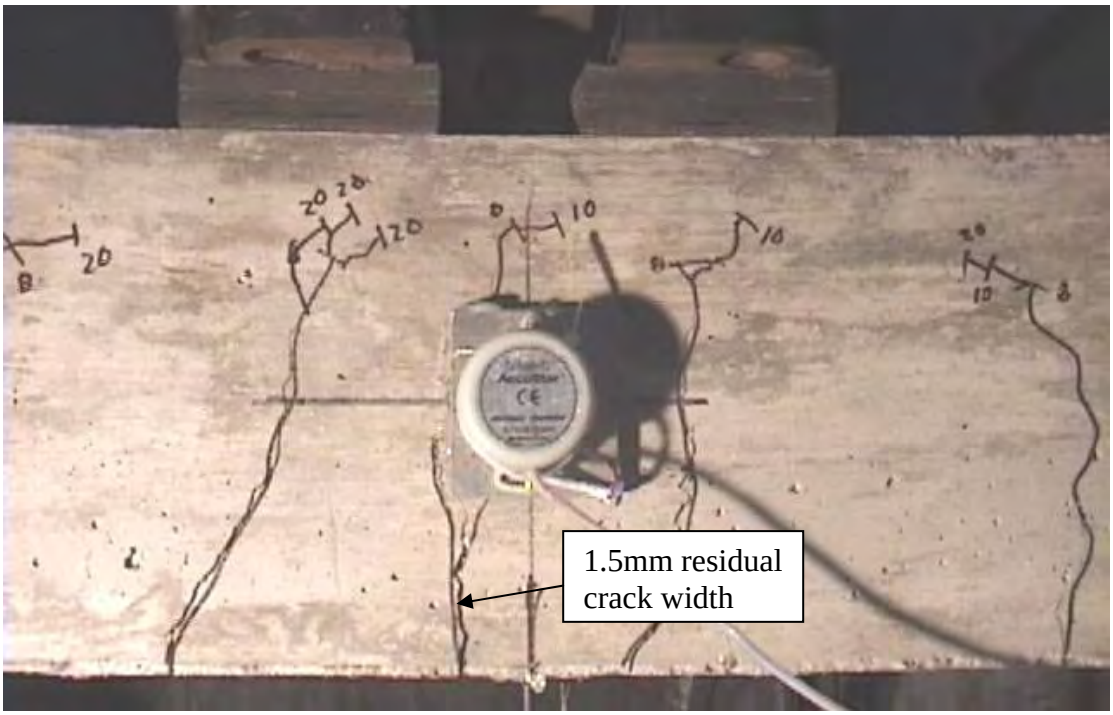

Figure 2-15: 1.5mm residual crack width (max beam deflection = 21.04mm)

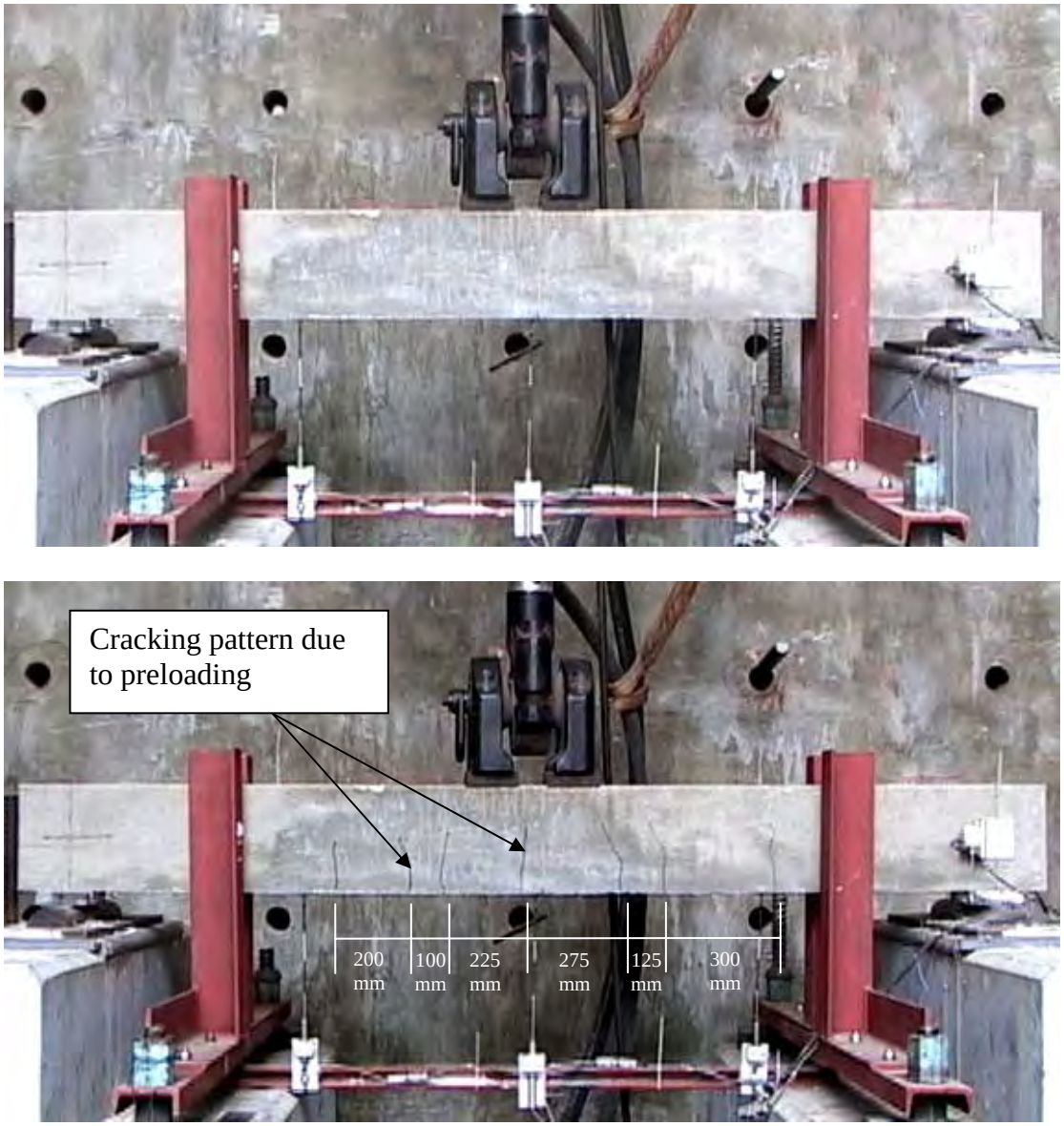

Figure 2-16: Picture before preloading and after preloading to 35.6kN.

2.9 Wet Layup Procedure

The FRP was applied to the test specimens using the wet lay-up method. In the wet lay-up procedure, the fabric is saturated, or wet out, with resin and placed on the specimen such that the epoxy-resin functions both as the matrix material as well as the adhesive bonding the FRP to the concrete. Figure 2-17 documents a series of steps detailing the procedure.

After the specimens were preloaded, they were taken outside and turned tension face up for the surface preparation procedure. Surface preparation involved moderate abrasive sandblasting of the tension face to remove laitance and expose the aggregate. For each casting, all specimens were sandblasted at once to minimize inconsistencies in surface preparation. However, since the two castings were sandblasted at different times, there existed noticeable differences between the surface preparations. The sandblasting of cast number one resulted in well exposed aggregates, but specimens from cast number two appeared to have more paste material remaining after the procedure was completed. Additionally, in both batches, differences in surface characteristics could be noted. After the sandblasting procedure, the specimens were moved back inside the laboratory, and the exposed surface was cleaned before lay-up using pressurized air to remove any remaining dust or other loose debris.

The Tyfo S epoxy resin was mixed at the manufacturer specified ratio of 100 parts of epoxy to 42 parts of hardener by volume for a period of 8 to 10 minutes to ensure full mixture of the two components. After mixture of the epoxy, a paint roller was utilized to wet the entire surface of the beam on which composite was to be

applied. Next, a precut strip of Hexcel GA090 carbon fiber fabric was saturated on a plastic sheet. The epoxy was applied using a paint roller to wet-out both sides of the fabric. The saturated fabric was then applied to the wet surface of the beam and compacted using a metal roller, followed by application of pressure using a plastic drywall spatula to remove voids and excess resin. A new layer of resin was then applied to the fabric surface and the second layer of carbon fabric was saturated and applied in an identical fashion to the first. Upon completion, the beams were left to cure undisturbed for at least seven days to ensure near full composite strength was achieved.

Sandblasting of the beam specimens	Cleaning the surface with compressed air
Resin saturation of concrete surface	Saturation of carbon fiber fabric
Application of fabric to beam surface	Compaction of material with metal roller

Figure 2-17: Wet lay-up procedure.

2.10 Final Testing

Final testing of the specimens occurred after sufficient time was given to ensure material strengths were near maximum. No final testing was conducted before the concrete and FRP had cured a minimum of 58 days and 7 days, respectively. The specimens were loaded using load cycles of 36kN, 75kN, and 90kN load limits. As each limit was reached, the test was paused at the corresponding displacement to make observations, measure cracks, and mark cracks. During these pauses the displacement would remain held constant, however, the load would drop slightly over time while it was being held in place. After observations were completed the specimen was then unloaded to near zero load (approximately 2.5 kN) at which point it was again paused for observations before proceeding to the next load cycle. This process was repeated for each load cycle until specimen failure.

The 36kN and 75kN load cycles were both run in load control at a loading rate of 0.22 kN per second. The remaining load cycles, however, were run in displacement control after a 75kN load was reached in order to have better control of the actuator when the specimen fails. Like the precracking phase, the loading rate in displacement control was set at 0.040mm/sec. Data was collected from the initiation of loading until the specimen was completely unloaded after global debonding had occurred.

References

ACI Committee 224, *Joints in Concrete Construction*, ACI 224.3R-95, American Concrete Institute, Famington Hills, MI, USA, p. 21, 2004.

ACI Committee 440, *Guide for the Design and Construction of Externally Bonded FRP Systems for Strengthening Concrete Structures*, ACI 440.2R-02, American Concrete Institute, Farmington Hills, MI, USA, pp. 103, 2002.

ASTM D-3039, *Standard Test Method for Tensile Properties of Polymer Matrix Composite Materials*, American Society for Testing and Materials, pp. 105-117, 2000.

Kaiser, H., *Assessment of Defect Criticality and Non-destructive Monitoring of CFRP-rehabilitated Civil Structures*, Masters Thesis *Department of Structural Engineering*, UCSD: La Jolla, CA, 2002.

Kaiser, H. and V.M. Karbhari, *Quality and Monitoring of Structural Rehabilitation Measures – Part 1: Description of Potential Defects*. University of California, San Diego: La Jolla, CA, p. 60, 2001.

Karbhari, V.M., *Materials Considerations in FRP Rehabilitation of Concrete Structures*, Journal of Materials in Civil Engineering, Vol. 13, No. 2, pp. 90-97, 2001.

Navada R., *An Experimental Assessment of Defect Criticality in FRP Rehabilitated Concrete using a Fracture Mechanics Approach*, Masters Thesis *Department of Structural Engineering*, UCSD: La Jolla, CA, 2004.

NCHRP Report 514, Transportation Research Board, Washington, D.C., Section II, p. 1-33, 2004.

Niu H., J. Delaney, V.M. Karbhari, *Effect of Defects on Performance of CFRP Strengthened RC Beams*, Sampe 2005 Long Beach Conference Proceedings, 2005.

3. DEFECT MODELING USING FEA

Issues of scale, amongst others, make the direct use of data obtained from the laboratory testing of the specimens in this project on larger specimens, such as bridge girders and slabs, a challenge. For example, it is difficult to test a defect on one of the laboratory specimens and be able to directly apply the results to determine how the same defect would behave on a structural member with different material and geometrical properties. The development of a finite element analysis model assists in enabling the laboratory testing results to be applied to appropriate situations in the field, using a local-global approach.

Several local bond-slip curves for bond performance between concrete and FRP have been suggested in recent years, as can be seen in figure 3-1, that have resulted from simple shear and flexural tests (Niu and Karbhari, 2006). The simplified bilinear softening model, as shown in figures 3-8 and 3-9, suggested by Yoshizawa et al. (2000) has been demonstrated to yield reliable behavior and results within a fracture-energy based approach and therefore, has been adopted for this investigation.

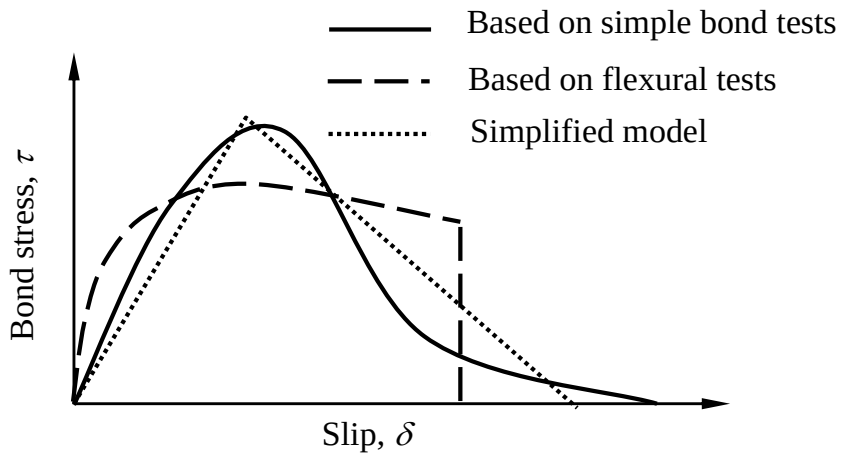

Figure 3-1: Local bond-slip curves for bond performance between concrete and FRP.

3.1 FE Analysis Program

The program utilized in this investigation is DIANA-8, a non-linear FE program designed specifically for use in civil engineering applications. For simplicity, the model was constructed in two dimensions. Therefore only defects (such as the rectangular disbonds described in Chapter 2) spanning the full 150mm width of the beam were modeled. Figure 3-2 is a graphical representation of the FE model displaying the mesh, incorporating concrete, reinforcing steel, FRP, and loading pads. A mesh sensitivity study was conducted that demonstrated that a medium mesh consisting of 10,639 elements was adequate for modeling purposes from the point of view of computational efficiency and accuracy. With this tool, the concrete was modeled using 4-node plane stress elements. During the development of the model, two commonly used cracking models were examined: The smeared cracking model

and the discrete cracking model (DIANA 2002). In the discrete cracking model, predefined cracks are assigned to the model based on experimental observations. The discrete cracking model is suitable for local cracking behavior and is modeled by separating the same nodal points to create the local displacement discontinuities with appropriate stress-displacement relationships for modeling the stress transfer along the crack surface. The disadvantages to the discrete cracking model are that the crack trajectory must be assigned in advance and crack locations must be predefined (DIANA 2002). It is noted that, comparisons between the discrete and the smeared crack model behavior have revealed very small differences in the program results for the specimens considered. The smeared crack model assumes fracture is distributed over a domain and, therefore, may be described using continuum models with the appropriate application of stress-strain relationships. With the presence of FRP, the principal stress axes rotate with the increase of loading, therefore a rotating crack model was utilized which is based on total strain formulation (Niu and Karbhari, 2005). Because of the above reasons, the smeared cracking method was the final choice in this investigation.

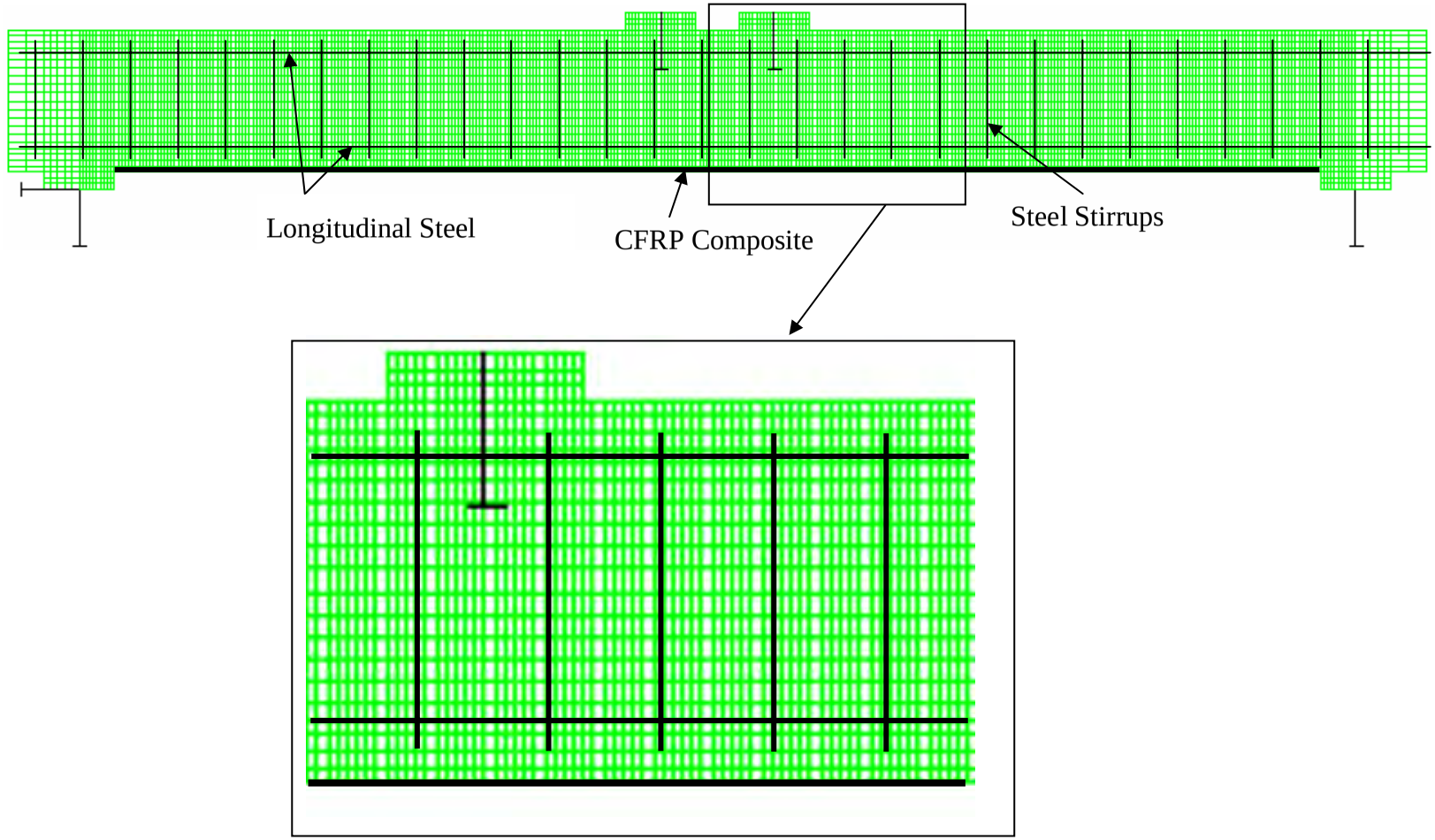

Figure 3-2: Graphical representation of the FE model.

The tensile behavior of the concrete is modeled as a linear tension-softening curve as can be seen in figure 3-4. The stress is assumed to increase linearly to the tensile strength f_t^c and then decreases linearly to zero (Hillerborg 1976). The area below the curve is related to the fracture energy, G_f^c and the crack band width, h_{cr}. The crack band width is defined as $h_{cr} = \sqrt{2A_{elem}}$ where A_{elem} is the area of the element. The stress-strain behavior for the compression behavior of the concrete is modeled with a modified Hognestad curve without limitations of strain capacity, also shown in figure 3-4 (Hognestad, 1951). The concrete properties derived by DIANA (E_c, f_t, and G_f^c) were calculated from $f_c^{'}$ using equations from CEB-FIP (1993) (DIANA, 2002), as can be seen in equations 3-1, 3-2, 3-3 and figure 3-3.

$$E_c = 2.15 \times 10^4 \left(\frac{f_c^{'}}{10} \right)^{\frac{1}{3}} \text{(MPa), (3-3)} \qquad (3\text{-}1)$$

$$f_t^c = 1.4 \left(\frac{f_c^{'} - 8}{10} \right)^{\frac{2}{3}} \text{(MPa),} \qquad (3\text{-}2)$$

$$G_f^c = G_f^0 \left(\frac{f_c^{'}}{10} \right)^{0.7} \text{(N/mm)} \qquad (3\text{-}3)$$

d_{max} [mm]	G_f^o [J/m^2]
8	25
16	30
32	58

Figure 3-3: Coefficients for determination of the fracture energy (CEB-FIP 1993).

where G_f^o is a function of the maximum aggregate size (d_{max} = 12.7mm) resulting in a value of 0.028 N/mm for this model (DIANA, 2002). In equation 3-2, f_t^c gives a value of 3.1 MPa which substantially over predicted the strengthened performance of the beam. The concrete tensile strength (f_t^c) is a very important parameter in the determination of the effectiveness of FRP strengthening because of its correlation to shear strength. It has been noted that concrete "tensile strength, however determined, does not correlate well with the compressive strength" (Nilson et al, 2004). Based on testing of the beam specimens in the laboratory, it was found necessary to change f_t^c from the value of equation 3-1, determined by CEB-FIP in DIANA to a more representative value of the concrete being utilized.

ACI Committee 318 (2002) suggests using equation 3-4 for concrete tensile strength.

$$f_t^{'} = 0.62\sqrt{f_c^{'}} \text{ (MPa)} \qquad (3\text{-}4)$$

This equation results in even a larger tensile strength of 3.96 MPa. JSCE (1996) suggests using equation 3-5 for determination of tensile strength.

$$f_t = 0.23 f_c^{2/3} \text{ (MPa)} \qquad (3\text{-}5)$$

Equation 3-5 yields a f_t of 2.72 MPa, which was still substantially too large to yield an accurate result. Because of this, the final f_t^c value chosen, which resulted in an excellent prediction of strengthened performance, was 1.5 MPa as determined by equation 3-6 suggested by Kata et al (1988).

$$f_t = 0.235\sqrt{f_c} \quad \text{in MPa} \tag{3-6}$$

Due to the difficulty calibrating f_t^c and the importance of this parameter, it is emphasized that more research is needed in determining concrete tensile strength for FRP strengthening applications.

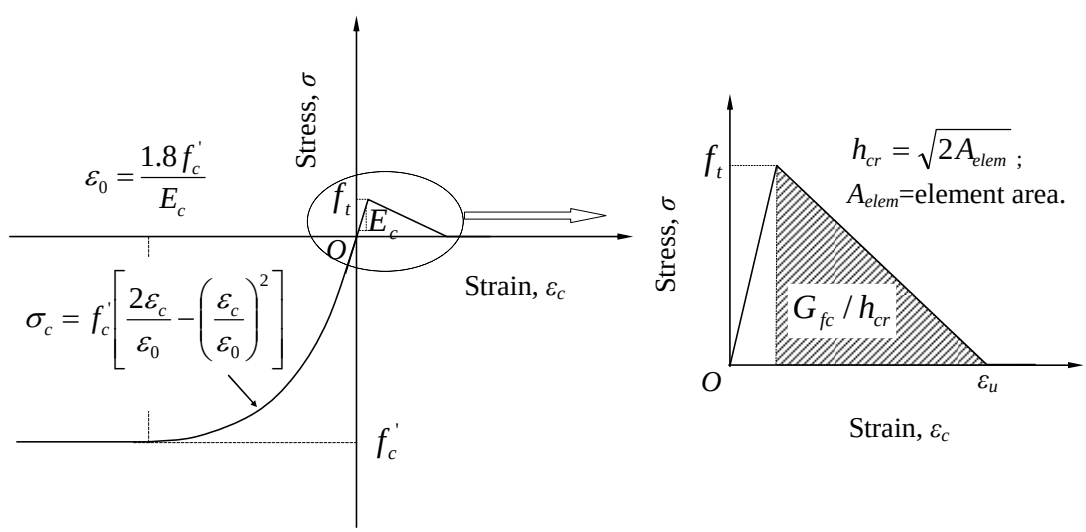

Figure 3-4: Stress-strain material model for concrete behavior

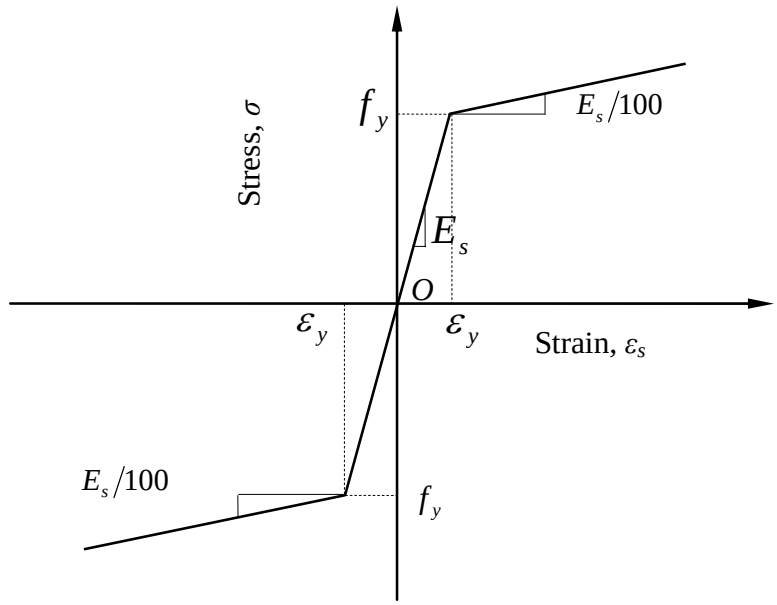

Figure 3-5: Steel material model utilized in the FE model

The reinforcing steel was modeled using 2-node linear truss elements with an elasto-plastic response with strain hardening of a slope that is 1% of the elastic modulus ($E_s/100$). Figure 3-5 gives a graphical representation of the steel material model utilized. The steel was connected to the concrete by zero-thickness line interface elements to model the bond in longitudinal bars according to the behavior model described by CEB-FIP MC90 (1993) as shown in figure 3-6. Perfect bond was assumed for transverse steel reinforcement.

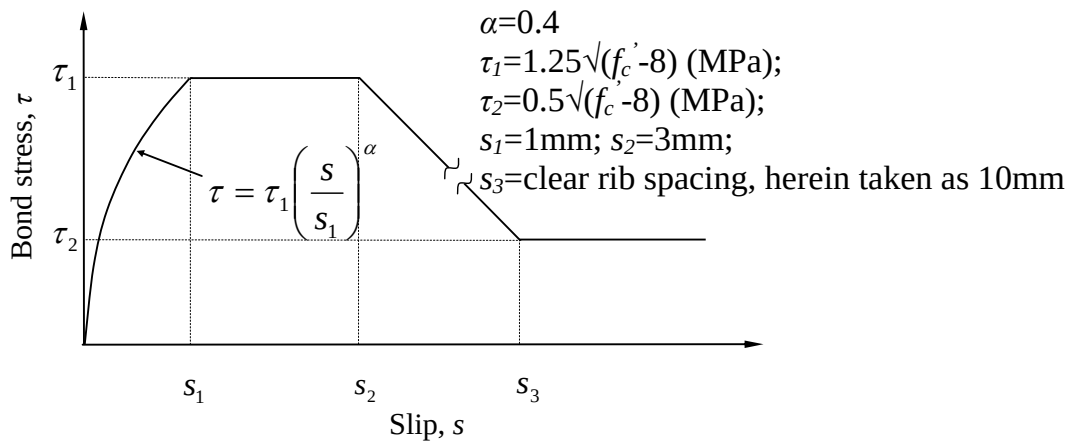

Figure 3-6: Model CEB-FIP MC90 describing steel-concrete bond behavior

The FRP was modeled based on the assumption that it behaved in a linear elastic fashion until rupture. This model is demonstrated in figure 3-8. Considering that the FRP in the beam is primarily loaded in tension, the model simulated the FRP using 2-node truss elements with zero-thickness interface elements to simulate the adhesive concrete-FRP bond. These interface elements modeled the adhesive layer between the concrete substrate and the FRP by using a bilinear curve proposed by Yoshizawa (2000) where the interfacial fracture energy, G_f^i, is the area under the stress-displacement curve shown in figure 3-9 (Niu and Karbhari, 2005). Values for interfacial stiffness (k_t), bond strength (τ_f), and G_f^i chosen for this model were 160 MPa/mm, 8 MPa, and 1.2 N/mm respectively as recommended by Yoshizawa (2000). It is pointed out that final debonding may occur either through the concrete or through the adhesive layer, as shown in figure 3-7. Debonding through the cover concrete is thought to be dominated by mode-I failure (Niu and Karbhari, 2006) and was modeled

by the smeared crack approach described previously following the fracture mechanics model described by figure 3-10. Debonding by shearing through the adhesive layer more closely resembles mode-II fracture (Niu and Karbhari, 2006) and is modeled using the simplified linear softening model shown in figure 3-7.

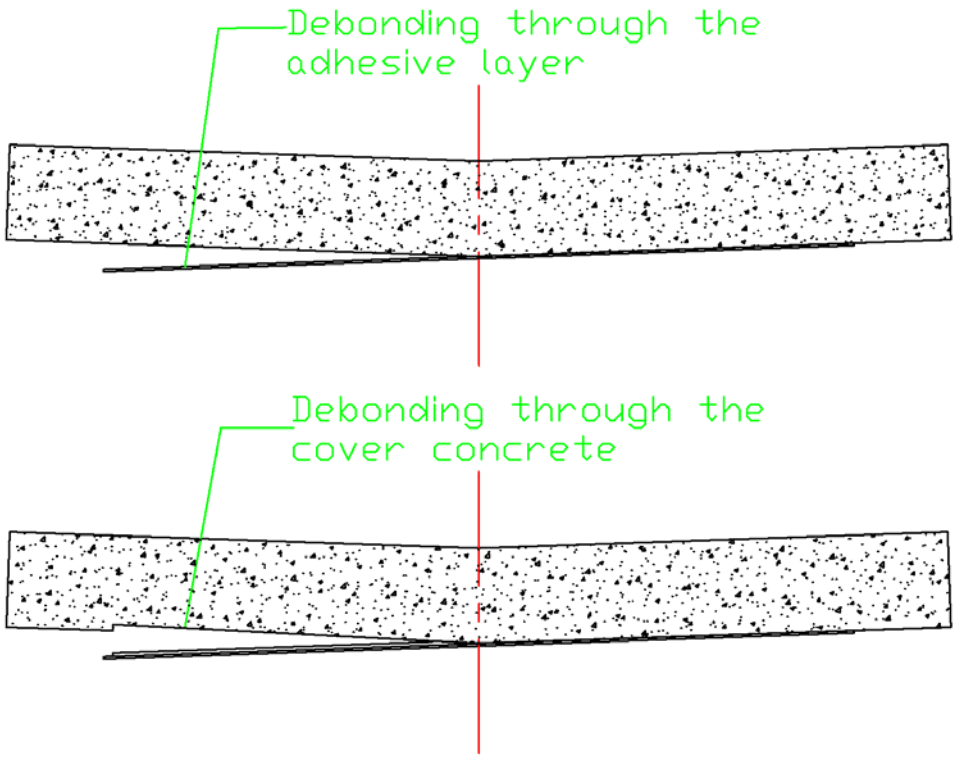

Figure 3-7: Failure modes: debonding through the adhesive layer and debonding through the concrete cover.

Laboratory experiments in this study indicate that local debonding eventually resulting in global failure is initiated from flexural or shear crack locations. In previous studies, it was noted that the application of preloading to cause these cracks to form prior to the application of FRP has a minimal effect on overall strengthening behavior in short duration tests (Sharif et al 1994, Arduini and Nanni 1997, Shahawy et al 2001, Seim et al 2001, and Chan and Niall 2001). However, this debonding

characteristic (initiating from concrete cracking) may have a noticeable impact on the long term effectiveness of the FRP rehabilitation and thus, this program emphasizes the determination of the effects at the materials level in an attempt to understand what local stress concentrations exist given a cracked or otherwise defective specimen. Table 3-1 illustrates the material properties used in the FEA model. Material properties f_t^c, G_f^c, G_f^i, τ_f, and k_t have all been discussed previously. All remaining properties listed in table 3-1 came from the material data obtained from the laboratory testing program as discussed in chapter two.

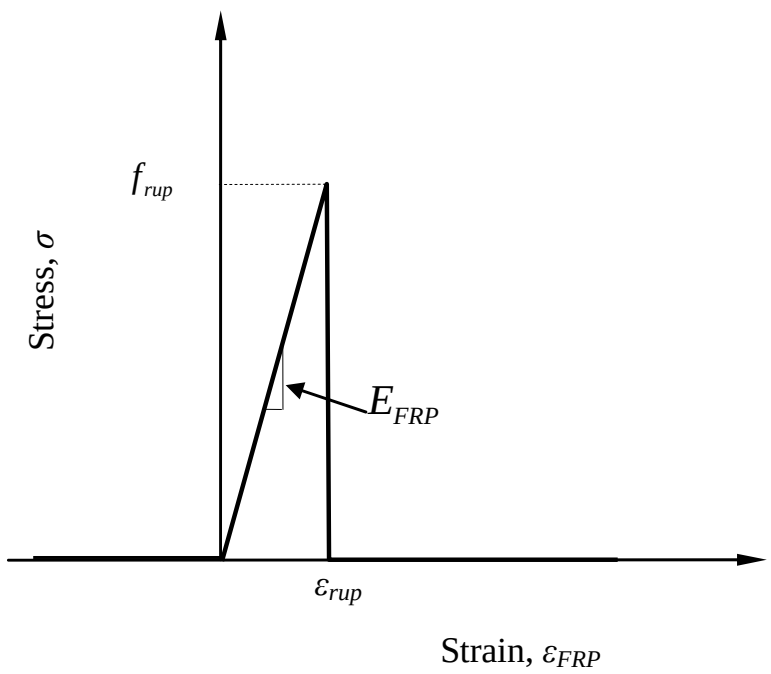

Figure 3-8: FRP stress-strain material model.

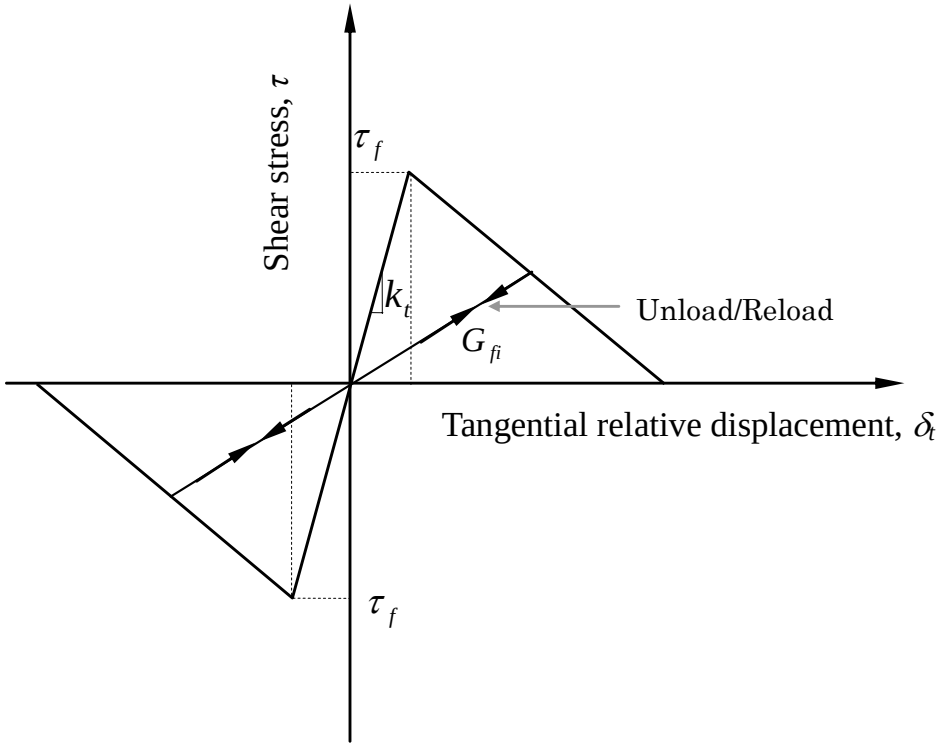

Figure 3-9: Simplified linear softening model for mode II fracture.

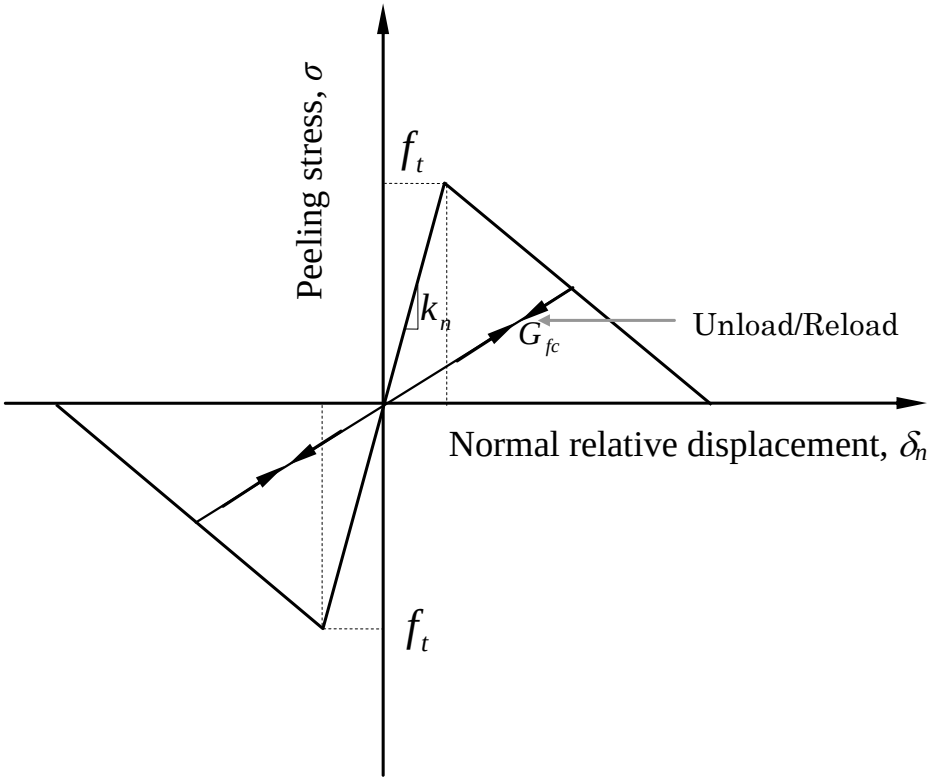

Figure 3-10: Simplified linear softening model for mode I fracture.

Table 3-1: Material Properties Used in the FEA

Constituent	Property	Value	Description
Concrete	f'_c	40.75 MPa	Concrete Compressive Strength
	f_t^c	1.5 MPa	Concrete Tensile Strength
	G_f^c	0.075 N/mm	Concrete Fracture Energy
FRP	t_{frp}	1.297 mm	FRP Thickness
	E_{frp}	104.3 GPa	FRP Modulus of Elasticity
	σ_{frp}	1646.39 MPa	FRP Tensile Strength
Longitudinal Steel	E_s	190 GPa	Steel Modulus
	$f_{y,s}$	476 MPa	Steel Yield Strength
	f_u	656 MPa	Steel Ultimate Strength
Transverse Steel	E_s	190 MPa	Steel Modulus
	$f_{y,s}$	476 MPa	Steel Yield Strength
	f_u	656 MPa	Steel Ultimate Strength
Adhesive Layer	k_t	160 MPa/mm	Interfacial Stiffness
	τ_f	8 MPa	Shear Strength
	G_f^i	1.2 N/mm	Adhesive Fracture Energy

To investigate the effect of preloading, some of the beams were loaded using displacement control in a two stage process in the FE analysis. The loading protocol was chosen in order to best simulate the actual loading process while utilizing the material behavior models as described above. The first step in the process was to load the beam to the predefined preload level, leaving the FRP elements and interface elements inactive. Once the preload level was reached, simulating the condition of the beam in the damaged state, the FRP elements and the interface elements were then activated while holding the load constant. Finally, the completed model was loaded to failure with all elements activated. This process was chosen because it simulates rehabilitation of a structure under service loads. In reality, the beams tested in

laboratory were not under service loads when FRP was applied, however there was still some permanent crack opening due to friction or steel yielding. The difficulty with following the exact loading process that was utilized in the testing program is that the secant path followed upon unloading in the concrete model returns back to the origin. Thus little preload effect could be observed upon activating the FRP and interface elements. For this reason, the two stage process was utilized to investigate the effect of preloading.

Since previous research, laboratory testing, as well as the FEA model all indicated that preload has little effect on structural performance of FRP rehabilitated structures, the final FEA model for determining the effect of a disbond ignored the preloading phase and only utilized the smeared crack model described earlier. The FEA program results presented in chapter four demonstrate and validate the relevance of this FEA program for analysis of the real structure.

References

ACI Committee 318, *Building Code Requirements for Reinforced Concrete*, ACI 318-02 and Commentary, American Concrete Institute, Farmington Hills, MI, USA, pp. 443, 2002.

Sharif A., G.J. Al-Sulaimani, I.A. Basunbul, M.H. Baluch and B.N. Ghaleb, "*Strengthening of Initially Loaded Reinforced Concrete Beams Using FRP Plates*", ACI Structural Journal, Vol. 91, No. 2, , pp. 160-168. 1994.

Arduini, M. and A. Nanni, *Behavior of Precracked RC Beams Strengthened with Carbon FRP Sheets*, Journal of Composites for Construction, Vol. 1, No. 2, p. 63-70, 1997.

Chan, T. K. and M. Niall, *Strengthening of One-way Slabs Using Carbon Fibre Plates: The Effect of Preload*, CSE Research Bulletin, No.14, 2001.

DIANA – Finite Element Analysis - User's Manual, release 8.1, TNO Building and Construction Research, The Netherlands, 2002.

Hillerborg, A., M. Modeer, and P.E. Petersson, *Analysis of crack formation and crack growth in concrete by means of fracture mechanics and finite elements*, Cement Concrete Research Vol. 6, pp. 773-782, 1976.

Nilson, A, D. Darwin, C. Dolan, Design of Concrete Structures (thirteenth edition), McGraw-Hill Companies, Inc., New York, NY, pp. 41-50, 2004.

Niu, H., J. Delaney, V.M. Karbhari, *Effect of Defects on Performance of CFRP Strengthened RC Beams*, Sampe 2005 Long Beach Conference Proceedings, 2005.

Niu, H., V.M. Karbhari, *FE Investigation of Material and Preload Parameters on FRP Strengthening Performance of RC Beams*, under review by the Journal of Structural Engineering and Mechanics, 2006.

Niu, H, Z. Wu, *Numerical Analysis of Debonding Mechanisms in FRP-Strengthened RC Beams*, Computer-Aided Civil and Infrastructure Engineering, Vol. 20, pp. 354-368, 2005.

Hognestad E. *A study of combined bending and axial load in reinforced concrete members*. University of Illinois Engineering Experimental Station, Bulletin Series No. 399, p128, 1951.

JSCE Standard Specification for Design and Construction of Concrete Structure, Japan Society of Civil Engineers, Tokyo, 1996.

Kata, I., S. Kawamata, *Mechanical Behavior of RC Concrete Slab Under In-plane Shear*, Journal of Japan Concrete Institute, Vol. 26, No. 10, pp. 97-110, 1988.

Seim, W., M. Horman, V. Karbhari, and F. Seible, *External FRP Poststrengthening of Scaled Concrete* Slabs, ACSE Journal of Composites for Construction, Vol. 5, No. 2, pp. 67-75, 2001.

Shahawy, M, O. Chaallal, T: E. Beitelman, and A. El-Saa, *Flexural Strengthening with Carbon Fiber-Reinforced Polymer Composites of Preloaded Full-Scale Girders*, ACI Structural Journal, Vol. 98, No. 5, p. 735, 2001.

Yoshizawa, H., Z.S. Wu, H. Yuan, T. Kanakubo, *Study on FRP-concrete interface bond Performance*, JSCE Jounal of Material, Concrete Structures and Pavements (in Japanese), Vol. 49, No. 662, pp. 105-119, 2000.

4. RESULTS

A total of sixty-one specimens were tested in this investigation. These specimens can be organized into five different sets according to the parameters being investigated. The sets are: 1) Control specimens; 2) Critical disbond size; 3) Critical disbond location; 4) Effect of excessive preload cracking; and 5) Effect of interlaminar disbonds. Some specimens fall into multiple categories. The basic breakdown of these sets was described in chapter 2 and can be seen in figure 2-1. Chapter four is organized such that these sets are discussed individually and, later, as a whole in an effort to describe the effect of defects. Finally, laboratory results are compared to results obtained from the finite element analysis program described in chapter three.

4.1. Control Specimens

Three varieties of control specimens were investigated in order to achieve appropriate baseline data for testing of the entire spectrum of defects analyzed. These three control specimen types were: 1) unstrengthened specimens; 2) non-preloaded, FRP strengthened specimens; and 3) preloaded, FRP strengthened control specimens.

The motivation for using the unstrengthened specimens was to determine the baseline behavior of the RC beam without the application of FRP. This baseline allows us to characterize the virgin beam strength and stiffness such that we can obtain the efficacy of the FRP strengthening of not only specimens with defects, but defect-free FRP strengthened specimens as well. Finally, the unstrengthened control specimens were also utilized to validate the finite element model. The non-preloaded,

strengthened control specimens were used to develop important baseline data for use in set four (effect of excessive of preload cracking) discussed in section 4.4. The final type of control specimen in this study (the preloaded, strengthened control specimen) provided important baseline data utilized in every portion of this investigation. Regardless of the specific defect being investigated, all the remaining specimens were preloaded to induce damage at least to the level of the 35.6kN load these control specimens were subjected to prior to the application of FRP.

4.1.1 Unstrengthened Control Specimens

This group consisted of four tested specimens in which no FRP was applied (specimens: 1, 2, 3, and 30). As can be seen in figure 4-1, all of these specimens had very similar initial stiffness, but varied from 48.6kN to 57.7kN in terms of maximum load. Control 1, Control 2, and Control 3 all came from the first concrete casting. Control 4 was from the second casting and the load displacement plot shows it to behave similar to those from the first casting. Figure 4-2 is a picture of failed specimen Control 2. The other unstrengthened control specimens exhibited very similar cracking patterns and spacing. Table 4-1 details the key beam response characteristics determined from each of these tests.

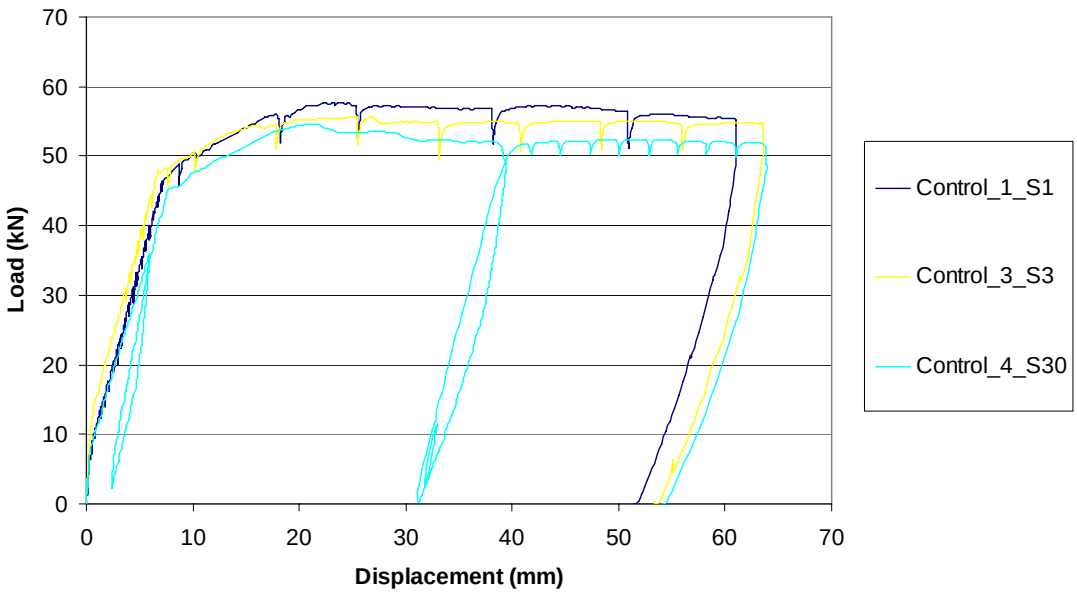

Figure 4-1: Load vs. Displacement plots for the unstrengthened control specimens.

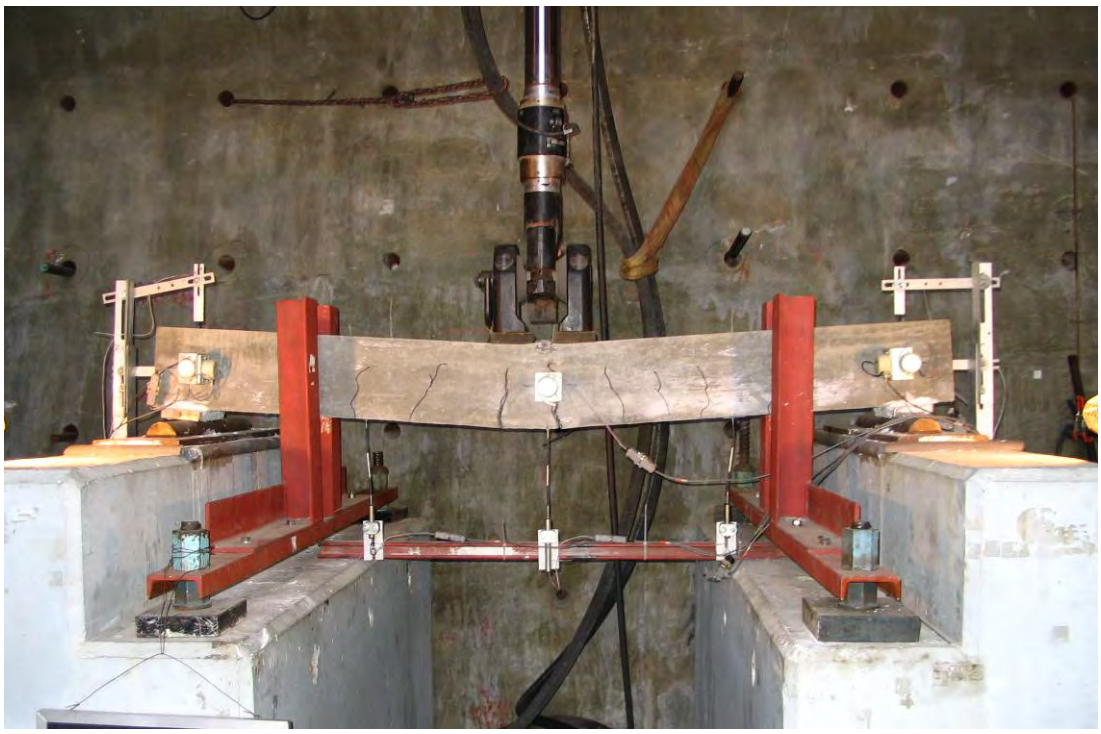

Figure 4-2: Typical failed unstrengthened control specimen.

Table 4-1: Unstrengthened control specimen beam characteristics.

Beam Characteristic	Control_1 (S1)	Control_2 (S2)	Control_3 (S3)	Control_4 (S30)	Average	Std Dev
Maximum Load (kN)	57.74	48.64	55.60	54.64	54.15	3.90
Steel Strain at Yield ($\mu\varepsilon$)	2236	2463	2512	2448	2414.75	122.26
Load at Steel Yield (kN)	46.8	41.64	47.62	45.32	45.35	2.65
Midspan Displacement at Steel Yield (mm)	7.33	7.21	6.98	8.02	7.39	0.45

4.1.2 Non-Preloaded, Strengthened Control Specimens

This subset of specimens consisted of four beams that had been strengthened with two layers of FRP material applied to the tension face of the beam (as described in Sections 2.5 and 2.9), but were not preloaded prior to the application of composite. Figure 4-3 is a picture of the crack pattern and debonding failure of a typical non-preloaded, strengthened beam. The non-preloaded, strengthened beam results in a relatively small, uniform crack spacing compared to the beams that are first preloaded before the application of FRP (as can be seen in Figure 4-3). A representative load-displacement curve can be seen in Figure 4-5. Figure 4-5 is a plot of typical control specimens of each of the three types described in this section. The specimens chosen in this plot and many of the plots in this section are representative specimens for a group of specimens, which will be explained further in the text for each section. Performance changes due to the application of FRP are easily noted in this figure where the non-precracked, strengthened beam reached an average ultimate load of 93.9kN compared to an average of 54.2kN ultimate load by the unstrengthened beam in conjunction with a greater initial stiffness. Figure 4-6 is a plot of the midspan steel

strain in each specimen vs. load. Again, differences in performance may be noted where, as expected, steel yielded at a much higher load in the FRP strengthened beam (73.0kN for the strengthened beam versus 45.4kN for the unstrengthened specimen).

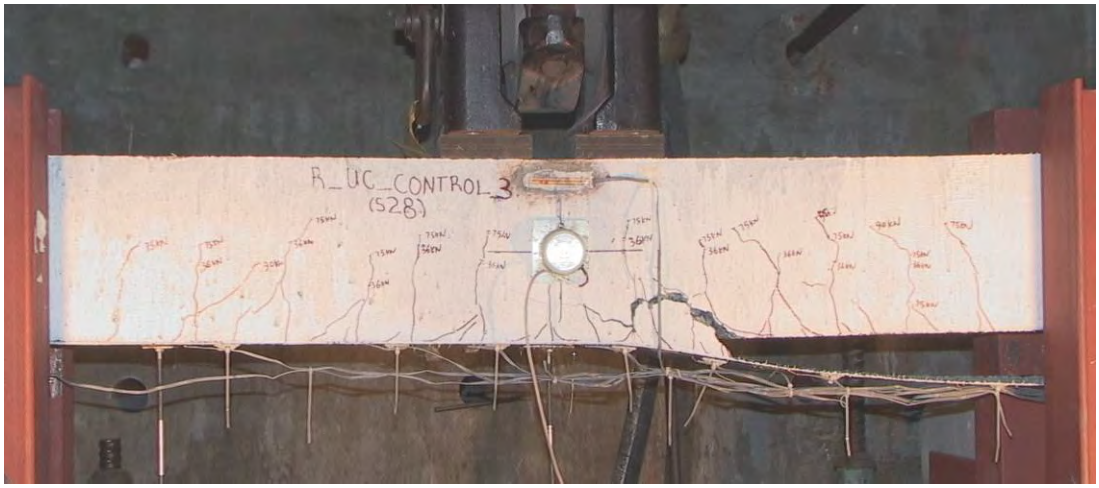

Figure 4-3: Crack pattern and debonding failure of a typical non-preloaded, strengthened beam.

4.1.3 Preloaded, Strengthened Control Specimens

A total of eight control specimens were tested in which the beams were preloaded and rehabilitated, but no defects were built into the specimens. Generally, a preloaded, strengthened control beam was made each time a set of beams were rehabilitated in order to ascertain baseline data for that specific set. After the first three rehabilitations it was found necessary to create a control specimen each time FRP was applied in order to account for the variability. Figure 4-4 shows a typical failed specimen of this type. It should be noted that the crack spacing is generally more variable in the specimens that were preloaded than the non-preloaded, strengthened

and unstrengthened beams. Additionally, average crack spacing and corresponding maximum crack width generally appeared to be greater than in the non-preloaded beams (see table 4-4, for details of crack width). Aside from slight differences in crack patterns, few behavioral differences can be noted between the preloaded and non-preloaded control specimens. In table 4-4, the measured crack widths during testing are shown in millimeters. Measurements of crack widths were taken when the loading process was paused at the top and bottom of each load cycle in the loading protocol (described in section 2.3) where the load returns to near zero after the maximum for each load cycle is reached. Figures 4-5, 4-6, and table 4-2 show how similar the two types of control specimens appeared to behave. Additionally, figure 4-7 shows typical FRP strain profiles for each control specimen type. Notice that the peak FRP strain was measured at or near the beam midspan, as anticipated. It should also be noted that the strain profile for the non-preloaded beam tends to be a more uniform curve, most likely due to the smaller, more uniform crack spacing.

Figure 4-4: Crack pattern and debonding failure of a typical precracked, rehabilitated beam.

Rehabilitation 1 had one uncracked, strengthened beam and one precracked, strengthened beam. Rehabilitation 2 constituted three of each type of control specimen. Because these two sets each had the same number of each type of control specimen, it is easy to compare the performance of the two types. The four non-preloaded, strengthened beams had average response characteristics of 93.9kN peak load, 16.4mm displacement at debonding, and 6886 microstrains in the FRP at debonding with standard deviations of 4.93kN, 0.76mm, and 492 microstrains, respectively. The preloaded beams had comparable average characteristics of 92.6kN peak load, 16.5mm displacement at debonding, and 7020 microstrains at debonding with standard deviations of 3.49kN, 1.63mm, and 267 microstrains, respectively. This data emphasizes the similarities in the global behavior of the two types of strengthened control specimens indicating that preloading at a level of 35.6kN does not appear to cause changes in behavior. It is shown that FRP rehabilitation is very effective in increasing structural performance and that bonding to mildly damaged concrete (due to cracking) may not have a large adverse effect on bond integrity and global performance. However, stress concentrations may exist due to substrate cracking. This is in support of data obtained from earlier investigations on rehabilitating precracked concrete members in which little or no effect of preloading was found (Sharif et al 1994, Arduini and Nanni 1997, Shahawy et al 2001, Seim et al 2001, and Chan and Niall 2001). However, the differences between the local cracking behavior in the two specimen types, as discussed earlier, should not be ignored due to the potential for

large cracks to degrade the bond response over time. The control specimens in set one gives valuable baseline data for the remainder of the results of this investigation.

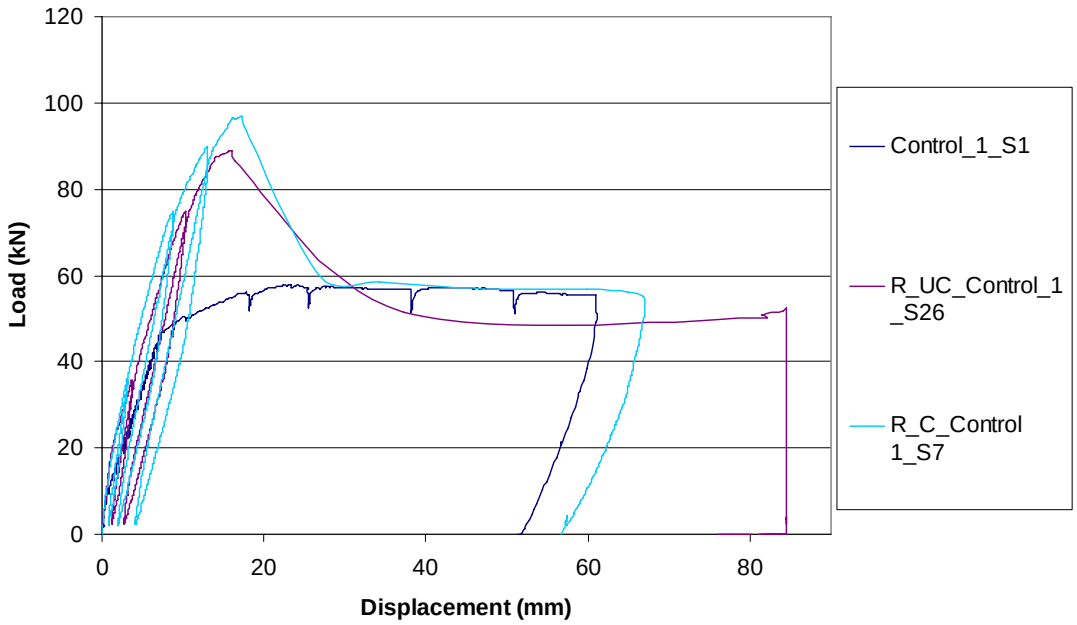

Figure 4-5: Representative Load vs. Displacement plots for the three types of control specimens.

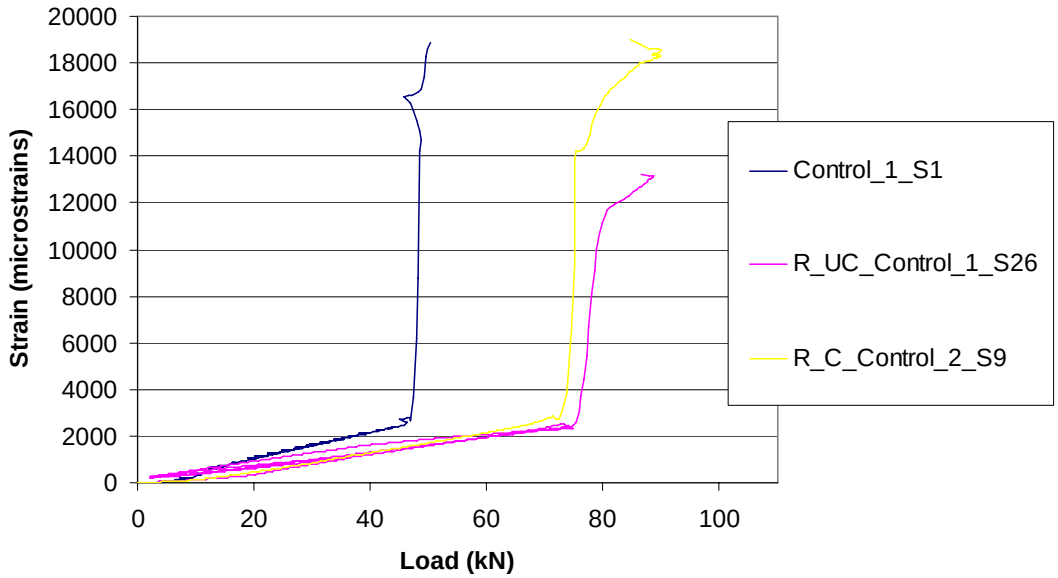

Figure 4-6: Representative Steel Strain vs. Load plots for the three types of control specimens.

Table 4-2: Strengthened control specimen beam characteristics.

Beam Characteristic	UC_1 (S26)	UC_2 (S27)	UC_3 (S28)	UC_4 (S29)	C_1 (S7)	C_2 (S9)
Maximum Load (kN)	88.83	99.03	90.6	97.04	96.8	89.7
Midspan Displacement at Max Load (mm)	16.00	16.97	15.56	17.15	17.25	14.14
Steel Strain at Yield ($\mu\varepsilon$)	2604	2677	2593	2705	2312	2487
Load at Steel Yield (kN)	75.36	75.22	70.34	71.26	76.51	69.14
Midspan Displacement at Steel Yield (mm)	9.56	9.50	8.72	8.80	9.45	7.54
FRP Strain at Steel Yield ($\mu\varepsilon$)	4143	poor data	3863	3580	4692	3740
FRP Strain at Debonding ($\mu\varepsilon$)	6385	poor data	6989	7285	7265	6959
Debonding Direction	Left	Left	Right	Left	Left	Left
Location of Debond Initiation	Left Load-point	Left Load-point	Right Load-point	Left Load-point	Midspan	Left Load-point
Failure Mode	Deep Concrete, Steel	Deep Concrete, Steel	Deep Concrete, Steel	Deep Concrete, Steel	Deep Concrete, Steel	Deep Concrete, Steel

UC = Uncracked (no preloading applied prior to application of FRP)
C = cracked (preloading was utilized to damage the structure)

Table 4-2 (continued): Strengthened control specimen beam characteristics.

Beam Characteristic	C_3 (S6)	C_4 (S10)	C_5 (S18)	C_6 (S36)	C_7 (S42)	C_8 (S47)
Maximum Load (kN)	94.18	89.78	95.87	80.28	89.76	89.95
Midspan Displacement at Max Load (mm)	17.01	17.74	15.65	12.77	16.99	16.42
Steel Strain at Yield ($\mu\varepsilon$)	2312	2417	2401	2453	2430	2558
Load at Steel Yield (kN)	73.1	67.69	70.03	67.2	70.68	69.84
Midspan Displacement at Steel Yield (mm)	8.41	7.88	7.53	7.83	8.00	7.88
FRP Strain at Steel Yield ($\mu\varepsilon$)	3886	3684	3262	3589	2465	3889
FRP Strain at Debonding ($\mu\varepsilon$)	7562	6748	7221	5644	6603	6695
Debonding Direction	Left	Left	Right	Left	Left	Right
Location of Debond Initiation	Right Load-point	Left Load point	Midspan	Left Load point	Left Load point	Right Load-point
Failure Mode	Deep Concrete, Steel	Deep Concrete, Steel	Deep Concrete, Steel	Resin Interface	Thick Concrete Bondline	Deep Concrete, Steel

UC = Uncracked (no preloading applied prior to application of FRP)
C = cracked (preloading was utilized to damage the structure)

Table 4-3: Average response characteristics for strengthened control specimens.

Beam Characteristic	Uncracracked, Strengthened		Preloaded, strengthened		Combined	
	Mean	Std Dev	Mean	Std Dev	Mean	Std Dev
Maximum Load (kN)	93.88	4.93	90.79	5.18	91.82	5.10
Midspan Displacement at Max Load (mm)	16.42	0.76	16.00	1.72	16.14	1.45
Steel Strain at Yield ($\mu\varepsilon$)	2644.75	54.80	2421.25	83.16	2495.75	131.64
Load at Steel Yield (kN)	73.05	2.62	70.52	3.03	71.36	3.04
Midspan Displacement at Steel Yield (mm)	9.15	0.45	8.07	0.62	8.43	0.76
FRP Strain at Steel Yield ($\mu\varepsilon$)	3862.00	281.50	3650.88	628.64	3708.45	549.73
FRP Strain at Debonding ($\mu\varepsilon$)	6886.33	458.70	6837.13	582.76	6850.55	529.47

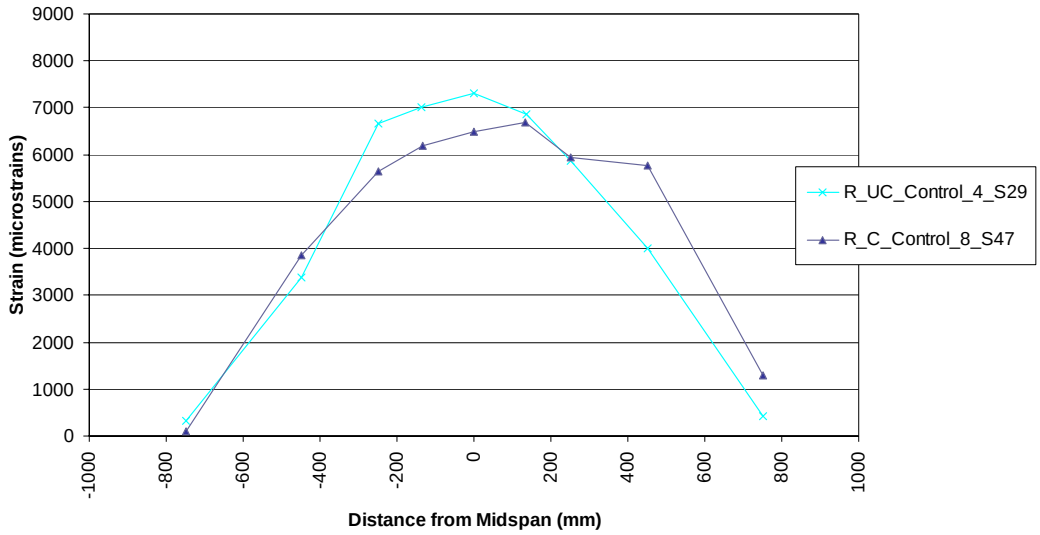

Figure 4-7: Representative strain profiles for preloaded and non-preloaded control specimens.

Table 4-4: Load vs. measured crack width (mm) during testing.

Load (kN)	Control_1 (S1)	Control_2 (S2)	Control_3 (S3)	Control_4 (S30)	UC_1 (S26)	UC_2 (S27)	UC_3 (S28)	UC_4 (S29)
0	0.0	0.0	0.0	0.0	0.0	0.0	0.0	0.0
36	0.20	0.28	0.2	0.22	< 0.1	< 0.1	< 0.1	< 0.1
2.5	-	-	-	-	< 0.1	< 0.1	< 0.1	<0.1
75	-	-	-	-	0.1	0.2	0.1	0.1
2.5	-	-	-	-	-	-	-	<0.1
90	-	-	-	-	-	-	-	0.3
2.5	-	-	-	-	-	-	-	0.1
Load (kN)	**C_1 (S7)**	**C_2 (S9)**	**C_3 (S6)**	**C_4 (S10)**	**C_5 (S18)**	**C_6 (S36)**	**C_7 (S42)**	**C_8 (S47)**
0	0.00	0	0	<0.1	<0.1	<0.1	<0.1	<0.1
36	< 0.10	< 0.1	< 0.1	<0.1	<0.1	< 0.1	< 0.1	< 0.1
2.5	< 0.10	< 0.1	< 0.1	<0.1	<0.1	< 0.1	< 0.1	< 0.1
75	0.1	0.2	0.2	0.1	0.1	0.3	0.3	~0.08
2.5	< 0.10	-	-	<0.1	<0.1	0.1	0.1	< 0.1
90	0.9	-	0.3	0.3	0.3	-	-	0.4
2.5	-	-	0.1	-	0.1	-	-	0.3

Control = Unstrengthened control specimen (no FRP applied)
UC = Uncracked (no preloading applied prior to application of FRP)
C = cracked (preloading was utilized to damage the structure)

A key limitation in the ability to determine the global influence of defects during this investigation was the existence of five different failure modes. These failure modes resulted in unexpected variations in behavior at near ultimate loads. For full descriptions of these five failure modes, see section 5.1 and appendix A. Three of these failure modes were observed during testing of the control specimens. From the strongest failure mode to weakest, they are debonding by “deep concrete, steel”, debonding through a “thick concrete bondline”, and debonding through the “resin interface” (see figure 5-1). Figure 4-8 shows the load versus midspan displacement for a typical specimen from each of these failure modes and figure 4-9 shows the FRP strain profile for these same specimens. Specimen 6 (R_C_Control_3_S6) failed by debonding through a “thick concrete bondline”. As expected from the specimen type, this specimen failed at the greatest load and at the greatest displacement. It also failed with the greatest measured FRP strain at ultimate load of 7562 microstrains. Specimen 42 (R_C_Control_7_S42) failed by debonding through a “thick concrete bondline”. This specimen failed at a slightly lower maximum load and midspan displacement and significantly lower maximum measured FRP strain than specimen 6. Specimen 36 (R_C_Control_6_S36) failed by debonding through the “resin interface”. Specimen 36 also failed at the lowest load and least displacement at debonding of the three specimens. The measured FRP debonding strain at 5644 microstrains was the least of the three specimens, 22.2% less than specimen 42. Often these debonding failure mode effects dominated the specimen behavior not only for the control specimens, but

also for specimens with defects, effectively masking some of their effects. Because of this influence, the specimens analyzed in each defect set described in this chapter are broken down further by failure mode to make comparisons more relevant.

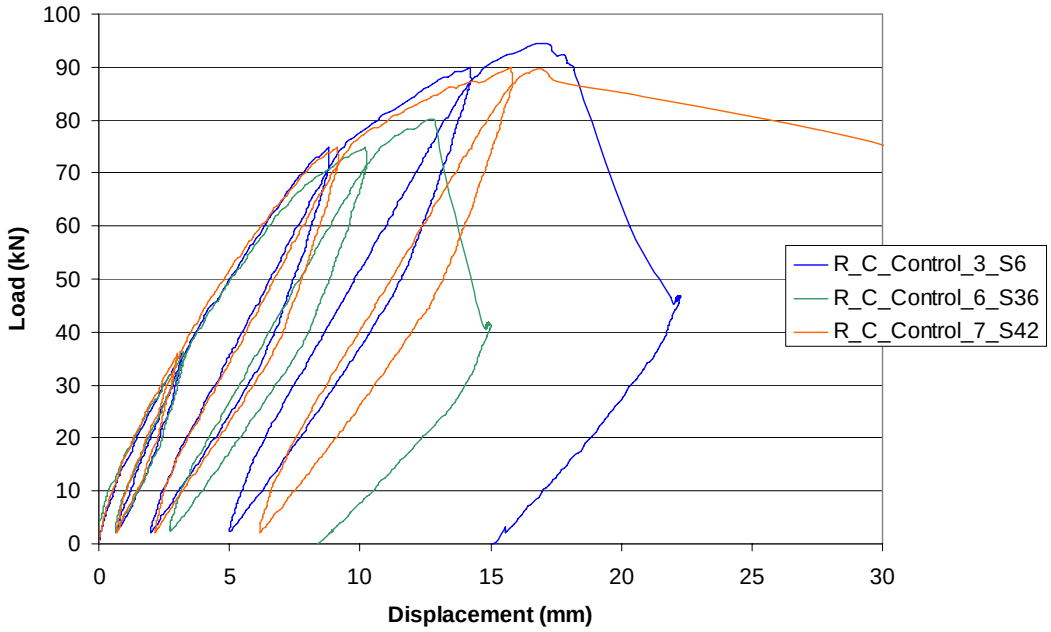

Figure 4-8: Representative load versus midspan displacement plots for the three different debonding failure modes observed during testing of the control specimens.

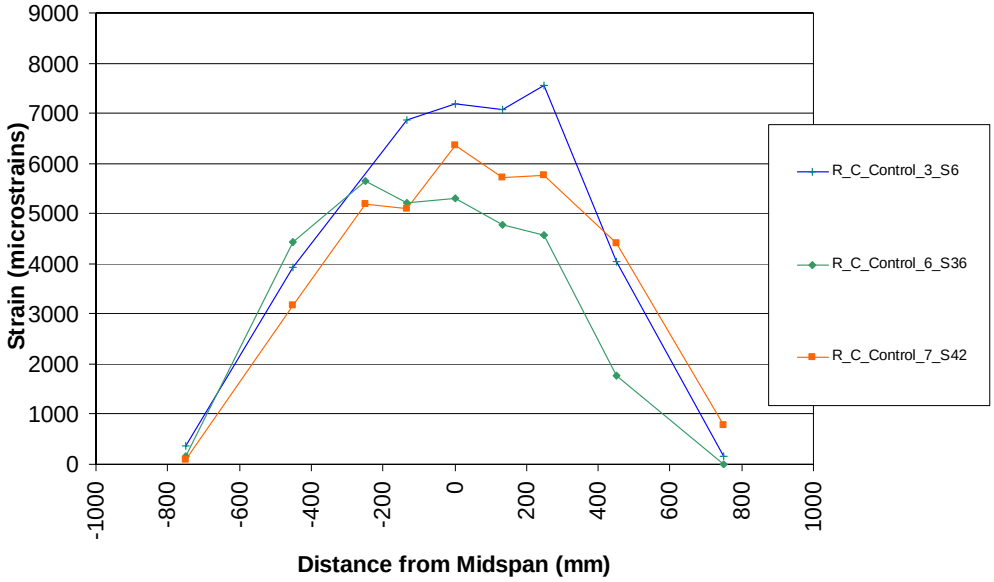

Figure 4-9: Representative strain profiles the three different debonding failure modes observed during testing of the control specimens.

4.2. Critical Disbond Size

In order to investigate the critical size of a disbond, a series of specimens were tested with varying sizes of disbonds all placed with a common centroidal location in the adhesive layer as described in section 2.4.1 and sketched as an example in figure 4-10. The location chosen for determining critical disbond size was 185mm from the midspan of the beam (see figure 2-4 for reference). This is a location in which the beam is subjected to high shear and moment and therefore is often the location in which debonding is observed to initiate in many of the control specimens discussed earlier. Two different configurations were used to investigate the effect of disbond size: Circular, and rectangular shaped disbonds.

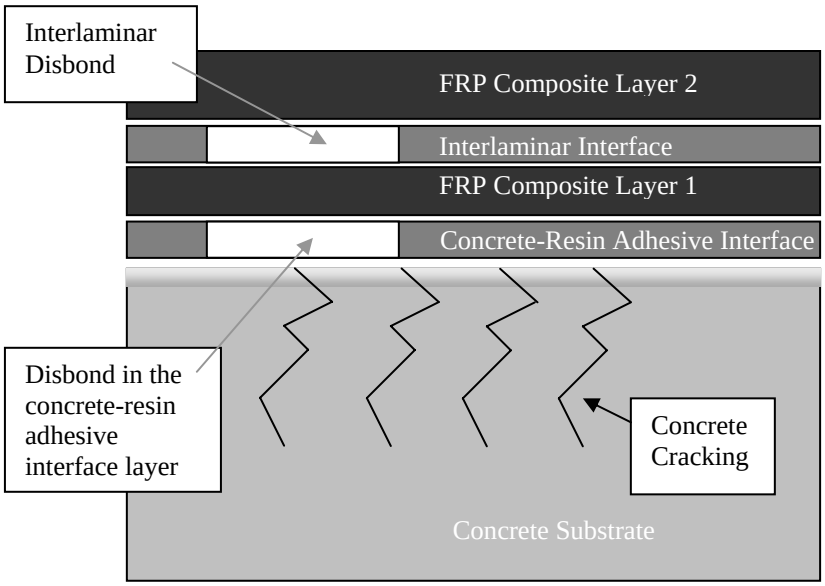

Figure 4-10: Sketch of disbond locations

4.2.1 Circular Disbond

The circular disbonds investigated in this study were placed in the center of the beams width, as shown in figure 4-11. This set constituted a total of nine beams, not including the baseline control specimens. The circular disbonds investigated ranged in size from 25mm to 150mm (the full width of the beam) in diameter. A summary of the beams tested and their behavior characteristics can be found in table 4-5.

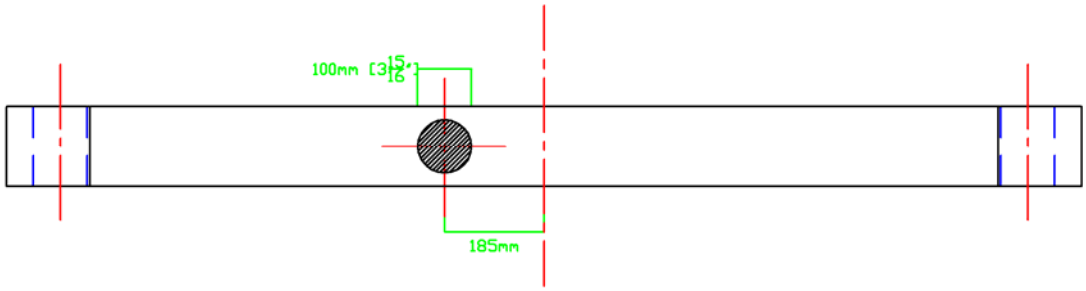

Figure 4-11: Example placement of a 100mm diameter circular disbond for investigating the critical defect size.

Table 4-5: Beam behavior characteristics for determination of critical circular disbond size.

Beam Characteristic	25mm (S12)	25mm (S59)	50mm (S21)	50mm (S60)	100mm (S15)	100mm (S16)	100mm (S5)	150mm (S17)	150mm (S22)
Maximum Load (kN)	98.88	100.23	100.85	96.54	84.5	86.27	85.63	92.2	89.78
Displacement at Maximum Load (mm)	19.21	16.58	17.95	14.97	19.7	14.86	14.19	15.26	15.47
Steel Strain at Yield ($\mu\varepsilon$)	2521	2398	2372	2343	2359	2463	2344	2389	2351
Load at Steel Yield (kN)	72.22	66.54	73.61	71.04	59.5	71.76	66.40	82.61	68.40
Midspan Displacement at Steel Yield (mm)	8.12	6.64	8.46	7.87	7.24	7.98	4.99	11.73	7.48
FRP Strain at Steel Yield ($\mu\varepsilon$)	3579	3221	3742	3482	3419	3708	3435	4955	3964
FRP Strain at Debonding ($\mu\varepsilon$)	7788	7708	6858	6483	8679	6330	6069	6082	6624
Debonding Direction	Left	Left	Right	Right	-	Left	Left	Right	Left
Location of Debond Initiation	Midspan	Left Load-Point	Right Load-Point	Right Load-Point	Right Load-Point	Left Load-Point	Midspan	Right Load-Point	Left Load-Point
Failure Mode	Deep Concrete, Steel	Deep Concrete, Steel	Deep Concrete, Steel	Deep Concrete, Steel	FRP Rupture	Thick Concrete Bondline	Deep Concrete, Steel	Deep Concrete, Steel	Thick Concrete Bondline

When considering the load vs. midspan displacement plots for this group of specimens, three different trends are evident: 1)beams that fail at a high load and a high displacement; 2) beams that fail at a relatively lower load and a lower displacement; and 3) those that fail at a low load, but a high displacement. Figure 4-12 is a plot containing a curve that represents each of these three behaviors. These three curves each represent a different failure mode observed during testing of this specimen set. These failure modes are “deep concrete, steel”, “thick concrete bondline”, and “FRP rupture”, respectively. The beam that represents the deep concrete, steel failure in figure 4-12 is specimen 12, the 25mm diameter disbond located 185mm from the midspan (25C_185_S12). The beams that fall in this category are specimen 59 (25mm), specimen 21 (50mm), specimen 12 (25mm), specimen 60 (50mm), specimen 5 (100mm), and specimen 17 (150mm). The low load and low displacement failure (thick concrete bondline failure) is represented by specimen 22 with a 150mm diameter disbond (150C_185_S22_2). The beams tested that fall in this category are specimen 16 (100mm) and specimen 22 (150mm). Only one specimen falls in the third category of failing at low load, but high displacement (due to FRP rupture): Specimen 15. This specimen behaved different from the others because it was inadvertently rehabilitated with only one layer of FRP, decreasing the structural stiffness, and changing the failure mode from debonding to FRP rupture. From the load displacement plots all of the beams from the first two sets had very similar initial stiffness of 9.00kN/mm.

Figure 4-13 is a plot of the typical steel strain vs. load data collected for specimens with the defects considered in this group as well as the two types of FRP strengthened control specimens. Specimen stiffness up to yield load is very similar for all of the specimens considered. However, after yield differences may be noted. The non-preloaded control beam (R_UC_Control_1_S26) in the figure has a lower slope after yield than the preloaded beams. This suggests that the load is being transferred to the FRP more effectively in the non-preloaded beam. The yield load in the two beams with disbonds occurred at loads lower than 75kN, whereas the yield in the control specimens occurred at a load greater than 75kN. Thus, the 75kN load cycle can be seen to occur between 6000 microstrains and 10,000 microstrains, whereas, this cycle follows the pre-yielding path for the control specimens.

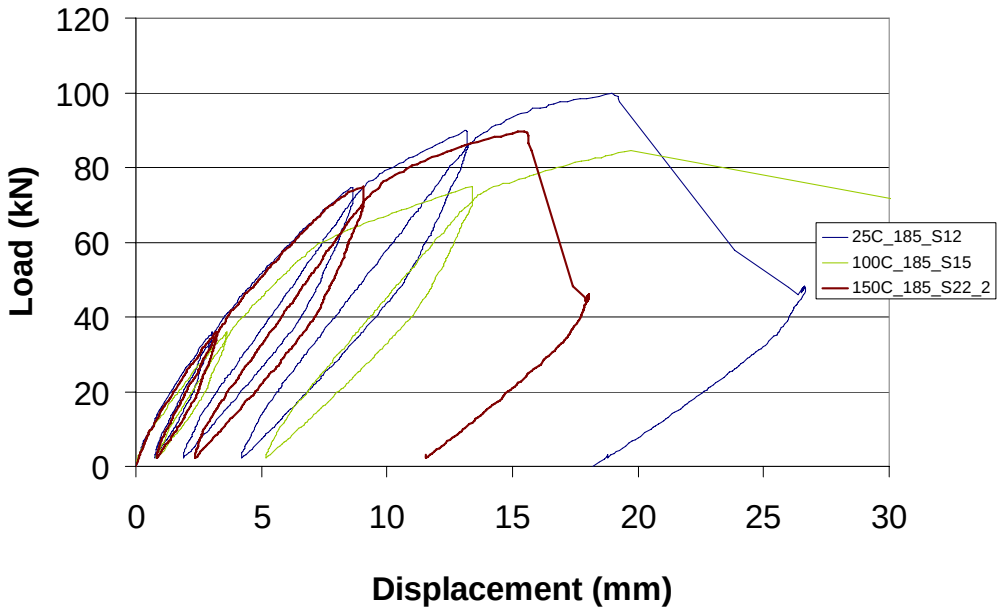

Figure 4-12: Characteristic load vs. midspan displacement plots for circular disbonds with different failure modes.

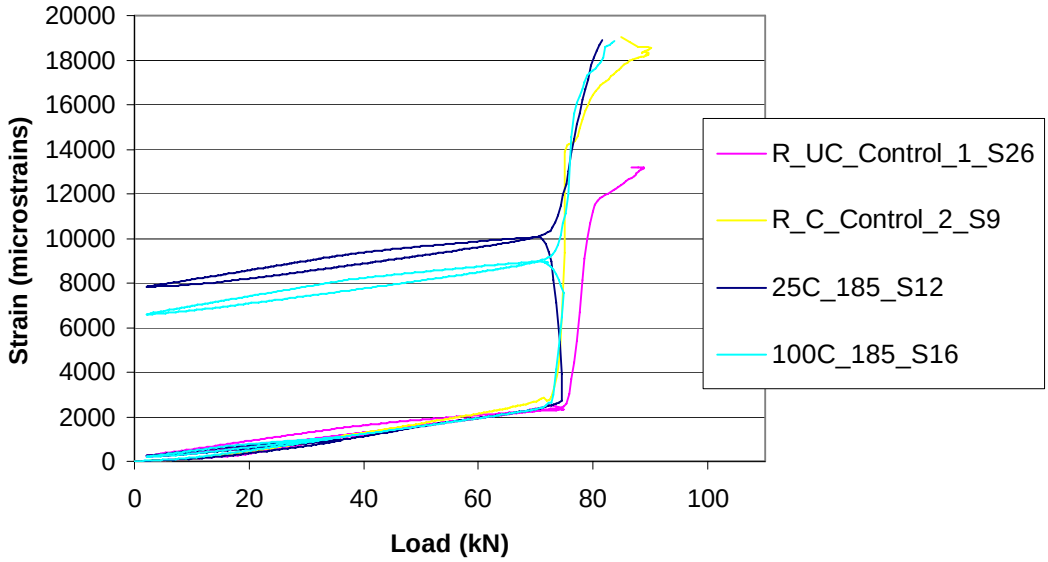

Figure 4-13: Representative Steel Strain vs. Load plots for representative circular disbond specimens and the control specimens.

Figure 4-14 shows pictures of two of the typical failed specimens. The top picture is of a beam with a 100mm diameter disbond while the bottom specimen had a disbond 150mm in diameter. Average crack spacing for these specimens is between 25mm to 50mm. The circled regions are the approximate locations of the disbonds. As can be seen in these pictures, often very little new cracking occurs during final testing within the length of the defect. Instead, large diagonal cracks tend to form on each side of the defect. These diagonal cracks were often observed to be at the same location from which debonding originated. This behavior was even more prominent in beams tested with rectangular shaped disbonds discussed in section 4.2.2.

Figure 4-14: Typical cracking patterns for specimens with circular disbond defects. The circled regions represent the approximate locations of the disbond(s).

Figure 4-15 shows characteristic FRP strain profiles for the specimens with circular disbonds considered in this section compared to a typical control specimen. The location of the center of the defect is 185mm to the left of the midspan, as noted earlier. At this location, a drop in FRP strain is apparent because no shear stress can be transferred. Instead only tension is carried. However, slight increases in strain were noted at each edge of the disbond where the bond resumed. This stress concentration in conjunction with the diagonal cracking seems to play a large role in the mechanism initiating debonding. Specimens with larger disbonds tend to result in larger crack

widths at ultimate load, despite having similar global stiffness. Table 4-6 show the maximum crack widths at the low load level and high load level of each load cycle for each specimen. The specimens in the table are labeled such that the first term is the defect size and the term in parenthesis underneath is the specimen number (example: (S12)) so each individual beam may be referenced in the appendix.

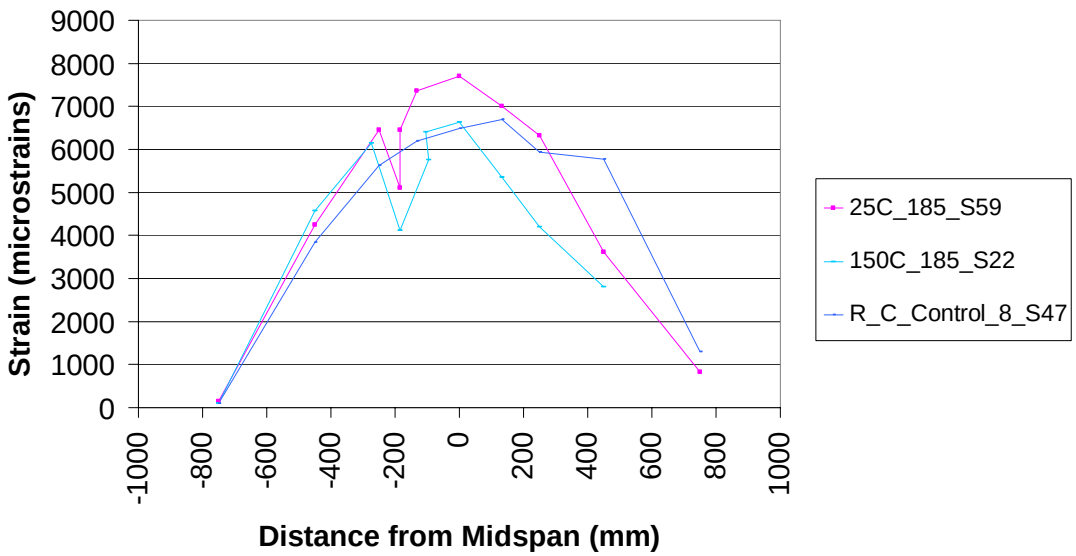

Figure 4-15: Representative strain profiles for beams with circular disbonds.

Table 4-6: Load vs. measured crack width (mm) during testing.

Load (kN)	25mm (S12)	25mm (S59)	50mm (S60)	50mm (S15)	100mm (S16)	100mm (S5)	150mm (S17)	150mm (S22)
0	<0.1	<0.1	<0.1	<0.1	<0.1	<0.1	0	<0.1
36	< 0.1	<0.1	< 0.1	< 0.1	<0.1	<0.1	< 0.1	0.1
2.5	< 0.1	<0.1	<0.1	<0.1	<0.1	<0.1	<0.1	<0.1
75	0.1	0.1	<0.1	0.4-0.5	0.1	0.3	0.2	0.4
2.5	< 0.1	<0.1	<0.1	0.1	<0.1	<0.1	0.1	-
90	0.3	0.3	0.2	0.5	-	-	0.5	-
2.5	-	0.15	0.1	-	-	-	0.2	-

Figures 4-16 and 4-17 show the maximum average load and maximum average displacement at debonding for each disbond diameter considered. Despite the crack patterns and local stress concentrations observed earlier, it is difficult to determine how the global performance of the beams is affected by the disbonds without accounting for the effect of the variable failure modes. One of the 100mm and one of the 150mm specimens debonded by the “thick concrete bondline” failure mode, whereas the other specimens (including all 25mm and 50mm diameter disbonds) failed by debonding through the “deep concrete, steel” failure mode causing a straight across comparison to be difficult. Still, the trend exists that the small disbonds (less than or equal to 50mm in diameter) and the control specimens without defects had greater maximum loads and greater displacements at debonding than the specimen with large circular disbonds (greater than or equal to 100mm).

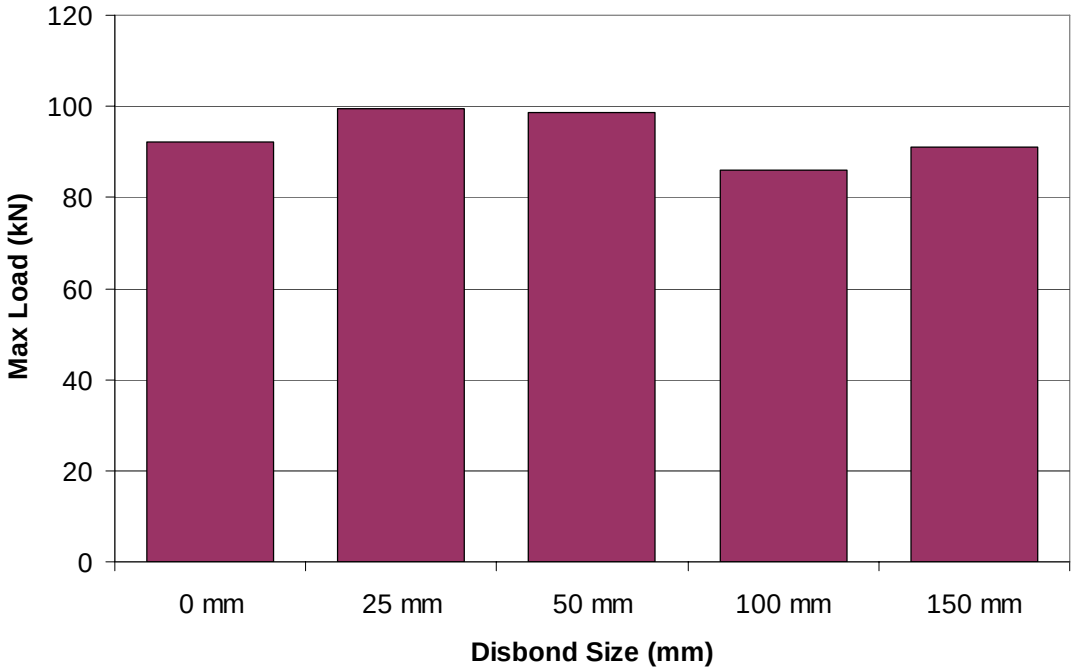

Figure 4-16: Max load vs. circular disbond diameter.

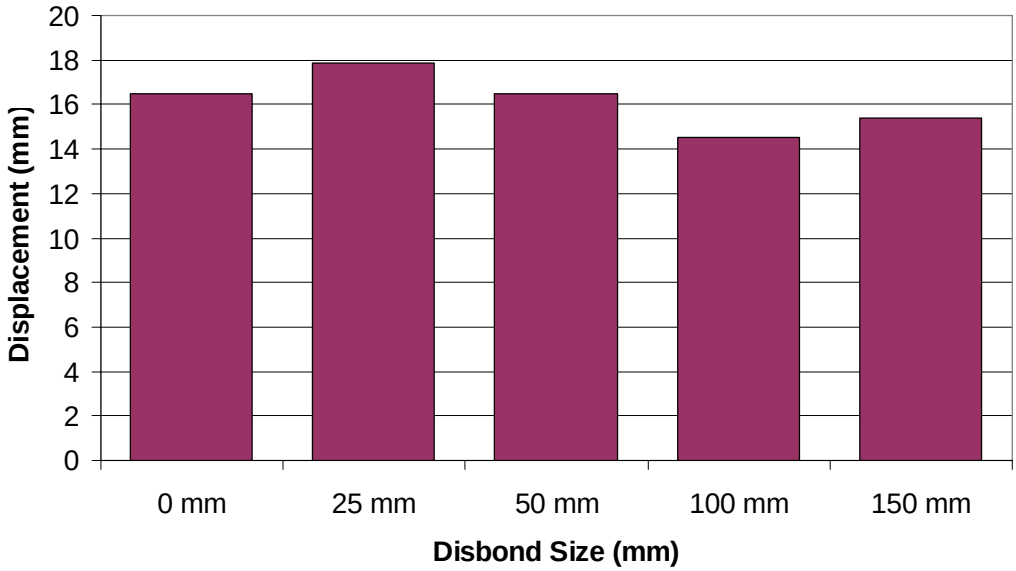

Figure 4-17: Displacement at debonding vs. circular disbond diameter.

In order to effectively eliminate the influence of the various failure modes, behavior of specimens failing by the “deep concrete, steel” failure mode only are compared in Figures 4-18 to 4-21. The average maximum load for each disbond diamter of 25mm, 50mm, 100mm, and 150mm are 99.6kN, 98.7kN, 85.6kN, and 92.2kN microstrains respectively as shown in figure 4-18, indicating decrease in capacity as disbond diameter increases. The displacement at debonding follows a similar trend shown in figure 4-19 where midspan displacements of 17.9, 16.5, 14.2, and 15.3mm were measured. The average values of FRP strain at debonding for each specimen for the 25mm, 50mm, 100mm, and 150mm diameter disbonds are 7748, 6670, 6069, and 6082 microstrains respectively as shown in figure 4-20, indicating that the maximum FRP strains decrease as the disbond size increases. In the same order, average steel strains at yield are 2460, 2357, 2344, and 2389 microstrains, suggesting a decreasing trend as well. Excluding specimen 5, the average load at steel yield for this subset increased with disbond diameter giving values of 69.4kN, 72.3kN, and 82.6kN for 25mm, 50mm, and 150mm specimens respectively, suggesting that the large disbonds may be changing the load path such that the FRP is being activated earlier in the loading process due to the large cracks found near the disbond edges. Evidence supporting this suggestion can be seen in figure 4-21, noting the FRP stress concentrations found near the defect location at steel yielding load. Generally, there seems to be a trend of decreased beam performance with the increased diameter of circular disbonds, although these trends do not suggest a large or critical influence on

specimen behavior despite the presence of relatively large unbonded areas compared to the specimen geometry.

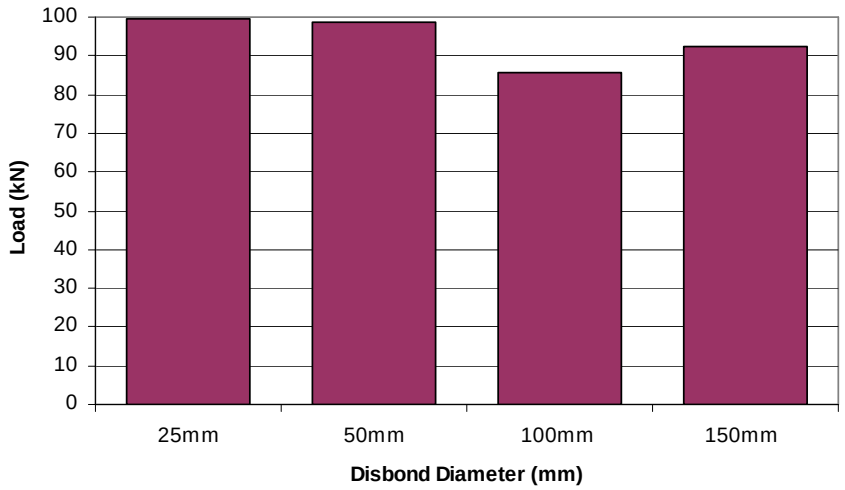

Figure 4-18: Maximum load vs. circular disbond diameter for "deep concrete, steel" failure mode.

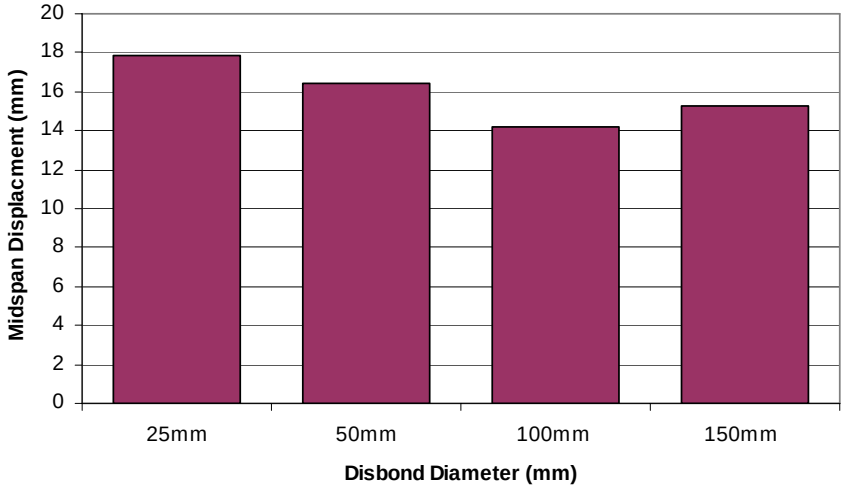

Figure 4-19: Displacement at debonding vs. circular disbond diameter for "deep concrete, steel" failure mode.

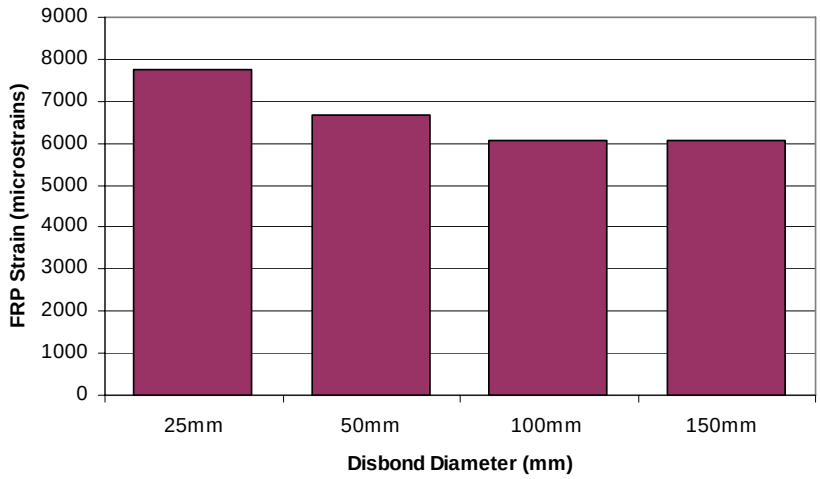

Figure 4-20: Peak FRP strain vs. circular disbond diameter for "deep concrete, steel" failure mode.

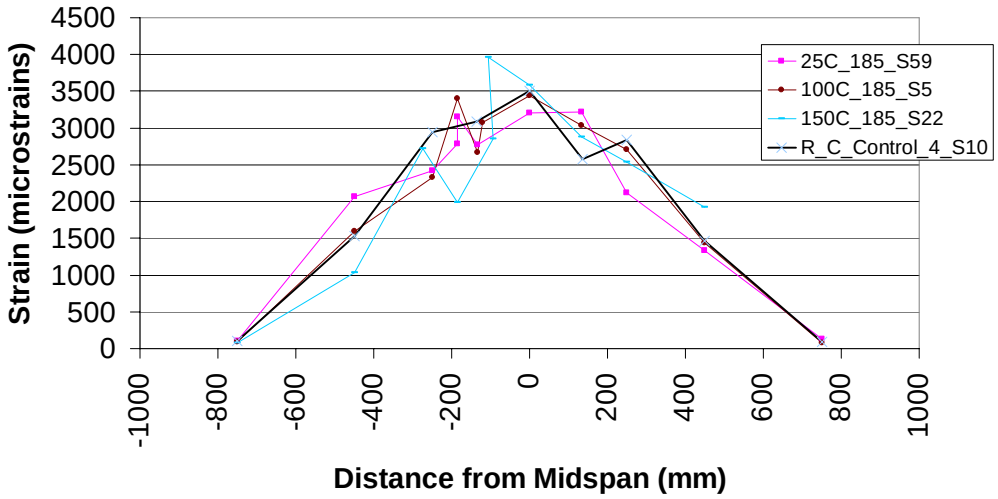

Figure 4-21: FRP strain profile at steel yielding load.

4.2.2 Rectangular Disbonds

Similar to the investigation described in section 4.2.1 for determining the effect of different sizes of circular disbonds, the centroid of the rectangular disbond was located 185mm from the midspan in the most critical debonding region of the beam as

shown in figure 4-22. As described in detail in section 2.4.1, the rectangular disbonds varied in length from 25mm to 250mm and spanned the full 150mm width of the beam. A summary of the beams tested in this set and their behavioral characteristics can be found in table 4-7. Further details pertaining to the individual test specimen results can be found in Appendix A.

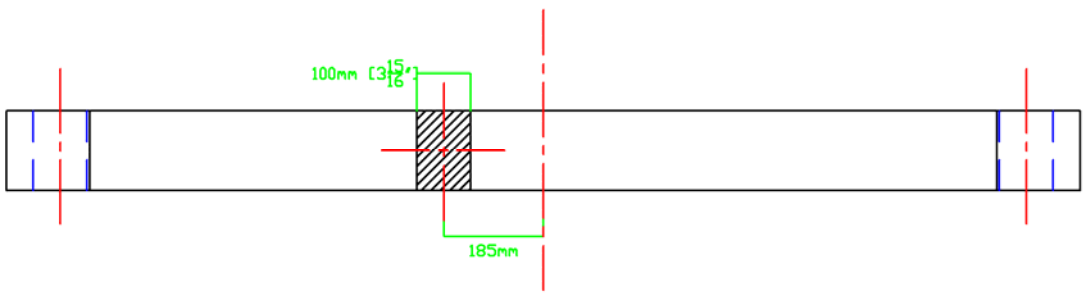

Figure 4-22: Placement of a 100mm rectangular disbond for investigating the critical defect size.

The load-displacement data for all of the specimens tested in this set is largely similar until the point at which debonding initiates. Figure 4-23 is a plot of two load vs. displacement curves that are representative of the common failures found in this set of beams. The specimens used as representative specimens in figure 4-23 are specimen 32 (full name: 50R_185_S32) and specimen 46 (full name: 50R_185_S46). From the figure it can be shown that until a load of 80kN is attained, the specimen stiffnesses are very similar. The point where the plots begin to diverge (approximately 80kN) is likely the point where local debonding began to occur and the specimen began losing

stiffness. The specimens that behaved most like the stronger curve (represented by specimen 50R_185_S46) in this set are defined as those that reached at least the peak of the 90kN load cycle. These specimens and their respective defect size include: specimen 13 (25mm), specimen 46 (50mm), specimen 8 (100mm), specimen 14 (150mm), specimen 33 (150mm), and specimen 61 (200mm). The failure modes observed for testing of these specimens consisted of two “deep concrete, steel,” three “thick concrete bondline,” and one “thin concrete bondline”. This group of specimens performed very similarly to control specimens S7, S9, S6, S10, S18, and S47 in which all of these control specimens failed with the failure mode defined earlier in table 4-3 as “deep concrete, steel,” in which debonding occurs by tearing the cover concrete down to the depth of the steel reinforcement. Further details on the various failure modes encountered and their significance during testing, can be found in appendix A and section 5.1. The remainder of the specimens which failed before reaching the top of the 90kN load cycle were specimen 19 (50mm), specimen 32 (50mm), specimen 4 (100mm), specimen 31 (100mm), specimen 38 (100mm), specimen 11 (150mm), specimen 34 (200mm), specimen 35 (250mm), and specimen 49 (250mm). In contrast to the stronger group of beams this group of beams comprised no beams failing by “deep concrete, steel,” but three through a “thick concrete bondline,” four through a “thin concrete bondline,” and two through the “resin interface.” It is important to realize that the two representive curves for each group in the load vs. displacement plots are of beams containing identical defects. They were shown to behave very similarly for most of their loading cycles and do not behave differently until near

ultimate load. At this point it seems the difference in behavior is dominated by the difference in failure mode due to material differences not related to the defect.

Table 4-7: Beam behavior characteristics for determination of critical rectangular disbond size.

Beam Characteristic	Size(S#) 25mm(S13)	50mm(S19)	50mm(S32)	50mm(S46)	100mm(S8)	100mm(S4)	100mm(S31)	100mm(S38)
Maximum Load (kN)	93.06	87.89	83.59	93.67	90.11	83.5	80.28	86.68
Displacement at Maximum Load (mm)	16.5	13.57	12.42	13.13	15.06	15.5	12.00	14.19
Steel Strain at Yield ($\mu\varepsilon$)	2487	2497	2395	2387	2437	2385	2353	2507
Load at Steel Yield (kN)	68.38	66.4	68.93	69.2	67.26	68.84	65.99	66.90
Midspan Displacement at Steel Yield (mm)	8.14	7.38	7.64	7.61	7.75	8.48	7.55	7.69
FRP Strain at Steel Yield ($\mu\varepsilon$)	3775	3308	3357	3708	3130	3568	3589	4176
FRP Strain at Debonding ($\mu\varepsilon$)	6894	6858	5804	7180	6787	6261	6658	7068
Debonding Direction	Left	Left	Left	Left	Left	Right	Left	Right
Location of Debond Initiation	Midspan	Left Load-Point	Defect	Right Load-Point	Right Load-Point / Defect	Right Load-Point	Left Load-Point	Left Load-Point
Failure Mode	Thick Concrete Bondline	Thick Concrete Bondline	Thin Concrete Bondline	Deep Concrete, Steel	Deep Concrete, Steel	Thick Concrete Bondline	Resin Interface	Resin Interface

Table 4-7 (continued): Beam behavior characteristics for determination of critical rectangular disbond size.

Beam Characteristic	150mm(S14)	150mm(S11)	150mm(S33)	200mm(S34)	200mm(S61)	250mm(S35)	250(S49)
Maximum Load (kN)	89.94	88.78	92.34	82.25	90.05	88.30	87.80
Displacement at Maximum Load (mm)	12.72	14.91	14.54	13.14	13.30	13.47	13.85
Steel Strain at Yield ($\mu\varepsilon$)	2735	2377	2316	2505	2227	2232	2318
Load at Steel Yield (kN)	73.18	72.15	68.12	66.00	65.30	57.60	66.00
Midspan Displacement at Steel Yield (mm)	8.45	8.92	7.05	7.51	6.93	5.36	7.06
FRP Strain at Steel Yield ($\mu\varepsilon$)	3483	4335	3225	3438	3167	4615	3573
FRP Strain at Debonding ($\mu\varepsilon$)	5858	8354	8600	6101	6684	7233	6790
Debonding Direction	Left	Left	Left	Left	Left	Left	Left
Location of Debond Initiation	Left Load-Point / Defect	Left Load-Point / Defect	Midspan / Defect	Defect	Defect	Midspan	Defect
Failure Mode	Thick Concrete Bondline	Thick Concrete Bondline	Thick Concrete Bondline	Thin Concrete Bondline	Thin Concrete Bondline	Thin Concrete Bondline	Thin Concrete Bondline

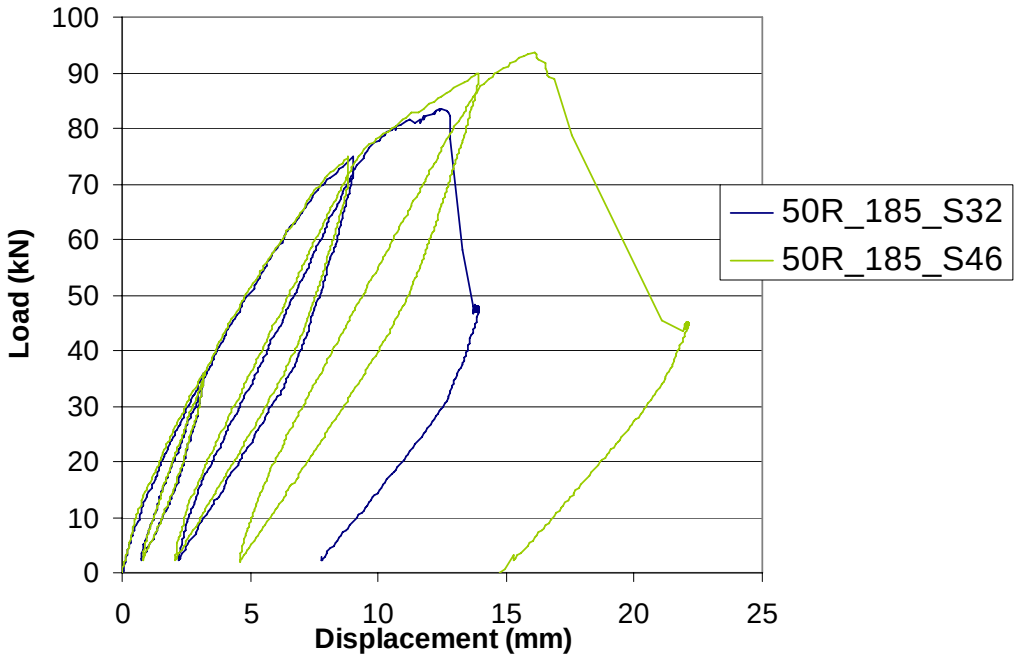

Figure 4-23: Characteristic load vs. displacement plots for rectangular disbond sets.

Figure 4-24 depicts representative steel strain vs. load plots for two of the uncracked control specimens, the precracked control specimens, and two beams from the rectangular disbond set (specimens 13 (25mm) and 34 (200mm)). There is very little difference to be noted between the specimens with defects plotted here. However, similar to the specimens with a circular disbond, the yield load is reached at a lower load level, indicating that perhaps the disbond causes more of the load to be distributed to the steel up to the point of steel yield. This was somewhat contradictory to what was suggested previously in section 4.2.1.

Figure 4-25 shows several of the failed specimens tested in this set of rectangular disbonds. In the pictures the approximate region in the beam where the

disbond was placed is circled. Due to the absence of shear load transfer between the FRP and the concrete across the unbonded region, often little or no new cracking would be observed in this region during final testing of the beams. However, to account for this absence of cracking within the disbond length, generally a large diagonal crack with a large crack width would occur near the left or right edge of the disbond where the stress concentration was measured in the FRP (see the strain profile in figure 4-26). These large cracks were typically observed to be the source of debonding initiation and are indicated in the photos in figure 4-21 by arrows pointing to them.

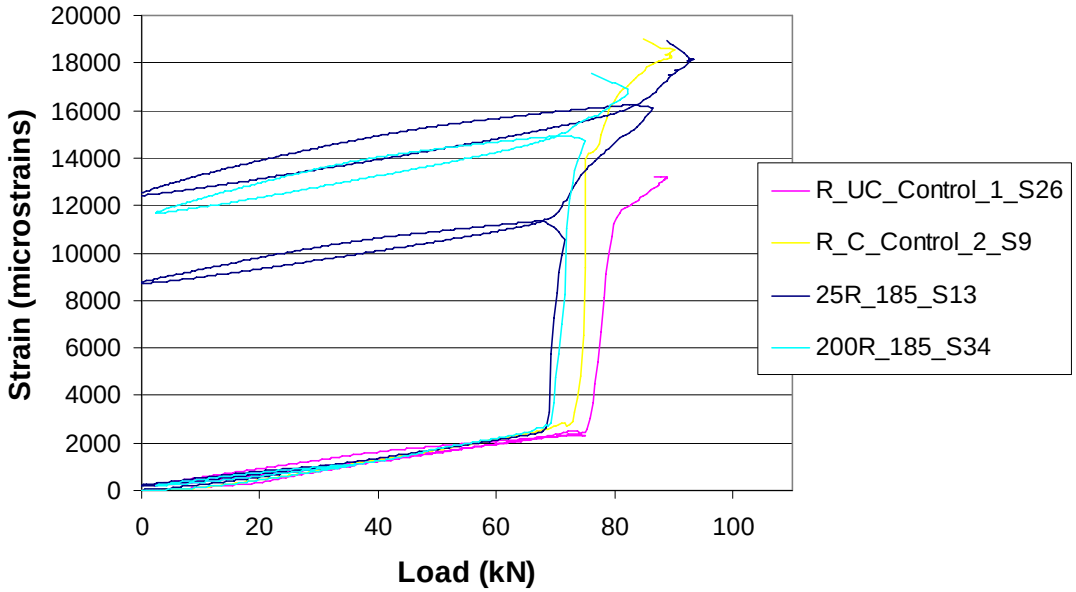

Figure 4-24: Representative Steel Strain vs. Load plots for representative rectangular disbond specimens and the control specimens.

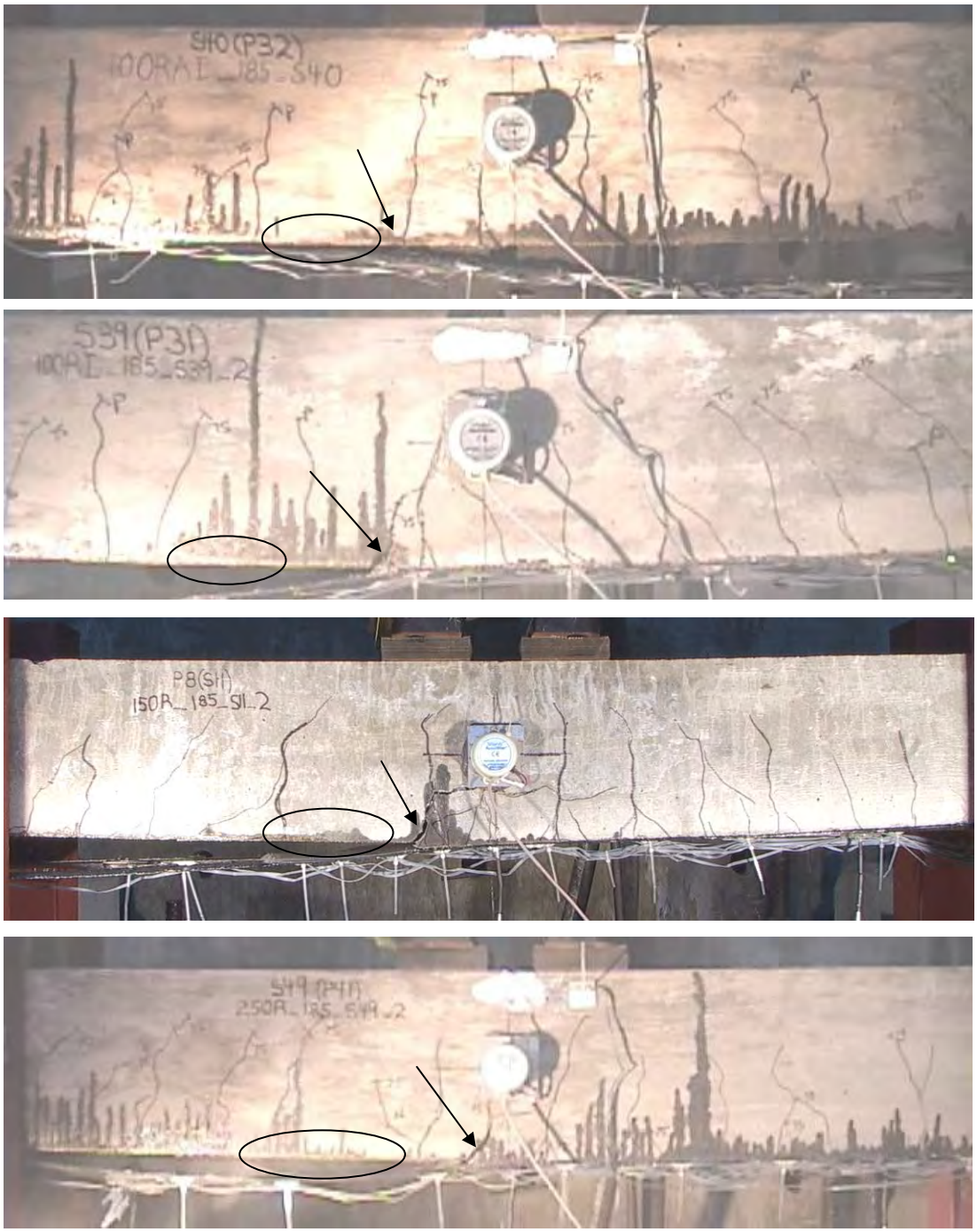

Figure 4-25: Typical cracking patterns for specimens with disbond defects. The circled regions represent the approximate locations of the disbond(s).

Figure 4-26 is a representative plot of strain profiles at ultimate load for typical specimens with rectangular disbonds compared to a typical control specimen. Specimens 11 and 49 were chosen here because they had large disbond sizes of 150mm and 250mm respectively. Specimens with large disbonds had particularly pronounced stress concentrations in the disbond region. The peak strains measured at ultimate load were located near the edges of the disbond as opposed to the control specimens which usually had peak strains near the midspan. Specimens with and without defects typically debonded at similar maximum strains, however the location of debonding was strongly influenced by the defect location.

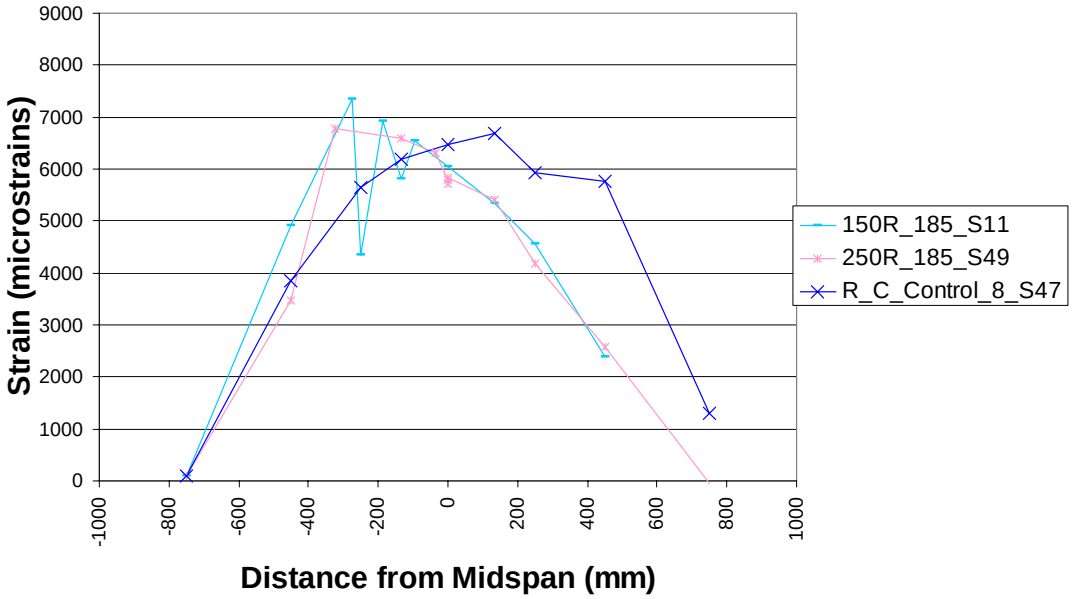

Figure 4-26: Representative strain profiles for beams with rectangular disbonds.

Table 4-8: Load vs. measured crack width (mm) during testing.

Load (kN)	25mm (S13)	50mm (S19)	50mm (S32)	50mm (S46)	100mm (S8)	100mm (S4)	100mm (S31)	100mm (S38)
0	0	0	<0.1	<0.1	0	0	<0.1	<0.1
36	< 0.1	< 0.1	<0.1	<0.1	< 0.1	< 0.1	0.1	<0.1
2.5	<0.1	<0.1	<0.1	<0.1	<0.1	<0.1	<0.1	<0.1
75	0.1	0.2	0.1	0.1	0.1	0.2	0.4	0.5
2.5	<0.1	<0.1	<0.1	<0.1	<0.1	0.1	<0.1	0.2
90	0.3			0.4	-	-	-	-
2.5	-	-	-	0.25	-	-	-	-

XXmm = Disbond length
(Sxx) = Specimen Number

Load (kN)	150mm (S14)	150mm (S11)	150mm (S33)	200mm (S34)	200mm (S61)	250mm (S35)	250mm (S49)
0	0	0.1	<0.1	<0.1	<0.1	<0.1	<0.1
36	< 0.1	<0.1	0.1	<0.1	<0.1	< 0.1	< 0.1
2.5	<0.1	0.5	<0.1	<0.1	<0.1	< 0.1	< 0.1
75	0.4	0.1	0.4	0.3	0.4	0.3	0.3
2.5	-	-	0.1	0.2	0.2	0.1	0.1
90	-	-	0.6	-	0.7	-	-
2.5	-	-	-	-	0.4	-	-

Table 4-8 shows the measured crack width at the peak and bottom of each load cycle for this set of specimens. Similar to the circular disbonds, it is noted that the larger disbond sizes generally results in larger crack widths, particularly near levels of ultimate load. These are often the same cracks that are referenced by the arrows in figure 4-21.

Figures 4-27 and 4-28 are plots of the maximum load vs. disbond length and displacement at debonding vs. disbond length, respectively. Although there appears to be a slight correlation between disbond length and peak load, it is difficult to quantify how strong this correlation may be due to multiple debonding failure modes existing. The 250mm disbonds reached an average maximum load of 88.1kN. This is a 4.6% drop in load from the control specimens. However, the beams with a 250mm disbond both had the failure mode “thin concrete bondline”, while the majority of the control specimens failed by the “deep concrete, steel” failure mode, making them difficult to

compare directly. As suggested in earlier sections, the debonding failure mode does not appear to be strongly related to the defect characteristics, but rather to material characteristics. Since the debonding failure mode has been strongly linked to the specimen strength (see appendix A) and given the large variability in maximum measured load in specimens containing the same defect, it is difficult to ascertain whether the disbond size is the cause of this difference. Figure 4-24, on the other hand shows more evidence of a correlation between displacement at debonding and rectangular disbond length. From the figure it would appear that a 25mm length disbond fails at about the same average displacement as the control specimens (0mm disbond length). However, the specimens with a 250mm disbond failed at an average displacement of 13.7mm which is 14.4% less than the control specimens.

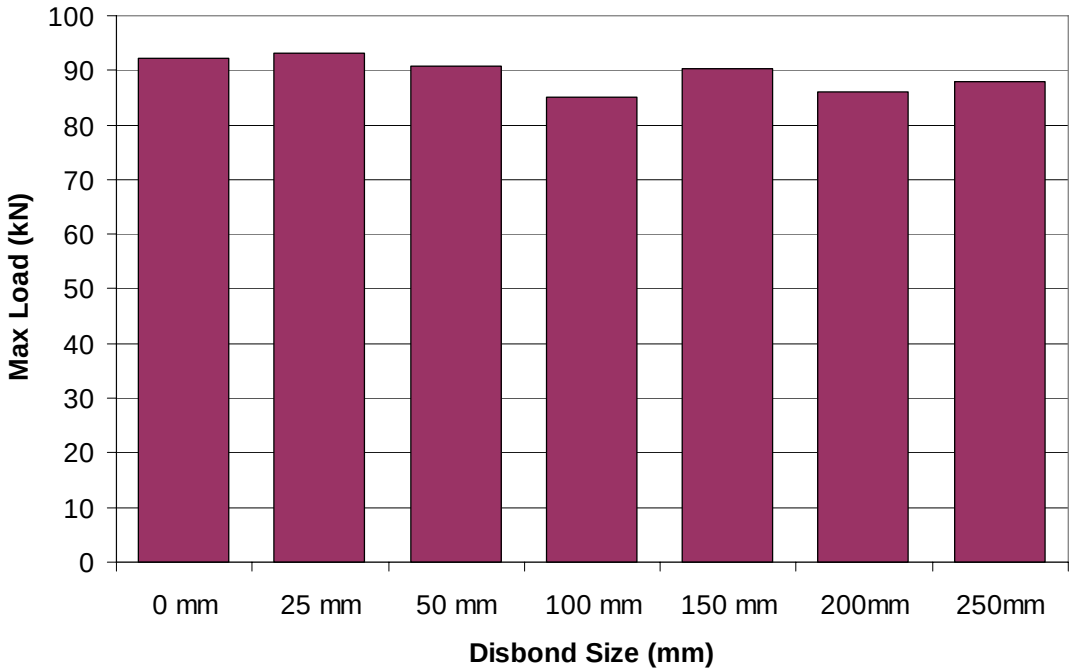

Figure 4-27: Max load vs. rectangular disbond length.

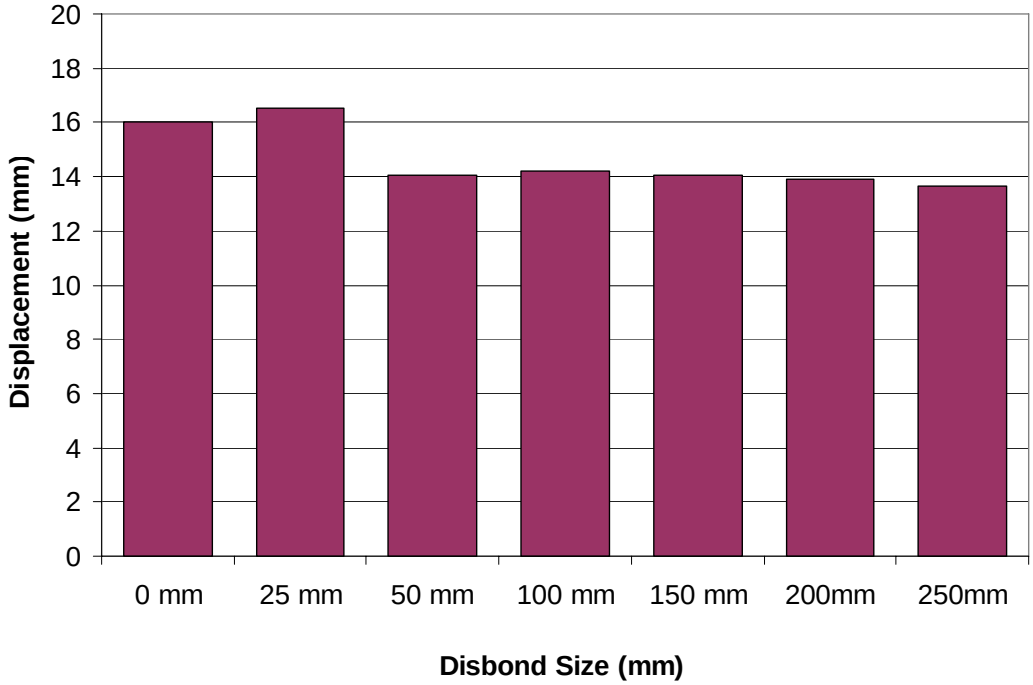

Figure 4-28: Displacement at debonding vs. rectangular disbond length.

The most common failure mode observed in this set of specimens was debonding through a thick concrete bondline. In order to better compare the behavior of specimens with various defects, specimens with this failure mode were isolated in a subset and compared with a control specimen with same failure mode (specimen 42). These specimens specifically were S13 (25mm), S19 (50mm), S4 (100mm), S14 (150mm), S11 (150mm), and S33 (150mm). Figures 4-29, 4-30, and 4-31 highlight data trends noticed in this subset. Figure 4-29 clearly demonstrates that the displacement at debonding decreased as disbond size increased for this subset of specimens. The FRP strain at debonding actually appears to increase with disbond size in this case with the exception of the 50mm specimen as shown in figure 4-31. Interestingly, the displacement at yield for this subset of specimens generally also increased with defect size as can be seen in figure 4-30.

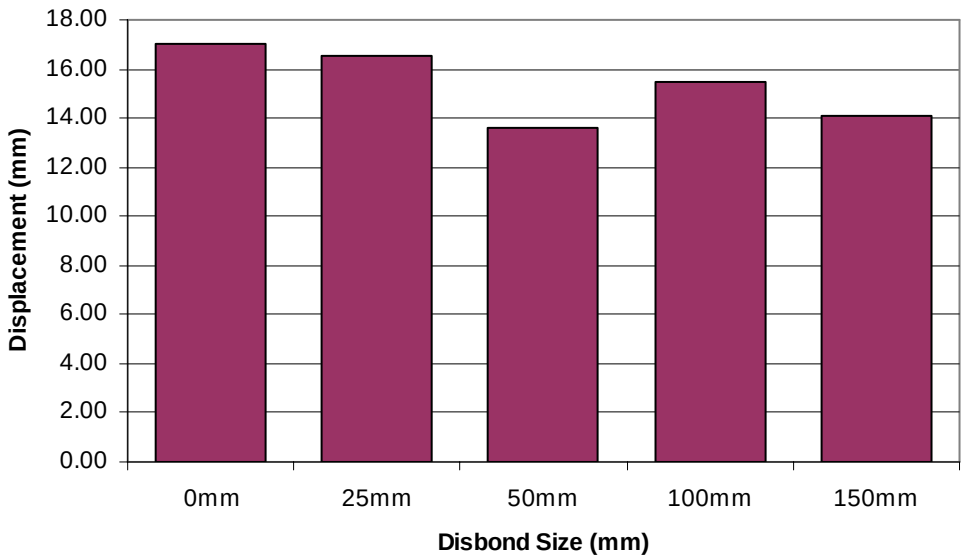

Figure 4-29: Displacement at debonding vs. rectangular disbond length with failure mode “thick concrete bondline”.

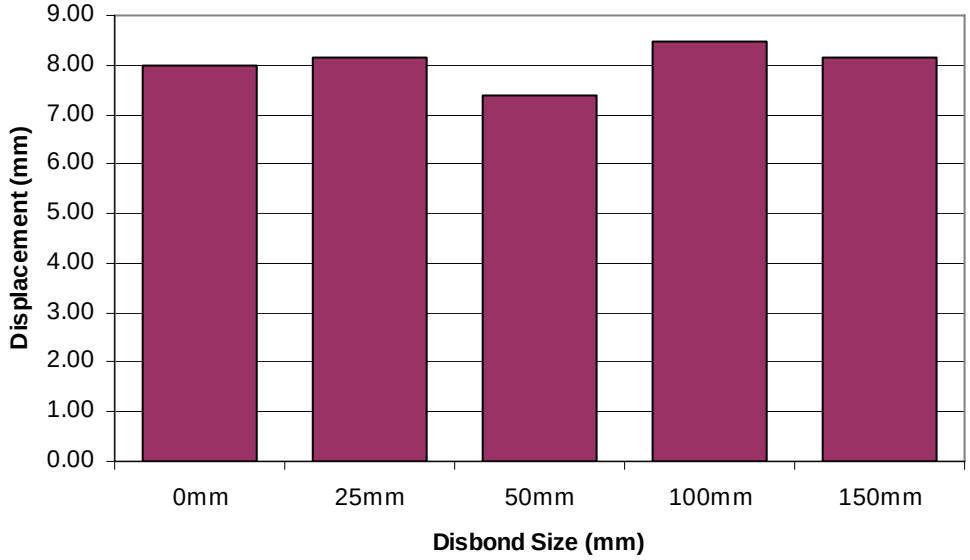

Figure 4-30: Displacement at steel yield vs. rectangular disbond length with failure mode “thick concrete bondline”.

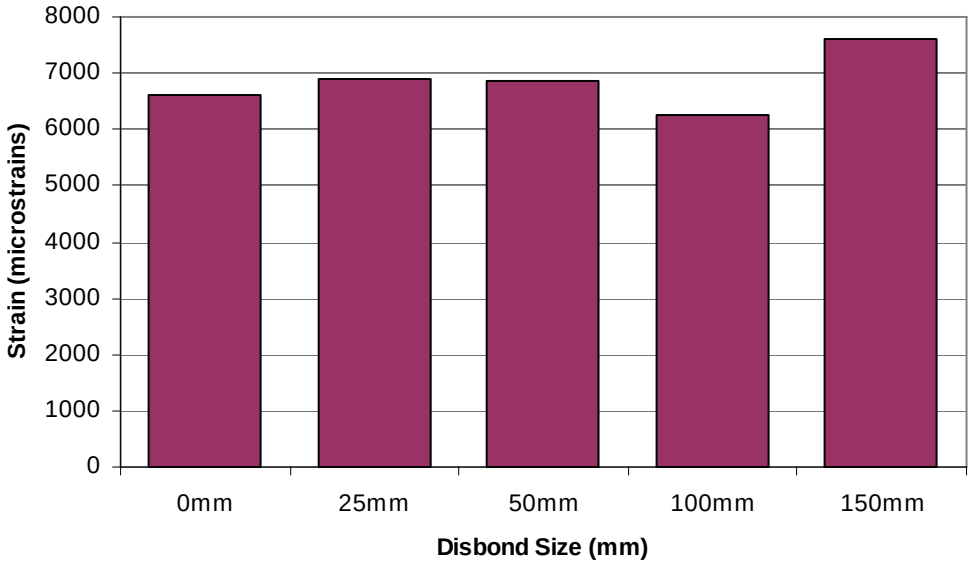

Figure 4-31: FRP strain at debonding vs. rectangular disbond length with failure mode “thick concrete bondline”.

4.3. Critical Disbond Location

In order to investigate the critical location of a disbond a series of specimens were tested with a set size of either 100mm diameter circular disbonds or 100mm length for rectangular disbonds. Disbonds were placed with varying centroidal locations from the midpoint in the adhesive layer as described in section 2.4.1. The disbond size chosen for determining critical disbond location was 100mm as chosen from preliminary results on the determination of critical disbond size.

4.3.1 Circular Disbond

The circular disbonds utilized for this portion of the investigation all consisted of 100mm diameter disbonds placed at locations of 0mm, 185mm, 428mm, and 660mm measured from the midspan to the center of the disbond. Details pertaining to the specimen behavior and the specific specimens considered in this portion of the investigation may be found in table 4-9. Terms in parenthesis in the heading of this table are the specimen numbers (used to reference the beams in appendix B). Figure 4-32 is a plot of the load vs. midspan displacement for this set of specimens. As found previously in this investigation, the global behavior based on the load versus midspan displacement of the specimens is nearly identical before the initiation of local or global debonding (which generally occurs at loads greater than 75kN). This behavior is apparent in figure 4-28 where the plotted lines begin to diverge between 75kN and 80kN, indicating a change in specimen stiffness. In figure 4-32, specimens with defects located 428mm and 660mm away from the midspan are seen to show a

stronger and stiffer response just prior to failure. This is expected because the disbonds in this case are located away from critical regions of high moment (see figure 2-4 in section 2.4.1). Figure 4-33 shows representative midspan steel strain vs. load plots for this set of specimens compared to a control specimen and to each other. It is noted that the steel strain behavior for all of the specimens containing defects is very similar. The steel strain behavior of this set compared to the control specimen is quite similar also. However, like the previous sets, steel yielding occurred just before the peak of the 75kN load cycle was reached, while yielding occurred just after this load for the control specimens.

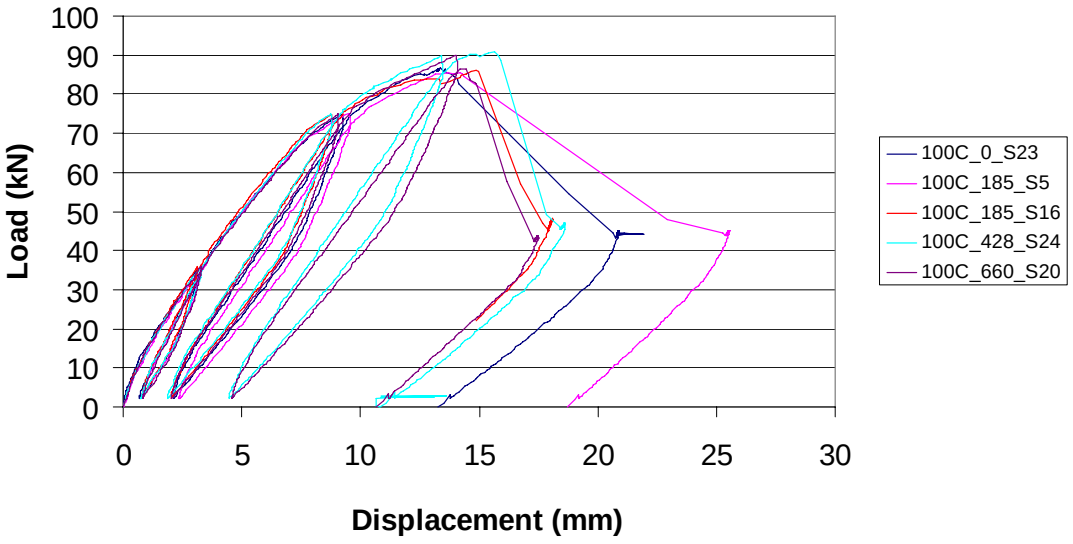

Figure 4-32: Characteristic load vs. displacement plots for various disbond locations.

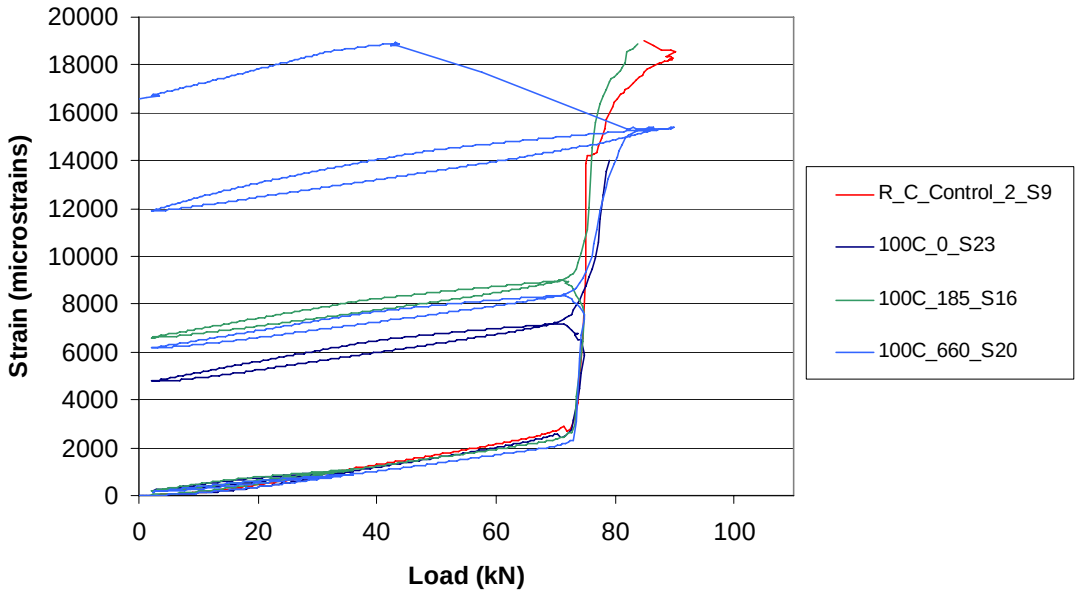

Figure 4-33: Representative Steel Strain vs. Load plots for various disbond locations.

Table 4-9: Beam behavior characteristics for determination of critical circular disbond locations.

Distance from Midspan/ Beam Characteristic	0mm(S23)	185mm(S16)	185mm(S5)	428mm(S24)	660mm(S20)
Maximum Load (kN)	86.74	86.27	85.63	90.72	89.90
Displacement at Maximum Load (mm)	13.36	14.86	14.19	16.62	14.05
Steel Strain at Yield ($\mu\varepsilon$)	2458	2463	2344	2414	2389
Load at Steel Yield (kN)	67.16	71.76	66.40	72.65	73.03
Midspan Displacement at Steel Yield (mm)	7.48	7.98	4.99	8.19	8.55
FRP Strain at Steel Yield ($\mu\varepsilon$)	3566	3708	3435	3244	4292
FRP Strain at Debonding ($\mu\varepsilon$)	5978	6330	6069	5845	6871
Debonding Direction	Right	Left	Left	Left	Right
Location of Debond Initiation	Defect / Midspan	Left Load-Point / Defect	Midspan	Defect	Right Load-Point
Failure Mode	Thick Concrete Bondline	Thick Concrete Bondline	Deep Concrete, Steel	Deep Concrete, Steel	Thick Concrete Bondline

Figure 4-34 shows a representative FRP strain profile at ultimate load for a disbond of each location considered. Much like the control specimens, the peak FRP strains for the specimen with a disbond located at the midspan are also near the

midspan location. The peak FRP strain at debonding in the disbonds located 185mm from the midspan are, as discussed previously at the edges of the disbond. For the disbonds located at 428mm and 660mm from the midspan, the peak FRP strains were not observed at the disbond location. Instead, they were located near the midspan, much like the control specimen. However, stress concentrations were still observed at the edges of the disbonds and may have had an influence on the direction of final debonding. The observation that maximum strains and debonding initiation did not occur near the disbonds, may explain why these two specimens seemed to behave slightly better than the others in this defect set.

Table 4-10 shows the measured concrete crack widths for each specimen at the peak and bottom of each load cycle. Interestingly, specimens 24 and 20 (located farthest from the defect at 428mm and 660mm, respectively) had the largest measured crack widths before failure. It is difficult to conclusively suggest, however, that this behavior was due to the defect location because these two specimens were the only two to reach the 90kN load where these large cracks were observed.

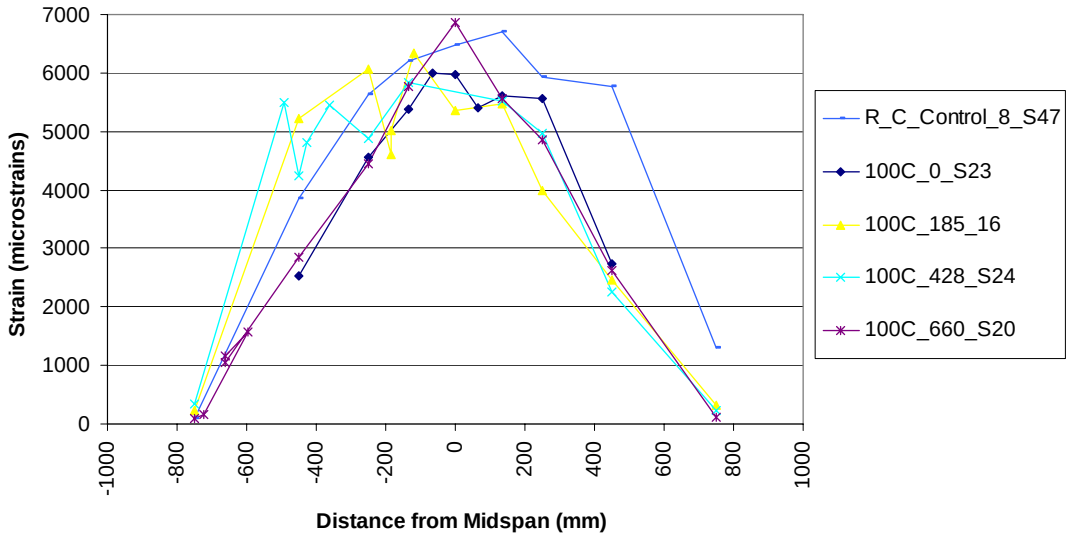

Figure 4-34: Representative strain profiles.

Table 4-10: Load vs. measured crack width (mm) during testing.

Load (kN)	0mm (S23)	185mm (S5)	185mm (S16)	428mm (S24)	660mm (S20)
0	<0.1	<0.1	<0.1	<0.1	<0.1
36	<0.1	<0.1	<0.1	<0.1	<0.1
2.5	<0.1	<0.1	<0.1	<0.1	<0.1
75	0.2	0.3	0.1	0.2	0.2
2.5	<0.1	<0.1	<0.1	<0.1	<0.1
90	-	-	-	0.8	0.4
2.5	-	-	-	0.7	<0.1

XXmm = Disbond location in mm from the midspan
(Sxx) = Specimen Number

Figures 4-35 and 4-36 show the maximum load vs. defect location and the displacement at debonding vs. defect location plots, respectively. As noted in the load vs. midspan displacement plots, specimens with defects furthest from the midspan were slightly stronger than those with defects located at the midspan or in the high moment, high shear region of the beam. The disbond located at the quarterspan deflected a sizeable amount more than the other beams before debonding occurred.

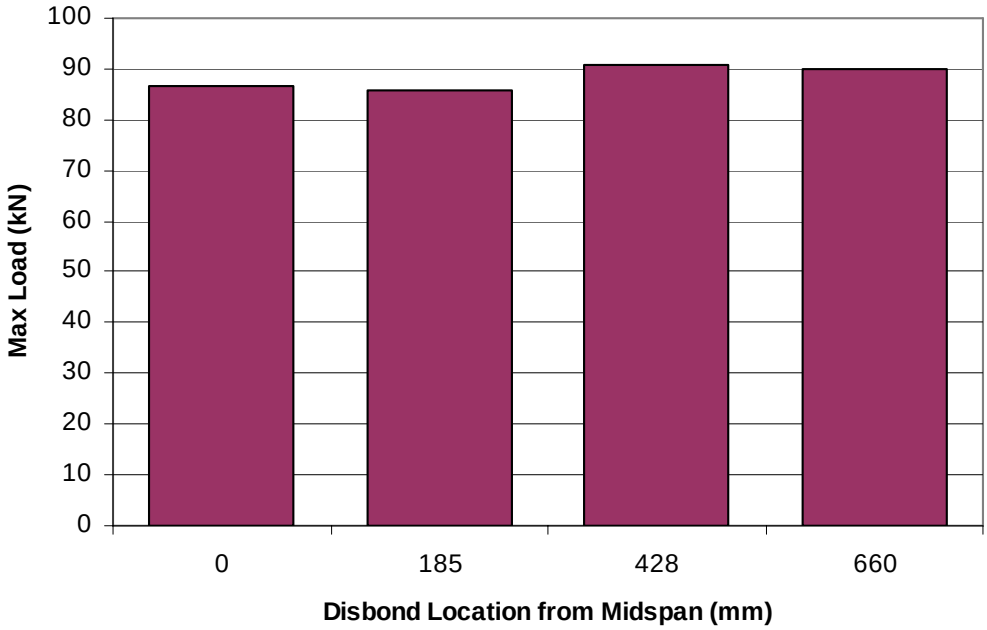

Figure 4-35: Max load vs. circular disbond location.

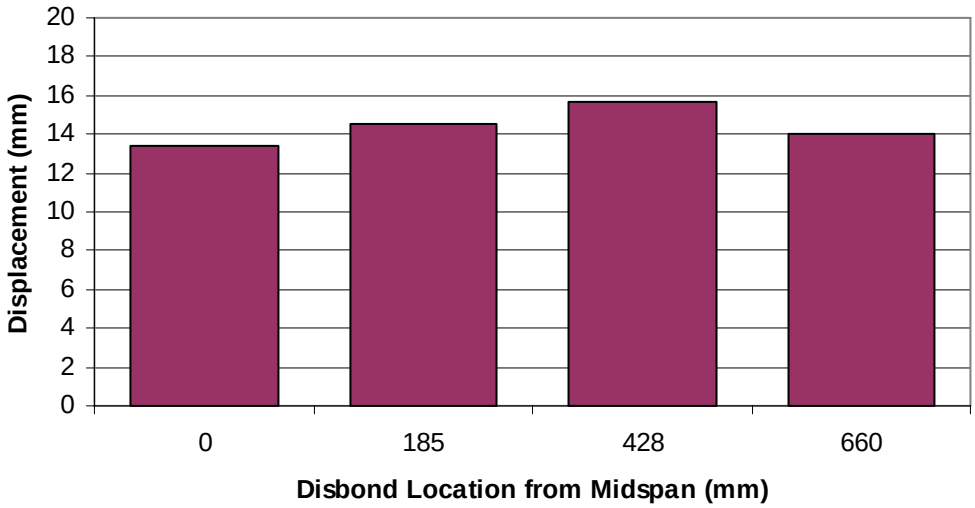

Figure 4-36: Displacement at debonding vs. circular disbond location.

As discussed in previous sections, direct comparisons between specimen behaviors are difficult due to the dissimilar debonding failure modes dominating behavioral parameters. Because of this occurrence, the set has been divided further into two subsets to make additional comparisons: Debonding through a “thick concrete bondline, and debonding through “deep concrete, steel” failure modes. Specimens 23 (0mm location), 16 (185mm location), and 20 (660mm location) all debonded by the “thick concrete bondline” failure mode, while specimens 5 (185mm location) and 24 (428mm location) debonded by the “deep concrete, steel” failure mode. Data trends observed for the “thick concrete bondline” failure mode are plotted below in figures 4-37 to 4-40. From these plots, it can be observed that the load at yield, midspan

displacement at yield, FRP strain at yield, and maximum FRP strains all increased as unbonded areas were moved farther from the high moment region near the midspan of the beam.

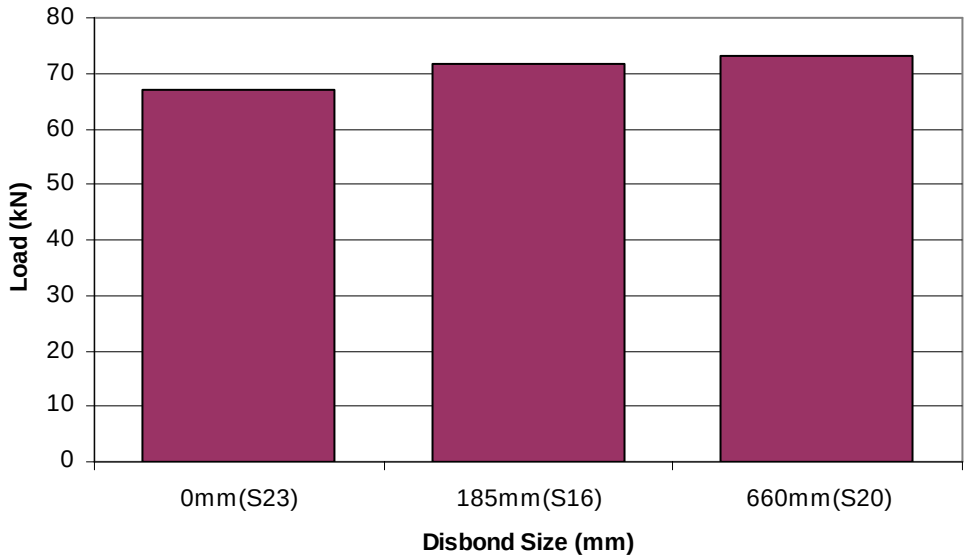

Figure 4-37: Load at steel yield vs. circular disbond location for “thick concrete bondline” debonding mode.

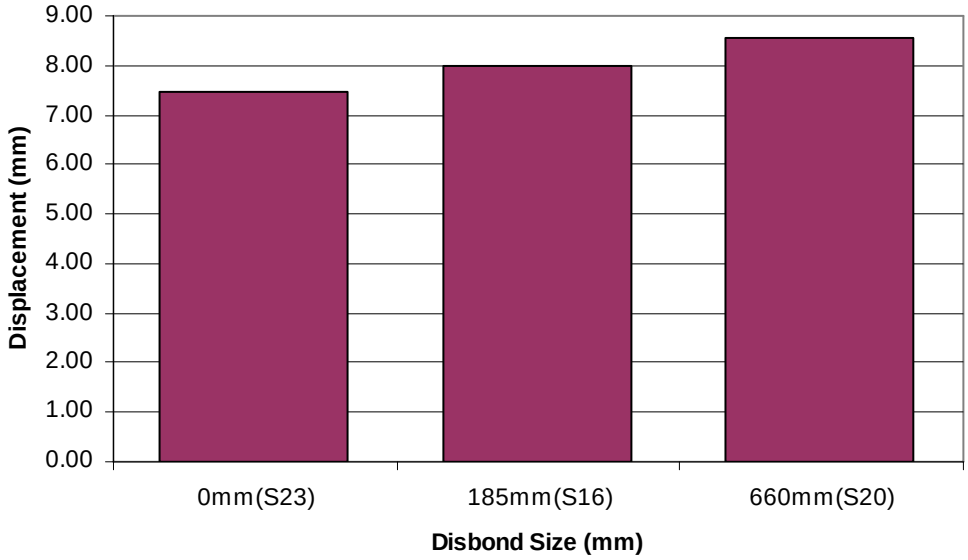

Figure 4-38: Displacement at steel yield vs. circular disbond location for "thick concrete bondline" debonding mode.

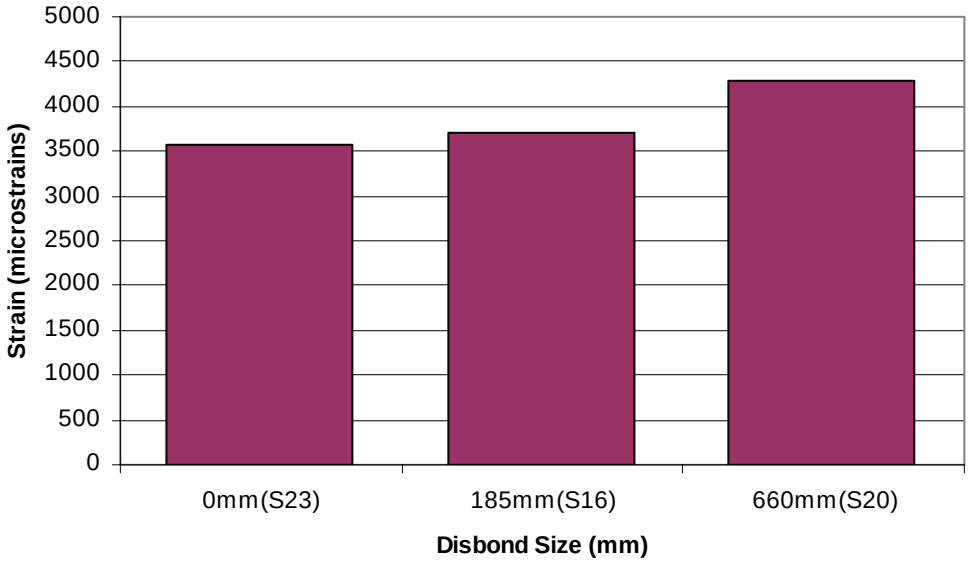

Figure 4-39: FRP strain at steel yield vs. circular disbond location for "thick concrete bondline" debonding mode.

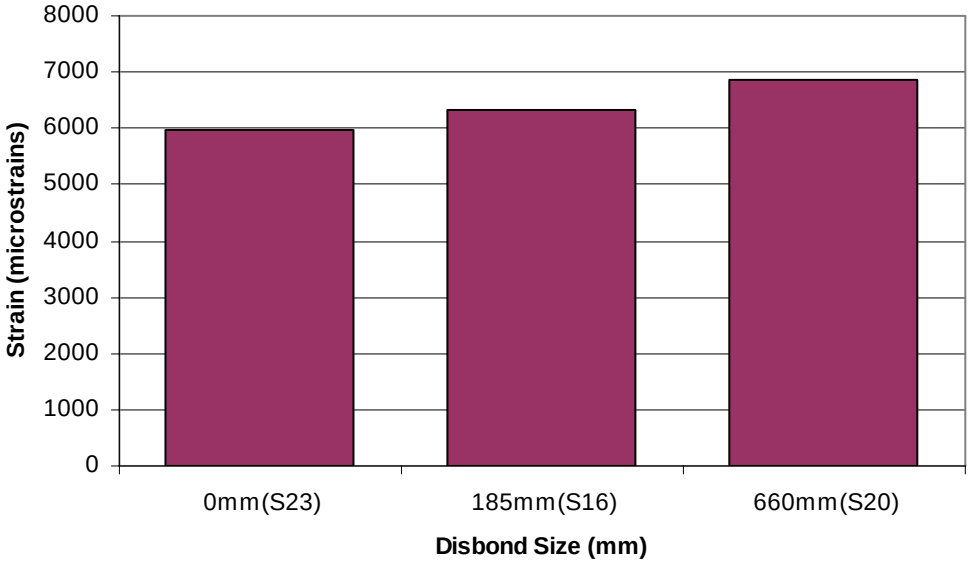

Figure 4-40: Maximum FRP strain vs. circular disbond location for "thick concrete bondline" debonding mode.

4.3.2 Rectangular Disbonds

This set of specimens consisted of strengthened beams with 100mm x 150mm rectangular disbonds located at various distances from the midspan of the beam. The centroids of these disbonds were placed at distances of 0mm, 185mm, or 428mm from the midspan. For details of the disbond layout and the strain gage layout, see appendix B for specimens 25, 8, 38, 45, 40, 41, and 44. This set of beams was divided into two categories with various disbond locations: those with defects located in the adhesive layer, and those with defects placed both in the adhesive layer and between FRP layers. Figure 4-41 shows the load vs. midspan displacement plots for the first groups of beams, those with defects located in the adhesive layer and the appropriate control specimen (S42) from the rehabilitation set. This group consists of five specimens: one

with a disbond located at the midspan (S25) and four with disbonds located 185mm from the midspan (S8, S4, S31, and S38). Of these five specimens, one failed by debonding in the “deep concrete, steel” mode (S8), two failed through a “thick concrete bondline” failure mode (S25 and S4), and two failed through the “resin interface” failure mode (S31 and S38). Three different failure modes in one set make direct comparisons inappropriate for the entire set. However, comparisons between S25 located at the midspan and S4 located 185mm from the midspan are more relevant because they have common debonding failure modes. From figure 4-41, the global performance of the beam with a disbond at the midspan (100R_0_S25) is slightly better than the control specimen corresponding to this rehabilitation, failing at a greater ultimate load. Specimen 4 (100R_185_S4) with a disbond at 185mm, however, failed significantly earlier than the control specimen and specimen 25, probably due to the disbonds being located in a more critical region of the beam. The curve for specimen 4 (100R_185_S4) in figure 4-41 shows the slightly lower initial stiffness and much lower stiffness after steel yield and initiation of local debonding preceding global debonding. Comparisons between specimen 25 and specimen 4 in table 4-11 highlights that specimen 4 failed at a load 9.7% less than specimen 25, but at nearly equal displacements at debonding. Additional comparisons between these two specimens suggest that an unbonded length in the critical high shear and high moment region (see figure 2-4) compared to one at the midspan results in a reduction in yield load, an increase in displacement at debonding and FRP strain at debonding

(indicating lower initial stiffness and earlier activation of FRP), and a reduction in FRP strain at debonding as can be seen in table 4-11.

Figure 4-42 is the load vs. midspan displacement plots of the remaining specimens in this set, with 100mm unbonded lengths located at the midspan (S45), at 185mm from the midspan (S40 and S41), and 428mm from the midspan (S44). Here, the control specimen is seen to behave significantly better than the specimens in this group. Specimens 45 and 44 failed prematurely by debonding through the adhesive "resin interface" layer. This change in failure mode was likely due to poor adhesive properties or inadequate surface preparation and application resulting in a weak bond between the concrete and FRP and not specifically due to the inserted disbonds. The three specimens that failed by debonding through the adhesive resin interface behaved so poorly that any trends were probably not reliable.

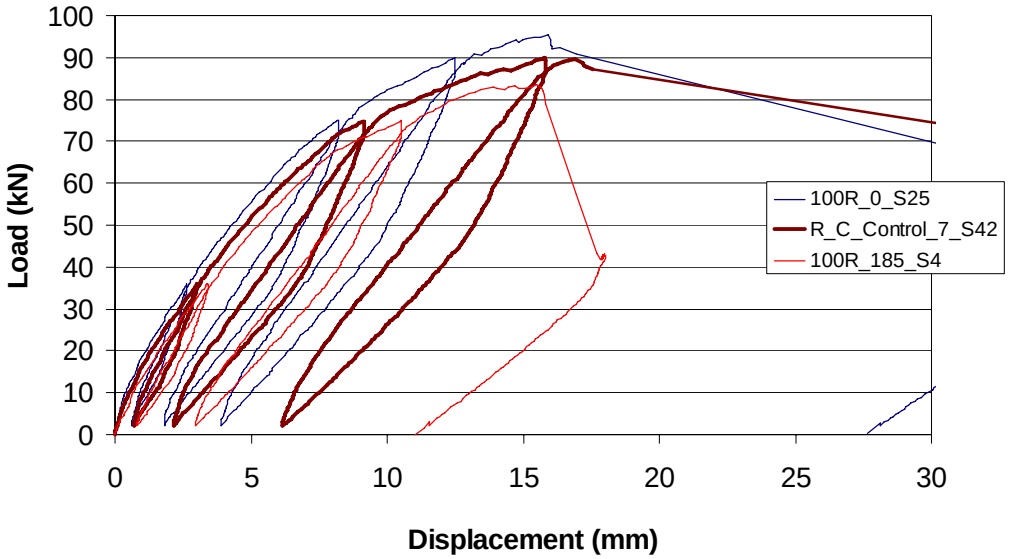

Figure 4-41: Characteristic load vs. displacement plots for various disbond locations.

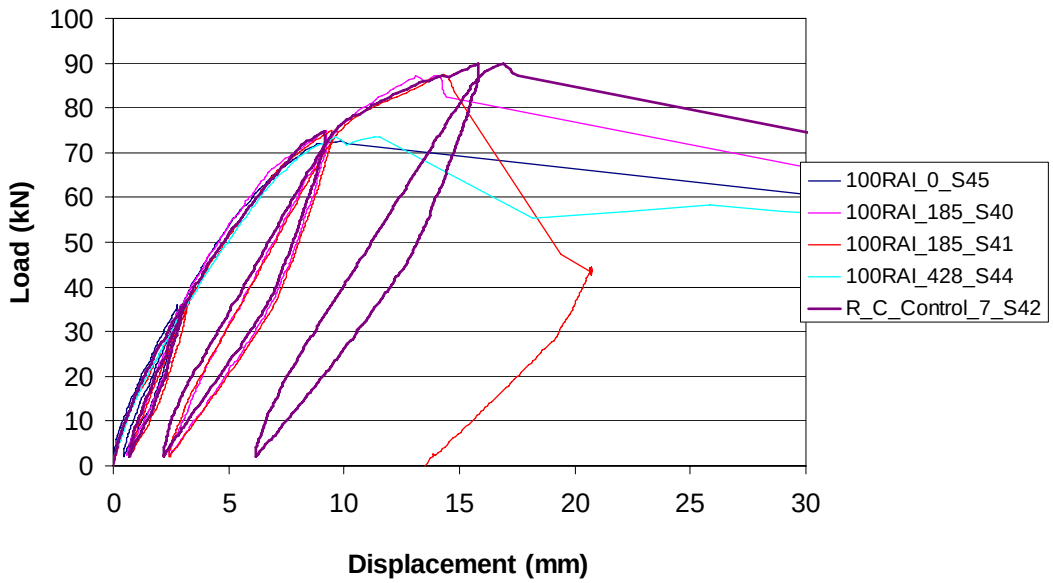

Figure 4-42: Characteristic load vs. displacement plots for various disbond locations.

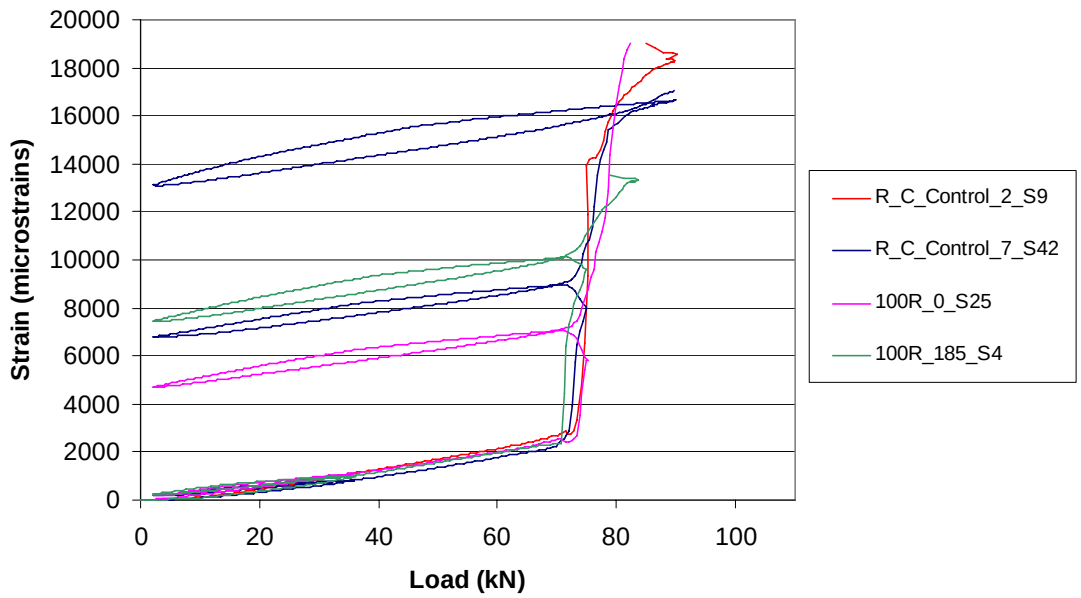

Figure 4-43: Representative Steel Strain vs. Load plots for various disbond locations.

Figure 4-43 show representative midspan steel strain vs. load curves for typical specimens in this investigation. As noted previously, steel yielding behavior for all of the specimens is fairly similar. Table 4-11 gives the beam behavior characteristics for each specimen in this set. More information about individual specimen behavior may be found in appendix B. Figure 4-45 is the FRP strain profiles at ultimate load for several typical specimens in this defect category. As with the case of the circular disbonds, stress concentrations in these plots can be found at the location of the disbond in the beam. The plot of specimen 44 (100RAI_185_S44) was included to emphasize how much lower the FRP debonding strains were in the specimens that failed entirely through the resin.

Table 4-11: Beam behavior characteristics for determination of critical rectangular disbond location.

	Disbonds in the Adhesive Layer					Interlaminar and Adhesive Interface Disbonds			
Distance from Midspan/ Beam Characteristic	**0mm(S25)**	**185(S8)**	**185(S4)**	**185(S31)**	**185(S38)**	**0mm(S45)**	**185(S40)**	**185(S41)**	**428(S44)**
Maximum Load (kN)	92.49	90.11	83.5	80.28	86.68	72.47	87.18	87.47	73.50
Displacement at Maximum Load (mm)	15.78	15.06	15.5	12.00	14.19	9.89	13.90		9.61
Steel Strain at Yield ($\mu\varepsilon$)	2529	2437	2385	2353	2507	2399	2582	2319	2234
Load at Steel Yield (kN)	70.62	67.26	68.84	65.99	66.90	57.50	68.17	67.84	63.50
Midspan Displacement at Steel Yield (mm)	7.27	7.75	8.48	7.55	7.69	5.57	7.31	7.45	6.92
FRP Strain at Steel Yield ($\mu\varepsilon$)	3248	3130	3568	3589	4176	3164	3931	4343	3155
FRP Strain at Debonding ($\mu\varepsilon$)	7187	6787	6261	6658	7068	4881	6940	7201	3997
Debonding Direction	Right	Left	Right	Left	Right	Left	Right	Left	Right
Location of Debond Initiation	Midspan	Right Load-Point / Defect	Right Load-Point	Left Load-Point	Left Load-Point	Defect / Midspan	Defect	Midspan	Midspan
Failure Mode	Thick Concrete Bondline	Deep Concrete, Steel	Thick Concrete Bondline	Resin Interface	Resin Interface	Resin Interface	Thin Concrete Bondline	Resin Interface	Resin Interface

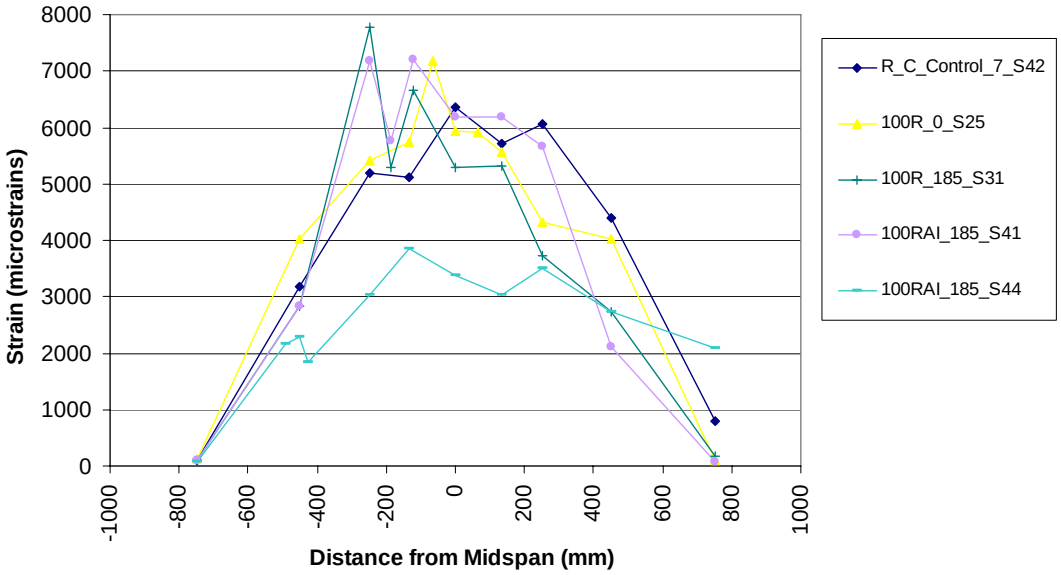

Figure 4-44: Representative strain profiles.

Table 4-12: Load vs. measured crack width (mm) during testing.

Load (kN)	0mm (S25)	185mm (S4)	185mm (S31)	185mm (S38)	0mm (S45)	185mm (S40)	185mm (S41)	428mm (S44)
0	<0.1	0	<0.1	<0.1	<0.1	<0.1	<0.1	<0.1
36	<0.1	< 0.1	0.1	<0.1	<0.1	<0.1	<0.1	-
2.5	<0.1	<0.1	<0.1	<0.1	<0.1	<0.1	<0.1	-
75	0.3	0.2	0.4	0.5	0.5	0.5		-
2.5		0.1	<0.1	0.2	0.2	0.2	0.1	-
90	0.5	-	-	-	-	-	-	-
2.5	-	-	-	-	-	-	-	-

XXmm = Disbond location in mm from the midspan
(Sxx) = Specimen Number

Figure 4-45 shows the maximum load versus disbond location for the specimens with disbonds located in the adhesive layer. Here it is clearly shown that the specimen with the disbond failed at a greater load than the control specimen, while specimens with defects away from the midspan all failed at loads from zero to eleven percent lower than the control specimen. Figure 4-46 is the midspan displacement at debonding versus disbond location for this same set. While final debonding occurred at a displacement less than the control specimen for all of the specimens, the beam with the defect located at the midspan again performed the best in this category failing at a greater displacement than the other specimens.

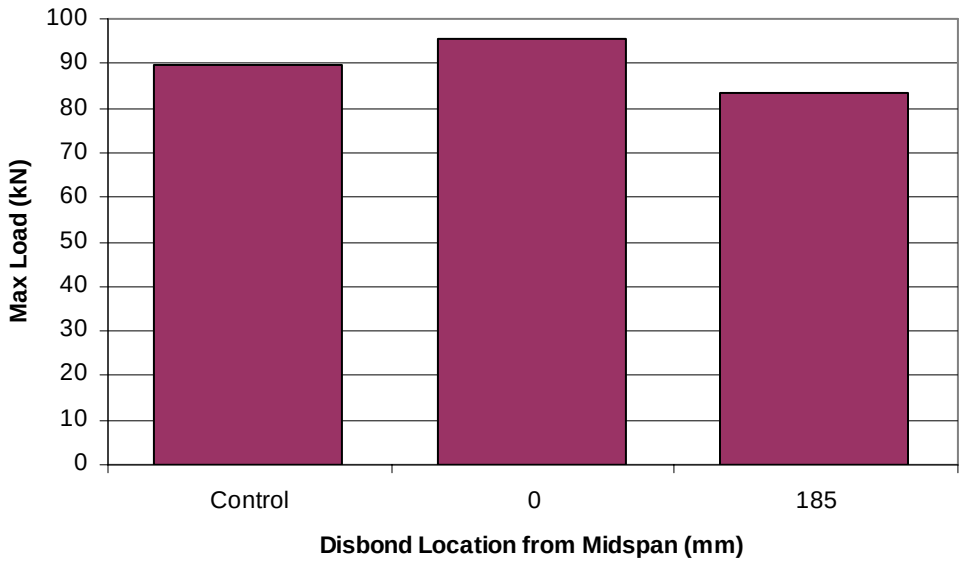

Figure 4-45: Max load vs. rectangular disbond location.

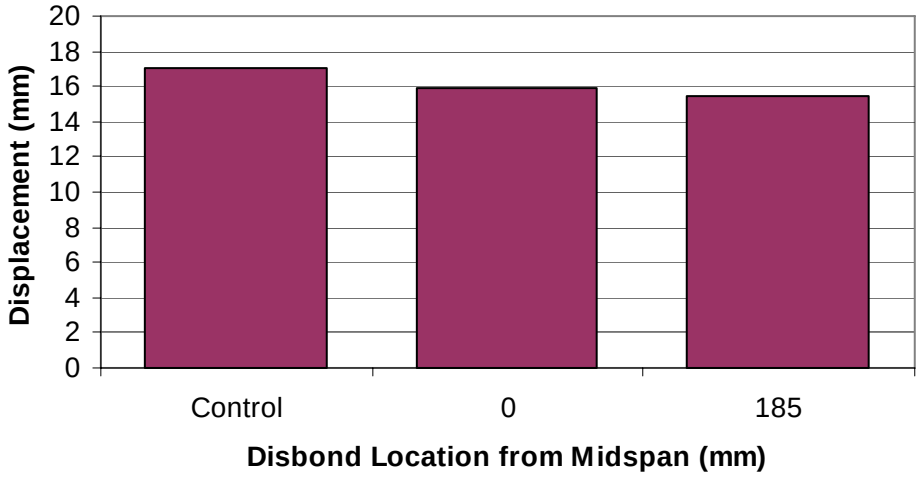

Figure 4-46: Displacement at debonding vs. rectangular disbond location.

Figures 4-47 and 4-48, respectively show the maximum load versus disbond location and displacement at debonding versus disbond location for the group of specimens containing disbonds in the adhesive layer as well as between FRP layers. Notice in both plots, the control specimen had superior behavior compared to the specimens with disbonds. Also, the beams with disbonds located at 185mm from the midspan of the beam performed better than those with defects located at 0mm or 428mm. However, it is difficult to suggest that these locations are more critical because these are the specimens that showed very poor behavior due to debonding failure propagating entirely through the adhesive “resin interface” layer (specimens 45 and 44, as mentioned earlier) making direct comparisons inappropriate.

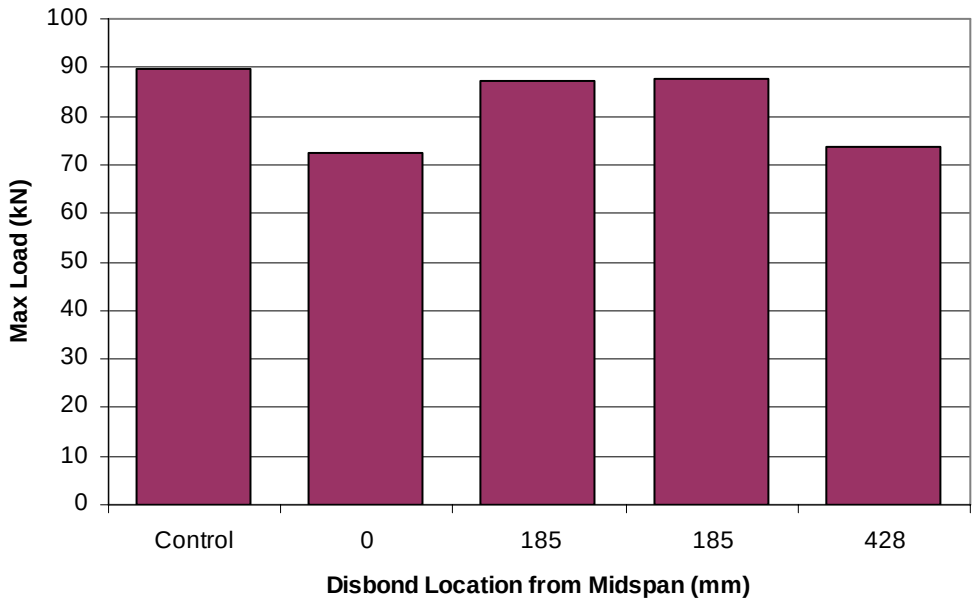

Figure 4-47: Max load vs. rectangular disbond location.

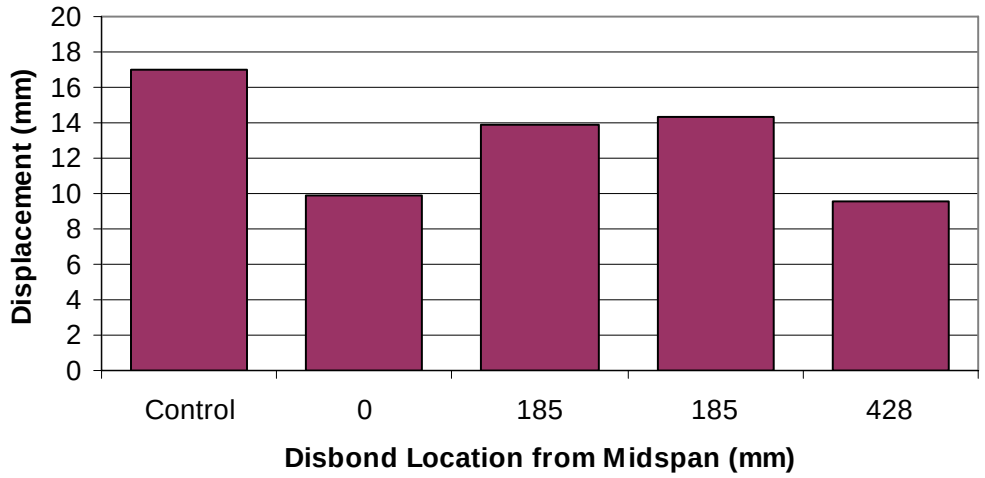

Figure 4-48: Displacement at debonding vs. rectangular disbond location.

Figures 4-49 and 4-50 show the load versus location and FRP debonding strains versus location for the three specimens in this subset that failed with a common failure mode. From figure 4-49 it is suggested that the 0mm and 428mm locations are more critical than the 185mm location near where debonding typically initiated. However, in figure 4-50 the debonding strains are shown to be excessively low for specimens 45 and 44, making it difficult to determine this relationship exists, or if it is more related to the extremely weak and variable nature of the "resin interface" debonding failure mode.

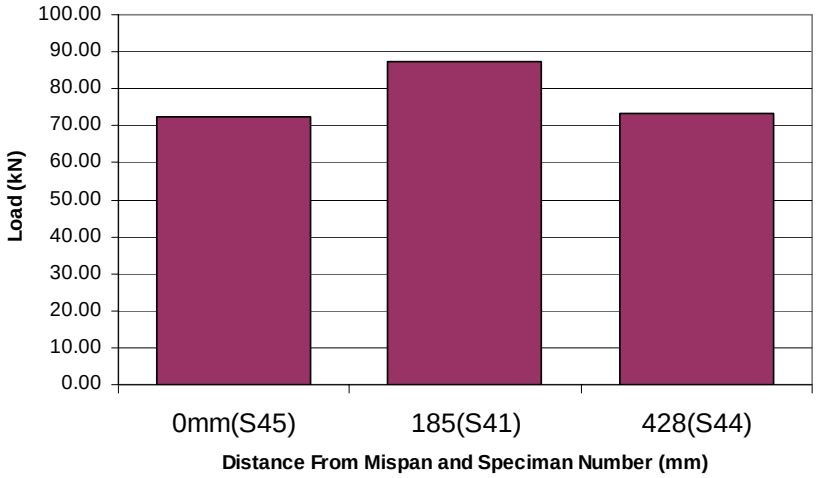

Figure 4-49: Displacement at debonding vs. rectangular disbond location.

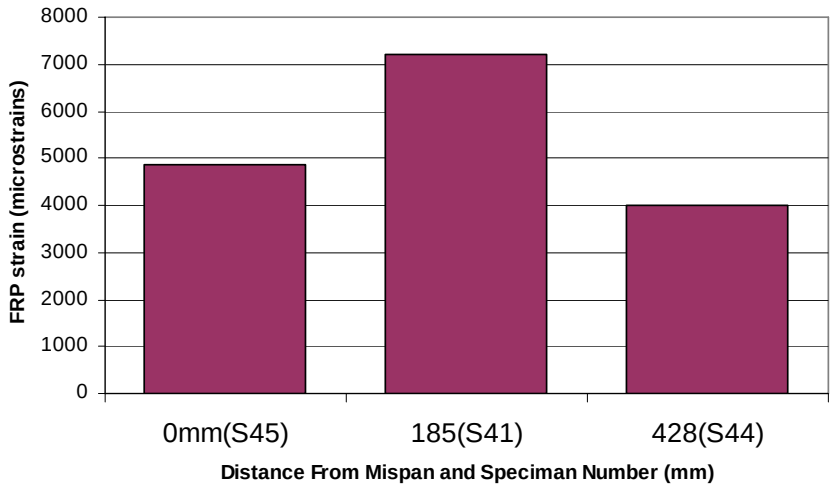

Figure 4-50: Displacement at debonding vs. rectangular disbond location.

4.4 Effect of Excessive Preload Cracking

In order to further investigate the effect of preloading on flexural strengthening, two different sets of specimens were manufactured: those with various levels of excessive preloading, and those preloaded to a predetermined residual crack width of 1.0mm and rehabilitated with various disbonds.

4.4.1 0mm to 1.5mm Crack Widths

As detailed in section 2.8, there were several different preload levels used in this portion of the investigation:

1) zero preloading
2) preloading to a maximum crack width of 0.2mm
3) preloading to a residual crack width of 0.2mm

4) preloading to a residual crack width of 0.6mm
5) preloading to a residual crack width of 1.0mm
6) and, preloading to a residual crack width of 1.5mm

This portion of the investigation focuses on the effect of these crack widths on the strengthened performance of the beams. The term “maximum crack width” refers to the crack width in a specimen at the point of maximum load during preloading. The term “residual crack width” refers to the crack width in a specimen that remains after the preload has been removed. Figure 4-51 is the load vs. midspan displacement plots for each of the preload cracking levels considered. The 0.2mm maximum preload cracking is the same preload that was utilized for all the other specimens in this study and is represented by specimen 47 (R_C_Control_8_S47), which is the precracked control specimen for rehabilitation number seven corresponding to this set of tests (see table 2-4 details pertaining to groups of specimens that were rehabilitated together). As seen in all the previous defect sets, the behavior of the specimens before the initiation of local debonding is very similar. However, after the initiation of local debonding (generally occurring between 75kN and 85kN) the specimen stiffness, peak load, and displacement at debonding vary greatly. Specimen 51 with the 0.6mm crack width was the strongest in the set, while specimen 52 with the 1.0mm crack width can be seen as significantly stiffer than the others after 75kN load was reached. Specimens 50 (0.2mm crack width) and 48 (1.5mm crack width) both performed similarly to the control specimen. The specimen 51 (0.6mm residual crack width) and specimen 52 (1.0mm residual crack width) may have failed at greater maximum loads than the

other specimens because they were preloaded to an extent that the steel was strained far past yield and strain hardened in addition to the wide cracks more effectively activating the FRP so it is utilized more effectively to greater strains before debonding. The subsequent drop in strengthening performance seen in specimen 48 (1.5mm residual crack width) is likely due to the loss of aggregate interlock due to the crack widths greatly exceeding 1.0mm as discussed by ACI Committee 224 (2004).

Figure 4-52 is the midspan steel strain versus load plot for specimen 50 (0.2mm residual crack width) and the control specimen. These are the only two specimens plotted in this figure because the large preload displacement damaged the steel strain gages on the other specimens. In this figure it can be seen that steel yielding occurred at a lower load of 68.9kN than the control specimen load of 76.5kN, but that the shape of the curve is still quite similar. Table 4-13 gives detailed beam performance characteristics relative to this investigation. More complete data on individual specimens can be found in appendix B.

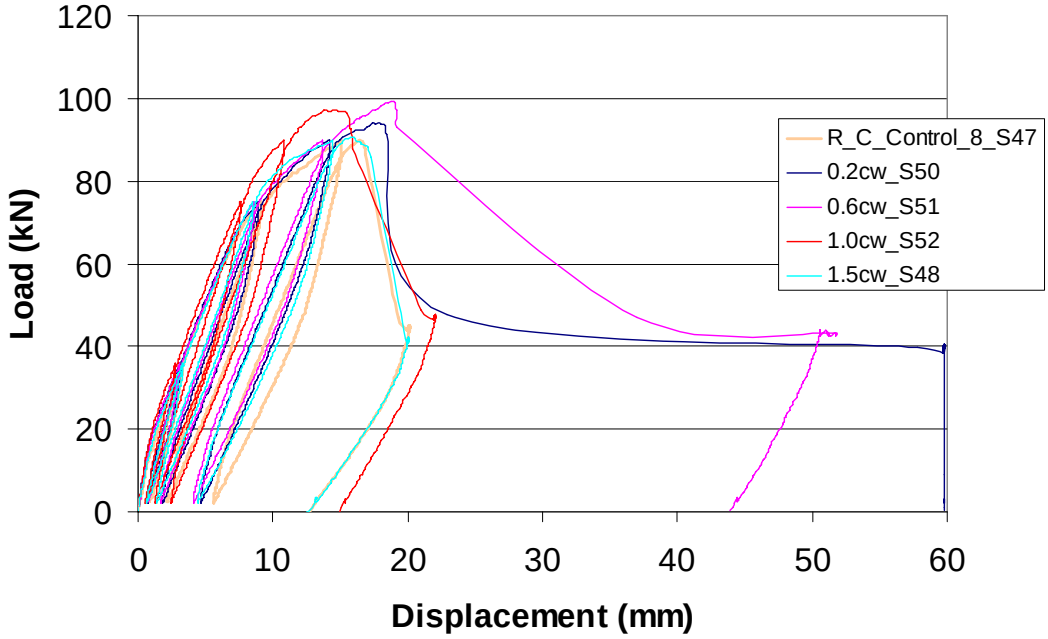

Figure 4-51: Characteristic load vs. displacement plots for various preload crack widths.

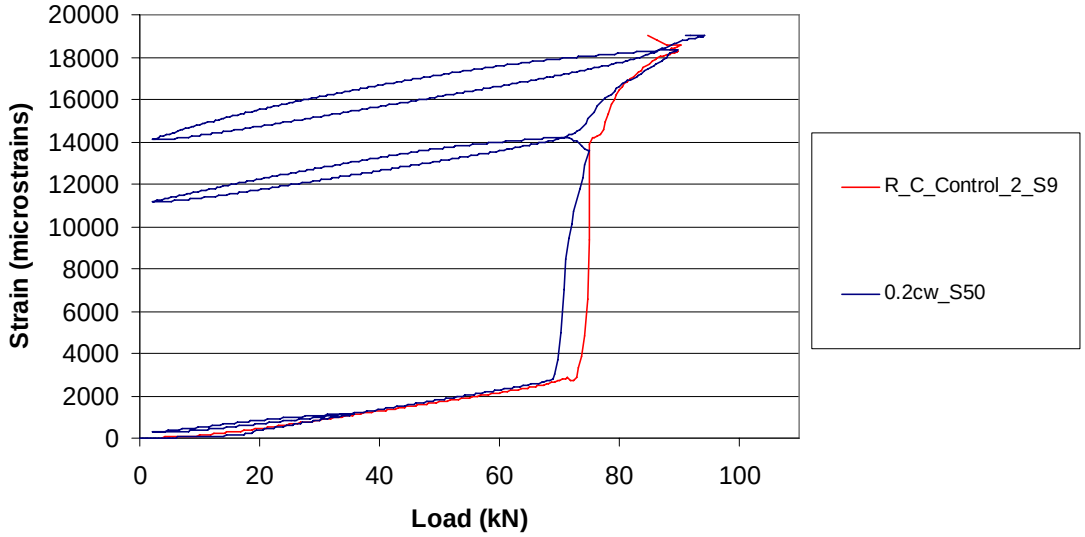

Figure 4-52: Representative Steel Strain vs. Load plots for various disbond locations

Table 4-13: Strengthened control specimen beam characteristics.

Crack Width (mm)/ Beam Characteristic	**0.2mm(S50)**	**0.6mm(S51)**	**1.0mm(S52)**	**1.5mm(S48)**
Maximum Load (kN)	94.17	99.35	97.32	90.58
Displacement at Maximum Load (mm)	17.90	18.77	14.03	16.05
Steel Strain at Yield ($\mu\varepsilon$)	2718	2744	no data	no data
Load at Steel Yield (kN)	68.88	79.55	80.42	~64.4
Midspan Displacement at Steel Yield (mm)	7.96	10.10	8.50	7.49
FRP Strain at Steel Yield ($\mu\varepsilon$)	4039	4870	4870	4028
FRP Strain at Debonding ($\mu\varepsilon$)	7163	8343	7742	7006
Debonding Direction	Left	Left	Left	Left
Location of Debond Initiation	Midspan	Left Load-Point	Left Load-Point	Left Load-Point
Failure Mode	Deep Concrete, Steel	Deep Concrete, Steel	Deep Concrete, Steel	Deep Concrete, Steel

Figure 4-53 is a plot of the FRP strain profiles at peak load for the specimens in this set. Since the beams are relatively symmetric about the midspan, the peak FRP strains were near the midspan. The reason for some deviation from the midspan is likely typically because a large crack is found at the same location of that strain gage, causing a stress concentration. Often final debonding was observed to occur from the location of the largest crack from preloading. Table 4-14 shows the measured crack widths for the testing of these specimens. As expected, the beams with the largest preload crack widths had the largest crack sizes during the tests.

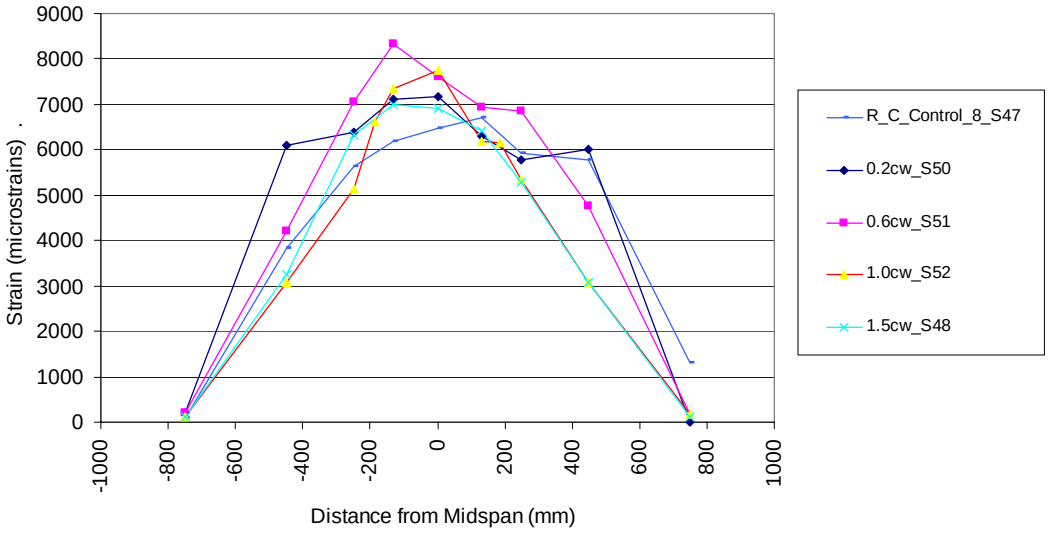

Figure 4-53: Representative strain profiles.

Table 4-14: Load vs. measured crack width (mm) during testing.

Load (kN)	0.2cw (S50)	0.6cw (S51)	1.0cw (S52)	1.5cw (S48)
0	0.15	0.5	1.4	1.5
36	0.15	0.6	1.5	1.6
2.5	0.15	0.5	1.4	1.5
75	0.2	0.6	1.6	1.6
2.5	0.15	0.5	1.5	1.5
90	0.3	0.8	1.7	1.8
2.5	0.2	0.6	1.5	1.5

XXcw = Approximate maximum crack width in mm
(Sxx) = Specimen Number

Figures 4-54 and 4-55 below show the max load versus the residual crack widths from preloading. Interestingly, all the specimens with excessive preload cracking held greater loads than the control specimen which was preloaded to the typical 35.6kN preload level used for testing, with the specimen with the 0.6mm crack width reaching the greatest load. This indicates that rehabilitating beams in which the steel has previously been yielded and large cracks may exist is still a very effective method of strengthening, and perhaps even slightly more beneficial than the application of FRP to specimens with only slight cracking damage. Despite carrying greater loads, the specimens loaded to residual preload crack widths of 1.0mm and 1.5mm showed a decrease in displacement at debonding. The reason for this was likely due to strain hardening in the steel during preloading causing greater specimen stiffness, or stress concentrations near the large cracks initiation global debonding prematurely.

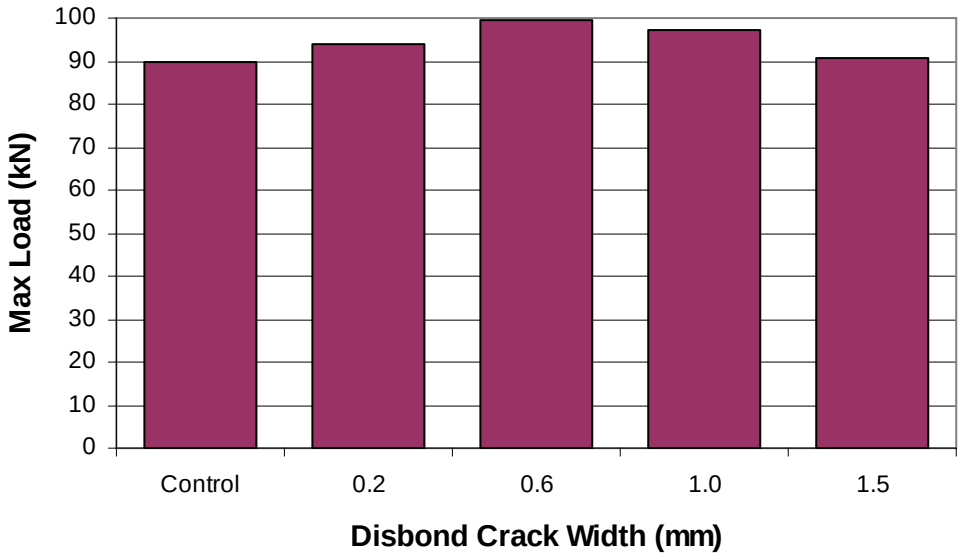

Figure 4-54: Max load vs. residual preload crack width.

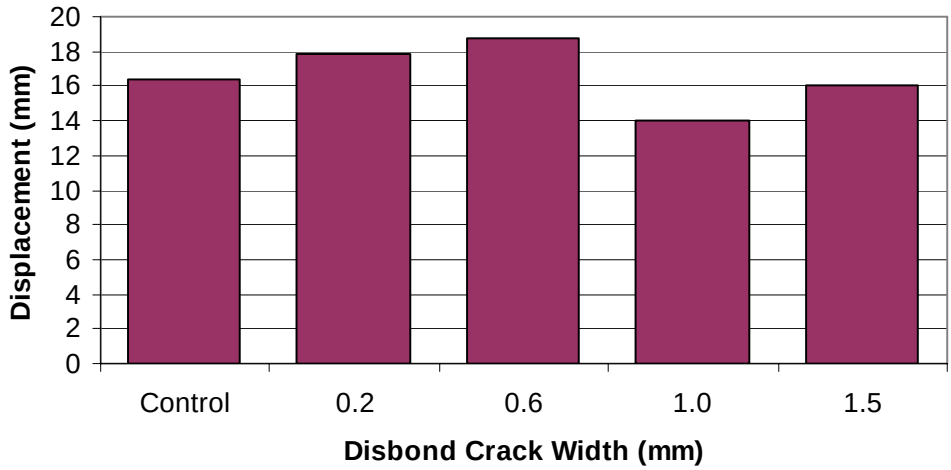

Figure 4-55: Displacement at debonding vs. residual preload crack width.

4.4.2 1.0mm Crack Widths with Disbonds

This set of specimens was created to investigate the effect of disbonds on specimens that have been preloaded past steel yield to a residual crack width of approximately 1.0mm. Additionally, this set includes specimens that include multiple defects to assess the combined effects of defects. Specimens 53, 58, and 56 were all preloaded to 1.0mm residual crack width, then rehabilitated with rectangular disbonds of lengths 100mm, 150mm, and 200mm, respectively at 185mm from the midspan. Specimen 57 (S57) was preloaded to a 1.0mm residual crack width, and had two disbonds inserted during rehabilitation: one 100mm rectangular disbond inserted at 185mm on each side of the midspan at the adhesive interface (see appendix B for more details). Specimens 55 and 54 were preloaded to 1.0mm residual crack width, rehabilitated with 100mm length rectangular disbonds at 185mm from the midspan, and submerged, tension-face down in approximately 25mm of water to soak for a period of 7 days and 21 days, respectively. Figure 4-56 show characteristic load versus displacement plots for this set of specimens. Most of the specimens' global performance seen in this figure is shown to behave quite similar to the control specimen (R_C_Control_8_S47) with the typical preloading of 35.6kN used for testing. However, if we consider specimen 52 (1.0cw_S52) from the section 4.4.1, preloaded to 1.0mm, as the control specimen for this set of specimens, the global performance of the specimens seems to be affected by the disbonds, as indicated in the figure by the seemingly premature failures. Key beam behavior characteristics in this

investigation may be seen in table 4-15 and additional individual test and specimen information may be found in appendix B.

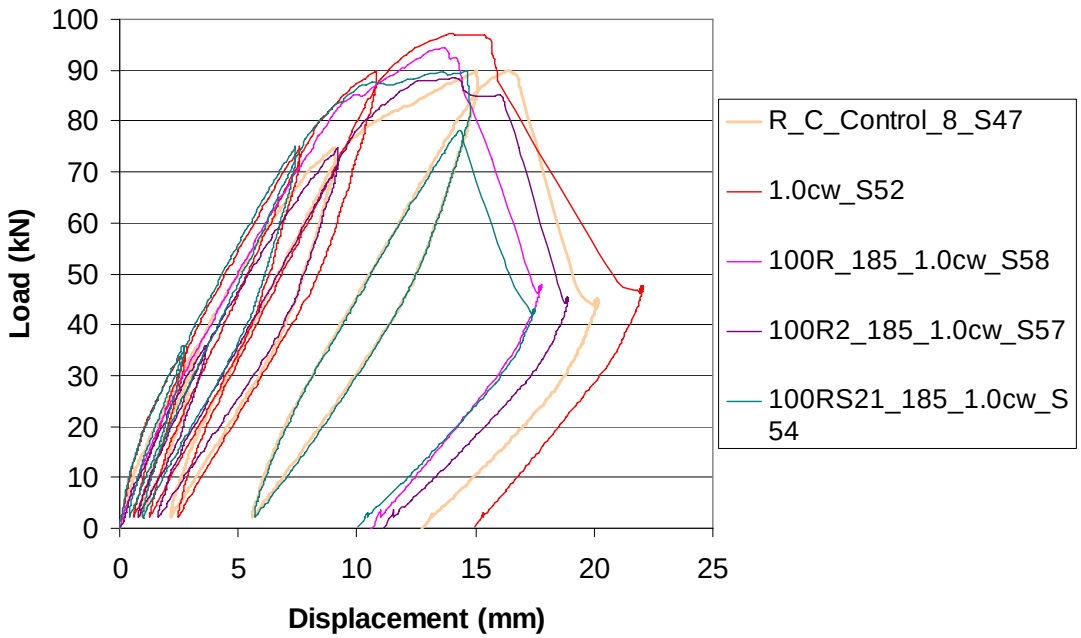

Figure 4-56: Characteristic load vs. displacement plots for various preload crack widths.

Table 4-15: Beam behavior characteristics for determination of critical rectangular disbond location.

Beam Characteristic	**1.0mm(S52)**	**100mm(S53)**	**100mm(S58)**	**200mm(S56)**	**2x100m(S57)**	**100mm, 7 day soak (S55)**	**100mm, 21 day soak (S54)**
Maximum Load (kN)	97.32	92.49	94.33	89.56	88.62	87.28	89.89
Displacement at Maximum Load (mm)	14.03	15.78	13.70	14.45	14.12	15.00	14.64
Steel Strain at Yield (me)	no data	2529	2147	2532	2737	2214	2920
Load at Steel Yield (kN)	80.42	76.07	70.34	67.43	78.68	62.90	91.62
Midspan Displacement at Steel Yield (mm)	8.50	7.89	7.48	7.51	10.08	6.39	6.94
FRP Strain at Steel Yield (me)	4870	4723	4000	3547	4507	3301	3726
FRP Strain at Debonding (me)	7742	7095	6685	7712	6890	7544	7222
Debonding Direction	Left	Left	Left	Left	Left	Left	Left
Location of Debond Initiation	Left Load-Point	Midspan	Left Load-Point / Defect	Left Load-Point / Defect	Left Load-Point	Left Load-Point / Defect	Left Load-Point
Failure Mode	Deep Concrete, Steel	Thick Concrete Bondline	Thin Concrete Bondline	Deep Concrete, Steel	Thin Concrete Bondline	Deep Concrete, Steel	Thick Concrete Bondline

Figure 4-57 show the characteristic FRP strain profiles for the specimens in this set. Like previously found in section 4.2.2 the FRP strain profiles reveal stress concentrations near disbond and crack locations, which are often the resulting location of debond initiation. Table 4-16 below shows the measured crack width for each of the specimens tested in this set. There is a large variation in the amount that a crack opens during loading in these specimens. This is because some specimens have only one large "primary" crack that opens very wide before debonding load is reached, while others will have multiple large cracks that either develop during preloading or during final testing of the rehabilitated beam.

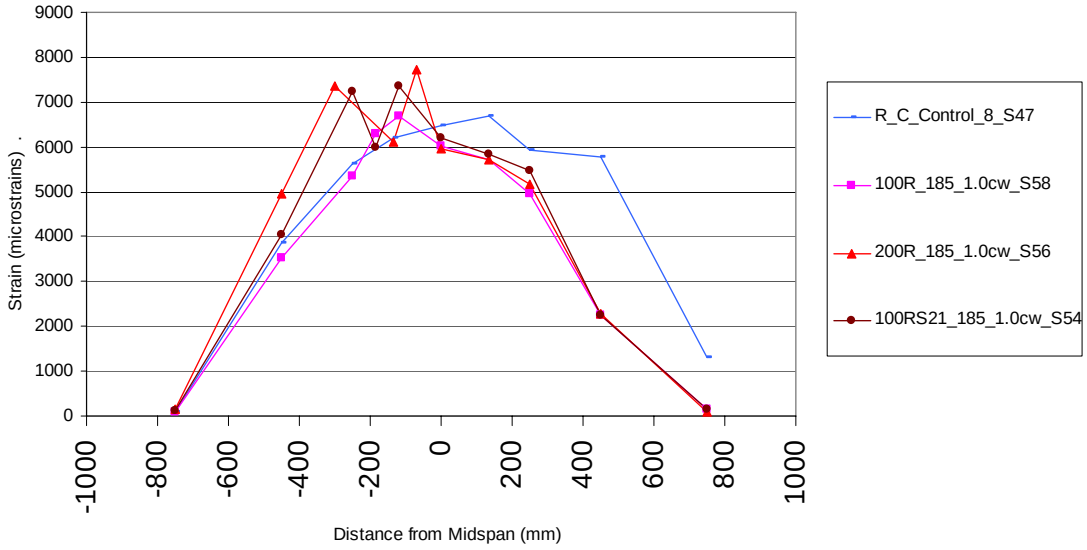

Figure 4-57: Representative strain profiles.

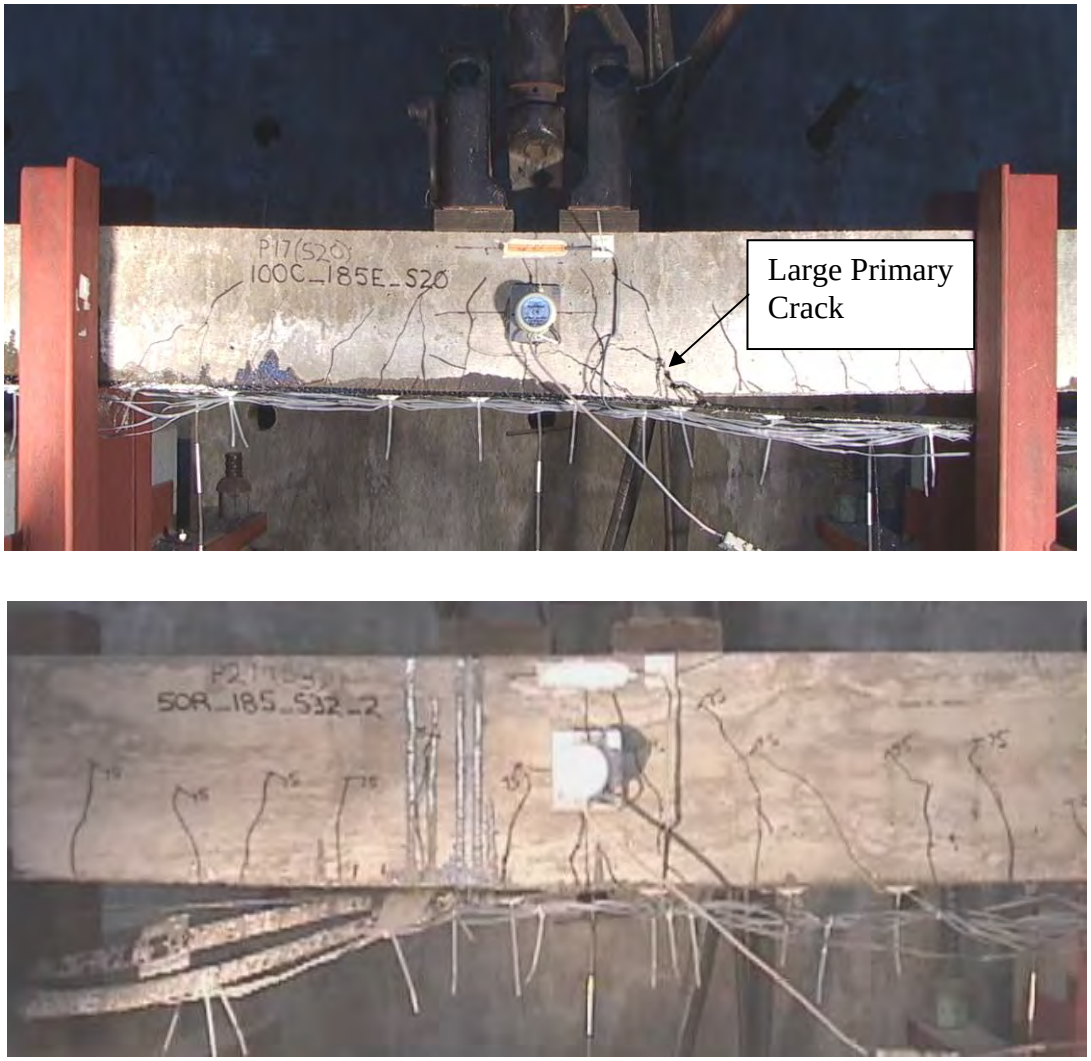

Figure 4-58: representative photos of large primary crack (top) and a multiple distributed cracks (bottom).

Table 4-16: Load vs. measured crack width (mm) during testing.

Load (kN)	100R (S53)	100R (S58)	200R (S56)	100Rx2 (S57)	100RS7 (S55)	100RS21 (S54)
0	1.2	1.1	1.0	0.8	1.8	1.0
36	1.8	-	1.1	0.8	2.4	1.1
2.5	1.4	-	1.0	0.8	1.9	1
75	1.8	-	1.2	0.9	2.5	1.2
2.5	1.6	-	1	0.8	2.3	1
90	1.8	-	-	-	2.7	1.2
2.5	1.6	-	-	-	2.3	1.1

xxxR = Disbond size in mm
(Sxx) = Specimen Number

Figure 4-59 shows the max load plotted for each specimen in this set. The specimens with disbonds are shown to fail at very near the same ultimate load as the control specimen that was manufactured in the same rehabilitation. However, when compared to specimen 52, which was a beam preloaded to 1.0 crack width without a disbond, they are in the range of 3% to 10% weaker. This behavior is in contrast to Figure 4-60, where the specimen displacement at failure is well aligned with specimen 52, but significantly less than the control specimen (S47). This set of specimens, much like the others shows several aspects of pertaining to the effect of defects at the local level by measuring strains and cracking behavior, yet in order to better asses the impact on global performance the specimens must be sorted by their respective failure modes due to material variability in the concrete and in the adhesive.

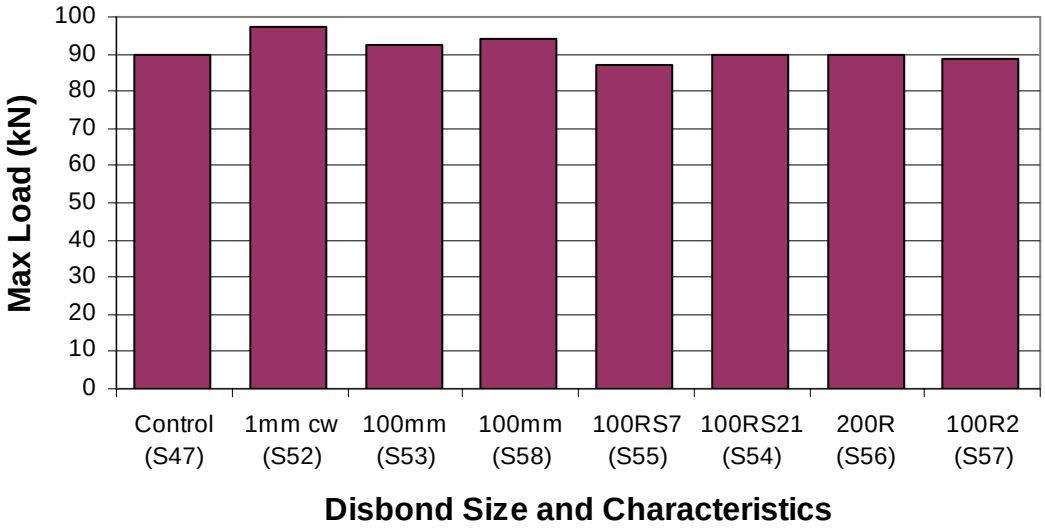

Figure 4-59: Max load versus defect(s) size and characteristics.

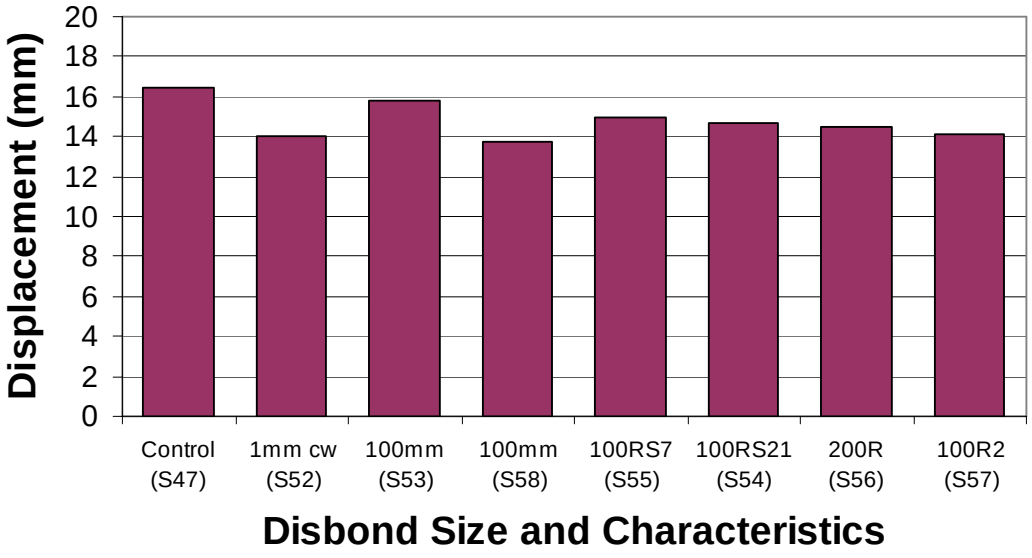

Figure 4-60: Displacement at debonding versus defect(s) size and characteristics.

Of the seven specimens in this set, three failed by debonding by the “deep concrete, steel” failure mode (specimens 52, 56, and 55), two debonded through a thick concrete bondline (specimens 53 and 54) and two debonded through a thin concrete bondline (specimens 57 and 58). Since three failed by “deep concrete, steel”, a subset for comparison of these three specimens behavior properties was chosen. Figures 4-61 through 4-66 show trends relating to the specimens’ load, displacement and FRP strain behavior at ultimate and steel yielding conditions. Specimen 52 had a greater ultimate load, load at steel yield, displacement at steel yield, FRP strain at steel yield and FRP strain at maximum load than the two specimens with disbonds and specimen 55 failed at the lowest load of the three. This suggests that these performance factors are affected significantly by the presence of disbonds in the specimens preloaded to a residual crack width of 1.0mm. The displacement at debonding shown in figure 4-62 actually shows the opposite trend as compared to the other performance factors with specimen 55 having the greatest displacement at debonding and specimen 52 having the least. However, all three values for displacement at debonding are very close (less than 1mm difference) suggesting the presence of unbonded lengths in this case may not have a large influence on this factor.

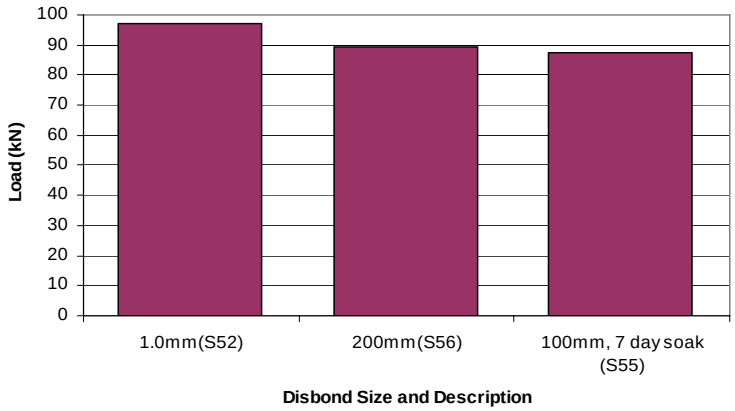

Figure 4-61: Max load versus defect(s) size and characteristics for specimens debonding by the “deep concrete, steel” failure mode.

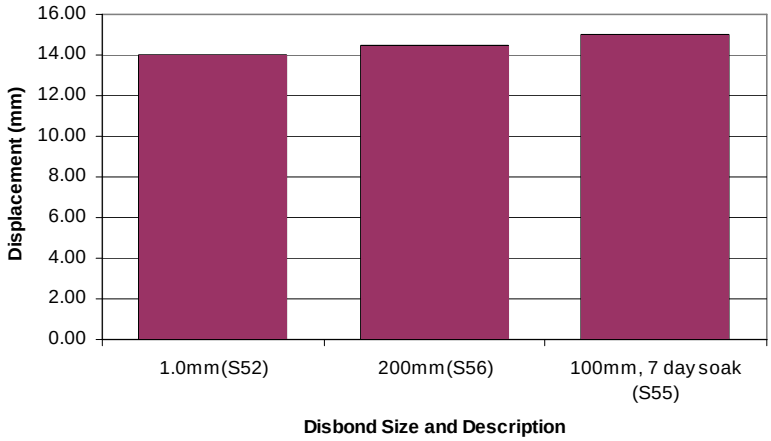

Figure 4-62: Displacement at debonding versus defect(s) size and characteristics for specimens debonding by the “deep concrete, steel” failure mode.

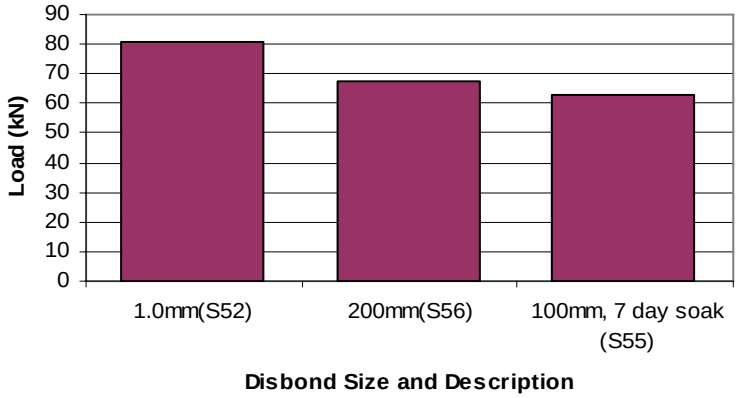

Figure 4-63: Load at steel yield versus defect(s) size and characteristics for specimens debonding by the “deep concrete, steel” failure mode.

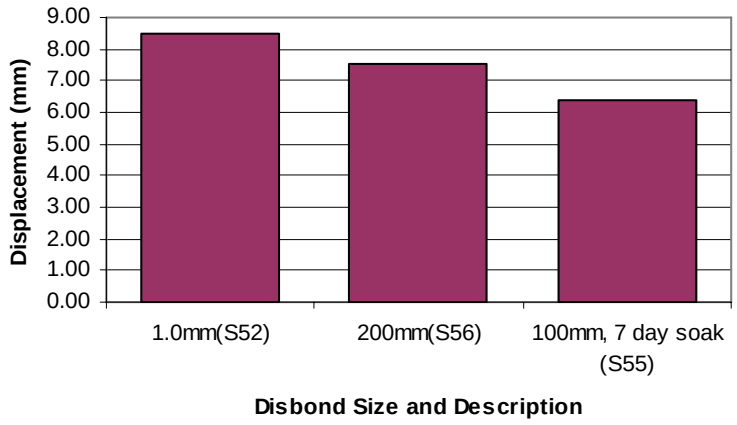

Figure 4-64: Midspan displacement at yield versus defect(s) size and characteristics for debonding by the “deep concrete, steel” failure mode.

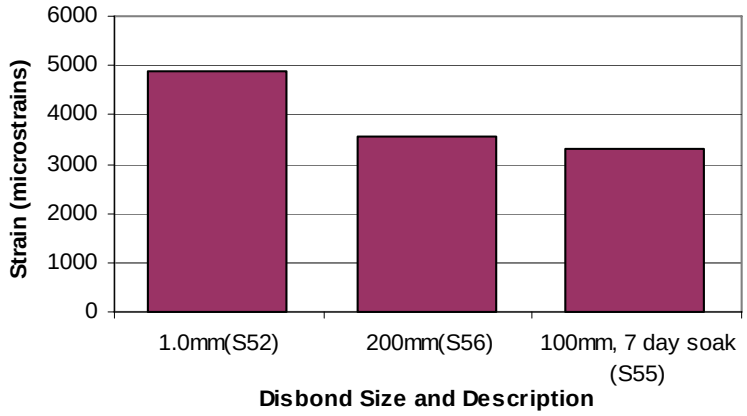

Figure 4-65: FRP strain at yield versus defect(s) size and characteristics for specimens debonding by the “deep concrete, steel” failure mode.

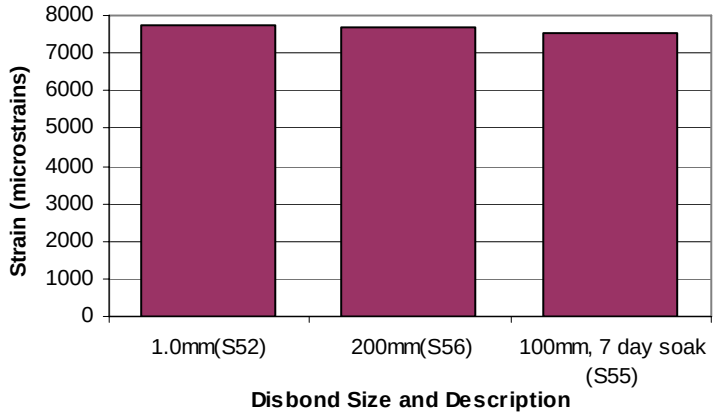

Figure 4-66: Maximum FRP strain versus defect(s) size and characteristics for specimens debonding by the “deep concrete, steel” failure mode.

4.4.3 Submerging FRP in Water

Figures 4-67 through 4-69 demonstrate the observed effect of submerging the tension face of specimens 55 and 54 in one inch of water one day after rehabilitation for periods of 7 and 21 days respectively. Note that the ultimate load of the specimens drops slightly from 93.4kN for the un-soaked beams to 87.3kN and 89.9kN for the specimens 55 and 54 respectively. Despite the loss in ultimate capacity displacement at debonding and FRP strain at debonding appear to be relatively unaffected.

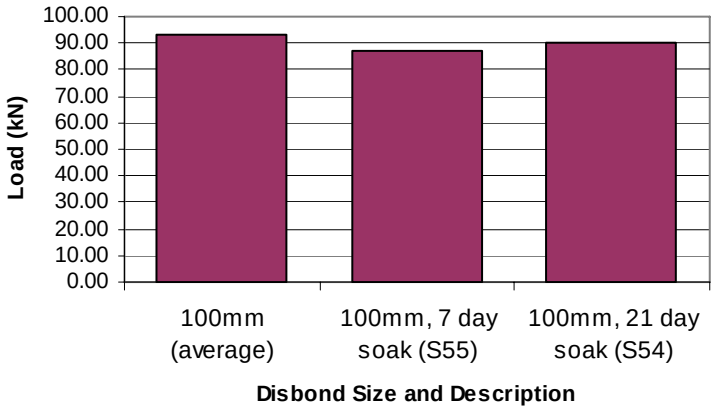

Figure 4-67: Ultimate load versus defect(s) size and characteristics for specimens soaked in water.

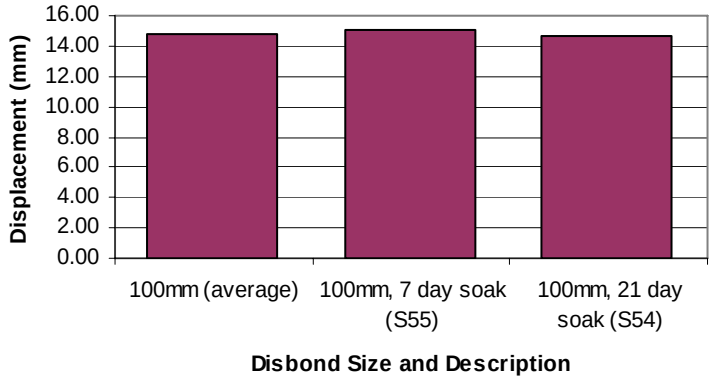

Figure 4-68: Ultimate load versus defect(s) size and characteristics for specimens soaked in water.

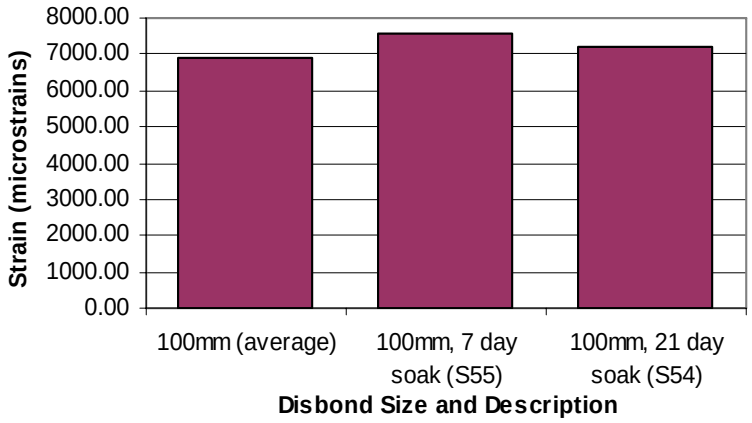

Figure 4-69: Maximum FRP strain versus defect(s) size and characteristics for specimens debonding by the "deep concrete, steel" failure mode.

4.5 Interlaminar Disbonds

This set of beams was created to investigate the differences in performance when disbonds occur at various locations in the FRP and adhesive material. As described in section 2.4.1, Circular and Rectangular 100mm disbonds were inserted in the adhesive interface, the interlaminar interface, and in both locations simultaneously at the critical location of 185mm from the midspan location. Figure 4-70 consists of plots of the load versus midspan displacement curves for this set of specimens. As has been typical for all the sets thus far, the global behavior is nearly identical until after the initiation of local debonding, at which point the specimen behavior quickly diverges. Figure 4-71 shows the typical midspan steel strain versus load plots for the specimens in this set and a control specimen. The steel strain behavior can be seen to be quite similar until debonding at which point the maximum useable range of the strain gage is exceeded for the specimen containing the disbond (S41).

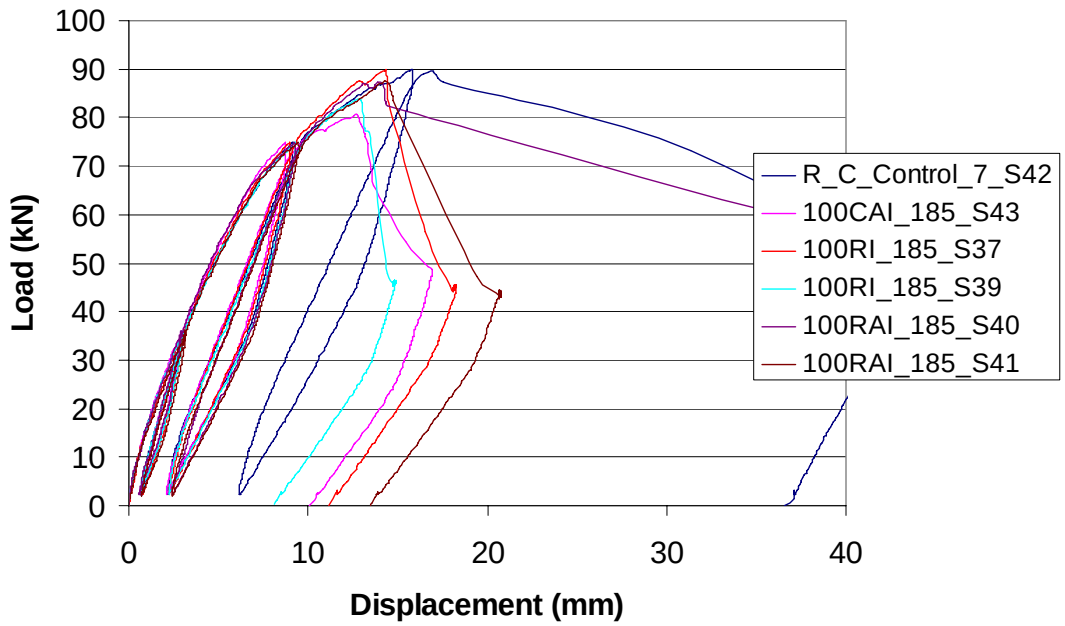

Figure 4-70: Characteristic load vs. displacement plots for various interface disbond locations.

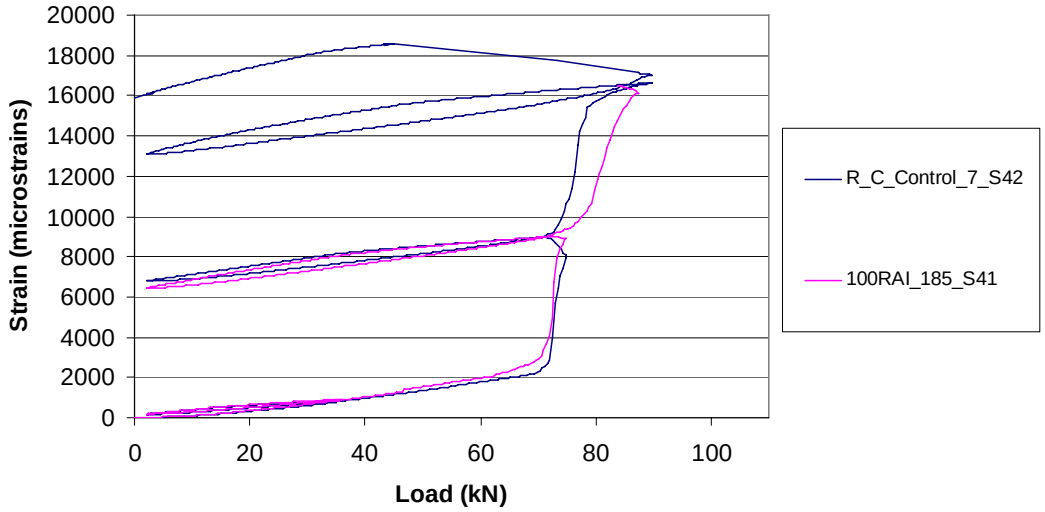

Figure 4-71: Representative steel strain vs. load plots for interlaminar disbonds.

Table 4-17: Beam behavior characteristics for determination of the effect of interlaminar disbonds.

Description / Beam Characteristic	Adhesive, (S8)	Adhesive, (S4)	Adhesive, (S31)	Adhesive, (S38)	Interlaminar Interface, (S37)	Interlaminar Interface, (S39)	Adhesive, Interface, (S40)	Adhesive, Interface, (S41)	Adhesive, Interface (S43)
Maximum Load (kN)	90.11	83.5	80.28	86.68	89.84	83.97	87.18	87.47	80.78
Displacement at Maximum Load (mm)	15.06	15.5	12.00	14.19	14.37	12.87	13.90	14.30	12.75
Steel Strain at Yield (me)	2437	2385	2353	2507	2287	2393	2582	2319	2277
Load at Steel Yield (kN)	67.26	68.84	65.99	66.90	68.90	62.10	68.17	67.84	67.90
Midspan Displacement at Steel Yield (mm)	7.75	8.48	7.55	7.69	7.46	6.59	7.31	7.45	7.12
FRP Strain at Steel Yield (me)	3130	3568	3589	4176	3483	3413	3931	4343	3205
FRP Strain at Debonding (me)	6787	6261	6658	7068	7127	6224	6940	7201	5979
Debonding Direction	Left	Right	Left	Right	Right	Left	Right	Left	Right
Location of Debond Initiation	Right Load-Point / Defect	Right Load-Point	Left Load-Point	Left Load-Point	Midspan	Left Load-Point	Defect	Midspan	Midspan
Failure Mode	Deep Concrete, Steel	Thick Concrete Bondline	Resin Interface	Resin Interface	Thick Concrete Bondline	Resin Interface	Thin Concrete Bondline	Resin Interface	Resin Interface

Figure 4-72 is the FRP strain profile for some of the typical specimens in this set. Like the specimens with disbonds located only in the adhesive investigated earlier in section 4.2.2, specimens with disbonds located in the interlaminar interface and in both locations develop stress concentrations near the edges of the disbonds. Table 4-18 shows the crack widths for each specimens at the top and bottom of each load cycle. The specimens with disbonds located in both the adhesive layer and between the FRP layers had the largest measured crack widths at the top of the various load cycles.

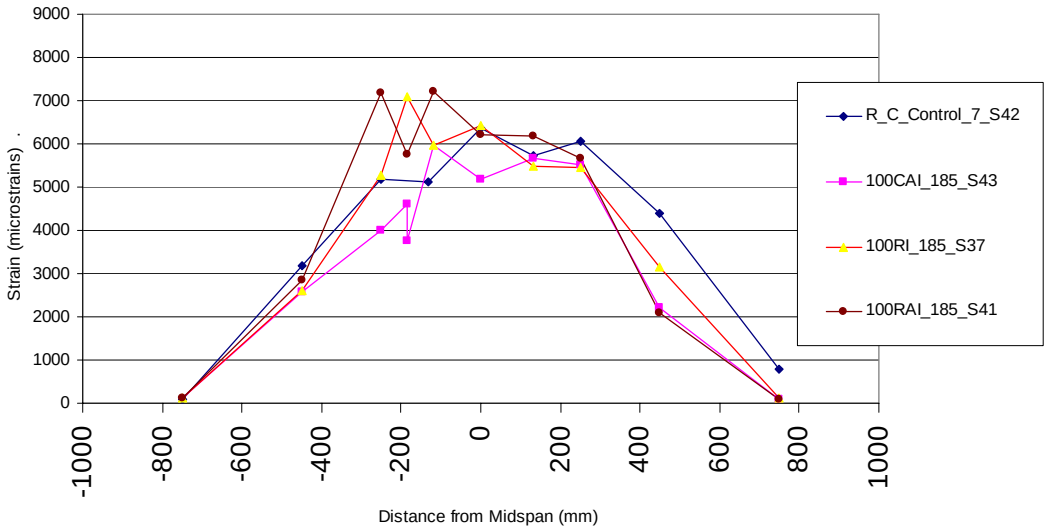

Figure 4-72: Representative strain profiles.

Table 4-18: Load vs. measured crack width (mm) during testing.

Load (kN)	100CAI (S43)	100RI (S37)	100RI (S39)	100RAI (S40)	100RAI (S41)
0	<0.1	<0.1	<0.1	<0.1	<0.1
36	0.1	<0.1	~0.05	<0.1	<0.1
2.5	<0.1	<0.1	<0.1	<0.1	<0.1
75	0.3	0.1	0.2	0.5	
2.5	0.1	<0.1	0.1	0.2	0.1
90	-	-	-	-	-
2.5	-	-	-	-	-

Figures 4-73 and 4-74 show the max loads for each specimen tested in this set. The specimens with disbonds considered in this set were found to carry a lower load than the control specimen, but there is no difference in peak load apparent between specimens with disbonds between FRP layers and those with disbonds in both locations. Figure 4-74 suggests that the displacement at debonding is not influenced by an additional disbond between the FRP layers either, although in this case, the displacements at debonding for all the specimens in this set were significantly less than their respective control specimen (S42) for this rehabilitation.

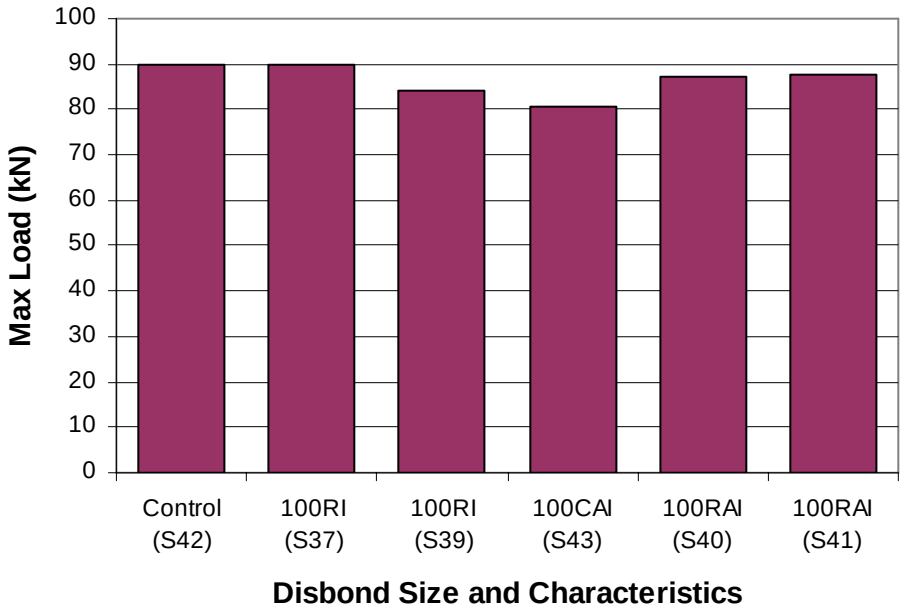

Figure 4-73: Max load vs. disbond characteristics

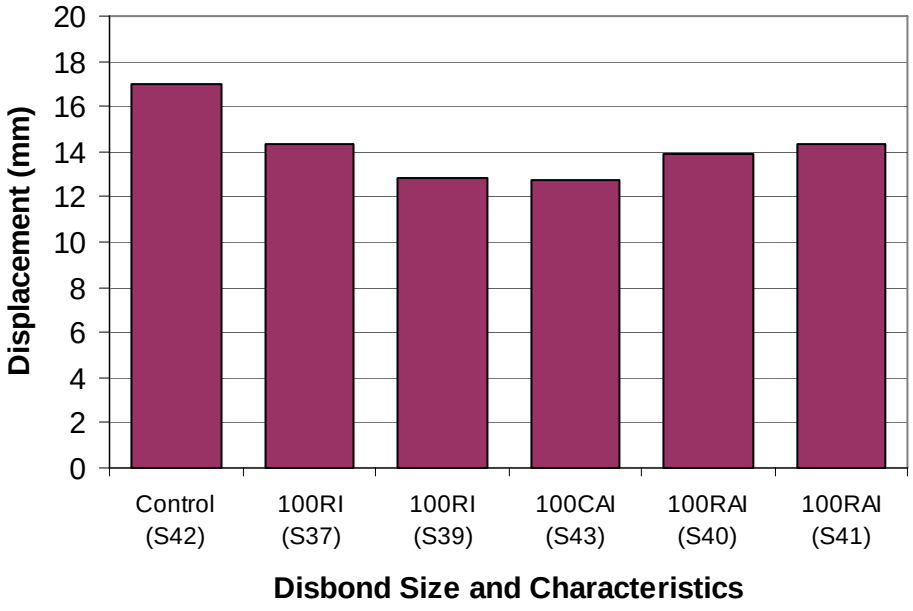

Figure 4-74: Displacement at debonding versus disbond characteristics

In order to better compare specimens, figures 4-75 through 4-77 show the individual results from four specimens in this set that failed with a common failure mode of debonding through the resin interface. Specimens 31 and 38 are both specimens that were rehabilitated with disbonds in the adhesive layer only. They have been left separate here instead of averaging their values so the variability between the two due to reasons unrelated to the defect can be seen. Specimen 39 is a rehabilitated beam with an unbonded region located between the two FRP layers only. Finally, specimen 41 is a beam rehabilitated with unbonded lengths in both the adhesive layer and between FRP layers. As can be seen in figures 4-75 through 4-77, the specimen behavior is difficult to differentiate in this case. The specimens 39 and 41 each performed very similarly to one of the two specimens with a disbond located in the

adhesive layer only, suggesting that differences in behavior cannot be detected due to the natural scatter occurring in this subset because of the inconsistent behavior associated with debonding through the adhesive resin interface discussed earlier. Therefore, based on this study a debond detected in the field should be considered to have an equally significant influence on structural behavior irrespective of whether it is detected in the adhesive layer, between FRP layers, or both locations.

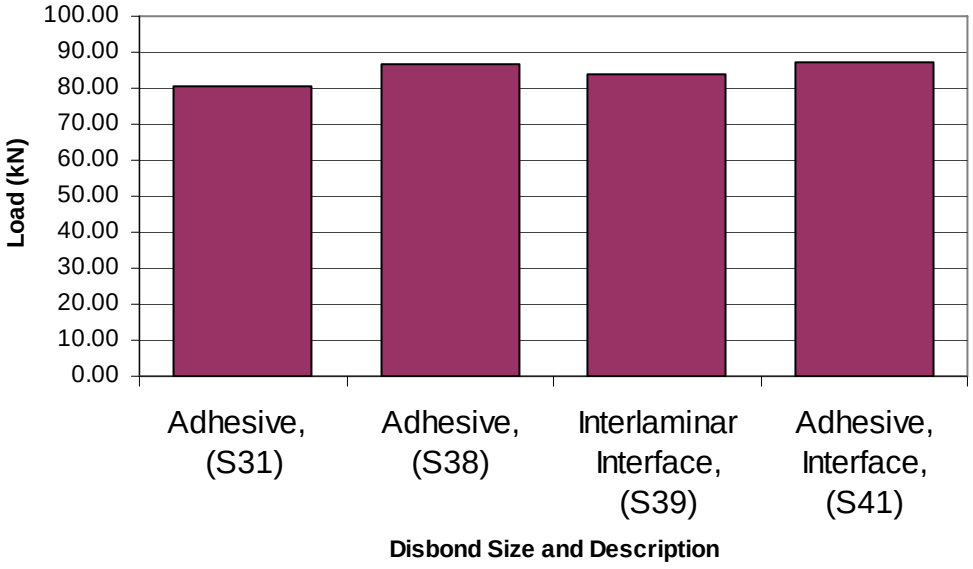

Figure 4-75: Max load vs. disbond characteristics for specimens debonding through the “resin interface” failure mode.

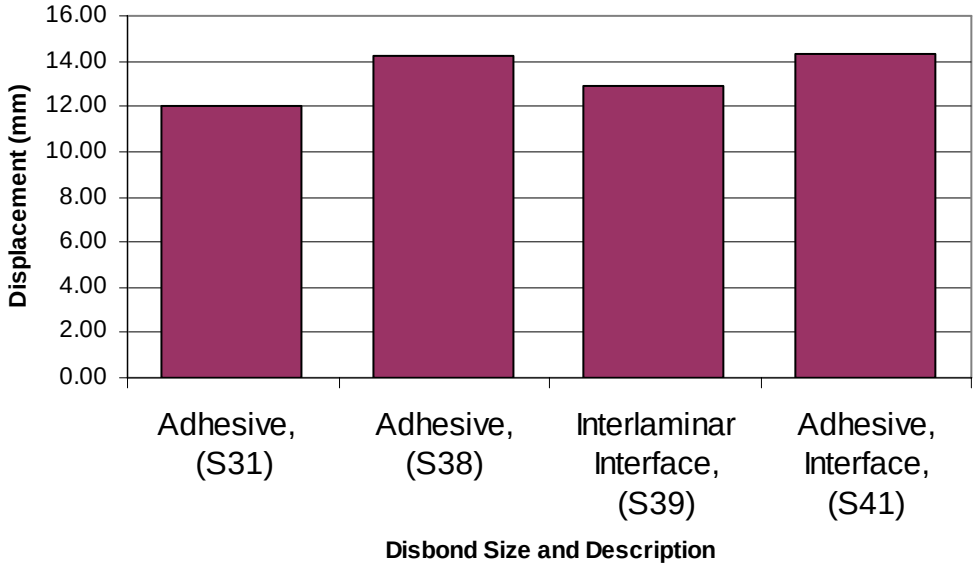

Figure 4-76: Displacement at debonding vs. disbond characteristics for specimens debonding through the "resin interface" failure mode.

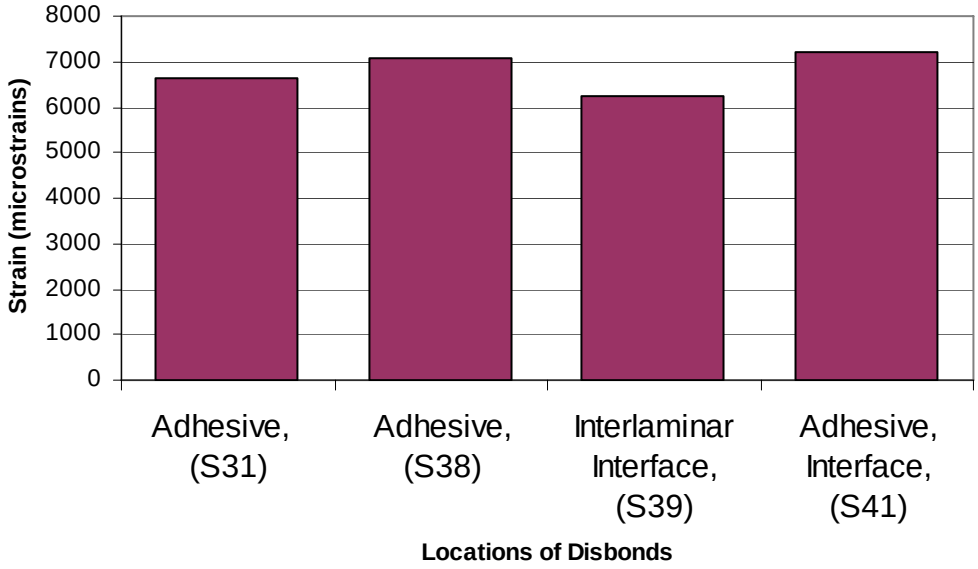

Figure 4-77: Maximum FRP strain vs. disbond characteristics for specimens debonding through the "resin interface" failure mode.

References

ACI Committee 224, *Joints in Concrete Construction*, ACI 224.3R-95, American Concrete Institute, Famington Hills, MI, USA, p. 21, 2004.

Arduini, M. and A. Nanni, *Behavior of Precracked RC Beams Strengthened with Carbon FRP Sheets*, Journal of Composites for Construction, Vol. 1, No. 2, p. 63-70, 1997.

Chan, T. K. and M. Niall, *Strengthening of One-way Slabs Using Carbon Fibre Plates: The Effect of Preload*, CSE Research Bulletin, No.14, 2001.

Seim, W., M. Horman, V. Karbhari, and F. Seible, *External FRP Poststrengthening of Scaled Concrete* Slabs, ACSE Journal of Composites for Construction, Vol. 5, No. 2, pp. 67-75, 2001.

Shahawy, M, O. Chaallal, T: E. Beitelman, and A. El-Saa, *Flexural Strengthening with Carbon Fiber-Reinforced Polymer Composites of Preloaded Full-Scale Girders*, ACI Structural Journal, Vol. 98, No. 5, p. 735, 2001.

Sharif A., G.J. Al-Sulaimani, I.A. Basunbul, M.H. Baluch and B.N. Ghaleb, "*Strengthening of Initially Loaded Reinforced Concrete Beams Using FRP Plates*", ACI Structural Journal, Vol. 91, No. 2, , pp. 160-168. 1994.

5. DISCUSSION OF RESULTS

5.1 Significant Observations of Results

The mean ultimate load of the four unstrengthened control specimens was 54.2kN. In contrast the mean ultimate loads of the non-preloaded and preloaded, strengthened control specimens were 93.9kN and 90.8kN, respectively. From these values, the FRP strengthening resulted in an average increased capacity between 68.8 percent and 73.2 percent. Additionally, the average increase in the load at longitudinal steel yield was 57.5 percent greater than the control specimens. The unstrengthened control specimens were designed to be very ductile and held near peak load for very large displacements until the specimen was considered failed by severe concrete crushing and cracking damage between 61mm and 71mm midspan displacement. However, with the application of FRP this ductility was lost and global debonding would occur in the range between 12.8mm and 17.7mm midspan displacement, resulting in an immediate large drop in capacity. The beams containing manufactured defects investigated in this study generally performed very close to the same as the strengthened control specimens relative to the unstrengthened specimens. Given the fairly small number of the specimens investigated in this study as well as the large variability in the performance of all three types of control specimens, differences in global performance were often difficult to quantify with certainty. However, local effects of the defects were generally much more observable and reveal some important considerations about the effect of defects on FRP strengthened concrete.

All of the defects investigated indicated that there were easily observable, significant local effects due to these defects. These local effects were observed with the assistance of strain data in the FRP, measured crack widths and noted crack patterns and characteristics. These characteristics likely had an effect on global performance. However, in this investigation these global effects due to short term loading were more difficult to determine due to the large variability in the materials in each test and the limitations of the number of specimens tested making it difficult to determine any statistical inference. In order to address this problem, specimens within a defect set were sorted and compared according to their respective failure modes.

Stress concentrations were a key local effect that was measured by strain gages near defects. This included regions of very high stress near the edges of disbonds, relatively less stress inside the unbonded area where no shear transfer exists, and high stress at locations of concrete cracks where the concrete stress continuum is interrupted. Additional effects observed in the region of a disbond included the concrete cracking patterns and crack widths. As can be seen in figures 4-13 and 4-25 in the previous chapter, generally very little new cracking occurred within the area of the disbond. However, usually the largest crack occurred within 25mm outside the edge of the unbonded region and extensive, tightly spaced cracks were often found within this region on each side of the disbond. Typically the largest crack in a beam with an unbonded region was a very large diagonal shear crack that propagates as denoted by the arrows in figure 4-25. These local effects were very pronounced in high-moment regions of the beam ranging from the left quarterspan to the right

quarterspan. Regions investigated outside the quarterspan area had minimal observable local effects.

As mentioned, specimen variability not related to the purposely manufactured defects was a limitation in this investigation for assessing the global influence of defects on behavior. The unstrengthened control specimens alone, for example, had a standard deviation in their mean strength of 3.9kN, while the strengthened control specimens strength varied with a standard deviation of 5.1kN. This variability in the control specimens is difficult to work with when assessing the performance of specimens with defects because often their peak loads fell well within one standard deviation of the strength of the control specimens. Figure 5-1 shows the mean strength of the four debonding failure modes defined in this investigation (see Appendix A for further details on the determination of the failure modes). This figure clearly shows how much more influential the specimen debonding failure mode was in contrast to the defects in the categories defined in chapter 4. It would be advantageous to find a relationship between the specimen debonding failure mode and the defects that were manufactured. However, if a relationship exists, it is not readily apparent in the data obtained in this study. Instead, the relationship determining the debonding failure mode seems to be much more closely tied to the rehabilitation set number. Shown in figure 5-2, is a schematic of the distribution of the debonding failure modes for each rehabilitation set conducted in this investigation. The sixty-one specimens investigated in this study were rehabilitated in seven different sets occurring on different dates throughout the investigation (see table 2-5). Notice how each rehabilitated set in figure

5-2 is dominated by a specific failure mode with the exception of set number five. Additionally, rehabilitation sets one through four were conducted on specimens from concrete cast number one (which was stronger concrete), while the rehabilitation sets five through seven were conducted on specimens from the second concrete casting. Notice that specimens tested from cast number one was largely dominated by debonding failure modes of “deep concrete, steel” and “thick concrete bondline,” while specimens from cast number two were dominated by failure modes “thin concrete bondline” and “resin interface.” There were two key differences between casts number one and number two: 1) Cast number one’s final concrete compression strength was 51.7MPa, while cast number two’s compressive strength was 46.8MPa; 2) After preloading, cast number one was sandblasted to a point where, visually, more aggregate was exposed than when cast number two was preloaded. Figure 5-3 shows a sketch of these four debonding failure modes and additional detail can be found in appendix A. Table 5-1 is a summary of the findings from the laboratory tests after considering the effects of the debonding failure modes.

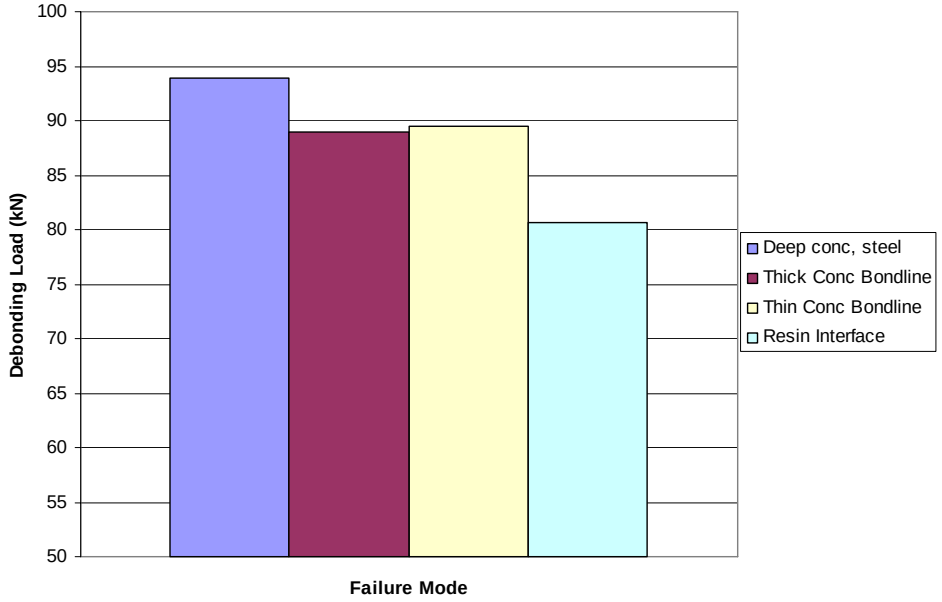

Figure 5-1: Debonding load versus failure mode

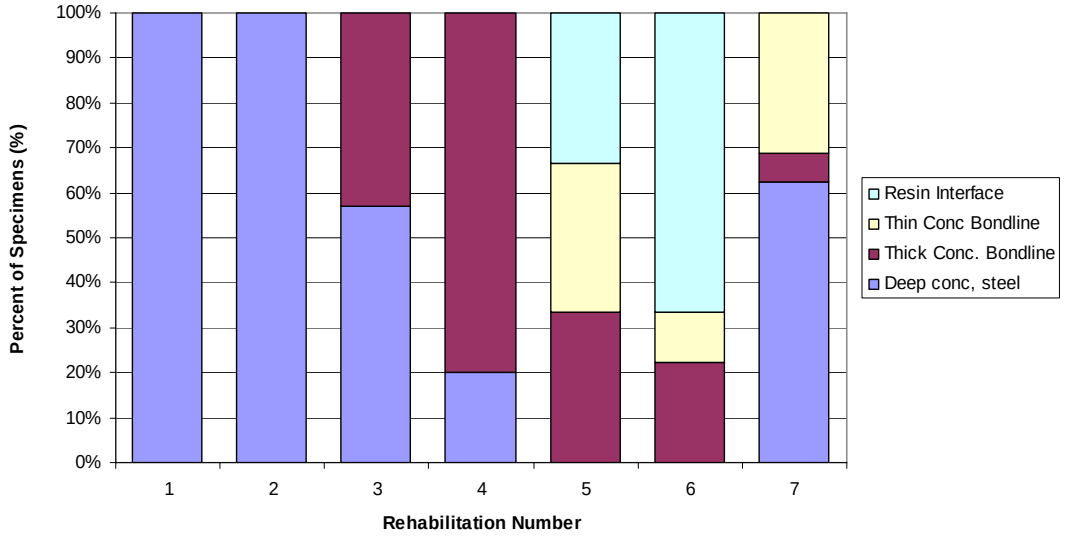

Figure 5-2: Specimen failure mode distribution in each rehabilitation set.

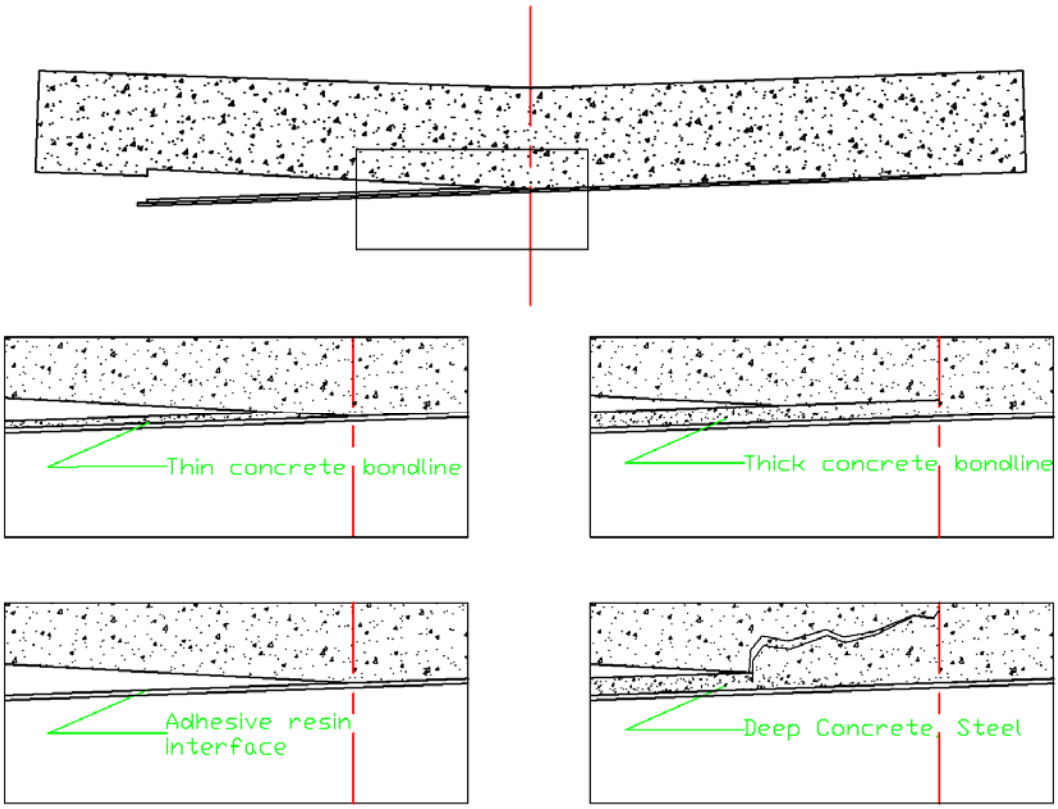

Figure 5-3: Four debonding failure modes that occurred.

Table 5-1: Summary of the Effect of Defects

Finding	Reference
1. Four debonding failure modes were observed. From best performing to worst, these modes were debonding through: a) deep concrete, steel b)thick concrete bondline c)thin concrete bondline d)resin interface	For details see: Section 4.1.3 Section 5.1 Appendix A
2. Effect of FRP strengthening: In the control specimens there was an average increase in ultimate load of 73.2% due to the application of FRP.	Section 4.1.2
3. Preloaded control specimens (preloaded to less than steel yield): No noticeable changes in specimen global response characteristics (peak load, displacement at debonding, FRP strain at debonding were all very similar). Thus the concern related to pre-existing cracks and the difference between results on uncracked and crack (to this extent) beam is shown to be minimal.	Section 4.1.3
4. Effect of circular disbond size: As disbond size increased from 25mm up to 150mm diameter a) peak load decreased b) displacement at debonding decreased c) FRP strain at debonding decreased d) stress concentrations in the FRP near disbond edges	Section 4.2.1
5. Effect of rectangular disbond size: For specimens with thick concrete bondline failure mode, as disbond size increased from 25mm to 250mm length a) displacement at debonding decreased b) displacement at steel yield remained the same c) FRP strain at debonding increased	Section 4.2.2

Table 5-1(continued): Summary of the Effect of Defects

6. Effect of circular disbond location: For specimens failing through a thick concrete bondline, as disbond locations varied from the midspan to 660mm from the midspan a) load at steel yield increased b) displacement at steel yield increased c) FRP strain at steel yield increased d) FRP strain at debonding increased Indicating that defects in high moment regions may be most critical	Section 4.3.1
7. Effect of rectangular disbond location: For specimens failing through a thick concrete bondline a disbond located 185mm from the midspan had a a) lower ultimate load b) lower displacement at debonding than the control specimen and a specimen with a disbond located at the midspan	Section 4.3.2
8. Effect of excessive preload cracking: Specimens preloaded to residual crack widths of 0mm, 0.2mm, 0.6mm, 1.0mm, 1.5mm failing with a deep concrete, steel failure mode had revealed a) the greatest peak load at 0.6mm and 1.0mm crack widths b) the greatest displacement at debonding at 0.6mm crack widths	Section 4.4.1
9. Effect of excessive preload cracking with disbonds: Disbonds caused a) maximum load to decrease b) load at yield to decrease c) FRP strain at yield to decrease d) FRP strain at debonding to remain unchanged	Section 4.4.2
10. Effect of excessive preload cracking with disbonds while soaking the tension face in water: a) maximum load decreased b) displacement at debonding remained unchanged c) FRP strain at debonding remained unchanged	Section 4.4.3
11. Effect of disbonds being located between FRP layers, at the adhesive interface, and both locations: a) no substantial differences in response were found	Section 4.5

5.2 Comparison with FEA

In an effort to validate the FEA model described in chapter 3, results were generated for the control specimens and compared to the test results. Also, adjustments were made in material properties to demonstrate the model could predict the changes in failure modes found in this testing procedure. Figure 5-4 is a comparison of the load versus midspan displacement of the unstrengthened control specimens tested in the laboratory to the FEA model prediction. This is a validation that the FEA model adequately simulates the concrete-steel behavior alone, without FRP. It is obviously important that this step be correct in order to have a reliable result when modeling specimens strengthened with FRP. As shown in the figure, the program models the initial stiffness, cracked stiffness, and yielded behavior of the unstrengthened control specimens quite well. Figure 5-5 shows a comparison of the load versus midspan displacement for non-preloaded control specimens compared to the results of the FEA model. Like the unstrenghtened control specimens, the specimen behavior was modeled quite well with the failure load occurring at very near the average peak load of the four control specimens.

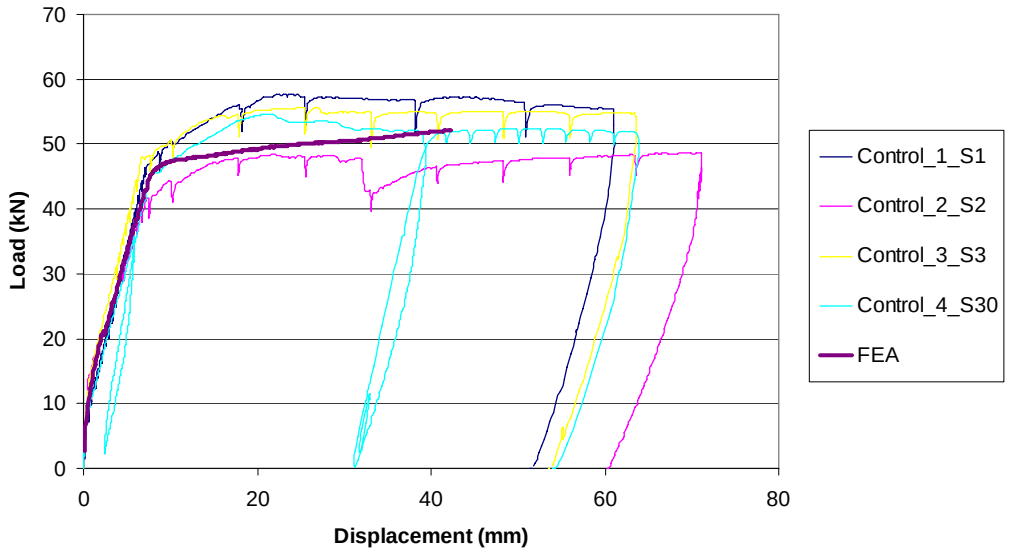

Figure 5-4: Load versus displacement comparison for unstrengthened control beams.

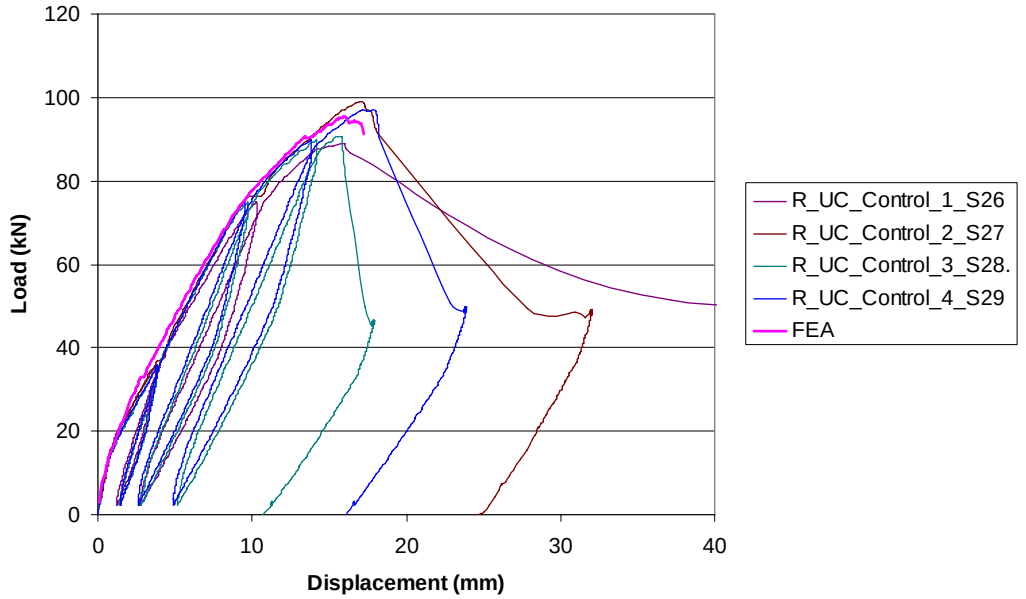

Figure 5-5: Load versus midspan displacement for specimens strengthened with FRP.

Figure 5-6 is a demonstration of the ability of the model to predict multiple failure modes depending on constituent material properties. The four curves demonstrate all combinations of high or low strength concretes and high and low adhesive fracture energies. Line number one represents the represents typical behavior in which the adhesive fracture energy is high relative to the strength of the concrete cover, but not great enough to cause FRP rupture. In this case failure is by debonding through the concrete cover, as was observed in 48 of the tests conducted in the laboratory. Line number two in figure 5-6 is the other common failure mode encountered in the laboratory tests in which the adhesive layer was weak and failed before the relatively strong concrete material. This failure mode was responsible for debonding in 12 of the beams tested in the laboratory as a result of low adhesive fracture energies. The curves labeled number three demonstrate the resulting failure in the case of an adequately strong adhesive layer to reach FRP rupture. This failure mode was only reached once during testing in the laboratory (specimen 15, in which only one layer of FRP was applied). Much of the difficulty encountered when attempting to assess the global effect of defects described in chapter four involved the large variability between the behaviors of lines one and two in figure 5-6, or some combination of the two failures. Section 5.1 and appendix A describe the failure modes encountered in the field further. The top beam shown in figure 5-7 is a graphic of the FEA program predicting this failure through the concrete cover, whereas the bottom graphic shows failure through the adhesive layer.

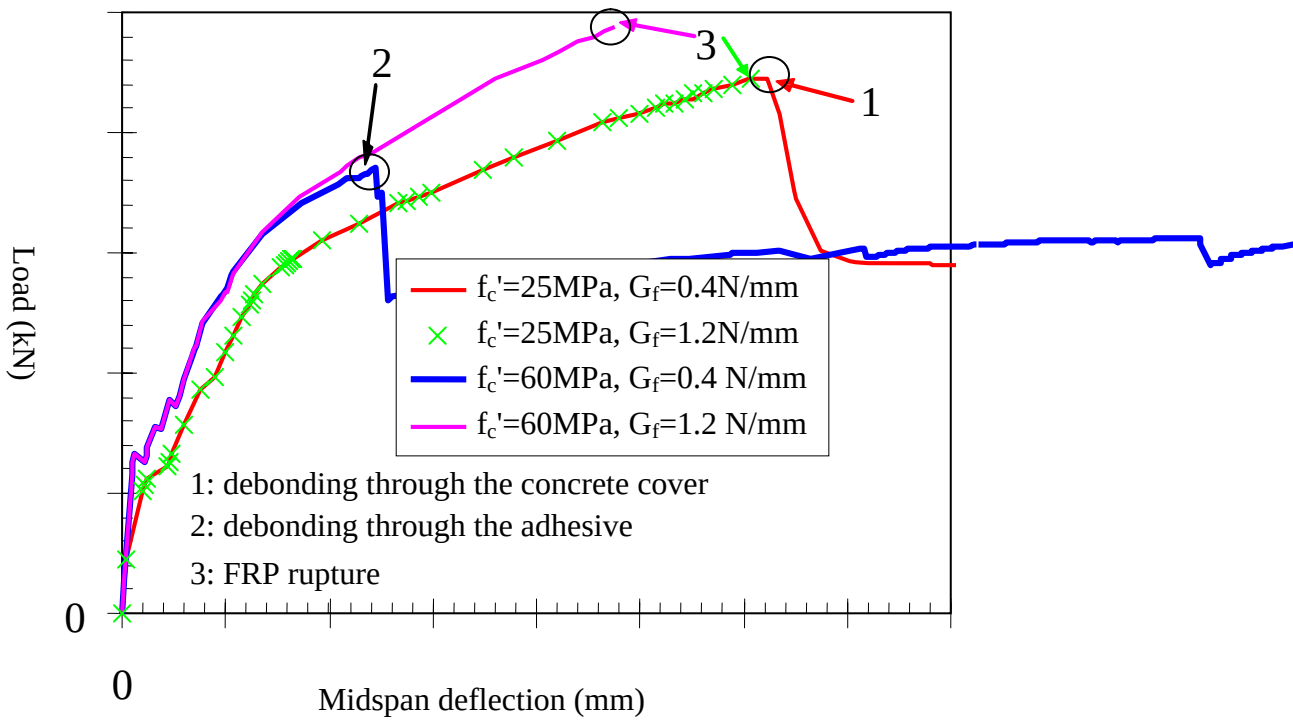

Figure 5-6: Behavior changes resulting from changes in material properties.

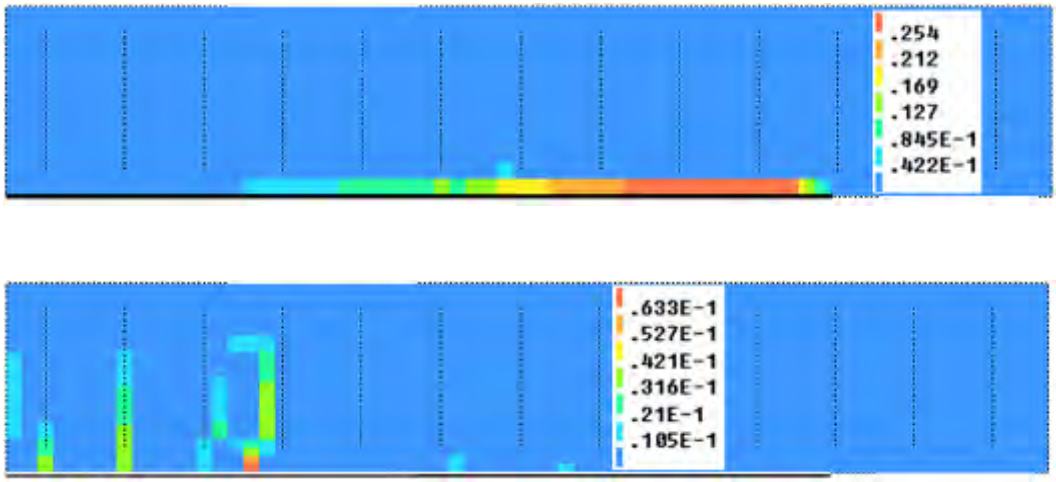

Figure 5-7: Changed debonding failure mode due to different material properties (top is debonding through the concrete substrate, while the bottom image is debonding through the adhesive).

Figures 5-8 through 5-11 show the load versus midspan displacement plots generated by the FEA model for specimens with disbonds located at the midspan, 185mm, 428mm, 660mm, and 750mm from the midspan, respectively. For each plot, curves for applicable disbond lengths of 100mm, 200mm, 250mm, and 400mm have been generated so the relative effect of a disbond at several locations and sizes can be compared.

In figure 5-7, the first term in each curve label in the key refers to the location of the defect in millimeters from the midspan (all are labeled “0” in figure 5-7 since the disbond is at the midspan). The second term refers to the disbond length in millimeters. For example, the blue dashed curve labeled “0_100mm” refers to a disbond located zero millimeters from the midspan that is 100mm in length. All cases considered in figures 5-7 through 5-11 are labeled similarly. Figure 5-7 demonstrates that the FEA model suggests very little influence due to unbonded sections at this point. The plots diverge only slightly at very near ultimate load. A slight loss in post yielding load stiffness can be seen for the 400mm unbonded length. The lack of influence of the disbonds located at the midspan is probably due to symmetry in the beam resulting in no gradient in FRP stress demand from one end of the disbond to the other. Additionally, these disbonds were inside the region of the beam’s span from which the diagonal shear cracks form that often were observed to initiate debonding, seemingly minimizing their influence. Figure 5-8 shows the FEA results for the defects’ centroid located 185mm from the midspan of the beam. As was suggested from the laboratory testing of the specimens, beam performance up to ultimate

conditions is minimal for all specimens regardless of disbond size. However, slight variations in behavior may be observed at near ultimate behavior. Losses in stiffness due to the unbonded lengths seemed to actually increase the displacement at global debonding in some cases. The maximum loads for the 0mm (control specimen), 100mm, 200mm, 250mm, and 400mm specimens, respectively, were 95.3kN, 94.9kN, 96.8kN, 94.4kN, and 92.9kN. Interestingly, the maximum loads did not decrease proportionately as the disbond size grew, but instead varied slightly depending on the disbond size. This behavior could be occurring either because the disbond size may have an influence on the diagonal crack debonding induced debonding method described by Niu et al (2006) or simply by slight variations due to computational deviations with the changed beam configurations. In figure 5-9 results for disbonds located 428mm from the midspan are shown. This is the quarterspan location of the length of the FRP laminate. Although still no large changes initial behavior are observed due to the size of the disbonds there is a larger variation in global performance noticed as ultimate loads are approached and, for the first time, a trend where unbonded length is related to strength. The maximum load for unbonded lengths of 0mm, 100mm, 200mm, 250mm, and 400mm are 95.3kN, 95.1kN, 93.4kN, 92.1kN, and 85.3kN respectively. The very large unbonded length of 250mm has a maximum load only 3.4% less than that of the control specimen with no unbonded length. This is a relatively small difference in strength compared to the variations suggested in section 5.1 pertaining to aspects of the various debonding failure modes in the laboratory tests, thus further demonstrating why the global influence of these

defects may have been difficult to measure in the laboratory. Despite debonding loads occurring in the intuitively expected sequence, displacements at debonding for unbonded lengths at 428mm from the midspan did not specifically decrease with increased size. The displacements at debonding this set were 15.9mm, 17.1mm, 17.1mm, 16.9mm, and 13.8mm for corresponding unbonded lengths of 0mm, 100mm, 200mm, 250mm, and 400mm. The trend of unbonded lengths of 250mm or less not affecting or even increasing the displacement at debonding was also observed several times during laboratory testing as discussed in chapter 4. Figure 5-10 shows the model results for beams with disbonds located 660mm from the midspan. Maximum loads decrease as expected as the unbonded length is increased in a similar trend to the previously described set. Maximum loads for 0mm, 100mm, 200mm, 250mm, and 300mm unbonded lengths were 95.3kN, 94.6kN, 93.4kN, 91.9kN, and 90.1kN respectively. In a similar trend, the consequently calculated displacements at debonding were 15.9mm, 15.8mm, 15.4mm, 15.2mm, and 15.0mm. Interestingly, the influence on debonding load is larger than those located at 185mm and 428mm from the midspan despite being a greater distance from the location of debonding initiation where unbonded lengths were originally assumed to have the greatest influence. Although no laboratory testing was conducted pertaining to unbonded regions at the ends of the FRP, this situation was explored using the FEA model to verify the prediction of an expected behavior. Figure 5-11 shows the effect of a 100mm and 200mm unbonded length located at 750mm from the midspan of the beam compared to the control specimen. It is important to realize here that the 100mm unbonded

length leaves 50mm of bond at the end of the FRP section while the 200mm unbonded length reaches the end of the FRP section, leaving the last 200mm unbonded. While behavior for the 100mm unbonded length remains largely the same as the control specimen, the performance losses for the 200mm unbonded length at the end of the FRP are very evident. Max loads for the 0mm, 100mm, and 200mm unbonded lengths at this location are 95.3kN, 94.9kN, and 87.8kN. Corresponding displacements at debonding are 15.9mm, 16.0mm, and 14.6mm. Here, the 200mm unbonded length shows losses of 7.9% of the load capacity and 8.2% of the ductility compared to the control specimen. These large losses are due to failure by debonding from the ends of the FRP section rather than the typical failure by debonding from the midspan. This behavior has been observed by other researchers (Taljsten 1997, Malek et al 1998) and functions as an additional validation of the FEA model.

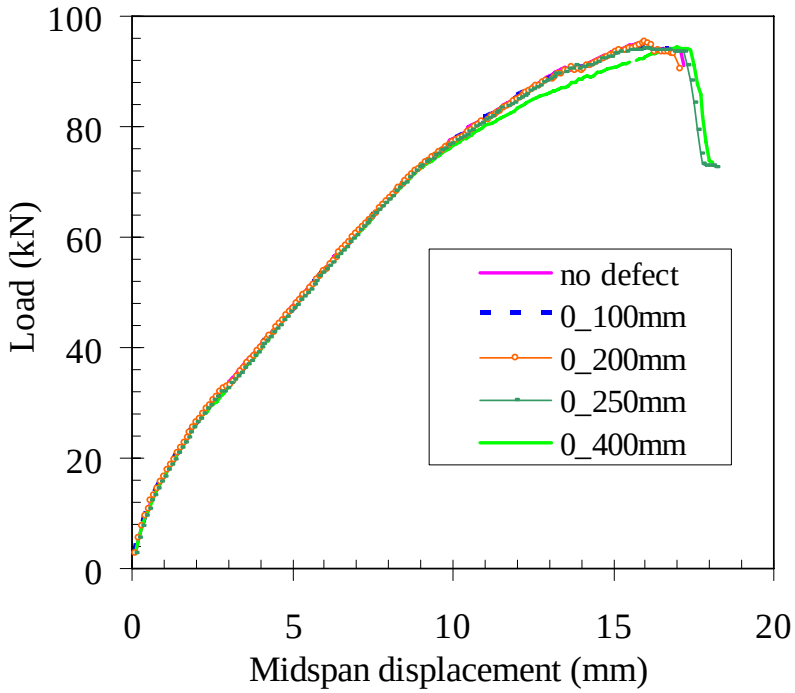

Figure 5-8: Load versus midspan displacement for disbonds located at the midspan.

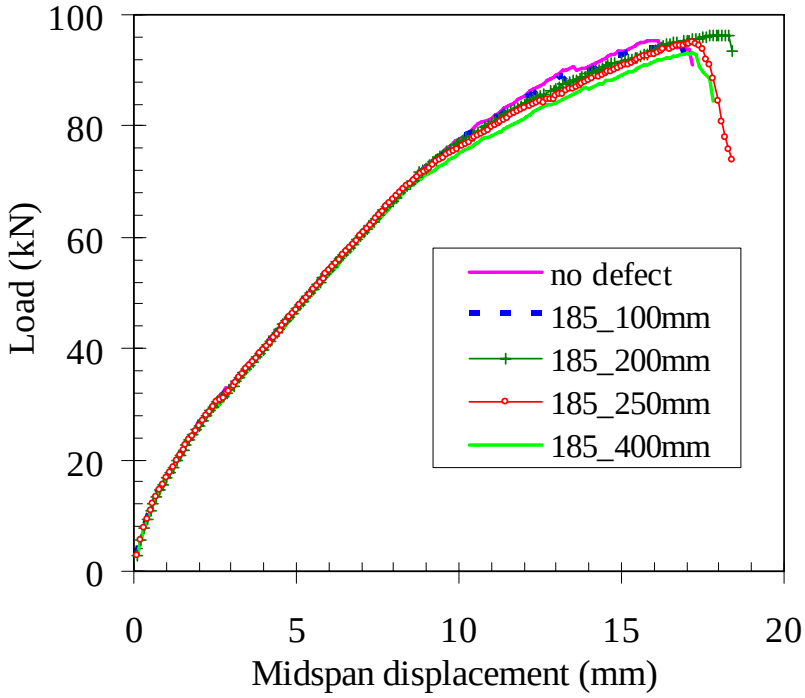

Figure 5-9: Load vs midspan displacement for disbonds located at 185mm from the midspan.

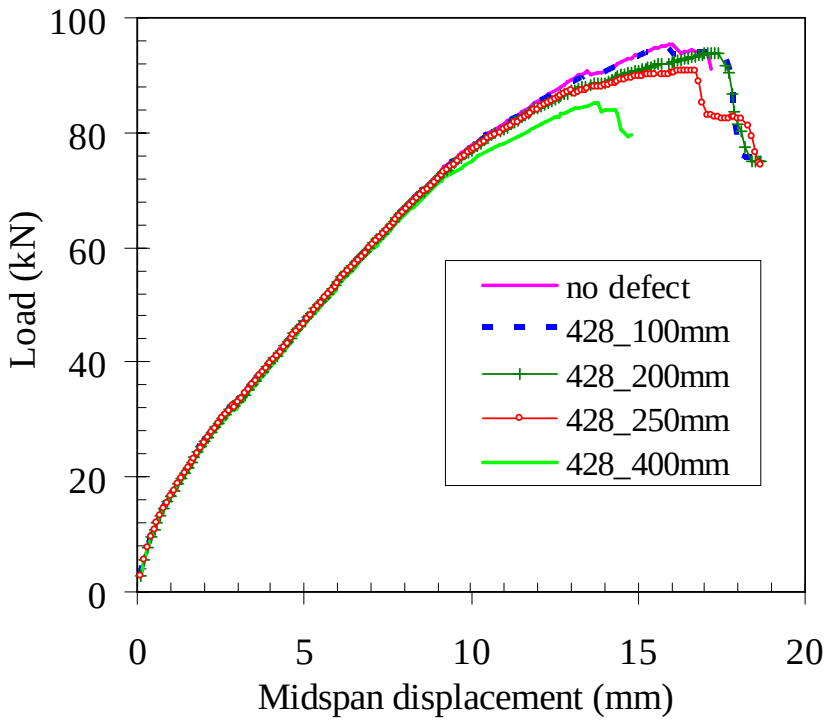

Figure 5-10: Load vs midspan displacement for disbonds located at 428mm from the midspan.

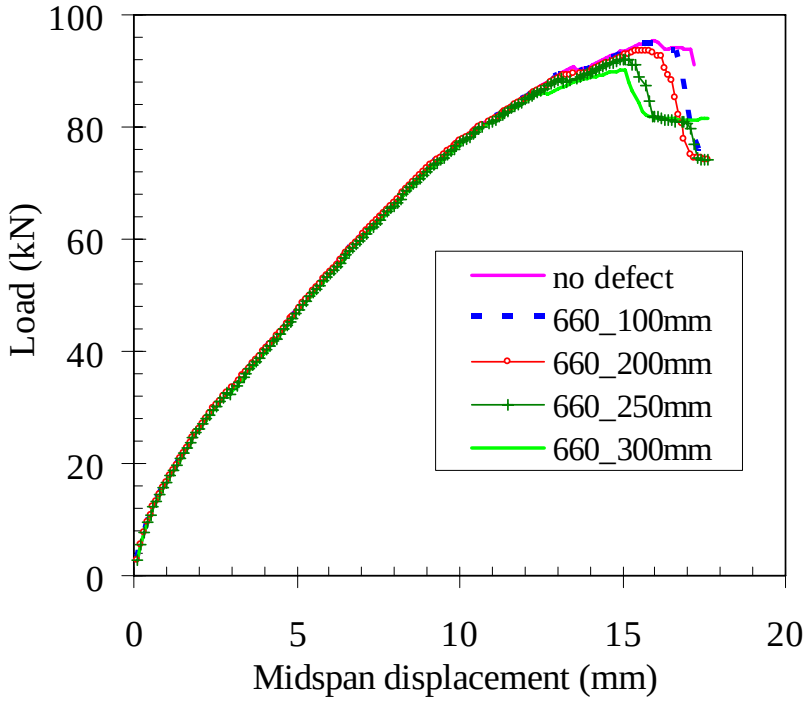

Figure 5-11: Load vs midspan displacement for disbonds located at 660mm from the midspan.

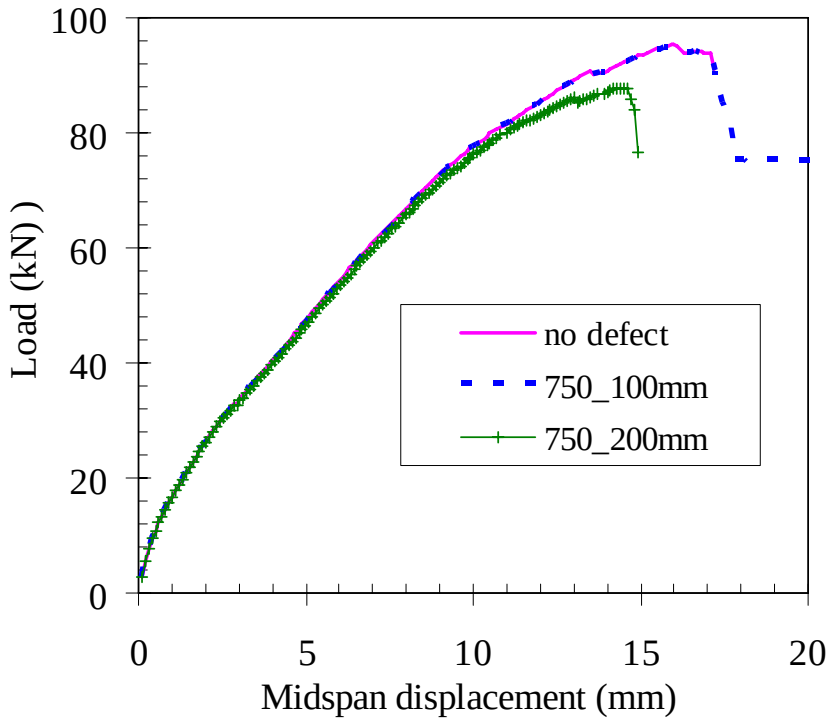

Figure 5-12: Load versus midspan displacement for disbonds located at 750mm from the midspan.

Figures 5-12 and 5-13 provide visual comparisons of the crack patterns obtained from the FEA model to pictures of the laboratory tests after failure. Figure 5-12 compares the cracking patterns for a control beam without defects. Note symmetrical crack pattern about the midspan both in the picture and the FEA graphic. Figure 5-13 shows the cracking patterns for a beam with a 250mm unbonded length located 185mm from the midspan. In this figure the approximate location of the disbond has been circled. No new cracking was observed in the region of the defect in both the FEA model and lab tests during final testing. Also, final debonding occurred on the side of the defect in both the FEA model and the tested specimen.

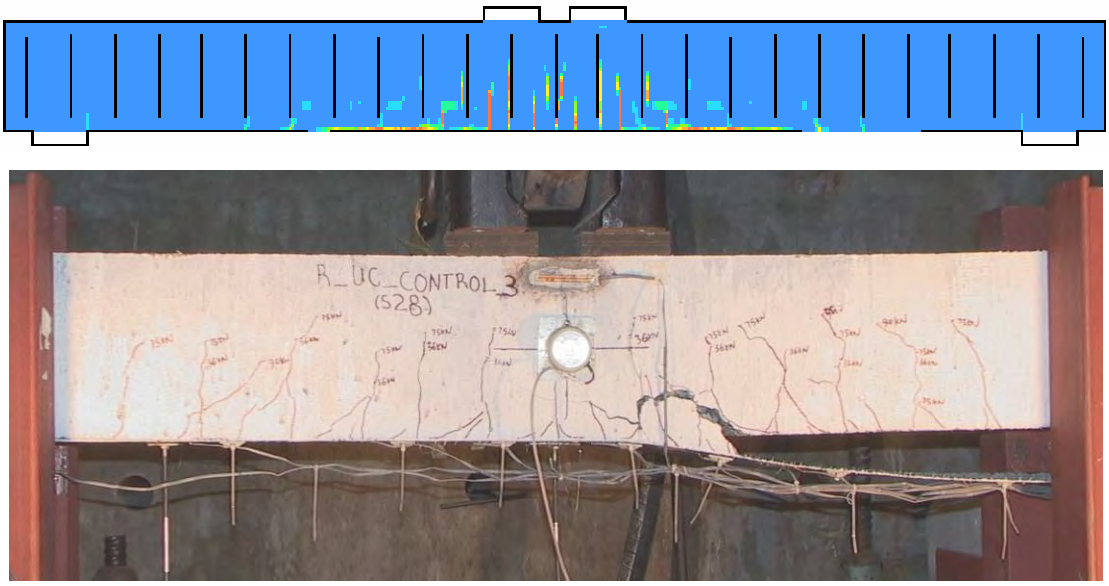

Figure 5-13: Comparison between FEA predicted cracking pattern for a rehabilitated beam without defects and a failed specimen without defects.

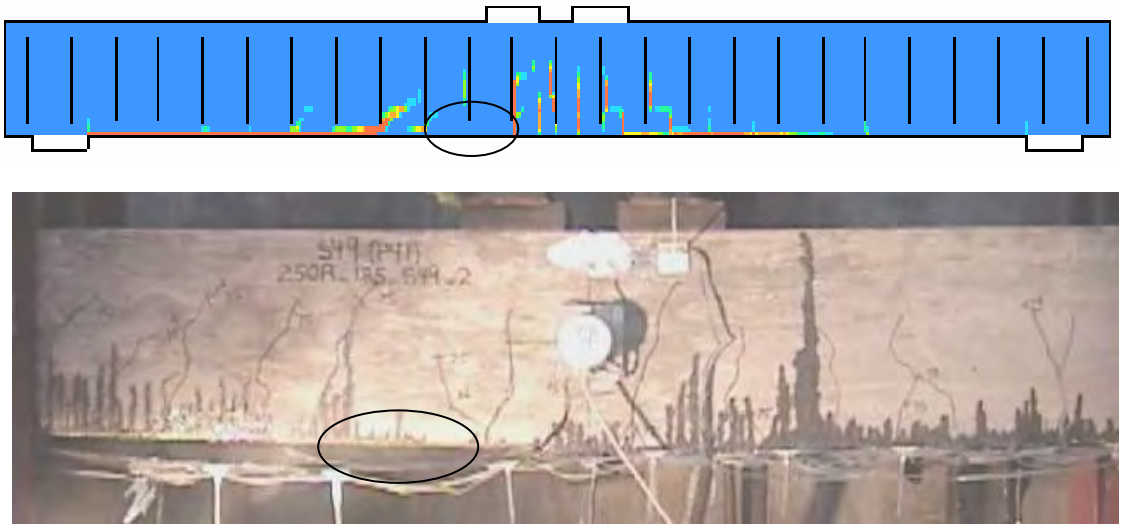

Figure 5-14: Comparison between FEA predicted cracking pattern of a beam and a failed specimen with a 250mm disbond located 185mm from the midspan.

Figures 5-14 and 5-15 compare the global performance characteristics of max load and displacement at debonding for the specimens tested in the laboratory to the scenarios tested by the FEA model. The figures emphasize how variable the laboratory results were when measuring parameters at ultimate conditions due to inconsistencies in bond quality. The large data points in the figure represent the lab data, while the thin lines represent the FEA model. The FEA model is validated to model quite adequately the behavior of the beams with and without defects. Even at ultimate conditions the model predicts the average behavior of the specimens well, as shown earlier in figures 5-4 and 5-5. The FEA model creates the ability to assess the effects of defects on ultimate behavior by eliminating the material inconsistencies encountered in the laboratory. There is still most likely some computational variations causing the choppy nature of the FEA curves generated in figures 5-12 and 5-13, however, this scatter is much less than that encountered in the laboratory. The displacement at debonding versus the disbond location from midspan shown in figure 5-12 reveals that the displacement at debonding decreases somewhat when an unbonded length is located in the exterior quarterspans of the beam and oddly, even seems to increase when the defect is located near the quarterspan location (between 250mm and 450mm). Although these trends seem somewhat pronounced in figure 5-12, the actual displacement at debonding varies only 3.0mm from the specimen with the greatest displacement at debonding to the specimen with the least. Considering the scale of the beams, the variability in the concrete control specimens alone, and that the deflection at debonding is small, it is no surprise that these differences are hard to

quantify in the laboratory. From figure 5-13, notice the maximum load for the 100mm specimen stays near constant for all locations investigated, while the very large unbonded lengths of 200mm and 250mm result in a decreased maximum load when the unbonded length is located outside the constant moment region. Excluding the last data point for the 250mm disbond, notice the maximum load for all specimens varies by 5% or less for all disbond sizes at any location. Given that this effect is so small, it is again not surprising this trend could not be extracted from the variable lab data. The final data point in the 200mm trend (located at 750mm from the midspan) shows a sharp drop in load because this is the previously noted unbonded length that results in the entire last 200mm of FRP being unbonded, changing the failure mode from interior FRP debonding to debonding from the plate end. A summary of the results obtained from the FEA is given in Table 5-2.

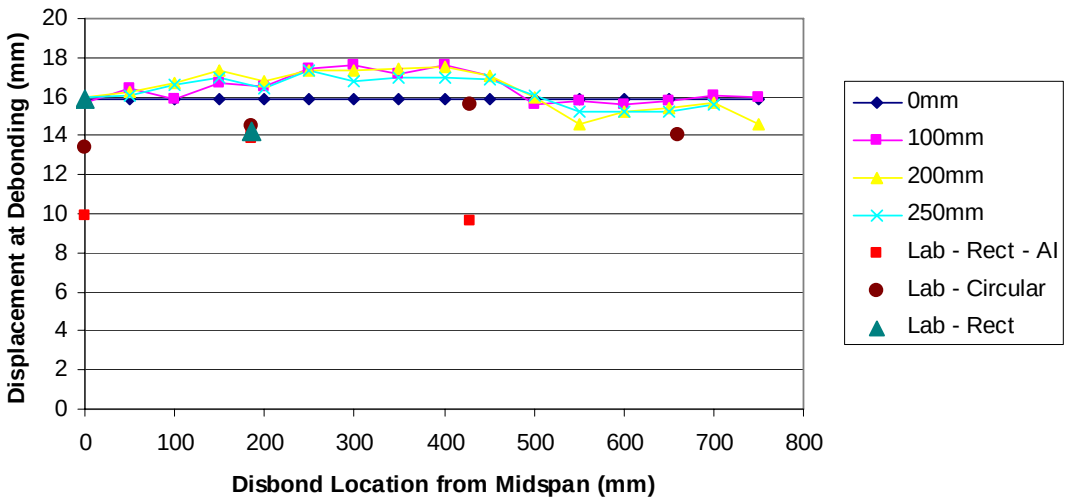

Figure 5-15: Displacement at debonding versus disbond location from midspan for FEA and laboratory results.

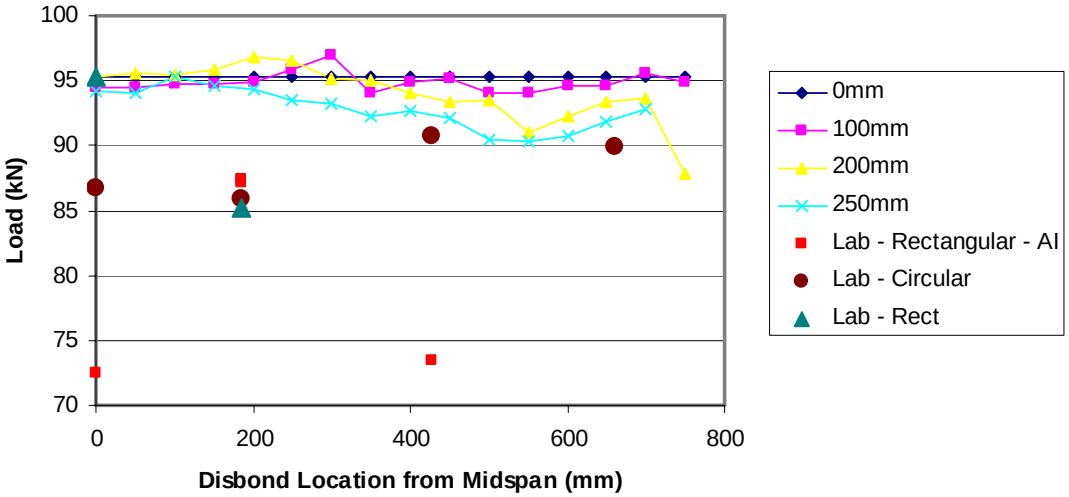

Figure 5-16: Load versus disbond location from midspan for FEA and laboratory results.

Table 5-2: Summary of FEA Results.

Finding	Reference
1. Unbonded lengths at the midspan greater than 250mm in length, showed a reduction in post-yield stiffness, but only small differences in final debonding load or displacement.	Figure 5-8
2. Unbonded lengths at 185mm from the midspan showed a reduced post-yield stiffness for disbonds larger than 100mm but only small differences in final debonding load or displacement.	Figure 5-9
3. Unbonded lengths at 428mm from the midspan showed a reduced post-yield stiffness for disbonds larger than 200mm in length and significant decreases in maximum load and displacement at debonding.	Figure 5-10
4. Unbonded lengths at 660mm from the midspan showed a reduced post-yield stiffness for disbonds larger than 100mm in length and significant decreases in maximum load and displacement at debonding.	Figure 5-11
5. Unbonded lengths at 750mm from the midspan (such that a portion of the unbonded length falls within one transfer length of the end of the FRP section) showed a reduced post-yield stiffness for disbonds larger than 100mm in length and large decreases in maximum load and displacement at debonding indicating a premature debonding failure.	Figure 5-12
6. The validated FEA model creates the ability to reduce much of the uncertainty related to the material variability when analyzing the effect of an unbonded length, making global performance changes more quantifiable.	Figure 5-15 Figure 5-16

References

Malek, A.M., H. Saadatmanesh, M.R. Ehsani, *Prediction of Failure Load of R/C Beams Strengthened with FRP Plate Due to Stess Concentration at the Plate End*, ACI Structural Journal, Vol. 95, No. 1, pp. 142-152, 1998.

Niu, H., V.M. Karbhari, Z. Wu, *Diagonal Macro-crack Induced Debonding Mechanisms in FRP Rehabilitated Concrete*, Composites, Part B, pp. 1-14, 2006.

Taljsten, B., *Strengthening of beams by plate bonding*, ASCE Journal of Materials in Civil Engineering, Vol. 9, No. 4, pp. 206-212, 1997.

6. CONCLUSIONS

This study investigated the effects of a small set of common defects influencing bond performance of FRP rehabilitated concrete structures. The results suggest that present guidelines assessing the aspects of critical defects, such as NCHRP Report 514 (2004) and ACI Committee 440 (2002) are conservative. Both the laboratory tests and the FEA analysis found that disbonds and cracking influence bond performance. However, this influence was often limited to local effects near the defect and the global influence was quite small compared to the scatter in the data intrinsic to aging, weak, and damaged concrete.

The largest influence on global behavior observed was not due to the defects that were purposely inserted into the beam specimens, but instead was due to the various debonding failure modes observed. From strongest to weakest, the debonding failure modes observed were given the names “deep concrete, steel”, “thick concrete bondline”, “thin concrete bondline”, and debonding through the “resin interface”. The first three failure modes were all ideal failures by shearing through the concrete material, where the FRP and the adhesive layer were left largely intact. However, failure by “deep concrete, steel” failed at noticeably greater loads than debonding through a “thick concrete bondline” or a “thin concrete bondline”. Failure by debonding through the resin interface occurred at relatively lower loads than any of those failures through the concrete materials. It was clear that these failure modes were influenced by minor variations in surface preparation and wet layup application techniques. The wet layup procedure used for all specimens adequately adhered to

recommended techniques described by NCHRP 514 (2004) and ACI 440 (2002). However slight variations in the amount of material removed during sandblasting and cleaning and the amount of epoxy applied to the concrete surface and the first layer of FRP during specimen rehabilitation seemed to have substantial influence on specimen behavior near ultimate loading conditions. Although previous research has been conducted on this topic and ACI 440 (2002) and NCHRP 514 (2004) give guidelines pertaining to surface preparation and application, it is evident from the laboratory test results that additional work relating to this topic is appropriate. Strict, quantifiable techniques for the wet layup process of rehabilitating concrete needs to be developed to ensure better quality control and more reliable bond performance.

The test results indicated that disbonds with diameters (for circular defects) or lengths (for rectangular defects) of 50mm or smaller had little or no effect on structural performance. Even very large unbonded sections with dimensions up to 250mm by 150mm or diameters reaching the entire width of a section (150mm) have limited measurable global influence on behavior. These large unbonded regions comprised 15% and 7% of the total laminate area, respectively, but seem to reduce the capacity of the beam by less then 5%. The ACI Committee 440 (2002) suggested limits for “small delaminations” of 2 square inches (1300mm^2) or 5% of the total laminate area are abundantly exceeded with minimal measurable influence. No repair was found necessary for debonds with dimensions smaller than 50mm or the ACI predefined 5% debonded area. Both the 250mm by 150mm rectangular (37,500mm^2) and the 150mm circular (17,700mm^2) disbonds also exceed the ACI defined threshold

for a medium sized disbond between 2 square inches (1300mm^2) and 25 square inches (16100mm^2). The ACI recommended repair of a medium sized delamination is by resin injection or ply replacement. Given the results of the laboratory tests and the FEA analysis, the recommendation is to only repair a medium disbond by resin injection and not use ply replacement due to the difficulty and cost of such a repair, unless the injection would cause progression of the disbond. The ACI defined threshold for a large delamination is an unbonded region greater than 25 square inches (16100mm^2). The 250mm by 150mm disbond is over twice this area. Given the minimal influence of this very large unbonded region, the ACI suggested repair of "selectively cutting away the affected sheet and applying an overlapping sheet patch," may be an excessive repair technique. More research is needed to determine if patching or simply repairing with epoxy injection is the more appropriate action. Although it was found that bond performance is not severely adversely affected by medium and large debonds they should be repaired by some technique such as epoxy injection to prevent moisture entrapment and to buffer the stress concentrations measured in the strain profiles described in chapter 4.

In search of critical disbond locations in FRP rehabilitated flexural members, unbonded regions were placed with centroids at the following distances from the beam midspan: 0mm, 185mm, 428mm, and 660mm. Global strength and displacement effects due to disbond location were difficult to ascertain due to scatter in the data at ultimate conditions. However, local effects were easily obtained at all locations and the FEA model was able to suggest the global performance of defects at various

locations and sizes. FRP stress concentrations were found in specimens with unbonded lengths located at the midspan, 185mm, and 428mm distances, whereas no stress concentrations were obtained at the 660mm location where the FRP strains are relatively low. The stress concentrations seemed to be the largest in specimens located at 185mm from the midspan where beam shear and moment forces are simultaneously near maximum. Tests indicated that a disbond located in the high moment regions of the beam appear to be slightly more critical than those located near the quarterspan, where the moment is less and at least one transfer length remains bonded until the end of the FRP section. Although global effects of disbond location were not reliably obtainable from the laboratory tests due to variations in material parameters and a limited number of specimens, the validated FEA model was able to suggest: Disbonds at the midspan had nearly no effect due to the lack of shear strain gradient due to symmetry, disbonds at 185mm had only a slight influence, while disbonds at 428mm and 660mm had small but measurable strength and displacement losses. This loss in performance at these locations was surprising because, unlike the beam at 185mm, they are away from the location of the diagonal macro-crack debonding mechanism (Niu, et al, 2006) from which debonding typically initiated. It was also surprising to note that no defect location away from the disbond ends (in which debonding may initiate from the ends of the FRP instead of from a diagonal crack) seems to have a large influence on specimen global performance. Specimens with unbonded regions placed at the interface between FRP layers as well as those with unbonded regions located both at the adhesive interface as well as between FRP layer seemed to behave

with very similar performance characteristics to those specimens with disbonds placed in the adhesive layer alone. In other words, similar behavior is seen due to an unbonded area irregardless of the interface in which it is placed.

All levels of preloading in which damage due to cracking was induced, stress concentrations were observed in the FRP at the crack location due to loss of continuity in the concrete material at that point causing all the tension force to be carried by the steel and the FRP. These stress concentrations were generally only apparent at moderate loads, however because as the strengthened specimen approached ultimate load, extensive new distributed cracks formed leading to more uniform distribution of strain in the FRP. ACI Committee 440 (2002) states, “some manufacturers have reported that the movement of crack 0.01 in. (0.3mm) and wider can affect the performance of externally bonded FRP system through delamination or fiber crushing.” Beams were investigated with crack widths of 0mm, 0.2mm maximum width, 0.2mm residual width, 0.6mm residual width, 1.0mm residual width, and 1.5mm residual width. From these tests and from the results of the FEA model, the loss of performance due to cracking was unsubstantiated. No decrease in beam load capacity or performance was measured due to excessive preload cracking. However, with very large residual crack widths of 1.0mm and 1.5mm a loss of deflection at debonding was measured perhaps due to strain hardening of steel during preloading or stress concentrations near the large cracks. ACI 440 suggests pressure injecting cracks wider than 0.3mm as a remedy to cracking induced premature delamination. The recommendation from this investigation is the same as ACI 440, or to seal the cracks

by some other appropriate method in order to prevent moisture penetration. However, the reason for this recommendation is not to prevent premature delamination of FRP, but to curtail additional steel degradation due to environmental exposure. Although several methods of crack repair are available, further research is recommended for determination of economical sealing and repair of these cracks in the presence of FRP rehabilitation. Specimens preloaded to a large crack width of 1.0mm residual crack width and rehabilitated with unbonded regions ranging from 100mm by 150mm to 200mm by 150mm in dimension behaved similar to those specimens corresponding with typical preloading. Beam performance appeared to be affected by the presence of these disbonds by showing decreased load and FRP strain capacity. Additionally, local effects in the form of FRP stress concentrations and location of debonding initiation due precracking as well as rehabilitation with unbonded regions were noted.

All the results derived in this investigation were based on short-term behavior only in which the specimens are loaded very quickly. No implications can be made about the long term behavior of these defects under sustained load, cyclic load, aging, or severe environmental exposure. Significantly more research is needed to determine the influence of the stress concentrations induced by cracking and disbonds with respect to such durability related issues.

The results of this investigation clearly indicate the current lacunae in criteria for inspection and repair. It is recommended that Caltrans initiate the development of both an inspection manual related to defects in FRP rehabilitated concrete components and a program to clearly establish, through use of an effects of defects methodology,

criteria for repair and rejection. Results from the present study should be implemented as initial guidelines.

References

ACI Committee 440, *Guide for the Design and Construction of Externally Bonded FRP Systems for Strengthening Concrete Structures*, ACI 440.2R-02, American Concrete Institute, Farmington Hills, MI, USA, pp. 103, 2002.

NCHRP Report 514, Transportation Research Board, Washington, D.C., Section II, p. 1-33, 2004.

Niu, H., V.M. Karbhari, Z. Wu, *Diagonal Macro-crack Induced Debonding Mechanisms in FRP Rehabilitated Concrete*, Composites, Part B, pp. 1-14, 2006.

Appendix A: Failure Modes

There were five different failure modes observed during this testing program:

1. Debonding by tearing large pieces of concrete cover away at the depth of the steel reinforcement. This failure was generally the result in the strongest specimens tested and is indicative of a very strong bond and FRP material.
2. Debonding through the concrete substrate in which a thick layer (approximately 1mm to 4mm in thickness) is left attached to the FRP and very little resin is exposed. This failure generally resulted from beams that performed much like expected. The failure was still largely due to the concrete strength and not to weakness in the adhesive or FRP material.
3. Debonding through the concrete substrate in which a thin layer (approximately 0.5mm to 2mm in thickness) is left attached to the FRP and often some small percentage of the failure occurred by shear through the adhesive material. This failure mode may have been a result of inadequate sandblasting to remove laitance from the concrete beam, inadequate application of resin during rehabilitation, or weak material in the adhesive layer.
4. Debonding through the adhesive layer where very little concrete is left attached to the FRP. However, there may be large amounts of adhesive material still attached to the concrete surface. This failure is a result of poor bonding either by inadequate application of resin during rehabilitation or due to the concrete

strength being superior to the adhesive material. This failure generally resulted in the weakest specimens tested.

5. Finally, failure by FRP rupture. This failure mode only resulted in one specimen in which only one layer of FRP as opposed to all other specimens which had two layers.

The pictures shown in figures A-1 through A-5 show typical failed beams for each of these five failure modes. Figure A-6 consists of pictures of the four debonding failure modes. The failure modes are labeled in the figure with the same terminology used to name the failure modes in the text: Deep concrete, steel; thick concrete bondline; thin concrete bondline; and resin interface. Figure A-7 shows the varying failure surface for beams from different rehabilitations. From top to bottom, the debonding surface is shown for specimens 22, 36, 45, and 56. These specimens resulted from rehabilitation sets 4 (fourth rehab of cast #1), 5 (First rehabilitation of cast #2), 6 (second rehabilitation of cast #2), and 7 (third rehabilitation of cast #2) respectively and sheared with the corresponding failure modes: Thick concrete bondline, resin interface, resin interface, and deep concrete, steel. The changes in failure mode seemed to have a large influence on the specimen behavior at ultimate load and displacement. Because this aspect was so influential, it was difficult to assess the impact a specific defect have on a beam’s capacity.

Figure A-1: “Deep Concrete, Steel” Debonding

Figure A-2: Debonding through a “Thick Concrete Bondline”

Figure A-3: Debonding through a “Thin Concrete Bondline”

Figure A-4: Debonding through the “Resin Interface”

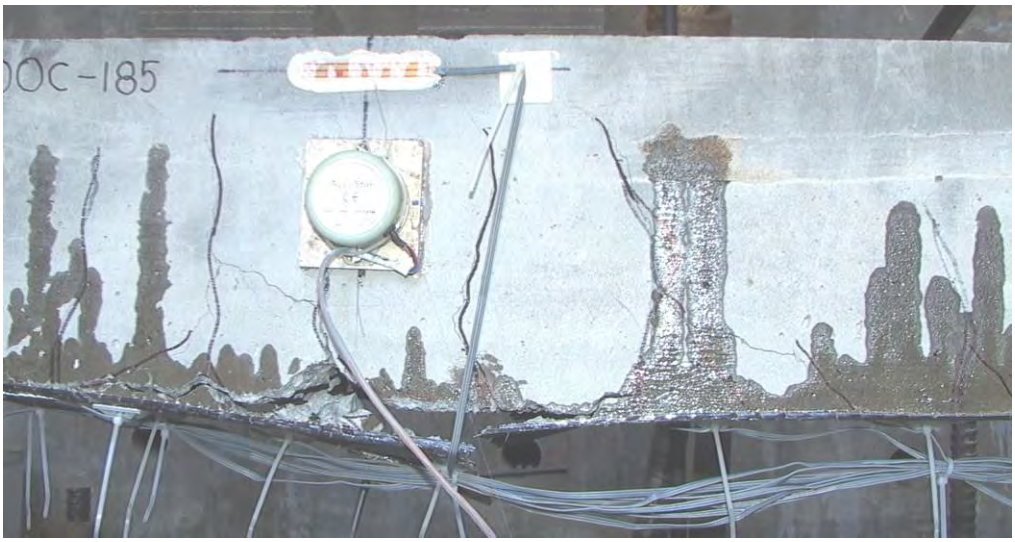

Figure A-5: “FRP Rupture”

Deep Concrete, Steel

Thick Concrete Bondline

Thin Concrete Bondline

Resin Interface

Figure A-6: Typical FRP debonding surface for the four different failure modes.

Figure A-7: Varying debonding failure surfaces between rehabilitations.

Appendix B: Specimen Test Synopsis

Each specimen and corresponding test in this appendix is described in this section in the chronological order tested. Refer to the index to reference the location of specific specimens in this appendix. Each specimen is provided with a brief description of important characteristics and any significant observations. Following this description for each specimen applicable behavior characteristics tables and load versus crack width and notes tables are shown. Additionally, figures showing applicable strain gage layouts and defect drawings, load versus displacement plots, steel strain versus load plots, strain profile plots, and failed specimen pictures are provided.

A.B.1: Control Specimens

Specimen 1: Unstrengthened control specimen tested 12/16/2004 (Control_1_S1)

Specimen 1 was the first beam tested to failure. It was an unstrengthened control specimen loaded monotonically to failure with several pauses during loading to observe and measure crack patterns. The specimen was loaded at a loading rate of 0.222 kN/sec until a change in slope in the load vs. midspan displacement plot was observed at 45.4 kN indicating the yield of longitudinal steel. At this point the actuator control was changed to displacement control at a loading rate of 0.04mm/sec which was chosen to maintain the loading speed of the actuator was the similar to when the test was in load control based on specimen stiffness. The test was paused at each loading increment shown load vs. crack width plot in order to record the crack width

and make observations. Test 1 has more pauses than all following tests which were simplified as deemed appropriate. The periodic 1 kN to 5 kN drops in load in the load versus midspan deflection curve are due to pauses in the test for crack measuring and observations. The specimen was loaded to a displacement of 61mm at which point, despite no large drops in load capacity the specimen was determined failed. The specimen held a large percentage of its maximum load (at least 95.9%) at displacements far past the peak load due to the ductile nature of the beam design. The maximum load sustained by Specimen 1 was 57.74 kN at a deflection of 23.3mm. From the midspan steel strain versus load plot, the yield strain of the midspan steel is determined to occur at 2236 microstrains by averaging the measured strains determined by the two midspan steel strain gages at the point of the initial change in slope. As with many of the tested specimens, the useable range of the strain gage was exceeded before the end of the test. Data collected beyond the useable range of the gauge is void of meaning and is not included in the plot in Figure 4-2.

Load (kN)	Crack Width (mm)	Notes
2.22	0.00	No cracks
4.45	0.00	No cracks
6.67	0.00	No cracks
8.90	0.00	No cracks
11.12	0.00	
14.19	0.00	
15.88	0.05	
18.33	0.05	
20.86	0.10	
22.64	0.10	
24.64	0.10	
26.78	0.10	
29.31	0.10	
31.67	0.10	
33.54	0.10	
35.94	0.20	
38.30	0.20	
40.39	0.25	
42.39	0.27	
44.48	0.27	
46.66	0.30	
49.11	0.60	

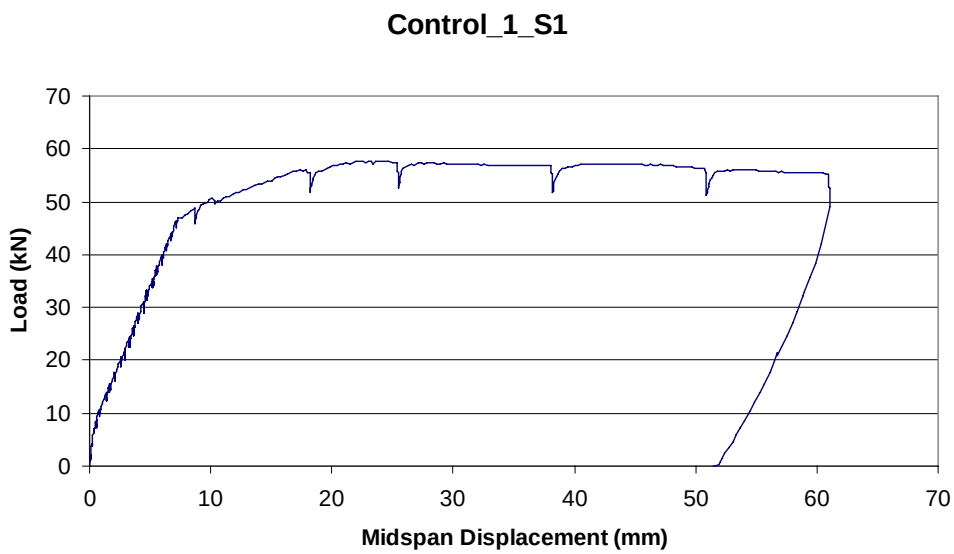

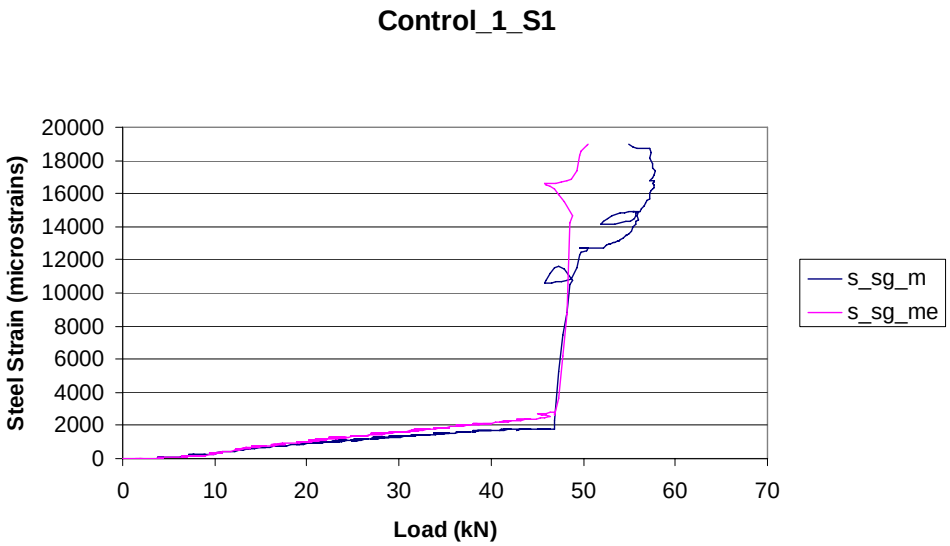

Specimen 2: Unstrengthened control specimen tested 1/7/2005 (Control_2_S2)

Specimen 2 was an unstrengthened control specimen loaded monotonically to failure with pauses during loading to observe and measure crack patterns. The data from Test 1 allowed for a reduced number of pauses for observation. Similar to Test 1,

the test actuator control was changed from load control to displacement control at 42.9kN after the initiation of steel yield. The test was paused at each loading increment shown in in order to record the crack width and make observations. The specimen was loaded to a displacement of 71mm at which point, the specimen was considered to be failed. Like Specimen 1, the specimen held near peak load at displacements far past steel yield due to the ductile nature of the beam design. The peak load was 48.64 kN at a deflection of 71.0mm. From the plot of the midspan steel strain versus load, the yield strain of the midspan steel is determined to occur at 2463 microstrains by averaging the measured strains determined by the two midspan steel strain gages at the point of the initial change in slope.

Load (kN)	Crack Width	Notes
0.00	0.00	
31.09	0.18	
33.27	0.20	
35.67	0.28	
37.72	0.32	
40.08	0.30	Yielding of steel
41.90	0.45	
44.53	1.40	

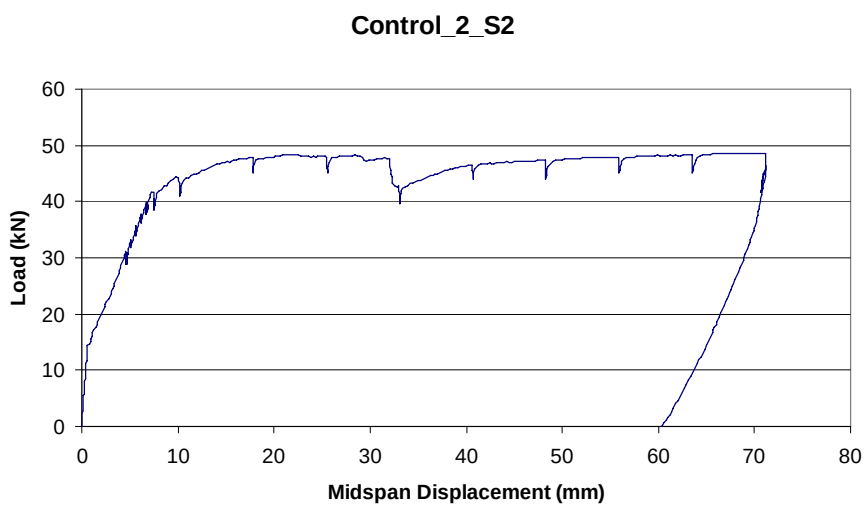

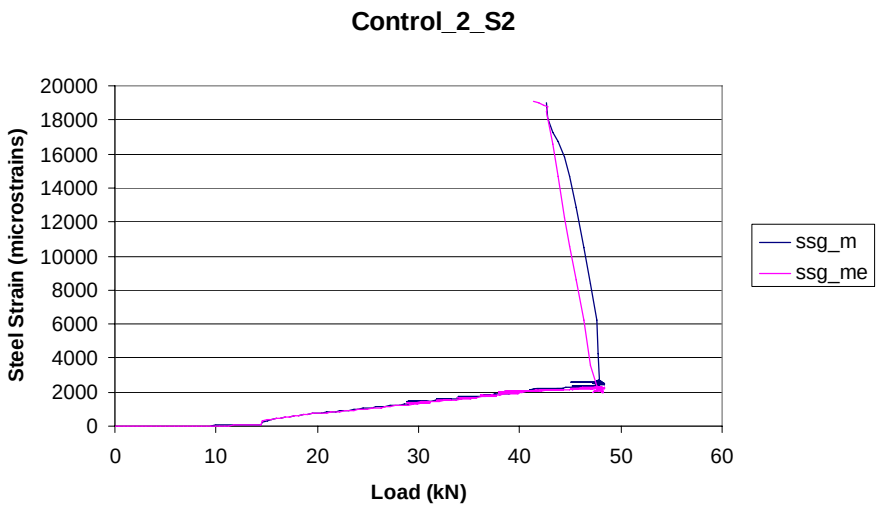

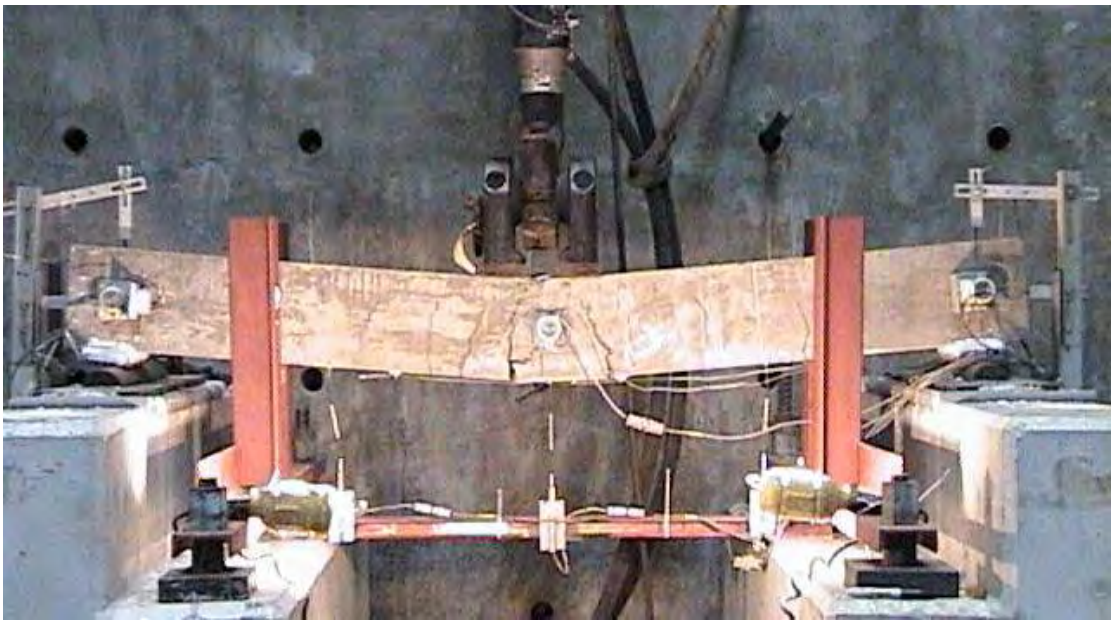

Specimen 3: Unstrengthened control specimen tested 1/14/2005 (Control_3)

Similar to specimens 1 and 2, specimen 3 was an unstrengthened control specimen loaded monotonically to failure with pauses during loading to observe and measure crack patterns. The test actuator control was changed from load control to displacement control at 48.6kN after the initiation of steel yield. The test was paused

at each loading increment shown in the load versus crack width table in order to record the crack width and make observations. The load vs. midspan deflection curve is plotted below. The specimen was loaded to a displacement of 63.5mm at which point, the specimen was considered to be failed. The specimen held near peak load at displacements far past steel yield due to the ductile nature of the beam design. The peak load was 55.60 kN at a deflection of 25.0mm. From the plot of the midspan steel strain versus load, the initial yielding strain of the midspan steel is determined to occur at 2512 microstrains by averaging the measured strains determined by the two midspan steel strain gages at the point of the initial change in slope.

Load (kN)	Crack Width	Notes
0.00	0.00	
31.23	0.10	Cracking to near quarterspan
33.36	0.18	
35.54	0.20	
37.45	0.25	
40.08	0.25	
42.08	0.25	
44.88	0.32	Crackin outside quarterspan
48.57	0.80	

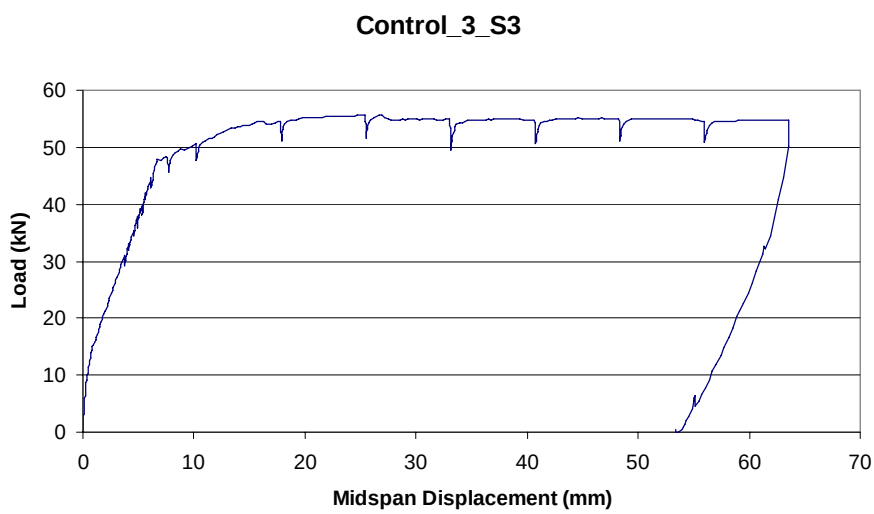

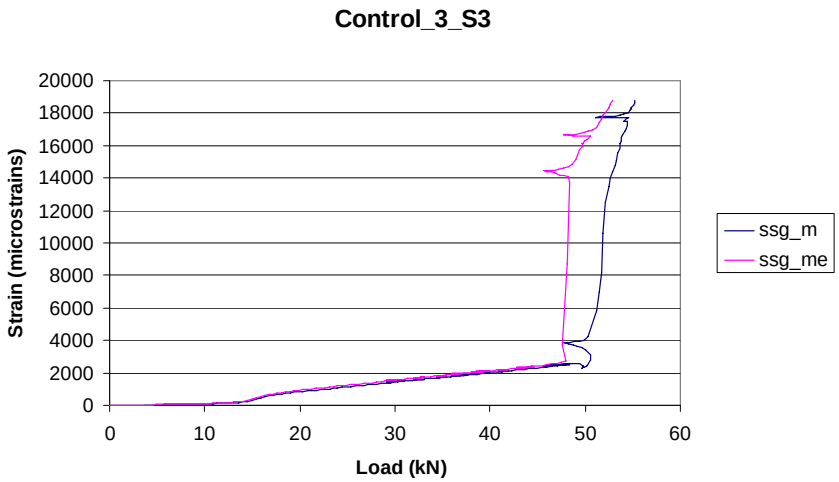

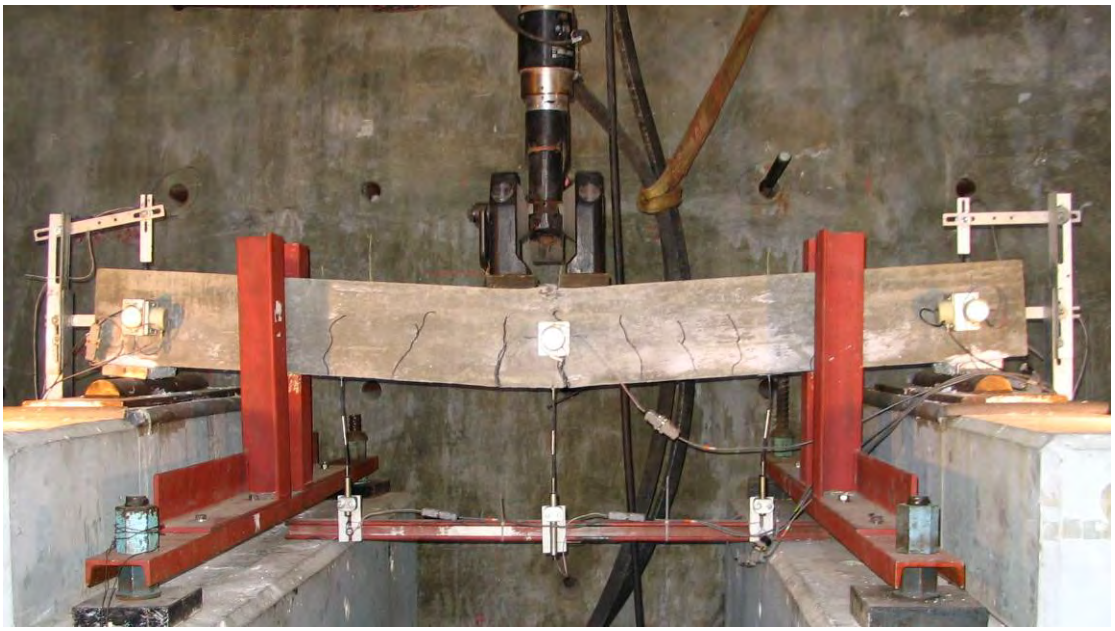

Specimen 7: Strengthened, preloaded control specimen tested 5/18/2005 (R_C_Control_1_S7)

Specimen 7 was the first test conducted on an FRP strengthened specimen. As discussed in section 2.9, the specimen was strengthened with two layers of the Hexel GA 090 carbon fabric using FYFE Co. Tyfo S Epoxy/Resin, which is consistent with

all the strengthened specimens from here on, unless otherwise noted. This specimen was classified as a control specimen because it did not have any purposely inserted defects. It was, however, precracked using the preloading protocol described in section 2.8 before the application of FRP. It should be noted, in this study the standard preload to 35.6 kN was not considered a defect, but was instead considered a method of more adequately replicating field conditions. At the time of testing, the FRP had been applied for 12 days to assure adequate cure time had occurred. As previously discussed in section 2.10, the load cycles were predetermined in order to document changes in specimen integrity as the loading progresses. The peak load held by this specimen was quite high at 96.80 kN and corresponding midspan displacement of 17.2mm. Final debonding occurred from near the midspan, propagating to the left. The debonding mechanism was classified as a deep concrete/steel debonding because, upon debonding a large chunk of concrete was tore out at the depth of the longitudinal steel (see figure 4-10). Even after the debonding had propagated to near the bond line, the failure plane was through a thick layer of concrete with very little of the failure occurring in the resin, or concrete-resin interface. As expected, global debonding occurred very rapidly upon initiation, as can be seen from the drop from peak load in the load displacement curve. Yielding at the midspan of the longitudinal steel occurred at 76.5 kN in the beam at a strain of 2312 microstrains. The yield strain was chosen by averaging the measured steel strain at the points where the strain-load became nonlinear.

The description for specimen 7 above is a typical summary of a tested, reinforced specimen. For brevity, when describing the remaining tests only important observations or deviations from the above testing description will be made.

Behavior Characteristic	Value
Test Date	5/18/2005
Rehab Date (number)	5/6/2005 (1) (1)
Concrete Cast Date (number)	10/19/04 (1)
Time from Rehab to Test	12 days
Maximum Load Held	96.8 kN
Displacement at Maximum Load	17.25 mm
Measured Steel Yield	2312 με
Load at Steel Yield	76.51 kN
Displacement at Steel Yield	9.45 mm
FRP Strain at Steel Yield	4692 με
FRP Strain at Debonding (Location)	7265 με
FRP Midspan Strain at Debonding	7265 με
Debonding Direction	Left
Failure Mode	Deep Concrete/Steel

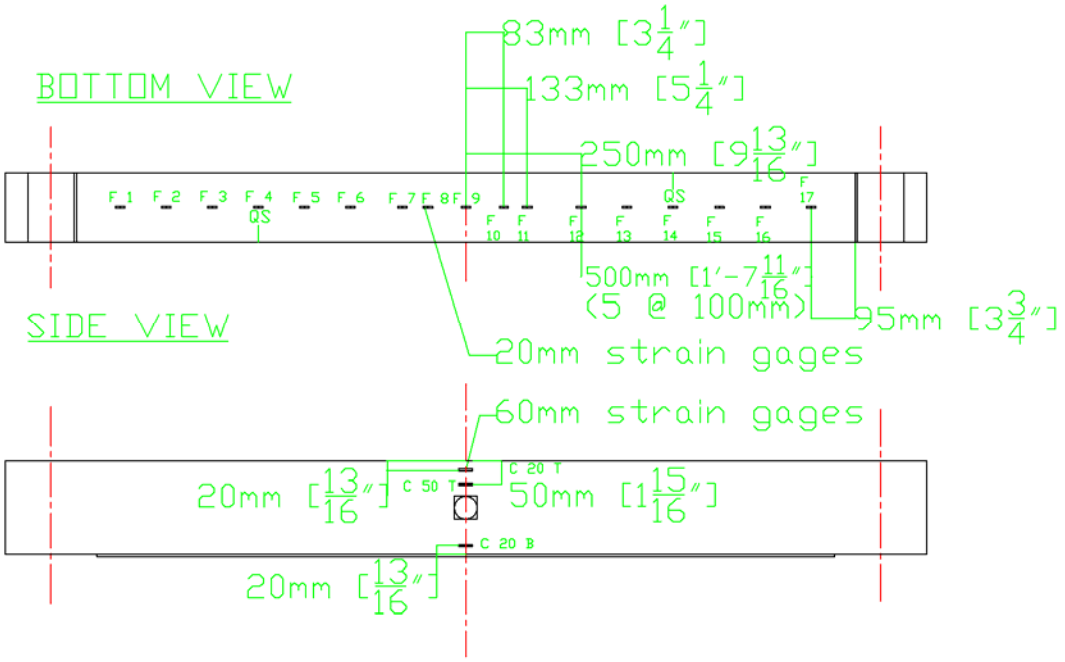

Load (kN)	Crack Width (mm)	Notes
0.00	0.00	
36.25	< 0.10	Existing cracks dialated somewhat and many small new cracks occurred (near surface) in the high moment region at approximately 1cm spacing.
2.49		
74.86	0.1	Formation of Larger Cracks Propagating to the N/A between existing cracks. Cracks still held closed at the interface.
2.45		All cracks still reclosing.
89.99	Vert - 0.40 Shear - 0.90	Occurance of localized debonding approximately 7-10cm in length at a point of edge discontinuity due to a chip in the concrete.
2.45		Shear crack remained open. The vertical cracks closed somewhat, but remained slightly open.
96.97		Debonding occurred rapidly from a different point than it initiated from. It began in the max moment region about 1.5" into the concrete, remained deep in the concrete for about 7" then migrated to the shallow conrete along the interface.

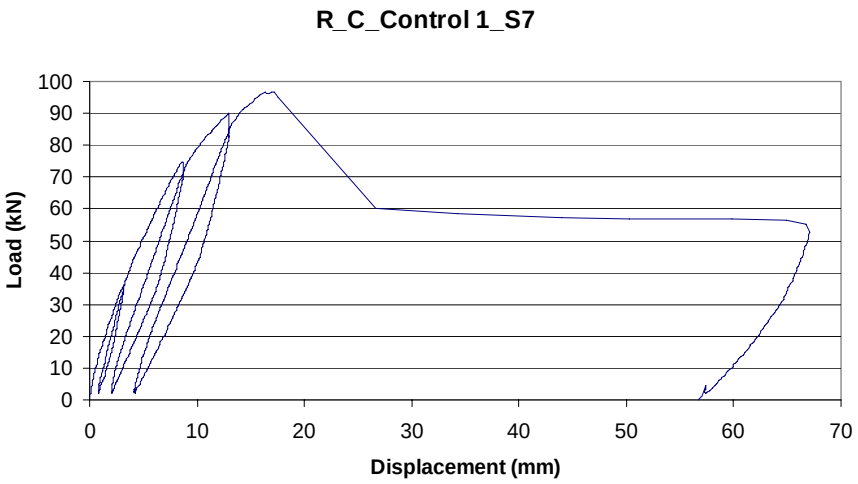
R_C_Control 1_S7
Load (kN)
Displacement (mm)
0
10
20
30
40
50
60
70
80
90
100

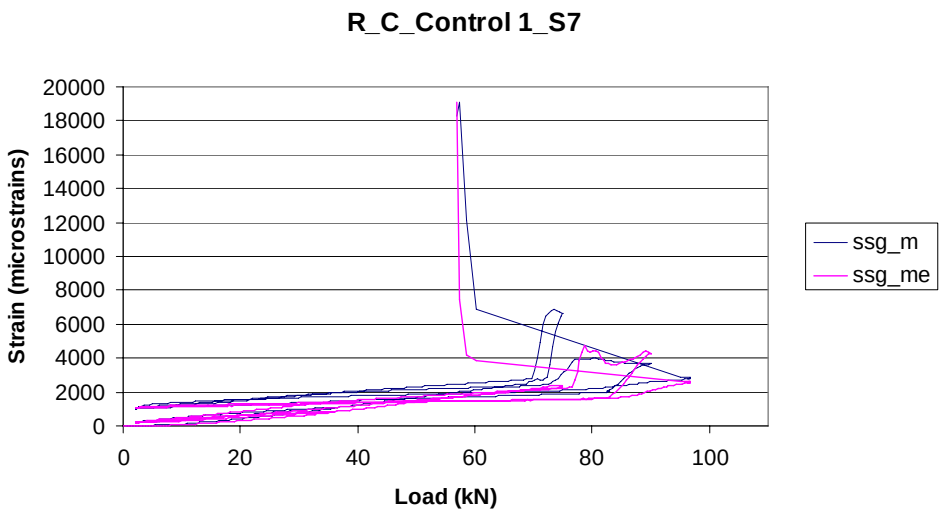
R_C_Control 1_S7
Strain (microstrains)
Load (kN)
ssg_m
ssg_me
0
2000
4000
6000
8000
10000
12000
14000
16000
18000
20000
0
20
40
60
80
100

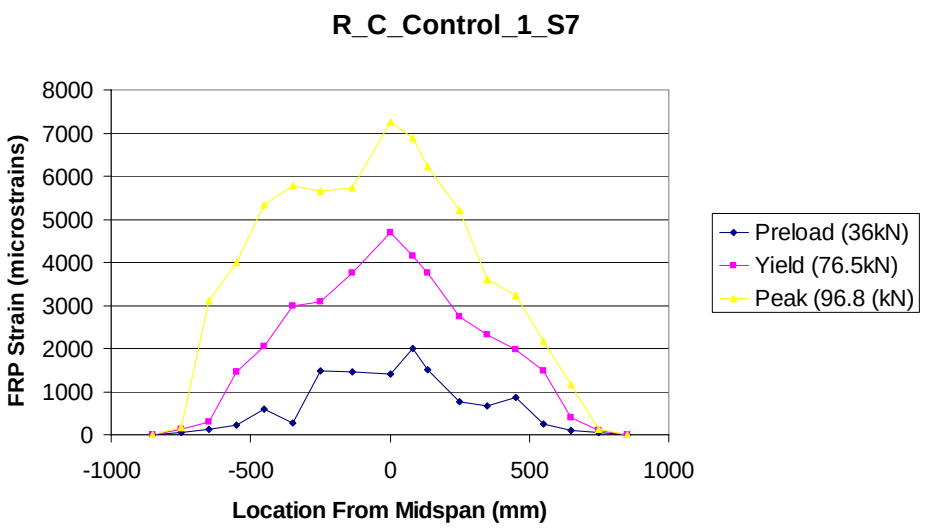
R_C_Control_1_S7
FRP Strain (microstrains)
Location From Midspan (mm)
Preload (36kN)
Yield (76.5kN)
Peak (96.8 (kN)
0
1000
2000
3000
4000
5000
6000
7000
8000
-1000
-500
0
500
1000

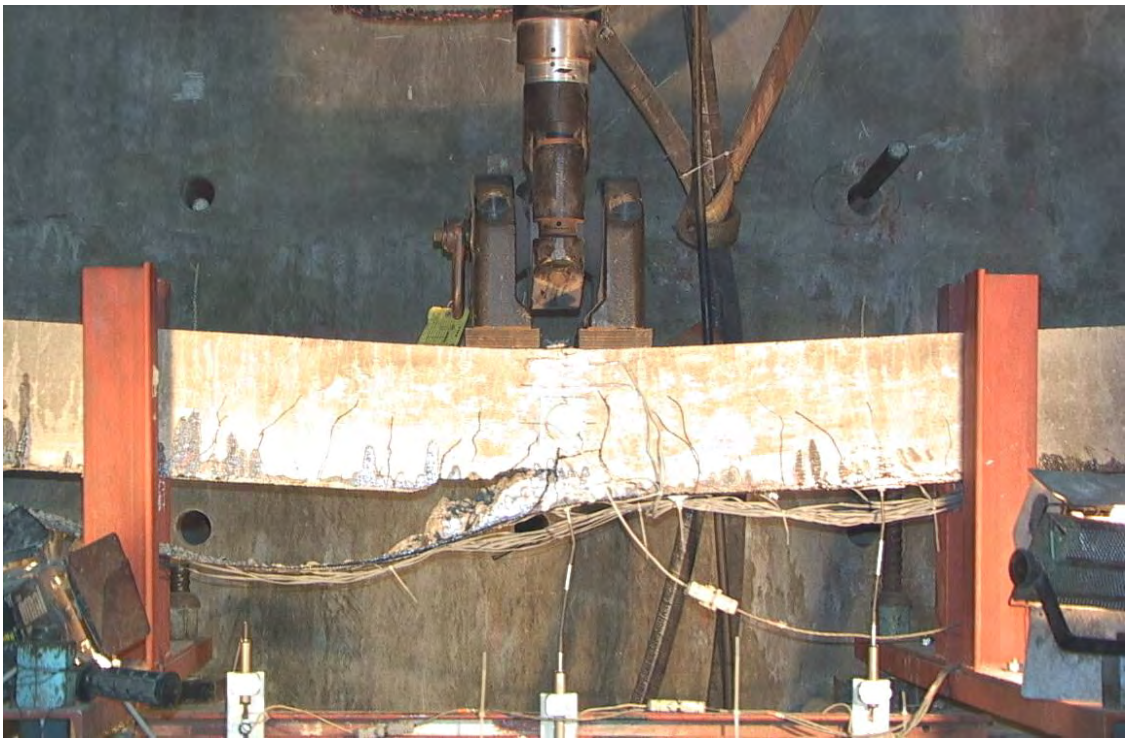

Specimen 26: Strengthened, non-preloaded control specimen tested 5/26/2005 (R_UC_Control_1_S26)

Specimen 26 is a control beam in which no preload (hence the term “UC” standing for uncracked) in the name) was applied before the application of FRP and no defect was purposely created in the specimen. Testing non-precracked specimens was done to quantify the impact damaging by preloading. The strain gauge layout for specimen 26 was the same as that in specimen 7 and is shown below. The peak load held by this specimen was significantly lower than the other specimen in rehab number one (specimen 7) at 88.83 kN and corresponding midspan displacement of

16.0mm. Final debonding occurred from near the midspan, propagating to the left (see picture).

Behavior Characteristic	Value
Test Date	5/26/2005
Rehab Date (number)	5/6/2005 (1)
Concrete Cast Date (number)	10/19/04 (1)
Time from Rehab to Test	20 days
Maximum Load Held	88.83 kN
Displacement at Maximum Load	16.00 mm
Measured Steel Yield	2398 με
Load at Steel Yield	71.75 kN
Displacement at Steel Yield	9.56 mm
FRP Strain at Steel Yield	4143 με
FRP Strain at Debonding (Location)	6385 (F7) με
FRP Midspan Strain at Debonding	6338 με
Debonding Direction	Left
Failure Mode	Deep Concrete/Steel

Load (kN)	Crack Width (mm)	Notes
0.00	0	
35.92	< 0.1	Many small cracks occurring at a small spacing (~1 cm) and larger cracks propagating to near the NA @ ~50 to ~75 cm spacing.
2.45		
74.91	0.1	Steel Yielding ~58kN. More cracking to approx 'd' from the supports. No debonding.
2.49		
88.93		Large crack propagating parallel to the longitudinal steel at ~2 inches depth just before debonding occurred.

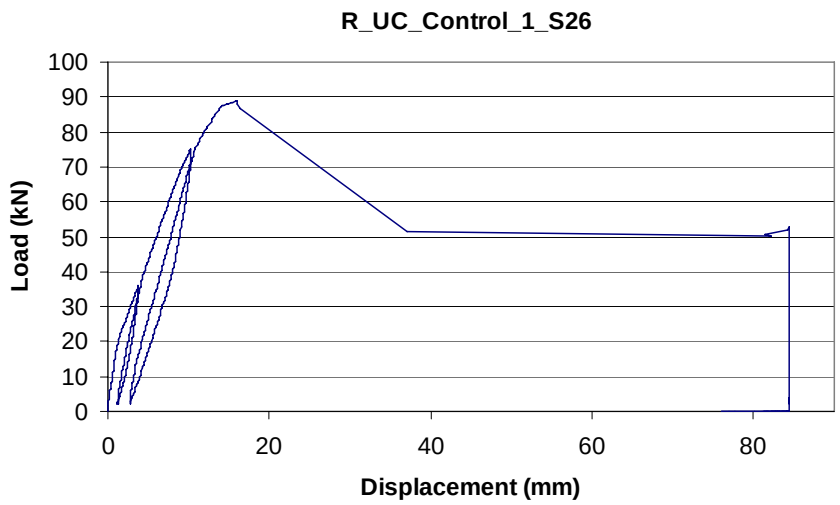
R_UC_Control_1_S26
Load (kN)
Displacement (mm)
0
10
20
30
40
50
60
70
80
90
100
0
20
40
60
80

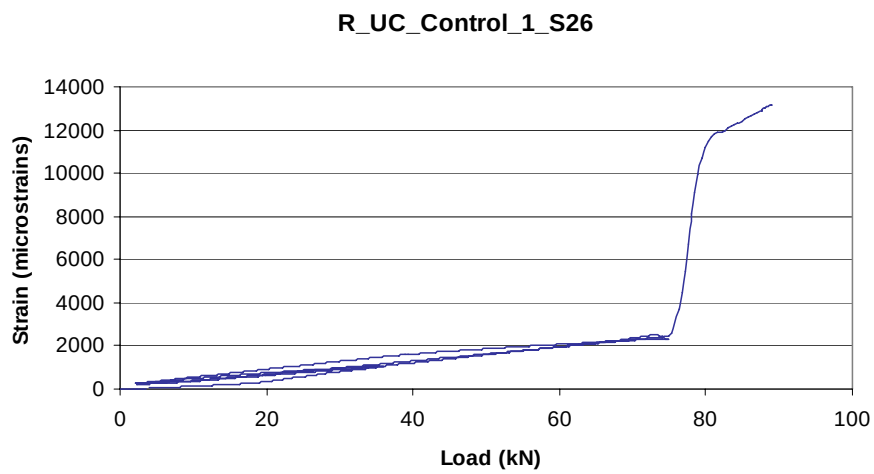
R_UC_Control_1_S26
Strain (microstrains)
Load (kN)
0
2000
4000
6000
8000
10000
12000
14000
0
20
40
60
80
100

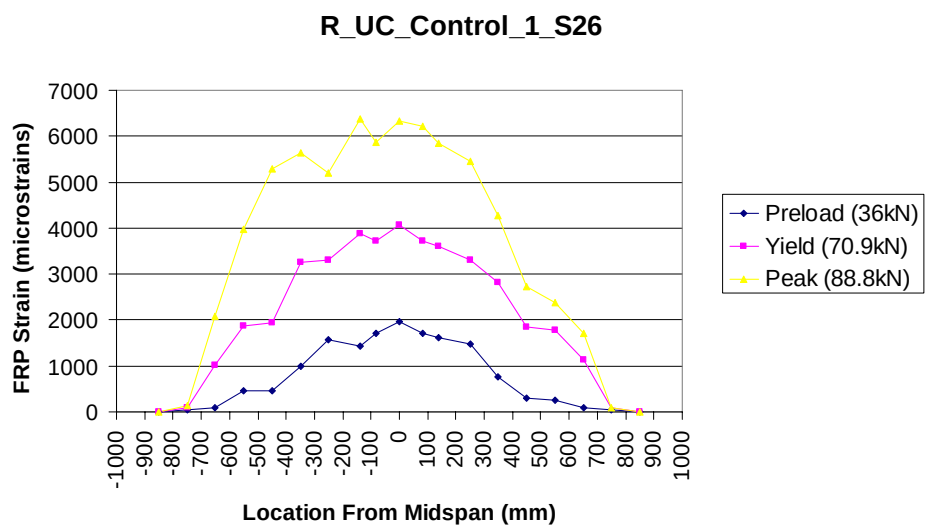
R_UC_Control_1_S26
FRP Strain (microstrains)
Location From Midspan (mm)
0
1000
2000
3000
4000
5000
6000
7000
-1000
-900
-800
-700
-600
-500
-400
-300
-200
-100
0
100
200
300
400
500
600
700
800
900
1000
Preload (36kN)
Yield (70.9kN)
Peak (88.8kN)

Specimen 9: Strengthened, preloaded control specimen tested 6/13/2005 (R_C_Control_2_S9)

Specimen 9 was another precracked, rehabilitated control specimen without any purposely inserted defects. Test 6 was ran monotonically to ensure the same behaviors are seen independent of whether the specimen is loaded monotonically or using a small number of cycles. Final debonding occurred from near the midspan, propagating to the left, as seen in the previous two tests.

Behavior Characteristic	Value
Test Date	6/13/2005
Rehab Date (number)	5/27/2005 (2)
Concrete Cast Date (number)	10/19/04 (1)
Time from Rehab to Test	17 days
Maximum Load Held	89.7 kN
Displacement at Maximum Load	14.14 mm
Measured Steel Yield	2487 με
Load at Steel Yield	69.14 kN
Displacement at Steel Yield	7.54 mm
FRP Strain at Steel Yield	3740 με
FRP Strain at Debonding (Location)	6959 (F9) με
FRP Midspan Strain at Debonding	6959 με
Debonding Direction	Left
Failure Mode	Deep Concrete/Steel

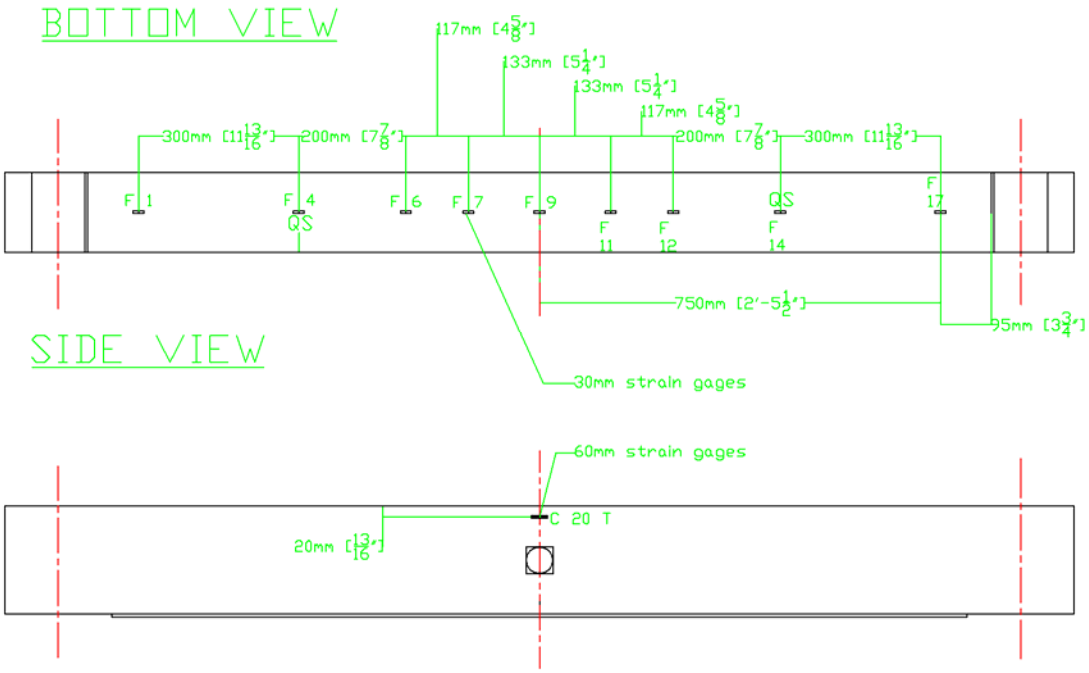

Load (kN)	Crack Width (mm)	Notes
0.00	0	
36.00	< 0.1	Slight reopening of existing cracks lost c_20_t right away.
75.10	0.2	Many small cracks formed.
89.70		Cracking sound at approximately 87kN. Debonding.

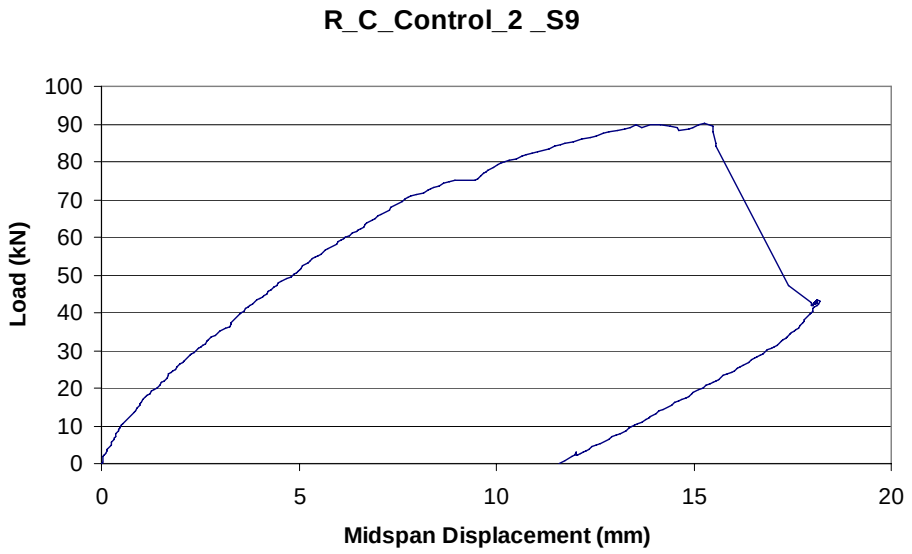

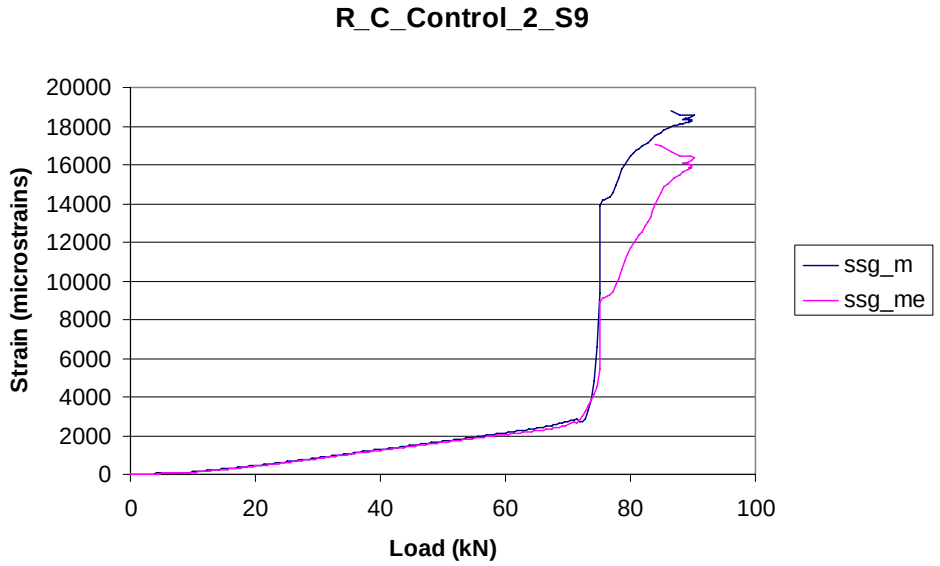

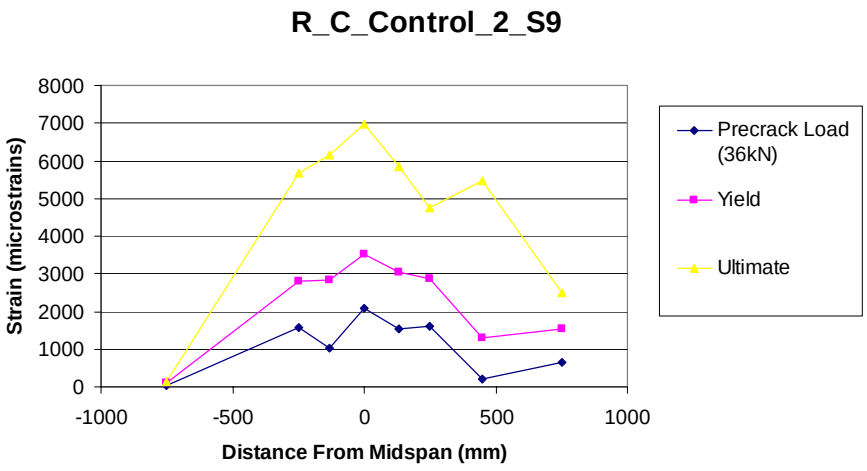

Specimen 27: Strengthened, non-preloaded control specimen tested 6/15/2005 (R_UC_Control_2_S27)

Specimen 27 is a control beam in which no preload was applied before the application of FRP and no defect was purposely created in the specimen. The strain gauge layout for specimen 27 is the same as that used for specimen 9. The peak load

held by this specimen was very high at 99.0 kN and corresponding midspan displacement of 17.0mm. Final debonding occurred from near the midspan, propagating to the left (see figure 4-24). The debonding mechanism was classified as a deep concrete/steel debonding. Observing this debonding mechanism in this specimen is not surprising because it was generally the strongest debonding failure mode observed during the testing process. Due to an error in data collection, most of the FRP strain data is not available for this specimen. Thus, no FRP strain values at ultimate or FRP strain profiles are provided.

Behavior Characteristic	Value
Test Date	6/15/2005
Rehab Date (number)	5/27/2005 (2)
Concrete Cast Date (number)	10/19/04 (1)
Time from Rehab to Test	19 days
Maximum Load Held	99.03 kN
Displacement at Maximum Load	16.97 mm
Measured Steel Yield	2677 με
Load at Steel Yield	75.22 kN
Displacement at Steel Yield	9.50 mm
FRP Strain at Steel Yield	Poor data.
FRP Strain at Debonding (Location)	
FRP Midspan Strain at Debonding	
Debonding Direction	Left
Failure Mode	Deep Concrete/Steel

Load (kN)	Crack Width (mm)	Notes
0.00	0.0	
36.00	< 0.1	Slight reopening of existing cracks lost c_20_t right away.
75.10	0.2	Many small cracks formed.
89.70		Cracking sound at approximately 87kN. Debonding.

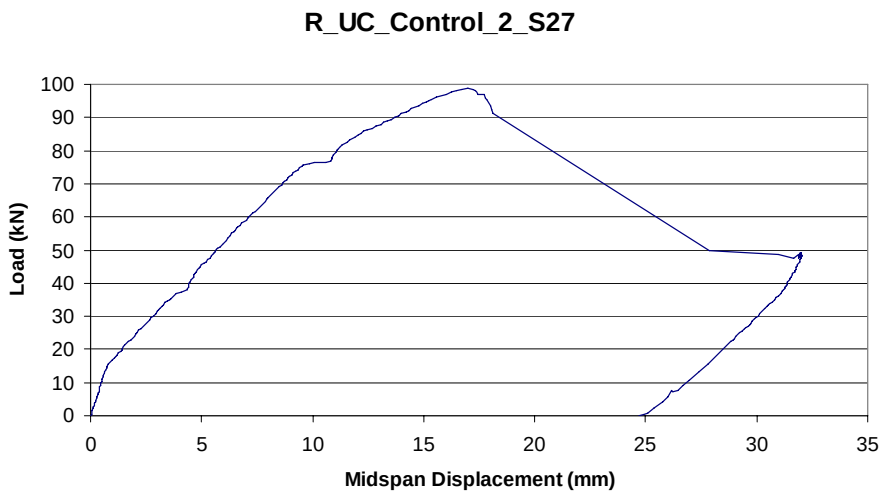
R_UC_Control_2_S27
Load (kN)
Midspan Displacement (mm)
0
10
20
30
40
50
60
70
80
90
100
0
5
10
15
20
25
30
35

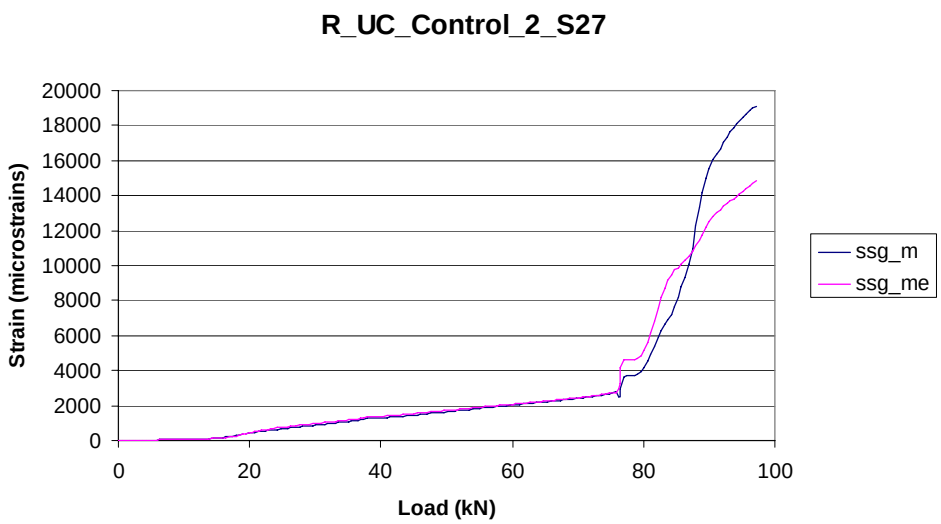
R_UC_Control_2_S27
Strain (microstrains)
Load (kN)
0
2000
4000
6000
8000
10000
12000
14000
16000
18000
20000
0
20
40
60
80
100
ssg_m
ssg_me

Specimen 6: Strengthened, non-preloaded control specimen tested 6/16/2005 (R_C_Control_3_S6)

Specimen 6 was an uncracked, strengthened control specimen without any purposely inserted defects. The peak load held by this specimen was 94.2 kN and corresponding midspan displacement of 17.0mm. Final debonding occurred from near the midspan, propagating to the right. This was the first specimen tested in which final debonding failed to the right. The debonding mechanism was classified as a deep concrete/steel debonding because, upon debonding a large chunk of concrete was tore out at the depth of the longitudinal steel (see picture). Even after the debonding had propagated to near the bondline, the failure plane was through a thick layer of concrete with little of the failure occurring in the resin, or concrete-resin interface.

Behavior Characteristic	Value
Test Date	6/16/2005
Rehab Date (number)	5/27/2005 (2)
Concrete Cast Date (number)	10/19/04 (1)
Time from Rehab to Test	20 days
Maximum Load Held	94.18 kN
Displacement at Maximum Load	17.01 mm
Measured Steel Yield	2312 με
Load at Steel Yield	73.1 kN
Displacement at Steel Yield	8.41 mm
FRP Strain at Steel Yield	3886 με
FRP Strain at Debonding (Location)	7562 (F12) με
FRP Midspan Strain at Debonding	7186 με
Debonding Direction	Left
Failure Mode	Deep Concrete/Steel

Load (kN)	Crack Width (mm)	Notes
0.0	0	
36.1	< 0.1	Lost F1 and F6. Small Reopening of Cracks
2.4	< 0.1	
75.1	0.2	Some shear cracking on left side. Crack spacing ~1" (small).
2.5		
90.0	0.3	Lost s_sg_m.
2.4	0.1	
94.2		Some debonding on the left side of beam, but global failure was debonding from the right side. Much slower debond than previous tests.

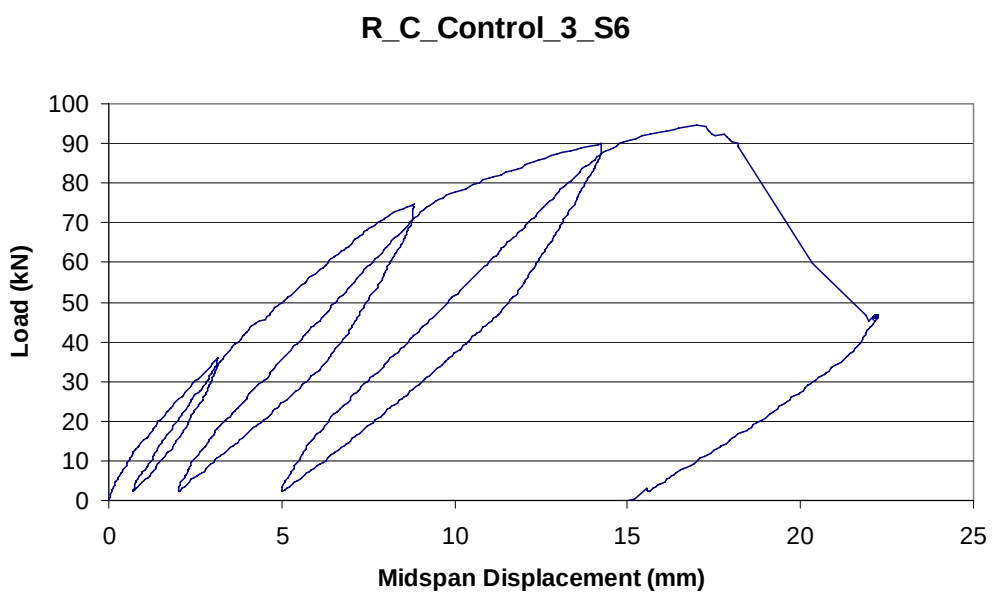

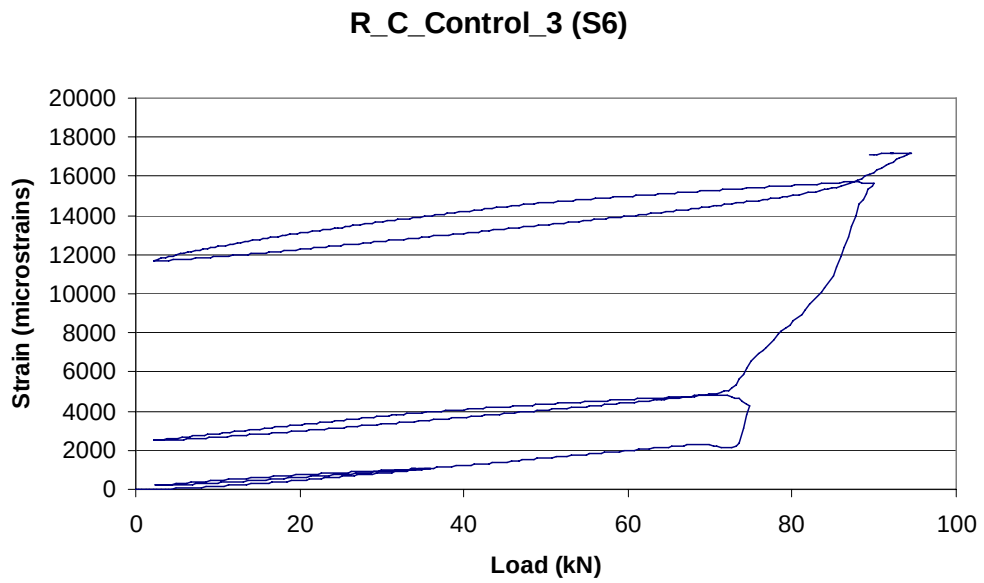
R_C_Control_3 (S6)
Strain (microstrains)
20000
18000
16000
14000
12000
10000
8000
6000
4000
2000
0
0
20
40
60
80
100
Load (kN)

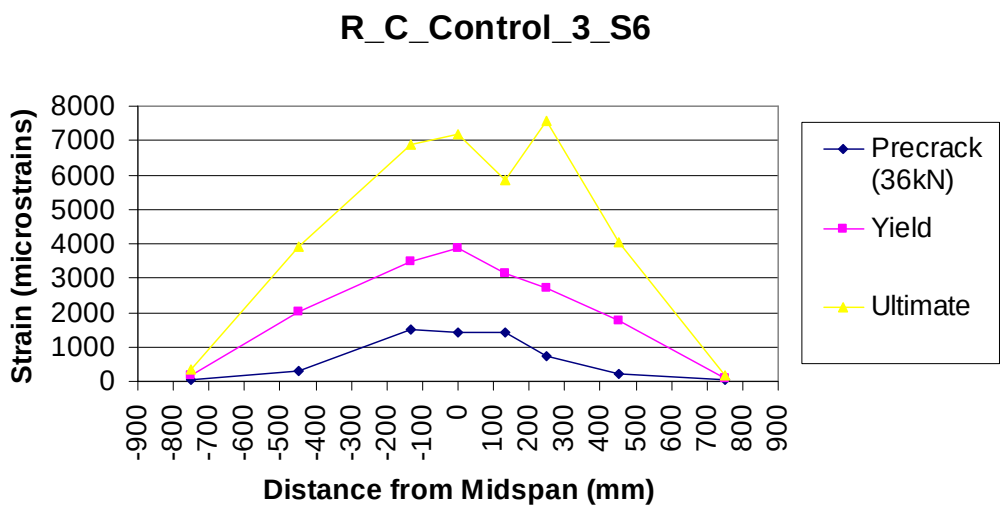
R_C_Control_3_S6
Strain (microstrains)
8000
7000
6000
5000
4000
3000
2000
1000
0
-900
-800
-700
-600
-500
-400
-300
-200
-100
0
100
200
300
400
500
600
700
800
900
Distance from Midspan (mm)
Precrack (36kN)
Yield
Ultimate

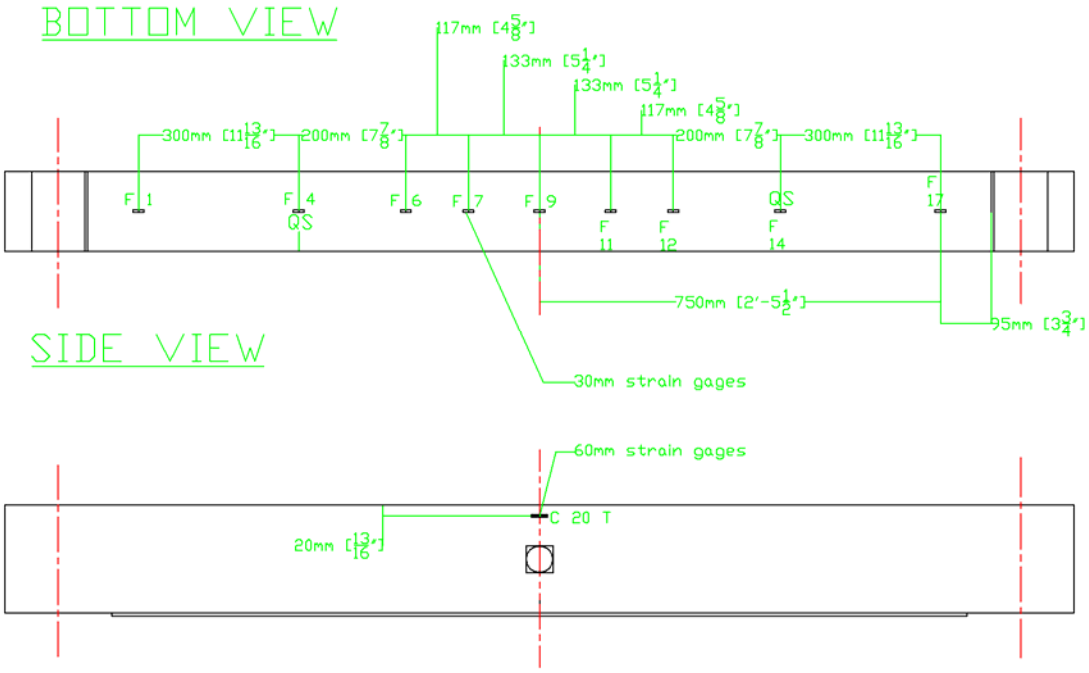
BOTTOM VIEW
117mm [4 5/8"]
133mm [5 1/4"]
133mm [5 1/4"]
117mm [4 5/8"]
300mm [11 13/16"]
200mm [7 7/8"]
200mm [7 7/8"]
300mm [11 13/16"]
F 1
F 4
QS
F 6
F 7
F 9
F 11
F 12
QS
F 14
F 17
750mm [2'-5 1/2"]
95mm [3 3/4"]
SIDE VIEW
30mm strain gages
60mm strain gages
C 20 T
20mm [13/16"]

P3(S6)
R_C_ CONTROL 3

Specimen 28: Strengthened, non-preloaded control specimen tested 6/17/2005 (R_UC_Control_3_S28)

Specimen 28 is a control beam in which no preload was applied before the application of FRP and no defect was purposely created in the specimen. The location of the strain gauges applied to the FRP surface is the same as that used for specimen 6. The peak load held by this specimen was typical at 90.6 kN and corresponding midspan displacement of 15.6mm. Final debonding occurred from near the right load-point, propagating to the right. The debonding mechanism was classified as a deep concrete/steel.

Behavior Characteristic	Value
Test Date	6/17/2005
Rehab Date (number)	5/27/2005 (2)
Concrete Cast Date (number)	10/19/04 (1)
Time from Rehab to Test	21 days
Maximum Load Held	90.6 kN
Displacement at Maximum Load	15.56 mm
Measured Steel Yield	2593 με
Load at Steel Yield	70.34 kN
Displacement at Steel Yield	8.72 mm
FRP Strain at Steel Yield	3863 με
FRP Strain at Debonding (Location)	6989 (F7) με
FRP Midspan Strain at Debonding	6582 με
Debonding Direction	Right
Failure Mode	Deep Concrete/Steel

Load (kN)	Crack Width (mm)	Notes
0.00	0	
35.92	< 0.1	Many small cracks occurring at a small spacing (~1 cm) and larger cracks propagating to near the NA @ ~50 to ~75 cm spacing.
2.45		
74.91	0.1	Steel Yielding ~58kN. More cracking to approx 'd' from the supports. No debonding.
2.49		
88.93		Large crack propagating parallel to the longitudinal steel at ~2 inches depth just before debonding occurred.

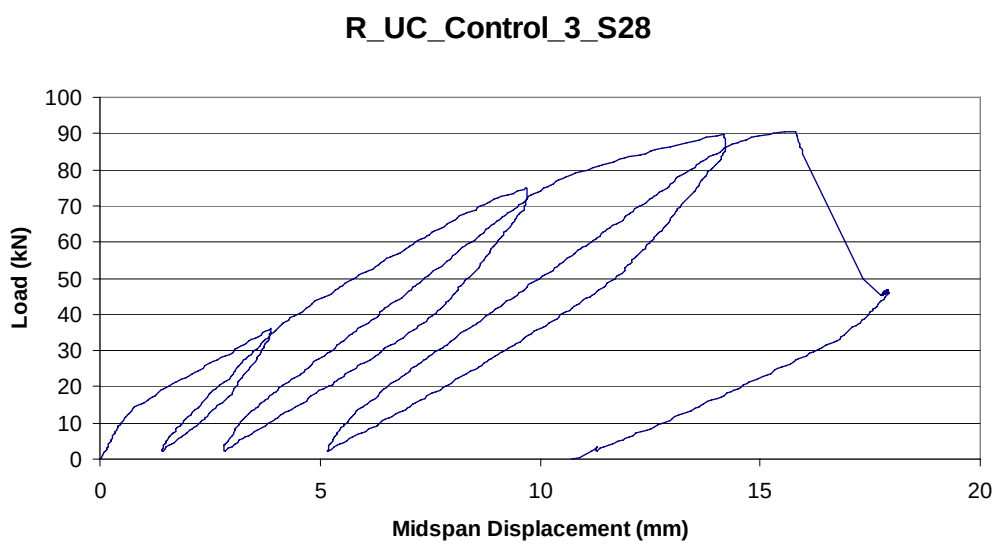

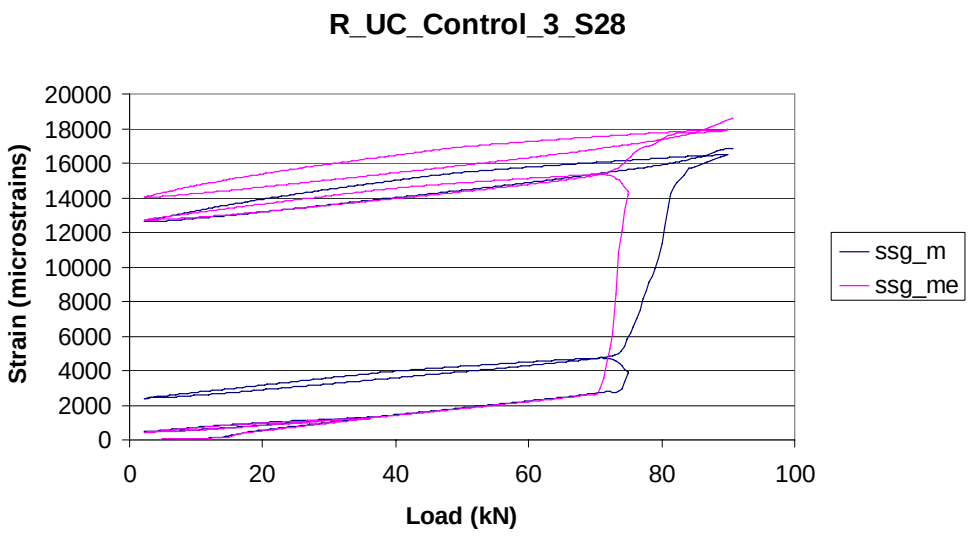
R_UC_Control_3_S28
Strain (microstrains)
20000
18000
16000
14000
12000
10000
8000
6000
4000
2000
0
0
20
40
60
80
100
Load (kN)
ssg_m
ssg_me

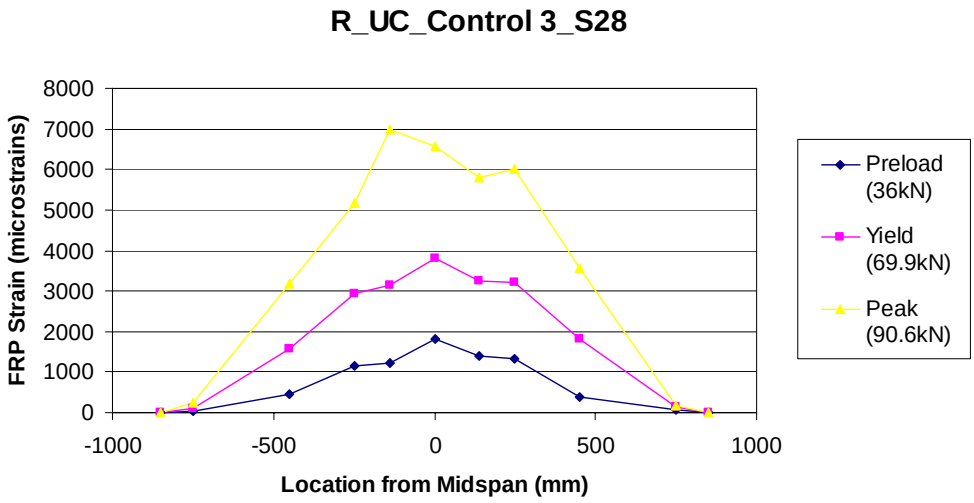
R_UC_Control 3_S28
FRP Strain (microstrains)
8000
7000
6000
5000
4000
3000
2000
1000
0
-1000
-500
0
500
1000
Location from Midspan (mm)
Preload (36kN)
Yield (69.9kN)
Peak (90.6kN)

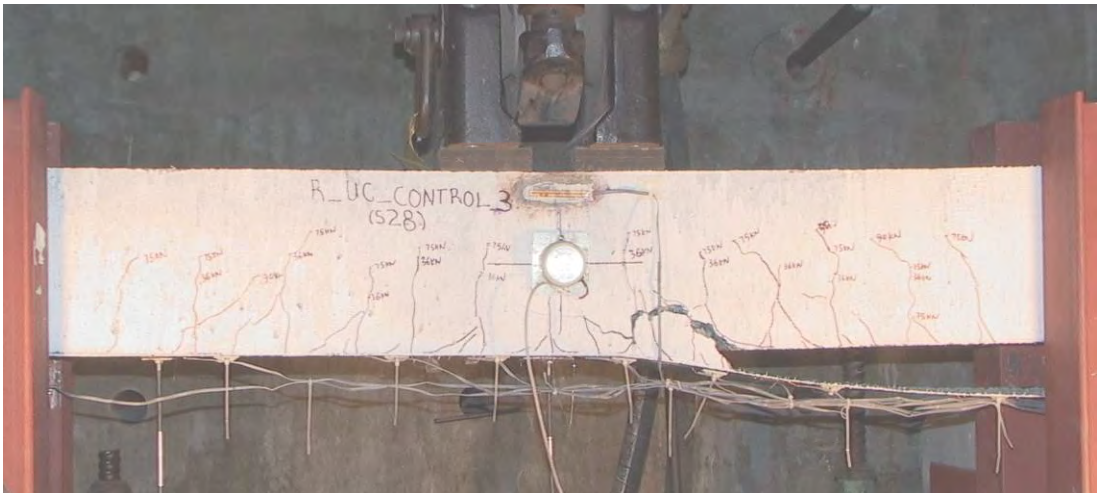
R_UC_CONTROL_3
(S28)

Specimen 29: Strengthened, non-preloaded control specimen tested 6/20/2005 (R_UC_Control_4_S29)

Specimen 29 is the fourth control beam in which no preload was applied before the application of FRP and no defect was purposely created in the specimen. The peak load held by this specimen was relatively high at 97.0 kN and occurred at a corresponding midspan displacement of 17.2mm. Final debonding occurred from near the left load-point, propagating to the left. The debonding mechanism was classified as a deep concrete/steel debonding because upon debonding a piece of concrete was torn out at the depth of the longitudinal steel. After the debonding had propagated from the steel depth to near the bondline, the failure plane was through a thick layer of concrete with little of the failure occurring in the resin, or concrete-resin interface. As expected, global debonding occurred very rapidly after initiation, as can be seen from the drop from peak load in the load-displacement plot. Yielding at the midspan of the longitudinal steel occurred at 70.8 kN in the beam at a strain of 2664 microstrains. The yield strain was chosen by averaging the measured steel strain at the points where the strain-load response becomes non-linear.

Behavior Characteristic	Value
Test Date	6/20/2005
Rehab Date (number)	5/27/2005 (2)
Concrete Cast Date (number)	10/19/04 (1)
Time from Rehab to Test	24 days
Maximum Load Held	97.04 kN
Displacement at Maximum Load	17.15 mm
Measured Steel Yield	2705 με
Load at Steel Yield	71.26 kN
Displacement at Steel Yield	8.80 mm
FRP Strain at Steel Yield	3580 με
FRP Strain at Debonding (Location)	7285 με
FRP Midspan Strain at Debonding	7285 με
Debonding Direction	Left
Failure Mode	Deep Concrete/Steel

Load (kN)	Crack Width (mm)	Notes
0.00	0	
36.20	< 0.1	Typical reopening of cracks at ~2-3" spacing
2.50	<0.1	
75.30	0.1	Typical decrease in crack spacing. Appearance of shear cracks on left hand side of the beam
2.50	<0.1	
90.00	0.3	Crackling sound @ 83kN. Local debonding near F7. Seems Close to failure. Debonded 12"-16" long on left side
2.50	0.1	
89.80		Relatively gradual debonding, but still sudden in the end

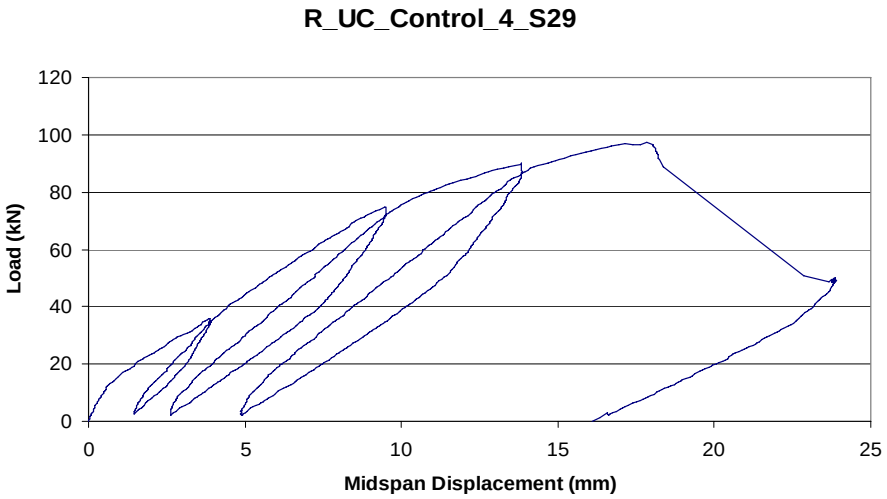
R_UC_Control_4_S29
Load (kN)
Midspan Displacement (mm)
0
20
40
60
80
100
120
0
5
10
15
20
25

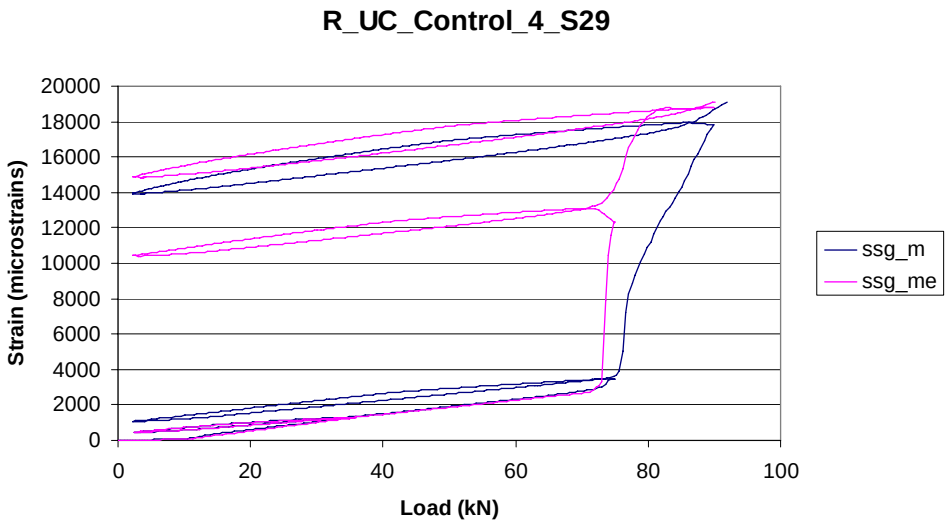
R_UC_Control_4_S29
Strain (microstrains)
Load (kN)
0
2000
4000
6000
8000
10000
12000
14000
16000
18000
20000
0
20
40
60
80
100
ssg_m
ssg_me

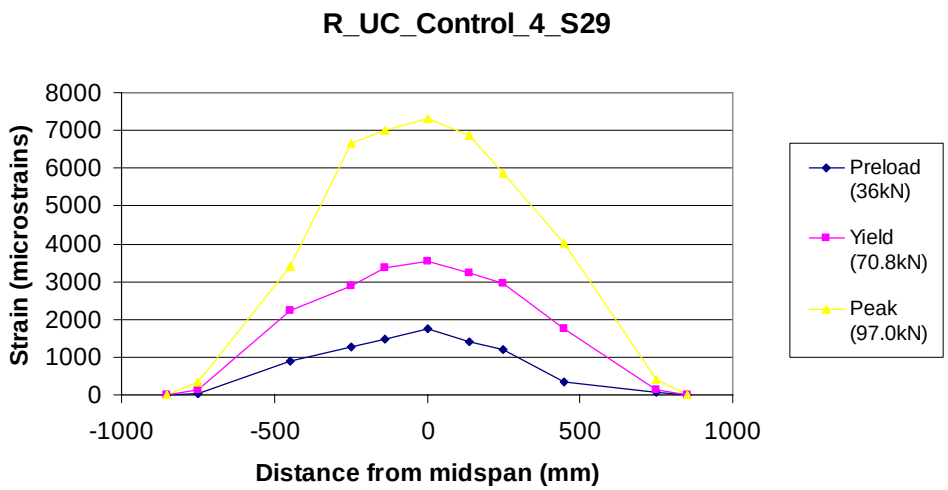
R_UC_Control_4_S29
Strain (microstrains)
Distance from midspan (mm)
0
1000
2000
3000
4000
5000
6000
7000
8000
-1000
-500
0
500
1000
Preload (36kN)
Yield (70.8kN)
Peak (97.0kN)

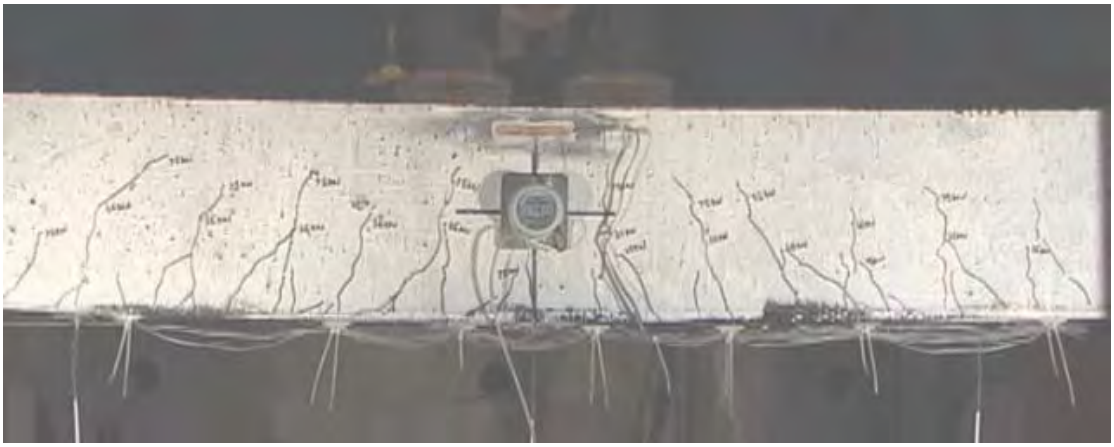

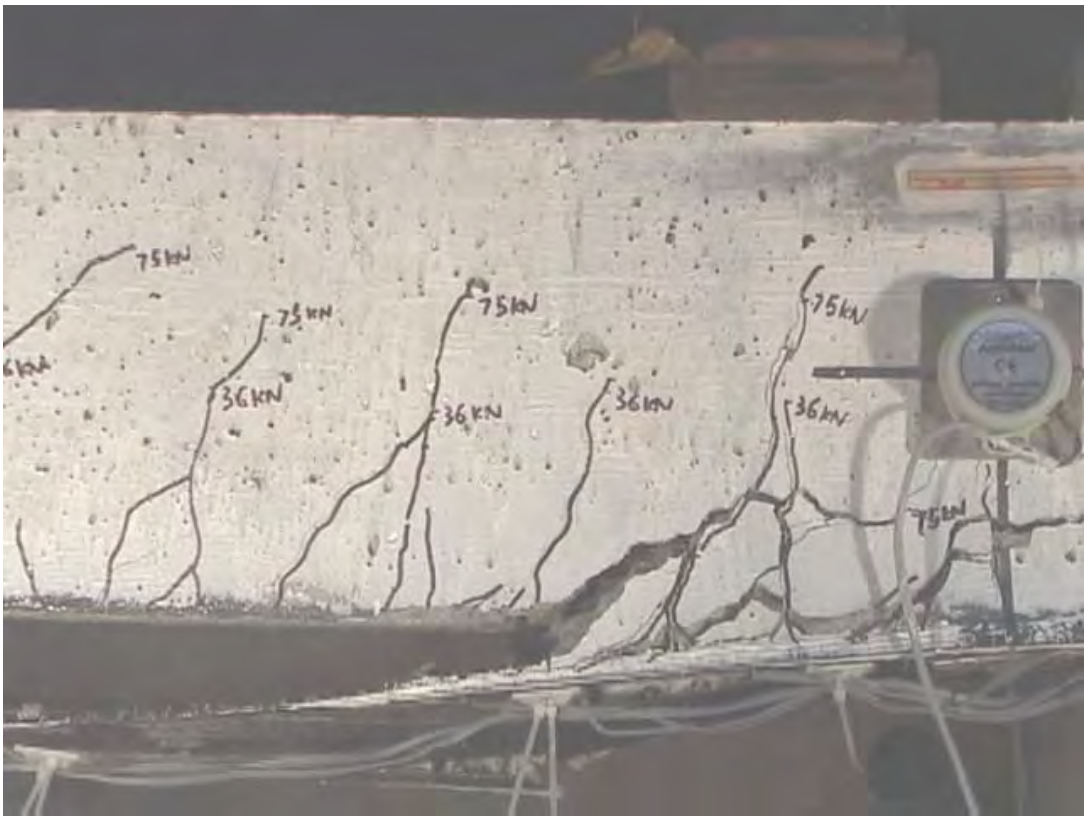
75kN
75kN
75kN
75kN
36kN
36kN
36kN
36kN
75kN

Specimen 10: Strengthened, preloaded control specimen tested 6/22/2005 (R_C_Control_4_S10)

Specimen 10 was a control specimen with standard preloading as discussed in section 2.8, but without any purposely inserted defects. At the time of testing, the FRP had been applied for 26 days. The peak load held by this specimen was modest at 89.78 kN and corresponding midspan displacement of 17.7mm. Final debonding occurred from approximately 2mm left of the midspan, propagating to the left. The debonding mechanism was classified as a deep concrete/steel debonding because, upon debonding a large chunk of concrete was tore out at the depth of the longitudinal steel. Even after the debonding had propagated to near the bondline, the failure plane was through a thick layer of concrete with little of the failure occurring in the resin, or concrete-resin interface. As usual, global debonding occurred very rapidly upon initiation, as can be seen from the drop from peak load in load-displacement plot. Yielding at the midspan of the longitudinal steel occurred at 64.5 kN in the beam at a strain of 2234 microstrains. The yield strain was determined by taking the measured steel strain at the points where the strain-load response becomes nonlinear.

Behavior Characteristic	Value
Test Date	6/22/2005
Rehab Date (number)	5/27/2005 (2)
Concrete Cast Date (number)	10/19/04 (1)
Time from Rehab to Test	24 days
Maximum Load Held	89.78 kN
Displacement at Maximum Load	17.74 mm
Measured Steel Yield	2417 με
Load at Steel Yield	67.69 kN
Displacement at Steel Yield	7.88 mm
FRP Strain at Steel Yield	3684 με
FRP Strain at Debonding (Location)	6748 (F11) με
FRP Midspan Strain at Debonding	6670 με
Debonding Direction	Right
Failure Mode	Deep Concrete/Steel

Load (kN)	Crack Width (mm)	Notes
0.00	0	
36.20	< 0.1	Typical reopening of cracks at ~2-3" spacing
2.50	<0.1	
75.30	0.1	Typical decrease in crack spacing. Appearance of shear cracks on left hand side of the beam
2.50	<0.1	
90.00	0.3	Crackling sound @ 83kN. Local debonding near F7. Seems Close to failure. Debonded 12"-16" long on left side
2.50	0.1	
89.80		Relatively gradual debonding, but still sudden in the end

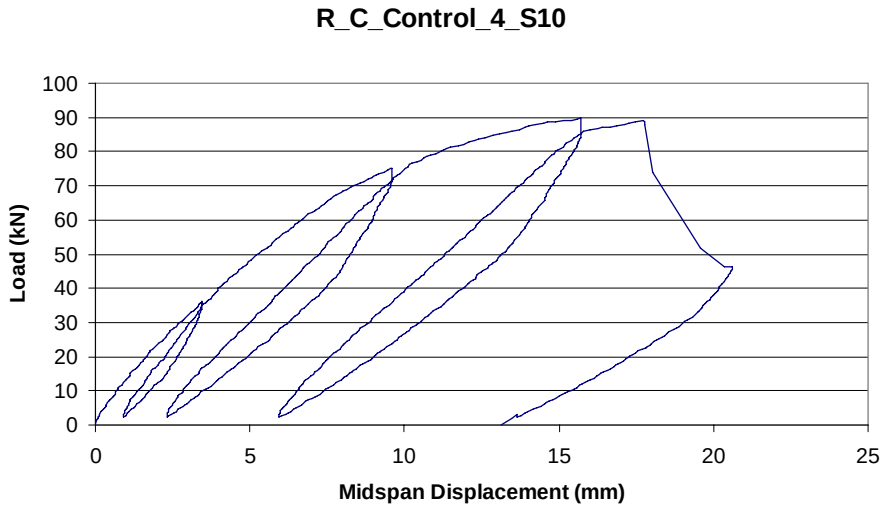
R_C_Control_4_S10
Load (kN)
100
90
80
70
60
50
40
30
20
10
0
0
5
10
15
20
25
Midspan Displacement (mm)

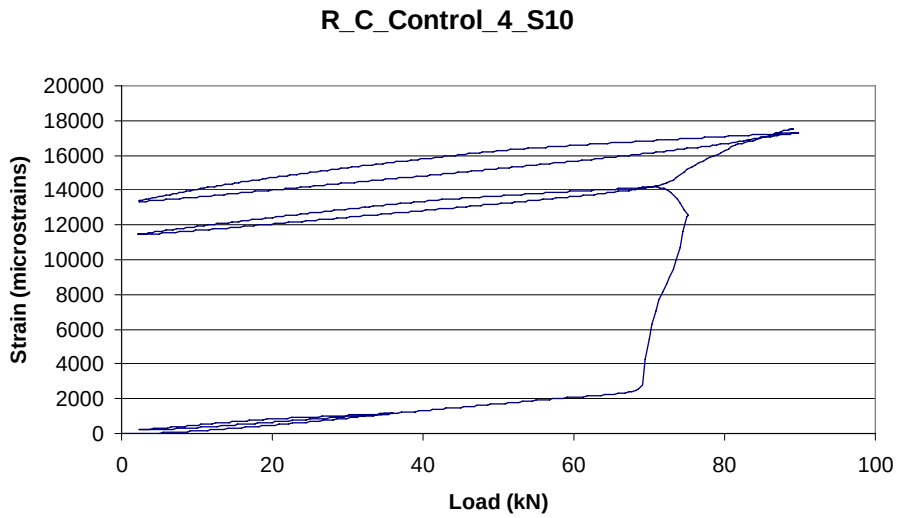
R_C_Control_4_S10
Strain (microstrains)
20000
18000
16000
14000
12000
10000
8000
6000
4000
2000
0
0
20
40
60
80
100
Load (kN)

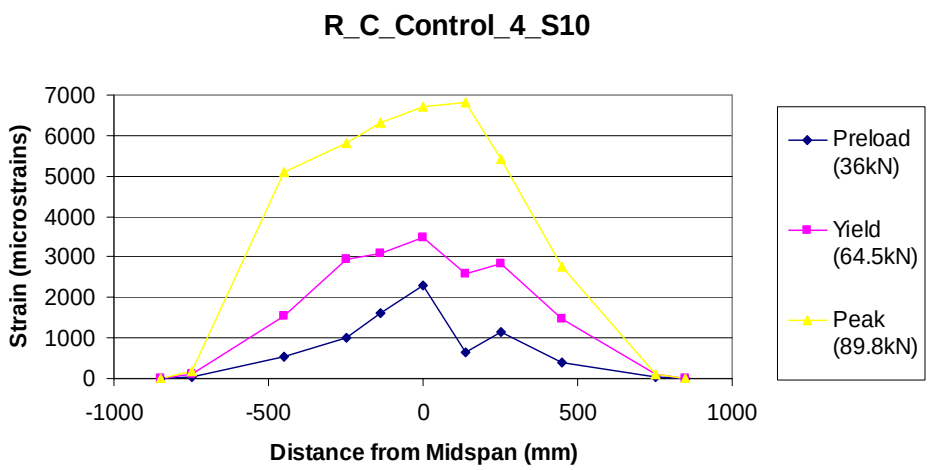
R_C_Control_4_S10
Strain (microstrains)
7000
6000
5000
4000
3000
2000
1000
0
-1000
-500
0
500
1000
Distance from Midspan (mm)
Preload (36kN)
Yield (64.5kN)
Peak (89.8kN)

A.B.2 Specimens with inserted defects

Specimen 14: 150x100mm rectangular disbond inserted in the adhesive interface 185mm from the midspan tested 6/22/2005 (150R_185_S14)

Specimen 14 was the first specimen tested in which a defect was manufactured into the rehabilitation process. The defect investigated was a rectangular disbond with a centroid located 185mm away from the midspan of the beam (see drawing). The disbond was created using three layers of thin Teflon sheets as discussed in section 2.4.1. The dimensions of the manufactured disbond were 150mm length by 150mm width (the full width of the beam). The beam was, precracked using the 35.6 kN preload level before the application of FRP. At the time of testing, the FRP had been applied for 6 days. The peak load held by this specimen was modest at 89.94 kN and corresponding midspan displacement of 12.72mm was much less than the control specimens. Final debonding occurred from approximately 125mm to the left of the

midspan, propagating to the left. The debonding mechanism was classified as a thick concrete bondline because the failure occurred by shearing a thick layer of concrete, but no large chunks of concrete were tore from the specimen (see picture). This failure mode was different from that of the control specimens that had been previously tested. This change in failure mode could have been caused by the presence of the disbond defect or by altered material properties because this specimen was rehabilitated on a different date. As usual, global debonding still occurred very rapidly, but was somewhat more gradual and less energetic than what was witnessed during testing of the control specimens.

Behavior Characteristic	Value
Test Date	6/22/2005
Rehab Date (number)	6/16/2005 (3)
Concrete Cast Date (number)	10/19/04 (1)
Time from Rehab to Test	6 days
Maximum Load Held	89.94 kN
Displacement at Maximum Load	12.72 mm
Measured Steel Yield	2735 με
Load at Steel Yield	73.18 kN
Displacement at Steel Yield	8.45 mm
FRP Strain at Steel Yield	3483 με
FRP Strain at Debonding (Location)	5858 (FD3) με
FRP Midspan Strain at Debonding	5682 με
Debonding Direction	Left
Failure Mode	Thick Concrete Bondline

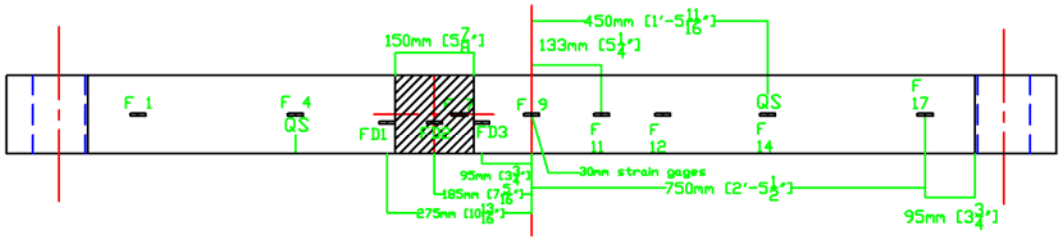

Load (kN)	Crack Width (mm)	Notes
0.00	0	
36.10	< 0.1	Slight reopening of existing cracks.
2.50	<0.1	
75.00	0.4	No new crackin gin the unbonded region. However, very large crack openings near the edges of the unbonded region. An asymmetric crack pattern is forming.
2.50		
90.00		Debonding Initiated and occurred while stopped at 90kN load. Initiation of the debond was at the lateral edge of the defect. Debonding was gradual at first then violent at the end. Much less energetic than preavious tests, but unclear if it is a product of the actuator holding constant or the presence of the defect.

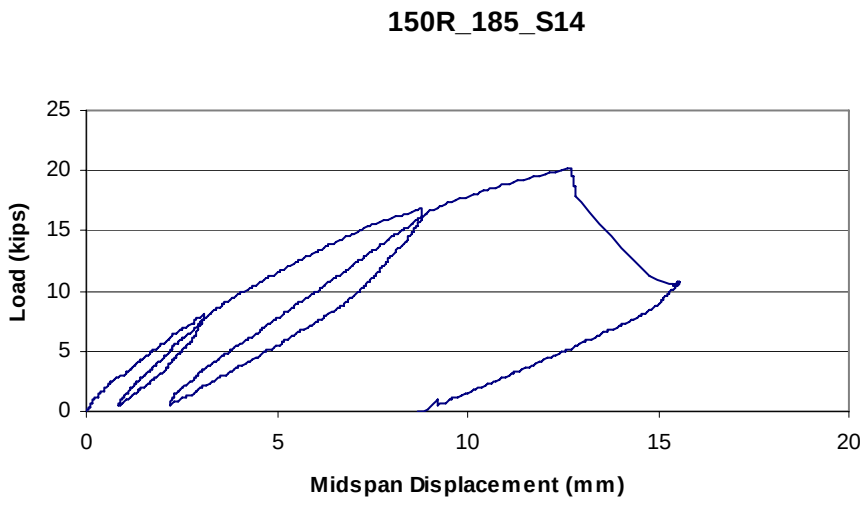
150R_185_S14
Load (kips)
Midspan Displacement (mm)
0
5
10
15
20
25

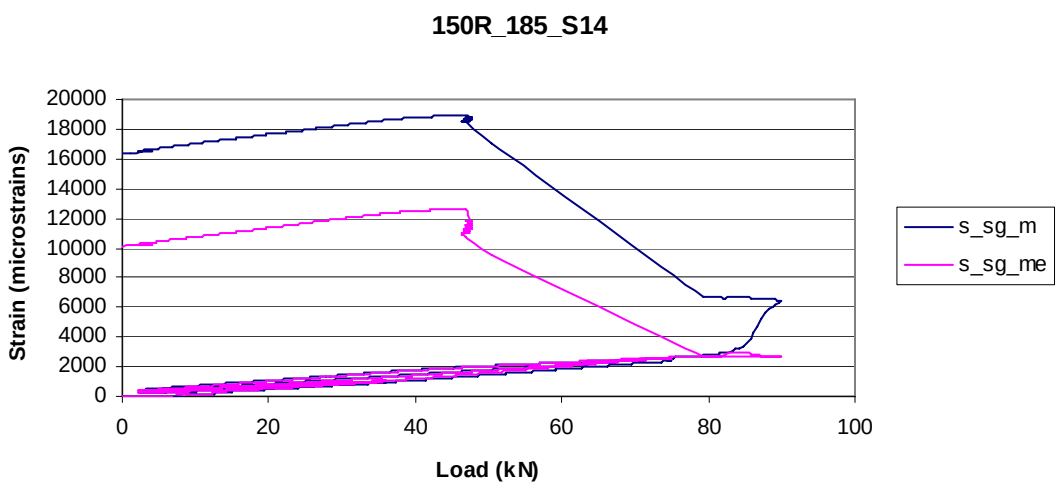
150R_185_S14
Strain (microstrains)
Load (kN)
s_sg_m
s_sg_me

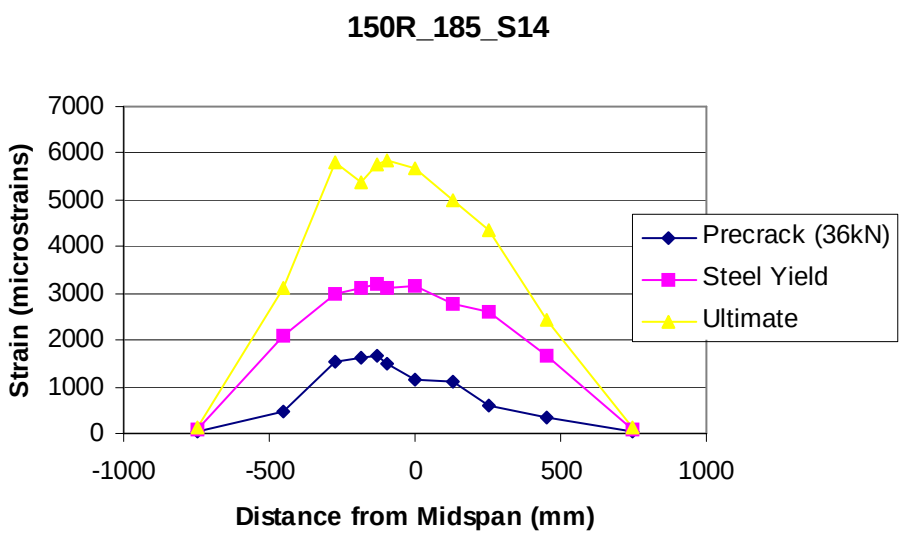
150R_185_S14
Strain (microstrains)
Distance from Midspan (mm)
Precrack (36kN)
Steel Yield
Ultimate

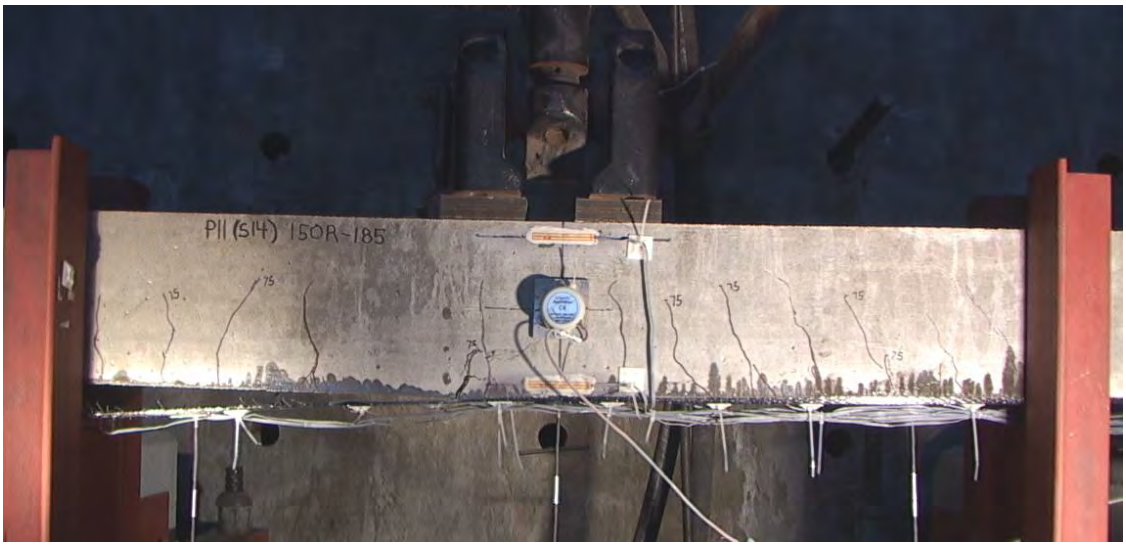

Specimen 17: 150mm diameter circular disbond inserted in the adhesive interface 185mm from the midspan tested 6/23/2005 (150C_185_S17)

Specimen 17 contained a defect with a circular disbond with a centroid located 185mm away from the midspan of the beam (see drawing). The disbond was created using three layers of thin, Teflon sheets. The size of the disbond was 150mm in diameter. This is the largest size of circular shaped disbond that could be tested in this investigation because the defect diameter is equal to the full width of the beam. The peak load held by this specimen was modest at 92.2kN and corresponding midspan displacement of 15.26mm was much less than the control specimens. Final debonding occurred from approximately 125mm to the left of the midspan, propagating to the left. The debonding mechanism was classified as a thick concrete bondline because the failure occurred by shearing a thick layer of concrete, but no large chunks of concrete were tore from the specimen (see picture). This failure mode was different from that of the control specimens that had been previously tested.

Behavior Characteristic	Value
Test Date	6/23/2005
Rehab Date (number)	6/16/2005 (3)
Concrete Cast Date (number)	10/19/04 (1)
Time from Rehab to Test	7 days
Maximum Load Held	92.2 kN
Displacement at Maximum Load	15.26 mm
Measured Steel Yield	2389 με
Load at Steel Yield	82.61 kN
Displacement at Steel Yield	11.73 mm
FRP Strain at Steel Yield	4955 με
FRP Strain at Debonding (Location)	6082 με
FRP Midspan Strain at Debonding	6082 με
Debonding Direction	Right
Failure Mode	Deep Concrete, Steel

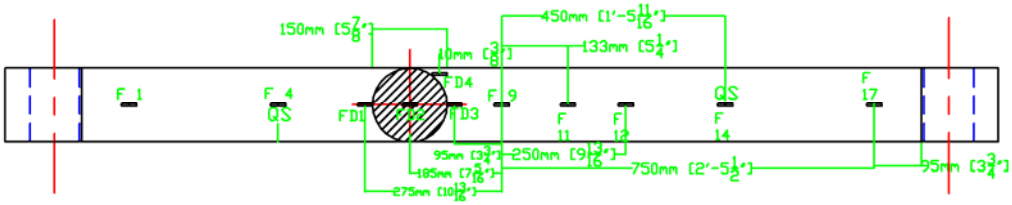

Load (kN)	Crack Width (mm)	Notes
0.00	0	
36.00	< 0.1	Typical crack reopening
2.50	<0.1	
75.10	0.2	Localized debonding occurring at the "corners" of the circular defect making it much like the rectangular disbond.
2.50	0.1	
90.00	0.5	Large crack opening in the area of localized debonding at circle edges.
2.50	0.2	
92.70		Although extensive debonding occurred on the left (defect) side macro debonding occurred on the right side (away from the defect).

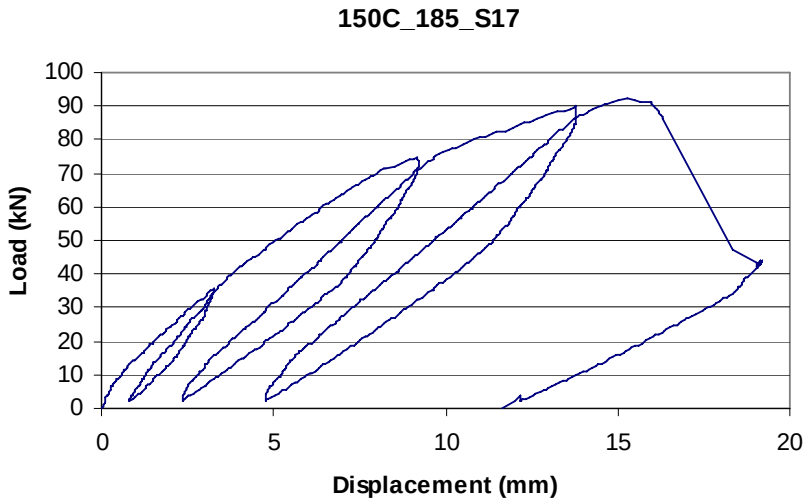
150C_185_S17
Load (kN)
Displacement (mm)
0
10
20
30
40
50
60
70
80
90
100
0
5
10
15
20

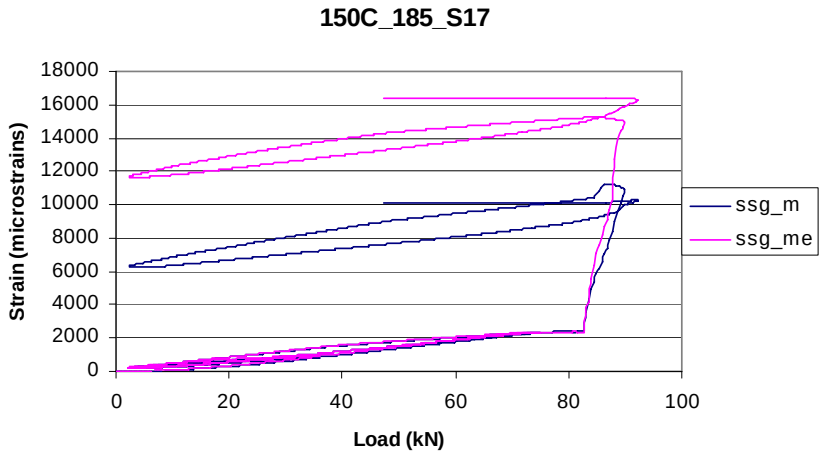
150C_185_S17
Strain (microstrains)
Load (kN)
0
2000
4000
6000
8000
10000
12000
14000
16000
18000
0
20
40
60
80
100
ssg_m
ssg_me

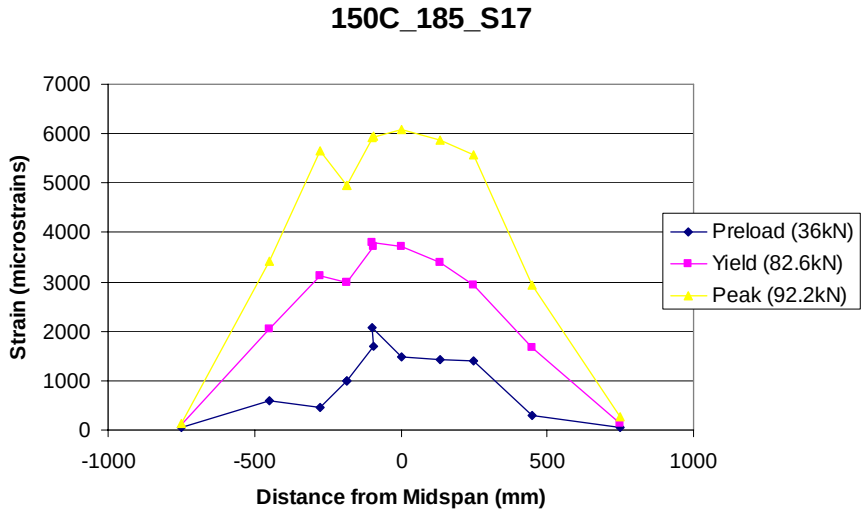
150C_185_S17
Strain (microstrains)
Distance from Midspan (mm)
0
1000
2000
3000
4000
5000
6000
7000
-1000
-500
0
500
1000
Preload (36kN)
Yield (82.6kN)
Peak (92.2kN)

Specimen 15: 100mm diameter circular disbond inserted in the adhesive interface 185mm from the midspan tested 6/23/2005 (100C_185_S15)

Specimen 15 contained a circular disbond defect with a centroid located 185mm away from the midspan of the beam. The size of the disbond was 100mm in diameter. Debonding began to occur on both sides of the midspan of the beam. However, final failure was by FRP rupture. This was not expected and upon inspection it was found that only one layer of fabric was placed on the specimen, rather than the two required for design. This is actually a defect that has great potential to occur in the field and is therefore still a useful test. Not only was the failure mode changed, but also the specimen failed at a low ultimate load compared to those that had been rehabilitated using two layers of FRP. This specimen was also very useful in the validation of the FEA model discussed in chapter 4.

Behavior Characteristic	Value
Test Date	6/24/2005
Rehab Date (number)	6/16/2005 (3)
Concrete Cast Date (number)	10/19/04 (1)
Time from Rehab to Test	8 days
Maximum Load Held	84.5 kN
Displacement at Maximum Load	19.7 mm
Measured Steel Yield	2359 με
Load at Steel Yield	59.5 kN
Displacement at Steel Yield	7.24 mm
FRP Strain at Steel Yield	3419 με
FRP Strain at Rupture (Location)	8679 (FD2) με
FRP Midspan Strain at Debonding	8322 με
Rupture Location	1.5" to the right of midspan
Failure Mode	FRP Rupture

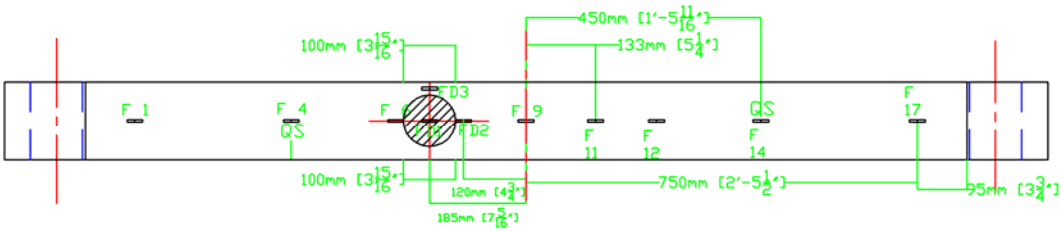

Load (kN)	Crack Width (mm)	Notes
0.00	0	
36.20	< 0.1	
2.50	<0.1	
75.10	0.4-0.5	Two large cracks formed near midspan with local debonding at the midspan and at the defect location, making it basically like the 100mm rectangular shaped defect.
2.50	0.1	
84.50	0.5	Debonding began to occur on both sides, but final failure was by FRP rupture. Upon inspection it appears only one layer of FRP was applied.

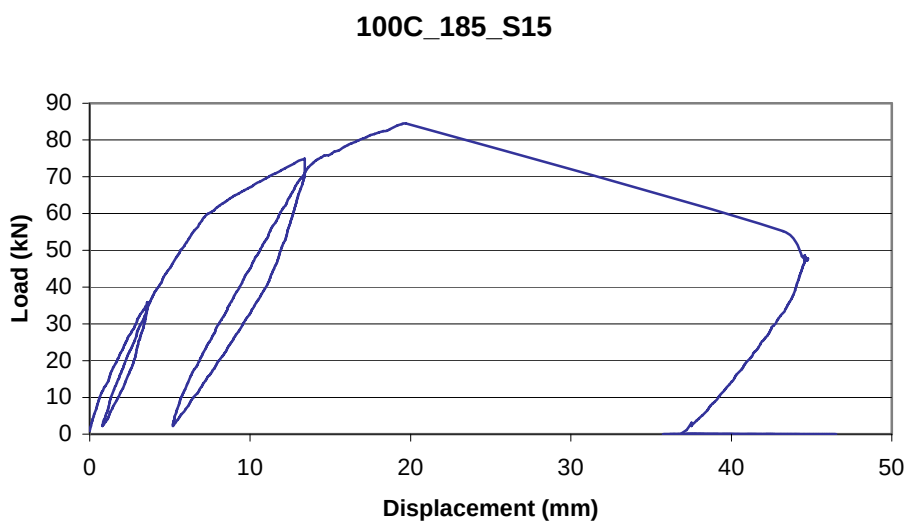

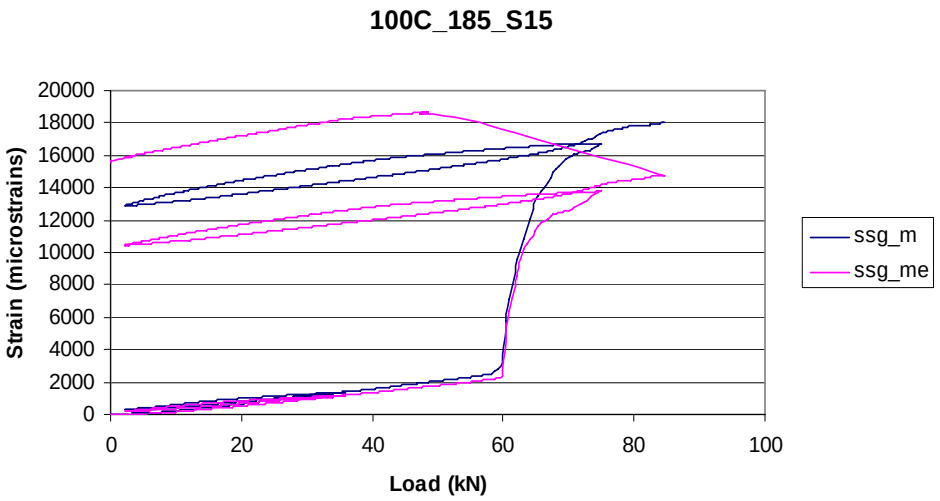
100C_185_S15
Strain (microstrains)
20000
18000
16000
14000
12000
10000
8000
6000
4000
2000
0
0
20
40
60
80
100
Load (kN)
ssg_m
ssg_me

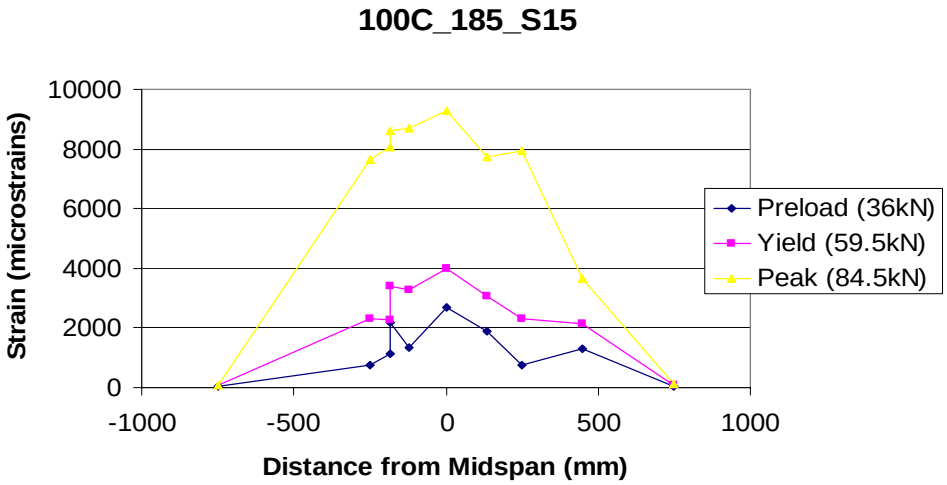
100C_185_S15
Strain (microstrains)
10000
8000
6000
4000
2000
0
-1000
-500
0
500
1000
Distance from Midspan (mm)
Preload (36kN)
Yield (59.5kN)
Peak (84.5kN)

P12(S15) 100C-185

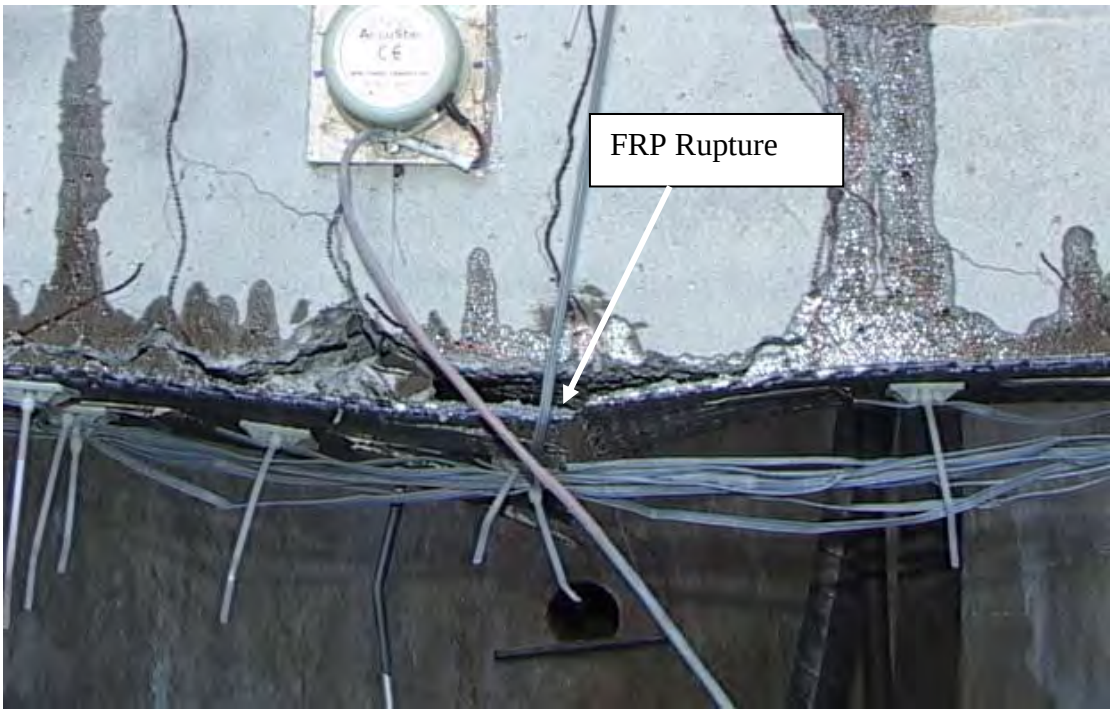

Specimen 8: 100mm x 150mm rectangular disbond inserted in the adhesive interface 185mm from the midspan tested 6/27/2005 (100R_185_S8)

Specimen 8 was manufactured with a defect consisting of a rectangular disbond with a centroid located 185mm away from the midspan of the beam (see figure x-xx). The dimensions of the manufactured disbond were 100mm length by 150mm width (the full width of the beam). The beam was, precracked using the 35.6 kN preload level before the application of FRP. Final debonding occurred from approximately 100mm to the left of the midspan, propagating to the left.

Behavior Characteristic	Value
Test Date	6/27/05
Rehab Date (number)	6/16/05 (3)
Concrete Cast Date (number)	10/19/04 (1)
Time from Rehab to Test	11 days
Maximum Load Held	90.11 kN
Displacement at Maximum Load	15.06 mm
Measured Steel Yield	2437 με
Load at Steel Yield	67.26 kN
Displacement at Steel Yield	7.75 mm
FRP Strain at Steel Yield	3130 με
FRP Strain at Debonding (Location)	6787 (FD2 με
FRP Midspan Strain at Debonding	5903 με
Debonding Direction	Left
Failure Mode	Deep Concrete, Steel

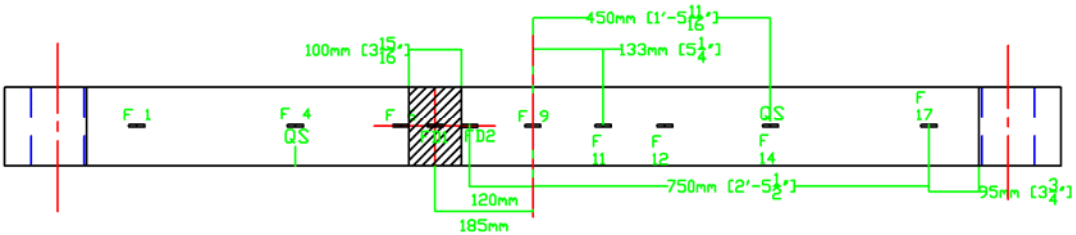

Load (kN)	Crack Width (mm)	Notes
0.00	0	
36.40	< 0.1	Typical crack reopening
2.50	<0.1	
74.90	0.1	Some local debonding near defect edges
2.50	<0.1	
90.00		Debonded while paused at 90kN

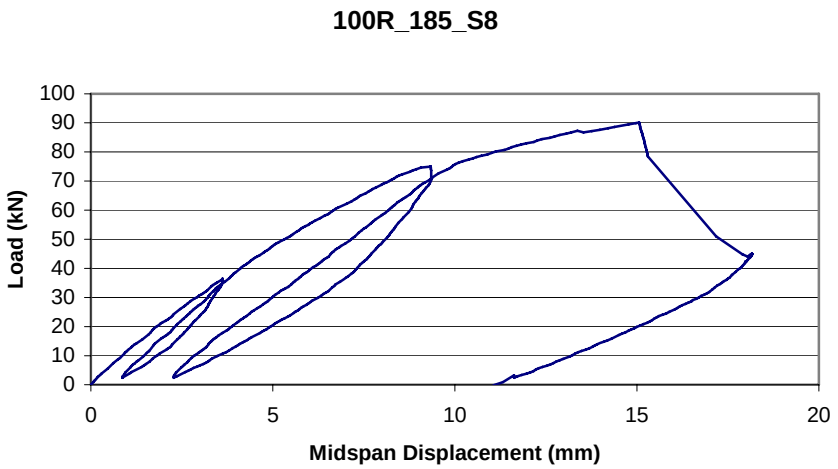
100R_185_S8
Load (kN)
100
90
80
70
60
50
40
30
20
10
0
0
5
10
15
20
Midspan Displacement (mm)

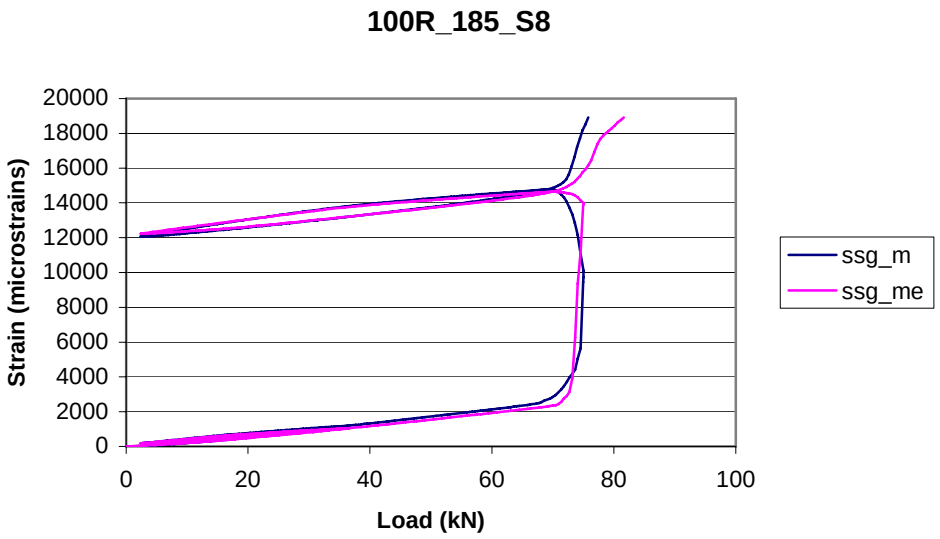
100R_185_S8
Strain (microstrains)
20000
18000
16000
14000
12000
10000
8000
6000
4000
2000
0
0
20
40
60
80
100
Load (kN)
ssg_m
ssg_me

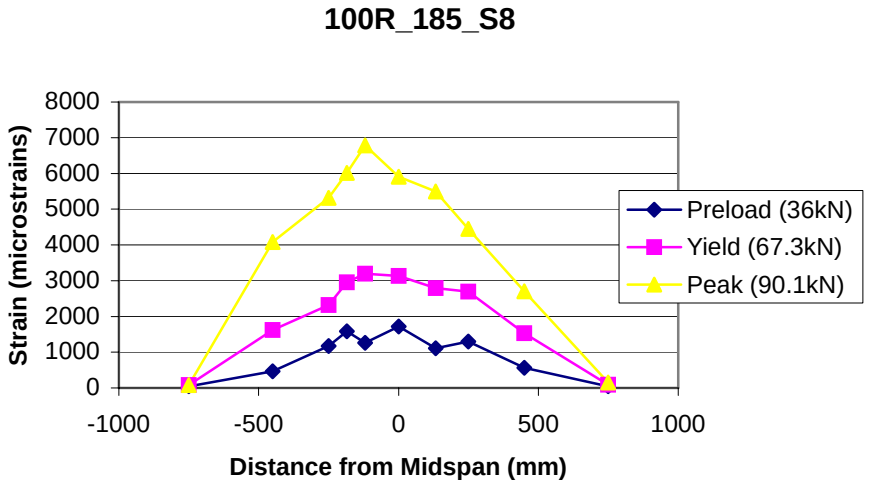
100R_185_S8
Strain (microstrains)
8000
7000
6000
5000
4000
3000
2000
1000
0
-1000
-500
0
500
1000
Distance from Midspan (mm)
Preload (36kN)
Yield (67.3kN)
Peak (90.1kN)

Specimen 19: 50mm x 150mm rectangular disbond inserted in the adhesive interface 185mm from the midspan tested 6/28/2005 (50R_185_S19)

Specimen 19 was manufactured with a defect consisting of a rectangular disbond with a centroid located 185mm away from the midspan of the beam. The dimensions of the manufactured disbond were 50mm length by 150mm width. The beam was, precracked using the 35.6 kN preload level before the application of FRP. Final debonding occurred from approximately 85mm to the left of the midspan, propagating to the left.

Behavior Characteristic	Value
Test Date	6/28/05
Rehab Date (number)	6/16/05 (3)
Concrete Cast Date (number)	10/19/04 (1)
Time from Rehab to Test	12 days
Maximum Load Held	87.89 kN
Displacement at Maximum Load	13.57 mm
Measured Steel Yield	2497 με
Load at Steel Yield	66.4 kN
Displacement at Steel Yield	7.38 mm
FRP Strain at Steel Yield	3308 με
FRP Strain at Debonding (Location)	6858 (F7) με
FRP Midspan Strain at Debonding	6095 με
Debonding Direction	Left
Failure Mode	Thick Conc. Bondline

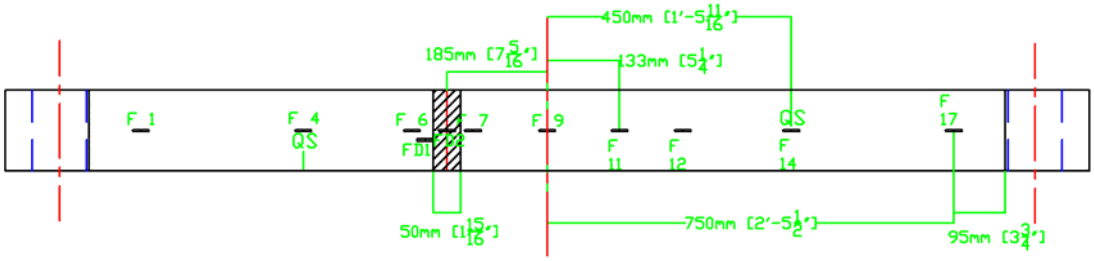

Load (kN)	Crack Width (mm)	Notes
0.00	0	
36.40	< 0.1	Typical crack reopening
2.50	<0.1	
75.00	0.2	Localized debonding occurring on each side of the defect (~40-50mm debond). Lost s_sg_m (midspan strain gage)
2.50	<0.1	
88.10		Debonded on the left side (defect side) from the defect location in the least energetic fashion seen yet.

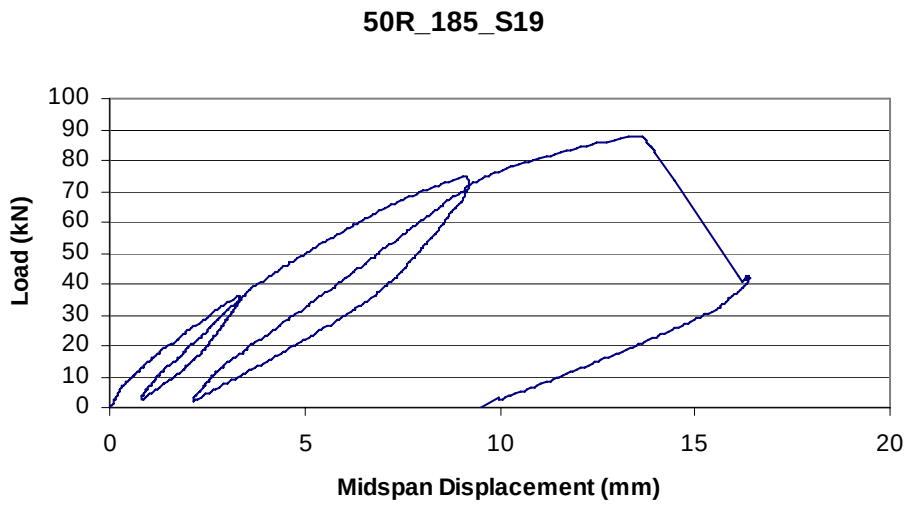
50R_185_S19
Load (kN)
100
90
80
70
60
50
40
30
20
10
0
0
5
10
15
20
Midspan Displacement (mm)

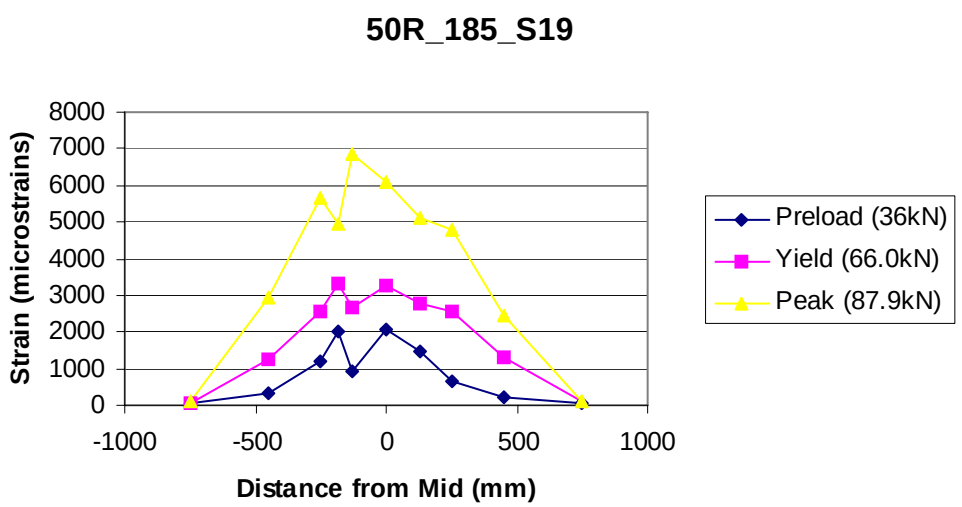
50R_185_S19
Strain (microstrains)
8000
7000
6000
5000
4000
3000
2000
1000
0
-1000
-500
0
500
1000
Distance from Mid (mm)
Preload (36kN)
Yield (66.0kN)
Peak (87.9kN)

Specimen 21: 50mm diameter circular disbond inserted in the adhesive interface 185mm from the midspan tested 6/29/2005 (50C_185_S21)

Specimen 21 was manufactured with a defect consisting of a circular disbond with a centroid located 185mm away from the midspan of the beam. The size of the manufactured disbond was 50mm in diameter. The beam was, precracked using the 35.6 kN preload level before the application of FRP. Final debonding occurred from approximately 125mm to the right of the midspan, propagating to the right. The defect in this specimen had been created on the right hand side of the midspan, so final debonding initiated near the disbond location.

Behavior Characteristic	Value
Test Date	6/29/05
Rehab Date (number)	6/16/05 (3)
Concrete Cast Date (number)	10/19/04 (1)
Time from Rehab to Test	13 days
Maximum Load Held	100.85 kN
Displacement at Maximum Load	17.95 mm
Measured Steel Yield	2372 με
Load at Steel Yield	73.61 kN
Displacement at Steel Yield	8.46 mm
FRP Strain at Steel Yield	3742 με
FRP Strain at Debonding (Location)	6858 (F7) με
FRP Midspan Strain at Debonding	6095 με
Debonding Direction	Right
Failure Mode	Deep Concrete, Steel

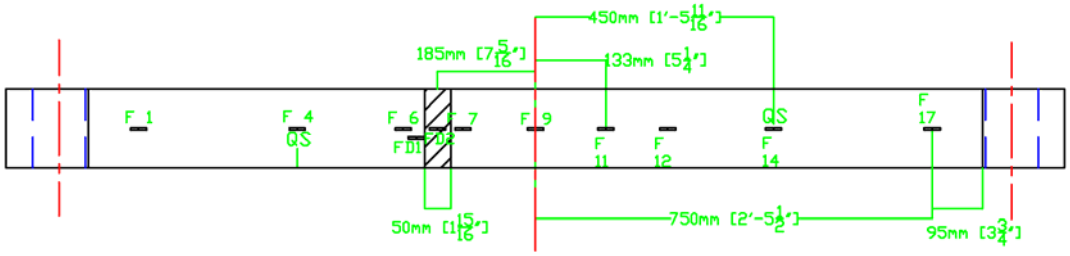

Load (kN)	Crack Width (mm)	Notes
0.00	0	
36.10	< 0.1	Typical crack reopening
2.50	<0.1	
75.00	<0.1	Crack opening is still quite small, but many sall cracks, no obvious local debonding yet.
2.50	<0.1	
90.00	0.2	Many cracks, some shear cracking. Some cracking heard. Maybe some local debonding.
2.50	0.1	Some small local debonding near the defect.
100.85		

50C_185_S21

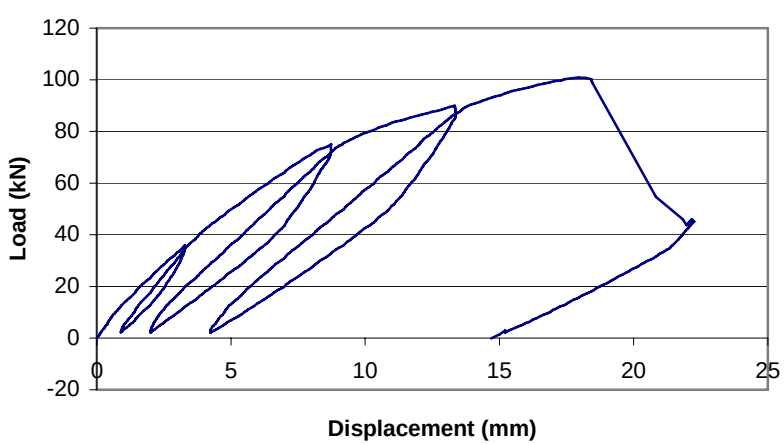

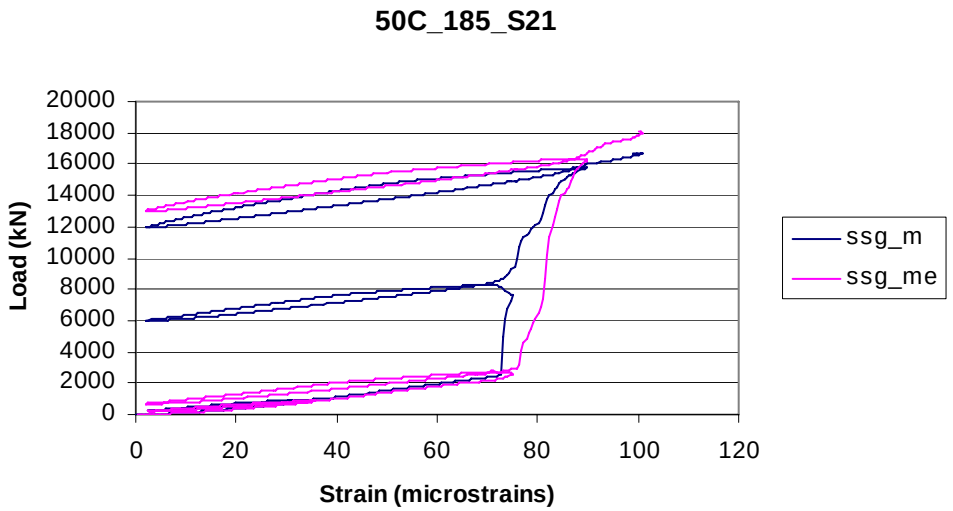
50C_185_S21
Load (kN)
20000
18000
16000
14000
12000
10000
8000
6000
4000
2000
0
0
20
40
60
80
100
120
Strain (microstrains)
ssg_m
ssg_me

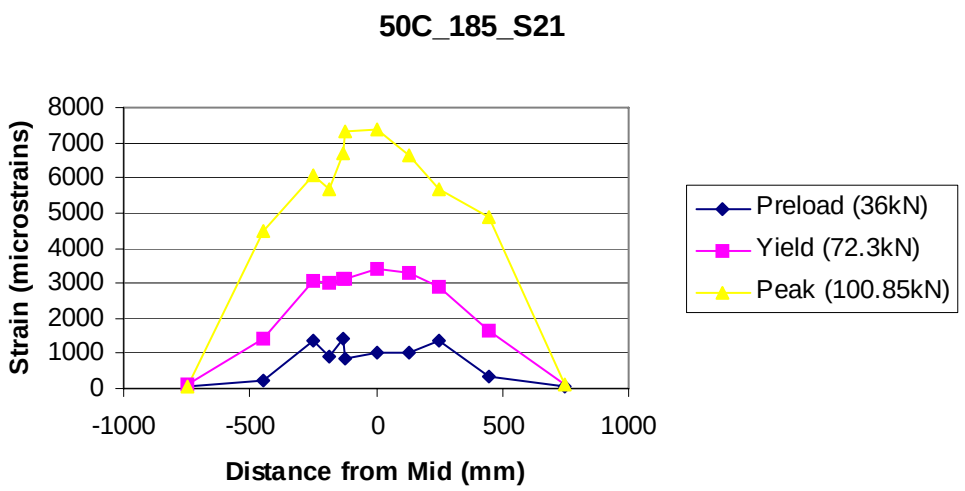
50C_185_S21
Strain (microstrains)
8000
7000
6000
5000
4000
3000
2000
1000
0
-1000
-500
0
500
1000
Distance from Mid (mm)
Preload (36kN)
Yield (72.3kN)
Peak (100.85kN)

P18(S21) 50C_185

Specimen 13: 25mm x 150mm rectangular disbond inserted in the adhesive interface 185mm from the midspan tested 7/6/2005 (25R_185_S13)

Specimen 13 was manufactured with a defect consisting of a rectangular disbond with a centroid located 185mm away from the midspan of the beam. The dimensions of the manufactured disbond were 50mm length by 150mm width. The beam was, precracked using the 35.6 kN preload level before the application of FRP. Final debonding occurred from approximately 75mm to the left of the midspan, propagating to the left.

Behavior Characteristic	Value
Test Date	7/6/05
Rehab Date (number)	6/16/05 (3)
Concrete Cast Date (number)	10/19/04 (1)
Time from Rehab to Test	20 days
Maximum Load Held	93.06 kN
Displacement at Maximum Load	16.5 mm
Measured Steel Yield	2487 με
Load at Steel Yield	68.38 kN
Displacement at Steel Yield	8.14 mm
FRP Strain at Steel Yield	3775 με
FRP Strain at Debonding (Location)	6894 (F9) με
FRP Midspan Strain at Debonding	6894 με
Debonding Direction	Left
Failure Mode	Thick Conc. Bondline

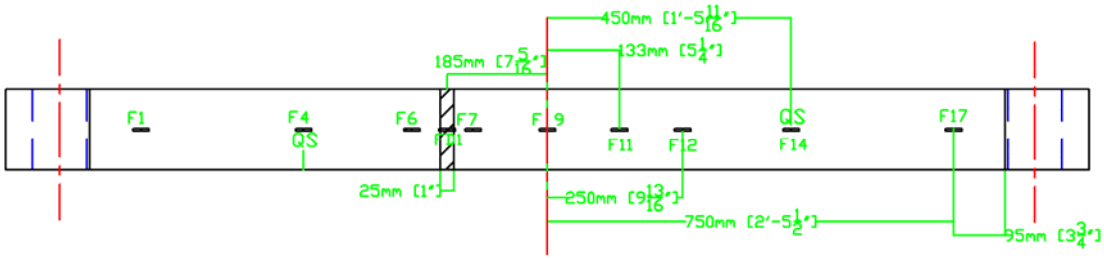

Load (kN)	Crack Width (mm)	Notes
0.00	0	
36.10	< 0.1	Typical crack reopening
2.50	<0.1	
75.10	0.1	Typical cracking
2.50	<0.1	
90.10	0.3	Approximately 50mm of local debonding in the constant moment region about 75mm to the left of the midspan. Cracking on each side of the defect
2.50		
96.90		Debonding from original point of observed local debonding

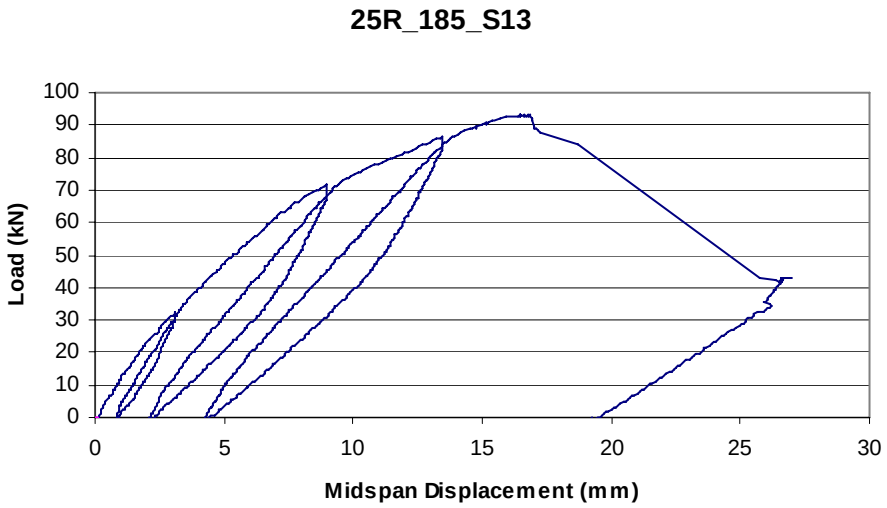
25R_185_S13
Load (kN)
100
90
80
70
60
50
40
30
20
10
0
0
5
10
15
20
25
30
Midspan Displacement (mm)

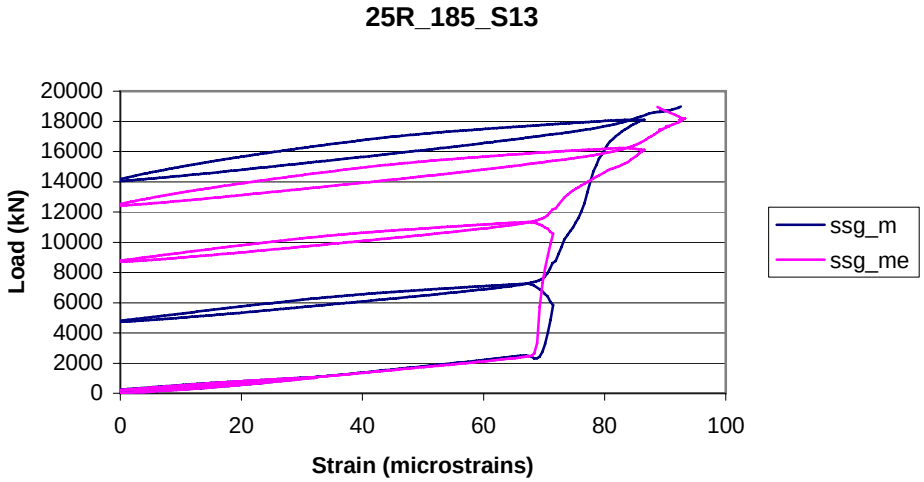
25R_185_S13
Load (kN)
20000
18000
16000
14000
12000
10000
8000
6000
4000
2000
0
0
20
40
60
80
100
Strain (microstrains)
ssg_m
ssg_me

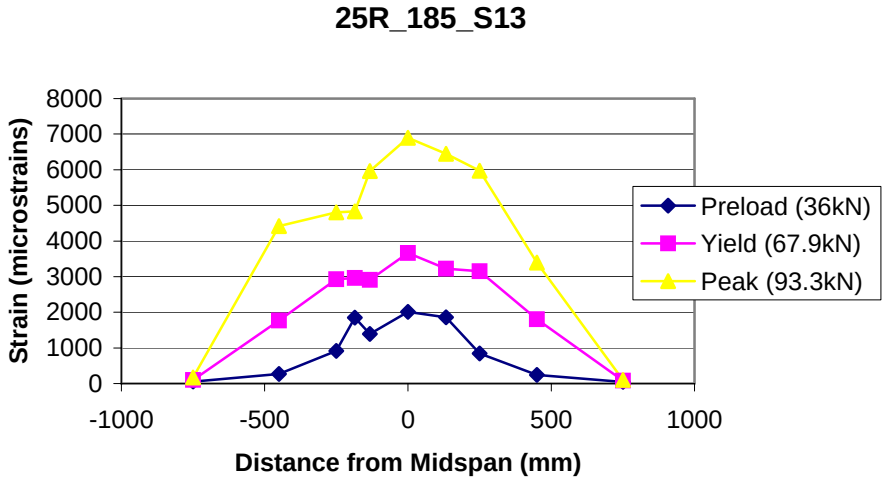
25R_185_S13
Strain (microstrains)
8000
7000
6000
5000
4000
3000
2000
1000
0
-1000
-500
0
500
1000
Distance from Midspan (mm)
Preload (36kN)
Yield (67.9kN)
Peak (93.3kN)

Specimen 12: 25mm diameter circular disbond inserted in the adhesive interface 185mm from the midspan tested 7/7/2005 (25C_185_S12)

Specimen 12 was manufactured with a defect consisting of a circular disbond with a centroid located 185mm away from the midspan of the beam (see figure x-xx). The size of the manufactured disbond was 25mm in diameter. Final debonding occurred from the midspan, propagating to the left.

Behavior Characteristic	Value
Test Date	6/29/05
Rehab Date (number)	6/16/05 (3)
Concrete Cast Date (number)	10/19/04 (1)
Time from Rehab to Test	13 days
Maximum Load Held	100.85 kN
Displacement at Maximum Load	17.95 mm
Measured Steel Yield	2372 με
Load at Steel Yield	73.61 kN
Displacement at Steel Yield	8.46 mm
FRP Strain at Steel Yield	3742 με
FRP Strain at Debonding (Location)	6858 (F7) με
FRP Midspan Strain at Debonding	6095 με
Debonding Direction	Right
Failure Mode	Deep Concrete, Steel

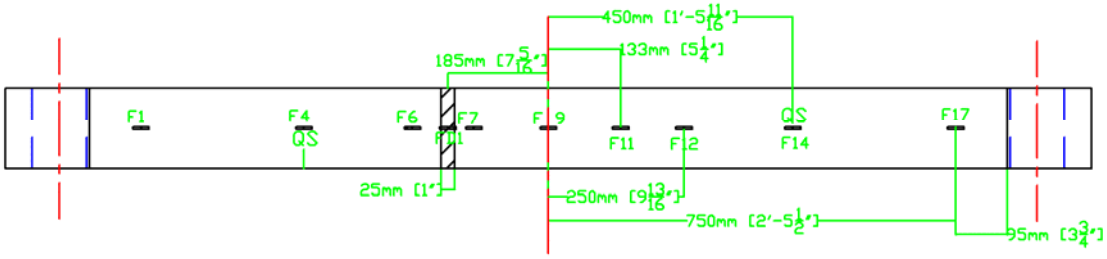

Load (kN)	Crack Width (mm)	Notes
0.00	0	
36.10	< 0.1	Typical crack reopening
2.50	<0.1	
75.00	<0.1	Crack opening is still quite small, but many sall cracks, no obvious local debonding yet.
2.50	<0.1	
90.00	0.2	Many cracks, some shear cracking. Some cracking heard. Maybe some local debonding.
2.50	0.1	Some small local debonding near the defect.
100.85		

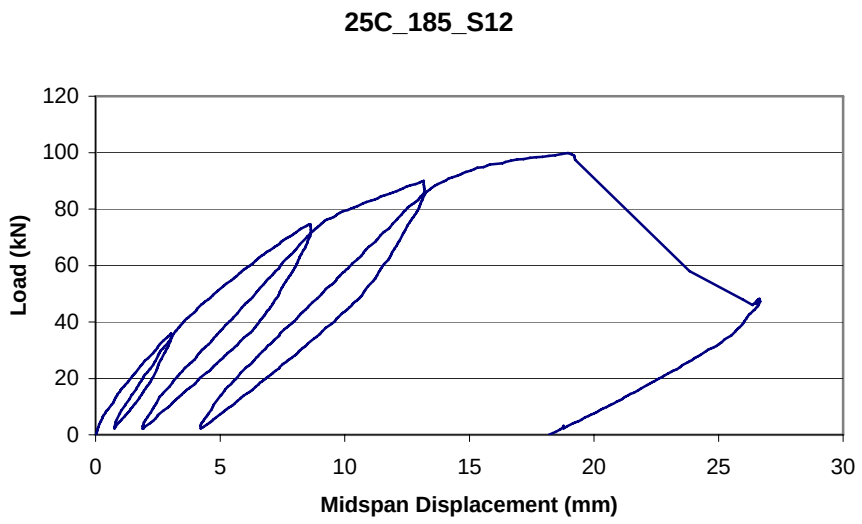
25C_185_S12
Load (kN)
Midspan Displacement (mm)
0
20
40
60
80
100
120
0
5
10
15
20
25
30

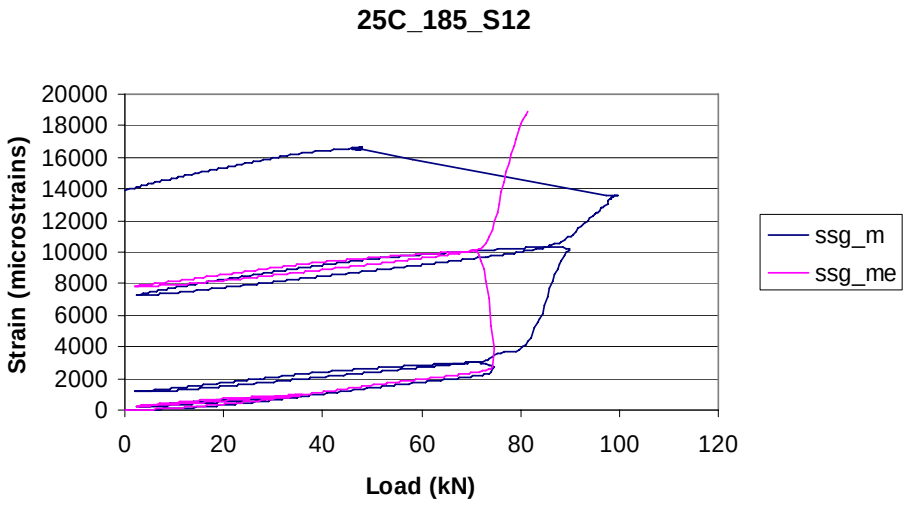
25C_185_S12
Strain (microstrains)
Load (kN)
ssg_m
ssg_me
0
2000
4000
6000
8000
10000
12000
14000
16000
18000
20000
0
20
40
60
80
100
120

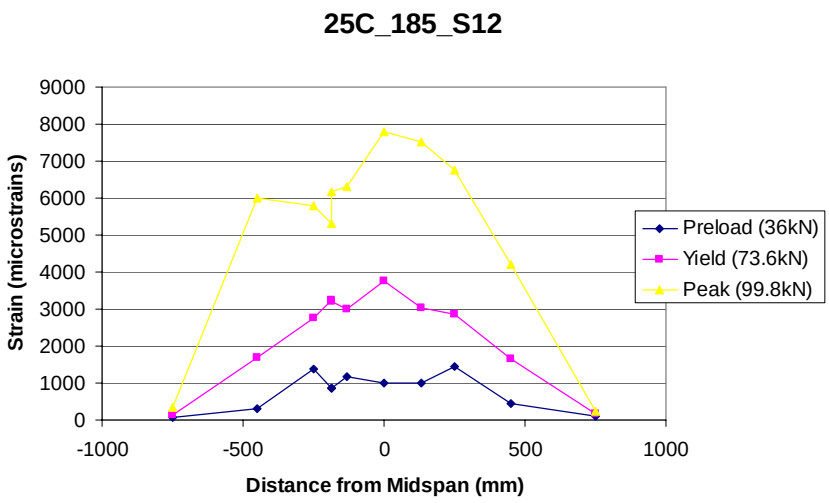
25C_185_S12
Strain (microstrains)
Distance from Midspan (mm)
Preload (36kN)
Yield (73.6kN)
Peak (99.8kN)
0
1000
2000
3000
4000
5000
6000
7000
8000
9000
-1000
-500
0
500
1000

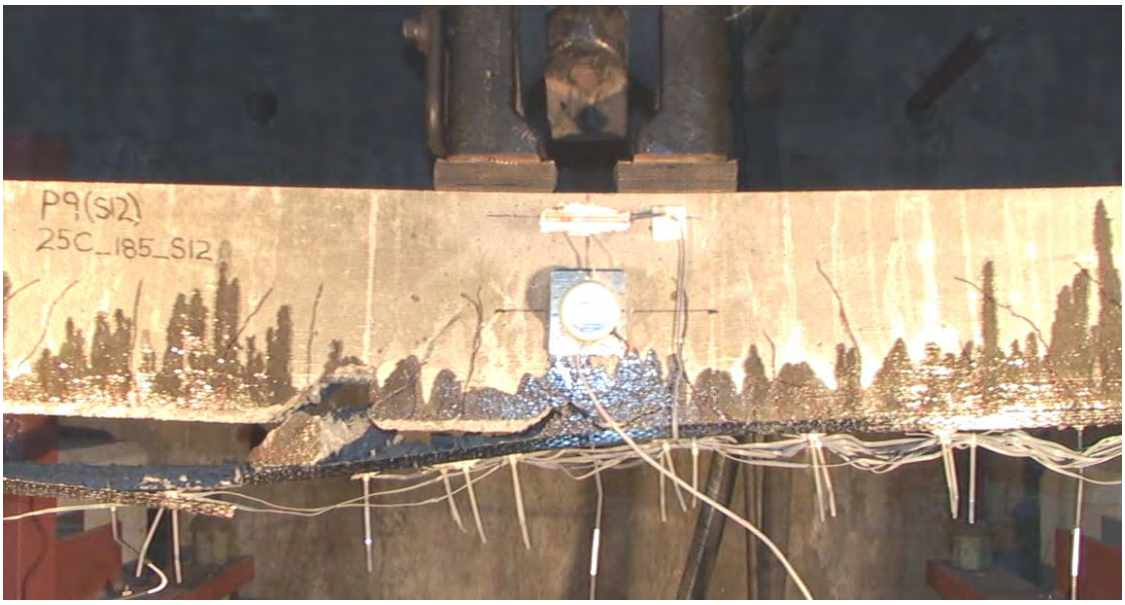

Specimen 4: 100mm x 150mm rectangular disbond inserted in the adhesive interface 185mm from the midspan tested 7/8/2005 (100R_185_S4)

Specimen 4 was manufactured with a defect consisting of a rectangular disbond with a centroid located 185mm away from the midspan of the beam. The size of the manufactured disbond was 100mm in length by 150mm in width. Final debonding occurred from the right load point, propagating to the right. Typically the disbonds were placed such that they were oriented on the left side of the midspan when the beam was placed in the test frame. However, in this specimen the disbond was placed on the right side inadvertently. This misplacement is inconsequential, however, as it should not effect the test in any way other than perhaps causing debonding to propagate in the opposite direction from typical.

Beam Characteristic	Value
Test Date	7/8/2005
Rehab Date (number)	7/1/2005 (4)
Concrete Cast Date (number)	10/19/04 (1)
Time from Rehab to Test	7 days
Maximum Load Held	83.5 kN
Displacement at Maximum Load	15.5 mm
Measured Steel Yield	2385 με
Load at Steel Yield	68.84 kN
Displacement at Steel Yield	8.48 mm
FRP Strain at Steel Yield	3568 με
FRP Strain at Debonding (Location)	6261 (FD2) με
FRP Midspan Strain at Debonding	5811 με
Debonding Direction	Right
Failure Mode	Thick Concrete Bondline

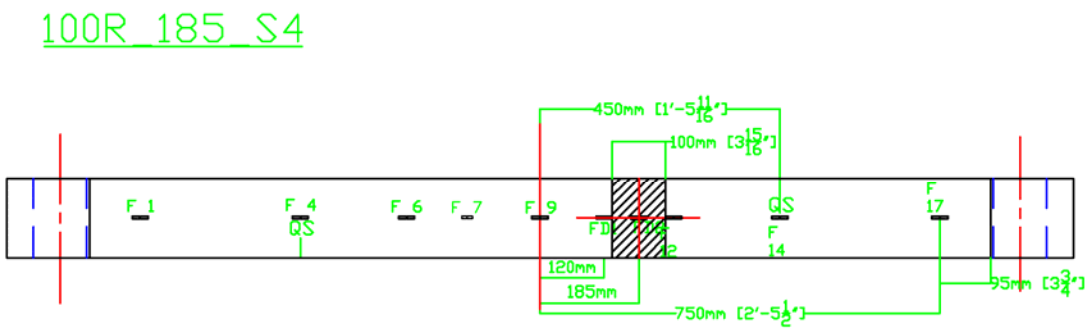

Load (kN)	Crack Width (mm)	Notes
0.00	0	
36.10	< 0.1	Typical crack reopening
2.50	<0.1	Strain gauge "F6" is reading quite high
75.10	0.2	Deboning (local) has already initiated. A lot of cracking heard beginning at ~69kN. Debonding is on each side of the defect (approximately 25mm on the left side and 50mm on the right side). Approximately 25mm debonding is also observed on the left side of the beam ~175mm to the left of the midspan
2.50	0.1	
83.80		Debonding occurred at a lower than expected load on the side of the defect. Less damage to the concrete than typical. The local debond on the left side grew to about 75mm long.

100R_185_S4_2

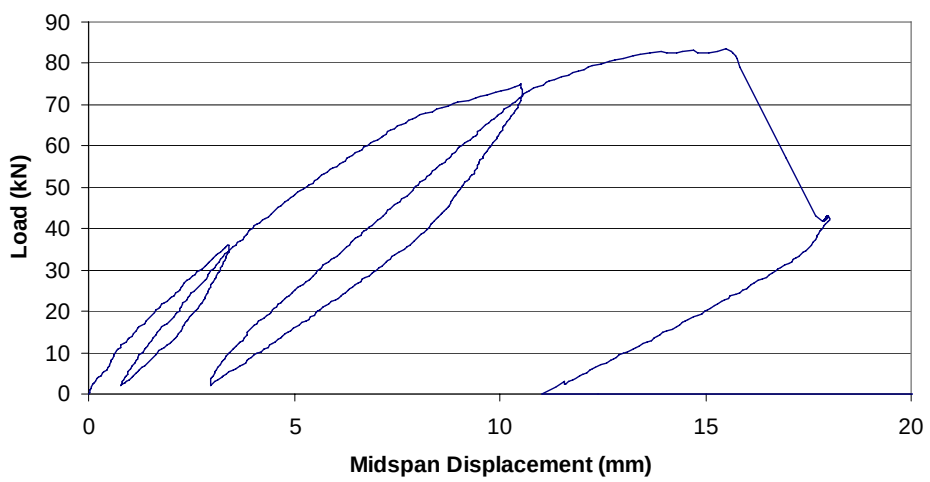

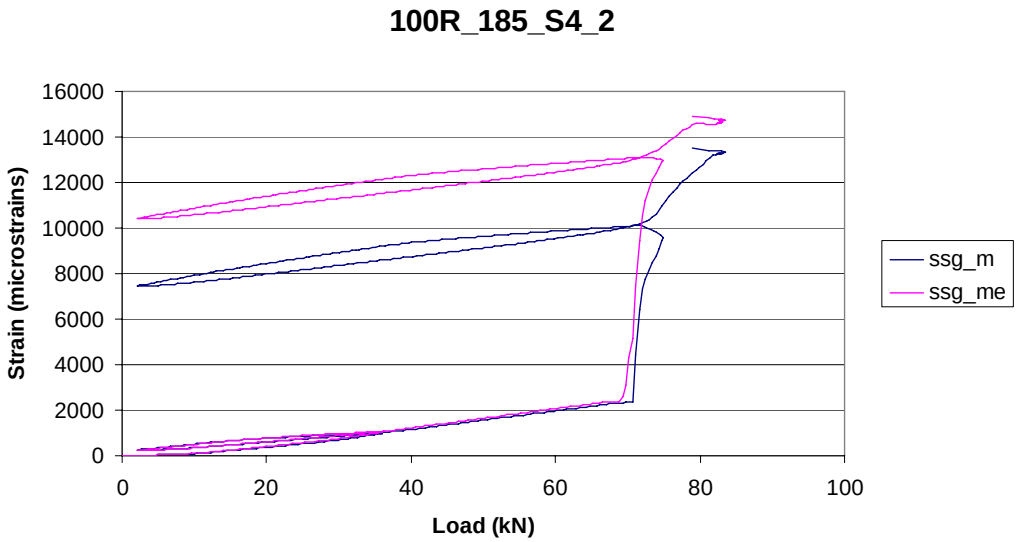
100R_185_S4_2
Strain (microstrains)
16000
14000
12000
10000
8000
6000
4000
2000
0
0
20
40
60
80
100
Load (kN)
ssg_m
ssg_me

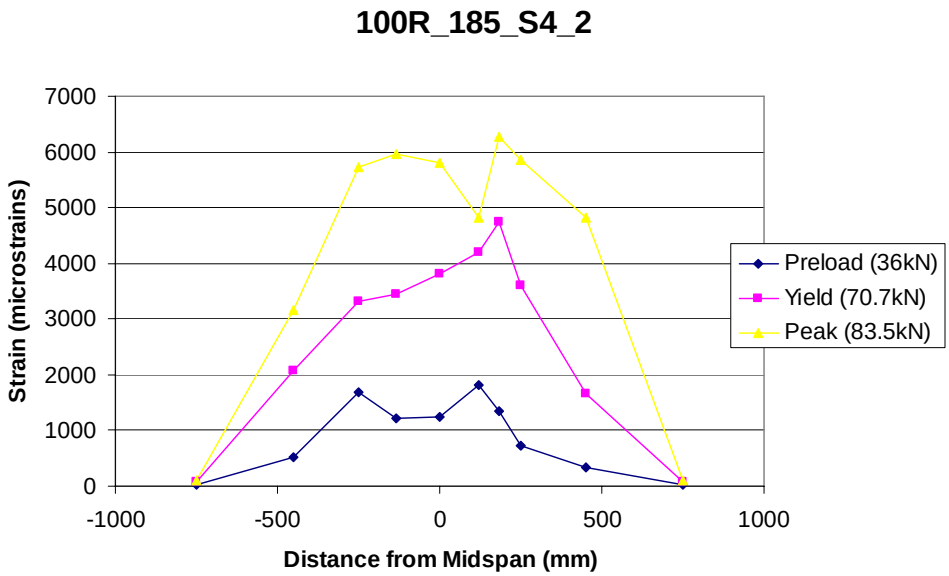
100R_185_S4_2
Strain (microstrains)
7000
6000
5000
4000
3000
2000
1000
0
-1000
-500
0
500
1000
Distance from Midspan (mm)
Preload (36kN)
Yield (70.7kN)
Peak (83.5kN)

P1(S4)
100R_185_S4_2

Specimen 16: 100mm diameter circular disbond inserted in the adhesive interface 185mm from the midspan tested 7/8/2005 (100C_185_S16_2)

Specimen 16 contained a circular disbond defect with a centroid located 185mm away from the midspan of the beam. The size of the disbond was 100mm in diameter. This is the second beam tested with this defect configuration (denoted by the '2' in the last term in the specimen name). As typically seen, failure occurred on the same side of the specimen as the disbond (the left side), debonding from a large diagonal crack. Final debonding occurred at a low load relative to the control specimens. The altered debonding mode of "thick concrete bondline" observed here was frequent in rehabilitation set number three and probably the key reason for the low strength.

Behavior Characteristic	Value
Test Date	7/8/05
Rehab Date (number)	7/1/05 (4)
Concrete Cast Date (number)	10/19/04 (1)
Time from Rehab to Test	7 days
Maximum Load Held	86.27 kN
Displacement at Maximum Load	14.86 mm
Measured Steel Yield	2463 με
Load at Steel Yield	71.76 kN
Displacement at Steel Yield	7.98 mm
FRP Strain at Steel Yield	3708 με
FRP Strain at Debonding (Location)	6330 (FD2) με
FRP Midspan Strain at Debonding	5359 με
Debonding Direction	Left
Failure Mode	Thick Concrete Bondline

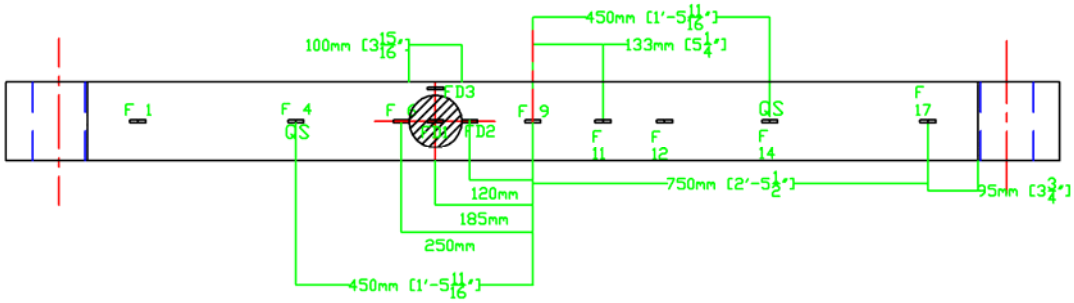

Load (kN)	Crack Width (mm)	Notes
0.00	<0.1	
36.10	<0.1	Typical crack reopening
2.40	<0.1	
75.10	0.1	Typical cracking. Some cracking sounds heard after 65 kN.
2.50	<0.1	
86.40		Failure was on the left (defect) side. A large diagonal crack was observed opening near the right side of the defect. Debonding appeared to propagate from this point. No debonding on the right side of the midspan.

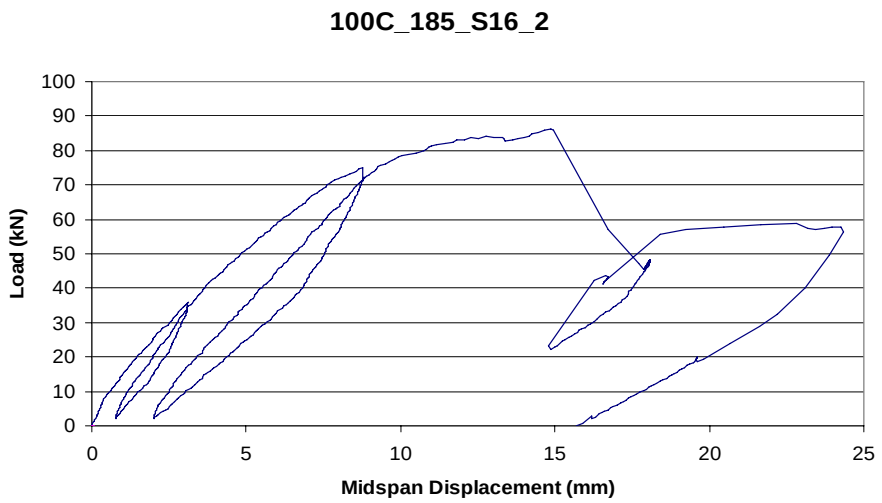
100C_185_S16_2
Load (kN)
Midspan Displacement (mm)
0
10
20
30
40
50
60
70
80
90
100
0
5
10
15
20
25

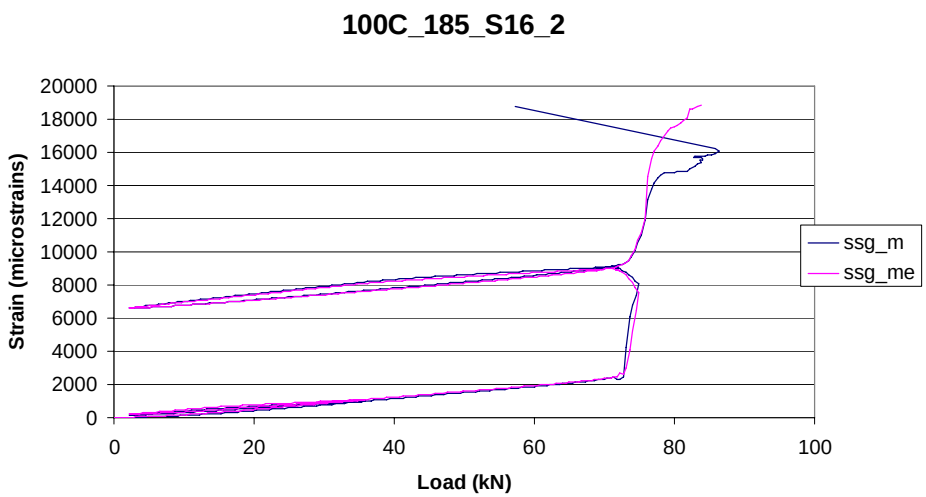
100C_185_S16_2
Strain (microstrains)
Load (kN)
ssg_m
ssg_me
0
2000
4000
6000
8000
10000
12000
14000
16000
18000
20000
0
20
40
60
80
100

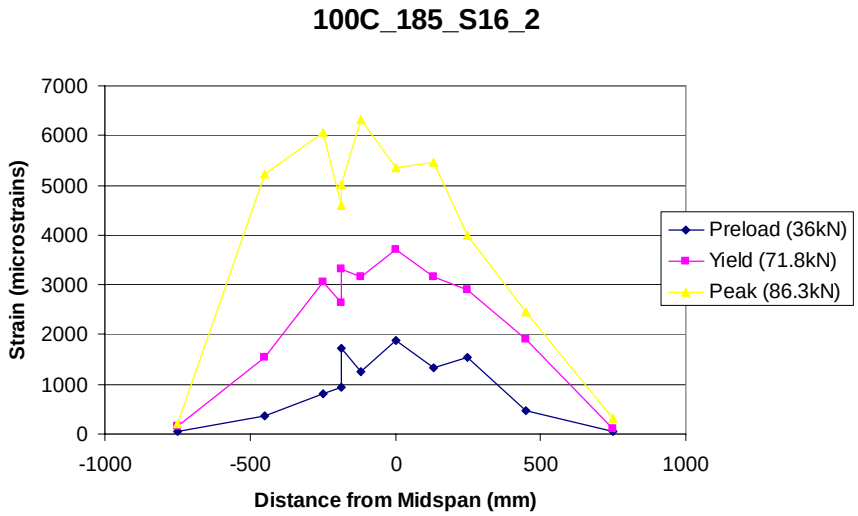
100C_185_S16_2
Strain (microstrains)
Distance from Midspan (mm)
Preload (36kN)
Yield (71.8kN)
Peak (86.3kN)
0
1000
2000
3000
4000
5000
6000
7000
-1000
-500
0
500
1000

Specimen 25: 100mm x 150mm rectangular disbond inserted in the adhesive interface located at the midspan tested 7/11/2005 (100R_0_S25)

Specimen 25 was manufactured with a defect consisting of a rectangular disbond with a centroid located at the midspan of the beam. The dimensions of the manufactured disbond were 100mm length by 150mm width. The beam was, precracked using the 35.6 kN preload level before the application of FRP. Local debonding occurred from the midspan outward in each direction. Final debonding occurred to the right end of the FRP. At an ultimate load of 95.5kN, this specimen was fairly strong.

Behavior Characteristic	Value
Test Date	7/11/2005
Rehab Date (number)	7/1/2005 (4)
Concrete Cast Date (number)	10/19/2004 (1)
Time from Rehab to Test	10 days
Maximum Load Held	95.30 kN
Displacement at Maximum Load	15.90 mm
Measured Steel Yield	2540 με
Load at Steel Yield	70.62 kN
Displacement at Steel Yield	7.27 mm
FRP Strain at Steel Yield	3248 με
FRP Strain at Debonding (Location)	7187 (FD1) με
FRP Midspan Strain at Debonding	5930 με
Debonding Direction	Right
Failure Mode	Thick Concrete Bondline

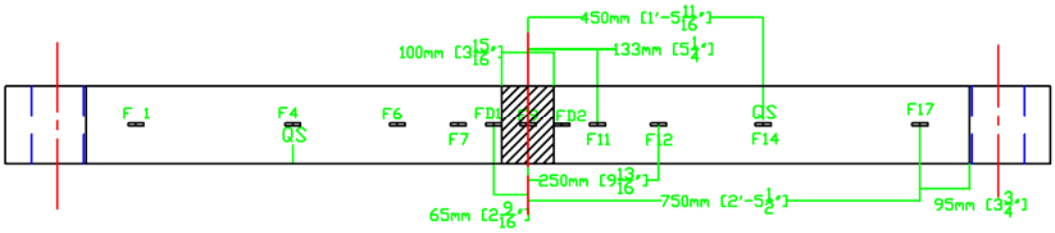

Load (kN)	Crack Width (mm)	Notes
0.00	<0.1	
36.00	<0.1	Typical crack reopening. There is a crack across F11, therefore, its strain appears to be higher at this location.
2.40	<0.1	
75.20	0.3	No debonding yet. 0.3mm crack opening at the edge of the defect. Only slight reopening of precracks located within the area of the defect. 3 large diagonal cracks formed on the left side of thhe beam, but non on the right.
2.50		Lost both midspan steel gauges.
90.10	0.5	First debonding heard at 80.4kN. Local debonding observed in two locations on the left side of the midspan. One is at the defect edge, the other is located at the large shear (diagonal) crack approximately 240mm from the left loading point. Both are about 25mm in length.
2.50		
95.50		Final debonding appeared to propagate from the midspan (defect location) outward in each direction. Final failure was debonding on the right side of the beam.

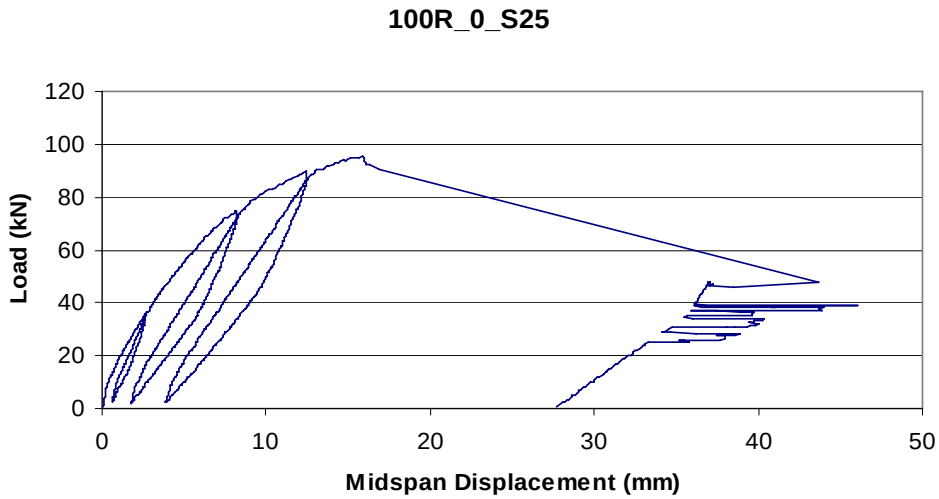
100R_0_S25
Load (kN)
Midspan Displacement (mm)
0
20
40
60
80
100
120
0
10
20
30
40
50

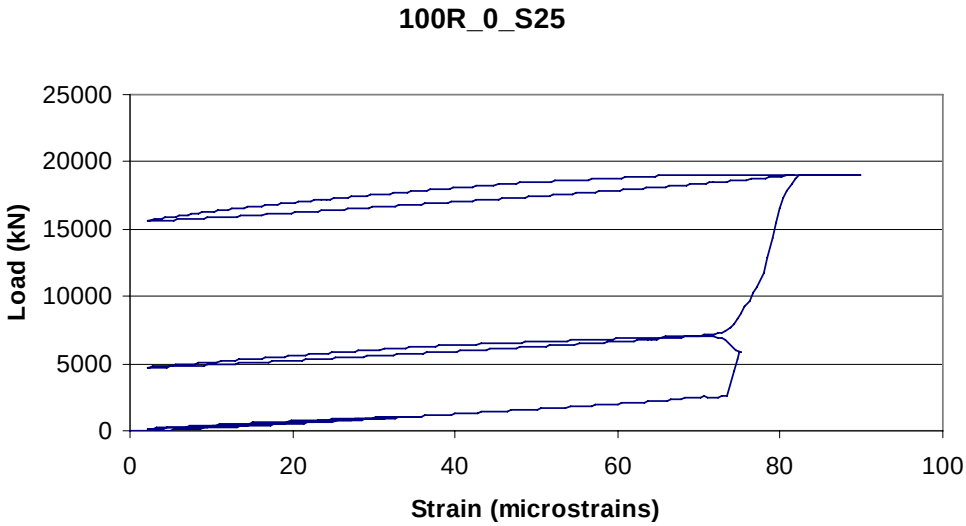
100R_0_S25
Load (kN)
Strain (microstrains)
0
5000
10000
15000
20000
25000
0
20
40
60
80
100

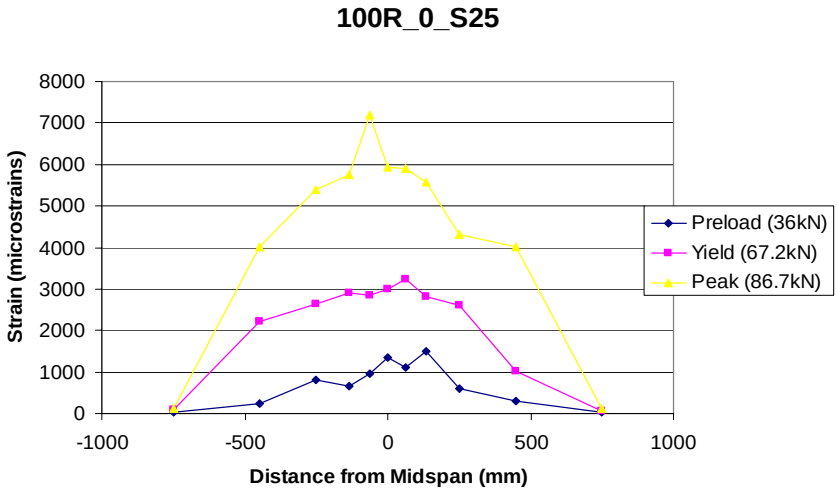
100R_0_S25
Strain (microstrains)
Distance from Midspan (mm)
Preload (36kN)
Yield (67.2kN)
Peak (86.7kN)
0
1000
2000
3000
4000
5000
6000
7000
8000
-1000
-500
0
500
1000

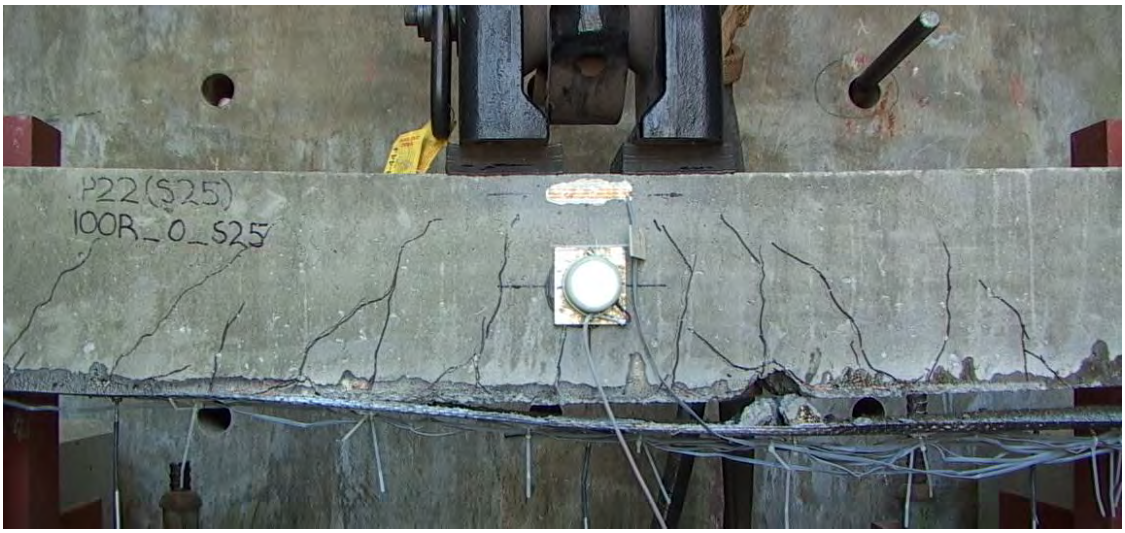

Specimen 18: Strengthened, preloaded control specimen tested 7/11/2005 (R_C_Control_5_S18)

Specimen 18 was a control specimen with standard preloading as discussed in section 2.8, but without any purposely inserted defects. It is the control specimen that was created in conjunction with the defective beams for rehabilitation set four. The peak load held by this specimen was modest at 95.9 kN and corresponding midspan displacement of 15.7mm. Final debonding occurred from approximately 50mm left of the midspan, propagating to the right end of the FRP through the midspan. The debonding mechanism was classified as a deep concrete/steel debonding, which was not the predominant failure mode for this set of specimens, making comparisons in this set difficult. As usual, global debonding occurred very rapidly upon initiation, as can be seen from the drop from peak load in the load-displacement plot. Yielding at

the midspan of the longitudinal steel occurred at 70.0 kN in the beam at a steel strain of 2401 microstrains.

Beam Characteristic	Value
Test Date	7/11/05
Rehab Date (number)	7/1/05 (4)
Concrete Cast Date (number)	10/19/04 (1)
Time from Rehab to Test	10 days
Maximum Load Held	95.87 kN
Displacement at Maximum Load	15.65 mm
Measured Steel Yield	2401 με
Load at Steel Yield	70.03 kN
Displacement at Steel Yield	7.53 mm
FRP Strain at Steel Yield	3262 με
FRP Strain at Debonding (Location)	7221 (F7) με
FRP Midspan Strain at Debonding	6900 με
Debonding Direction	Right
Failure Mode	Deep Concrete, Steel

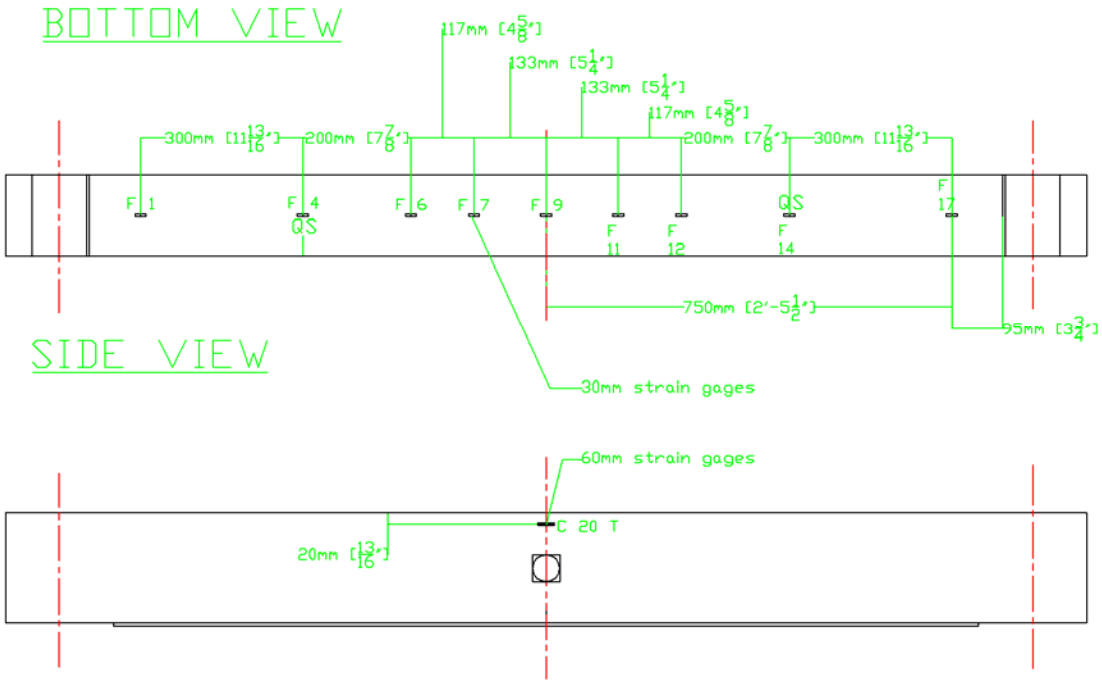

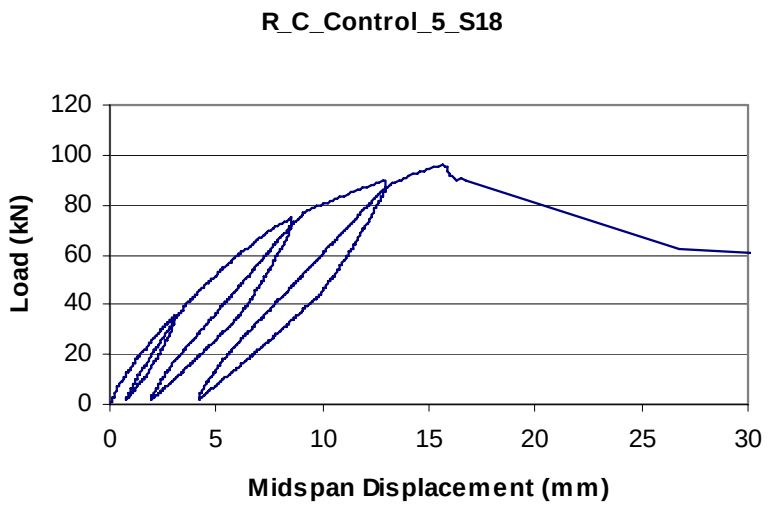
R_C_Control_5_S18
Load (kN)
120
100
80
60
40
20
0
0
5
10
15
20
25
30
Midspan Displacement (mm)

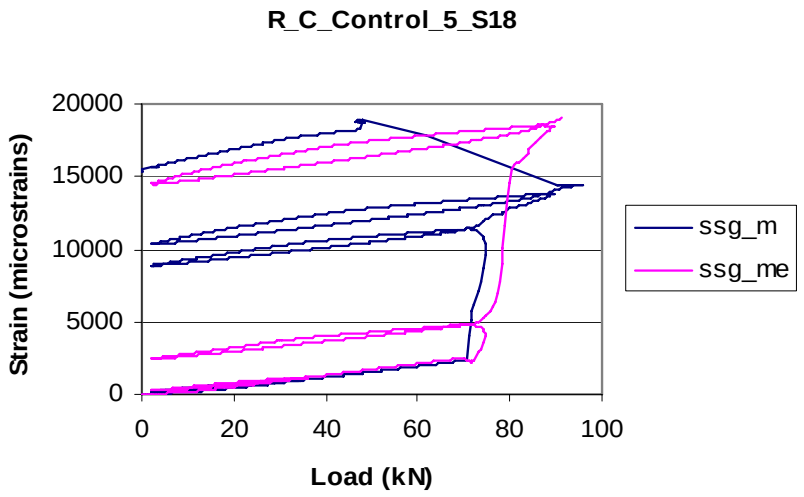
R_C_Control_5_S18
Strain (microstrains)
20000
15000
10000
5000
0
0
20
40
60
80
100
Load (kN)
ssg_m
ssg_me

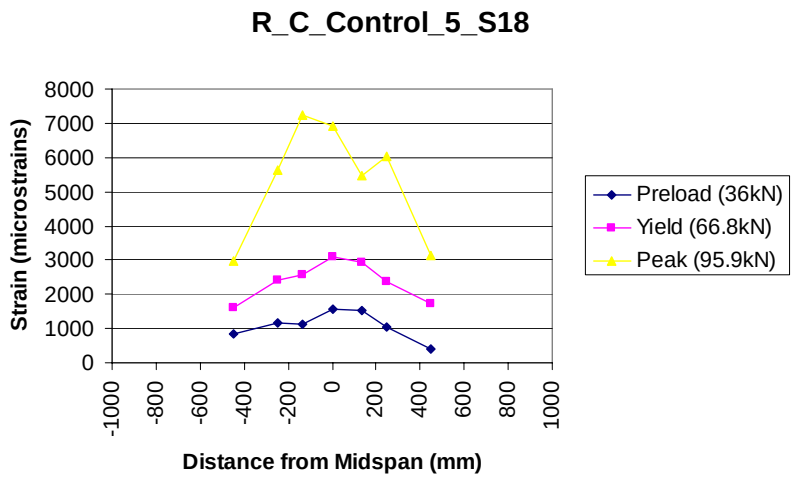
R_C_Control_5_S18
Strain (microstrains)
8000
7000
6000
5000
4000
3000
2000
1000
0
-1000
-800
-600
-400
-200
0
200
400
600
800
1000
Distance from Midspan (mm)
Preload (36kN)
Yield (66.8kN)
Peak (95.9kN)

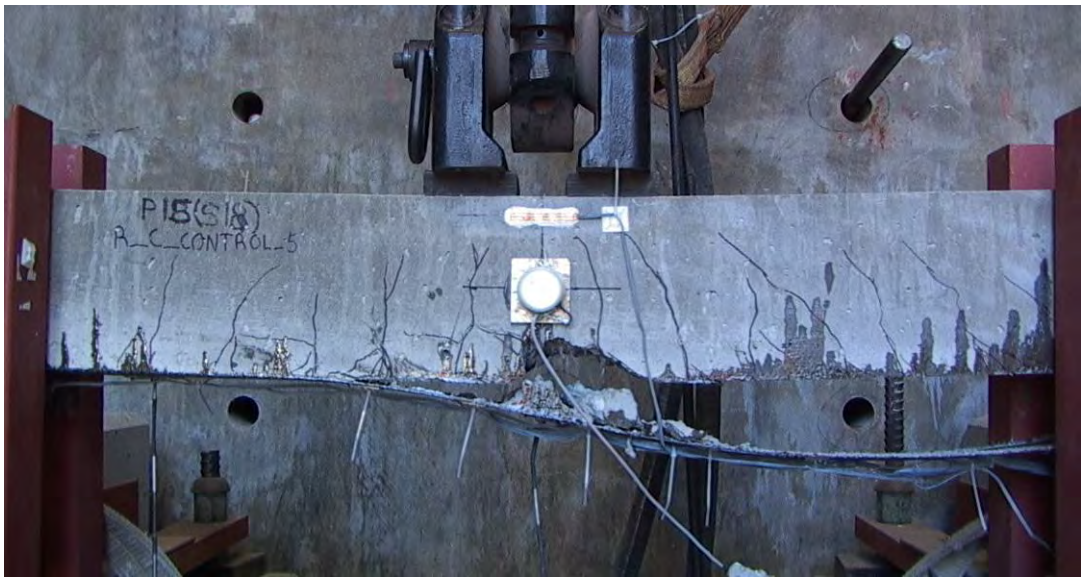

Specimen 24: 100mm diameter circular disbond inserted in the adhesive interface 428mm from the midspan tested 7/12/2005 (100C_428_S24)

Specimen 24 contained a circular disbond defect with a centroid located 428mm away from the midspan of the beam. The size of the disbond was 100mm in diameter. Debonding occurred to the left through the disbonded region initiating from a diagonal shear crack that can be seen in the picture below.

Behavior Characteristic	Value
Test Date	7/12/05
Rehab Date (number)	7/1/05 (4)
Concrete Cast Date (number)	10/19/04 (1)
Time from Rehab to Test	11 days
Maximum Load Held	90.72 kN
Displacement at Maximum Load	16.62 mm
Measured Steel Yield	2414 με
Load at Steel Yield	72.65 kN
Displacement at Steel Yield	8.19 mm
FRP Strain at Steel Yield	3244 με
FRP Strain at Debonding (Location)	5845 (F7) με
FRP Midspan Strain at Debonding	bad data
Debonding Direction	Left
Failure Mode	Deep Concrete, Steel

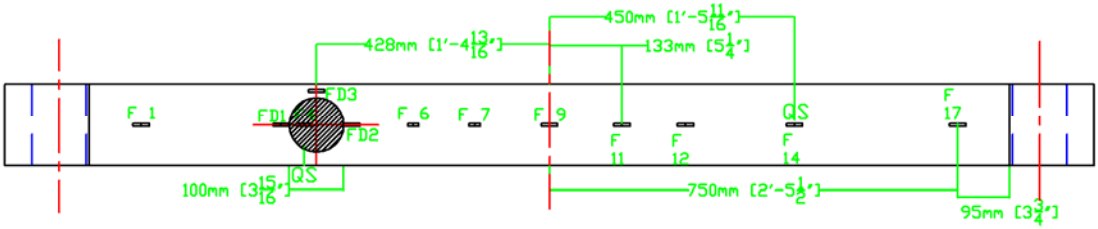

Load (kN)	Crack Width (mm)	Notes
0.00	<0.1	
36.00	<0.1	Typical crack reopening except one new crack at the dial edge of the defect.
2.40	<0.1	
75.30	0.2	Extensive cracking near the midspan. A large diagonal crack has opened up from near the medial edge of the defect. Strains on the side of the defect are significantly larger than on the defect free side.
2.40	<0.1	
90.00	0.8	A large local debond occurred while holding the load at 90kN. Debond is about 150mm in length and spans from the medial edge of the defect to a large diagonal crack (0.8mm width). Also, some small local debonding on the right side of the beam.
2.60	0.7	
91.10		Final failure was debonding from the defect (previous local debond) outward to the FRP end. Final debond was quite gradual. Debonding could be easily observed over several seconds until it propagated to near the ends.

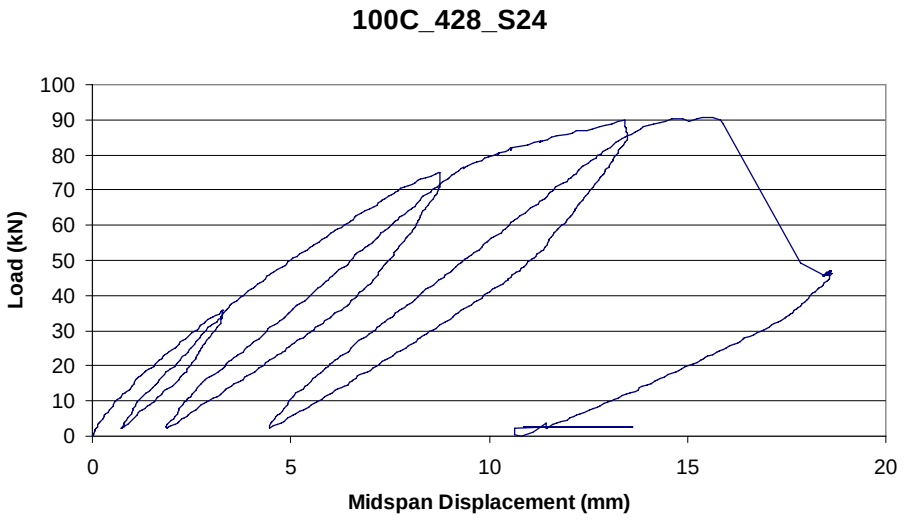
100C_428_S24
Load (kN)
Midspan Displacement (mm)
0
10
20
30
40
50
60
70
80
90
100
0
5
10
15
20

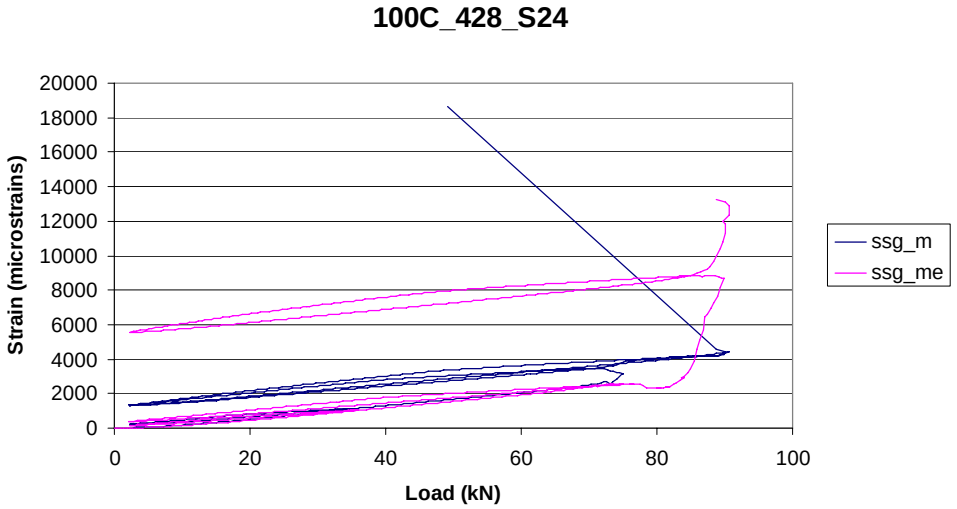
100C_428_S24
Strain (microstrains)
Load (kN)
0
2000
4000
6000
8000
10000
12000
14000
16000
18000
20000
0
20
40
60
80
100
ssg_m
ssg_me

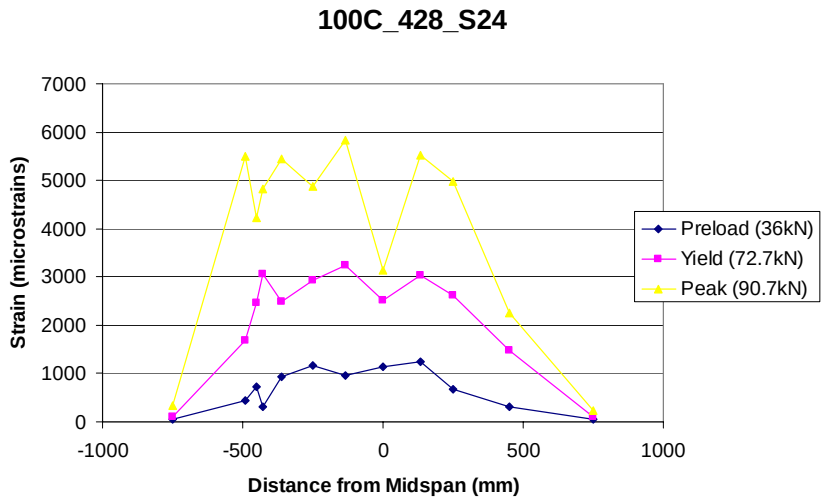
100C_428_S24
Strain (microstrains)
Distance from Midspan (mm)
0
1000
2000
3000
4000
5000
6000
7000
-1000
-500
0
500
1000
Preload (36kN)
Yield (72.7kN)
Peak (90.7kN)

Specimen 20: 100mm diameter circular disbond inserted in the adhesive interface 185mm from the end of the FRP tested 7/12/2005 (100C_185E_S20)

Specimen 20 contained a circular disbond defect with a centroid located 660mm away from the midspan of the beam. The size of the disbond was 100mm in diameter. This defect location is only 185mm from the end of the FRP section (as denoted by the second term in the specimen name: “185E”). Debonding occurred to the right propagating away from the defect initiating about 75mm from the outside of the right loading pad at the location of a diagonal shear crack.

Beam Characteristic	Value
Test Date	7/12/05
Rehab Date (number)	7/1/05 (4)
Concrete Cast Date (number)	10/19/04 (2)
Time from Rehab to Test	11 days
Maximum Load Held	89.90 kN
Displacement at Maximum Load	14.05 mm
Measured Steel Yield	2389 με
Load at Steel Yield	73.03 kN
Displacement at Steel Yield	8.55 mm
FRP Strain at Steel Yield	4292 με
FRP Strain at Debonding (location)	6871 (F9) με
FRP Midspan Strain at Debonding	6871 με
Debonding Direction	Right
Failure Mode	Thick Concrete Bondline

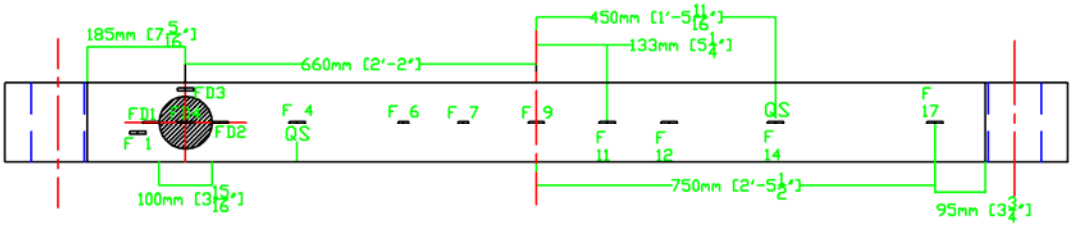

Load (kN)	Crack Width (mm)	Notes
0.00	<0.1	
36.20	<0.1	Typical crack reopening
2.40	<0.1	
75.10	0.2	Typical cracking.
2.40	<0.1	
90.00	0.4	A large diagonal crack has opened about 75mm outside the lateral edge of the right loading pad.
2.60	<0.1	
		Final debonding was <90kN and occurred away from the defect. No debonding was observed near the defect location.

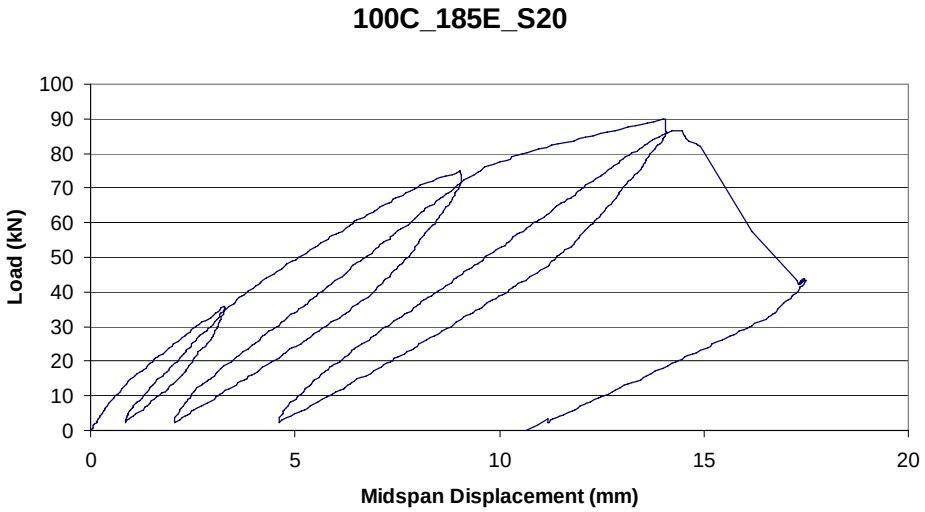
100C_185E_S20
Load (kN)
Midspan Displacement (mm)
0
10
20
30
40
50
60
70
80
90
100
0
5
10
15
20

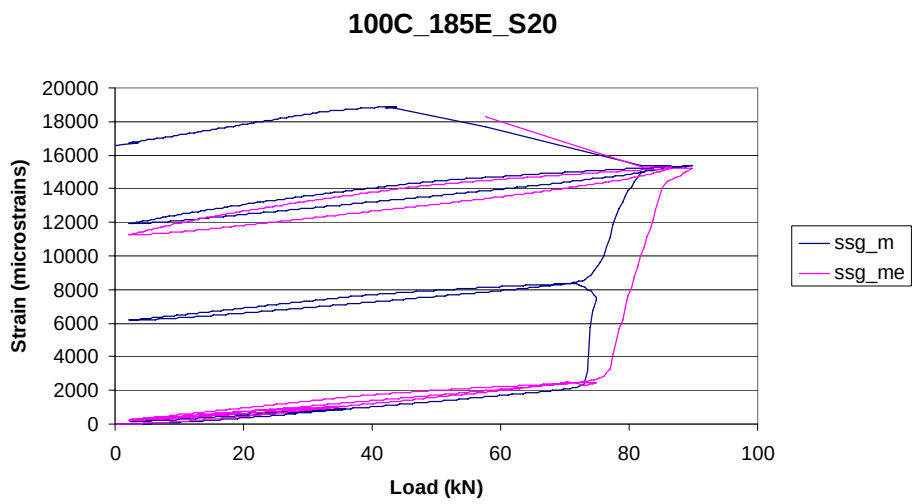
100C_185E_S20
Strain (microstrains)
Load (kN)
ssg_m
ssg_me
0
2000
4000
6000
8000
10000
12000
14000
16000
18000
20000
0
20
40
60
80
100

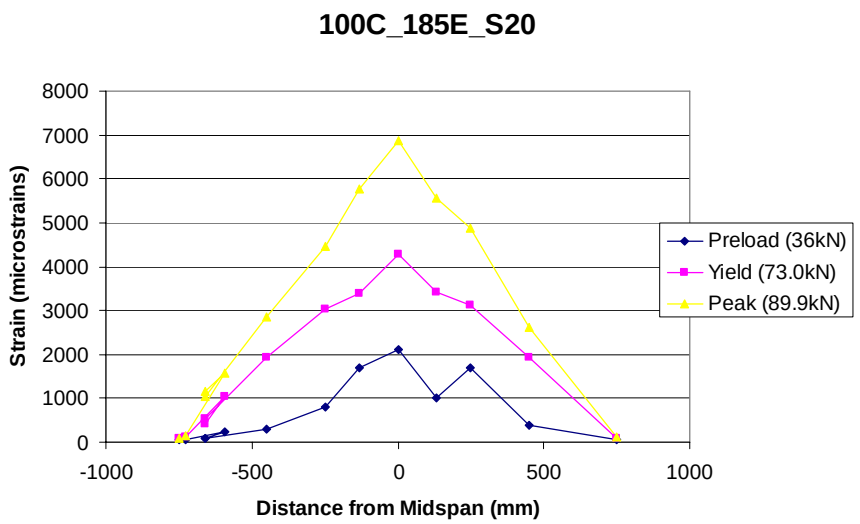
100C_185E_S20
Strain (microstrains)
Distance from Midspan (mm)
Preload (36kN)
Yield (73.0kN)
Peak (89.9kN)
0
1000
2000
3000
4000
5000
6000
7000
8000
-1000
-500
0
500
1000

Specimen 11: 150mm x 150mm rectangular disbond inserted in the adhesive interface located 185mm from the midspan, tested 7/13/2005 (150R_185_S11_2)

Specimen 11 contained a rectangular disbond with a centroid located 185mm away from the midspan of the beam (see drawing). The dimensions of the manufactured disbond were 150mm length by 150mm width (the full width of the beam). This was the second beam tested in with this defect configuration (as denoted by the term ‘2’ at the end of the specimen name). The beam was, precracked using the typical 35.6 kN preload level before the application of FRP. Final debonding occurred from the defect location with some debonding occurring through the resin. Stress concentrations due to the disbond are very apparent in the strain profile.

Beam Characteristic	Value
Test Date	7/13/05
Rehab Date (number)	7/1/05 (4)
Concrete Cast Date (number)	10/19/04 (1)
Time from Rehab to Test	12 days
Maximum Load Held	88.78 kN
Displacement at Maximum Load	14.91 mm
Measured Steel Yield	2377 με
Load at Steel Yield	72.15 kN
Displacement at Steel Yield	8.92 mm
FRP Strain at Steel Yield	4335 με
FRP Strain at Debonding (Location)	8354 (FD1) με
FRP Midspan Strain at Debonding	6049 με
Debonding Direction	Left
Failure Mode	Thick Concrete Bondline

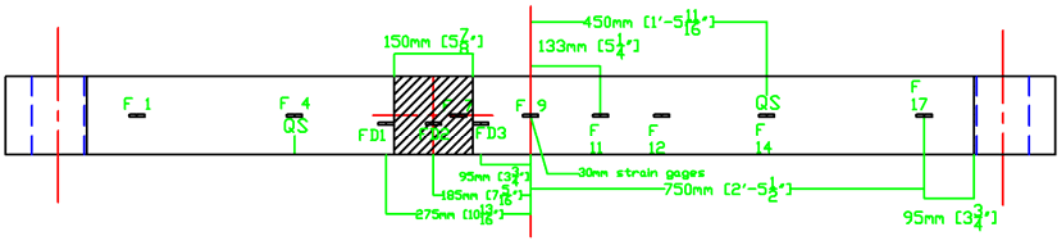

Load (kN)	Crack Width (mm)	Notes
0.00	<0.1	
36.10	0.1	Typical crack reopening.
2.40	<0.1	
75.10	0.5	Very large flexural crack opened near the right edge of the disbond. Local debonding (~25mm) has initiated on the left side of the defect. Much smaller crack spacing in the right span than in the left span (defect in in the left span).
2.40	0.1	
89.00		Final debonding occurred from the defect location. Propagating to the end in the left direction. Much of the failure occurred in the resin instead of the concrete. Perhaps the primer layer was too thin.

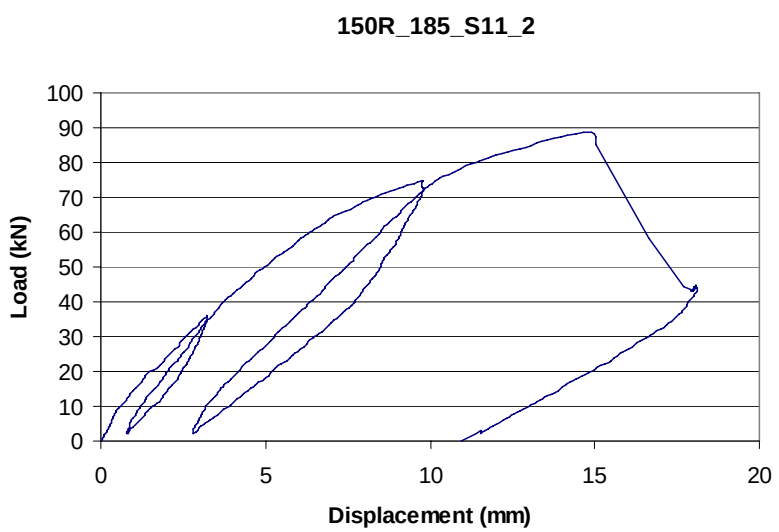

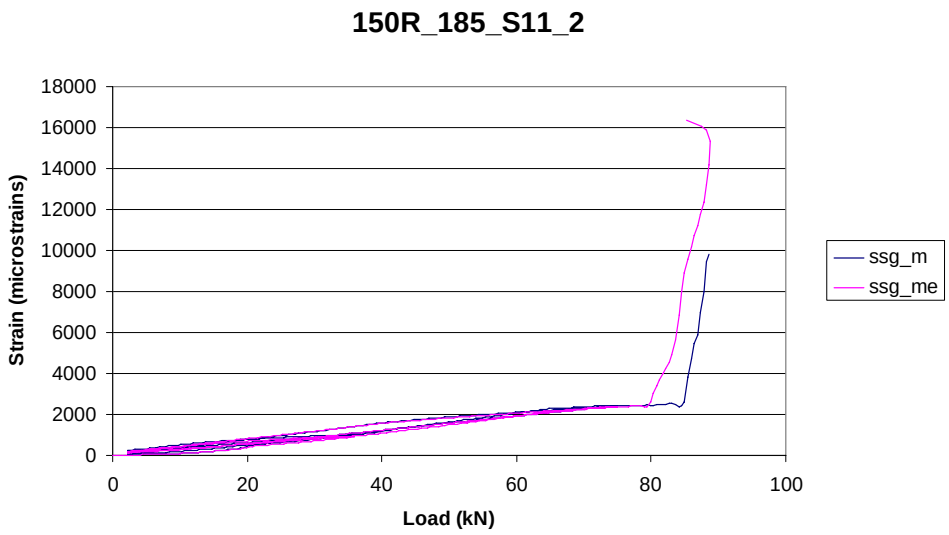
150R_185_S11_2
Strain (microstrains)
18000
16000
14000
12000
10000
8000
6000
4000
2000
0
0
20
40
60
80
100
Load (kN)
ssg_m
ssg_me

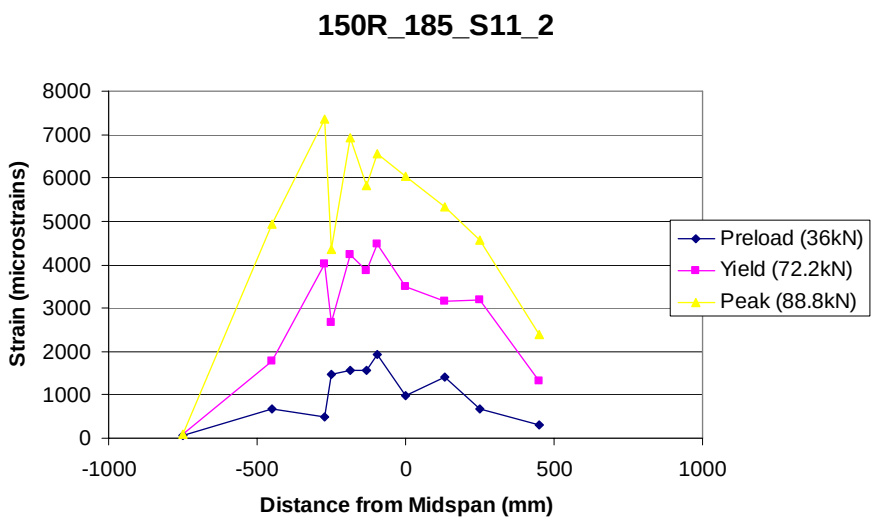
150R_185_S11_2
Strain (microstrains)
8000
7000
6000
5000
4000
3000
2000
1000
0
-1000
-500
0
500
1000
Distance from Midspan (mm)
Preload (36kN)
Yield (72.2kN)
Peak (88.8kN)

P8(SH)
150R_185_S11_2

Specimen 5: 100mm diameter circular disbond inserted in the adhesive interface 185mm from the midspan tested 7/13/2005 (100C_185_S5_3)

Specimen 5 contained a circular disbond defect with a centroid located 185mm away from the midspan of the beam. The size of the disbond was 100mm in diameter. This is the third beam tested with this defect configuration (denoted by the '3' in the last term in the specimen name). As often seen, failure occurred on the same side of the specimen as the disbond (the left side), debonding from near the midspan of the beam. Final debonding occurred at a low load relative to the control specimens of 85.6kN despite have a debonding failure mode of "deep concrete, steel", which is typically the strongest failure mode.

Beam Characteristic	Value
Test Date	7/13/05
Rehab Date (number)	7/1/05 (4)
Concrete Cast Date (number)	10/19/04 (2)
Time from Rehab to Test	12 days
Maximum Load Held	85.63 kN
Displacement at Maximum Load	14.19 mm
Measured Steel Yield	2344 με
Load at Steel Yield	66.40 kN
Displacement at Steel Yield	4.99 mm
FRP Strain at Steel Yield	3435 με
FRP Strain at Debonding (Location)	6069 (F7) με
FRP Midspan Strain at Debonding	5365 με
Debonding Direction	Left
Failure Mode	Deep Concrete, Steel

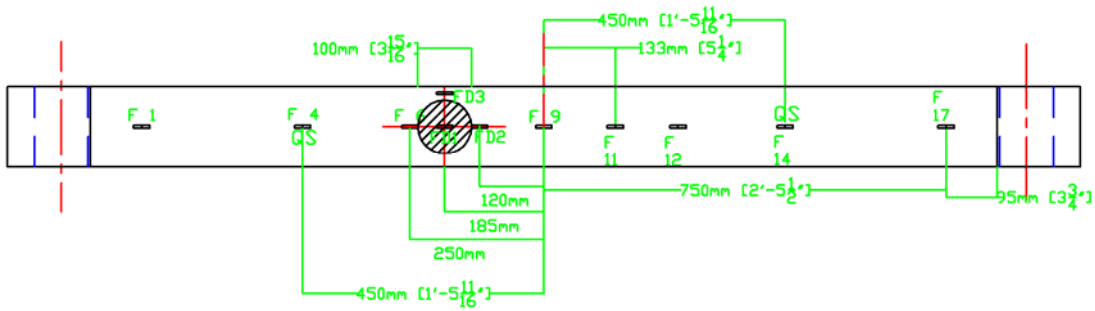

Load (kN)	Crack Width (mm)	Notes
0.00	<0.1	
36.10	<0.1	Typical crack reopening
2.40	<0.1	
75.30	0.3	Cracking heard at about 70kN. The largest crack is at the midspan.
2.50	<0.1	
85.80		Final debonding on the same side as the defect (the left side).

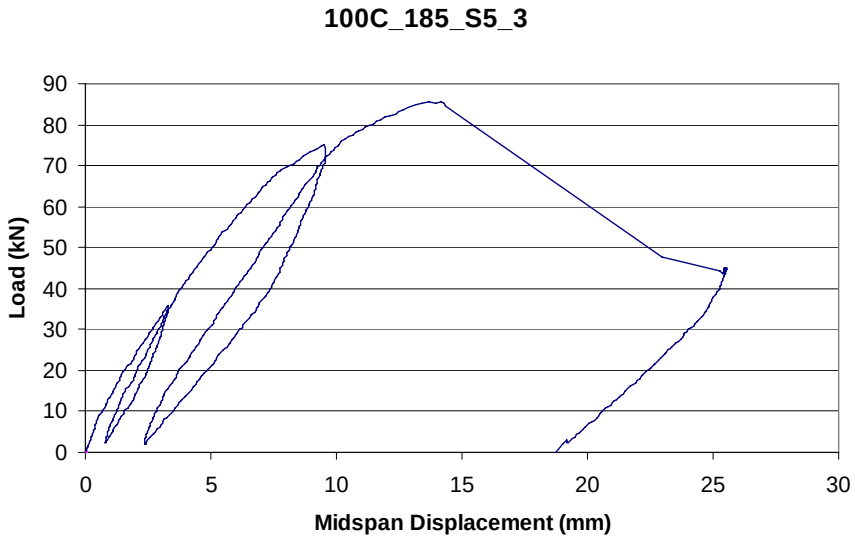
100C_185_S5_3
Load (kN)
Midspan Displacement (mm)
0
10
20
30
40
50
60
70
80
90
0
5
10
15
20
25
30

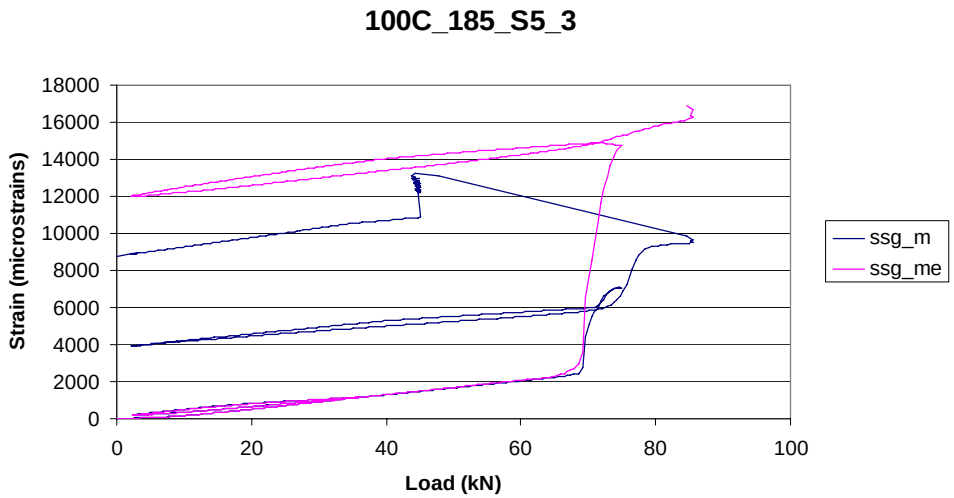
100C_185_S5_3
Strain (microstrains)
Load (kN)
0
2000
4000
6000
8000
10000
12000
14000
16000
18000
0
20
40
60
80
100
ssg_m
ssg_me

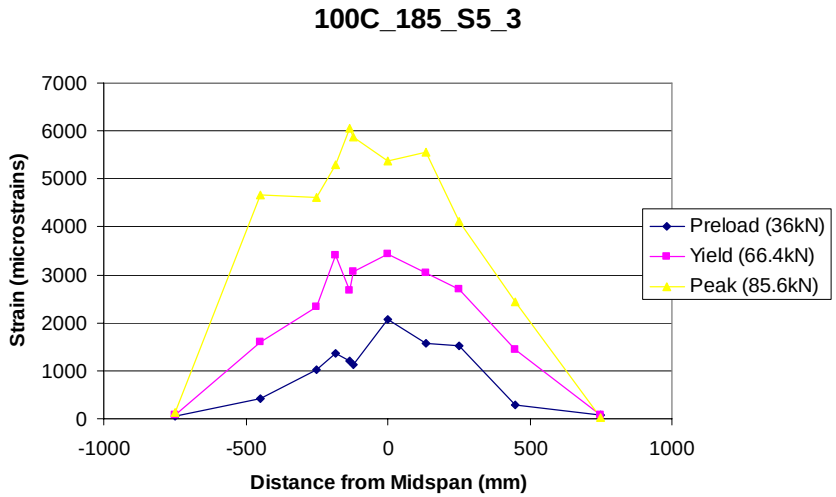
100C_185_S5_3
Strain (microstrains)
Distance from Midspan (mm)
0
1000
2000
3000
4000
5000
6000
7000
-1000
-500
0
500
1000
Preload (36kN)
Yield (66.4kN)
Peak (85.6kN)

Specimen 23: 100mm diameter circular disbond inserted in the adhesive interface located at the midspan tested 7/14/2005 (100C_0_S23)

Specimen 23 contained a circular disbond defect with a centroidal location at the midspan of the beam. The size of the disbond was 100mm in diameter. Debonding occurred to the right propagating from the defect location at the midspan. Relatively low failure load of 86.7kN.

Beam Characteristic	Value
Test Date	7/14/05
Rehab Date (number)	7/1/05 (4)
Concrete Cast Date (number)	10/19/04 (1)
Time from Rehab to Test	13 days
Maximum Load Held	86.74 kN
Displacement at Maximum Load	13.36 mm
Measured Steel Yield	2458 με
Load at Steel Yield	67.16 kN
Displacement at Steel Yield	7.48 mm
FRP Strain at Steel Yield	3566 με
FRP Strain at Debonding (Location)	5978 (F9) με
FRP Midspan Strain at Debonding	5978 με
Debonding Direction	Right
Failure Mode	Thick Concrete Bondline

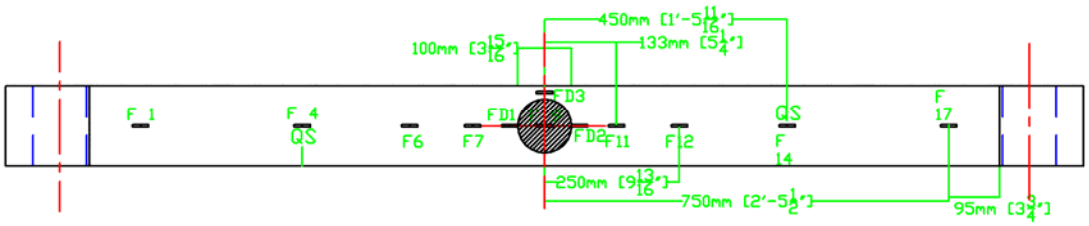

Load (kN)	Crack Width (mm)	Notes
0.00	<0.1	
36.10	<0.1	Small crack reopening.
2.50	<0.1	
75.30	0.2	Debonding through the width of the section at the defect location (the midspan), essentially making it a rectangular section. Many small cracks.
2.40	<0.1	
87.20		Weak specimen. Debonding occurred from the defect to the right side.

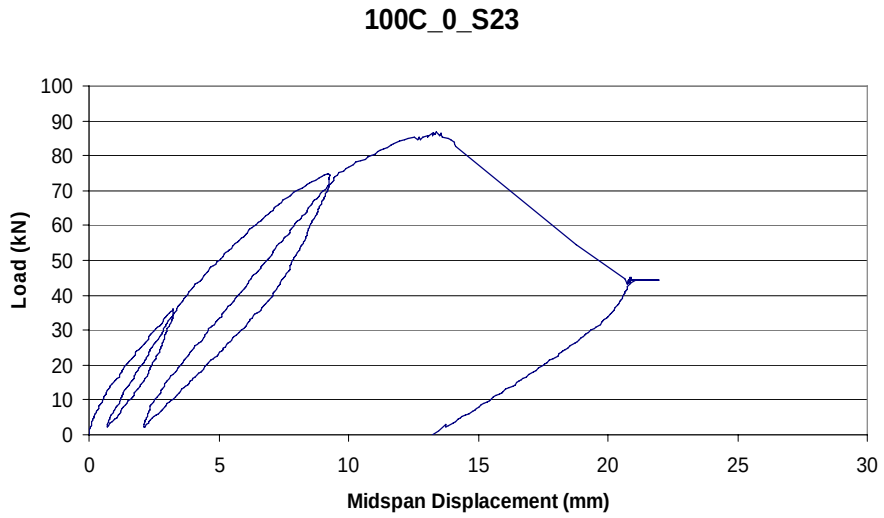
100C_0_S23
Load (kN)
Midspan Displacement (mm)
0
10
20
30
40
50
60
70
80
90
100
0
5
10
15
20
25
30

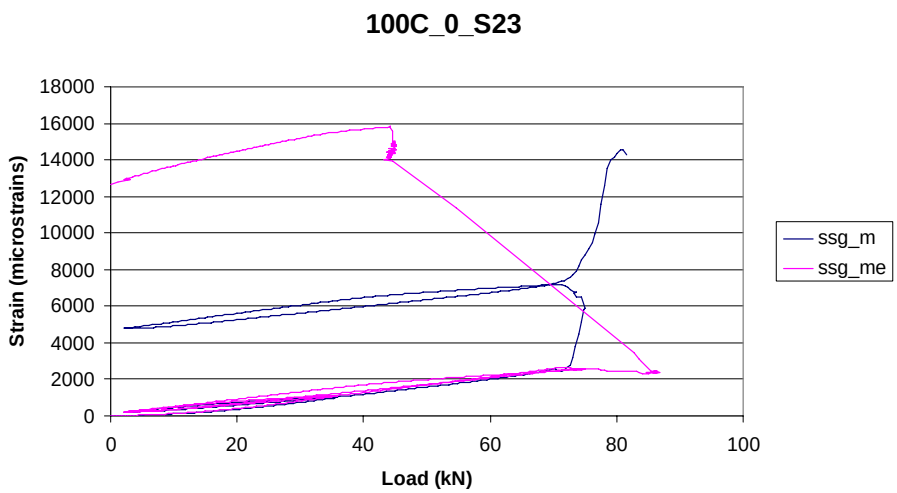
100C_0_S23
Strain (microstrains)
Load (kN)
0
2000
4000
6000
8000
10000
12000
14000
16000
18000
0
20
40
60
80
100
ssg_m
ssg_me

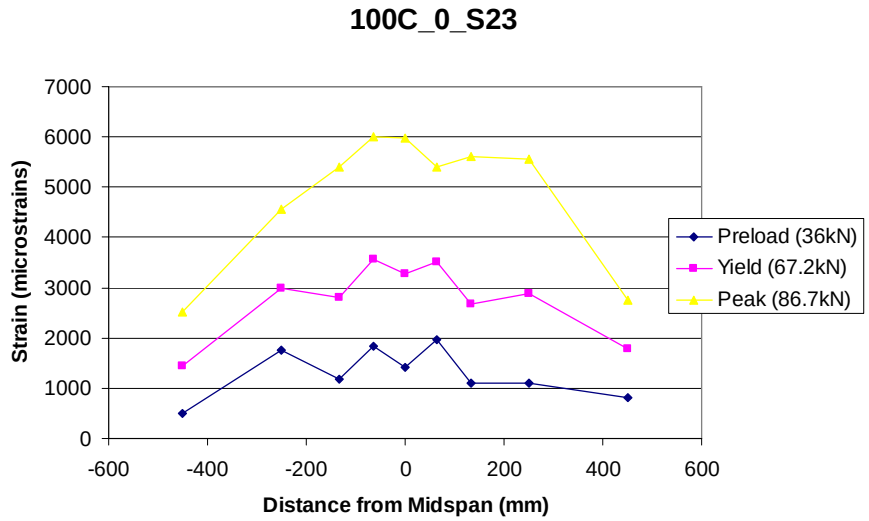
100C_0_S23
Strain (microstrains)
Distance from Midspan (mm)
0
1000
2000
3000
4000
5000
6000
7000
-600
-400
-200
0
200
400
600
Preload (36kN)
Yield (67.2kN)
Peak (86.7kN)

Specimen 22: 150mm diameter circular disbond inserted in the adhesive interface 185mm from the midspan tested 7/14/2005 (150C_185_S22_2)

Specimen 22 contained a defect with a circular disbond with a centroid located 185mm away from the midspan of the beam (see drawing). The size of the disbond was 150mm in diameter. This is the largest size of circular shaped disbond that could be tested in this investigation because the defect diameter is equal to the full width of the beam. Specimen 22 is the second specimen tested with this defect configuration. The peak load held by this specimen was modest at 89.8kN and corresponding midspan displacement of 15.5mm was much less than the control specimens. Which is not surprising since the failure mode is debonding through a “thick concrete bondline”. Final debonding occurred from the defect location propagating to the left end of the beam.

Beam Characteristic	Value
Test Date	7/14/05
Rehab Date (number)	7/1/05 (4)
Concrete Cast Date (number)	10/19/04 (1)
Time from Rehab to Test	13 days
Maximum Load Held	89.78 kN
Displacement at Maximum Load	15.47 mm
Measured Steel Yield	2351 με
Load at Steel Yield	68.40 kN
Displacement at Steel Yield	7.48 mm
FRP Strain at Steel Yield	3964 με
FRP Strain at Debonding (Location)	6624 (F9) με
FRP Midspan Strain at Debonding	6624 με
Debonding Direction	Left
Failure Mode	Thick Concrete Bondline

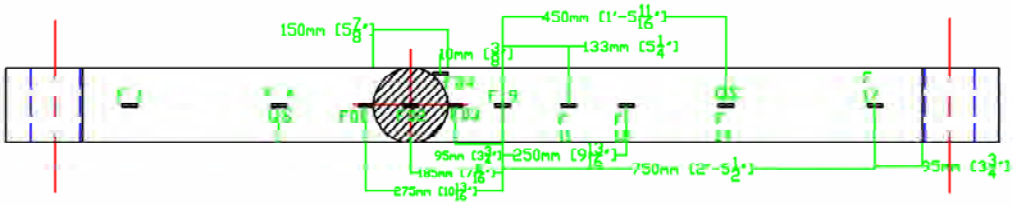

Load (kN)	Crack Width (mm)	Notes
0.00	<0.1	
36.20	0.1	Typical crack reopening.
2.50	<0.1	
75.00	0.4	Debonding at the edges of the disbond causing it to become essentially a rectangular unbonded region. Debonding is several inches long at each corner. It appears to have been initiated by a large diagonal crack near the defect edge.
2.30		
90.00		Final debonding occurred almost immediately after 90kN load level was reached. Debonding occurred on the left side (side with the defect) of the structure, initiating at the defect location.

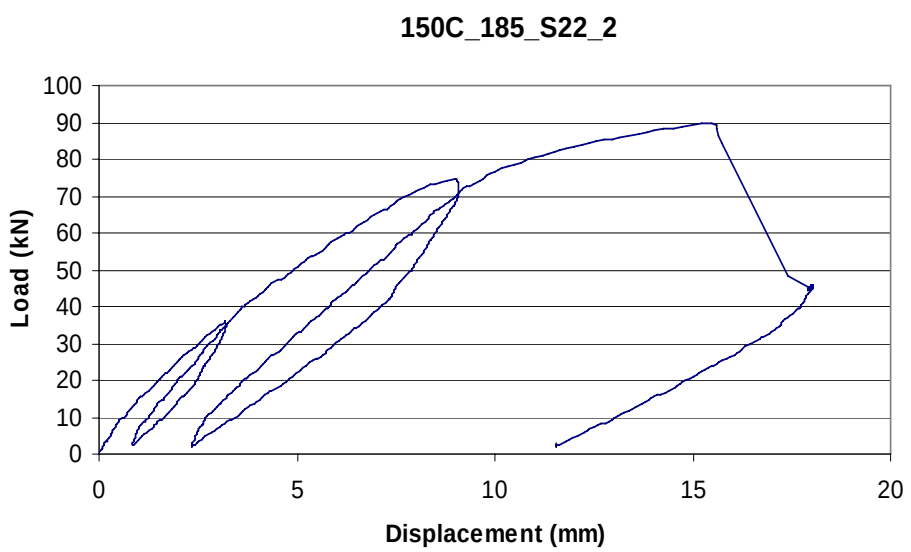

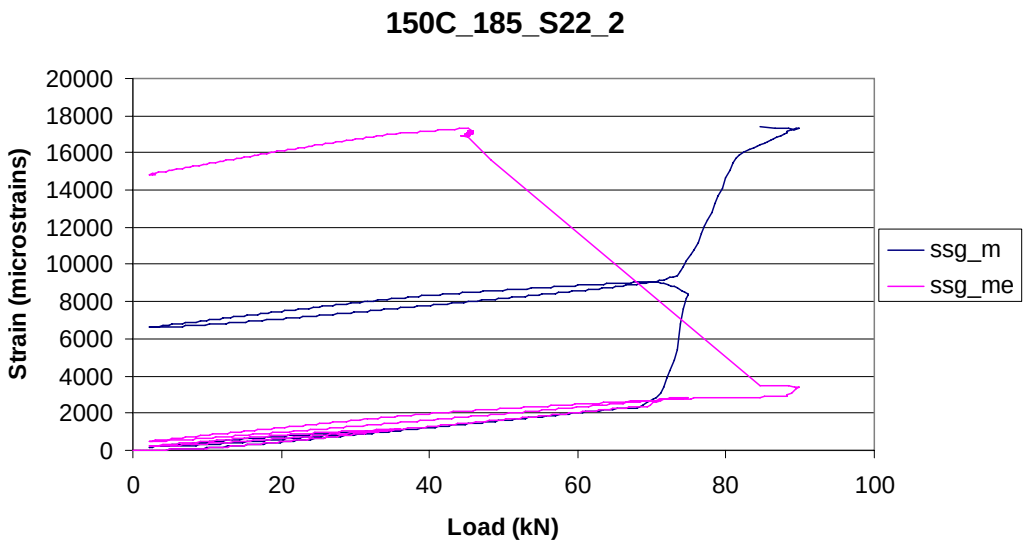
150C_185_S22_2
Strain (microstrains)
20000
18000
16000
14000
12000
10000
8000
6000
4000
2000
0
0
20
40
60
80
100
Load (kN)
ssg_m
ssg_me

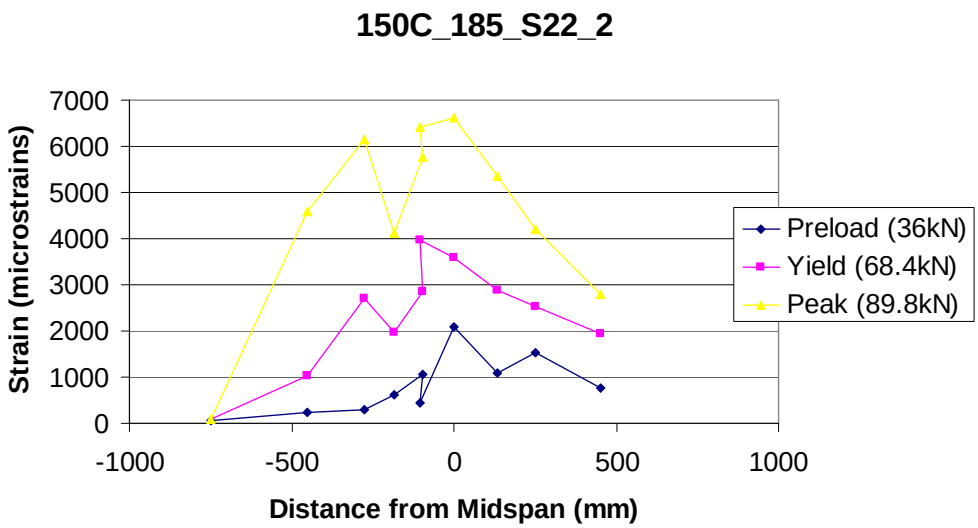
150C_185_S22_2
Strain (microstrains)
7000
6000
5000
4000
3000
2000
1000
0
-1000
-500
0
500
1000
Distance from Midspan (mm)
Preload (36kN)
Yield (68.4kN)
Peak (89.8kN)

150C_185_S22_2

Specimen 30: Unstrengthened control specimen tested 7/28/2005 (Control_4_S30)

Specimen 4 was an unstrengthened control specimen loaded to failure with pauses during loading to observe and measure crack patterns. This specimen was the only unstrengthened control of concrete cast number two. Only one was found to be necessary since the behavior was very similar to the unstrengthened specimens tested from cast number one. The specimen held near peak load at displacements far past steel yield due to the ductile nature of the beam design. The peak load was 54.60 kN at a deflection of 22.0mm. From the plot of the midspan steel strain versus load, the initial yielding strain of the midspan steel is determined to occur at 2448 microstrains by averaging the measured strains determined by the two midspan steel strain gages at the point of the initial change in slope.

Load (kN)	Crack Width	Notes
0.00	0.00	
36.20	0.22	Typical cracking. Widest cracking is at the midspan. Midspan steel strain is 2090 microstrains.

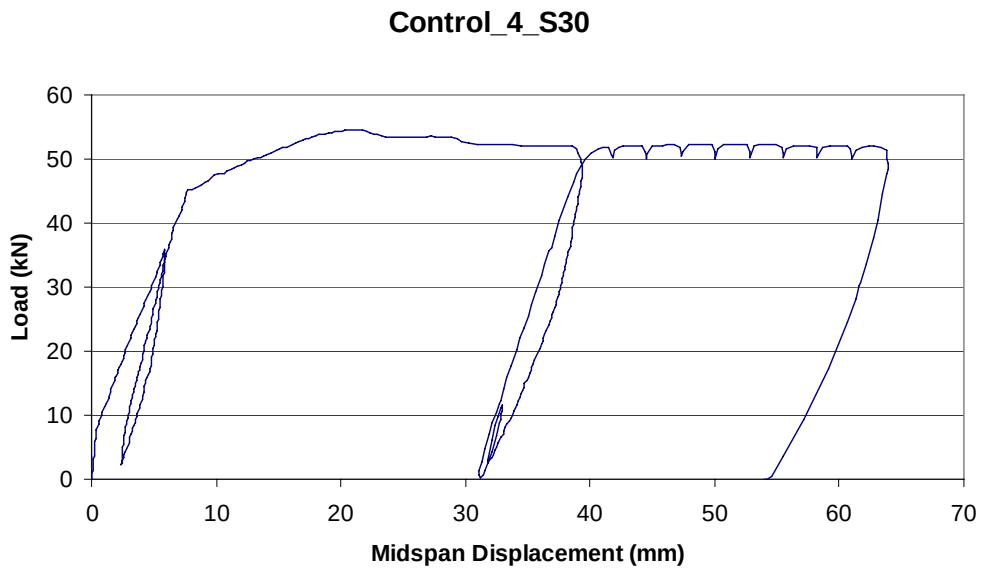
Control_4_S30
Load (kN)
Midspan Displacement (mm)
0
10
20
30
40
50
60
70

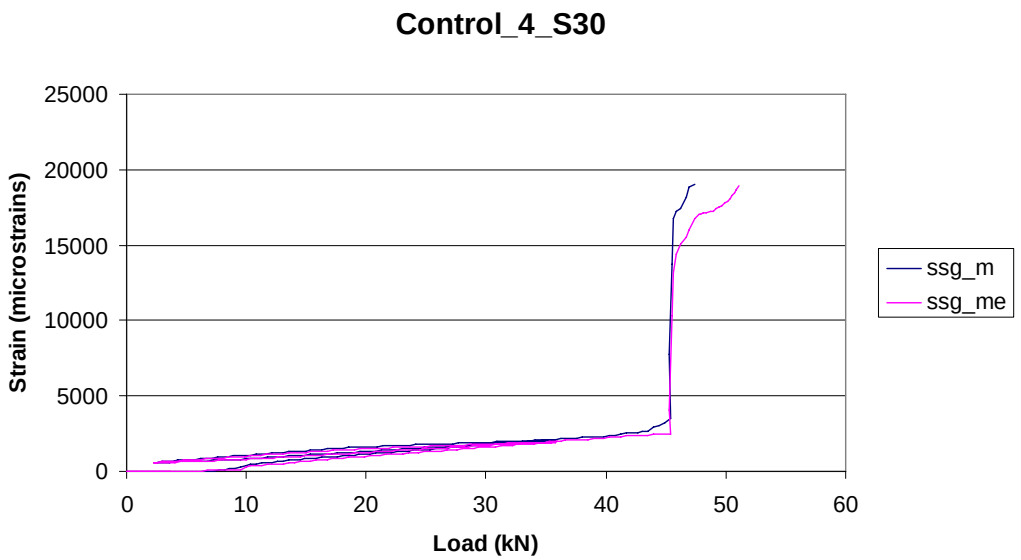
Control_4_S30
Strain (microstrains)
Load (kN)
ssg_m
ssg_me
0
5000
10000
15000
20000
25000
10
20
30
40
50
60

Specimen 31: 100mm x 150mm rectangular disbond inserted in the adhesive interface 185mm from the midspan tested 9/2/2005 (100R_185_S31)

Specimen 31 was manufactured with a defect consisting of a rectangular disbond with a centroid located 185mm away from the midspan of the beam. The dimensions of the manufactured disbond were 100mm length by 150mm width (the full width of the beam). This specimen was the third manufactured with this defect configuration. The beam was, precracked using the 35.6 kN preload level before the application of FRP. Final debonding occurred from the location of a diagonal shear crack located under the left load point near the disbond. The failure load was very low due to debonding occurring through the adhesive resin interface.

Beam Characteristic	Value
Test Date	9/2/05
Rehab Date (number)	8/19/05 (5)
Concrete Cast Date (number)	2/8/05 (2)
Time from Rehab to Test	14 days
Maximum Load Held	80.28 kN
Displacement at Maximum Load	12.00 mm
Measured Steel Yield	2353 με
Load at Steel Yield	65.99 kN
Displacement at Steel Yield	7.55 mm
FRP Strain at Steel Yield	3589 με
FRP Strain at Debonding (Location)	6658 (FD2) με
FRP Midspan Strain at Debonding	5293 με
Debonding Direction	Left
Failure Mode	Resin Interface

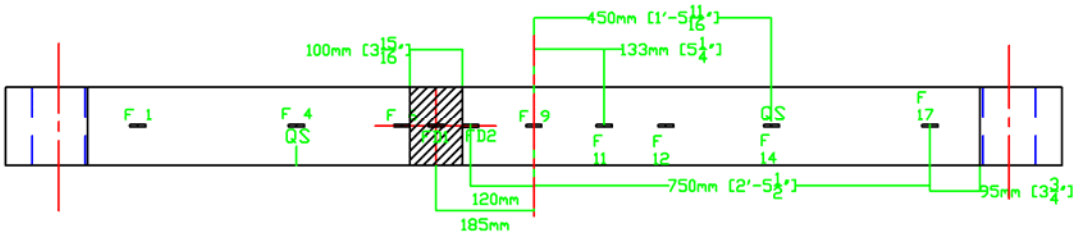

Load (kN)	Crack Width (mm)	Notes
0.00	<0.1	
36.10	0.1	Specimen was loaded monotonically. Final debonding was relatively non-violent propagating from the defect to the left through a thin concrete layer.
0.00	<0.1	
75.20	0.4	Largest crack is just to the right (~25mm) of the defect. Local Debonding has occurred about 50mm to the left of the defect and 30mm to the right (began at 72kN).
0.00	<0.1	
80.30		Very low failure load. Much of the failure was in the adhesive layer.

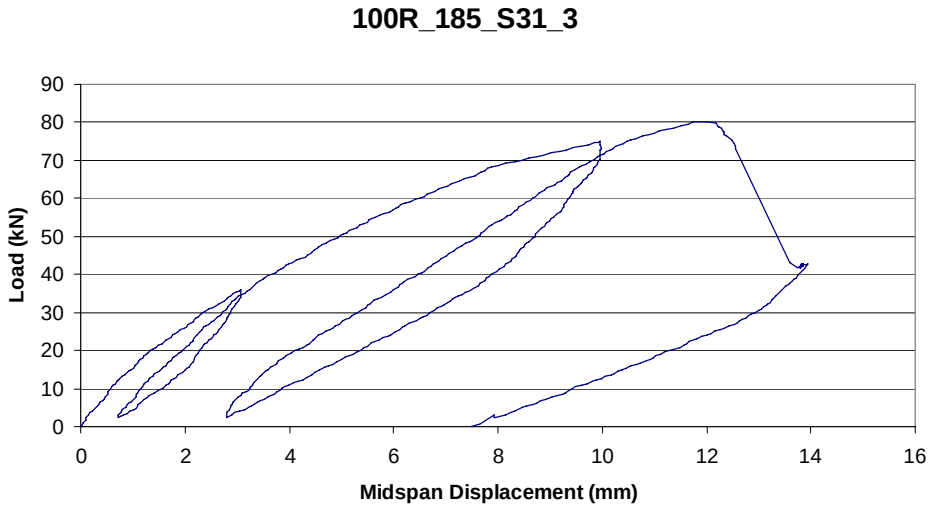
100R_185_S31_3
Load (kN)
Midspan Displacement (mm)
0
10
20
30
40
50
60
70
80
90
0
2
4
6
8
10
12
14
16

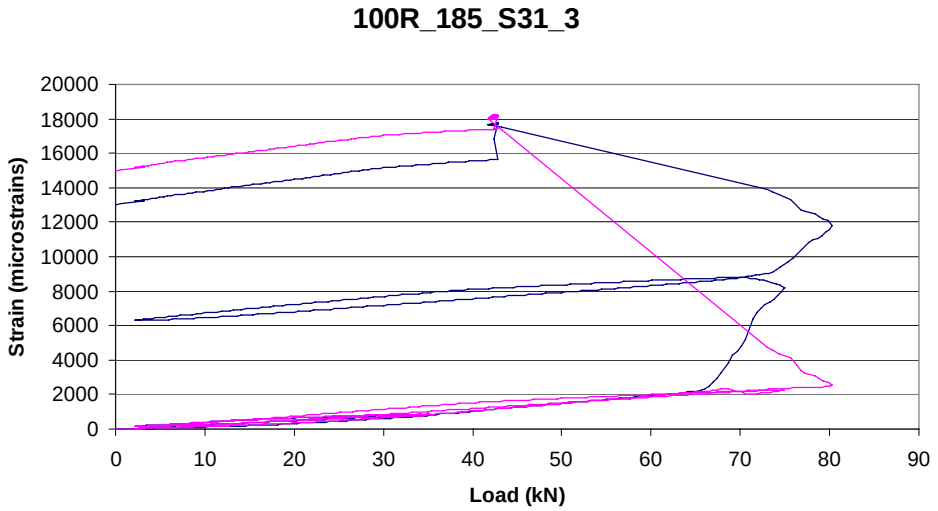
100R_185_S31_3
Strain (microstrains)
Load (kN)
0
2000
4000
6000
8000
10000
12000
14000
16000
18000
20000
0
10
20
30
40
50
60
70
80
90

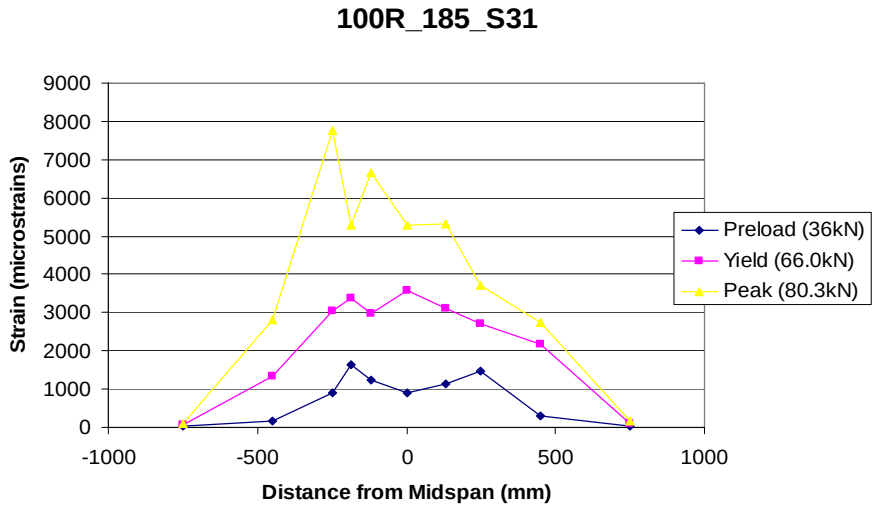
100R_185_S31
Strain (microstrains)
Distance from Midspan (mm)
0
1000
2000
3000
4000
5000
6000
7000
8000
9000
-1000
-500
0
500
1000
Preload (36kN)
Yield (66.0kN)
Peak (80.3kN)

Specimen 36: Strengthened, preloaded control specimen tested 9/13/2005 (R_C_Control_6_S36)

Specimen 36 was a control specimen with standard preloading as discussed in section 2.8, but without any purposely inserted defects. It is the control specimen that was created in conjunction with the defective beams for rehabilitation set five. The peak load held by this specimen was very low relative to the other control specimens at 80.28kN and corresponding midspan displacement of 12.8mm. Local debonding initiated during the 75kN load cycle at the location of a diagonal shear crack to the left of the midspan as can be seen in the photo. Final debonding occurred from this point and propagated to the left end of the FRP. left of the midspan, propagating to the right end of the FRP through the midspan. The debonding mechanism observed was failure through the resin interface, which is probably the main contributing factor for failure occurring at such low ultimate conditions. Yielding at the midspan of the longitudinal steel occurred at 67.2 kN in the beam at a steel strain of 2453 microstrains.

Beam Characteristic	Value
Test Date	9/13/05
Rehab Date (number)	8/19/05 (5)
Concrete Cast Date (number)	2/8/05 (2)
Time from Rehab to Test	25 days
Maximum Load Held	80.28 kN
Displacement at Maximum Load	12.77 mm
Measured Steel Yield	2453 με
Load at Steel Yield	67.2 kN
Displacement at Steel Yield	7.83 mm
FRP Strain at Steel Yield	3589 με
FRP Strain at Debonding (Location)	5644 (F6) με
FRP Midspan Strain at Debonding	5307 με
Debonding Direction	Left
Failure Mode	Resin Interface

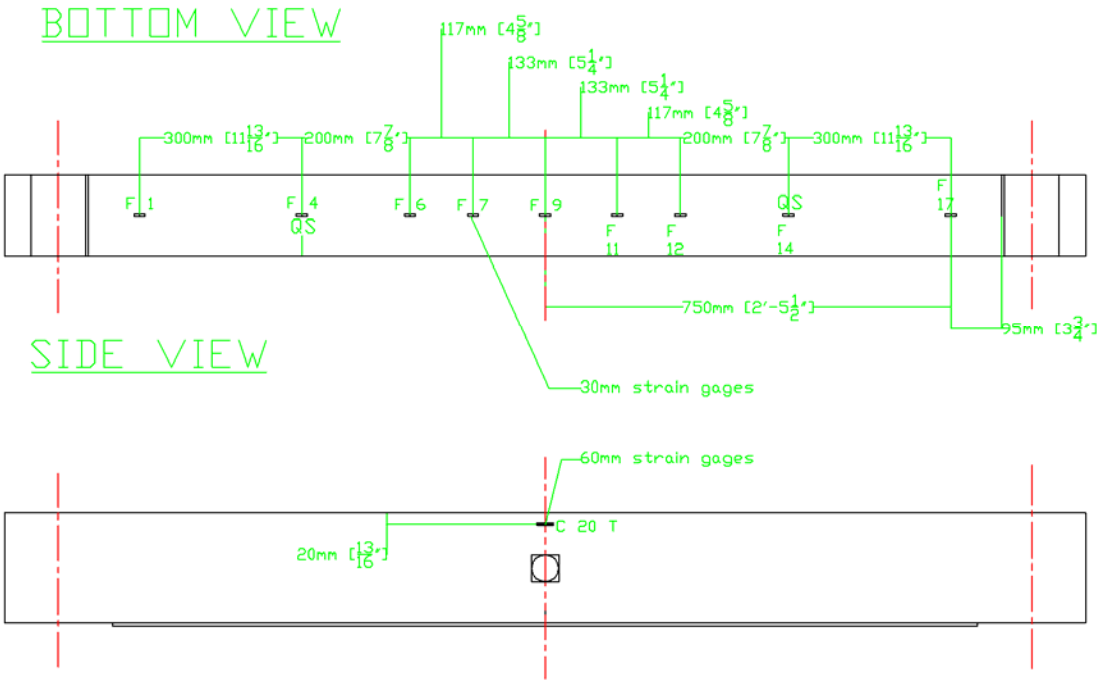

Load (kN)	Crack Width (mm)	Notes
0.00	<0.1	
36.50	< 0.1	Typical crack reopening
2.60	< 0.1	
75.00	0.3	A lot of noise heard during loading (cracking sound). A Large diagonal crack has occurred on the left side and local debonding has occurred at the diagonal crack propagating outward. Debonding is about 75mm long on the left side of the midspan and 25mm long on the on the right side.
2.00	0.1	
80.70		Debonding continued slowly until it was about 150mm in length, the macro debonding occurred on the left side of the midspan. Debonding occurred primarily through the adhesive.

R_C_Control_6

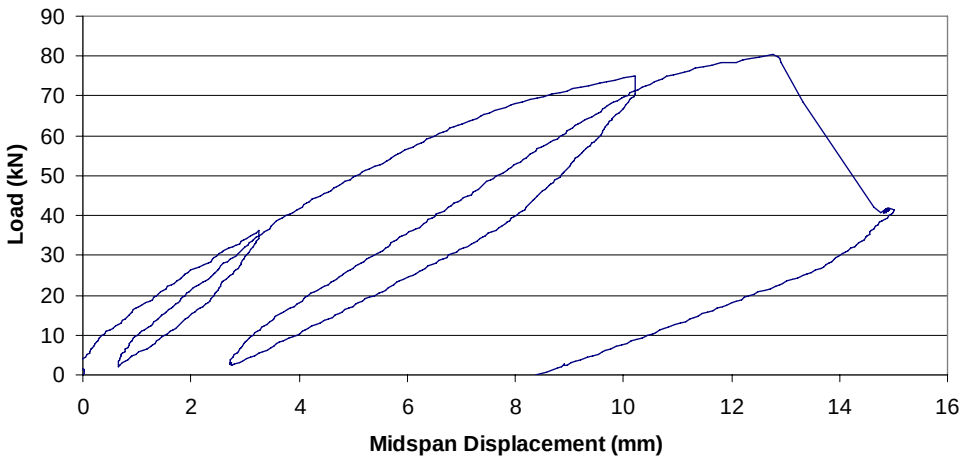

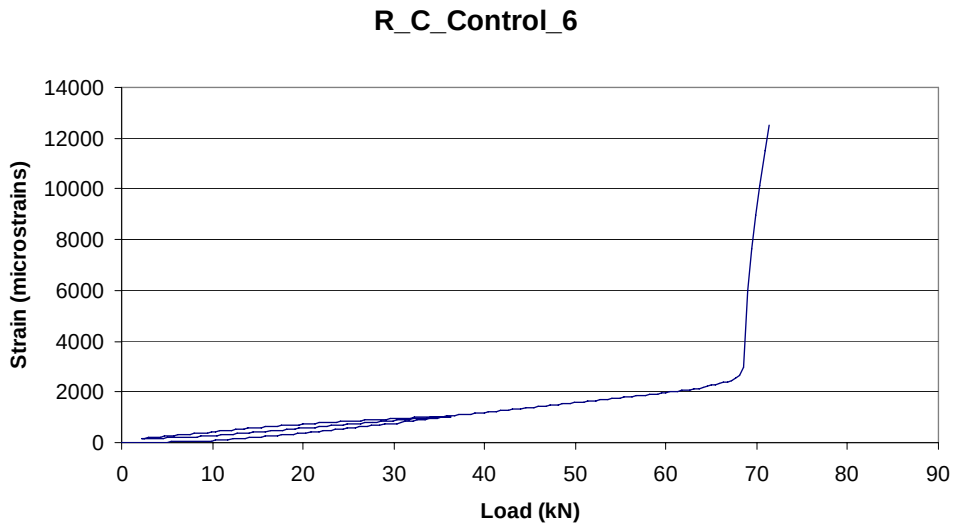
R_C_Control_6
Strain (microstrains)
14000
12000
10000
8000
6000
4000
2000
0
0
10
20
30
40
50
60
70
80
90
Load (kN)

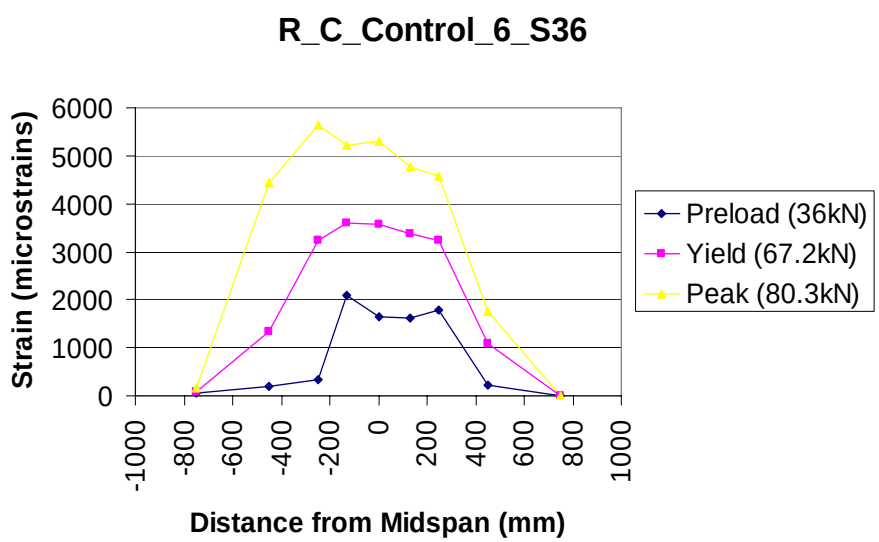
R_C_Control_6_S36
Strain (microstrains)
6000
5000
4000
3000
2000
1000
0
-1000
-800
-600
-400
-200
0
200
400
600
800
1000
Distance from Midspan (mm)
Preload (36kN)
Yield (67.2kN)
Peak (80.3kN)

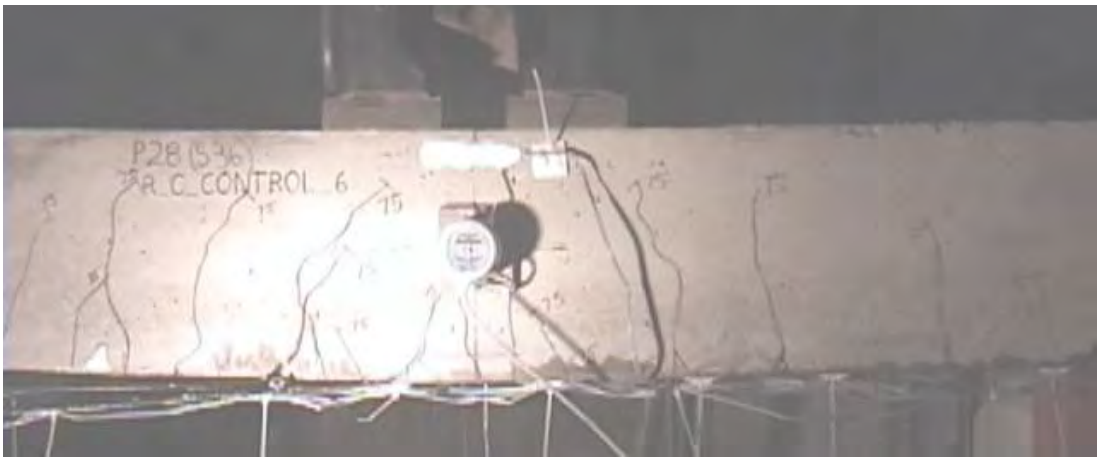
P28 (S36)
R_C_CONTROL_6

Specimen 35: 250mm x 150mm rectangular disbond inserted in the adhesive interface located 185mm from the midspan, tested 9/20/2005 (250R_185_S35)

Specimen 35 was manufactured with a defect consisting of a rectangular disbond with a centroid located 185mm away from the midspan of the beam. The dimensions of the manufactured disbond were 250mm length by 150mm width (the full width of the beam). This specimen is the largest sized disbond that was investigated in the laboratory. The beam was, precracked using the 35.6 kN preload level before the application of FRP. Final debonding occurred from the midspan where a large crack was observed. The initial debonding propagated about 100mm until it reached another crack at which point debonding halted and the specimen reloaded some before final debonding occurred. This was the first test in which a crack was definitely observed to stop debonding until additional load was added. About 20% of the debonding was observed to propagate through the adhesive layer and the remainder through a thin concrete bondline, effectively mixing two of the debonding failure modes defined in appendix A.

Beam Characteristic	Value
Test Date	9/20/05
Rehab Date (number)	8/19/05 (5)
Concrete Cast Date (number)	2/8/05 (2)
Time from Rehab to Test	32 days
Maximum Load Held	88.30 kN
Displacement at Maximum Load	13.47 mm
Measured Steel Yield	2232 με
Load at Steel Yield	57.60 kN
Displacement at Steel Yield	5.36 mm
FRP Strain at Steel Yield	4615 με
FRP Strain at Debonding (Location)	7233 (F11) με
FRP Midspan Strain at Debonding	5075 με
Debonding Direction	Left
Failure Mode	Thin Concrete Bondline

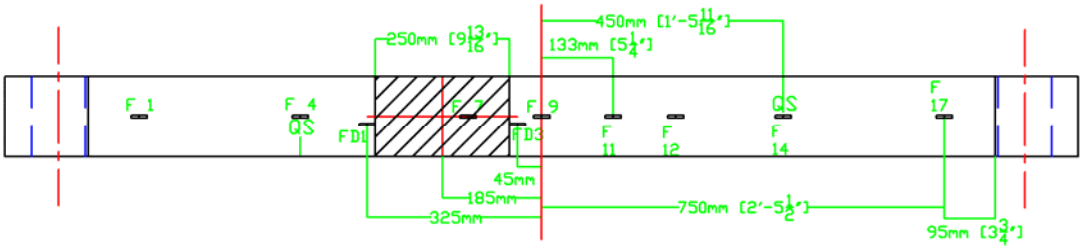

Load (kN)	Crack Width (mm)	Notes
0.00	<0.1	
36.50	<0.1	Typical crack reopening.
2.50	<0.1	
75.50	0.5	A massive crack has opened near the right edge of the defect. A large diagonal crack has opened near the left side of the defect. F11 is reading quite high.
2.60	0.1	
88.70		Debonding initiated, propagated for ~100mm, then halted at a crack about 100mm outside the quarter span before continuing on after picking up some load again. First time macro-debonding has been halted. Approximately 20% of the debonding occurred in the adhesive layer.

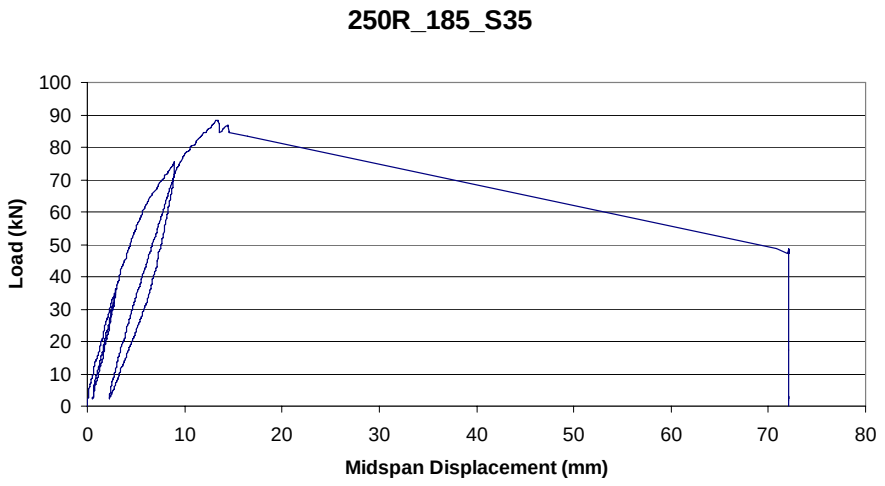
250R_185_S35
Load (kN)
Midspan Displacement (mm)
0
10
20
30
40
50
60
70
80
90
100

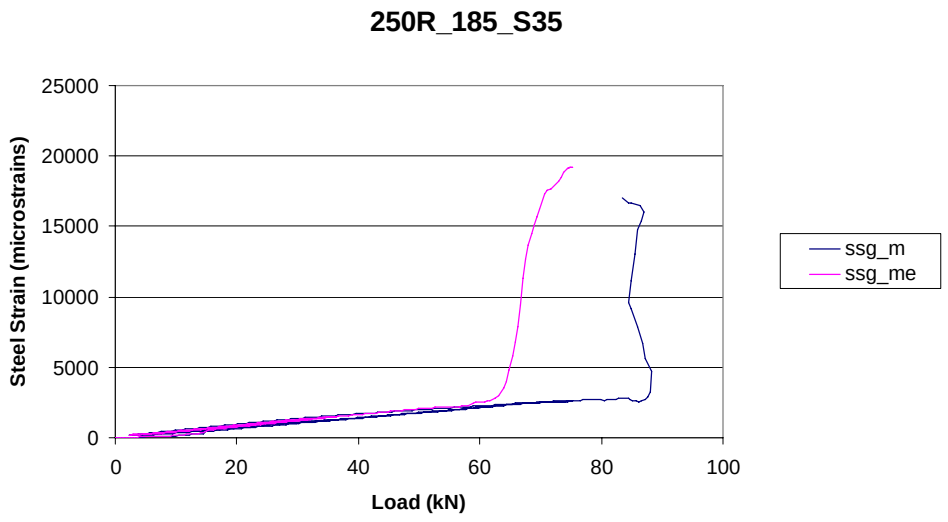
250R_185_S35
Steel Strain (microstrains)
Load (kN)
ssg_m
ssg_me
0
5000
10000
15000
20000
25000
0
20
40
60
80
100

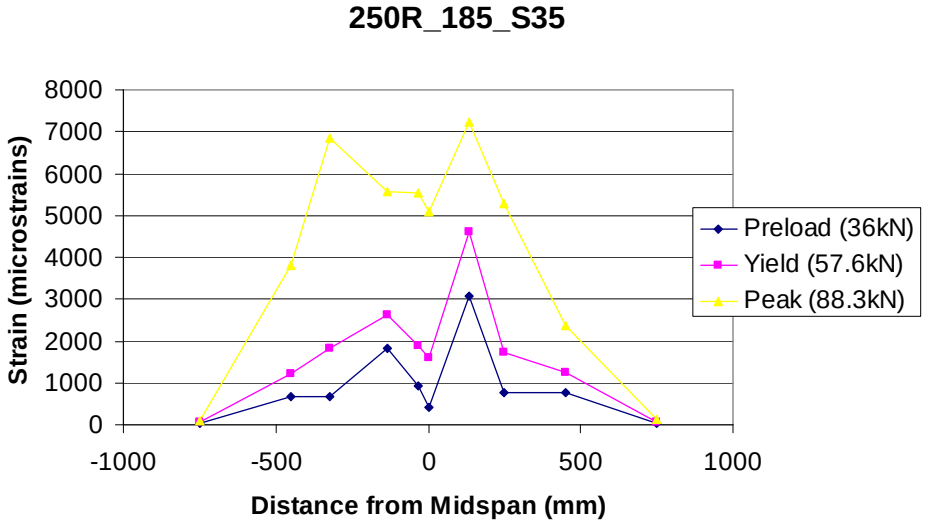
250R_185_S35
Strain (microstrains)
Distance from Midspan (mm)
Preload (36kN)
Yield (57.6kN)
Peak (88.3kN)
0
1000
2000
3000
4000
5000
6000
7000
8000
-1000
-500
0
500
1000

Specimen 32: 50mm x 150mm rectangular disbond inserted in the adhesive interface 185mm from the midspan tested 9/20/2005 (50R_185_S32_2).

Specimen 32 was manufactured with a defect consisting of a rectangular disbond with a centroid located 185mm away from the midspan of the beam. The dimensions of the manufactured disbond were 50mm length by 150mm width. This specimen was the second manufactured with this defect configuration. The beam was, precracked using the 35.6 kN preload level before the application of FRP. Final debonding occurred from the location of the disbond. The failure load was very low due to much of the debonding occurring through the adhesive resin interface. Approximately 30% of the failure was observed to be a failure through the adhesive, suggesting that the bond strength and the concrete strength are similar.

Beam Characteristic	Value
Test Date	9/20/2005
Rehab Date (number)	8/19/2005 (5)
Concrete Cast Date (number)	2/8/2005 (2)
Time from Rehab to Test	32 days
Maximum Load Held	83.59 kN
Displacement at Maximum Load	12.42 mm
Measured Steel Yield	2395 με
Load at Steel Yield	68.93 kN
Displacement at Steel Yield	7.64 mm
FRP Strain at Steel Yield	3357 με
FRP Strain at Debonding (Location)	5804 (F11) με
FRP Midspan Strain at Debonding	5201 με
Debonding Direction	Left
Failure Mode	Thin Concrete

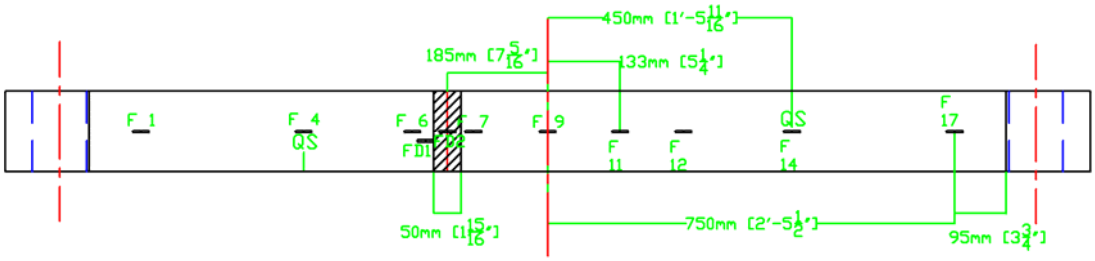

Load (kN)	Crack Width (mm)	Notes
0.00	<0.1	
36.20	<0.1	Typical crack reopening
2.50	<0.1	
75.00	0.1	Some cracking noise heard over 70kN.
2.50	<0.1	Some long, narrow, local debonding away from the defect location.
84.20		Long, slow, gradual debonding. Local debonding occurred at about 150mm on both sides of the midspan. Also, extensive local debonding on the left side of the defect before macro-debonding. ~30% of failure was through the adhesive.

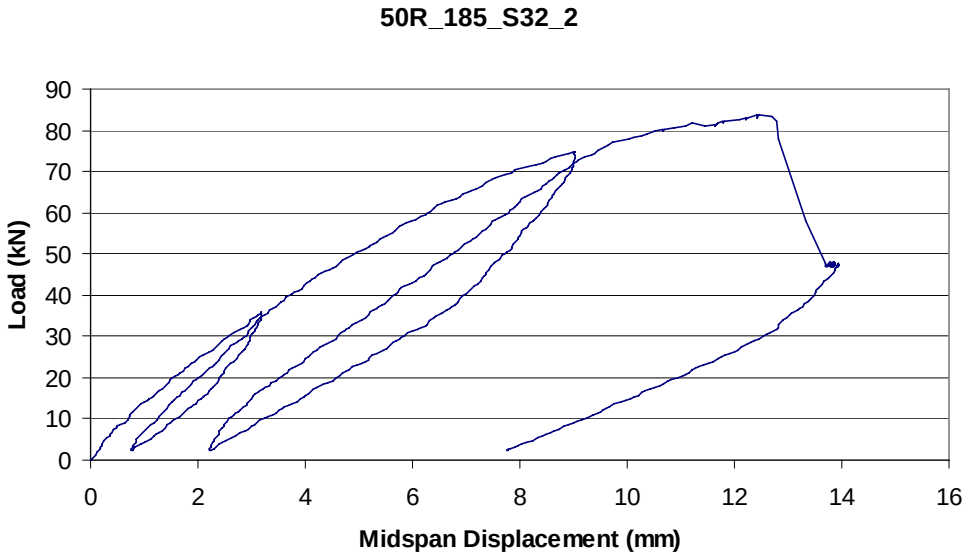

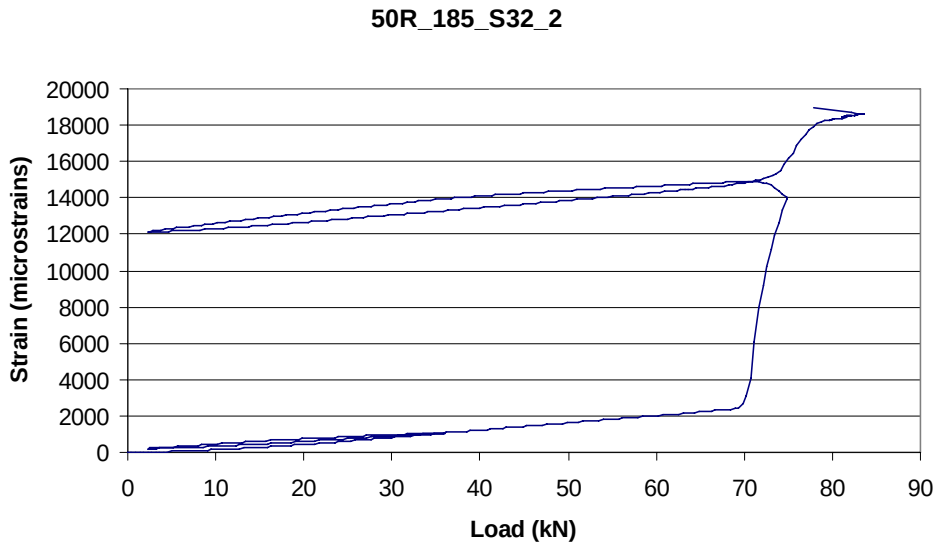
50R_185_S32_2
Strain (microstrains)
20000
18000
16000
14000
12000
10000
8000
6000
4000
2000
0
0
10
20
30
40
50
60
70
80
90
Load (kN)

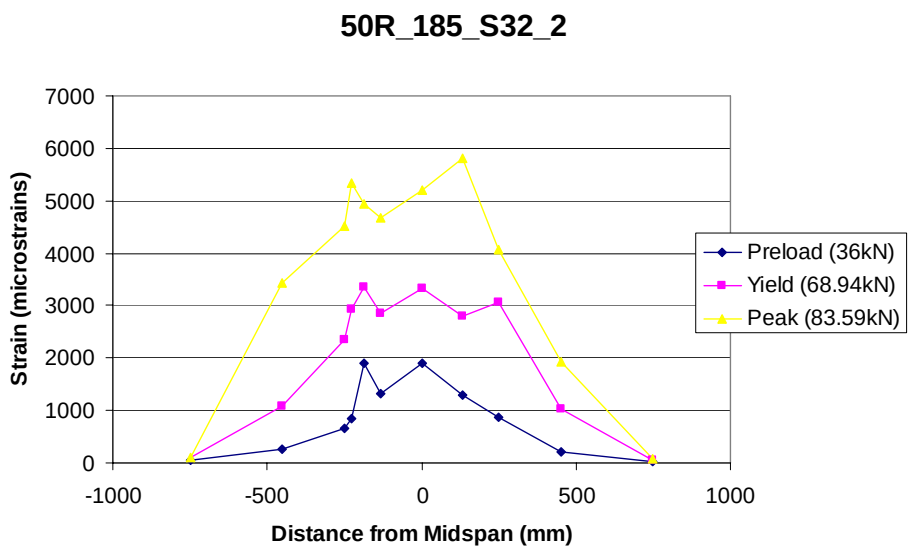
50R_185_S32_2
Strain (microstrains)
7000
6000
5000
4000
3000
2000
1000
0
-1000
-500
0
500
1000
Distance from Midspan (mm)
Preload (36kN)
Yield (68.94kN)
Peak (83.59kN)

50R_185_S32_2

Specimen 33: 150x100mm rectangular disbond inserted in the adhesive interface 185mm from the midspan tested 9/20/2005 (150R_185_S33_3)

Specimen 33 was manufactured with a defect consisting of a rectangular disbond with a centroid located 185mm away from the midspan of the beam. The dimensions of the manufactured disbond were 150mm length by 150mm width. This specimen was the third manufactured with this defect configuration. The beam was, precracked using the 35.6 kN preload level before the application of FRP. Initial debonding during the 75kN load cycle propagated from the defect to the right through the midspan, but halted at a crack. Final debonding occurred to the left from the

location of the disbond (the opposite direction initial local debonding was propagating). The debonding failure mode was through a thick concrete bondline, which was not typical for this rehabilitation set (rehabilitation set #5).

Beam Characteristic	Value
Test Date	9/20/05
Rehab Date (number)	8/19/05 (5)
Concrete Cast Date (number)	2/8/05 (2)
Time from Rehab to Test	32 days
Maximum Load Held	92.34 kN
Displacement at Maximum Load	14.54 mm
Measured Steel Yield	2316 με
Load at Steel Yield	68.12 kN
Displacement at Steel Yield	7.05 mm
FRP Strain at Steel Yield	3225 με
FRP Strain at Debonding (Location)	8600 (FD2) με
FRP Midspan Strain at Debonding	6654 με
Debonding Direction	Left
Failure Mode	Thick Concrete Bondline

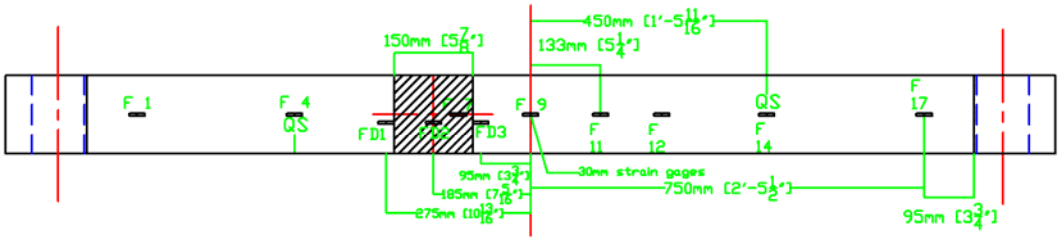

Load (kN)	Crack Width (mm)	Notes
0.00	<0.1	
36.00	0.1	Typical crack reopening.
2.60	<0.1	
75.00	0.4	Large flexural crack opening at the right edge of the defect. Local debonding about 35mm long occurring to the right of the disbond.
2.50	0.1	
90.10	0.6	Local debonding from the defect through the midspan and about 185mm to the right of the midspan.
2.50		
92.60		Good, thick concrete layer. No failure in the epoxy this time.

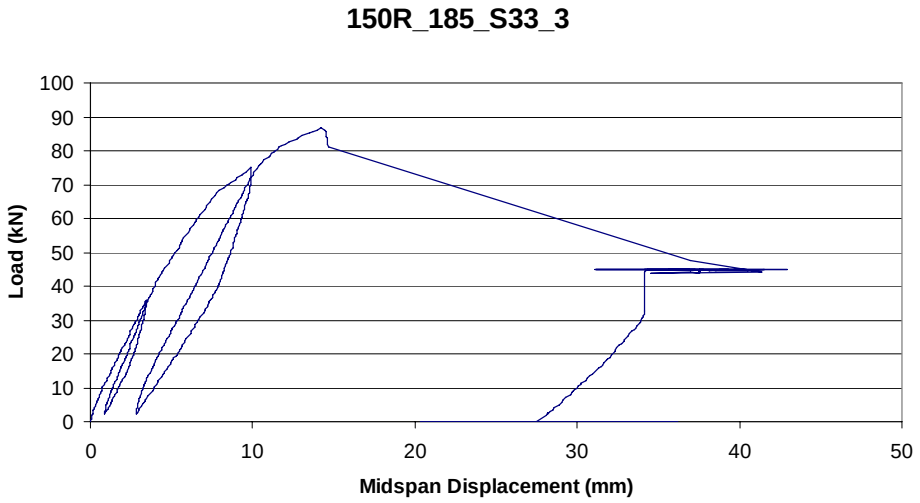
150R_185_S33_3
Load (kN)
Midspan Displacement (mm)
0
10
20
30
40
50
60
70
80
90
100
0
10
20
30
40
50

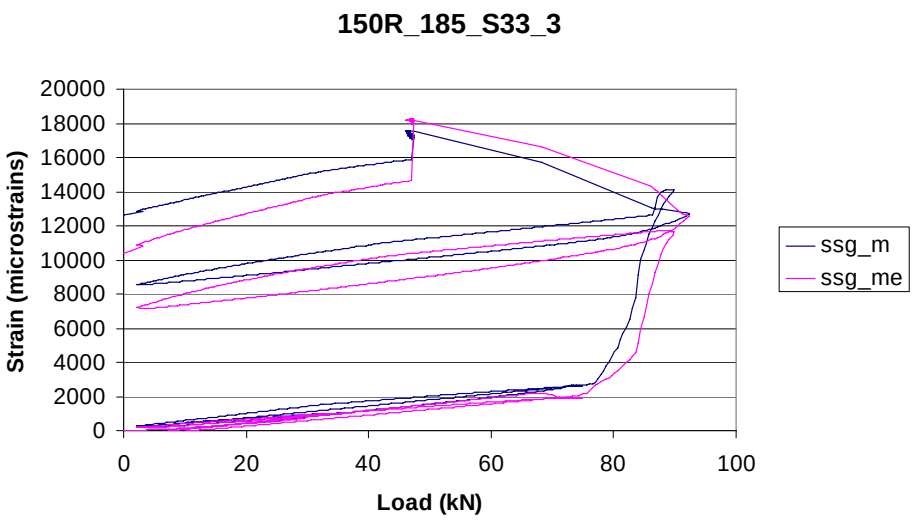
150R_185_S33_3
Strain (microstrains)
Load (kN)
0
2000
4000
6000
8000
10000
12000
14000
16000
18000
20000
0
20
40
60
80
100
ssg_m
ssg_me

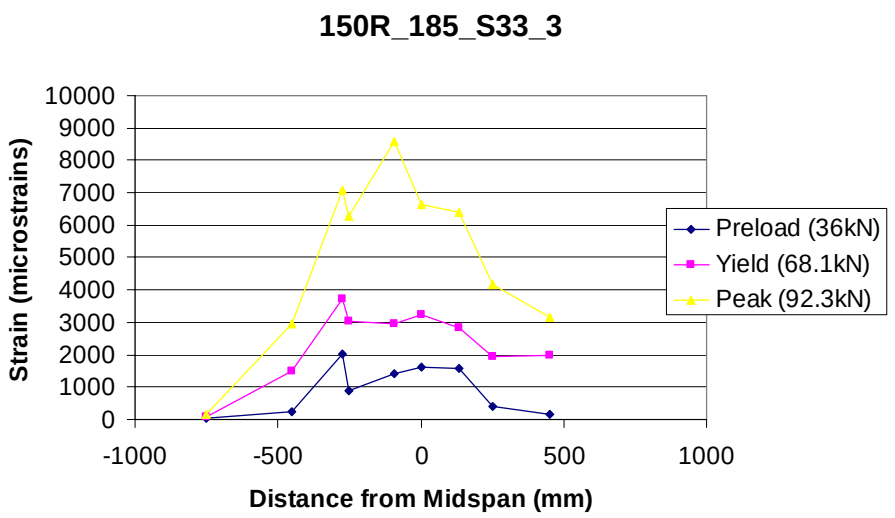
150R_185_S33_3
Strain (microstrains)
Distance from Midspan (mm)
0
1000
2000
3000
4000
5000
6000
7000
8000
9000
10000
-1000
-500
0
500
1000
Preload (36kN)
Yield (68.1kN)
Peak (92.3kN)

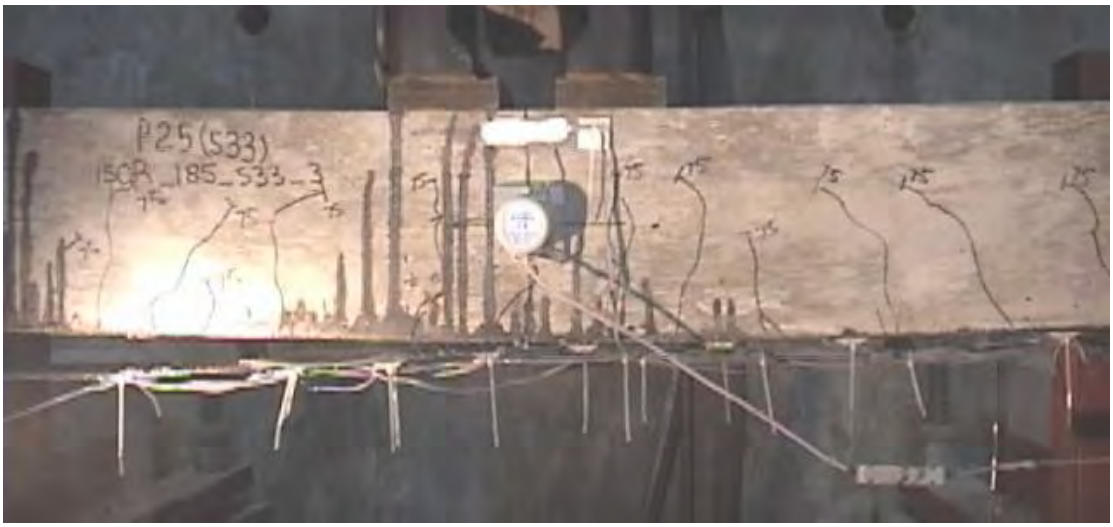

Specimen 34: 200mm by 150mm rectangular disbond inserted in the adhesive interface 185mm from the midspan tested 9/22/2005 (200R_185_S34)

Specimen 34 was manufactured with a defect consisting of a rectangular disbond with a centroid located 185mm away from the midspan of the beam. The dimensions of the manufactured disbond were 200mm length by 150mm width (the full width of the beam). This is the second largest disbond that was tested in the laboratory. The beam was, precracked using the 35.6 kN preload level before the application of FRP. Similar to specimen 33, initial debonding during the 75kN load cycle propagated from the defect to the right through the midspan, but halted at a crack. Final debonding occurred to the left from the location of the disbond (the opposite direction initial local debonding was propagating). The debonding failure mode was through a thin concrete bondline, but the debonding load and deflection were atypically low for this failure mode.

Beam Characteristic	Value
Test Date	9/22/05
Rehab Date (number)	8/19/05 (5)
Concrete Cast Date (number)	2/8/05 (2)
Time from Rehab to Test	34 days
Maximum Load Held	82.25 kN
Displacement at Maximum Load	13.14 mm
Measured Steel Yield	2505 με
Load at Steel Yield	66.00 kN
Displacement at Steel Yield	7.51 mm
FRP Strain at Steel Yield	3438 με
FRP Strain at Debonding (Location)	6101 (FD2) με
FRP Midspan Strain at Debonding	4312 με
Debonding Direction	Left
Failure Mode	Thin Concrete Bondline

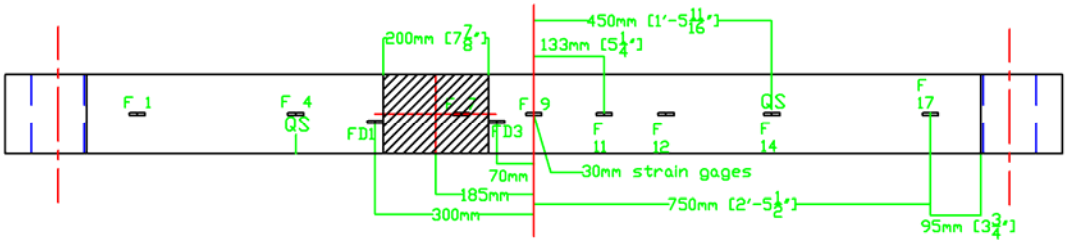

Load (kN)	Crack Width (mm)	Notes
0.00	<0.1	
36.20	<0.1	Typical crack reopening.
2.60	<0.1	
75.10	0.3	Extensive new cracking throughout the beam. Debonding occurred from the defect towards the midspan beginning at about 69kN. A large diagonal crack appeared about 25mm from the defect's right edge.
2.50	0.2	
82.50		The failure was decent. Almost exclusively in the concrete. Still a very low load, however.

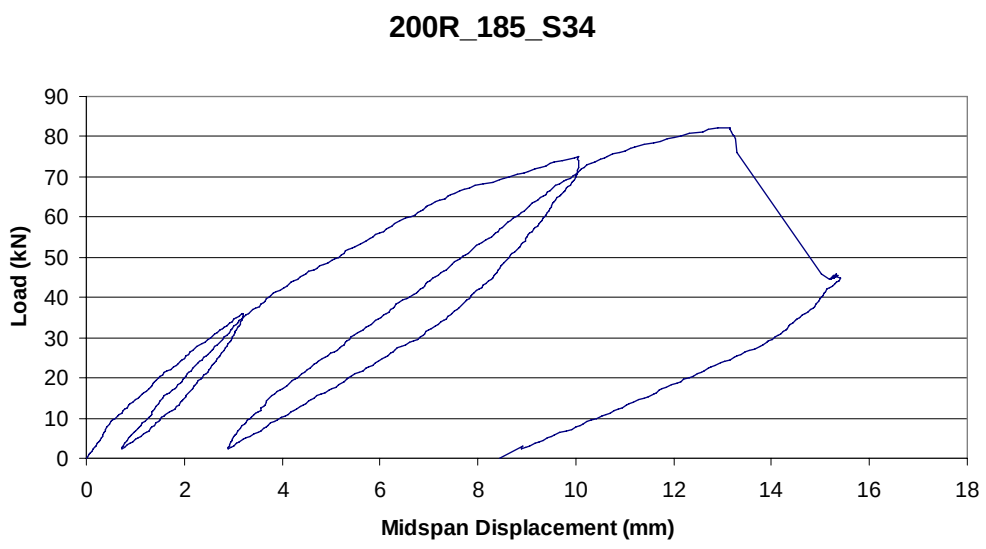

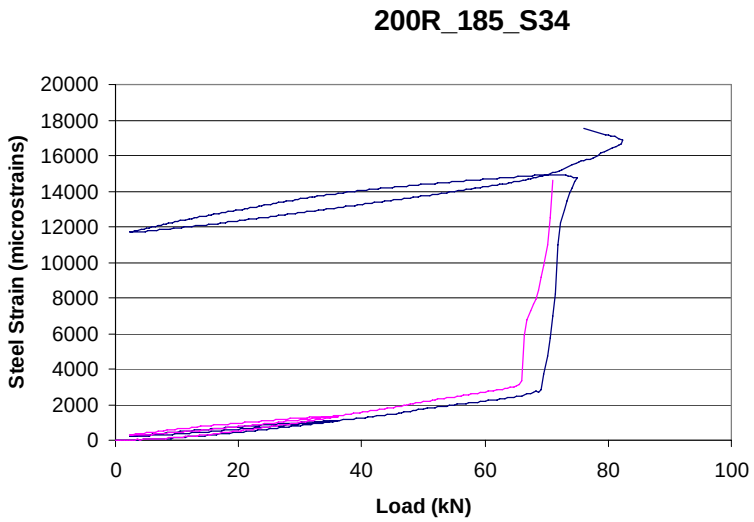
200R_185_S34
Steel Strain (microstrains)
20000
18000
16000
14000
12000
10000
8000
6000
4000
2000
0
0
20
40
60
80
100
Load (kN)

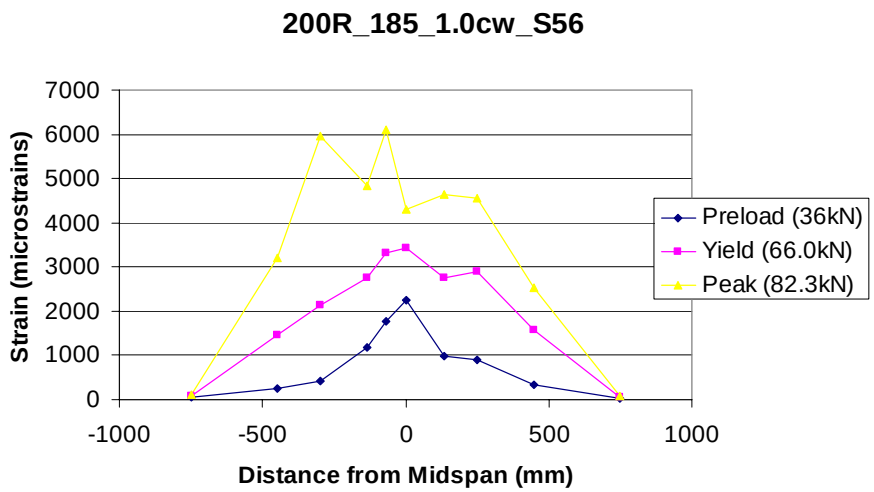
200R_185_1.0cw_S56
Strain (microstrains)
7000
6000
5000
4000
3000
2000
1000
0
-1000
-500
0
500
1000
Distance from Midspan (mm)
Preload (36kN)
Yield (66.0kN)
Peak (82.3kN)

Specimen 37: 100mm x 150mm rectangular disbond inserted in the interface between FRP layers located 185mm from the midspan tested 9/27/2005 (100RI_185_S37)

Specimen 37 was manufactured with a defect consisting of a rectangular disbond located between FRP layers (interlaminar) with a centroidal location 185mm away from the midspan of the beam. The dimensions of the manufactured disbond were 100mm length by 150mm width. This was the first specimen investigated with an interlaminar disbond. The beam was, precracked using the 35.6 kN preload level before the application of FRP. Debonding occurred to the right end of the FRP, away from the defect, after initiating from a diagonal shear crack under the right load support. The debonding propagated while paused at the peak of the 90kN load cycle. The debonding failure mode was through a thick concrete bondline, and therefore, it was not surprising the specimen failed around 90kN (see figure 5-1).

Beam Characteristic	Value
Test Date	9/27/05
Rehab Date (number)	9/20/05 (6)
Concrete Cast Date (number)	2/8/05 (2)
Time from Rehab to Test	7 days
Maximum Load Held	89.84 kN
Displacement at Maximum Load	14.37 mm
Measured Steel Yield	2287 με
Load at Steel Yield	68.90 kN
Displacement at Steel Yield	7.46 mm
FRP Strain at Steel Yield	3483 με
FRP Strain at Debonding (Location)	7127 (FD2) με
FRP Midspan Strain at Debonding	6458 με
Debonding Direction	Right
Failure Mode	Thick Concrete Bondline

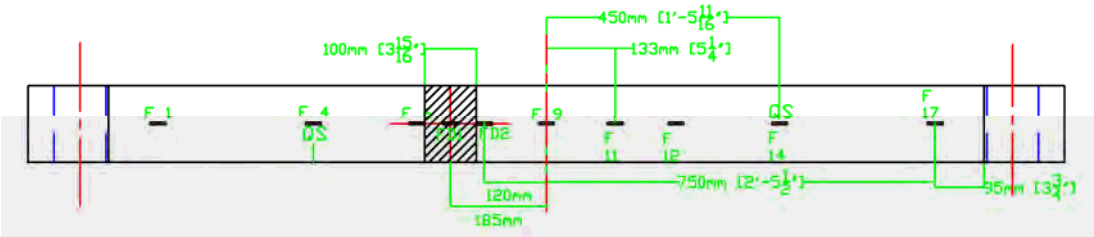

Load (kN)	Crack Width (mm)	Notes
0.00	<0.1	
36.40	<0.1	Typical reopening of cracks.
2.60	<0.1	
75.00	0.1	Tight crack spacing. No local debonding yet. Largest crack (0.1mm) is near the center of the defect.
2.70	<0.1	
90.00		Failure occurred very slowly after the actuator had paused at the peak of the 90kN load cycle. Debonding propagated to the right away from the defect. Some local debonding to the right of the defect.

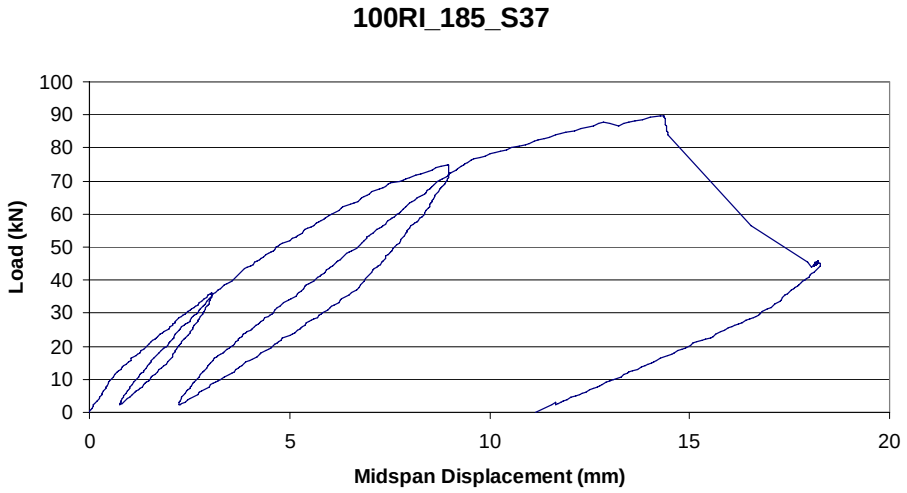
100RI_185_S37
Load (kN)
Midspan Displacement (mm)
0
10
20
30
40
50
60
70
80
90
100
0
5
10
15
20

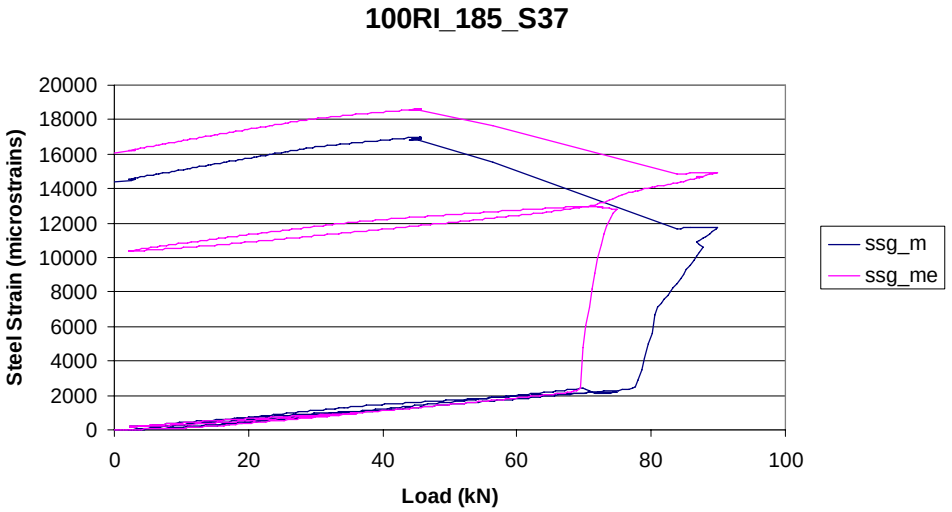
100RI_185_S37
Steel Strain (microstrains)
Load (kN)
0
2000
4000
6000
8000
10000
12000
14000
16000
18000
20000
0
20
40
60
80
100
ssg_m
ssg_me

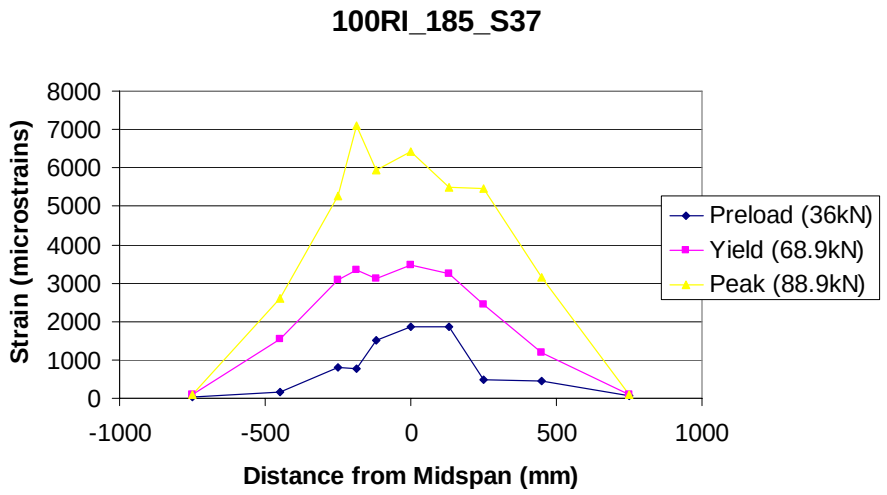
100RI_185_S37
Strain (microstrains)
Distance from Midspan (mm)
0
1000
2000
3000
4000
5000
6000
7000
8000
-1000
-500
0
500
1000
Preload (36kN)
Yield (68.9kN)
Peak (88.9kN)

Specimen 40: 100mm x 150mm rectangular disbond inserted in the interface between FRP layers and in the adhesive located 185mm from the midspan tested 9/28/2005 (100RAI_185_S40)

Specimen 40 was manufactured with a defect consisting of one rectangular disbond located between FRP layers (interlaminar) and one in the adhesive interface with a centroidal location 185mm away from the midspan of the beam. The dimensions of the manufactured disbond were 100mm length by 150mm width. This was the first specimen investigated with both interlaminar and adhesive interface disbonds. The beam was, precracked using the 35.6 kN preload level before the application of FRP. Debonding occurred to the right end of the FRP, initiating from the defect location and propagating through the midspan. There was also approximately 25mm to 35mm of local debonding to the left of the disbond. The debonding failure mode was through a thin concrete bondline, but a small amount of the failure surface (approximately 10%) was observed to have failed through the adhesive layer.

Beam Characteristic	Value
Test Date	9/28/05
Rehab Date (number)	9/20/05 (6)
Concrete Cast Date (number)	2/8/05 (2)
Time from Rehab to Test	8 days
Maximum Load Held	87.18 kN
Displacement at Maximum Load	13.90 mm
Measured Steel Yield	2582 με
Load at Steel Yield	68.17 kN
Displacement at Steel Yield	7.31 mm
FRP Strain at Steel Yield	3931 με
FRP Strain at Debonding (Location)	6940 (FD1) με
FRP Midspan Strain at Debonding	6471 με
Debonding Direction	Right
Failure Mode	Thin Concrete Bondline

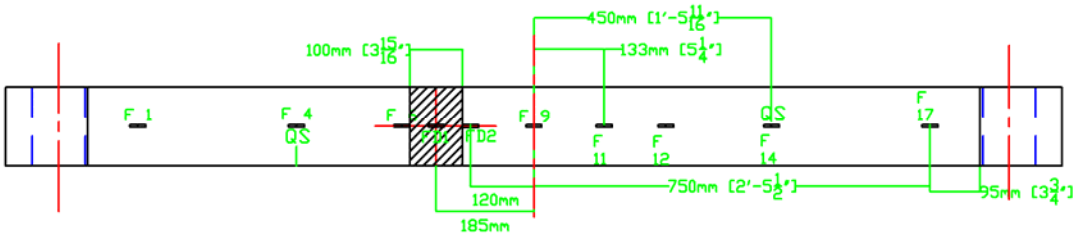

Load (kN)	Crack Width (mm)	Notes
0.00	<0.1	
36.10	<0.1	Typical reopening of cracks.
2.50	<0.1	
75.00	0.5	Extensive new cracking. Largest crack opening is located at the right edge of the defect. It is much larger than the others.
2.30	0.2	Crack width is <0.1mm at the FRP, but is ~0.2mm at the steel depth.
87.60		FRP strains are much higher on the side of the midspan with the defect. Final debonding occurred from the defect to the right (through the midspan). There was also about 25-35mm of debonding to the left of the defect. Failure was not bad, but some was in the interface.

100RAI_185_S40

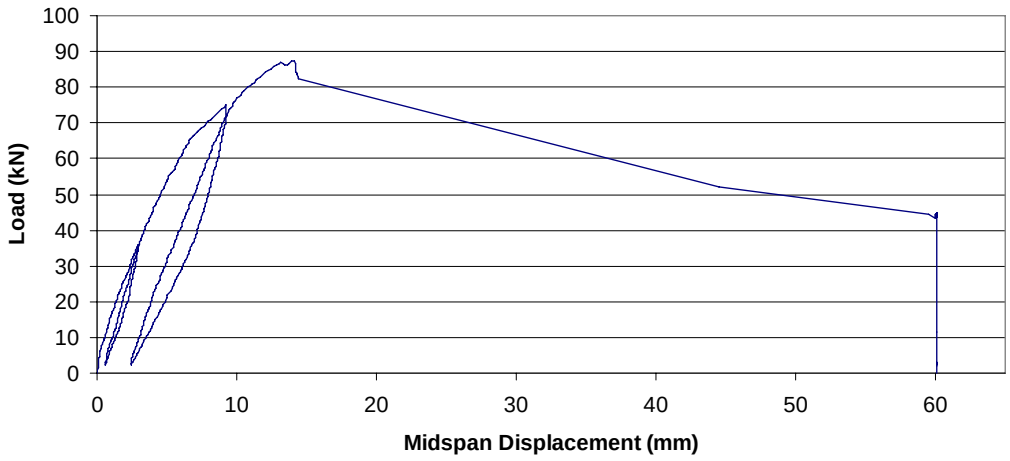

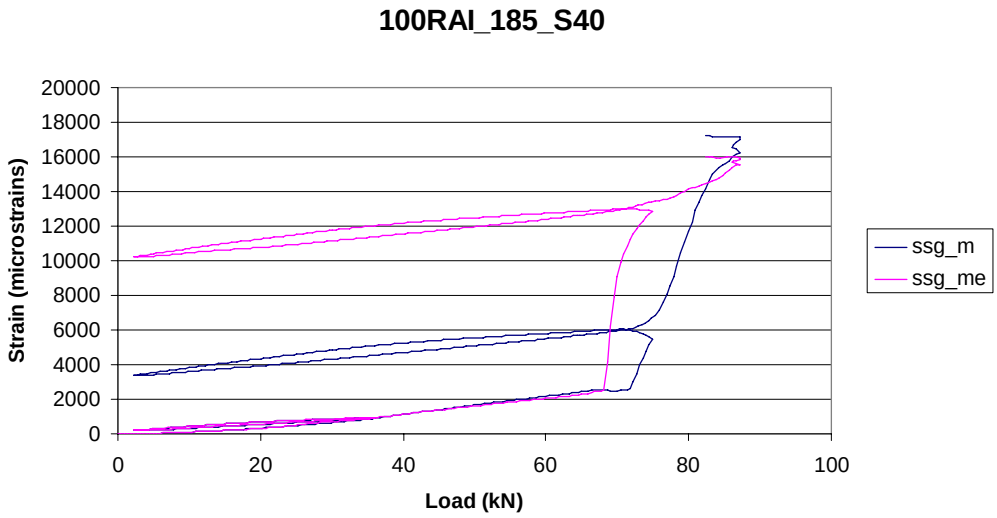
100RAI_185_S40
Strain (microstrains)
20000
18000
16000
14000
12000
10000
8000
6000
4000
2000
0
0
20
40
60
80
100
Load (kN)
ssg_m
ssg_me

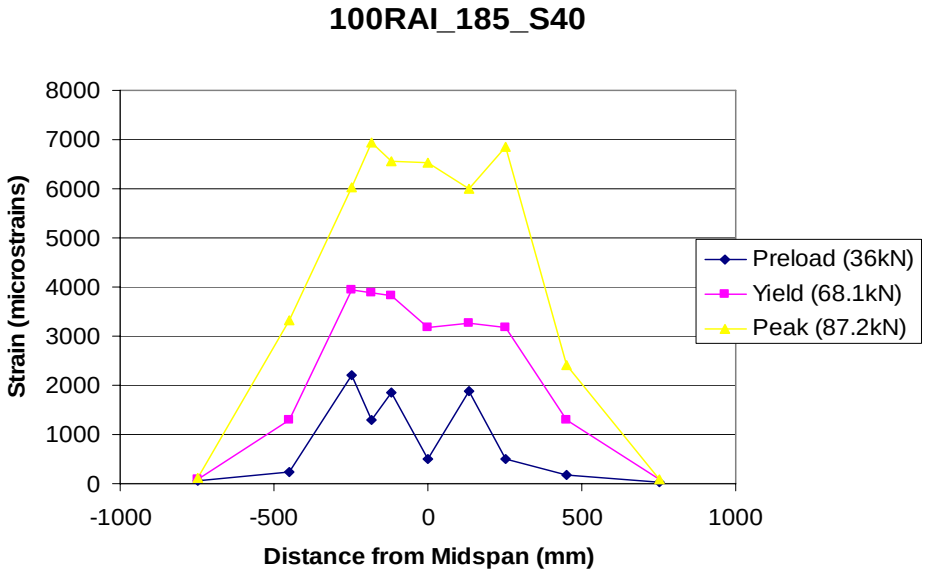
100RAI_185_S40
Strain (microstrains)
8000
7000
6000
5000
4000
3000
2000
1000
0
-1000
-500
0
500
1000
Distance from Midspan (mm)
Preload (36kN)
Yield (68.1kN)
Peak (87.2kN)

S10(P32)
100RAI_185_S40

Specimen 38: 100mm x 150mm rectangular disbond inserted in the adhesive interface 185mm from the midspan tested 9/28/2005 (100R_185_S38_4)

Specimen 38 was manufactured with a defect consisting of a rectangular disbond in the adhesive layer with a centroid located 185mm away from the midspan of the beam. The size of the manufactured disbond was 100mm in length by 150mm in width. This was the fourth specimen manufactured with this defect configuration. It was manufactured in order to compare it to other specimens in this rehabilitation set with interlaminar disbonds. Final debonding occurred from the defect, propagating to

the right through the midspan. The failure was poor occurring through the adhesive resin interface resulting in a fairly low ultimate load and displacement.

Beam Characteristic	Value
Test Date	9/28/05
Rehab Date (number)	9/20/05 (6)
Concrete Cast Date (number)	2/8/05 (2)
Time from Rehab to Test	8 days
Maximum Load Held	86.68 kN
Displacement at Maximum Load	14.19 mm
Measured Steel Yield	2507 με
Load at Steel Yield	66.90 kN
Displacement at Steel Yield	7.69 mm
FRP Strain at Steel Yield	4176 με
FRP Strain at Debonding (Location)	7068 (F9) με
FRP Midspan Strain at Debonding	7068 με
Debonding Direction	Right
Failure Mode	Resin Interface

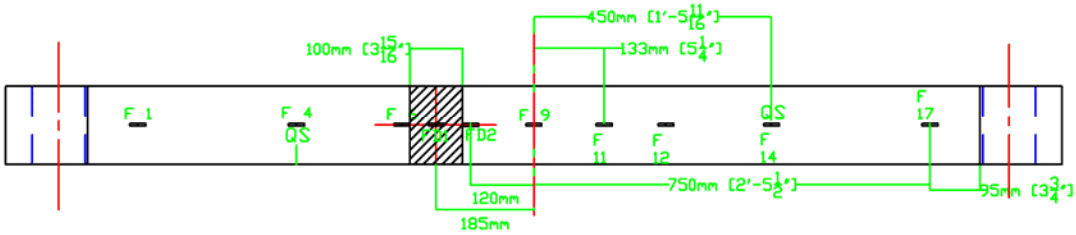

Load (kN)	Crack Width (mm)	Notes
0.00	<0.1	
36.10	<0.1	Typical crack reopening
2.30	<0.1	
75.30	0.5	Cracking sound at 47kN (very low load). Some local debonding on both sides of the defect. Largest crack opening is about 25mm to the right of the defect. Extensive cracking at the bondline near the midspan.
2.80	0.2	
87.00		Failure was again through the adhesive (primarily). Debonding propagated from the defect through the midspan to the right end of the FRP.

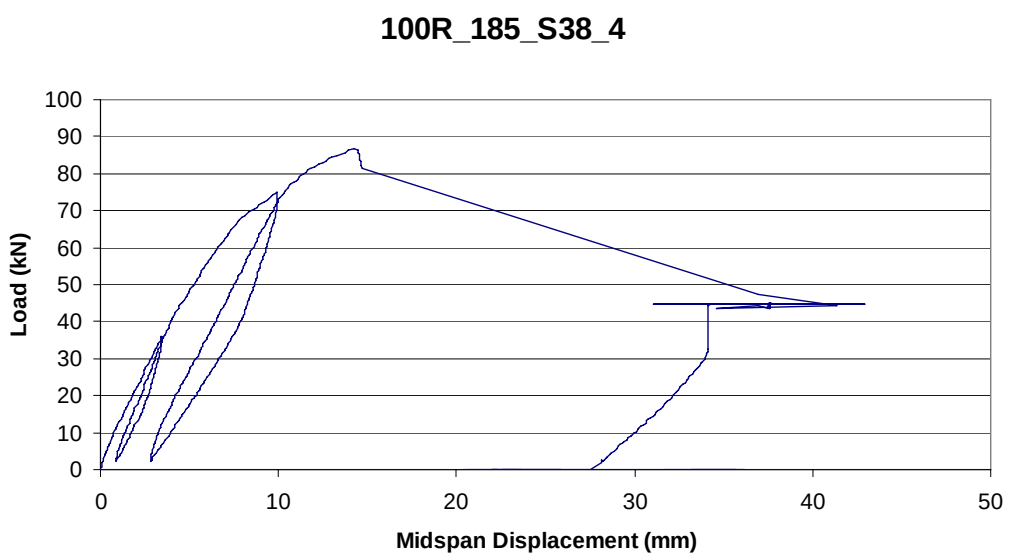

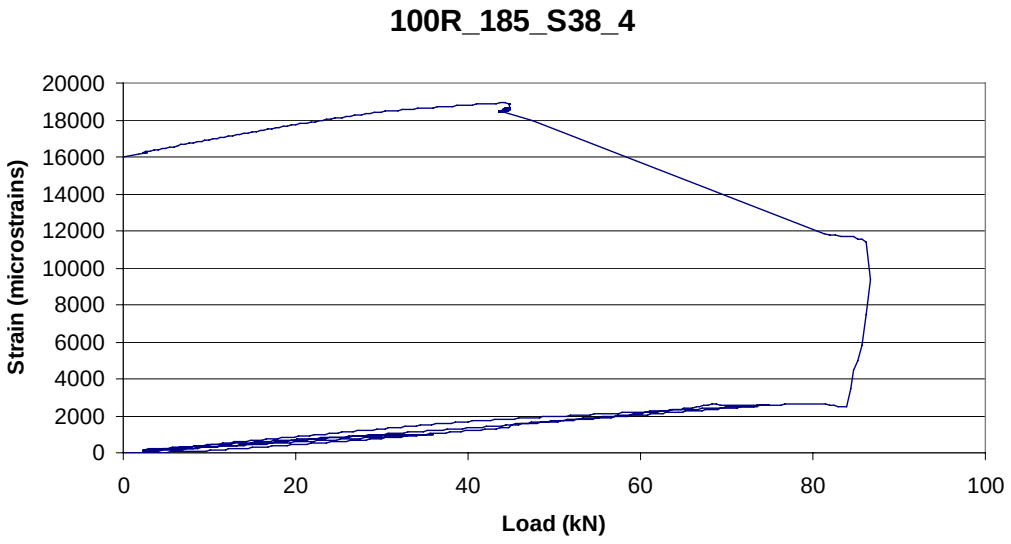
100R_185_S38_4
Strain (microstrains)
20000
18000
16000
14000
12000
10000
8000
6000
4000
2000
0
0
20
40
60
80
100
Load (kN)

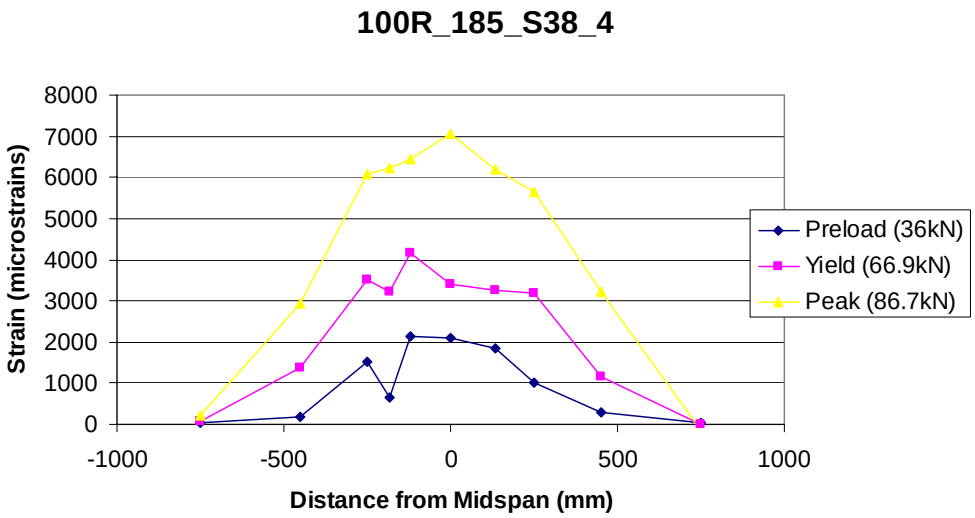
100R_185_S38_4
Strain (microstrains)
8000
7000
6000
5000
4000
3000
2000
1000
0
-1000
-500
0
500
1000
Distance from Midspan (mm)
Preload (36kN)
Yield (66.9kN)
Peak (86.7kN)

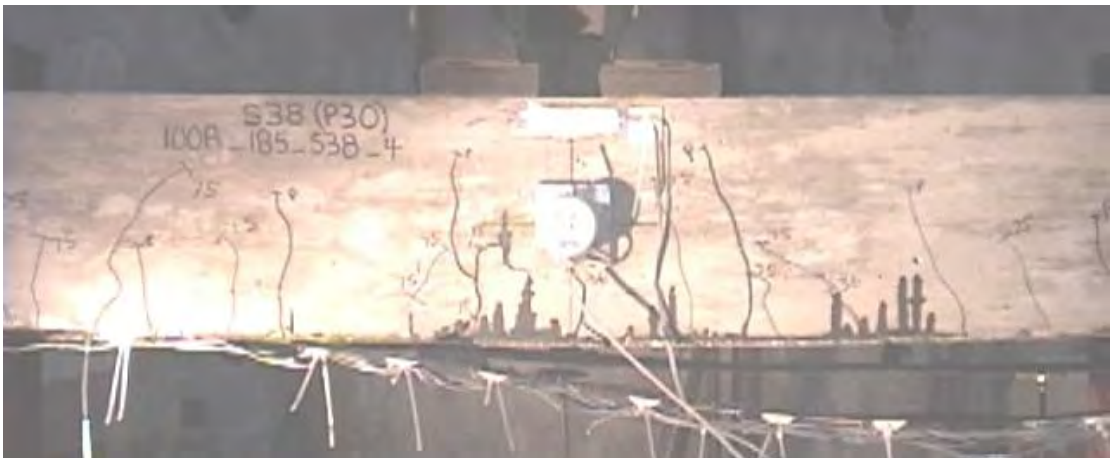
S38 (P30)
100R_185_S38_4

Specimen 43: 100mm diameter circular disbond inserted in the interface between FRP layers and in the adhesive interface, located 185mm from the midspan tested 9/30/2005 (100CAI_185_S43)

Specimen 43 contained a circular disbond defect with a centroid located 185mm away from the midspan of the beam. The disbond was manufactured in both the adhesive interface layer and in the interlaminar location. The size of the disbond was 100mm in diameter. During the 75kN load cycle, approximately 200mm of local debonding occurred at the midspan of the beam, but not reach the defect location. Debonding was almost exclusively through the adhesive layer, with very little concrete left attached to the FRP. The failure propagated to the right away from the defect in a very gradual manner and after reaching a very low ultimate load.

Beam Characteristic	Value
Test Date	9/30/2005
Rehab Date (number)	9/20/2005 (6)
Concrete Cast Date (number)	2/8/2005 (2)
Time from Rehab to Test	10 days
Maximum Load Held	80.78 kN
Displacement at Maximum Load	12.75 mm
Measured Steel Yield	2277 με
Load at Steel Yield	67.90 kN
Displacement at Steel Yield	7.12 mm
FRP Strain at Steel Yield	3205 με
FRP Strain at Debonding (Location)	5979 (FD2) με
FRP Midspan Strain at Debonding	5178 με
Debonding Direction	Right
Failure Mode	Resin Interface

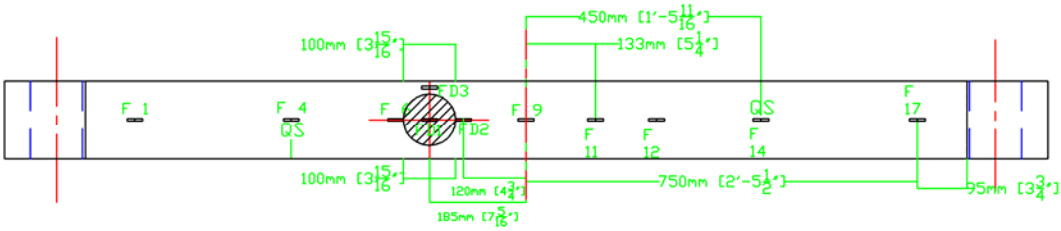

Load (kN)	Crack Width (mm)	Notes
0.00	<0.1	
36.20	0.1	Typical crack reopening. No new cracks.
2.50	<0.1	
75.00	0.3	Large debond through the midspan (~200mm long). No debonding at the defect location yet.
2.50	0.1	
81.00		Debonding was again almost entirely through the adhesive layer. No debonding ever occurred near the defect. The debonding through the adhesive was very slow as the FRP gradually peeled off. The past two tests in this batch have failed through the adhesive, while the first two were in the concrete.

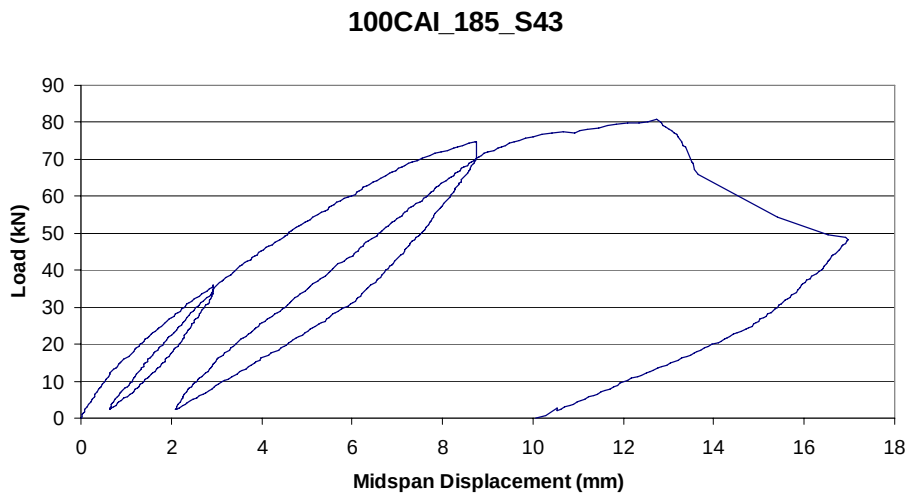
100CAI_185_S43
Load (kN)
Midspan Displacement (mm)
0
10
20
30
40
50
60
70
80
90
0
2
4
6
8
10
12
14
16
18

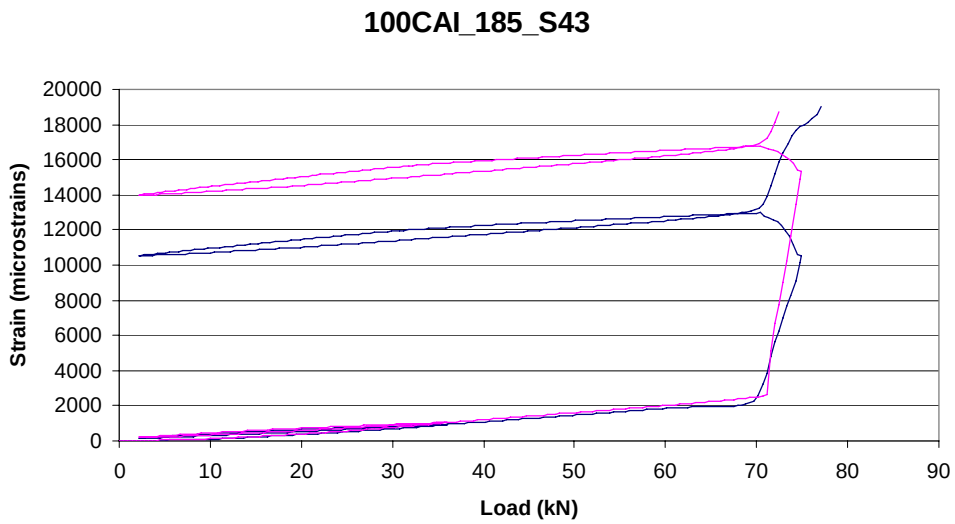
100CAI_185_S43
Strain (microstrains)
Load (kN)
0
2000
4000
6000
8000
10000
12000
14000
16000
18000
20000
0
10
20
30
40
50
60
70
80
90

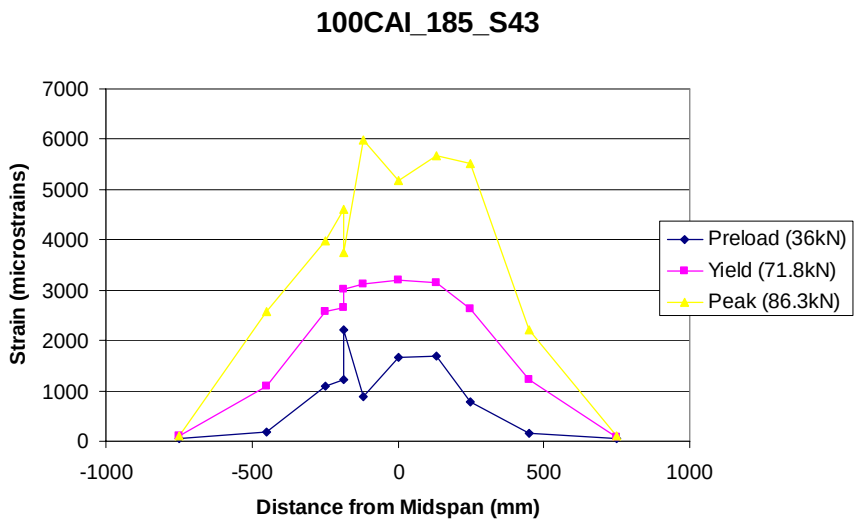
100CAI_185_S43
Strain (microstrains)
Distance from Midspan (mm)
0
1000
2000
3000
4000
5000
6000
7000
-1000
-500
0
500
1000
Preload (36kN)
Yield (71.8kN)
Peak (86.3kN)

Specimen 42: Strengthened, preloaded control specimen tested 9/30/2005 (R_C_Control_7_S42)

Specimen 42 was a control specimen with standard preloading as discussed in section 2.8, but without any purposely inserted defects. It is the control specimen that was created in conjunction with the defective beams for rehabilitation set six. The peak load held by this specimen was modest at 89.76kN and corresponding midspan displacement of 16.99mm. Local debonding initiated as the actuator approached the peak of the 90kN load cycle at the midspan location. Final debonding occurred when a 90kN load was approached on the 105kN load cycle. Debonding propagated to the left end of the beam. The debonding mechanism observed was failure through a thick concrete bondline with little failure through the resin interface.

Beam Characteristic	Value
Test Date	9/30/05
Rehab Date (number)	9/20/05 (6)
Concrete Cast Date (number)	2/8/05 (2)
Time from Rehab to Test	10 days
Maximum Load Held	89.76 kN
Displacement at Maximum Load	16.99 mm
Measured Steel Yield	2430 με
Load at Steel Yield	70.68 kN
Displacement at Steel Yield	8.00 mm
FRP Strain at Steel Yield	2465 με
FRP Strain at Debonding (Location)	6603 (F9) με
FRP Midspan Strain at Debonding	6603 με
Debonding Direction	Left
Failure Mode	Thick Concrete Bondline

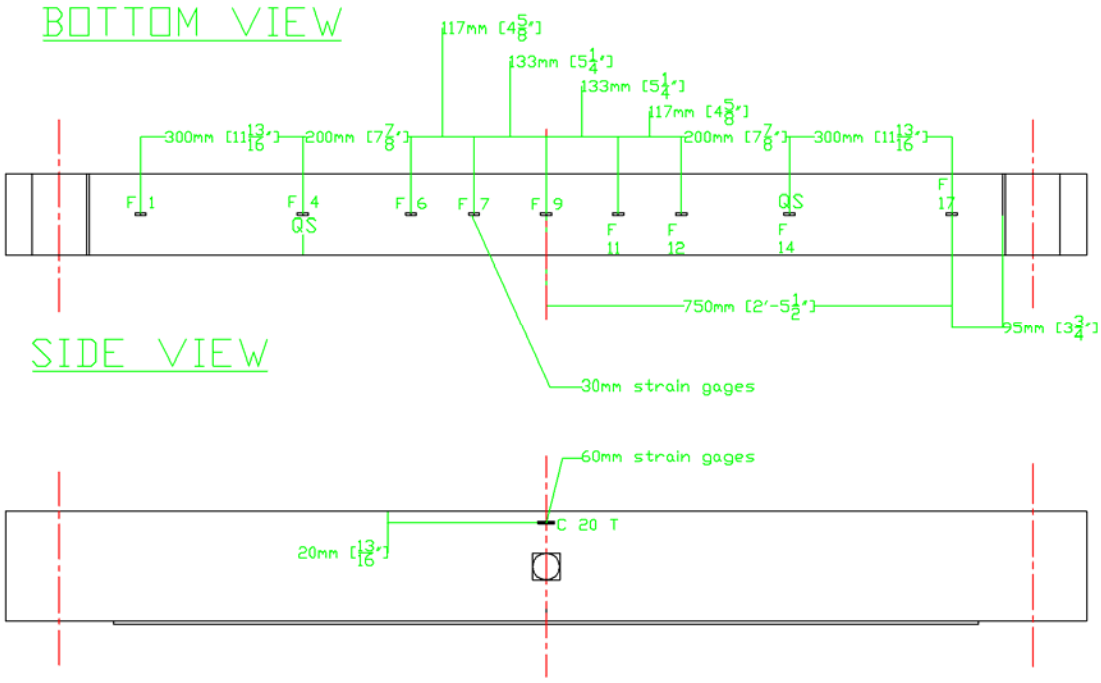

Load (kN)	Crack Width (mm)	Notes
0.00	<0.1	
36.20	< 0.1	Typical crack reopening
2.60	< 0.1	
75.00	0.3	Typical cracking
2.50	0.1	
90.00		Debonding was once again somewhat gradual, but it was a good failure, primarily through the concrete.

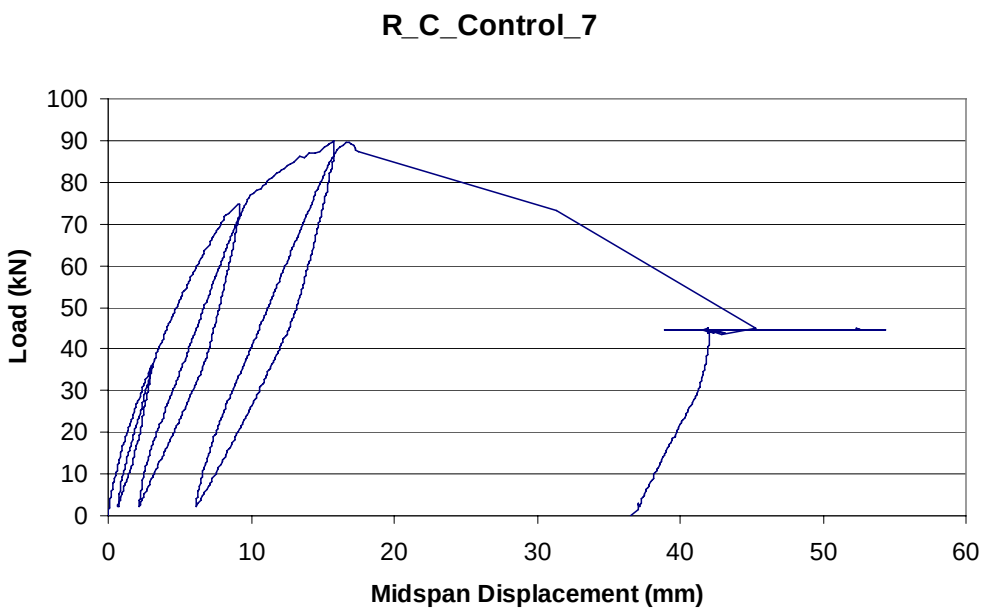

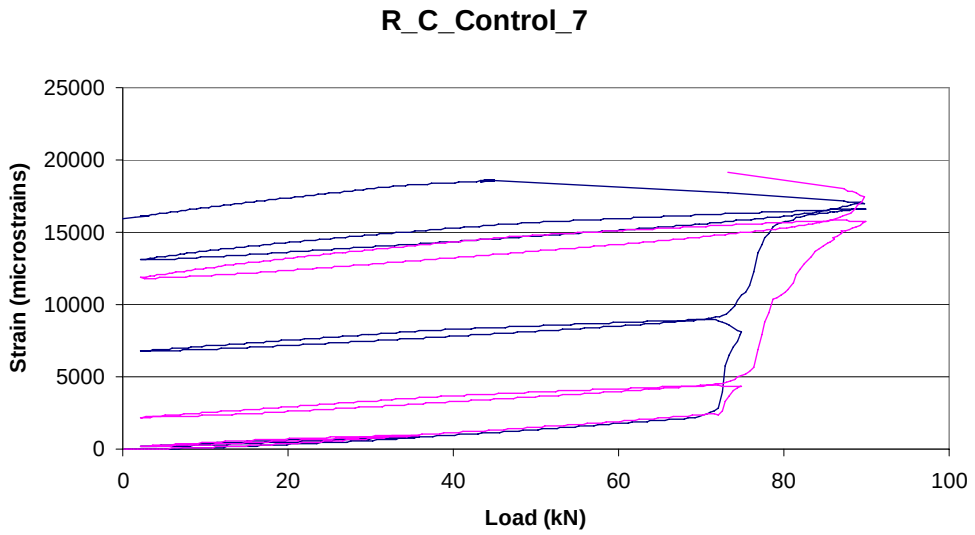
R_C_Control_7
Strain (microstrains)
25000
20000
15000
10000
5000
0
0
20
40
60
80
100
Load (kN)

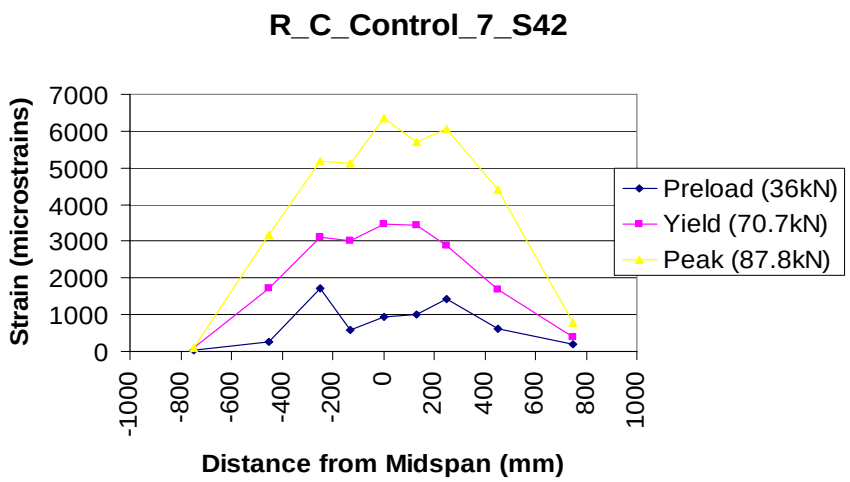
R_C_Control_7_S42
Strain (microstrains)
7000
6000
5000
4000
3000
2000
1000
0
-1000
-800
-600
-400
-200
0
200
400
600
800
1000
Distance from Midspan (mm)
Preload (36kN)
Yield (70.7kN)
Peak (87.8kN)

S42 (P34)
R_C_CONTROL_7

Specimen 45: 100mm x 150mm rectangular disbond inserted in the interface between FRP layers and in the adhesive interface located at the midspan tested 10/25/2005 (100RAI_0_S45)

Specimen 45 was manufactured with a defect consisting of one rectangular disbond located between FRP layers (interlaminar) and one in the adhesive interface with a centroidal location at the midspan of the beam. The dimensions of the manufactured disbond were 100mm length by 150mm width. The beam was, precracked using the 35.6 kN preload level before the application of FRP. Debonding occurred toward the left end of the FRP, initiating from the defect location. This specimen failed at a very low load (72.47kN) through the adhesive resin interface.

Beam Characteristic	Value
Test Date	10/25/05
Rehab Date (number)	9/20/05 (6)
Concrete Cast Date (number)	2/8/05 (2)
Time from Rehab to Test	35 days
Maximum Load Held	72.47 kN
Displacement at Maximum Load	9.89 mm
Measured Steel Yield	2399 με
Load at Steel Yield	57.50 kN
Displacement at Steel Yield	5.57 mm
FRP Strain at Steel Yield	3164 με
FRP Strain at Debonding (Location)	4881 (F7) με
FRP Midspan Strain at Debonding	3235 με
Debonding Direction	Left
Failure Mode	Resin Interface

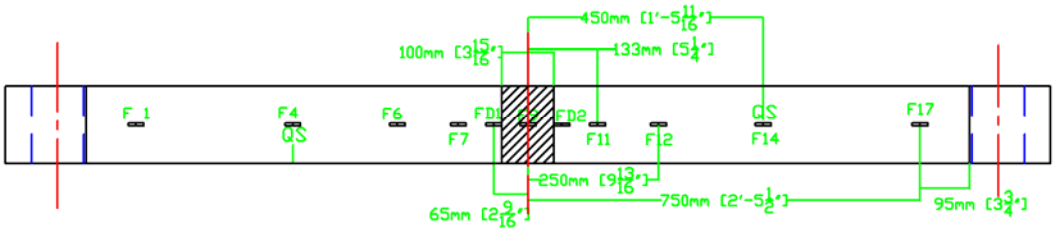

Load (kN)	Crack Width (mm)	Notes
0.00	<0.1	
36.10	<0.1	Typical crack reopening
2.30	<0.1	
75.30	0.5	Cracking sound at 47kN (very low load). Some local debonding on both sides of the defect. Largest crack opening is about 25mm to the right of the defect. Extensive cracking at the bondline near the midspan.
2.80	0.2	
87.00		Failure was again through the adhesive (primarily). Debonding propagated from the defect through the midspan to the right end of the FRP.

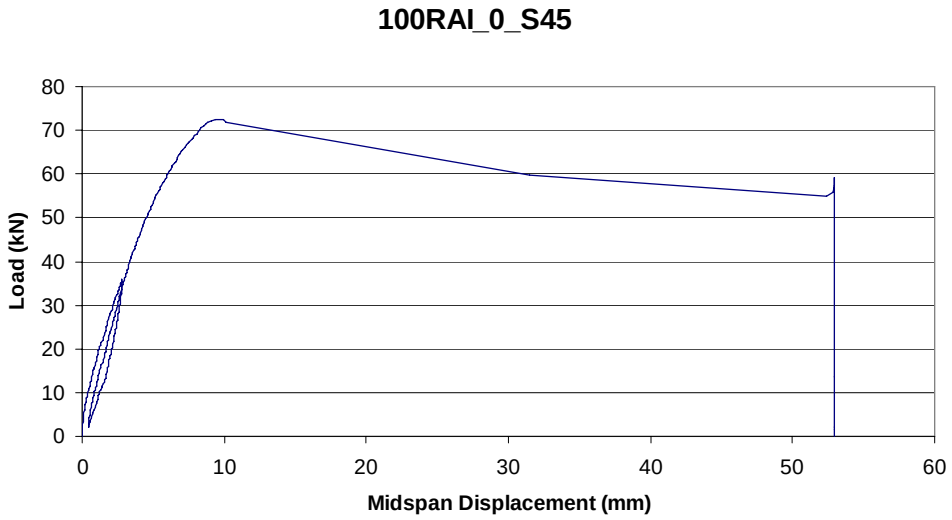
100RAI_0_S45
Load (kN)
Midspan Displacement (mm)
0
10
20
30
40
50
60
70
80

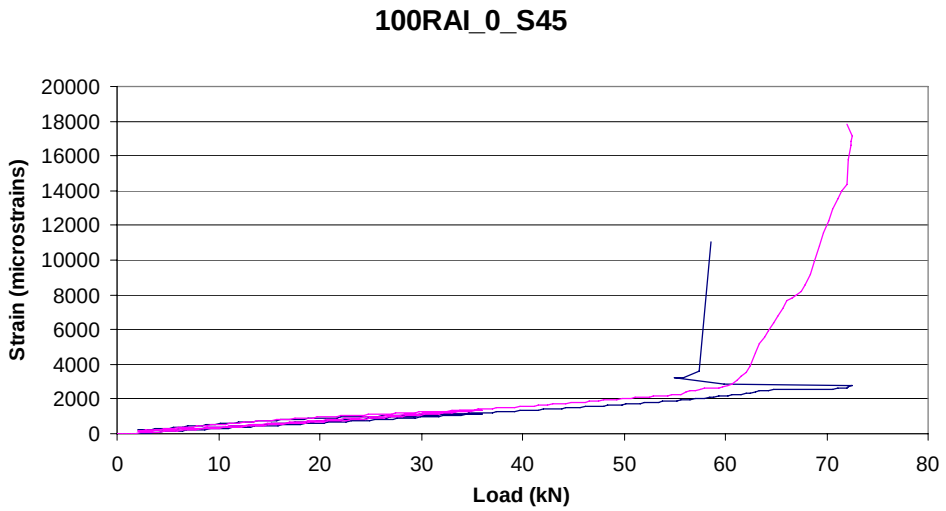
100RAI_0_S45
Strain (microstrains)
Load (kN)
0
2000
4000
6000
8000
10000
12000
14000
16000
18000
20000
0
10
20
30
40
50
60
70
80

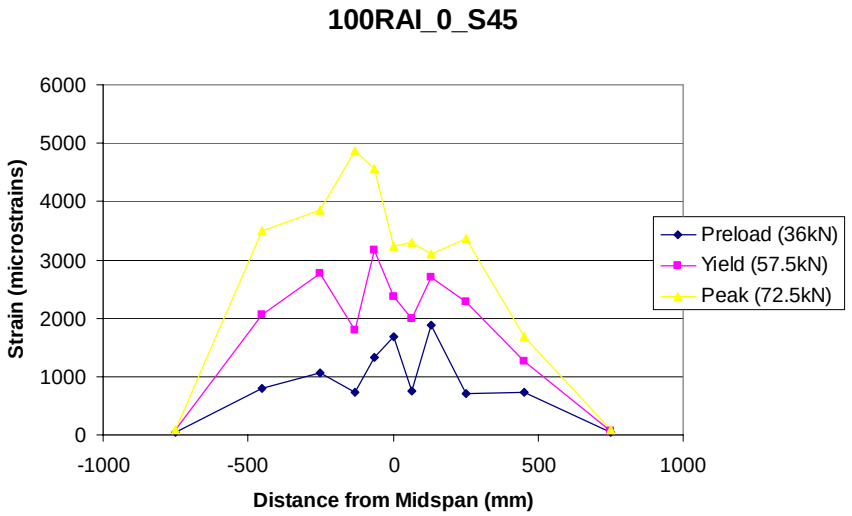
100RAI_0_S45
Strain (microstrains)
Distance from Midspan (mm)
0
1000
2000
3000
4000
5000
6000
-1000
-500
0
500
1000
Preload (36kN)
Yield (57.5kN)
Peak (72.5kN)

Specimen 44: 100mm x 150mm rectangular disbond inserted in the interface between FRP layers and in the adhesive interface located at the midspan tested 10/26/2005 (100RAI_428_S44)

Specimen 44 was manufactured with a defect consisting of one rectangular disbond located between FRP layers (interlaminar) and one in the adhesive interface with a centroidal location 428mm away from the midspan of the beam. The dimensions of the manufactured disbond were 100mm length by 150mm width. The beam was, precracked using the 35.6 kN preload level before the application of FRP. Similar to specimen 45 tested previously, this specimen failed at a very low load (73.8kN) through the adhesive resin interface.

Beam Characteristic	Value
Test Date	10/26/05
Rehab Date (number)	9/20/05 (6)
Concrete Cast Date (number)	2/8/05 (2)
Time from Rehab to Test	36 days
Maximum Load Held	73.50 kN
Displacement at Maximum Load	9.61 mm
Measured Steel Yield	2234 με
Load at Steel Yield	63.50 kN
Displacement at Steel Yield	6.92 mm
FRP Strain at Steel Yield	3155 με
FRP Strain at Debonding (Location)	3997 (F12) με
FRP Midspan Strain at Debonding	3739 με
Debonding Direction	Right
Failure Mode	Resin Interface

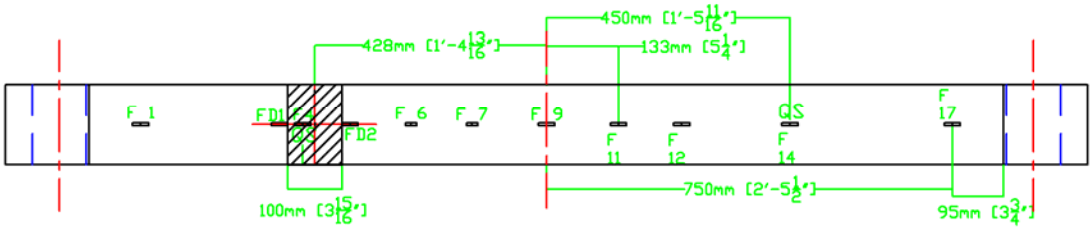

Load (kN)	Crack Width (mm)	Notes
0.00	<0.1	
73.80		Very poor failure occurring to the right (away from the defect) debonding throught the adhesive.

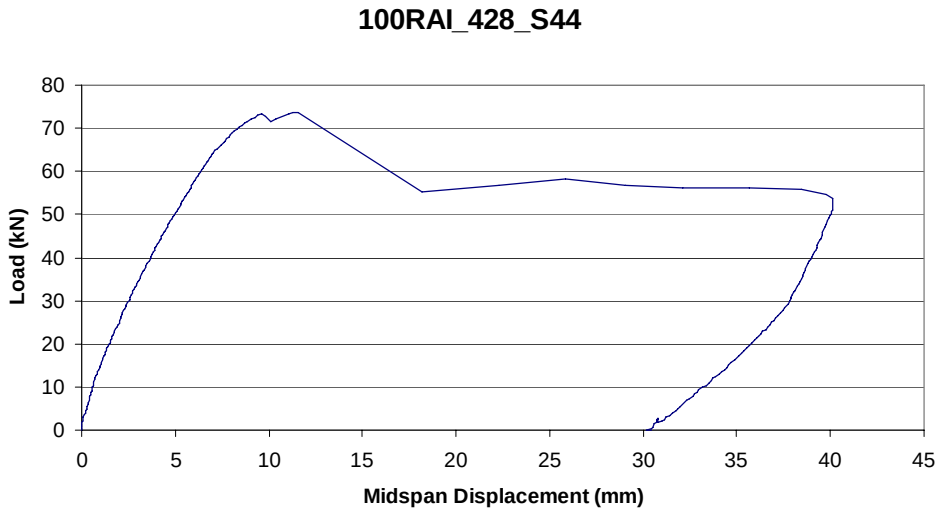
100RAI_428_S44
Load (kN)
Midspan Displacement (mm)
0
10
20
30
40
50
60
70
80
0
5
10
15
20
25
30
35
40
45

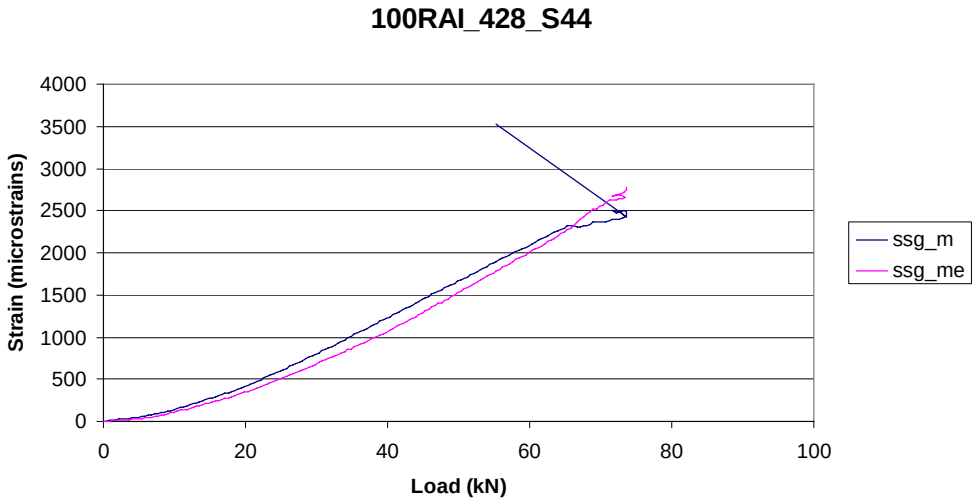
100RAI_428_S44
Strain (microstrains)
Load (kN)
0
500
1000
1500
2000
2500
3000
3500
4000
0
20
40
60
80
100
ssg_m
ssg_me

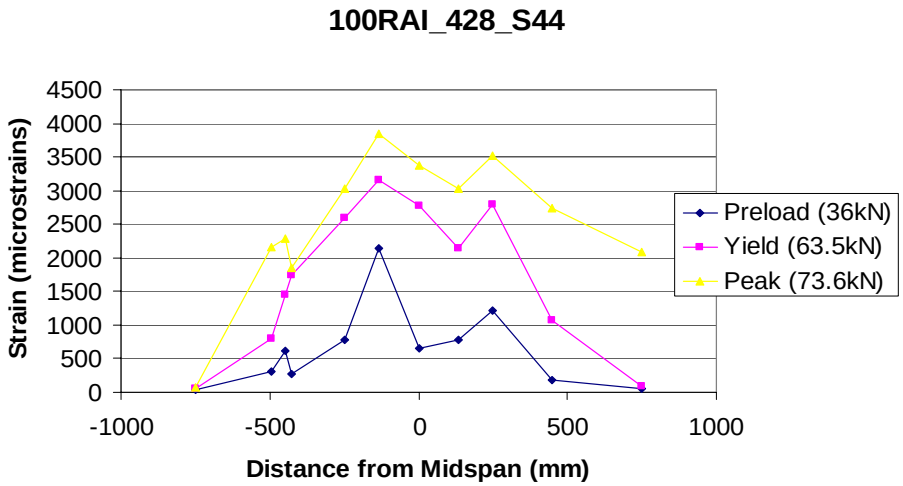
100RAI_428_S44
Strain (microstrains)
Distance from Midspan (mm)
0
500
1000
1500
2000
2500
3000
3500
4000
4500
-1000
-500
0
500
1000
Preload (36kN)
Yield (63.5kN)
Peak (73.6kN)

544(P36)
100RAT.-428.544

Specimen 41: 100mm x 150mm rectangular disbond inserted in the interface between FRP layers and in the adhesive located 185mm from the midspan tested 10/26/2005 (100RAI_185_S41_2)

Specimen 41 was manufactured with a defect consisting of one rectangular disbond located between FRP layers (interlaminar) and one in the adhesive interface with a centroidal location 185mm away from the midspan of the beam. The dimensions of the manufactured disbond were 100mm length by 150mm width. This was the second beam tested with this defect configuration. The beam was, precracked using the 35.6 kN preload level before the application of FRP. Despite debonding through the adhesive resin interface, the specimen maximum load of 87.5kN was significantly greater than the previous two specimens (S44 and S45). Debonding propagated to the left initiating from the midspan.

Beam Characteristic	Value
Test Date	10/26/05
Rehab Date (number)	9/20/05 (6)
Concrete Cast Date (number)	2/8/05 (2)
Time from Rehab to Test	36 days
Maximum Load	87.47 kN
Displacement at Maximum Load	14.30 mm
Measured Steel Yield	2319 με
Load at Steel Yield	67.84 kN
Displacement at Steel Yield	7.45 mm
FRP Strain at Steel Yield	4343 με
FRP Strain at Debonding (Location)	7201 (FD2) με
FRP Midspan Strain at Debonding	6198 με
Debonding Direction	Left
Failure Mode	Resin Interface

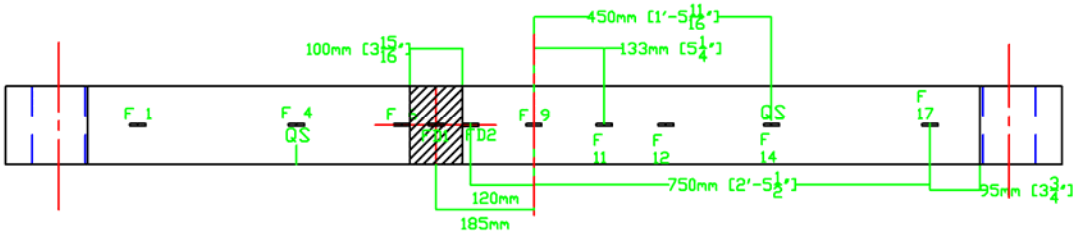

Load (kN)	Crack Width (mm)	Notes
0.00	<0.1	
36.00	<0.1	Some new cracking near the defect
2.40	<0.1	
75.00		Seems unstable, so didn't approach for observation until unloading. Local debonding occurred as low as 47kN.
2.40	0.1	Local debonding near the defect in the direction of the midspan (to the right). Debonding is about 50mm long. Largest cw is in this region.
87.90		Local debonding slowly propagated for a long time. Final debonding occurred from the midspan through the defect to the left end of the FRP. Failure is largely through the adhesive interface, but much more concrete is left on the FRP than in S44 or S45.

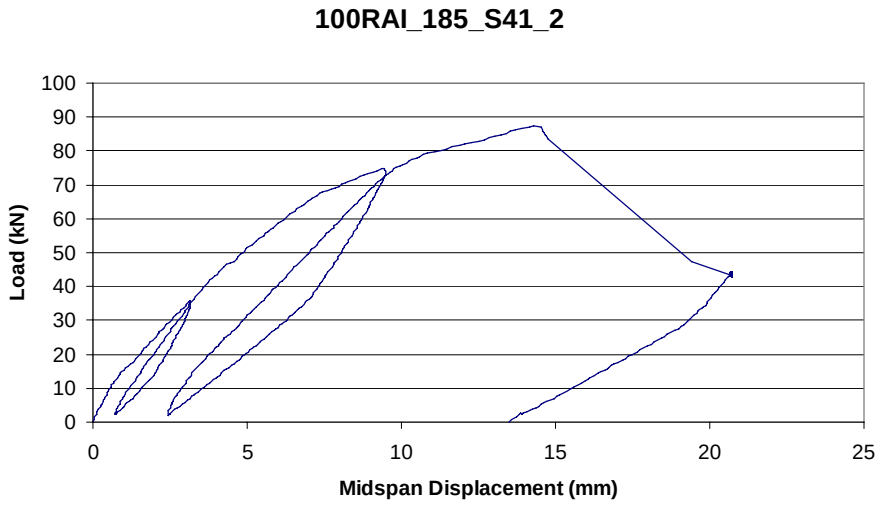
100RAI_185_S41_2
Load (kN)
Midspan Displacement (mm)
0
10
20
30
40
50
60
70
80
90
100
0
5
10
15
20
25

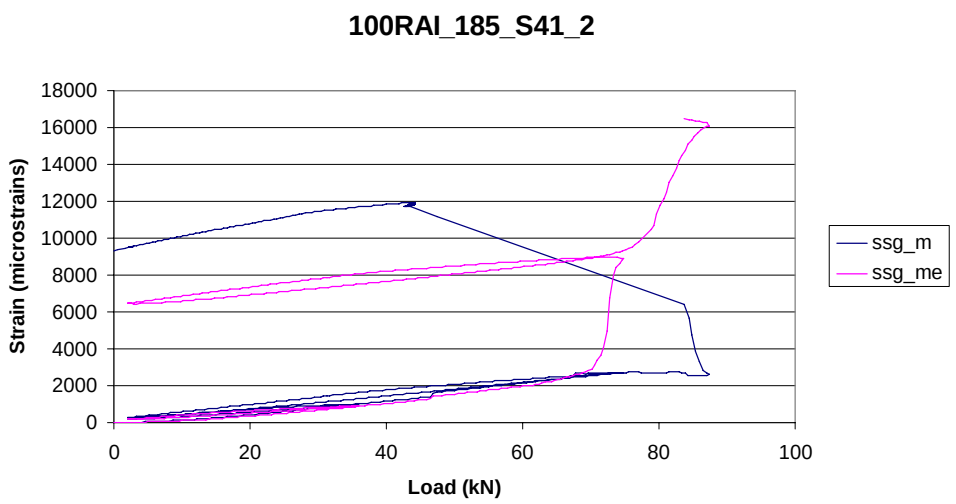
100RAI_185_S41_2
Strain (microstrains)
Load (kN)
0
2000
4000
6000
8000
10000
12000
14000
16000
18000
0
20
40
60
80
100
ssg_m
ssg_me

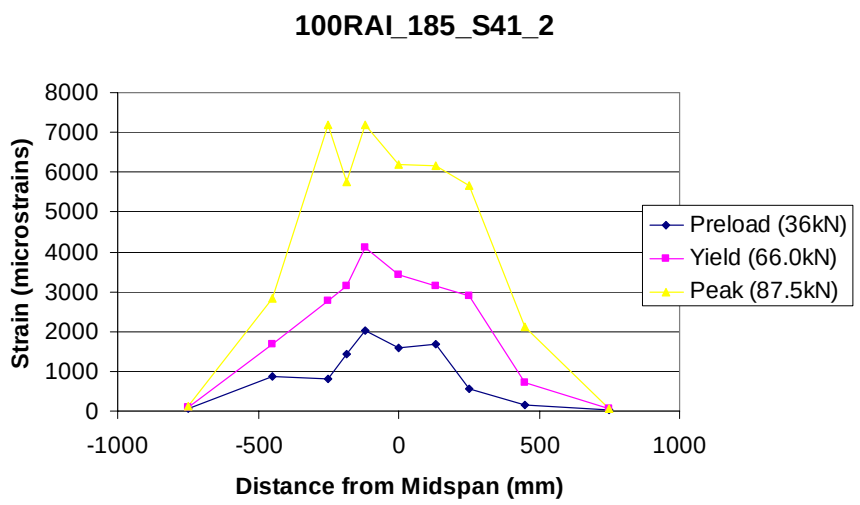
100RAI_185_S41_2
Strain (microstrains)
Distance from Midspan (mm)
0
1000
2000
3000
4000
5000
6000
7000
8000
-1000
-500
0
500
1000
Preload (36kN)
Yield (66.0kN)
Peak (87.5kN)

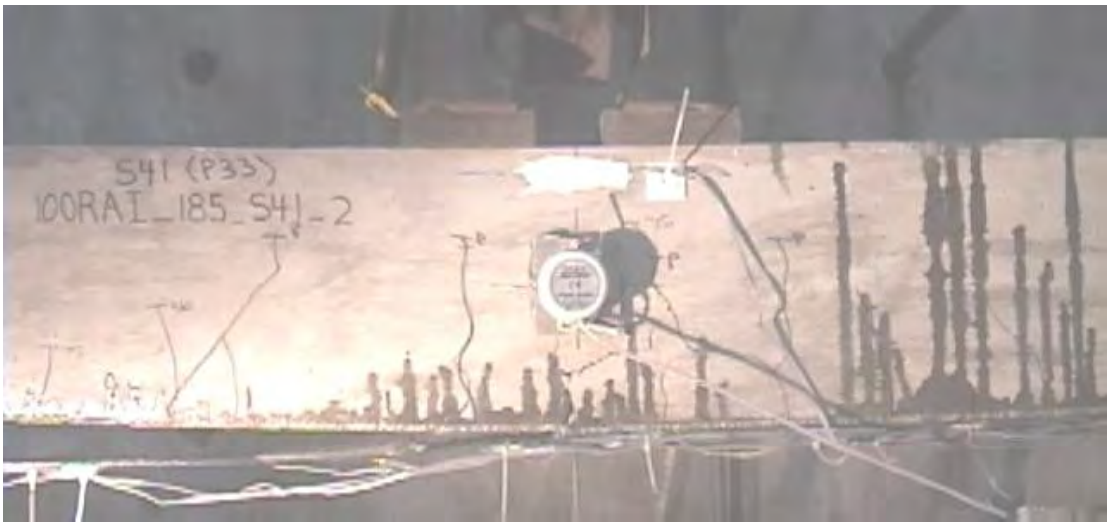
S41 (P33)
100RAI_185_S41-2

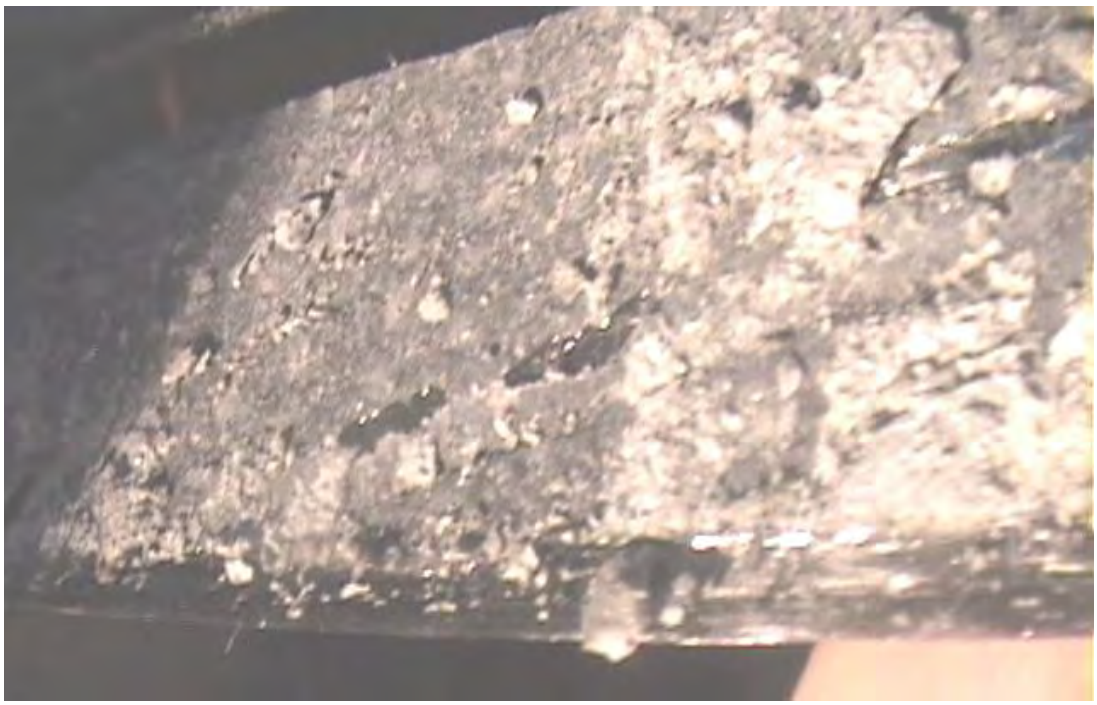

Specimen 39: 100mm x 150mm rectangular disbond inserted in the interface between FRP layers located 185mm from the midspan tested 10/28/2005 (100RI_185_S39_2)

Specimen 39 was manufactured with a defect consisting of a rectangular disbond located between FRP layers (interlaminar) with a centroidal location 185mm away from the midspan of the beam. The dimensions of the manufactured disbond were 100mm length by 150mm width. This was the second specimen investigated with this defect orientation. The beam was, precracked using the 35.6 kN preload level before the application of FRP. Debonding occurred from the left load point, through the defect to the left end of the FRP. The maximum load was 83.97kN, which is a fairly weak specimen, but not surprising because the debonding failure mode was through the resin interface.

Beam Characteristic	Value
Test Date	10/28/05
Rehab Date (number)	9/20/05 (6)
Concrete Cast Date (number)	2/8/05 (2)
Time from Rehab to Test	38 days
Maximum Load Held	83.97 kN
Displacement at Maximum Load	12.87 mm
Measured Steel Yield	2393 με
Load at Steel Yield	62.10 kN
Displacement at Steel Yield	6.59 mm
FRP Strain at Steel Yield	3413 με
FRP Strain at Debonding (Location)	6224 (FD2) με
FRP Midspan Strain at Debonding	5851 με
Debonding Direction	Left
Failure Mode	Resin Interface

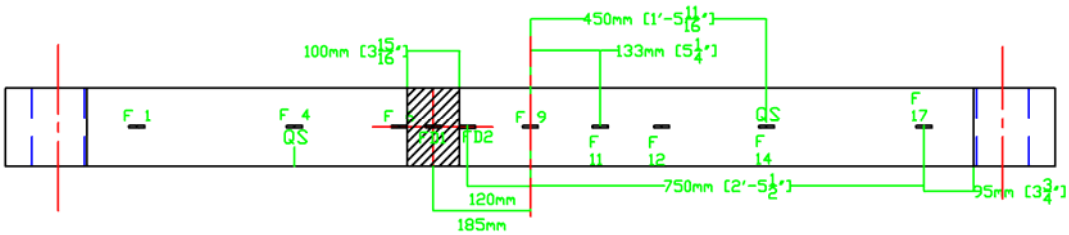

Load (kN)	Crack Width (mm)	Notes
0.00	<0.1	
36.10	~0.05	Typical reopening of cracks. No apparent damage.
2.50	<0.1	
75.20	0.2	Extensive new cracking. Some slight local debonding on the right side. Many new diagonal cracks on the right.
2.40	0.1	
84.20		Final debonding occurred from the left load point to the left end of the FRP (through the defect). Failure is still shallow, but the majority is through the concrete. Only about 5% to 10% of failure is through the resin.

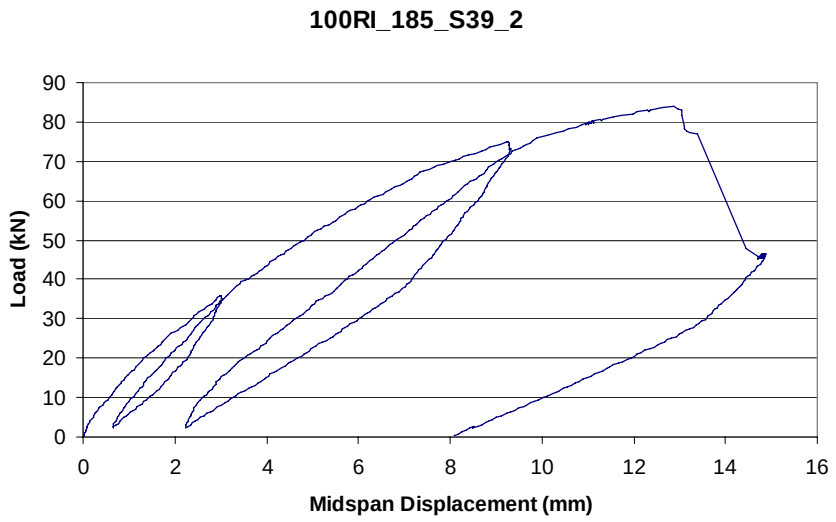
100RI_185_S39_2
Load (kN)
Midspan Displacement (mm)
0
10
20
30
40
50
60
70
80
90
0
2
4
6
8
10
12
14
16

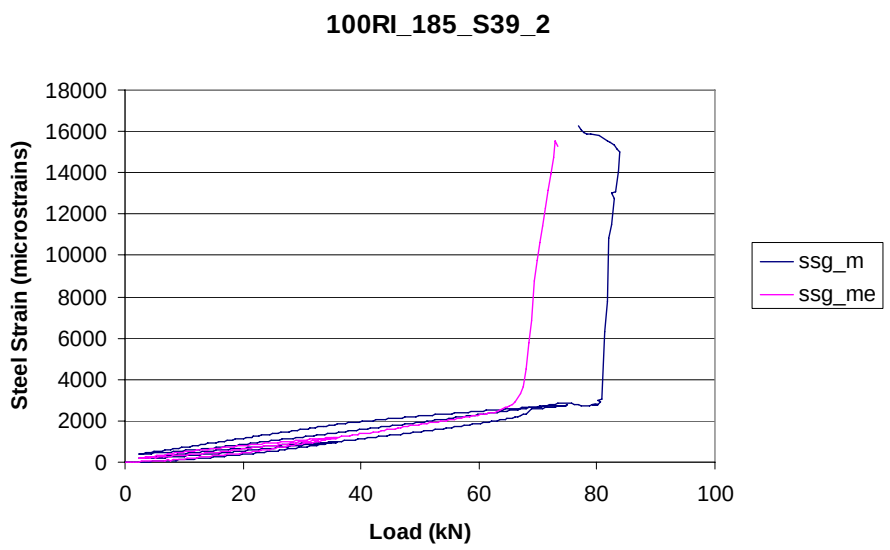
100RI_185_S39_2
Steel Strain (microstrains)
Load (kN)
0
2000
4000
6000
8000
10000
12000
14000
16000
18000
0
20
40
60
80
100
ssg_m
ssg_me

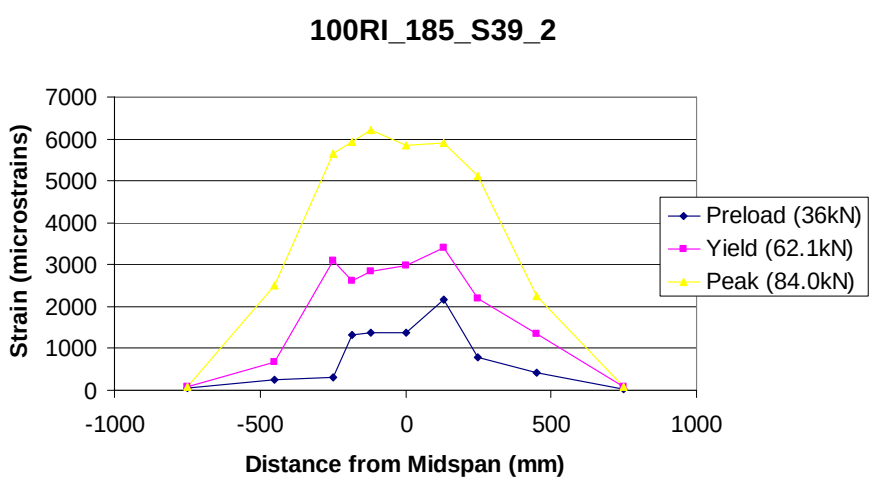
100RI_185_S39_2
Strain (microstrains)
Distance from Midspan (mm)
0
1000
2000
3000
4000
5000
6000
7000
-1000
-500
0
500
1000
Preload (36kN)
Yield (62.1kN)
Peak (84.0kN)

Specimen 55: 100mm x 150mm rectangular disbond inserted in the adhesive interface, submerged in water for seven days, located 185mm from the midspan, tested 11/2/2005 (100RS7_185__1.0cw_S55)

Specimen 55 was preloaded such that a residual crack width of 1.0mm resulted (see section 2.8 for details). No steel strain data is available for final testing of this specimen due to the damage sustained to the strain gauges during preloading. This specimen consisted of a combination of three different defects in an effort to assess their cumulative effects: 1) excessive preload cracking to a 1.0mm residual maximum crack width; 2) a 100mm long by 150mm wide unbonded rectangular region in the adhesive interface located 185mm from the midspan; and 3) after initial curing the tension face was submerged in one inch of water for a period of seven days. Given the large amount of damage that was manufactured into this beam, it performed quite well

failing with a maximum load of 87.3kN at a midspan displacement of 15.0mm. The failure mode was ideal being “deep concrete, steel”. Debonding occurred to the left propagating from near the right edge of the defect where a large diagonal crack opened prior to failure.

Beam Characteristic	Value
Test Date	11/2/05
Rehab Date (number)	10/21/05 (7)
Concrete Cast Date (number)	2/8/05 (2)
Time from Rehab to Test	12 days
Maximum Load Held	87.28 kN
Displacement at Maximum Load	15.00 mm
Measured Steel Yield	2214 με
Load at Steel Yield	62.90 kN
Displacement at Steel Yield	6.39 mm
FRP Strain at Steel Yield	3301 με
FRP Strain at Debonding (Location)	7544 (FD2) με
FRP Midspan Strain at Debonding	5809 με
Debonding Direction	Left
Failure Mode	Deep Concrete, Steel

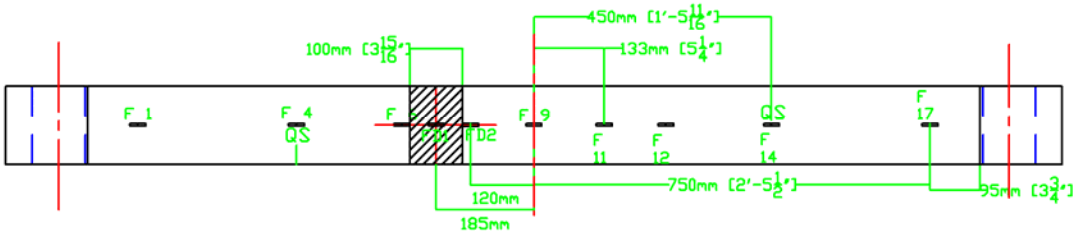

Load (kN)	Crack Width (mm)	Notes
0.00	1.8	
36.10	2.4	The largest crack reopened quite a bit more than the others.
2.50	1.9	
75.20	2.5	Local debonding from the left edge of the defect propagating about 25mm toward the left end of the FRP.
2.40	2.3	
90.10	2.7	The largest FRP strain is in C50_f (placed 50mm to the left of the midspan across the largest crack from preloading).
2.50	2.3	
		Global debonding occurred before the beam reached the 90kN load obtained in the previous load cycle. Final debonding occurred when a huge diagonal crack opened near the right edge of the disbond, peeling the FRP. Good failure through the concrete.

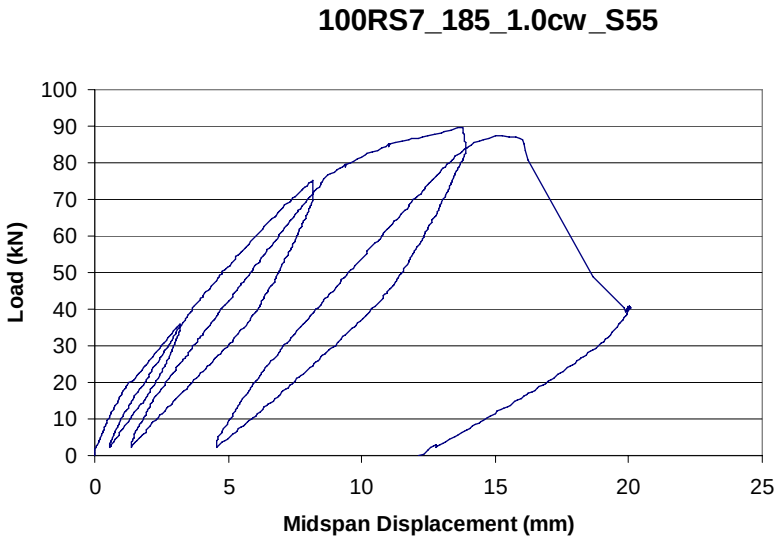

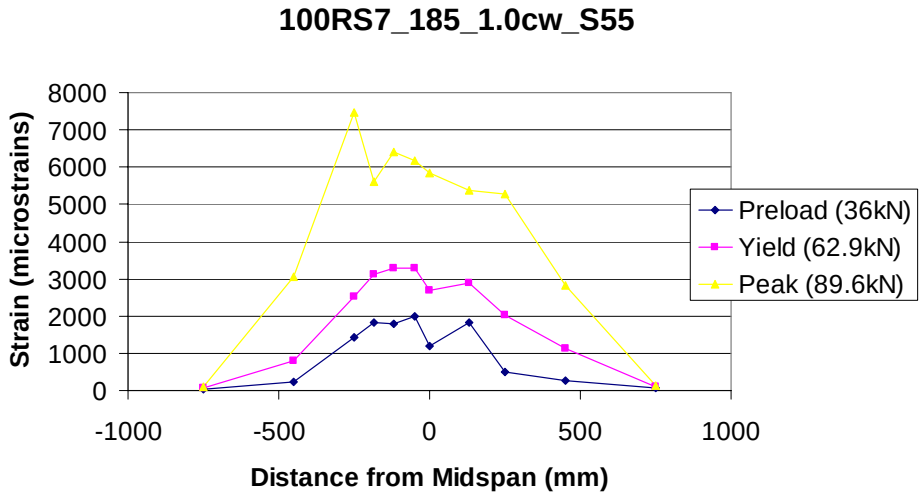

Specimen 61: 200mm by 150mm rectangular disbond inserted in the adhesive interface 185mm from the midspan tested 11/2/2005 (200R_185_S61_2)

Specimen 61 was manufactured with a defect consisting of a rectangular disbond with a centroid located 185mm away from the midspan of the beam. The

dimensions of the manufactured disbond were 200mm length by 150mm width (the full width of the beam). This is the second largest disbond that was tested in the laboratory. Specimen 61 is the second beam tested with this defect configuration. The beam was, precracked using the 35.6 kN preload level before the application of FRP. At the peak of the 75kN load cycle, extensive new cracking was noted including a large shear crack on the right side of the beam (away from the defect), despite no sign of local debonding. At the peak of the 90kN load cycle some local debonding was noted. The specimen failed at 90.1kN and 13.3mm midspan displacement while loading on the 105kN load cycle. The debonding occurred to the left from the defect location where another shear crack had opened near the right edge of the disbond. The failure mode of debonding through a thin concrete bondline was typical given the specimen's ultimate load.

Beam Characteristic	**Value**
Test Date	11/2/05
Rehab Date (number)	10/21/05 (7)
Concrete Cast Date (number)	2/8/05 (2)
Time from Rehab to Test	12 days
Maximum Load Held	90.05 kN
Displacement at Maximum Load	13.30 mm
Measured Steel Yield	2227 με
Load at Steel Yield	65.30 kN
Displacement at Steel Yield	6.93 mm
FRP Strain at Steel Yield	3167 με
FRP Strain at Debonding (Location)	6684 (FD1) με
FRP Midspan Strain at Debonding	6091 με
Debonding Direction	Left
Failure Mode	Thin Concrete Bondline

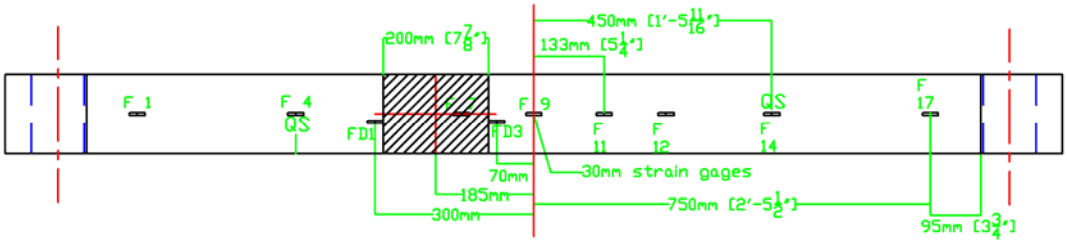

Load (kN)	Crack Width (mm)	Notes
0.00	<0.1	
36.20	<0.1	Typical crack reopening.
2.60	<0.1	
75.10	0.4	Extensive new cracking. A large shear crack has opened near the right side of the defect. No apparent local debonding yet.
2.50	0.2	
90.30	0.7	Crackling and local debonding.
2.50	0.4	
90.30		Just reached previous peak when macro-debonding occurred. Good failure through the concrete. Debonding initiated at the defect propagating to the left end of the FRP.

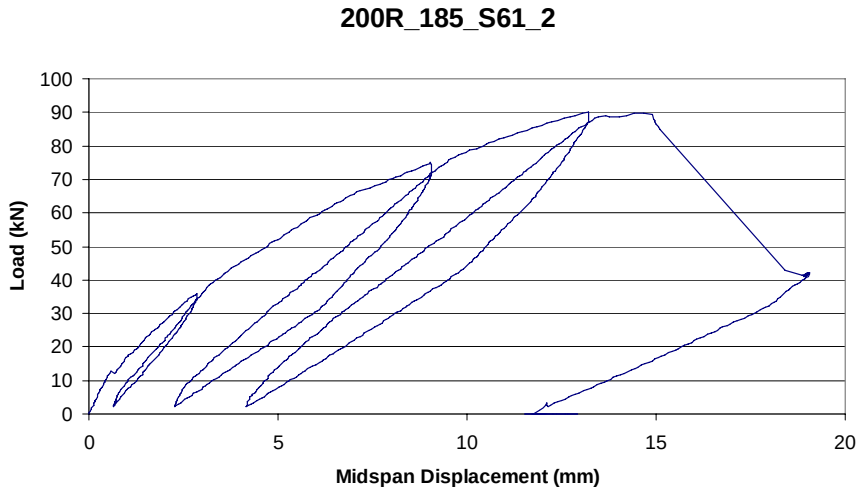
200R_185_S61_2
Load (kN)
Midspan Displacement (mm)
0
10
20
30
40
50
60
70
80
90
100
0
5
10
15
20

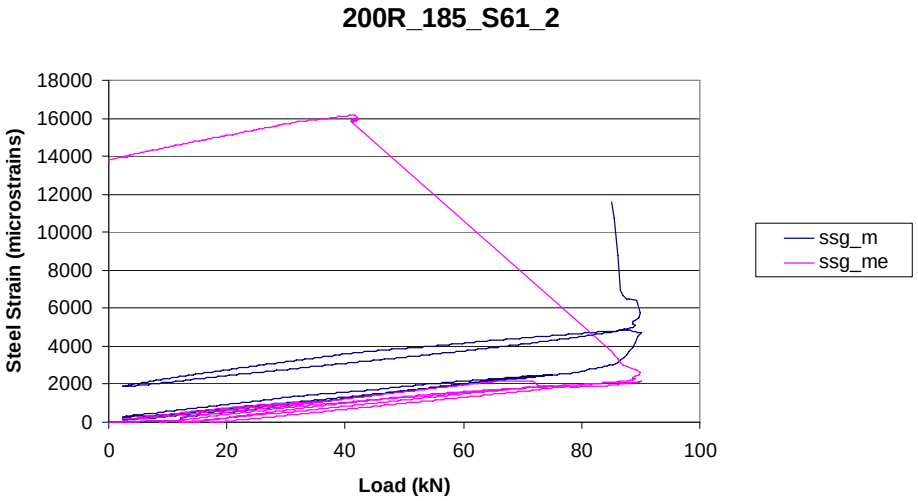
200R_185_S61_2
Steel Strain (microstrains)
Load (kN)
0
2000
4000
6000
8000
10000
12000
14000
16000
18000
0
20
40
60
80
100
ssg_m
ssg_me

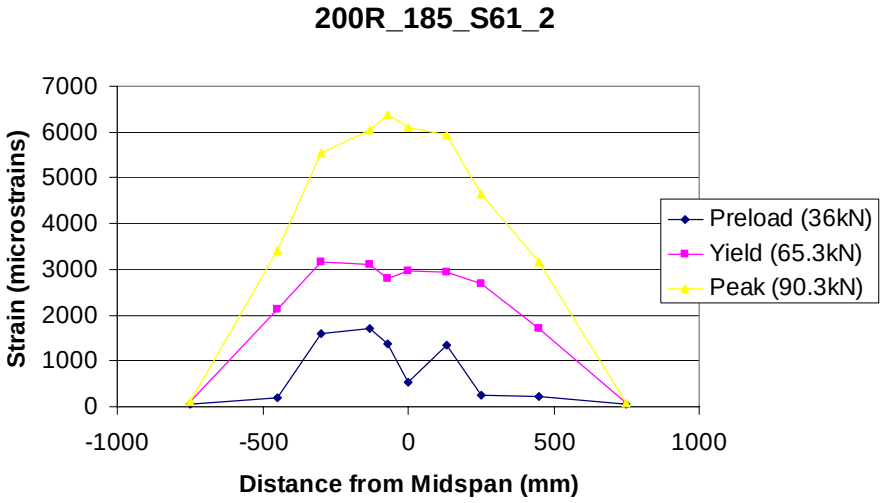
200R_185_S61_2
Strain (microstrains)
Distance from Midspan (mm)
0
1000
2000
3000
4000
5000
6000
7000
-1000
-500
0
500
1000
Preload (36kN)
Yield (65.3kN)
Peak (90.3kN)

Specimen 46: 50mm x 150mm rectangular disbond inserted in the adhesive interface 185mm from the midspan tested 11/4/2005 (50R_185_S46_3)

Specimen 46 was manufactured with a defect consisting of a rectangular disbond with a centroid located 185mm away from the midspan of the beam. The dimensions of the manufactured disbond were 50mm length by 150mm width. This specimen was the third manufactured with this defect configuration. The beam was, precracked using the 35.6 kN preload level before the application of FRP. Final debonding initiated from a diagonal shear crack located just outside the right loading point and propagated to the right. The failure load was high at 93.7kN and, as expected from this load, the failure mode observed was debonding by “deep concrete, steel”.

Beam Characteristic	Value
Test Date	11/4/2005
Rehab Date (number)	10/21/2005 (7)
Concrete Cast Date (number)	2/8/2005 (2)
Time from Rehab to Test	14 days
Maximum Load	93.67 kN
Displacement at Maximum Load	13.13 mm
Steel Strain at Yield	2387 με
Load at Steel Yield	69.2 kN
Displacement at Steel Yield	7.61 mm
FRP Strain at Steel Yield	3708 με
FRP Strain at Debonding (Location)	7180 (F7) με
FRP Midspan Strain at Debonding	6683 με
Debonding Direction	Right
Failure Mode	Deep Concrete, Steel

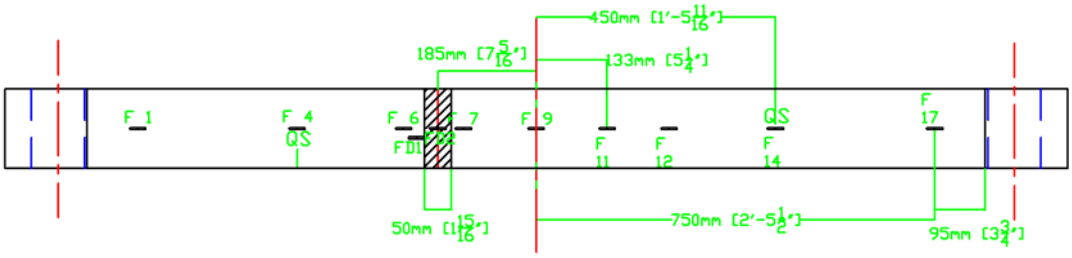

Load (kN)	Crack Width (mm)	Notes
0.00	0	
36.40	< 0.1	Typical crack reopening
2.50	<0.1	
75.00	0.2	Localized debonding occurring on each side of the defect (~40-50mm debond). Lost s_sg_m (midspan strain gage)
2.50	<0.1	
88.10		Debonded on the left side (defect side) from the defect location in the least energetic fashion seen yet.

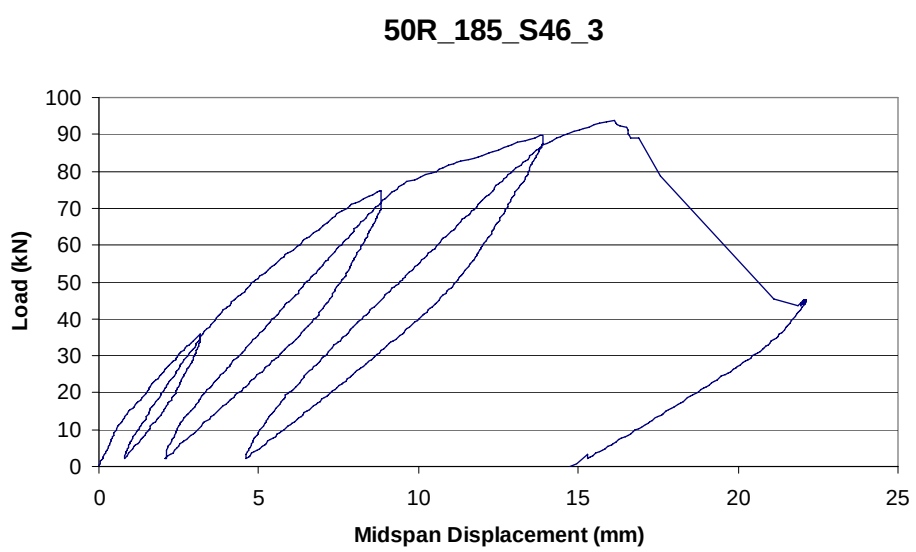

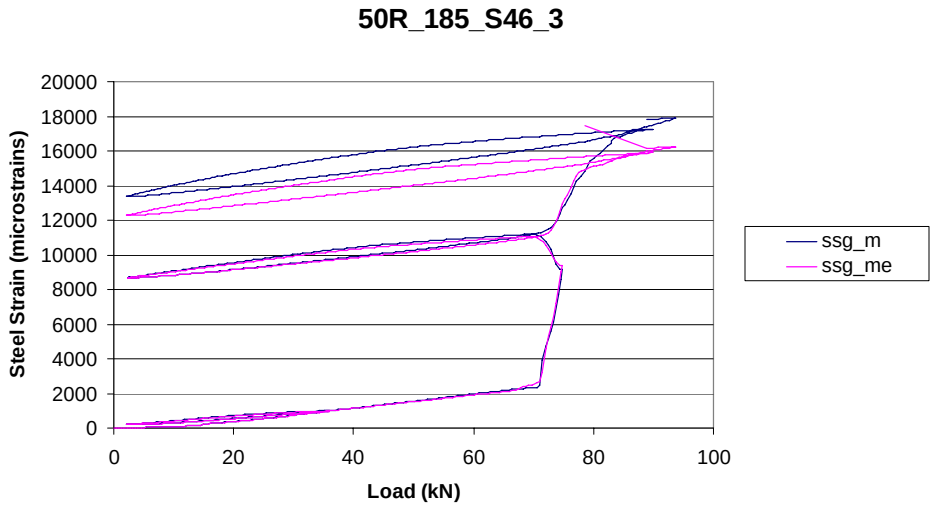
50R_185_S46_3
Steel Strain (microstrains)
20000
18000
16000
14000
12000
10000
8000
6000
4000
2000
0
0
20
40
60
80
100
Load (kN)
ssg_m
ssg_me

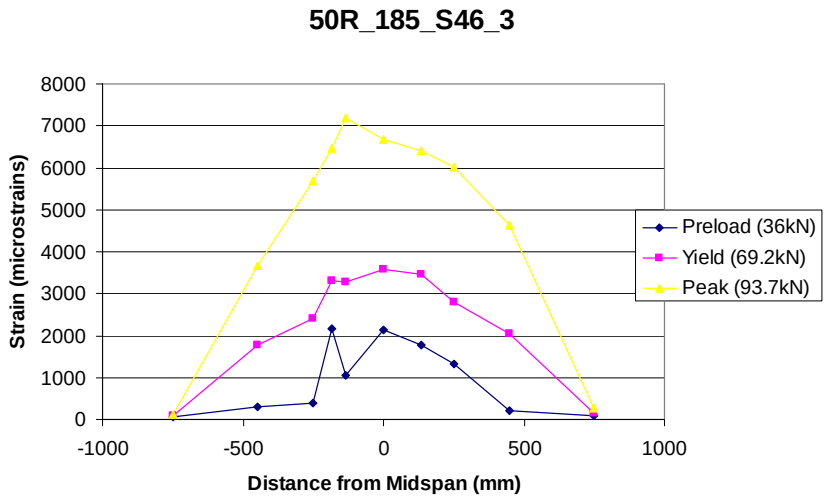
50R_185_S46_3
Strain (microstrains)
8000
7000
6000
5000
4000
3000
2000
1000
0
-1000
-500
0
500
1000
Distance from Midspan (mm)
Preload (36kN)
Yield (69.2kN)
Peak (93.7kN)

S46(P38)
50R_185_S46_3

Specimen 53: 100mm x 150mm rectangular disbond inserted in the adhesive interface 185mm from the midspan tested 11/4/2005 (100R_185_1.0cw_S53)

Specimen 53 was preloaded such that a 1.0mm approximate residual crack width remained (see section 2.8 for details). This specimen consisted of two distinct defect types: 1) excessive preload cracking to 1.0mm; and 2) a 100mm by 150mm rectangular disbond in the adhesive interface located 185mm from the midspan. Debonding occurred to the left originating from the midspan. The failure was through a thick concrete bondline resulting in a strong specimen with reaching a maximum load of 92.5kN at a typical midspan displacement of 15.8mm.

Beam Characteristic	Value
Test Date	11/4/2005
Rehab Date (number)	10/21/2005 (7)
Concrete Cast Date (number)	2/8/2005 (2)
Time from Rehab to Test	14 days
Maximum Load Held	92.49 kN
Displacement at Maximum Load	15.78 mm
Measured Steel Yield	2529 με
Load at Steel Yield	76.07 kN
Displacement at Steel Yield	7.89 mm
FRP Strain at Steel Yield	4723 με
FRP Strain at Debonding (Location)	7095 (FD2) με
FRP Midspan Strain at Debonding	6148 με
Debonding Direction	Left
Failure Mode	Thick Concrete Bondline

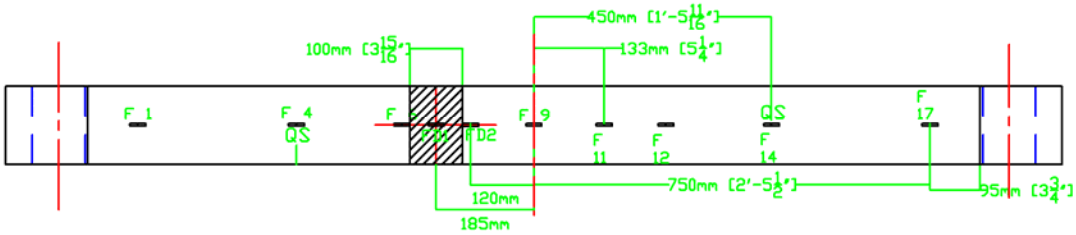

Load (kN)	Crack Width (mm)	Notes
0.00	1.2	
36.10	1.8	Typical concrete crack reopening
2.40	1.4	
75.40	1.8	Extensive new cracking. No local debonding yet.
2.50	1.6	
90.10	1.8	About 25mm of local debonding to the left of the midspan. Approximately 35mm of local debonding to the right of the defect.
2.50	1.6	
93.00		Good failure to the left through the defect. Sheared through the concrete.

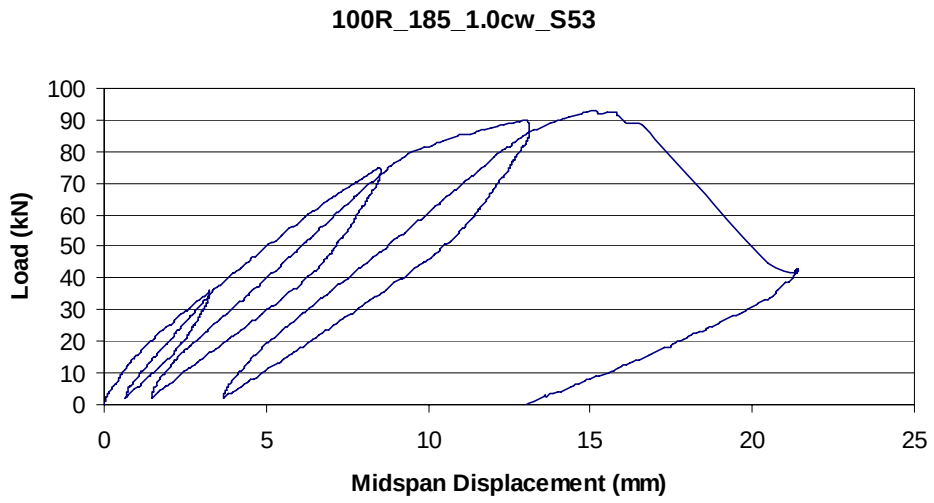
100R_185_1.0cw_S53
Load (kN)
Midspan Displacement (mm)
0
10
20
30
40
50
60
70
80
90
100
0
5
10
15
20
25

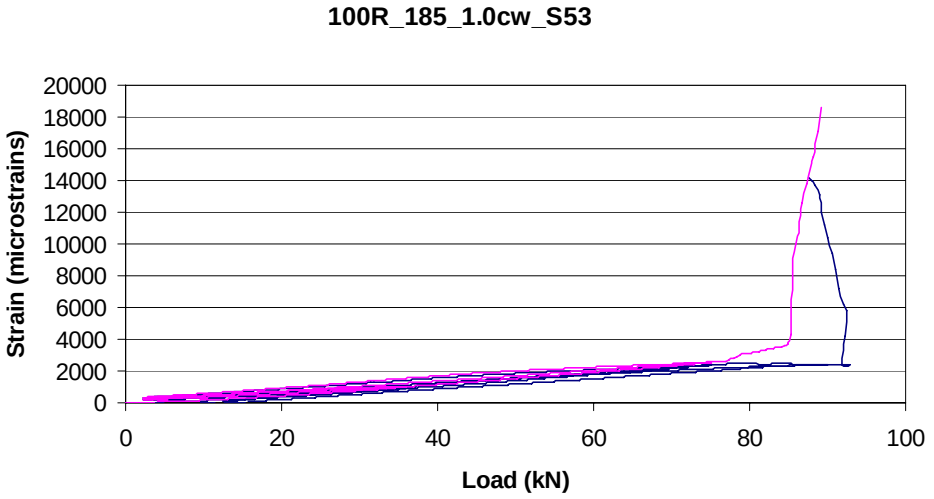
100R_185_1.0cw_S53
Strain (microstrains)
Load (kN)
0
2000
4000
6000
8000
10000
12000
14000
16000
18000
20000
0
20
40
60
80
100

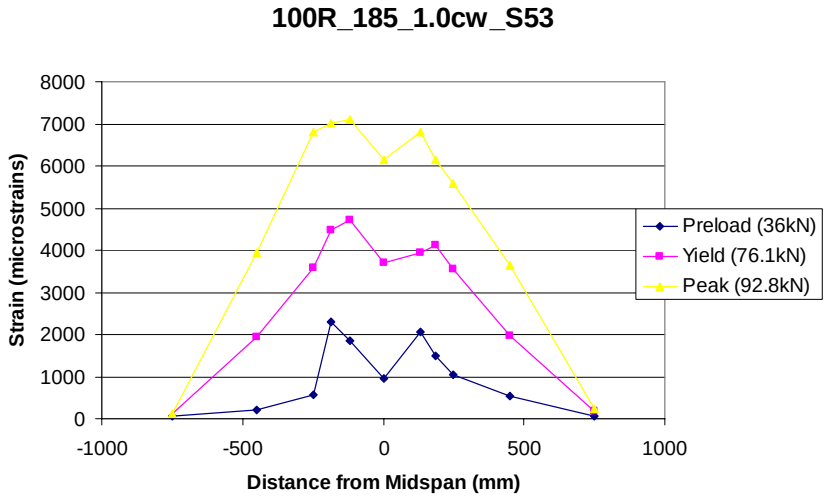
100R_185_1.0cw_S53
Strain (microstrains)
Distance from Midspan (mm)
0
1000
2000
3000
4000
5000
6000
7000
8000
-1000
-500
0
500
1000
Preload (36kN)
Yield (76.1kN)
Peak (92.8kN)

Specimen 52: Specimen preloaded to a 1.0mm residual maximum crack width 11/7/2005 (1.0cw_S52)

This specimen was preloaded such that the residual crack width after the beam was unloaded was approximately 1.0mm. The midspan displacement necessary to yield this residual crack width was determined during preloading of specimen 48 where the beam was cycled to various preload displacements and then the cracks were measured after the load was released. The displacement necessary to achieve this residual crack width was also determined from FEA model. No unbonded regions were manufactured into this specimen. The large maximum crack width is the only defect. Final debonding occurred to the left initiating under the left load point with a “deep concrete, steel” failure mode, as can be seen in the photo below.

In addition to the 14 gauge layout used for strain gauging the FRP, two additional gauges were utilized to investigate the effect of the crack on the FRP strain. FRP strain gage C185f was a strain gauge added across the largest crack due to preloading. C185n was a strain gage added at the corresponding location on the opposite side of the midspan, away from a concrete crack. The increased strain due to the crack can be seen in the FRP strain profile.

Beam Characteristic	Value
Test Date	11/7/2005
Rehab Date (number)	10/21/2005 (7)
Concrete Cast Date (number)	2/8/2005 (2)
Time from Rehab to Test	17 days
Maximum Load Held	97.32 kN
Displacement at Maximum Load	14.03 mm
Measured Steel Yield	no data
Load at Steel Yield	80.42 kN
Displacement at Steel Yield	8.50 mm
FRP Strain at Steel Yield	4870 με
FRP Strain at Debonding (Location)	7742 (F9) με
FRP Midspan Strain at Debonding	7742 με
Debonding Direction	Left
Failure Mode	Deep Concrete, Steel

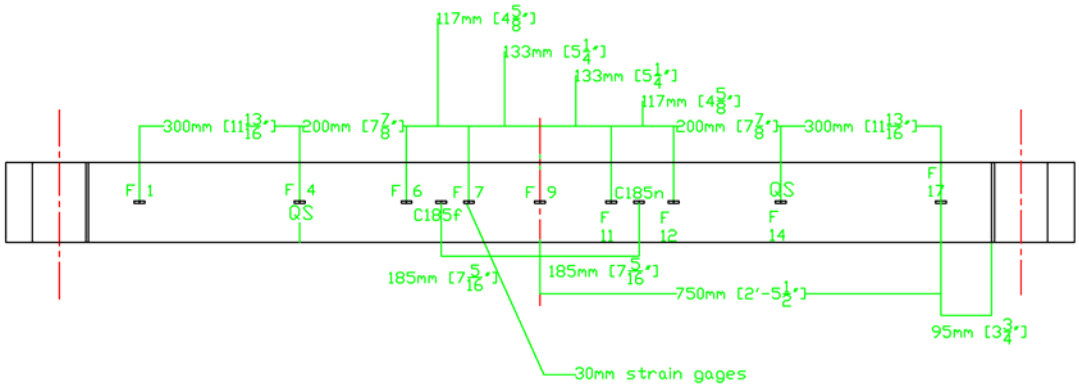

Load (kN)	Crack Width (mm)	Notes
0.00	1.4	Both midspan steel strain gauges have been broken.
36.10	1.5	C185f is reading greater than C185n as expected.
2.40	1.4	
75.00	1.6	Several new cracks.
2.50	1.5	No local debonding yet.
90.00	1.7	
2.50	1.5	Approximately 50mm of local debonding centering about a pre-existing (from preload) crack just to the left of the left edge of the load point.
97.60		Macro debonding from previously mentioned debond to the left side of the beam. Tore out a large chunk of concrete. Good failure through the concrete. Final debonding was not near the location of the largest flexural crack.

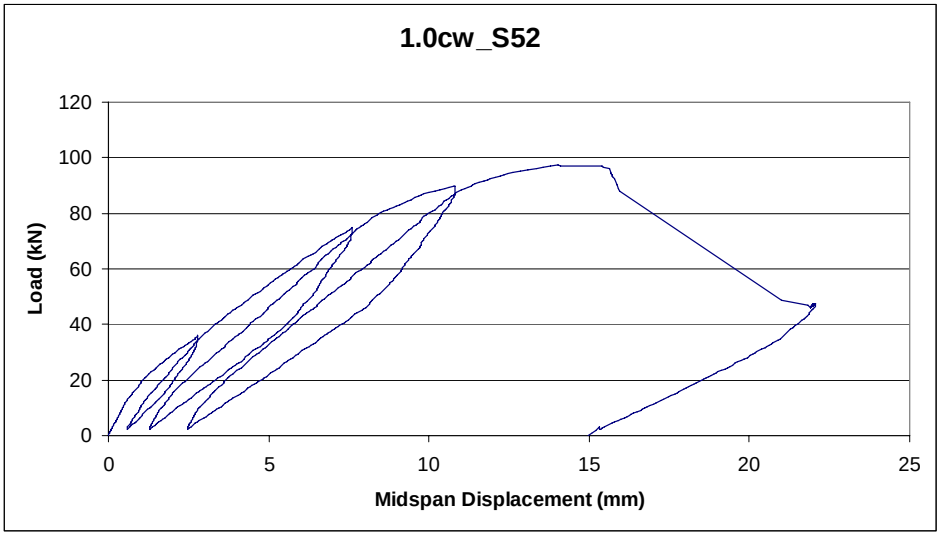
1.0cw_S52
Load (kN)
Midspan Displacement (mm)
0
20
40
60
80
100
120
0
5
10
15
20
25

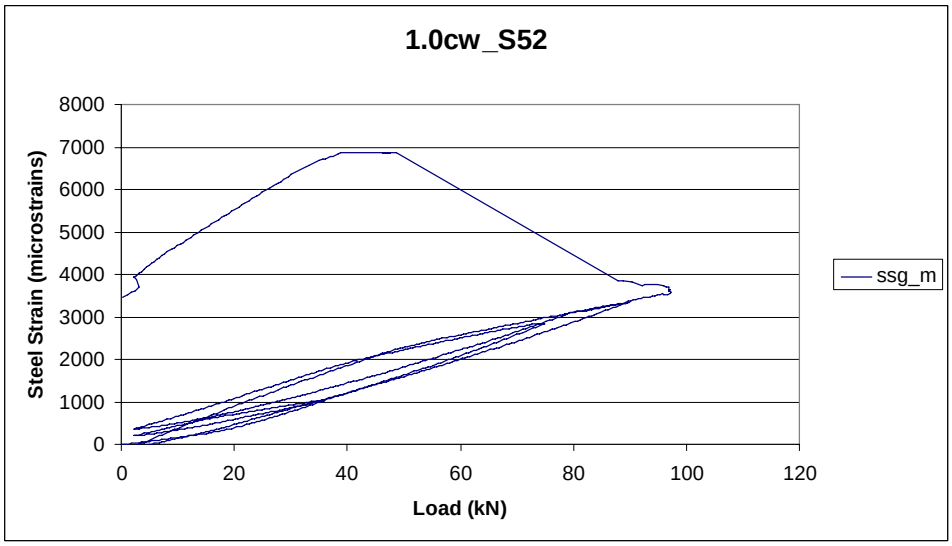
1.0cw_S52
Steel Strain (microstrains)
Load (kN)
ssg_m
0
1000
2000
3000
4000
5000
6000
7000
8000
0
20
40
60
80
100
120

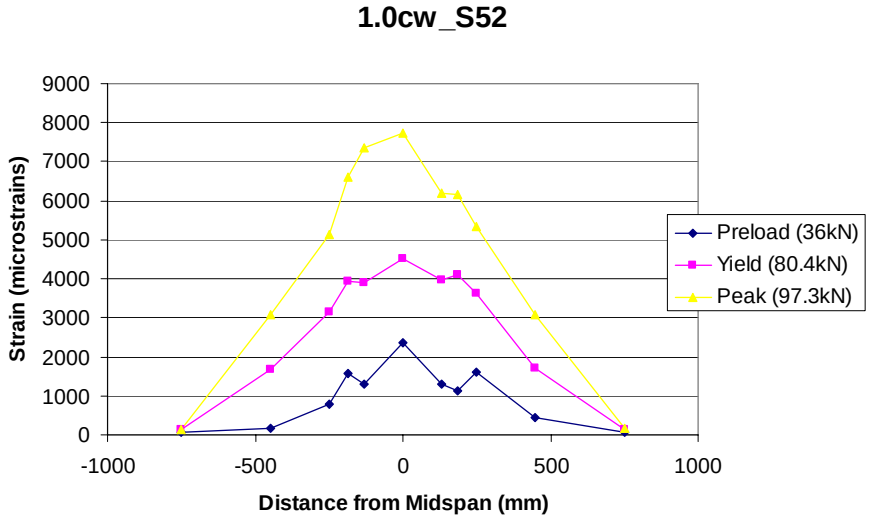
1.0cw_S52
Strain (microstrains)
Distance from Midspan (mm)
Preload (36kN)
Yield (80.4kN)
Peak (97.3kN)
0
1000
2000
3000
4000
5000
6000
7000
8000
9000
-1000
-500
0
500
1000

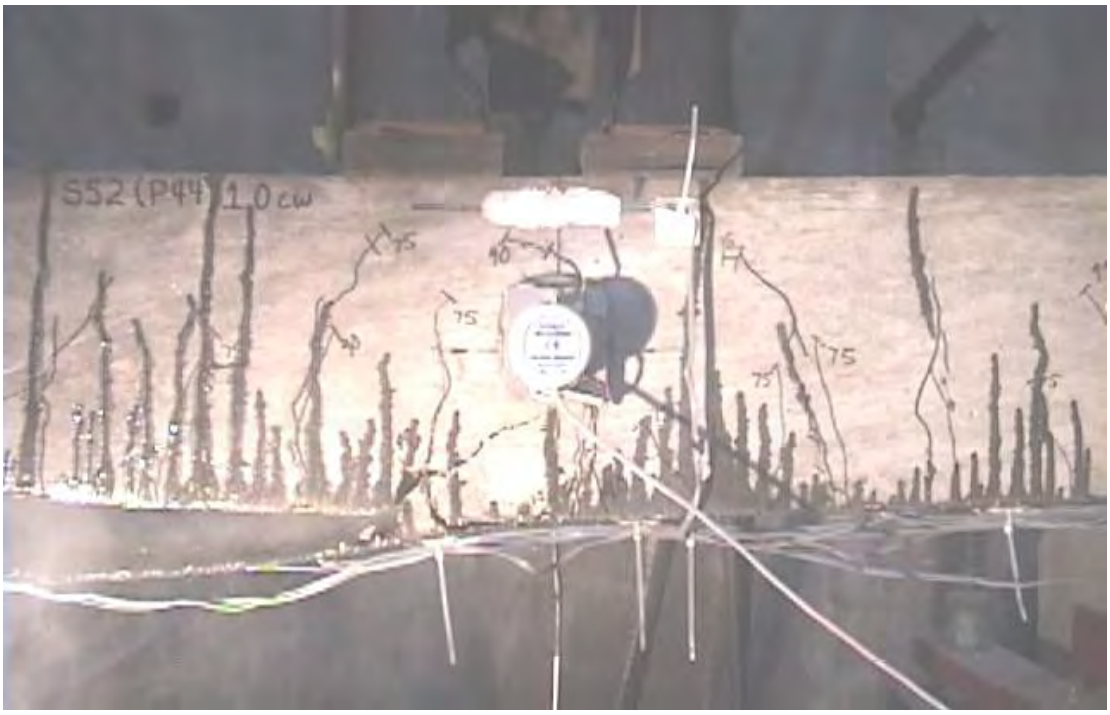
S52 (P44) 1.0 cw

Specimen 51: Specimen preloaded to a 0.6mm residual maximum crack width 11/8/2005 (0.6cw_S51)

This specimen was preloaded such that the residual crack width after the beam was unloaded was approximately 0.6mm. The midspan displacement necessary to yield this residual crack width was determined during preloading of 48 where the beam was cycled to various preload displacements and then the cracks were measured after the load was released. Like specimen 52 tested previously, no unbonded regions were manufactured into this specimen. The relatively large maximum residual crack width is the only defect. Final debonding occurred to the left initiating under the left load point with a "deep concrete, steel" failure mode, as can be seen in the photo below. Despite having a very large residual crack width from preloading, the peak load was 99.4kN at a large displacement of 18.8mm and the failure mode was deep concrete, steel debonding.

Beam Characteristic	Value
Test Date	11/8/2005
Rehab Date (number)	10/21/2005 (7)
Concrete Cast Date (number)	2/8/2005 (2)
Time from Rehab to Test	18 days
Maximum Load Held	99.35 kN
Displacement at Maximum Load	18.77 mm
Measured Steel Yield	2744 με
Load at Steel Yield	79.55 kN
Displacement at Steel Yield	10.10 mm
FRP Strain at Steel Yield	4870 με
FRP Strain at Debonding (Location)	8343 (F7) με
FRP Midspan Strain at Debonding	7616 με
Debonding Direction	Left
Failure Mode	Deep Concrete, Steel

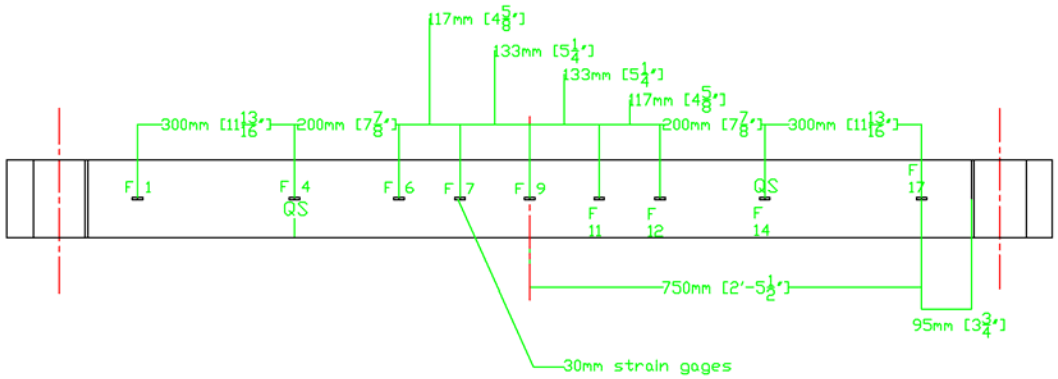

Load (kN)	Crack Width (mm)	Notes
0.00	0.5	
36.00	0.6	Typical crack reopening. Some slight new cracking
2.50	0.5	
75.00	0.6	Many new cracks. No local debonding yet.
2.50	0.5	
90.10	0.8	~150mm long section of local debonding through the midspan between the two largest flexural crack from the preload.
2.50	0.6	
99.35		Very strong rehab. Final debonding tore a 300mm long section of concrete down to the rebar from the midspan toward the left end of the FRP. After 300mm it migrated to the interface, but still failed deep in the concrete (no adhesive failure).

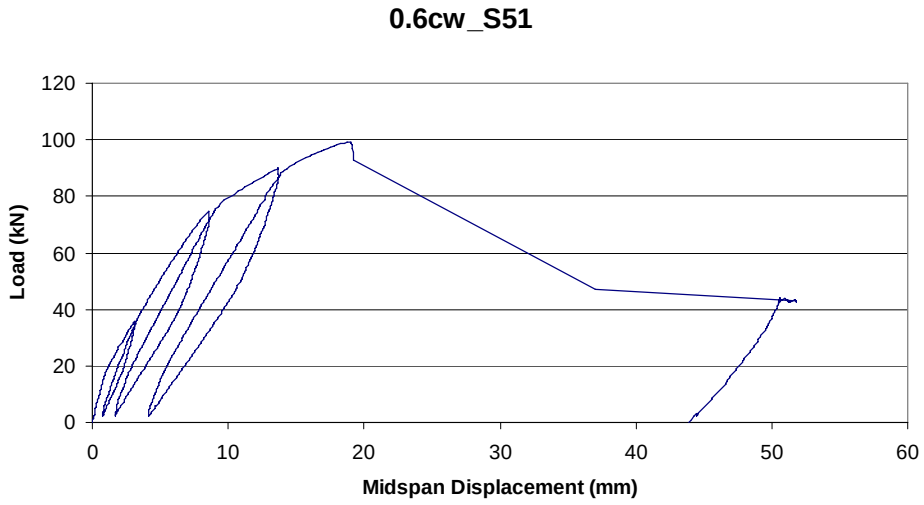
0.6cw_S51
Load (kN)
Midspan Displacement (mm)
0
20
40
60
80
100
120
0
10
20
30
40
50
60

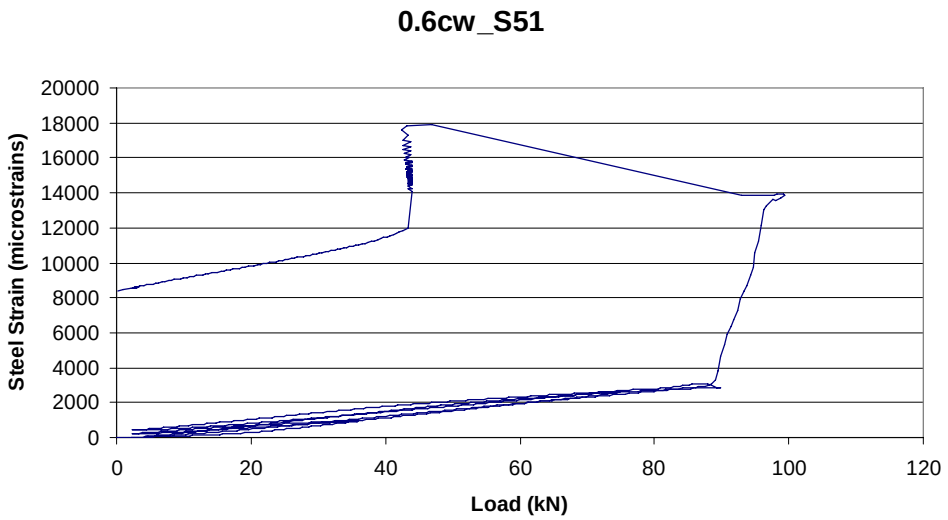
0.6cw_S51
Steel Strain (microstrains)
Load (kN)
0
2000
4000
6000
8000
10000
12000
14000
16000
18000
20000
0
20
40
60
80
100
120

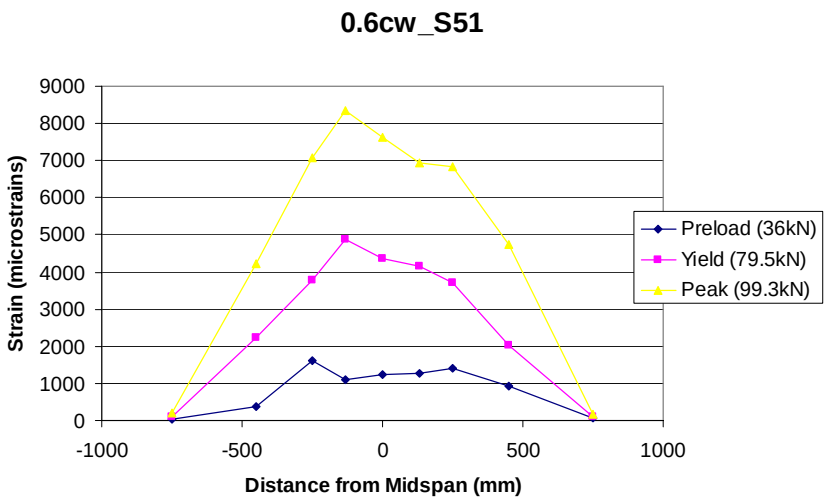
0.6cw_S51
Strain (microstrains)
Distance from Midspan (mm)
0
1000
2000
3000
4000
5000
6000
7000
8000
9000
-1000
-500
0
500
1000
Preload (36kN)
Yield (79.5kN)
Peak (99.3kN)

S51 (P43) 0.625

Specimen 50: Specimen preloaded to a 0.2mm residual maximum crack width 11/9/2005 (0.2cw_S50)

This specimen was preloaded such that the residual crack width after the beam was unloaded was approximately 0.2mm. The midspan displacement necessary to yield this residual crack width was determined during preloading of 48 where the beam was cycled to various preload displacements and then the cracks were measured after the load was released. This was the lowest preload level tested in which the steel had been yielded during loading. Like specimens 52 and 51 tested previously, no unbonded regions were manufactured into this specimen. The relatively large maximum residual crack width is the only defect. Final debonding occurred to the left initiating under the left load point at a diagonal crack location with a "deep concrete, steel" failure mode, as can be seen in the photo below. Note that a very large reagion of concrete was left attached to the FRP as the concrete debonded away from the steel, rather than the FRP. The peak load was 94.2kN at a midspan displacement of 17.9mm and the failure mode was deep concrete, steel debonding. These are typical load and midspan displacements for specimens debonding by this failure mode.

Beam Characteristic	Value
Test Date	11/9/2005
Rehab Date (number)	10/21/2005 (7)
Concrete Cast Date (number)	2/8/2005 (2)
Time from Rehab to Test	19 days
Maximum Load Held	94.17 kN
Displacement at Maximum Load	17.90 mm
Measured Steel Yield	2718 με
Load at Steel Yield	68.88 kN
Displacement at Steel Yield	7.96 mm
FRP Strain at Steel Yield	4039 με
FRP Strain at Debonding (Location)	7163(F9) με
FRP Midspan Strain at Debonding	7163 με
Debonding Direction	Left
Failure Mode	Deep Concrete, Steel

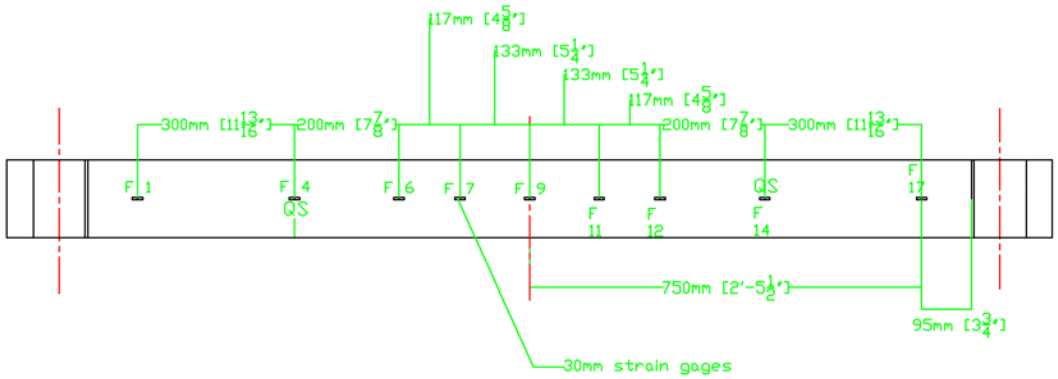

Load (kN)	Crack Width (mm)	Notes
0.00	0.15	
36.00	0.15	Some small new cracks
2.50	0.15	
75.10	0.2	Some new cracking. Very small local debonding in the constant moment region
2.50	0.15	
90.00	0.3	Several new diagonal cracks. Slight local debonding under the left load point
2.50	0.2	
95.30		Final failure tore a huge section of concrete (~18") down to the steel. Deep failure was to the left from the midspan to the quarter span

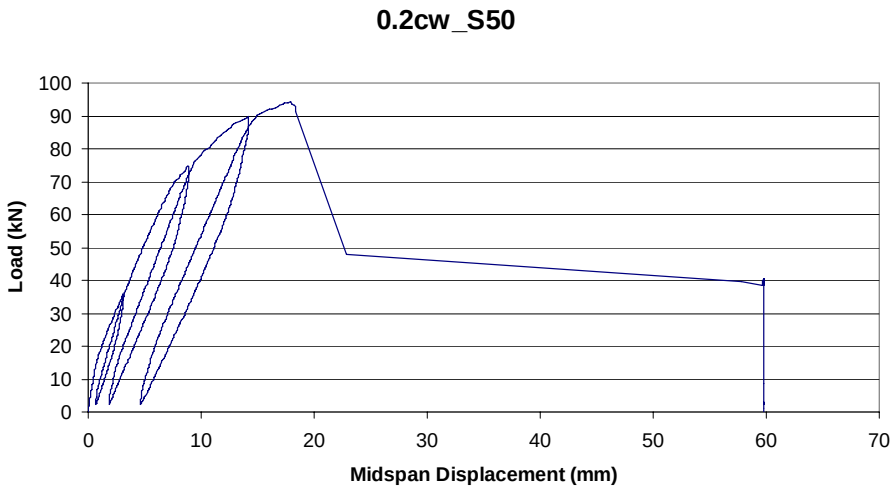
0.2cw_S50
Load (kN)
Midspan Displacement (mm)
0
10
20
30
40
50
60
70
80
90
100

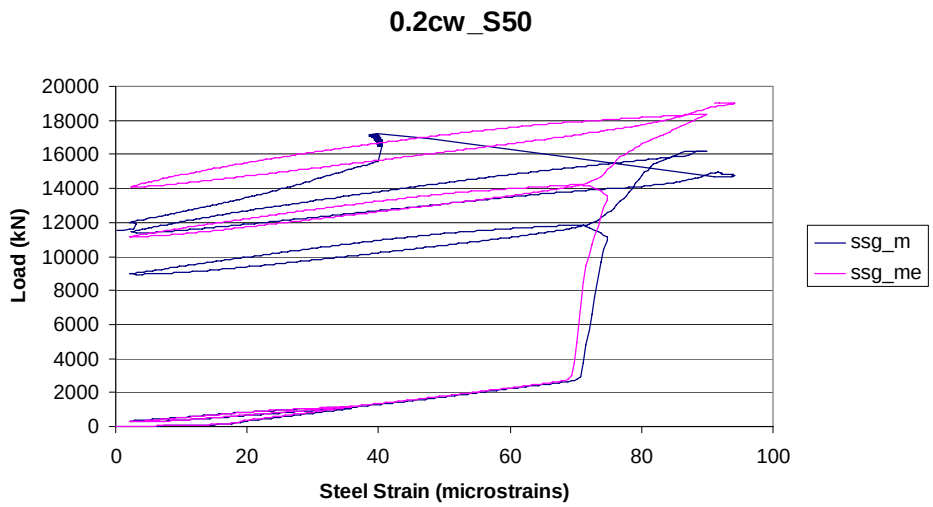
0.2cw_S50
Load (kN)
Steel Strain (microstrains)
ssg_m
ssg_me

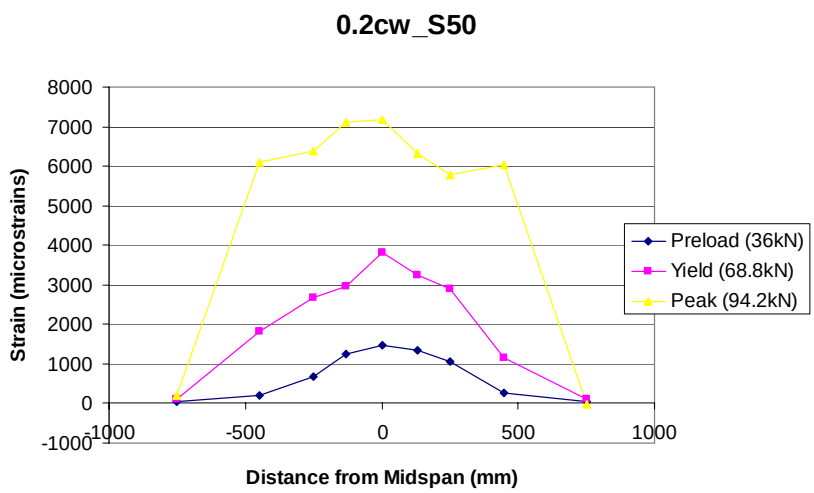
0.2cw_S50
Strain (microstrains)
Distance from Midspan (mm)
Preload (36kN)
Yield (68.8kN)
Peak (94.2kN)

Specimen 47: Strengthened, preloaded control specimen tested 11/9/2005 (R_C_Control_8_S47)

Specimen 47 was a control specimen with standard preloading as discussed in section 2.8, but without any purposely inserted defects. It is the control specimen that was created in conjunction with the defective beams for rehabilitation set seven. The peak load held by this specimen was modest at 90.0kN and corresponding midspan displacement of 16.42mm. Several inches of local debonding developed as the actuator approached the peak of the 90kN load cycle on both sides of the midspan. Final debonding occurred when a 90kN load was approached on the 105kN load cycle.

Debonding propagated to the right end of the beam. The debonding mechanism observed was failure debonding through deep concrete, and at the steel.

Beam Characteristic	Value
Test Date	11/9/05
Rehab Date (number)	10/21/05 (7)
Concrete Cast Date (number)	2/8/05 (2)
Time from Rehab to Test	19 days
Maximum Load Held	89.95 kN
Displacement at Maximum Load	16.42 mm
Measured Steel Yield	2558 με
Load at Steel Yield	69.84 kN
Displacement at Steel Yield	7.88 mm
FRP Strain at Steel Yield	3889 με
FRP Strain at Debonding (Location)	6695 (F11) με
FRP Midspan Strain at Debonding	6482 με
Debonding Direction	Right
Failure Mode	Deep Concrete, Steel

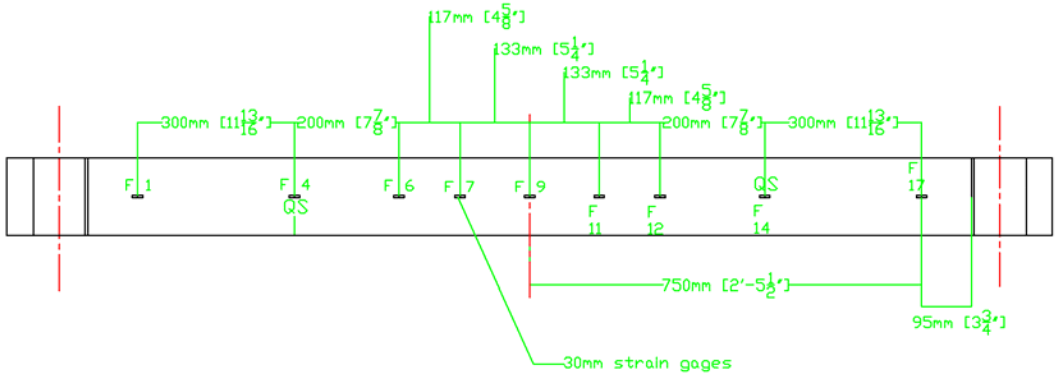

Load (kN)	Crack Width (mm)	Notes
0.00	<0.1	
36.30	< 0.1	Typical crack reopening
2.50	< 0.1	
75.00	~0.08	Typical new cracking
2.50	< 0.1	
90.00	0.4	A lot of noise during loading. Curve has a pretty low slope. Shear cracks have caused several inches of local debonding on both sides of the beam outside the constant moment region.
2.50	0.3	
90.20		Final debonding to the right side from the location of the shear crack approx 100mm to the right side of the loading point. Good failure through the concrete. The beam was somewhat weaker than anticipated, however.

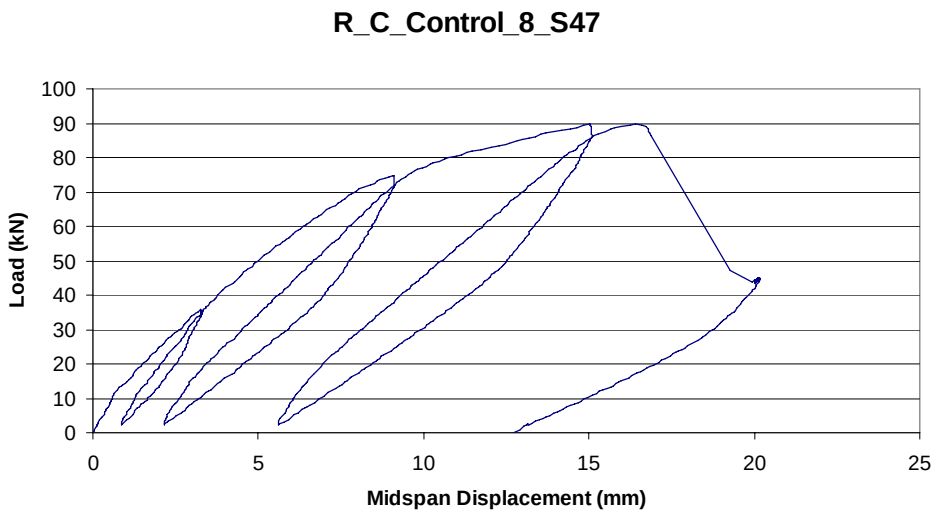
R_C_Control_8_S47
Load (kN)
Midspan Displacement (mm)
0
10
20
30
40
50
60
70
80
90
100
0
5
10
15
20
25

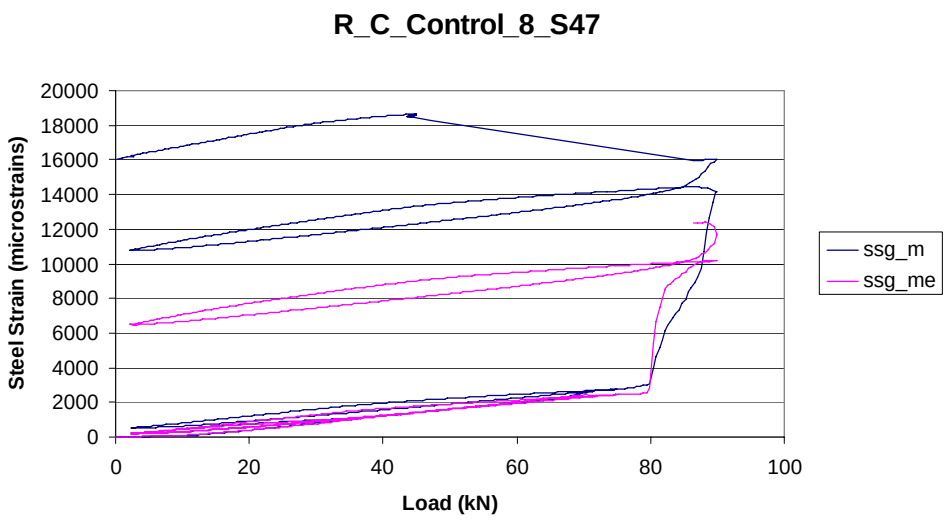
R_C_Control_8_S47
Steel Strain (microstrains)
Load (kN)
0
2000
4000
6000
8000
10000
12000
14000
16000
18000
20000
0
20
40
60
80
100
ssg_m
ssg_me

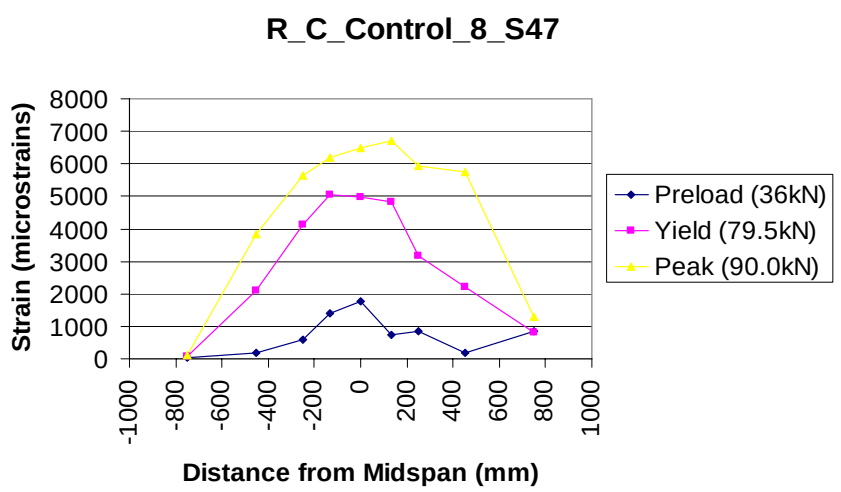
R_C_Control_8_S47
Strain (microstrains)
Distance from Midspan (mm)
0
1000
2000
3000
4000
5000
6000
7000
8000
-1000
-800
-600
-400
-200
0
200
400
600
800
1000
Preload (36kN)
Yield (79.5kN)
Peak (90.0kN)

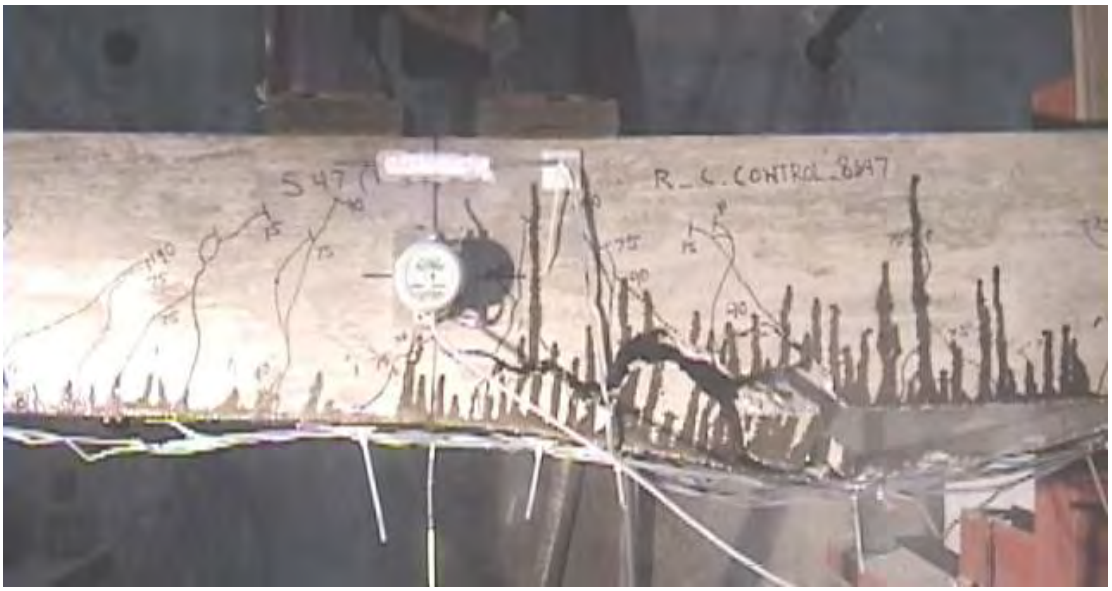

Specimen 48: Specimen preloaded to a 1.5mm residual maximum crack width 11/10/2005 (1.5cw_S48)

No steel strain gauge data was available during final testing due to damage during preloading. Specimen 48 was preloaded to the largest residual crack width investigated. This specimen was preloaded such that the residual crack width after the beam was unloaded was approximately 1.5mm. Like specimens 52, 51, and 50 tested previously, no unbonded regions were manufactured into this specimen. The relatively large maximum residual crack width is the only defect. Final debonding occurred to the left initiating a diagonal crack about 75mm to the left of the loading point. A “deep concrete, steel” failure mode was observed, as can be seen in the photo below. The peak load was 90.6kN at a midspan displacement of 16.05mm.

Beam Characteristic	Value
Test Date	11/10/2005
Rehab Date (number)	10/21/2005 (7)
Concrete Cast Date (number)	2/8/2005 (2)
Time from Rehab to Test	20 days
Maximum Load Held	90.58 kN
Displacement at Maximum Load	16.05 mm
Measured Steel Yield	no data
Load at Steel Yield	~64.4 kN
Displacement at Steel Yield	7.49 mm
FRP Strain at Steel Yield	4028 με
FRP Strain at Debonding (Location)	7006 (F7) με
FRP Midspan Strain at Debonding	6897 με
Debonding Direction	Left
Failure Mode	Deep Concrete, Steel

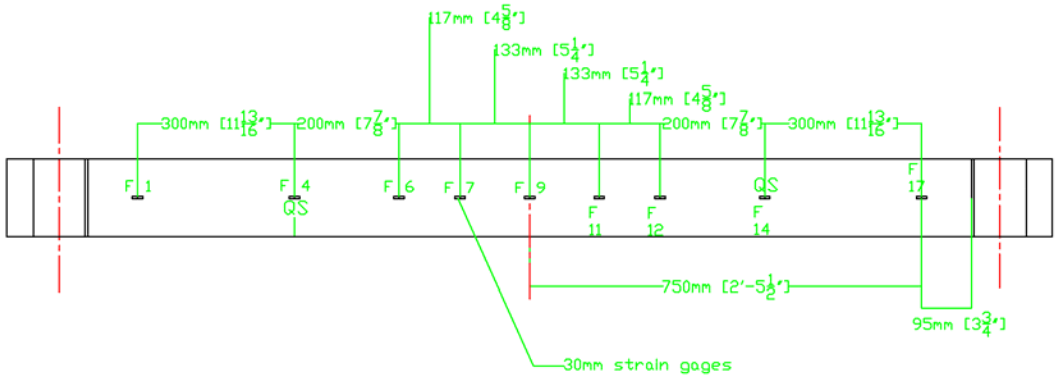

Load (kN)	Crack Width (mm)	Notes
0.00	1.5	Both midspan steel strain gauges have been broken.
36.00	1.6	Some slight new cracking. Appears to have relatively low initial stiffness.
2.50	1.5	
75.00	1.6	More new cracking.
2.40	1.5	
90.00	1.8	Large shear crack opened on the left side just outside the constant moment region. About 50mm of local debonding at this point.
2.40	1.5	
90.90	1.8	Still an excellent failure propagating to the left from the shear crack. Deep break near the shear crack, but most of the failure is through the concrete at the interface.

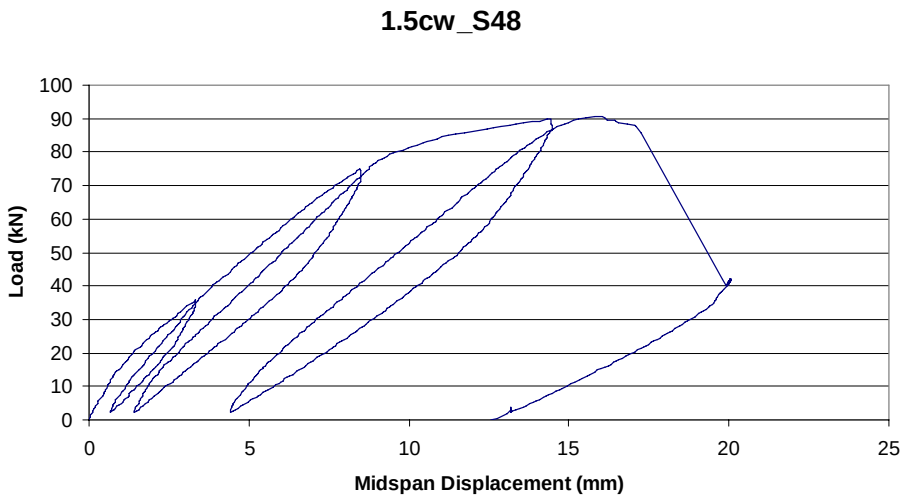
1.5cw_S48
Load (kN)
100
90
80
70
60
50
40
30
20
10
0
0
5
10
15
20
25
Midspan Displacement (mm)

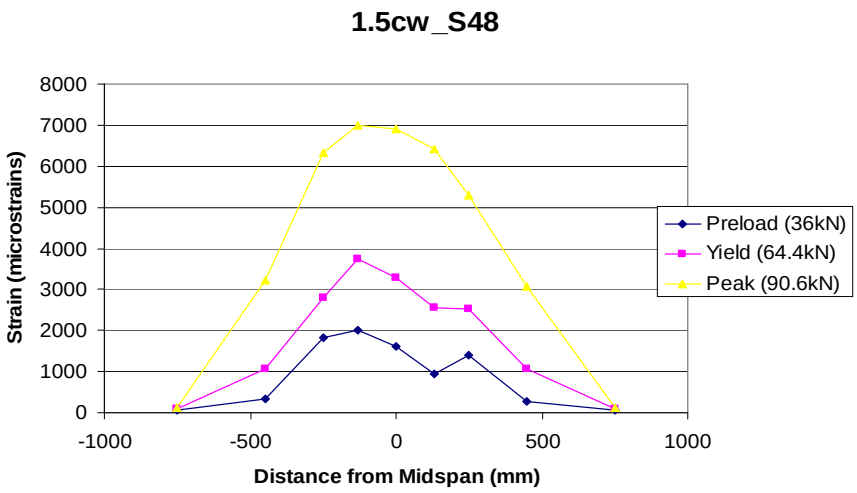
1.5cw_S48
Strain (microstrains)
8000
7000
6000
5000
4000
3000
2000
1000
0
-1000
-500
0
500
1000
Distance from Midspan (mm)
Preload (36kN)
Yield (64.4kN)
Peak (90.6kN)

Specimen 54: 100mm x 150mm rectangular disbond inserted in the adhesive interface, submerged in water for twenty-one days, located 185mm from the midspan, tested 11/14/2005 (100RS21_185_1.0cw_S54)

Specimen 54 was preloaded such that a residual crack width of 1.0mm resulted (see section 2.8 for details). No steel strain data is available for final testing of this specimen due to the damage sustained to the strain gauges during preloading. This specimen consisted of a combination of three different defects in an effort to assess their cumulative effects: 1) excessive preload cracking to a 1.0mm residual maximum crack width; 2) a 100mm long by 150mm wide unbonded rectangular region in the adhesive interface located 185mm from the midspan; and 3) after initial curing the tension face was submerged in one inch of water for a period of twenty-one days. Given the large amount of damage that was manufactured into this beam, it performed quite well failing with a maximum load of 88.9kN at a midspan displacement of 14.6mm. The failure mode was debonding through a thick concrete bondline. Debonding occurred to the left propagating from near the right edge of the defect where a large crack opened prior to failure.

Beam Characteristic	Value
Test Date	11/14/05
Rehab Date (number)	10/21/05 (7)
Concrete Cast Date (number)	2/8/05 (2)
Time from Rehab to Test	24 days
Maximum Load Held	89.89 kN
Displacement at Maximum Load	14.64 mm
Measured Steel Yield	2920 με
Load at Steel Yield	91.62 kN
Displacement at Steel Yield	6.94 mm
FRP Strain at Steel Yield	3726 με
FRP Strain at Debonding (Location)	7222 (F6) με
FRP Midspan Strain at Debonding	6192 με
Debonding Direction	Left
Failure Mode	Thick Concrete Bondline

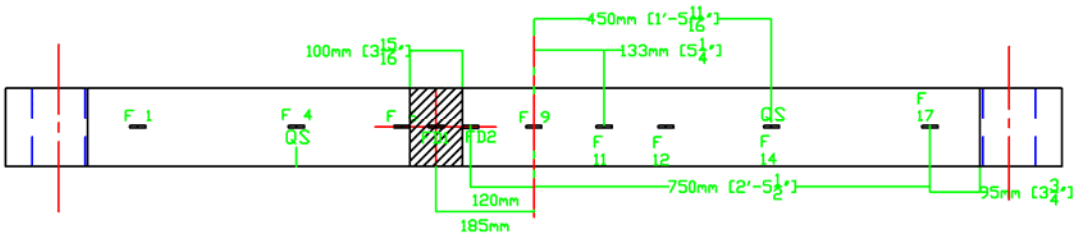

Load (kN)	Crack Width (mm)	Notes
0.00	1.0	The tension face of this specimen was submerged in ~25mm of water for 21 days.
36.10	1.1	
2.50	1	
75.20	1.2	Some new cracking. No obvious local debonding.
2.40	1	No new cracks at the defect location yet.
90.10	1.2	Massive local debonding from the defect to about 25mm to the left of the quarter span. Extensive concrete crushing at the midspan.
2.50	1.1	
		Global debonding occurred before the beam reached the 90kN load obtained in the previous load cycle. Final debonding was a good failure (~90% though the concrete).

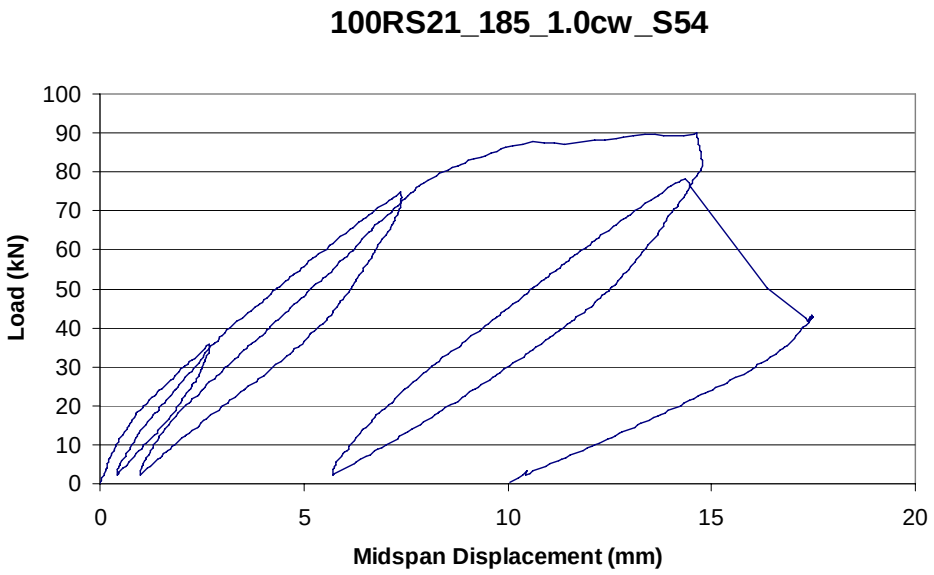
100RS21_185_1.0cw_S54
Load (kN)
100
90
80
70
60
50
40
30
20
10
0
0
5
10
15
20
Midspan Displacement (mm)

S54 (P46)
100RS_185_1.0cw_S54

Specimen 57: 100mm x 150mm rectangular disbond inserted in the adhesive interface 185mm from the midspan in both directions tested 11/15/2005 (100R2_185_1.0cw_S57)

Specimen 57 was preloaded such that a 1.0mm approximate residual crack width remained (see section 2.8 for details). This specimen consisted of two distinct defect types: 1) excessive preload cracking to 1.0mm; and 2) a 100mm by 150mm rectangular disbond in the adhesive interface located 185mm from the midspan in each direction (see drawing below). Debonding occurred to the left originating from the left side disbond. The failure was through a thin concrete bondline resulting in a typical specimen reaching a maximum load of 88.6kN at a typical midspan displacement of 14.1mm.

Beam Characteristic	Value
Test Date	11/15/05
Rehab Date (number)	10/21/05 (7)
Concrete Cast Date (number)	2/8/05 (2)
Time from Rehab to Test	25 days
Maximum Load Held	88.62 kN
Displacement at Maximum Load	14.12 mm
Measured Steel Yield	2737 με
Load at Steel Yield	78.68 kN
Displacement at Steel Yield	10.08 mm
FRP Strain at Steel Yield	4507 με
FRP Strain at Debonding (Location)	6890 (F6) με
FRP Midspan Strain at Debonding	5955 με
Debonding Direction	Left
Failure Mode	Thin Concrete Bondline

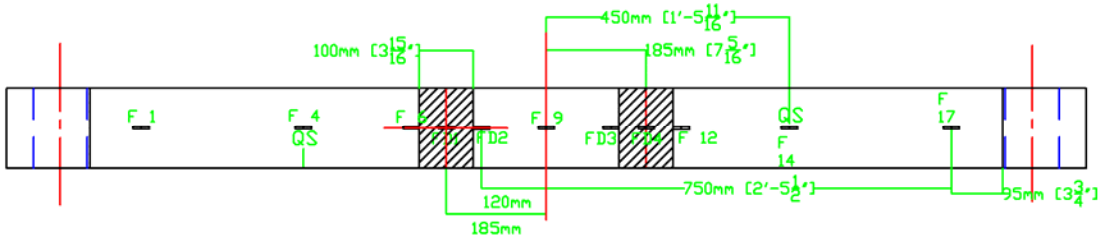

Load (kN)	Crack Width (mm)	Notes
0.00	0.8	
36.10	0.8	
2.40	0.8	
75.10	0.9	Some new cracking. No obvious local debonding
2.50	0.8	
88.80	0.5	Very gradual debonding propagating from the left defect in the left direction. Debonded through a thin concrete layer, but not through the adhesive. FRP ruptured, but I think it happened on the recoil as the composite snapped off due to global debonding.
2.50		
95.50		Final debonding appeared to propagate from the midspan (defect location) outward in each direction. Final failure was debonding on the right side of the beam.

100R2_185_1.0cw_S57

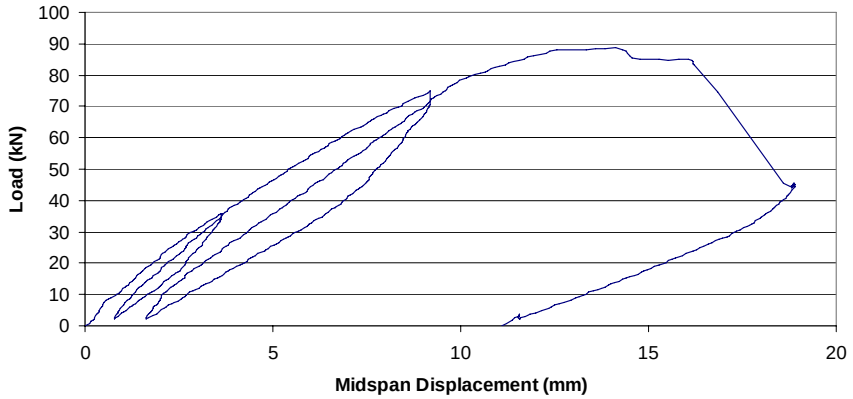

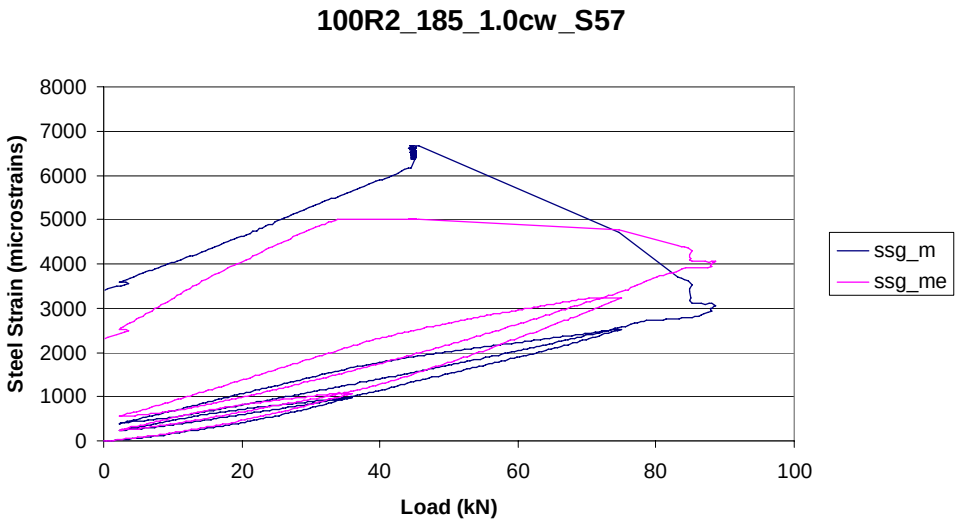
100R2_185_1.0cw_S57
Steel Strain (microstrains)
8000
7000
6000
5000
4000
3000
2000
1000
0
0
20
40
60
80
100
Load (kN)
ssg_m
ssg_me

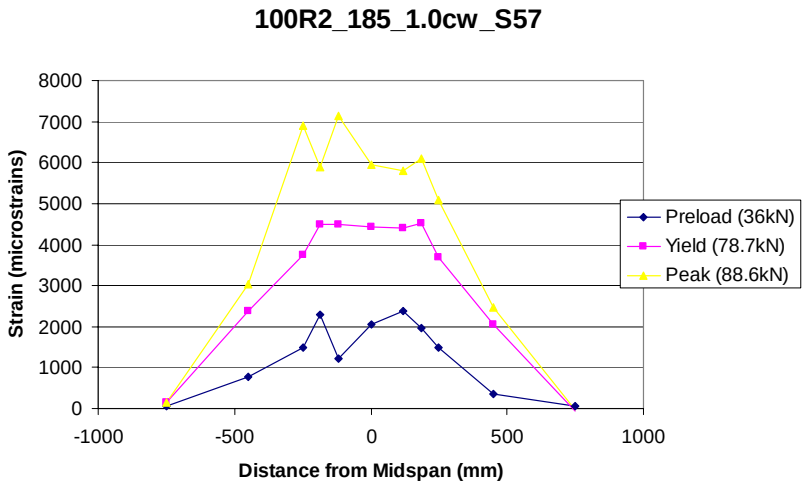
100R2_185_1.0cw_S57
Strain (microstrains)
8000
7000
6000
5000
4000
3000
2000
1000
0
-1000
-500
0
500
1000
Distance from Midspan (mm)
Preload (36kN)
Yield (78.7kN)
Peak (88.6kN)

S57 (P49)
100R2-185.1.0cw_S57

Specimen 58: 100mm x 150mm rectangular disbond inserted in the adhesive interface 185mm from the midspan tested 11/16/2005 (100R_185_1.0cw_S58)

Specimen 54 was preloaded such that a residual crack width of 1.0mm resulted (see section 2.8 for details). The specimen was loaded monotonically to verify similar behavior compared to those loaded with low level cycling. Specimen 54 consisted of two distinct defect types: 1) excessive preload cracking to 1.0mm; and 2) a 100mm by 150mm rectangular disbond in the adhesive interface located 185mm from the midspan. Debonding occurred to the left originating from the left side of the disbond from a diagonal crack. The failure was through a thin concrete bondline resulting in a strong specimen reaching a maximum load of 94.3kN at a typical midspan displacement of 13.7mm.

Beam Characteristic	Value
Test Date	11/16/2005
Rehab Date (number)	10/21/2005 (7)
Concrete Cast Date (number)	2/8/2005 (2)
Time from Rehab to Test	26 days
Maximum Load Held	94.33 kN
Displacement at Maximum Load	13.70 mm
Measured Steel Yield	2147 με
Load at Steel Yield	70.34 kN
Displacement at Steel Yield	7.48 mm
FRP Strain at Steel Yield	4000 με
FRP Strain at Debonding (Location)	6685 (FD2) με
FRP Midspan Strain at Debonding	6008 με
Debonding Direction	Left
Failure Mode	Thin Concrete Bondline

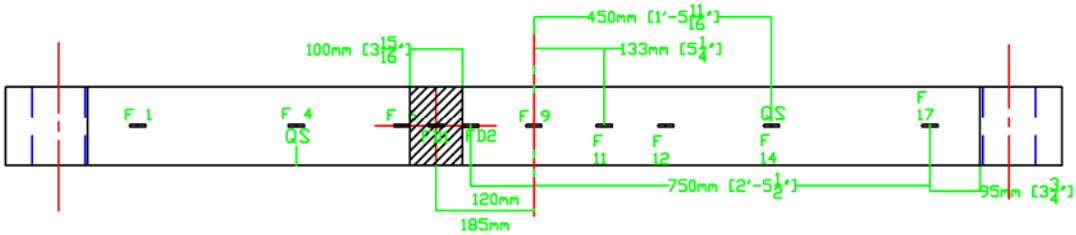

Load (kN)	Crack Width (mm)	Notes
0.00	1.1	
94.60		Final debonding was relatively non-violent propagating from the defect to the left through a thin concrete layer.

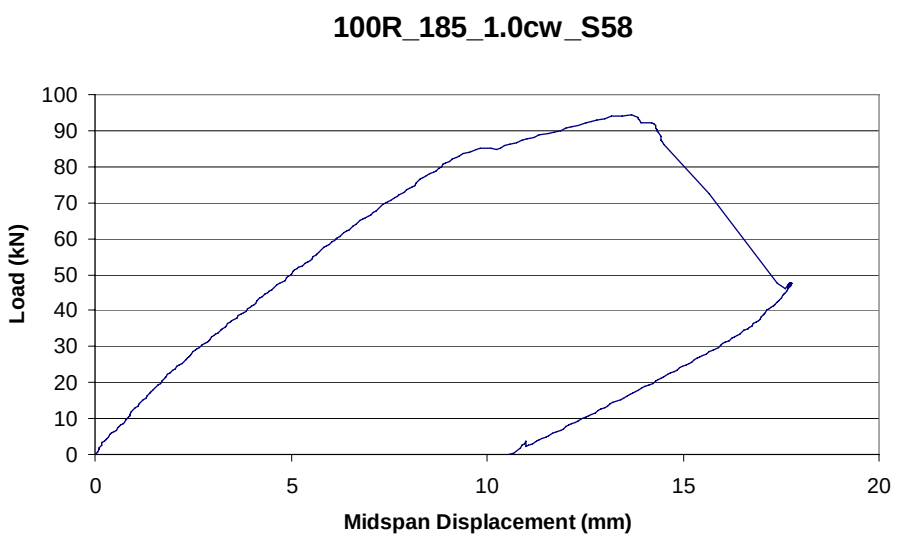

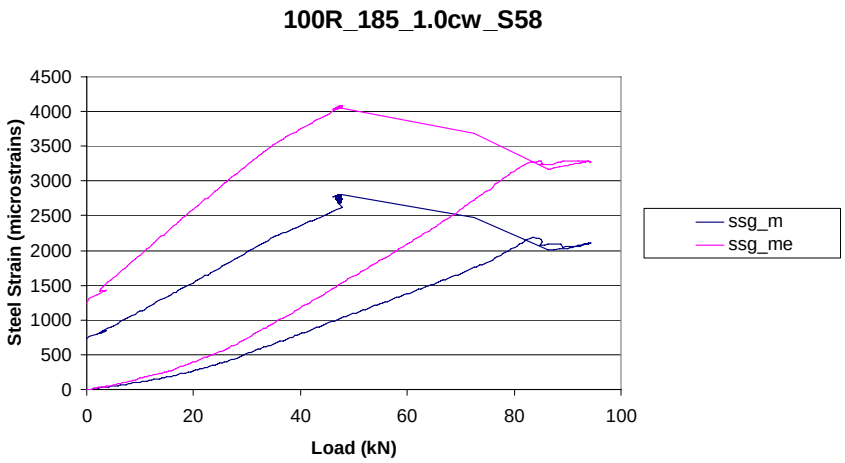
100R_185_1.0cw_S58
Steel Strain (microstrains)
4500
4000
3500
3000
2500
2000
1500
1000
500
0
0
20
40
60
80
100
Load (kN)
ssg_m
ssg_me

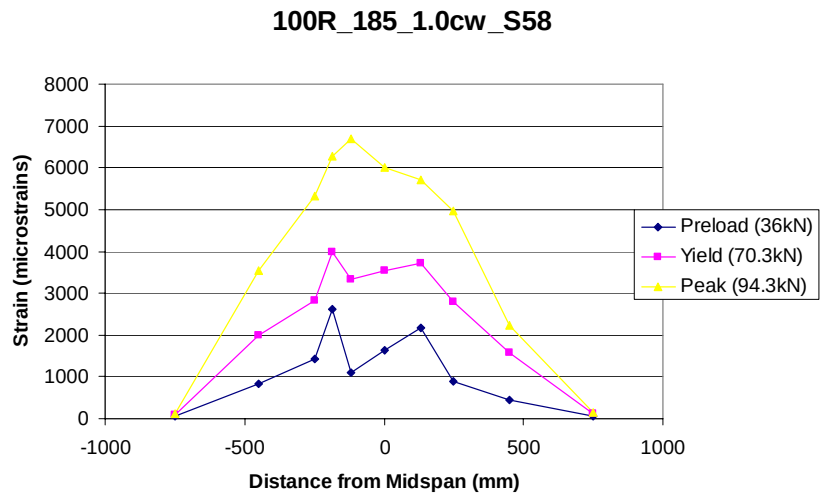
100R_185_1.0cw_S58
Strain (microstrains)
8000
7000
6000
5000
4000
3000
2000
1000
0
-1000
-500
0
500
1000
Distance from Midspan (mm)
Preload (36kN)
Yield (70.3kN)
Peak (94.3kN)

S58 (P50)
100R_185_S58

Specimen 60: 50mm diameter circular disbond inserted in the adhesive interface 185mm from the midspan tested 11/17/2005 (50C_185_S60_2)

Specimen 60 was manufactured with a defect consisting of a circular disbond with a centroid located 185mm away from the midspan of the beam. The size of the manufactured disbond was 50mm in diameter. This was the second specimen tested with this defect configuration. The beam was, precracked using the 35.6 kN preload level before the application of FRP. Final debonding occurred from approximately 100mm to the right of the right loading point (on the opposite side of the midspan as the disbond), propagating to the right.

Beam Characteristic	Value
Test Date	11/17/05
Rehab Date (number)	10/21/05 (7)
Concrete Cast Date (number)	2/8/05 (2)
Time from Rehab to Test	27 days
Maximum Load Held	96.54 kN
Displacement at Maximum Load	14.97 mm
Measured Steel Yield	2343 με
Load at Steel Yield	71.04 kN
Displacement at Steel Yield	7.87 mm
FRP Strain at Steel Yield	3482 με
FRP Strain at Debonding (Location)	6483 (F9) με
FRP Midspan Strain at Debonding	6483 με
Debonding Direction	Right
Failure Mode	Deep Concrete, Steel

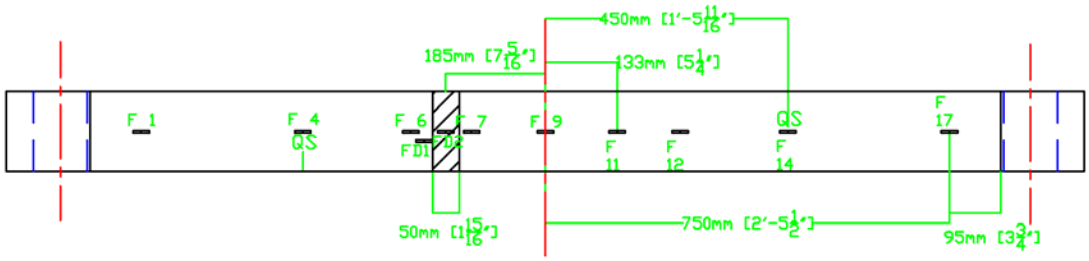

Load (kN)	Crack Width (mm)	Notes
0.00	<0.1	
36.30	~0.05	
2.40	<0.1	
75.20	0.1	Typical new cracking, but no apparent debonding.
2.30	<0.1	
90.00	0.3	More new cracking. Largest crack is just to the right of the defect.
2.50	0.1	largest crack width is at the steel depth.
96.80		Final failure was to the right (away from the defect location), starting from the outside edge of the right load point. Tore out a large chunk of concrete, shearing a good layer of concrete.

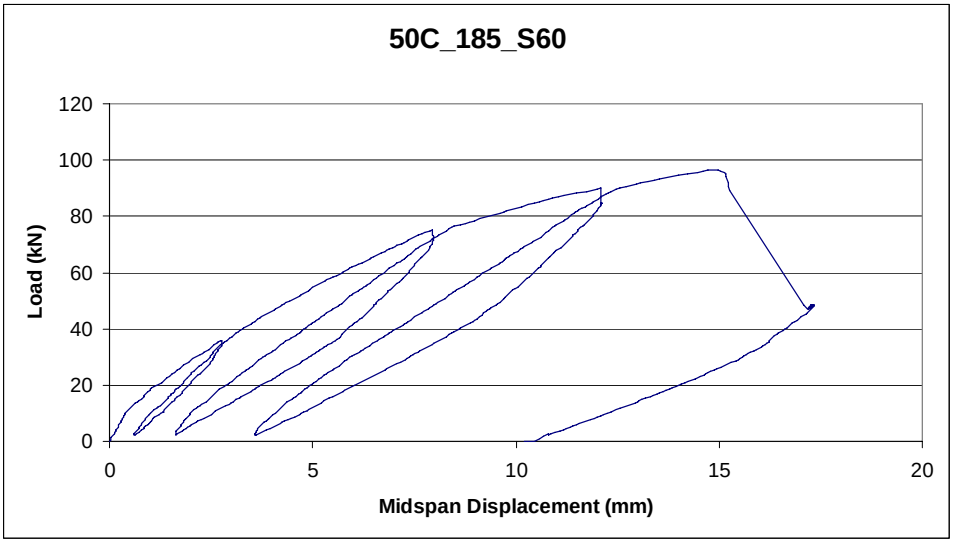
50C_185_S60
Load (kN)
120
100
80
60
40
20
0
0
5
10
15
20
Midspan Displacement (mm)

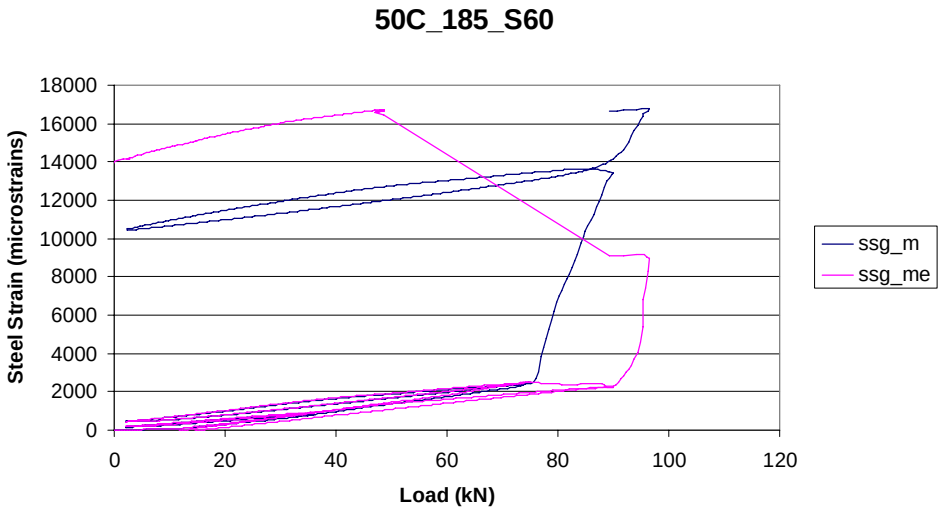
50C_185_S60
Steel Strain (microstrains)
18000
16000
14000
12000
10000
8000
6000
4000
2000
0
0
20
40
60
80
100
120
Load (kN)
ssg_m
ssg_me

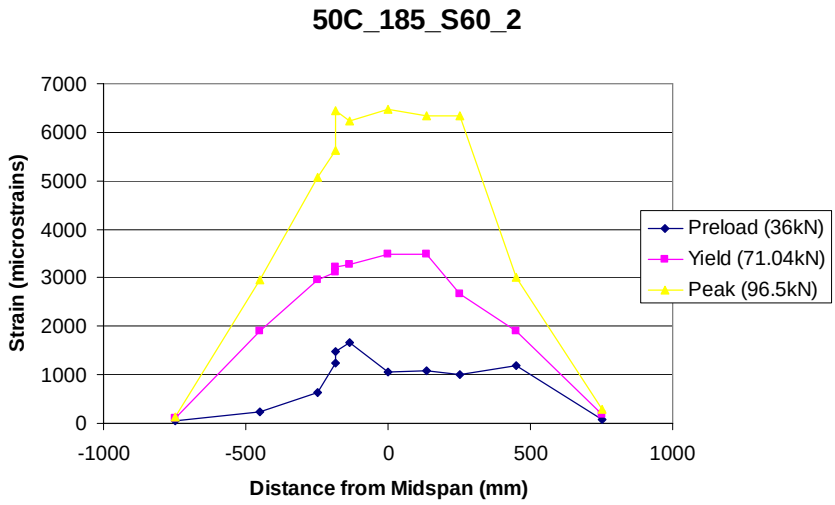
50C_185_S60_2
Strain (microstrains)
7000
6000
5000
4000
3000
2000
1000
0
-1000
-500
0
500
1000
Distance from Midspan (mm)
Preload (36kN)
Yield (71.04kN)
Peak (96.5kN)

Specimen 59: 25mm diameter circular disbond inserted in the adhesive interface 185mm from the midspan tested 11/17/2005 (25C_185_S59_2)

Specimen 59 was manufactured with a defect consisting of a circular disbond with a centroid located 185mm away from the midspan of the beam. The size of the manufactured disbond was 25mm in diameter. This was the second specimen tested with this defect configuration. The beam was, precracked using the 35.6 kN preload level before the application of FRP. Final debonding occurred at the defect location, failing by the "deep concrete, steel" debonding failure mode. This specimen failed at a very high load of 100.2kN at a corresponding midspan deflection of 16.6mm.

Beam Characteristic	Value
Test Date	11/17/05
Rehab Date (number)	10/21/05 (7)
Concrete Cast Date (number)	2/8/05 (2)
Time from Rehab to Test	27 days
Maximum Load Held	100.23 kN
Displacement at Maximum Load	16.58 mm
Measured Steel Yield	2398 με
Load at Steel Yield	66.54 kN
Displacement at Steel Yield	6.64 mm
FRP Strain at Steel Yield	3221 με
FRP Strain at Debonding (Location)	7708 (F9) με
FRP Midspan Strain at Debonding	7708 με
Debonding Direction	Left
Failure Mode	Deep Concrete, Steel

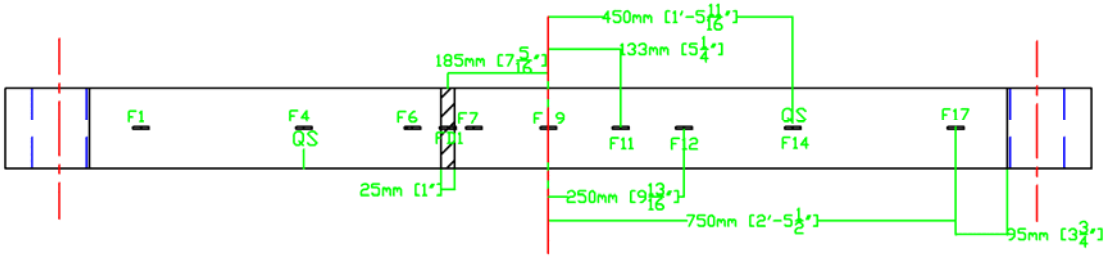

Load (kN)	Crack Width (mm)	Notes
0.00	<0.1	
36.00	<0.1	Some slight new cracking. Appears to have relatively low initial stiffness.
2.50	<0.1	
75.20	0.1	Moderate new cracking. No debonding. Both midspan strain gauges are lost.
2.40	<0.1	
90.00	0.3	Some crackling sound. Largest crack is located near the defect. Slight local debonding on both sides of the disbond.
2.40	0.15	
100.50		Very strong specimen tearing a large amount of concrete cover down to the steel.

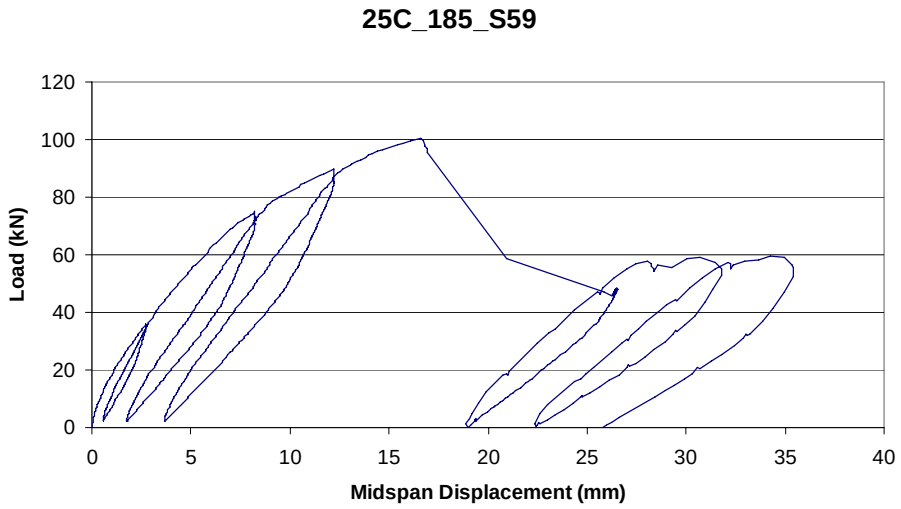
25C_185_S59
Load (kN)
Midspan Displacement (mm)
0
20
40
60
80
100
120
0
5
10
15
20
25
30
35
40

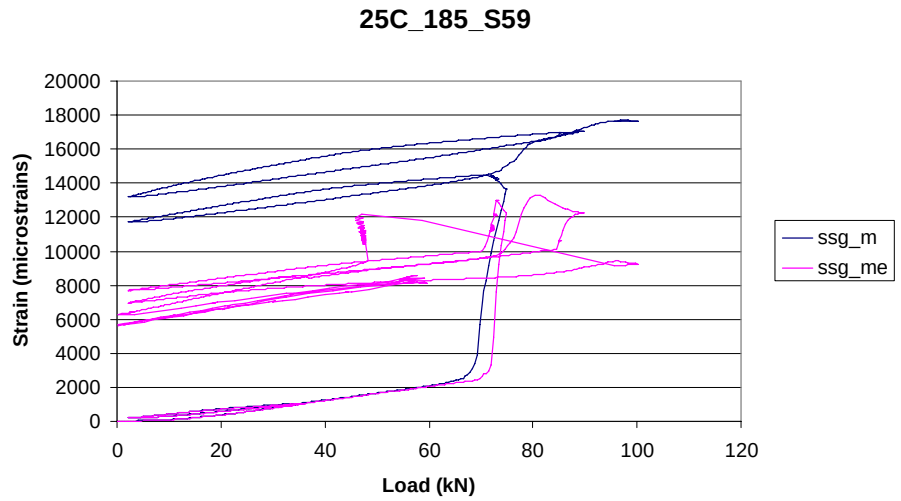
25C_185_S59
Strain (microstrains)
Load (kN)
ssg_m
ssg_me
0
2000
4000
6000
8000
10000
12000
14000
16000
18000
20000
0
20
40
60
80
100
120

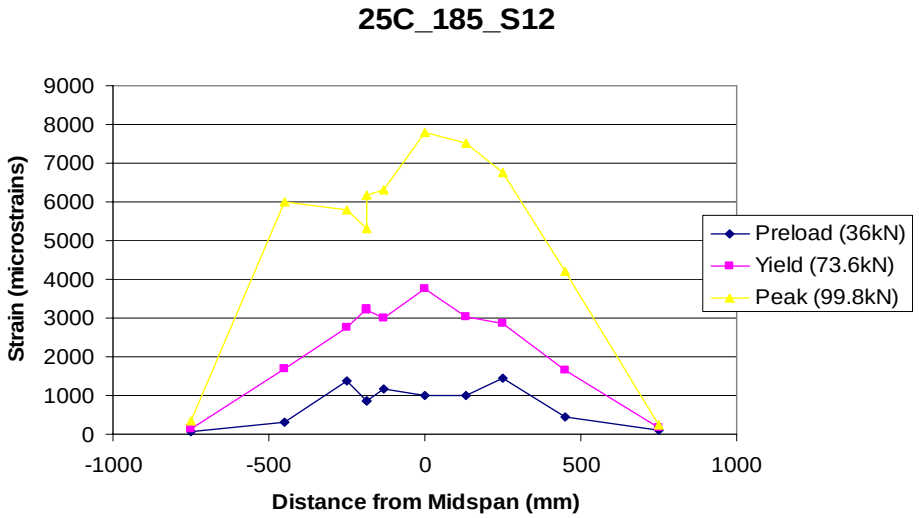
25C_185_S12
Strain (microstrains)
Distance from Midspan (mm)
Preload (36kN)
Yield (73.6kN)
Peak (99.8kN)
0
1000
2000
3000
4000
5000
6000
7000
8000
9000
-1000
-500
0
500
1000

Specimen 56: 200mm by 150mm rectangular disbond inserted in the adhesive interface 185mm from the midspan tested 11/18/2005 (200R_185_1.0cw_S56)

Specimen 54 was preloaded such that a 1.0mm approximate residual crack width remained (see section 2.8 for details). This specimen consisted of two distinct defect types: 1) excessive preload cracking to 1.0mm; and 2) a 200mm by 150mm rectangular disbond in the adhesive interface located 185mm from the midspan. Debonding occurred to the left originating from the midspan. The failure mode was deep concrete, steel debonding reaching a modest maximum load for this failure mode of 89.6kN at a somewhat low midspan displacement of 14.5mm.

Beam Characteristic	Value
Test Date	11/18/05
Rehab Date (number)	10/21/05 (7)
Concrete Cast Date (number)	2/8/05 (2)
Time from Rehab to Test	28 days
Maximum Load Held	89.56 kN
Displacement at Maximum Load	14.45 mm
Measured Steel Yield	2532 με
Load at Steel Yield	67.43 kN
Displacement at Steel Yield	7.51 mm
FRP Strain at Steel Yield	3547 με
FRP Strain at Debonding (Location)	7712 (FD2) με
FRP Midspan Strain at Debonding	5971 με
Debonding Direction	Left
Failure Mode	Deep Concrete, Steel

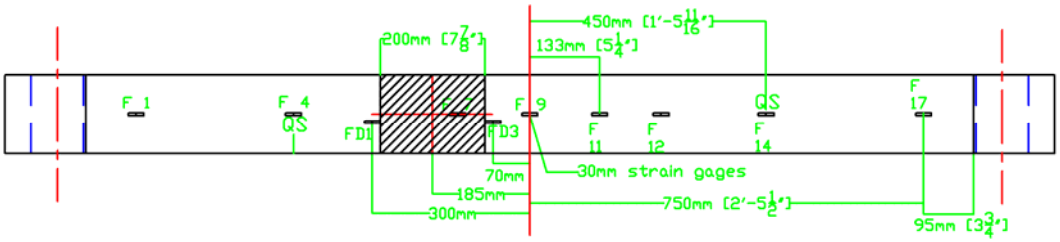

Load (kN)	Crack Width (mm)	Notes
0.00	1.0	
36.00	1.1	Some popping sound in defect region during loading. Two new cracks.
2.60	1.0	
75.40	1.2	Typical new cracking.
2.40	1	
89.90		More popping on loading. Failure was, as expected, debonding to the left from the defect location. Good failure by shearing through a thick layer of concrete.

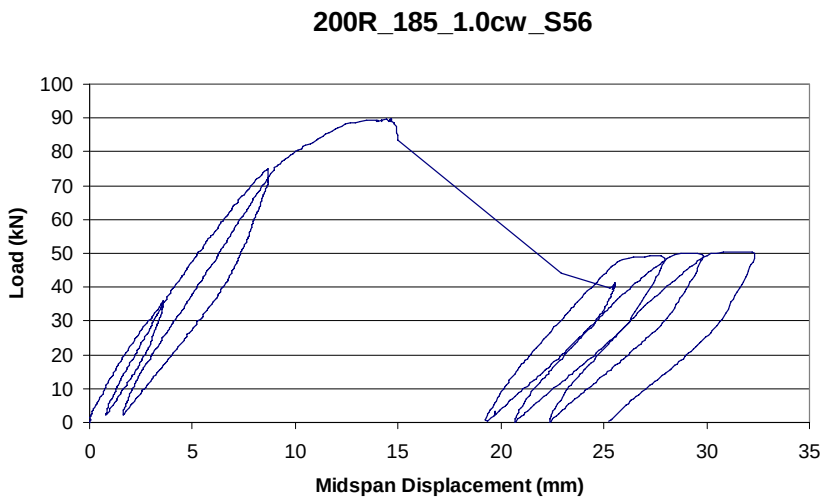
200R_185_1.0cw_S56
Load (kN)
Midspan Displacement (mm)
0
10
20
30
40
50
60
70
80
90
100
0
5
10
15
20
25
30
35

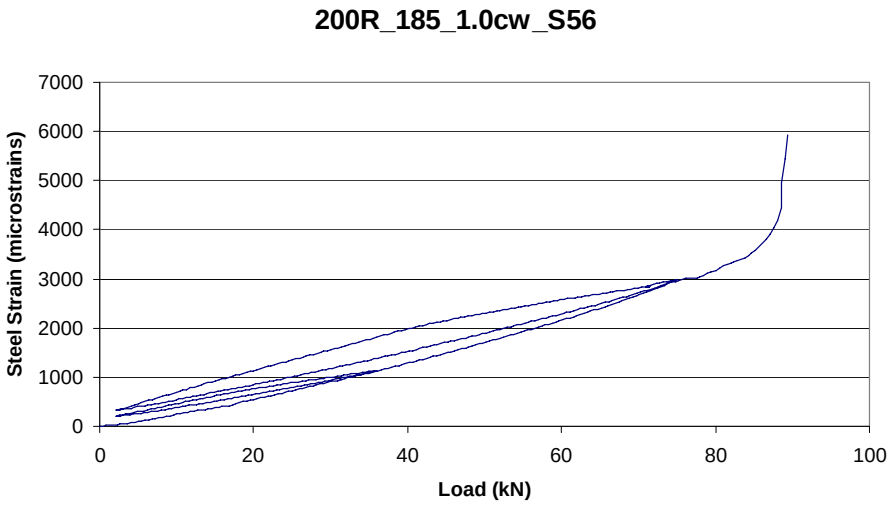
200R_185_1.0cw_S56
Steel Strain (microstrains)
Load (kN)
0
1000
2000
3000
4000
5000
6000
7000
0
20
40
60
80
100

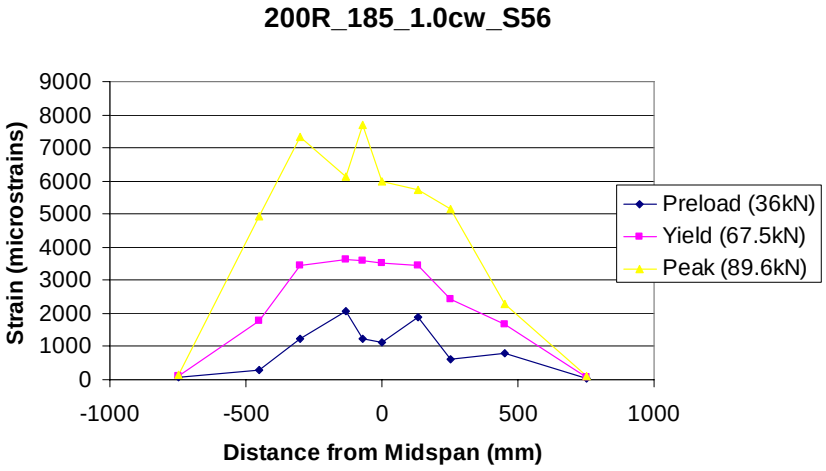
200R_185_1.0cw_S56
Strain (microstrains)
Distance from Midspan (mm)
0
1000
2000
3000
4000
5000
6000
7000
8000
9000
-1000
-500
0
500
1000
Preload (36kN)
Yield (67.5kN)
Peak (89.6kN)

Specimen 49: 250mm x 150mm rectangular disbond inserted in the adhesive interface located 185mm from the midspan, tested 11/18/2005 (250R_185_S49_2)

Specimen 49 was manufactured with a defect consisting of a rectangular disbond with a centroidal location 185mm away from the midspan of the beam. The dimensions of the manufactured disbond were 250mm length by 150mm width (the full width of the beam). This specimen is the largest sized disbond that was investigated in the laboratory. Specimen 49 is the second specimen tested with this defect configuration. The beam was, precracked using the 35.6 kN preload level before the application of FRP. Final debonding occurred from the defect where a large diagonal crack was observed. The specimen failed at 87.8kN and at a midspan deflection of 13.9mm by the thin concrete bondline debonding failure mode.

Beam Characteristic	Value
Test Date	11/18/05
Rehab Date (number)	10/21/05 (7)
Concrete Cast Date (number)	2/8/05 (2)
Time from Rehab to Test	24 days
Maximum Load Held	87.80 kN
Displacement at Maximum Load	13.85 mm
Measured Steel Yield	2318 με
Load at Steel Yield	66.00 kN
Displacement at Steel Yield	7.06 mm
FRP Strain at Steel Yield	3573 με
FRP Strain at Debonding (Location)	6790 (FD1) με
FRP Midspan Strain at Debonding	5776 με
Debonding Direction	Left
Failure Mode	Thin Concrete Bondline

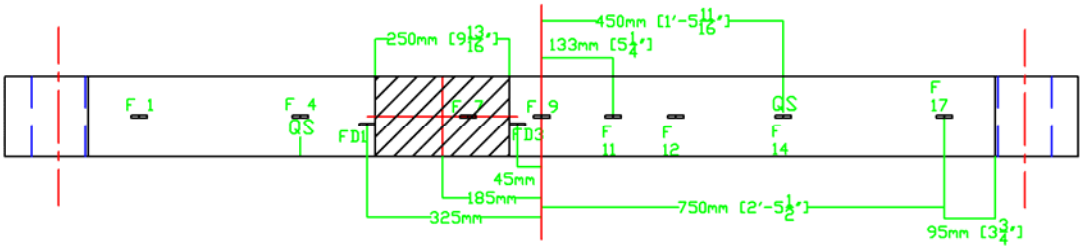

Load (kN)	Crack Width (mm)	Notes
0.00	<0.1	
36.10	<0.1	Typical crack reopening.
2.50	<0.1	
75.50	0.5	Largest crack is at the defect location.
2.60	0.15	
88.00		Debonding to the left from the defect location. Failed by shearing a thin concrete layer.

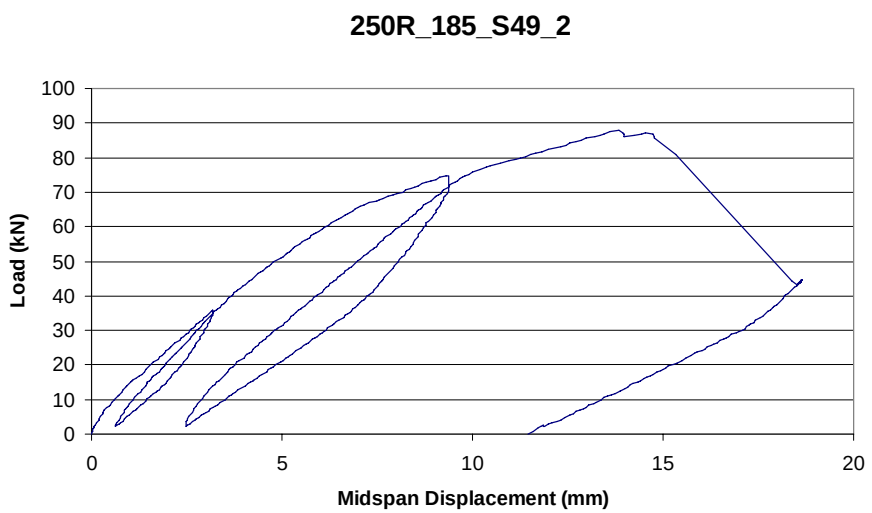

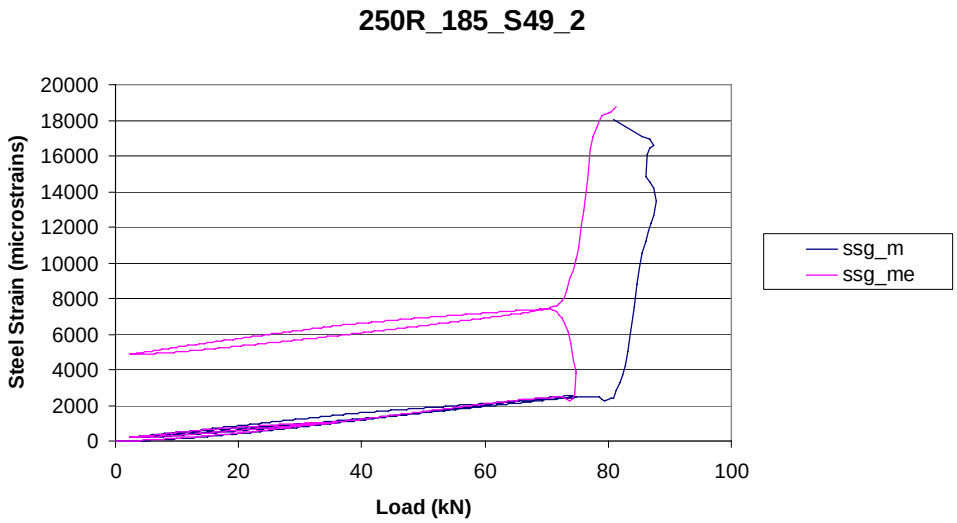
250R_185_S49_2
Steel Strain (microstrains)
20000
18000
16000
14000
12000
10000
8000
6000
4000
2000
0
0
20
40
60
80
100
Load (kN)
ssg_m
ssg_me

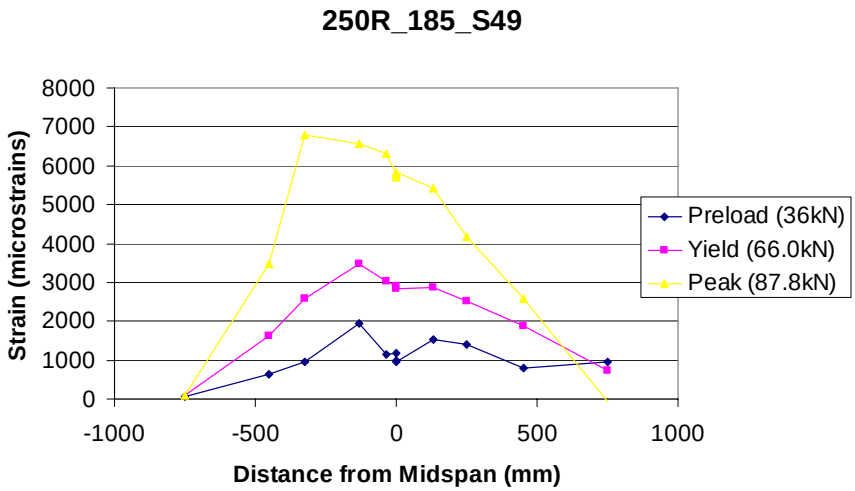
250R_185_S49
Strain (microstrains)
8000
7000
6000
5000
4000
3000
2000
1000
0
-1000
-500
0
500
1000
Distance from Midspan (mm)
Preload (36kN)
Yield (66.0kN)
Peak (87.8kN)